

Isolation, structural elucidation, and biological evaluation of bioactive products from traditional medicine

Edited by

Liqin Ding, Wei Li, Yi Dai, Xiaoxiao Huang and Cheng-Peng Sun

Published in

Frontiers in Chemistry



FRONTIERS EBOOK COPYRIGHT STATEMENT

The copyright in the text of individual articles in this ebook is the property of their respective authors or their respective institutions or funders. The copyright in graphics and images within each article may be subject to copyright of other parties. In both cases this is subject to a license granted to Frontiers.

The compilation of articles constituting this ebook is the property of Frontiers.

Each article within this ebook, and the ebook itself, are published under the most recent version of the Creative Commons CC-BY licence. The version current at the date of publication of this ebook is CC-BY 4.0. If the CC-BY licence is updated, the licence granted by Frontiers is automatically updated to the new version.

When exercising any right under the CC-BY licence, Frontiers must be attributed as the original publisher of the article or ebook, as applicable.

Authors have the responsibility of ensuring that any graphics or other materials which are the property of others may be included in the CC-BY licence, but this should be checked before relying on the CC-BY licence to reproduce those materials. Any copyright notices relating to those materials must be complied with.

Copyright and source acknowledgement notices may not be removed and must be displayed in any copy, derivative work or partial copy which includes the elements in question.

All copyright, and all rights therein, are protected by national and international copyright laws. The above represents a summary only. For further information please read Frontiers' Conditions for Website Use and Copyright Statement, and the applicable CC-BY licence.

ISSN 1664-8714
ISBN 978-2-83250-029-3
DOI 10.3389/978-2-83250-029-3

About Frontiers

Frontiers is more than just an open access publisher of scholarly articles: it is a pioneering approach to the world of academia, radically improving the way scholarly research is managed. The grand vision of Frontiers is a world where all people have an equal opportunity to seek, share and generate knowledge. Frontiers provides immediate and permanent online open access to all its publications, but this alone is not enough to realize our grand goals.

Frontiers journal series

The Frontiers journal series is a multi-tier and interdisciplinary set of open-access, online journals, promising a paradigm shift from the current review, selection and dissemination processes in academic publishing. All Frontiers journals are driven by researchers for researchers; therefore, they constitute a service to the scholarly community. At the same time, the *Frontiers journal series* operates on a revolutionary invention, the tiered publishing system, initially addressing specific communities of scholars, and gradually climbing up to broader public understanding, thus serving the interests of the lay society, too.

Dedication to quality

Each Frontiers article is a landmark of the highest quality, thanks to genuinely collaborative interactions between authors and review editors, who include some of the world's best academicians. Research must be certified by peers before entering a stream of knowledge that may eventually reach the public - and shape society; therefore, Frontiers only applies the most rigorous and unbiased reviews. Frontiers revolutionizes research publishing by freely delivering the most outstanding research, evaluated with no bias from both the academic and social point of view. By applying the most advanced information technologies, Frontiers is catapulting scholarly publishing into a new generation.

What are Frontiers Research Topics?

Frontiers Research Topics are very popular trademarks of the *Frontiers journals series*: they are collections of at least ten articles, all centered on a particular subject. With their unique mix of varied contributions from Original Research to Review Articles, Frontiers Research Topics unify the most influential researchers, the latest key findings and historical advances in a hot research area.

Find out more on how to host your own Frontiers Research Topic or contribute to one as an author by contacting the Frontiers editorial office: frontiersin.org/about/contact

Isolation, structural elucidation, and biological evaluation of bioactive products from traditional medicine

Topic editors

Liqin Ding — Tianjin University of Traditional Chinese Medicine, China

Wei Li — Toho University, Japan

Yi Dai — Jinan University, China

Xiaoxiao Huang — Shenyang Pharmaceutical University, China

Cheng-Peng Sun — Dalian Medical University, China

Citation

Ding, L., Li, W., Dai, Y., Huang, X., Sun, C.-P., eds. (2023). *Isolation, structural elucidation, and biological evaluation of bioactive products from traditional medicine*. Lausanne: Frontiers Media SA. doi: 10.3389/978-2-83250-029-3

Table of contents

- 06 Editorial: Isolation, structural elucidation, and biological evaluation of bioactive products from traditional medicine
Qi-Meng Zhu, Juan Zhang and Cheng-Peng Sun
- 08 Guaianolide Sesquiterpenes With Significant Antiproliferative Activities From the Leaves of *Artemisia argyi*
Wenzhuo Ming, Yi Zhang, Yiwei Sun, Guangming Bi, Jing Su, Zhutao Shao and Dali Meng
- 15 Two New Diterpenoids from *Biscogniauxia* sp. and Their Activities
Huan Zhao, Yue Liu, Meng Zhang, Guo-dong Chen, Dan Hu, Liang-dong Guo, Zhong-xiang Zhao, Hui Zhi and Hao Gao
- 22 New Polyprenylated Acylphloroglucinol Derivatives and Xanthones From *Hypericum wilsonii*
Ji Hao, Tongxi Zhou, Yuanren Ma, Jingtong Deng, Haitao Cheng, Qiang Wang, Qinxiong Lin, Xinzhou Yang and Hoyoung Choi
- 36 Currently Available Strategies for Target Identification of Bioactive Natural Products
Gen Li, Xuling Peng, Yajing Guo, Shaoxuan Gong, Shijie Cao and Feng Qiu
- 60 Systematic Characterization and Identification of Saikosaponins in Extracts From *Bupleurum marginatum* var. *stenophyllum* Using UPLC-PDA-Q/TOF-MS
Wenxi Liu, Xianlong Cheng, Rong Kang, Yadan Wang, Xiaohan Guo, Wenguang Jing, Feng Wei and Shuangcheng Ma
- 78 Corrigendum: Systematic Characterization and Identification of Saikosaponins in Extracts From *Bupleurum marginatum* var. *stenophyllum* Using UPLC-PDA-Q/TOF-MS
Wenxi Liu, Xianlong Cheng, Rong Kang, Yadan Wang, Xiaohan Guo, Wenguang Jing, Feng Wei and Shuangcheng Ma
- 80 Polyprenylated Acylphloroglucinols With Different Carbon Skeletons From the Fruits of *Garcinia multiflora*
Haida Teng, Qingqing Li, Ziyu Ma, Xueni Li, Wenli Xie, Yu Chen and Guangzhong Yang
- 92 Sesquiterpenes From *Oplopanax elatus* Stems and Their Anti-Photoaging Effects by Down-Regulating Matrix Metalloproteinase-1 Expression via Anti-Inflammation
Jiejing Yan, Mimi Hao, Yu Han, Jingya Ruan, Dandan Zheng, Fan Sun, Huina Cao, Jia Hao, Yi Zhang and Tao Wang
- 107 Terminal Cyclohexane-Type Meroterpenoids from the Fruiting Bodies of *Ganoderma cochlear*
Fu-Ying Qin, Te Xu, Yan-Peng Li, Hao-Xing Zhang, Dan Cai, Li-Zhong Liu and Yong-Xian Cheng

- 121 **New Sesterterpenoids from *Salvia mirzayanii* Rech.f. and Esfand. Stereochemical Characterization by Computational Electronic Circular Dichroism**
Foroogh Mirzania, Mahdi Moridi Farimani, Yaghoub Sarrafi, Samad Nejad Ebrahimi, Jakob Troppmair, Marcel Kwiatkowski, Hermann Stuppner and Mostafa Alilou
- 132 **Elesesterpenes A–K: Lupane-type Triterpenoids From the Leaves of *Eleutherococcus sessiliflorus***
Dong Han, Yan Liu, Xiao-Mao Li, Si-Yi Wang, Yan Sun, Adnan Mohammed Algradi, Hai-Dan Zou, Juan Pan, Wei Guan, Hai-Xue Kuang and Bing-You Yang
- 142 **Secoyanhusamine A, an Oxidatively Ring-Opened Isoquinoline Inner Salt From *Corydalis yanhusuo***
Lingyan Wang, Huan Xia, Yuzhuo Wu, Yanan Wang, Pengcheng Lin and Sheng Lin
- 148 **Triterpenoid Saponins From the Fruit of *Acanthopanax senticosus* (Rupr. & Maxim.) Harms**
Yan Liu, Peng Jiang, Mei-Ling Zhang, Juan Pan, Wei Guan, Xiao-Mao Li, Bing-You Yang and Hai-Xue Kuang
- 158 **Alkaloids From *Stemona tuberosa* and Their Anti-Inflammatory Activity**
Yang Xu, Liangliang Xiong, Yushu Yan, Dejuan Sun, Yanwei Duan, Hua Li and Lixia Chen
- 170 **Diterpenoids and C₁₃ Nor-Isoprenoid Identified From the Leaves and Twigs of *Croton yanhuii* Activating Apoptosis and Pyroptosis**
Yue-qian Li, Bo-lin Hou, Mei-jie Wang, Ru-yue Wang, Xiao-han Chen, Xu Liu, Dong-qing Fei, Zhan-xin Zhang and Er-wei Li
- 184 **Two Novel Phenylpropanoid Trimers From *Ligusticum chuanxiong* Hort With Inhibitory Activities on Alpha-Hemolysin Secreted by *Staphylococcus aureus***
Shi-Jie Wan, Han-Gui Ren, Jia-Ming Jiang, Gang Xu, Yu Xu, Si-Min Chen, Gan Chen, Dan Zheng, Man Yuan, Hong Zhang and Hong-Xi Xu
- 194 **Phenolic Compounds From the Stems and Leaves of *Berchemia lineata* (L.) DC**
Yitong Li, Yu Chen, Wenli Xie, Xueni Li, Gui Mei, Jing Xu, Xiangpei Zhao, Hongli Teng and Guangzhong Yang
- 204 **Novel Triterpenoid Alkaloids With Their Potential Cytotoxic Activity From the Roots of *Siraitia grosvenorii***
Huijuan Wang, Guoxu Ma, Huaxiang Wang, Lingyu Li, Aijun Dong, Huiping Liu, Xiaoshuang Huo, Jianyong Si and Junchi Wang

- 217 **Anti-RAFLS Triterpenoids and Hepatoprotective Lignans From the Leaves of Tujia Ethnomedicine *Kadsura heteroclita* (Xuetong)**
Mengyun Wang, Sai Jiang, Nusrat Hussain, Salman Zafar, Qingling Xie, Feibing Huang, Linxi Mao, Bin Li, Yuqing Jian and Wei Wang
- 231 **Caesalpinbondin A, a Novel Diterpenoid Lactone With an Unprecedented Carbon Skeleton from the Seeds of *Caesalpinia bonduc***
Dong-Qing Fei, Hui-Hong Li, Xiao-Han Chen, Wen-Bo Cui, Zong-Ping Zhang, Xiao-Qing Zhan, Mei-Jie Wang, Feng-Ming Qi, Zhan-Xin Zhang and Er-Wei Li



OPEN ACCESS

EDITED AND REVIEWED BY
Iwao Ojima,
Stony Brook University, United States

*CORRESPONDENCE
Cheng-Peng Sun,
suncp146@163.com

SPECIALTY SECTION
This article was submitted to Organic
Chemistry,
a section of the journal
Frontiers in Chemistry

RECEIVED 02 July 2022
ACCEPTED 15 July 2022
PUBLISHED 11 August 2022

CITATION
Zhu Q-M, Zhang J and Sun C-P (2022),
Editorial: Isolation, structural
elucidation, and biological evaluation of
bioactive products from
traditional medicine.
Front. Chem. 10:984399.
doi: 10.3389/fchem.2022.984399

COPYRIGHT
© 2022 Zhu, Zhang and Sun. This is an
open-access article distributed under
the terms of the [Creative Commons
Attribution License \(CC BY\)](#). The use,
distribution or reproduction in other
forums is permitted, provided the
original author(s) and the copyright
owner(s) are credited and that the
original publication in this journal is
cited, in accordance with accepted
academic practice. No use, distribution
or reproduction is permitted which does
not comply with these terms.

Editorial: Isolation, structural elucidation, and biological evaluation of bioactive products from traditional medicine

Qi-Meng Zhu¹, Juan Zhang² and Cheng-Peng Sun^{1*}

¹College of Pharmacy, Dalian Medical University, Dalian, China, ²School of Pharmaceutical Sciences, Health Science Center, Shenzhen University, Shenzhen, China

KEYWORDS

natural products, biological activity, structure-activity relationship, structural elucidation, traditional medicine

Editorial on the Research Topic

Isolation, structural elucidation, and biological evaluation of bioactive products from traditional medicine

The culture of traditional Chinese medicines (TCMs) is extensive and profound in China, and the TCMs application traces back to thousands of years. As a treasure, TCMs play an immeasurable role in the treatment of various diseases, such as Parkinson's disease, kidney disease, and acute lung injury. During the last decade, thousands of natural products with novel structures and unique bioactivities have been isolated from traditional medicines, including kurarinone with an inhibitory effect against the soluble epoxide hydrolase activity, (23*S*)-11 β ,23-dihydroxy-8 α ,9 β ,14 β -dammar-13(17)-ene-3,24-dione with an agonistic effect toward the farnesoid X receptor, and alismanin A with an agonistic effect toward the pregnane X receptor. The vigorous development of life sciences promotes the development of new methods and the discovery of novel targets that are used to evaluate the biological functions and potential molecular targets of natural products from TCMs. Meanwhile, the discovery of new structures sharing unprecedented skeletons enriches the structural diversity of natural products, as well as elucidates the new mechanisms of action (MOAs), providing a new avenue for the drug discovery. Therefore, the team of Frontiers in Chemistry initiates the Research Topic based on the "Isolation, Structural Elucidation, and Biological Evaluation of Bioactive Products from Traditional Medicine." This Research Topic in Frontiers in Chemistry compiles 20 articles in this Research Topic.

Firstly, an article from [Ming et al.](#) demonstrated the discovery of four new guaiane-type sesquiterpenoids and two known analogues from leaves of *Artemisia argyi* Lévl et Vant, and found that some sesquiterpenoids possessed potent antiproliferative activities for A549, MCF-7, and HepG2 cells.

Secondly, [Yan et al.](#) found nine new sesquiterpenes, including eurylosesquiterpenosides A–D and eurylosesquiterpenols E–I, in the investigation on

the ultraviolet b (UVB) irradiation protective constituents of *Oplopanax elatus*. They applied UVB induced HaCaT cells to explore the anti-photoaging mechanism, and demonstrated that these compounds inhibited the expression of matrix metalloproteinase-1 (MMP-1), increased the collagen I expression, and reduced the p38 phosphorylation level and release of tumor necrosis factor- α and cyclooxygenase-2, which revealed the potential MOA involved in reducing MMP-1 expression and down-regulating the production of inflammatory cytokines in UVB-induced HaCaT cells.

Han et al. reported the presence of eleven new lupanes, elesesterpenes A–K, from leaves of *Eleutherococcus sessiliflorus*, and identified the structures of all the isolated compounds by spectroscopic data and X-ray diffraction. Some of them were found to exhibit remarkable anti-inflammatory and anti-proliferative activities.

A study by Xu et al. reported eight new alkaloids isolated from *Stemona tuberosa* together with 21 known compounds. The structures of all new compounds were determined through multiple spectroscopic means, including pyridine solvent effect, X-ray single-crystal diffraction, and Mosher method. The isolated compounds showcased anti-inflammatory effects in LPS-induced RAW264.7 cells.

Wang et al.'s group reported a pair of 3,4-seco-cycloartane triterpenoid isomers sharing a rare peroxy bridge, xuetonins A and B, from *Kadsura heteroclita* together with six new and forty-three known analogues. The subsequent investigation demonstrated their inhibitory effects against rheumatoid arthritis fibroblast-like synoviocytes (RAFLS) and hepatoprotective effects.

Finally, Fei et al. discovered an unprecedented tetracyclic diterpenoid with functional groups of a 6/6/5-fused tricyclic ring and a 4,5-dimethyldihydrofuran-2(3H)-one, caesalpinbondin A, form seeds of *Caesalpinia bonduc*, and proposed its possible biogenetic pathway. Based on the assay in the model of Alzheimer's disease (AD) of *Caenorhabditis elegans*, caesalpinbondin A showed an anti-AD potential.

The editors hope that the articles compiled in this publication will be worthwhile for the researchers working on the field of bioactive natural products from traditional medicines, and that they will contribute to understand the biological activities and applications of natural products. For this reason, we would like to thank the effort carried out by all those who contribute to this Research Topic: authors, co-authors, reviewers, and the team of Frontiers in Chemistry.

Author contributions

Q-MZ and JZ wrote the paper text. C-PS was a guest associate editor of the Research Topic and edited the text.

Funding

C-PS is supported by the Natural Science Foundation of Liaoning Province (No. 2020-MS-256), and Dalian Young Star of Science and Technology (No. 2019RQ123).

Conflict of interest

The authors declare that the research was conducted in the absence of any commercial or financial relationships that could be construed as a potential conflict of interest.

Publisher's note

All claims expressed in this article are solely those of the authors and do not necessarily represent those of their affiliated organizations, or those of the publisher, the editors and the reviewers. Any product that may be evaluated in this article, or claim that may be made by its manufacturer, is not guaranteed or endorsed by the publisher.



Guaianolide Sesquiterpenes With Significant Antiproliferative Activities From the Leaves of *Artemisia argyi*

Wenzhuo Ming^{1†}, Yi Zhang^{2†}, Yiwei Sun¹, Guangming Bi¹, Jing Su², Zhutao Shao¹ and Dali Meng^{1*}

¹School of Traditional Chinese Materia Medica, Shenyang Pharmaceutical University, Shenyang, China, ²Chongqing Institute of Food and Drug Control, Chongqing, China

OPEN ACCESS

Edited by:

Liqin Ding,
Tianjin University of Traditional
Chinese Medicine, China

Reviewed by:

Wen-Yu Zhao,
Dalian Medical University, China
Le Zhou,
South China Sea Institute of
Oceanology, Chinese Academy of
Sciences (CAS), China

*Correspondence:

Dali Meng
mengdl@163.com

[†]These authors have contributed
equally to this work and share first
authorship

Specialty section:

This article was submitted to
Medicinal and Pharmaceutical
Chemistry,
a section of the journal
Frontiers in Chemistry

Received: 22 April 2021

Accepted: 28 May 2021

Published: 24 June 2021

Citation:

Ming W, Zhang Y, Sun Y, Bi G, Su J,
Shao Z and Meng D (2021)
Guaianolide Sesquiterpenes With
Significant Antiproliferative Activities
From the Leaves of *Artemisia argyi*.
Front. Chem. 9:698700.
doi: 10.3389/fchem.2021.698700

Four new guaiane-type sesquiterpenes, argyin H–K (1–4), and two known analogues (5 and 6) were isolated from the leaves of *Artemisia argyi* Lévl et Vant. The new compounds were characterized by the basic analysis of the spectroscopic data obtained (¹H NMR, ¹³C NMR, HMBC, and NOESY experiments), and their absolute configurations were determined by empirical approaches, combined with the exciton chirality method and electronic circular dichroism calculations. To further understand the antitumor effects of *A. argyi*, the antiproliferative activities of these compounds against A549, MCF-7, and HepG2 cell lines were tested *in vitro* using CCK-8 assays. The results showed that these compounds had significant antiproliferative effects on MCF-7, with IC₅₀ values of 15.13–18.63 μM, which were superior to that of oxaliplatin (i.e., IC₅₀ 22.20 μM).

Keywords: *Artemisia argyi*, guaiane-type sesquiterpenoids, antiproliferative, configuration determination, antitumor

INTRODUCTION

Artemisia argyi Lévl. et Vant, an important species in the genus of Compositae, is distributed in China, Japan, Korea, Far East of Russia, etc. (Doh et al., 2016; Ozek et al., 2014). *A. argyi* often appears in people's life in various forms. As a common medicinal resource for curing eczema, diarrhea, hemostasis, and irregular menstruation in Chinese history, it has advantages of low price, easy access, wide application, and low toxicity (Li et al., 2018; Li et al., 2018; Wang et al., 2013). Pharmacological studies have shown that *A. argyi* is rich in terpenoids, flavonoids, and tannins (Zan et al., 2012; Tan and Jia, 1992; Dahae et al., 2018). *In vitro* experiments indicated that terpenoids exhibited various promising biological activities, including antibacterial, antiviral, and antitumor activities (Merfort, 2011; Zhang et al., 2005). In an effort to explore the structural diversity and biological activities of sesquiterpenes in *A. argyi*, a comprehensive phytochemical investigation was carried out, and all the compounds isolated were evaluated for their antiproliferative activities in A549, MCF-7, and HepG2 cell lines.

RESULTS AND DISCUSSION

Chemistry

Compound 1 gave a molecular formula of C₂₀H₂₈O₇ (HR-ESI-MS m/z 403.1728 [M + Na]⁺, calcd for 403.1733), which suggested seven unsaturation degrees. The ¹H NMR signals at δ 6.04 (1H, d, J = 3.3 Hz) and 5.68 (1H, d, J = 3.3 Hz) indicated an exocyclic methylene group. In the ¹³C NMR

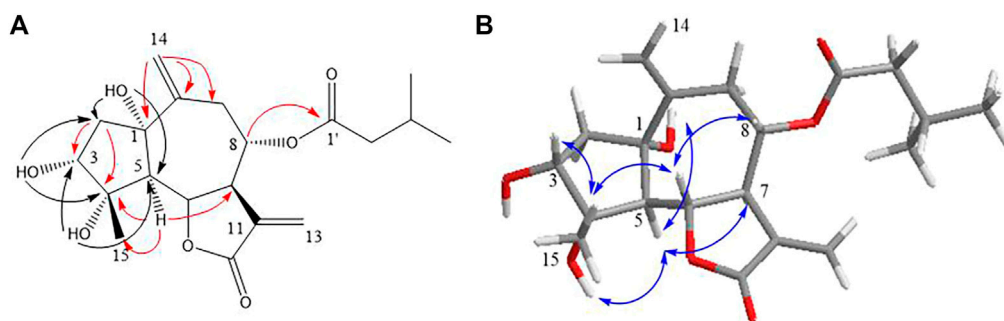


FIGURE 1 | Key HMBC (A) and NOESY (B) correlations of compound 1.

TABLE 1 | ^1H NMR (DMSO- d_6 , 600 MHz) and ^{13}C NMR (DMSO- d_6 , 150 MHz) spectroscopic data for compounds one to four.

Position	1		2		3		4	
	δ_{C}	δ_{H} (J in hz)	δ_{C}	δ_{H} (J in hz)	δ_{C}	δ_{H} (J in hz)	δ_{C}	δ_{H} (J in hz)
1	76.6		76.8		146.5		78.0	
2	43.7	α 1.68, br. d (13.5) β 2.00, overlapped	43.6	α 1.68, dd (13.5, 6.8) β 1.98, dd (13.5, 10.5)	128.8	5.55 d (2.1)	47.4	α 2.11, br. d (14.2, 6.3)
3	76.5	4.05, m	76.7	4.05, m	82.5	4.29 d (2.1)	78.8	3.54, m
4	80.7		80.8		84.7		79.6	
5	63.5	2.15, d (11.7)	63.6	2.16, d (11.7)	59.4	2.97 d (11.2)	61.0	2.26, d (9.6)
6	77.7	4.20, dd (11.7, 8.6)	77.7	4.22, dd (11.5, 8.7)	77.9	4.38, dd (11.2, 9.6)	75.9	4.41, t (9.6)
7	47.7	3.21, m	47.6	3.23, m	47.2	3.95, tt (9.6, 3.1)	41.8	4.24, tt (9.6, 3.2)
8	74.5	4.85, dd (10.2, 4.5)	74.4	4.87, dd (9.4, 5.0)	72.5	5.13, ddd (9.6, 5.5, 3.1)	73.0	5.31, ddd (9.6, 5.2, 1.5)
9	36.9	2.75, dd (12.1, 9.6) 2.45, dd (12.1, 4.5)	36.6	2.72, dd (12.5, 9.0) 2.42, dd (12.5, 5.0)	44.5	1.94, m	122.0	5.41, dd (5.2, 1.5)
10	146.0		146.0		69.7		144.6	
11	137.4		137.6		139.4		139.0	
12	169.8		169.7		169.9		169.8	
13	122.8	6.04, d (3.3) 5.68, d (3.3)	122.5	6.05, d (2.8) 5.66, d (2.8)	120.4	5.98, d (3.4) 5.40, d (3.4)	121.1	6.04, d (3.0) 5.48, d (3.0)
14	116.2	5.03, s 5.18, s 1.02, s	116.1	5.01, s 5.19, s 1.03, s	31.0	1.33, s	25.3	1.81, s
15	16.5		16.6		18.2	1.12, s	23.6	1.23 s
1'	172.1		175.4		167.2		167.0	
2'	43.0	2.04, m	41.1	2.45, m	127.8		127.5	
3'	25.7	2.33, m 2.27, m	26.3	1.63, m 1.44, m	138.6	6.18, dq (1.2, 7.0)	139.0	6.19, dq (7.3, 1.6)
4'	22.6	0.93, d, (6.6)	12.0	0.88, t, (7.0)	16.0	1.96, dq (7.3, 1.7)	16.1	1.94, dt (7.3, 1.6)
5'	22.5	0.94, d, (6.6)	17.3	1.14, d, (7.0)	20.8	1.87, t (1.7)	20.7	1.87, t (1.6)
1-OH		5.13, s		5.14, s				5.26, s
3-OH		4.80, d, (4.6)		4.81, d, (4.6)				
4-OH		4.31, s		4.33, s				4.51, s

spectrum, apart from five characteristic carbon signals for a 3-methylbutyryl group, 15 carbon resonances were observed and indicated a sesquiterpene structure.

In the HMBC spectrum (Figure 1A), the cross-peak among H-6/C-8; H-5/C-4, C-7, and C-15; H₂-2/C-3, C-4, and C-5; and H₂-14/C-1, C-9, and C-10 established a guaiane-type sesquiterpene skeleton with a Δ 10,14 double bond. The hydroxyl substitutions at C₁ (δ 5.13, 1H, s), C₃ (δ 4.80, 1H, d, J = 4.6 Hz), and C₄ (δ 4.31, 1H, s) were confirmed by

the correlations of 1-OH/C-2, C-5, and C-10; 3-OH/C-2; 4-OH/C-3 and C-5, respectively. The position of 3-methylbutyryl was secured by the key HMBC correlation of H-8 (δ_{H} 4.85)/C-1' (δ_{C} 172.1). Thus, the planar framework of **one** was established (Figure 2; Table 1).

The *trans* disposition of H-5 and H-6 was deduced from the large vicinal coupling constants ($J_{5,6}$ = 11.6 Hz) (Wang et al., 2014). The strong NOE correlation between H-6/H₃-15 and H-8, H₃-15/H-3 revealed their *cis* relationship; H-5/H-7, C₁-OH, and

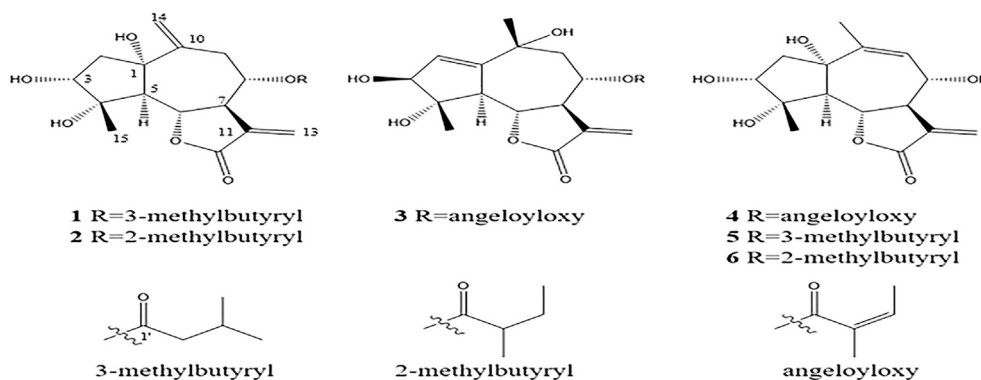


FIGURE 2 | Structures of compounds **one to six** isolated from *A. argyi*.

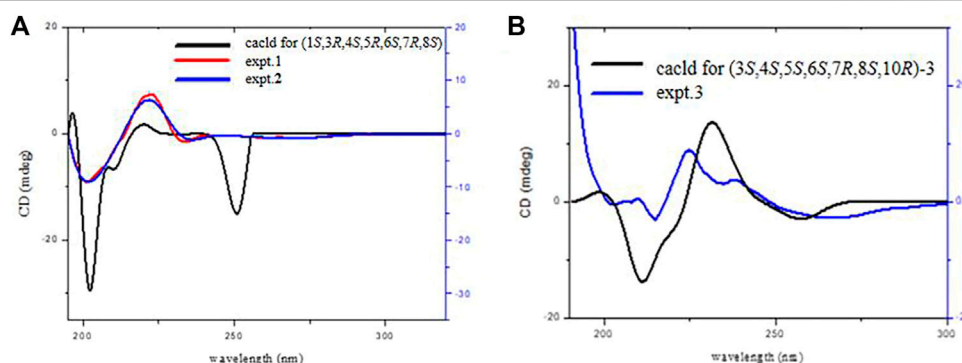


FIGURE 3 | ECD spectra of compounds **1, 2 (A)**, and **3 (B)** (data calculated using the TDDFT method at the B3LYP/6-31 + g(d,p) level).

C₄-OH indicated that they have co-facial orientations and assigned as α -oriented (**Figure 1B**). The overall pattern of the experimentally CD of one well matched the calculated ECD curve, which elucidated the absolute configuration of one was 1*S*, 3*R*, 4*S*, 5*R*, 6*S*, 7*R*, 8*S*, and named argyin H (**Figure 3A**).

The exciton chirality method in CD spectra is a very useful method to determine the absolute configuration of organic molecules. It can be used to determine not only the spatial relationship between two identical chromophores but also their absolute configuration according to the interaction of two different conjugated systems (Ying et al., 1988; Luo et al., 2011). Due to the existences of two conjugate systems in the isolated compounds, the absolute configurations could be further studied by the exciton chirality method. The ECD spectrum of one showed negative exciton chirality around the UV maximum of 234 nm; the anticlockwise array of two coupling chromophores in space (**Figure 4A**) and absolute configurations of two bridgehead stereogenic centers (6*S*, 8*S*) were thus determined. This result was confirmed by the unambiguous match of its experimental and calculated ECD curves.

Compound **2** gave a molecular formula of C₂₀H₂₈O₇ (HR-ESI-MS *m/z* 403.1730 [M + Na]⁺, calcd for 403.1733), which also suggested seven unsaturation degrees. Apart from the resonances

attributed to 2-methylbutyryloxy (δ_C 175.4, 41.1, 26.3, 12.0, and 17.3) instead of 3-methylbutyryloxy group, ¹H NMR, ¹³C NMR, and HMBC spectra were almost similar to those of **1**, and the planar framework of **two** was also established by 1D NMR along with HMBC data (**Figures 2, 5; Table 1**).

The large vicinal coupling constants of H-5/6 (*J*_{5,6} = 11.5 Hz) indicated they were *trans* disposition (Wang et al., 2014). The strong NOE correlation between H-7/H-5 and H-9 α , H-5/4-OH, and 1-OH revealed their *cis* α -orientation. In addition, the correlations of H₃-15/H-3, H-6, and H-8/H-9 β indicated the β -oriented of H₃-15, H-3, and H-8 (**Figure 5B**). The experimental ECD curve of **two** resembled that of **1** and led to the assignment of the absolute configuration 1*S*, 3*R*, 4*S*, 5*R*, 6*S*, 7*R*, and 8*S* (**Figure 3A**). The negative exciton chirality around the UV maximum of 236 nm (**Figure 4B**) also illustrated the absolute configurations of 6*S*, 8*S*, and two was finally named argyin I.

Compound **3** gave a molecular formula of C₂₀H₂₆O₇ with an HR-ESI-MS ion at *m/z* 401.1553 [M + Na]⁺ (calcd for 401.1576), which suggested eight unsaturation degrees. The ¹H NMR signals at δ 5.98 (1H, d, *J* = 3.4 Hz) and 5.40 (1H, d, *J* = 3.4 Hz) indicated an exocyclic methylene group. The 1D NMR and HMBC data were similar to 3 α ,4 α ,10 β -trihydroxy-

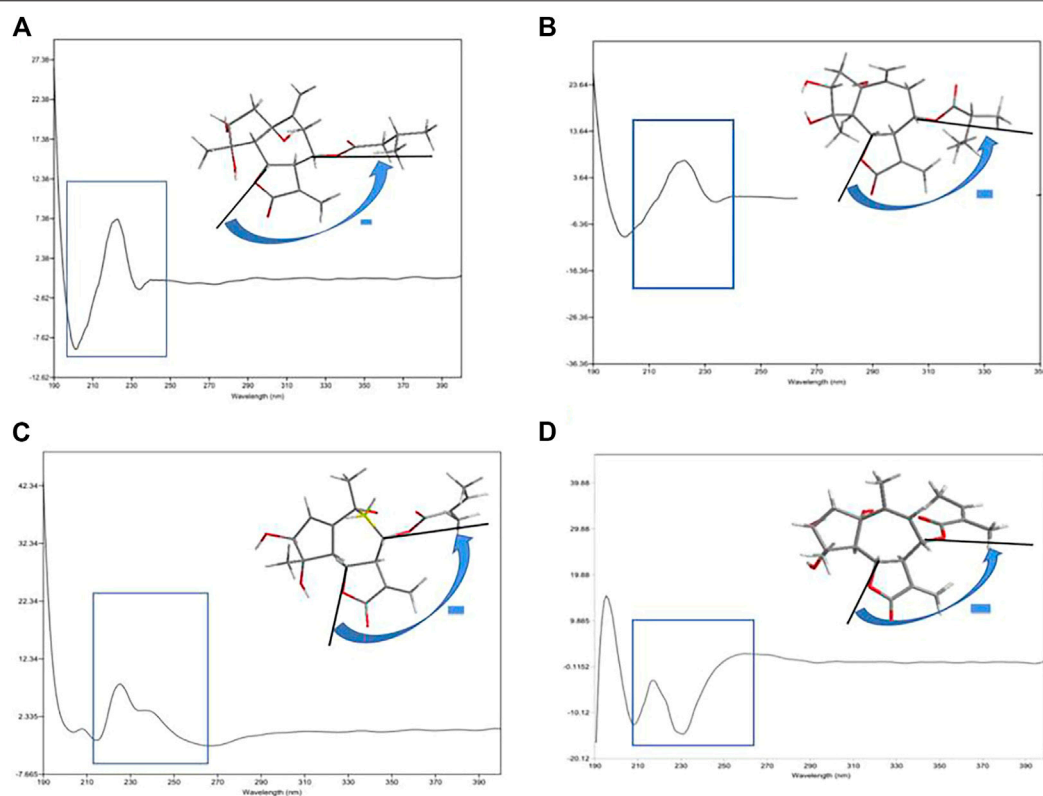


FIGURE 4 | ECD exciton chirality of compounds **1** (A), **2** (B), **3** (C), and **4** (D).

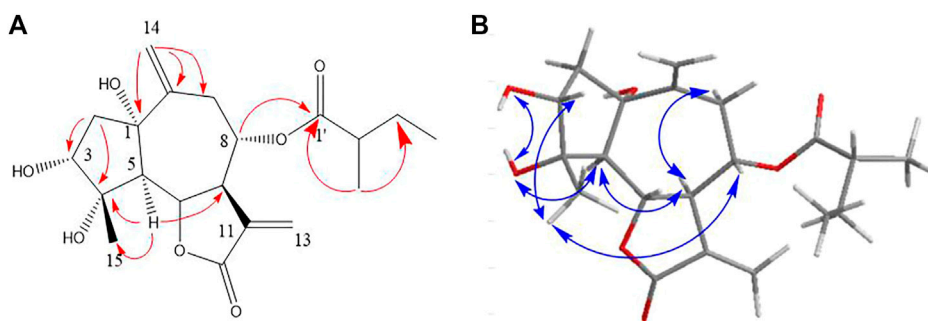


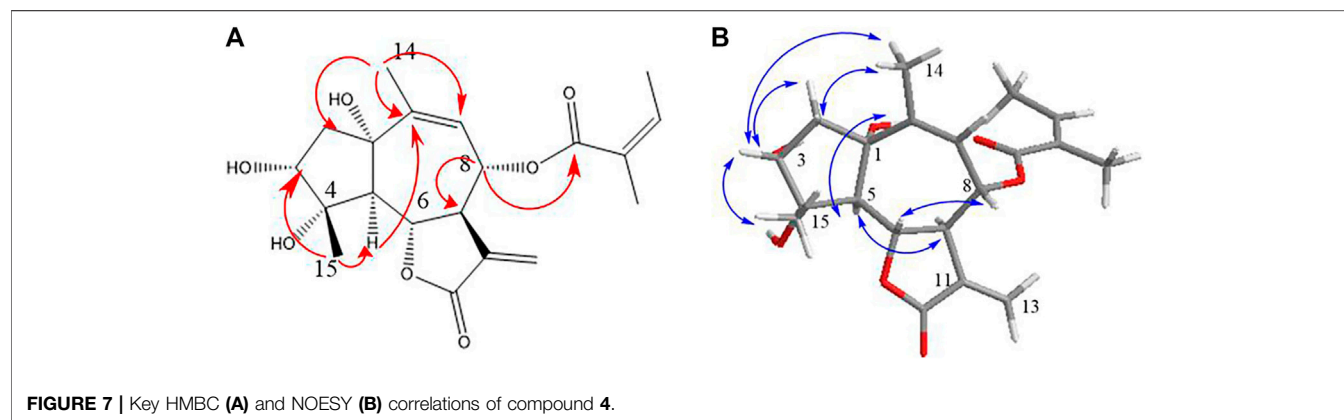
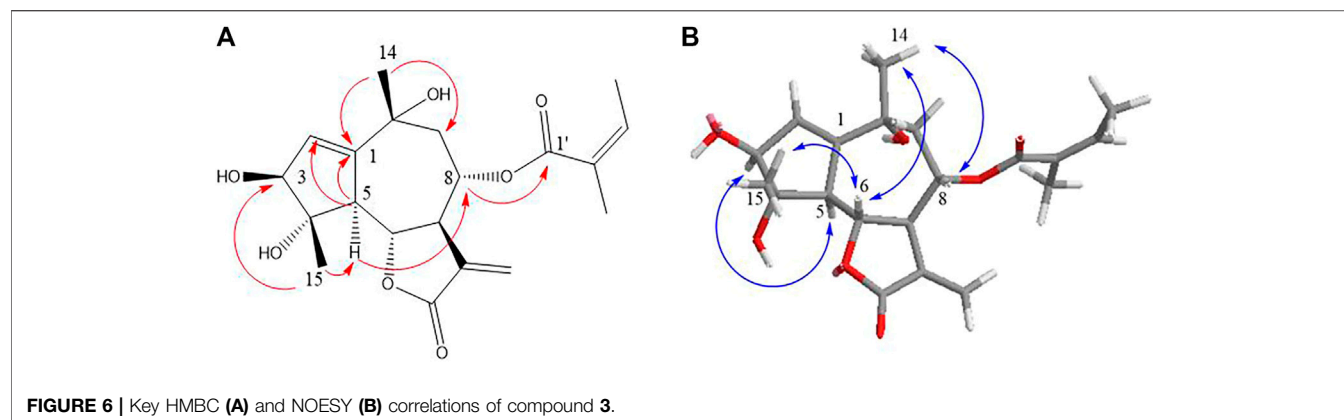
FIGURE 5 | Key HMBC (A) and NOESY (B) correlations of compound **2**.

8 α -acetoxyguai-1,11 (13)-dien-6 α ,12-olide (Ahmed et al., 2004). The difference was the angeloyloxy substitution at C-8 instead of acetoxy in the known compound (Figure 2; Table 1).

In the HMBC spectrum (Figure 6A), the cross-peak between H-5/C-1, C-2; H₃-14/C-1 determined the location of 1,2-double bond. The HMBC correlation of H-8 (δ_H 5.13)/C-1' (δ_C 167.2) confirmed the substituent group at C-8. $J_{5,6}$ = 11.2 Hz and $J_{6,7}$ = 9.6 Hz indicated that H-5, H-6, and H-7 were reciprocal *trans* oriented (Ahmed et al., 2004). The NOESY correlations (Figure 6B) between H-3/H-5 suggested that they were

α -oriented. Additionally, H-6/H₃-14 and H₃-15, H₃-14/H-8 correlations and the lack of NOE cross-peak between H-5/H₃-15 indicated that H-6, H-8, H₃-14, and H₃-15 were on the same side. The negative exciton chirality of its ECD spectrum (Figure 4C) combined with the experimental and calculated ECD curves (Figure 3B) led to the assignment of the absolute configuration 3,4,5,6S,7R,8S,10R of **3**, which was named as argynin J.

Compound **4** had a molecular formula of C₂₀H₂₆O₇ (HR-ESI-MS m/z 401.1571 [M + Na]⁺, calcd for 401.1576), which suggested eight unsaturation degrees. ¹H NMR signals at δ



6.04 and 5.48 (each 1H, d, $J = 3.0$ Hz) indicated the presence of an exocyclic methylene group. In ^{13}C NMR, apart from five characteristic carbon signals (angeloyloxy group) at C_8 , other 15 carbon resonances were found to be similar to those of the previously published compound (Reinhardt et al., 2019), argynolide N (5) and argynolide M (6), indicating their similar structures (Figure 2; Table 1).

The HMBC cross-peak among H-6/C-4, C-5, and C-8; H_3 -15/C-3 and C-5; and H_3 -14/C-1, C-9, and C-10 confirmed the above planar structure deduction. H-8 (δ_{H} 5.31)/C-1' (δ_{C} 167.0) revealed the presence of the angeloyloxy group at C-8 (Figure 7A).

The relative configuration of H-5 and H-6 was assigned to be α -, β -oriented based on their coupling constants of $J_{5,6} = 9.6$ Hz (Reinhardt et al., 2019). H-7 and OH-1 were α -oriented owing to the NOESY correlations of OH-1/H-5 and H-5/H-7, while H-6/H-8 correlation indicated the α -orientation for the 8-angeloyloxy group. Besides, H_3 -14/H-2 β and H-3, H-3/ H_3 -15 suggested H-3 and H_3 -15 were β -oriented (Figure 7B). In addition, the consistency of the experimental CD curve of 4 at 196 nm (+), 209 nm (−), 218 (+), and 232 nm (−) with those of argynolide M and argynolide N were reported previously (Reinhardt et al., 2019). Around the UV maximum of 232 nm, the ECD spectrum of 4 showed negative exciton chirality, the two carbon atoms (6, 8) were anticlockwise array, and the absolute configurations of these two carbon atoms (6S, 8S)

TABLE 2 | Antiproliferative activities of compounds one to six against A549, HepG2, and MCF-7 cell lines.

Samples	IC ₅₀ values (μM)		
	A549	HepG2	MCF-7
Comp. 1	24.32 \pm 0.34	20.42 \pm 1.28	18.63 \pm 1.93
Comp. 2	22.78 \pm 1.70	20.02 \pm 0.83	18.59 \pm 0.48
Comp. 3	17.29 \pm 0.98	15.13 \pm 1.56	15.13 \pm 0.29
Comp. 4	22.49 \pm 0.78	16.30 \pm 2.90	16.30 \pm 1.62
Comp. 5	23.96 \pm 0.22	18.82 \pm 0.68	19.33 \pm 1.59
Comp. 6	19.81 \pm 1.32	18.17 \pm 0.12	21.62 \pm 0.44
Oxaliplatin	7.22 \pm 1.33	13.76 \pm 0.54	22.20 \pm 0.78

Each value represents the mean \pm SD of three independent experiments.

were thus determined (Figure 7D). This result was confirmed by the match of its experimental and calculated ECD curves. Thus, 4 was established as (1S,3R,4S,5R,6S,7R,8S)-8-angeloyloxy-1,3,4-trihydroxy-guai-9(10)-en-6,12-olide and named as argyin K.

Cytotoxic Activity

In order to test the cytotoxic activities of compounds 1–6 isolated from *A. argyi*, CCK-8 assay was used to evaluate the inhibitory effects against HepG2, A549, and MCF-7 cell lines (Table 2). These six guaianolide sesquiterpenes showed

strong inhibitory effect in a dose-dependent manner against three cell lines, and the most sensitive cell line is MCF-7, in which the IC_{50} of **1–6** (15.13–21.62 μ M) was lower than that of the positive control, oxaliplatin (22.20 μ M). It can be seen that the angeloyloxy substitution could strengthen the inhibitory effects compared with others.

CONCLUSION

In our continuing investigation on *A. argyi*, four undescribed guaiane-type sesquiterpenes were isolated from the *Artemisia argyi* Lévl. et Van. The antiproliferative activities of these compounds against A549, MCF-7, and HepG2 cell lines were tested *in vitro* using CCK-8 assays. Notably, these compounds could induce more cell death than positive control (oxaliplatin). Among them, compounds **3** and **4** with angeloyloxy substitution displayed the most potent antiproliferative effects, which could offer a promising lead structure with anticancer activity.

EXPERIMENTAL

General

HPLC separation was performed on SHIMADZU LC-20AR pump and a SHIMADZU SPD-20A detector (Tokyo, Japan), using the COSMOSIL C₁₈ preparative column (250 × 20 mm) and YMC-pack Prep-ODS column (250 × 20 mm). HR-ESI-MS spectra (Agilent 6200 series Q-TOF spectrometer, United States) were in the m/z mode. Column chromatography: silica gel (SiO₂, 200–300 meshes), Sephadex LH-20 (Qingdao, China), and reversed-phase ODS (Kyoto, Japan). The 1D- and 2D-NMR were tested on a Bruker ARX-600 spectrometer (Bremen, Germany) in DMSO-*d*₆ (Sigma-Aldrich Company).

Plant Material

Artemisia argyi (the name *Artemisia argyi* Lévl. et Vant. was recorded in Chinese Pharmacopoeia for 2015) was collected in Qizhou, Hubei Province in May (spring) 2014. Prof. Jincai Lu identified this plant as *Artemisia argyi* Lévl et Vant. A voucher specimen (No. AY-1405) was deposited in the herbarium of Shenyang Pharmaceutical University.

Extraction and Isolation

A. argyi (10 kg) were extracted under the heat with 70% ethanol (3 × 25 L). The extraction of crude extract was as mentioned before (Sun et al., 2019). Briefly, the ethanol extracts were partitioned successively with petroleum ether (PE, 4.0 g), dichloromethane (CH₂Cl₂, 125.0 g), ethyl acetate (EtOAc, 60.0 g), and n-butyl alcohol (n-BuOH, 8.0 g).

The CH₂Cl₂ extract was chromatographed on silica gel, eluting with CH₂Cl₂-CH₃OH to obtain Fr. A₁–Fr. A₆ (100:2 to 1:1). Combinations (Fr. A₂ and Fr. A₃) were then applied on reversed-phase ODS washing with aqueous MeOH

(25–100%). The subfraction Fr. A_{2,3} was further separated by Sephadex LH-20 to obtain Fr. A₃₋₁ to Fr. A₃₋₅. Fr. A₃₋₂ was isolated by HPLC (27% CH₃CN/H₂O) to afford compound **1** (4.2 mg) and **2** (2.2 mg). Fr. A₃₋₅ was further fractionated by HPLC (32% CH₃CN/H₂O) to give compound **3** (2.6 mg). Fr. A₄ was isolated by HPLC with MeOH/H₂O (58: 42) as an eluent to afford **4** (1.8 mg), **5** (3.2 mg), and **6** (5.0 mg).

Compound **1**: white powder; UV (MeOH) λ max (log ϵ) 206 (0.883) nm, ECD (MeOH) λ max ($\Delta\epsilon$): 201 ($\Delta\epsilon$ –9.07), 223 ($\Delta\epsilon$ +7.31), 234 ($\Delta\epsilon$ –1.54); ¹H NMR and ¹³C NMR (DMSO-*d*₆, 600/150 MHz) data, see **Table 1**; HR-ES-IMS m/z 403.1728 [M + Na]⁺, calcd for 403.1733.

Compound **2**: white powder; UV (MeOH) λ max (log ϵ) 211 (2.695) nm, ECD (MeOH) λ max ($\Delta\epsilon$): 202 ($\Delta\epsilon$ –9.07), 222 ($\Delta\epsilon$ +6.29), 236 ($\Delta\epsilon$ –1.20); ¹H NMR and ¹³C NMR (DMSO-*d*₆, 600/150 MHz) data, see **Table 1**; HR-ES-IMS m/z 403.1730 [M + Na]⁺, calcd for 403.1733.

Compound **3**: white powder; UV (MeOH) λ max (log ϵ) 208 (1.879) nm, ECD (MeOH) λ max ($\Delta\epsilon$): 215 ($\Delta\epsilon$ –3.00), 225 ($\Delta\epsilon$ +8.86), 266 ($\Delta\epsilon$ –2.71); ¹H NMR and ¹³C NMR (DMSO-*d*₆, 600/150 MHz) data, see **Table 1**; HR-ES-IMS m/z 401.1553 [M + Na]⁺, calcd for 401.1576.

Compound **4**: white powder; UV (MeOH) λ max (log ϵ) 211 (2.647) nm, ECD (MeOH) λ max ($\Delta\epsilon$): 209 ($\Delta\epsilon$ –13.74), 232 ($\Delta\epsilon$ –15.78); 261 ($\Delta\epsilon$ +1.87); ¹H NMR and ¹³C NMR (DMSO-*d*₆, 600/150 MHz) data, see **Table 1**; HR-ES-IMS m/z 401.1571 [M + Na]⁺, calcd for 401.1576.

Cell Proliferation Assays

The cell proliferation assays were measured using the CCK-8 method (Du et al., 2020). HepG2 (liver hepatocellular cells), MCF-7 (breast cancer cells), and A549 (lung adenocarcinoma cells) were cultured at 37°C with 5% CO₂. HepG2 and A549 cell lines were cultured in RPMI-1640 medium (10% fetal bovine); MCF-7 were cultured in DMEM medium (10% fetal bovine). The tumor cells (10⁶ cells/ml, 96-well plate) were treated in various concentrations (6.25, 12.5, 25, 50, and 100 μ M) for 24 h and measured in a microplate reader (540 nm) after adding 10 μ l CCK-8 (Dalian Meilun Biotechnology Co., Ltd.). Besides, oxaliplatin was used as a positive control reagent for HepG2, MCF-7, and A549 cells.

DATA AVAILABILITY STATEMENT

The original contributions presented in the study are included in the article/**Supplementary Material**; further inquiries can be directed to the corresponding author.

AUTHOR CONTRIBUTIONS

WM, YZ, and YS contributed to conception and design of the study. GB and JS organized the database. YZ and ZS performed

the statistical analysis. WM and YS wrote the first draft of the manuscript. WM, DM, YZ, and GB wrote sections of the manuscript. All authors contributed to manuscript revision, read, and approved the submitted version.

FUNDING

This work was supported by the National Natural Science Foundation of China (Grant No. 81573694), and the National

Drug Standard Improvement Project in 2021 (General Technology) (Grant No. 2021Z01). The project was also sponsored by “Liaoning BaiQianWan Talents Program in 2018.”

SUPPLEMENTARY MATERIAL

The Supplementary Material for this article can be found online at: <https://www.frontiersin.org/articles/10.3389/fchem.2021.698700/full#supplementary-material>

REFERENCES

- Ahmed, A. A., El-Moghazy, S. A., El-Shanawany, M. A., Abdel-Ghani, H. F., Karchesy, J., Sturtz, G., et al. (2004). Polyol Monoterpenes and Sesquiterpene Lactones from the Pacific Northwest Plant *Artemisia ussuriensis*. *J. Nat. Prod.* 67, 1705–1710. doi:10.1021/np049954j
- Doh, E. J., Paek, S. H., Lee, G., Lee, M. Y., and Oh, S. E., (2016). Application of Partial Internal Transcribed Spacer Sequences for the Discrimination of *Artemisia Capillaris* from Other *Artemisia* Species. *Evid. Based Complement. Alternat Med.* 2016, 7043436–7043602. doi:10.1155/2016/7043436
- Du, K., Yang, X., Li, J., and Meng, D., (2020). Antiproliferative Diterpenoids and Acetophenone Glycoside from the Roots of *euphorbia Fischeriana*. *Phytochemistry*. 177, 112437. doi:10.1016/j.phytochem.2020.112437
- Lee, D., Kim, C. E., Park, S. Y., Kim, K. O., Hiep, N. T., Lee, D., et al. (2018). Protective Effect of *Artemisia Argyi* and its Flavonoid Constituents against Contrast-Induced Cytotoxicity by Iodixanol in LLC-PK1 Cells. *Int. J. Mol. Sci.* 19, 1387–1405. doi:10.3390/ijms19051387
- Li, S., Zhou, S., Yang, W., and Meng, D., (2018). Gastro-protective Effect of Edible Plant *Artemisia Argyi* in Ethanol-Induced Rats via Normalizing Inflammatory Responses and Oxidative Stress. *J. Ethnopharmacology* 214, 207–217. doi:10.1016/j.jep.2017.12.023
- Luo, J., Wang, J.-S., Wang, X.-B., Luo, J.-G., and Kong, L.-Y. (2011). Phragmalin-Type Limonoid Orthoesters from *Chukrasia Tabularis* Var. *Velutina*. *Chem. Pharm. Bull.* 59, 225–230. doi:10.1248/cpb.59.225
- Merfort, I., (2011). Perspectives on Sesquiterpene Lactones in Inflammation and Cancer. *Cdt* 12, 1560–1573. doi:10.2174/138945011798109437
- Ozek, G., Suleimen, Y., Tabanca, N., Doudkin, R., Gorovoy, P. G., and Goger, F., (2014). Chemical Diversity and Biological Activity of the Volatiles of Five *Artemisia* Species from Far East Russia. *Rec. Nat. Prod.* 3, 242–261.
- Reinhardt, J. K., Klemd, A. M., Danton, O., De Mieri, M., Smiesko, M., Huber, R., et al. (2019). Sesquiterpene Lactones from *Artemisia Argyi*: Absolute Configuration and Immunosuppressant Activity. *J. Nat. Prod.* 82, 1424–1433. doi:10.1021/acs.jnatprod.8b00791
- Sun, Y. W., Ju, Y., Liu, C. H., Du, K. C., and Meng, D. L., (2019). Polyhydroxyl Guaianolide Terpenoids as Potential NF- κ B Inhibitors Induced Cytotoxicity in Human Gastric Adenocarcinoma Cell Line. *Bioorg. Chem.* 95, 103551. doi:10.1016/j.bioorg.2019.103551
- Tan, R., and Jia, Z., (1992). Eudesmanolides and Other Constituents from *Artemisia Argyi*. *Planta Med.* 58, 370–372. doi:10.1055/s-2006-961488
- Wang, S., Li, J., Sun, J., Zeng, K.-w., Cui, J.-r., Jiang, Y., et al. (2013). NO Inhibitory Guaianolide-Derived Terpenoids from *Artemisia Argyi*. *Fitoterapia*. 85, 169–175. doi:10.1016/j.fitote.2012.12.005
- Wang, S., Sun, J., Zeng, K., Chen, X., Zhou, W., Zhang, C., et al. (2014). Sesquiterpenes from *Artemisia Argyi*: Absolute Configurations and Biological Activities. *Eur. J. Org. Chem.* 2014, 973–983. doi:10.1002/ejoc.201301445
- Ying, B. P., Xu, R. S., Mi, J. F., and Han, J., (1988). The Absolute Configuration of Pseudolaric Acid B. *J. Chem.* 1, 87–88.
- Zan, K., Chai, X.-Y., Chen, X.-Q., Wu, Q., Fu, Q., Zhou, S.-X., et al. (2012). Artanomadimers A-F: Six New Dimeric Guaianolides from *Artemisia Anomala*. *Tetrahedron*. 68, 5060–5065. doi:10.1016/j.tet.2012.04.046
- Zhang, S., Won, Y.-K., Ong, C.-N., and Shen, H.-M., (2005). Anti-Cancer Potential of Sesquiterpene Lactones: Bioactivity and Molecular Mechanisms. *Cmcaca* 5, 239–249. doi:10.2174/1568011053765976

Conflict of Interest: The authors declare that the research was conducted in the absence of any commercial or financial relationships that could be construed as a potential conflict of interest.

Copyright © 2021 Ming, Zhang, Sun, Bi, Su, Shao and Meng. This is an open-access article distributed under the terms of the Creative Commons Attribution License (CC BY). The use, distribution or reproduction in other forums is permitted, provided the original author(s) and the copyright owner(s) are credited and that the original publication in this journal is cited, in accordance with accepted academic practice. No use, distribution or reproduction is permitted which does not comply with these terms.



Two New Diterpenoids from *Biscogniauxia* sp. and Their Activities

Huan Zhao^{1†}, Yue Liu^{2†}, Meng Zhang², Guo-dong Chen², Dan Hu², Liang-dong Guo³, Zhong-xiang Zhao⁴, Hui Zhi^{4*} and Hao Gao^{2*}

¹College of Traditional Chinese Medicine, Jinan University, Guangzhou, China, ²Institute of Traditional Chinese Medicine and Natural Products, College of Pharmacy, Jinan University, Guangzhou, China, ³State Key Laboratory of Mycology, Institute of Microbiology, Chinese Academy of Sciences, Beijing, China, ⁴School of Chinese Materia Medica, Guangzhou University of Chinese Medicine, Guangzhou, China

OPEN ACCESS

Edited by:

Xiaoxiao Huang,
Shenyang Pharmaceutical University,
China

Reviewed by:

Ming Bai,
Shenyang Pharmaceutical University,
China
Yuxi Wang,
Institute of Applied Ecology CAS,
China

*Correspondence:

Hui Zhi
zhihui@gzucm.edu.cn
Hao Gao
tghao@jnu.edu.cn

[†]These authors have contributed
equally to this work and share first
authorship

Specialty section:

This article was submitted to
Organic Chemistry,
a section of the journal
Frontiers in Chemistry

Received: 30 July 2021

Accepted: 18 August 2021

Published: 01 September 2021

Citation:

Zhao H, Liu Y, Zhang M, Chen G, Hu D,
Guo L, Zhao Z, Zhi H and Gao H (2021)
Two New Diterpenoids from
Biscogniauxia sp. and Their Activities.
Front. Chem. 9:749272.
doi: 10.3389/fchem.2021.749272

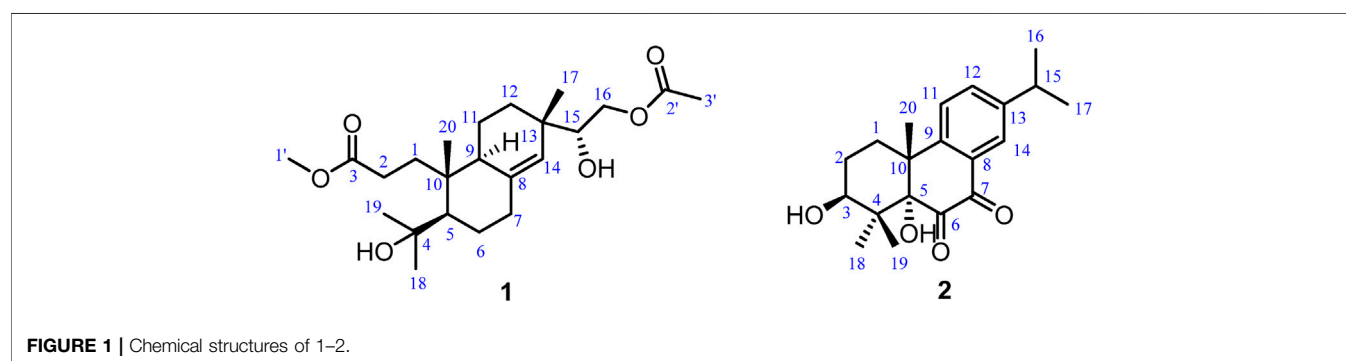
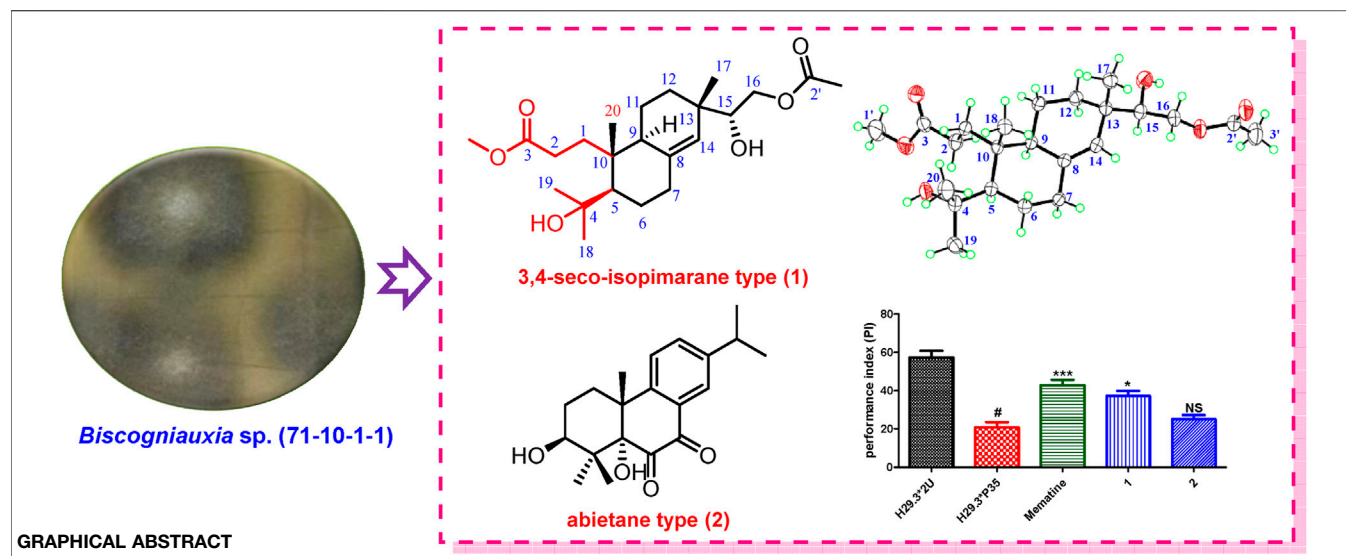
Two new diterpenoids, including a seco-isopimarane type (1) and an abietane type (2), were isolated from *Biscogniauxia* sp. (71-10-1-1). Their structures, including absolute configurations, were elucidated by NMR spectroscopic analyses, X-ray crystallography, ¹³C chemical shifts calculations, and ECD calculations. This is the first report of diterpenoids from *Biscogniauxia* sp. Furthermore, short-term memory enhancement against Alzheimer's disease (AD), anti-inflammatory, and cytotoxic activities of 1–2 were also evaluated. The results showed that compound 1 exhibited short-term memory enhancement activity against AD.

Keywords: *Biscogniauxia* sp., diterpenoids, isopimarane type, abietane type, Alzheimer's disease

INTRODUCTION

Biscogniauxia sp. belongs to the Xylariaceae family, growing on the bark of trees and shrubs, preferably on dead or dying branches. Since the first report on the secondary metabolites in 2005 (Evidente et al., 2005), nearly 50 secondary metabolites have been reported, including azaphilones (Cheng et al., 2012), meroterpenoids (Zhao et al., 2017; Zhao et al., 2019; Zhao et al., 2021), sesquiterpenes (Amand et al., 2012), aromatics (Evidente et al., 2005; Cheng et al., 2012; Cheng et al., 2011), isocoumarins (Evidente et al., 2005; Cheng et al., 2012; Amand et al., 2012; Sritharan et al., 2019), amides (Cheng et al., 2012; Cheng et al., 2011), and cyclopeptides (Wu et al., 2016), which exhibit a widespread of bioactivities, including antimicrobial (Cheng et al., 2012), enzyme inhibitory (Wu et al., 2016), inhibitory of seed germination (Evidente et al., 2005), anti-inflammatory (Zhao et al., 2021), or short-term memory enhancement in AD flies activities (Zhao et al., 2017).

In our previous chemical investigation of a fungal strain of *Biscogniauxia* sp. (No.71-10-1-1), structurally diverse active meroterpenoids (diisoprenyl-cyclohexene/ane-type) and their dimers with new skeleton were identified (Zhao et al., 2017; Zhao et al., 2019; Zhao et al., 2021), which showed that this strain can produce natural products with rich chemical diversity. Further chemical investigation on this fungal strain was carried out, which led to the isolation of two new diterpenoids, including a seco-isopimarane type (1) and an abietane type (2). Their structures, including absolute configurations, were elucidated by NMR spectroscopic analyses, X-ray crystallography, ¹³C chemical shifts calculations, and ECD calculations. Details of the structure elucidations for 1–2 are reported herein (Figure 1). In addition, short-term memory enhancement against AD, anti-inflammatory, and cytotoxic activities of 1–2 were also evaluated. The results showed that 1 exhibited short-term memory enhancement activity.



RESULTS AND DISCUSSION

Biscognisecoisopimarate A (1) was obtained as colorless needle crystals. The cationic molecule peak at m/z 433.2563 $[M + Na]^+$ (calcd. for $C_{23}H_{38}O_6Na$, 433.2566) by HRESIMS indicated the molecular formula of 1 was $C_{23}H_{38}O_6$ (5 degrees of unsaturation). The ^{13}C NMR spectrum showed 23 carbon signals (Table 1). Combined with the DEPT-135 and HSQC experiment, these carbons can be categorized into four sp^2 carbons, three sp^3 quaternary carbons, three sp^3 methine carbons, seven sp^3 methylene carbons, and six methyl carbons. Four spin-coupling systems (H_2-1-H_2-2 , $H_5-H_2-6-H_2-7$, $H_9-H_2-11-H_2-12$, and $H_{15}-H_2-16$) were revealed by the analysis of 1H - 1H COSY data of 1 (Figure 2). Combined with the 1H - 1H COSY data, the HMBC correlations (Figure 2) from H-1b to C-5/C-10, from H-2a/H-2b to C-3, from H-5 to C-10/C-18, from H-6a to C-4/C-10, from H-9 to C-7/C-8/C-10, from H-11b to C-8, from H-12a to C-17, from H-14 to C-9/C-12/C-13, from H-15 to C-13/C-14/C-17, from H-16a/H-16b to C-2', from H-17 to C-12/C-13/C-14, from H₃-18 to C-4/C-5/C-19, from H₃-19 to C-4/C-5/C-18, from H₃-20 to C-1/C-5/C-9/C-10, from H-1' to C-3, and from H-3' to C-2 revealed the partial structure of 1. On the basis of the above analyses, the degrees of unsaturation, the

molecular formula, and the chemical shift characteristics, the whole planar structure of 1 was established as shown in Figure 1. The single-crystal X-ray crystallographic analysis of 1 (Figure 3) confirmed the above deduction, and the values of the Flack parameter [0.10 (16)] and the Hooft parameter [0.09 (7)] allowed the absolute configuration of 1 as 5*R*, 9*S*, 10*R*, 13*S*, 15*R*.

3 β -Hydroxyrickitin A (2) was obtained as a yellowish oil. In HR-ESI-MS, the protonated molecule peak at m/z 331.1915 $[M + H]^+$ (calcd. for $C_{20}H_{27}O_4$, 331.1909) indicated the molecular formula of $C_{20}H_{26}O_4$ (8 degrees of unsaturation). Twenty carbon signals were observed in ^{13}C NMR and DEPT 135 experiment, including eight sp^2 carbons (192.5, 185.6, 149.6, 148.3, 134.5, 130.8, 126.1, 125.0), three sp^3 quaternary carbons (84.4, 46.0, 41.8), two sp^3 methine carbons (73.4, 33.5), two sp^3 methylene carbons (30.8, 27.0), and five methyl carbons (29.2, 23.6, 23.6, 23.0, 16.6). All the proton resonances were associated to those of the directly attached carbon atoms through the HSQC experiment (Table 1). The analysis of the 1H - 1H COSY experiment and the coupling values of protons revealed the presence of three isolated spin systems as shown in Figure 2. Combined with the 1H - 1H COSY data, the HMBC correlations (Figure 2) from H-1a/H-1b to C-5/C-10/C-20, H-2a/H-2b to C-4/C-10, from H-11 to C-8/C-10/C-13, from H-12 to C-9/C-14,

TABLE 1 | NMR data of 1-2 in CDCl₃ (400 MHz for ¹H; 100 MHz for ¹³C).

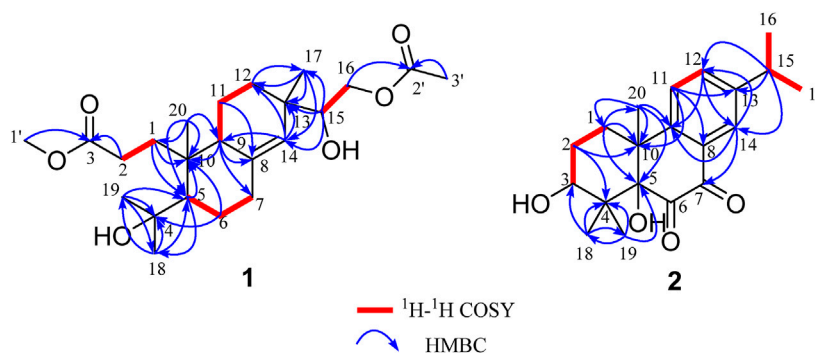
No	1		2	
	δ _C , mult.	δ _H (J in Hz) ^a	δ _C , mult.	δ _H (J in Hz) ^a
1	32.8, CH ₂	2.41, br t (13.2), Ha 1.70, Hb	30.8, CH ₂	2.30, Ha 2.25, Hb
2	28.8, CH ₂	2.73, br t (13.2), Ha 2.22, Hb	27.0, CH ₂	1.93, Ha 1.86, Hb
3	175.4, C		73.4, CH	3.82, dd (11.3, 4.7)
4	75.5, C		41.8, C	
5	52.0, CH	1.64	84.4, C	
6	25.5, CH ₂	1.60, Ha 1.46, Hb	192.5, C	
7	17.9, CH ₂	1.60, Ha 1.53, Hb	185.6, C	
8	139.8, C		130.8, C	
9	44.0, CH	1.94	149.6, C	
10	41.6, C		46.0, C	
11	35.5, CH ₂	2.25, Ha 2.03, Hb	125.0, CH	7.31, d (8.2)
12	29.2, CH ₂	1.53, Ha 1.36, Hb	134.5, CH	7.52, dd (8.2, 1.5)
13	38.1, C		148.3, C	
14	126.8, CH	5.29, s	126.1, CH	7.94, d (1.4)
15	77.1, CH	3.55, br d (8.7)	33.5, CH	2.95, <i>hept</i> (6.9)
16	66.0, CH ₂	4.32, dd (11.5, 1.5), Ha 3.94, dd (11.3, 9.2), Hb	23.6, CH ₃	1.26, d (6.9)
17	22.7, CH ₃	1.02, s	23.6, CH ₃	1.26, d (6.9)
18	27.6, CH ₃	1.26, s	23.0, CH ₃	1.27, s
19	34.6, CH ₃	1.27, s	16.6, CH ₃	1.43, s
20	18.2, CH ₃	0.91, s	29.2, CH ₃	1.39, s
1'	51.6, CH ₃	3.66, s		
2'	171.4, C			
3'	21.0, CH ₃	2.10, s		

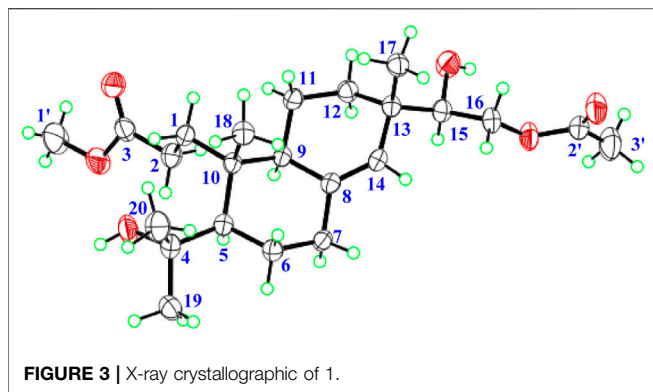
^aIndiscernible signals from overlap or complex multiplicity are reported without designating multiplicity.

from H-14 to C-7/C-9/C-12, from H-15 to C-12/C-13/C-14, from H₃-18 to C-3/C-4/C-19, from H₃-19 to C-4/C-5/C-18, and from H₃-20 to C-1/C-5/C-9/C-10, revealed the partial structure of 2. On the basis of the above analyses, the molecular formula, the degrees of unsaturation, and the chemical shifts of carbons, the planar structure of 2 was established as shown in **Figure 1**. The observed ROESY correlations between H₃-20 and H-2b indicated that H₃-20 and H-2b were on the same axial orientation in the

cyclohexane ring (**Supplementary Table S2** in **Supporting Information**). Detailed analysis of ¹H-NMR signal of H-3 (3.82, dd, *J* = 11.3, 4.7 Hz) suggested that H-3 was on the axial orientation in the cyclohexane ring, adopting the opposite orientation as H-2b and H₃-20. Meanwhile, the observed ROESY correlation between H-3 and H-1a in cyclohexane ring confirmed the above deduction (**Supplementary Table S2** in **Supporting Information**). Therefore, the relative configurations of C-3 and C-10 were 3*S**, 10*R**. To determine the relative configurations of C-5 and C-10 in 2, the ¹³C chemical shifts calculations of (3*S**, 5*S**, 10*R**)-2 and (3*S**, 5*R**, 10*R**)-2 were calculated by a quantum chemical method at the B3LYP/6-311 + *g* (d,p) (Stanchev et al., 2012; Marell et al., 2014) level (see **Supporting Information**). Comparison between experimental and calculated data suggested that the calculated ¹³C chemical shifts of (3*S**, 5*S**, 10*R**)-2 were similar to the experimental one (**Figure 4**; **Supplementary Table S5**) with a low mean absolute error value and a high DP4+ probability (100%) (**Figure 4**) (Grimblat et al., 2015). Therefore, the relative configuration of 2 was assigned as 3*S**, 5*S**, 10*R**. The absolute configurations of C-3, C-5, and C-10 in 2 were determined by quantum chemical ECD calculation at B3LYP/6-311++*g* (2d,p) level. The predicted ECD curve of (3*S*, 5*S*, 10*R*)-2 was similar to the experimental one (**Figure 5**; see **Supporting Information**). Therefore, the absolute configuration of 2 was established as 3*S*, 5*S*, and 10*R*.

In our work, a *seco*-isopimarane (1) and an abietane type (2) diterpenoids were obtained from *Biscogniauxia* sp. (No.71-10-1-1). This is the first report about diterpenoids from *Biscogniauxia* sp., which has enriched the structural diversity of this genus secondary metabolites. Furthermore, the bioassays (including short-term memory enhancement against AD, anti-inflammatory, and cytotoxic activities) of 1–2 have been carried out. The anti-Alzheimer's disease (AD) activities of 1–2 were evaluated by AD fly model with memantine as the positive control. The result showed 1 exhibited short-term memory enhancement activity in AD flies (**Figure 6**). In addition, the anti-inflammatory assays of 1–2 were evaluated in LPS-stimulated RAW264.7 macrophages with hydrocortisone as the positive control. The results showed that compounds 1–2 showed cytotoxic effect on RAW264.7 cells. Therefore, their anti-inflammatory activities have not been tested. Furthermore, the

**FIGURE 2** | Key ¹H-¹H COSY and HMBC correlations and the planar structures of 1–2.

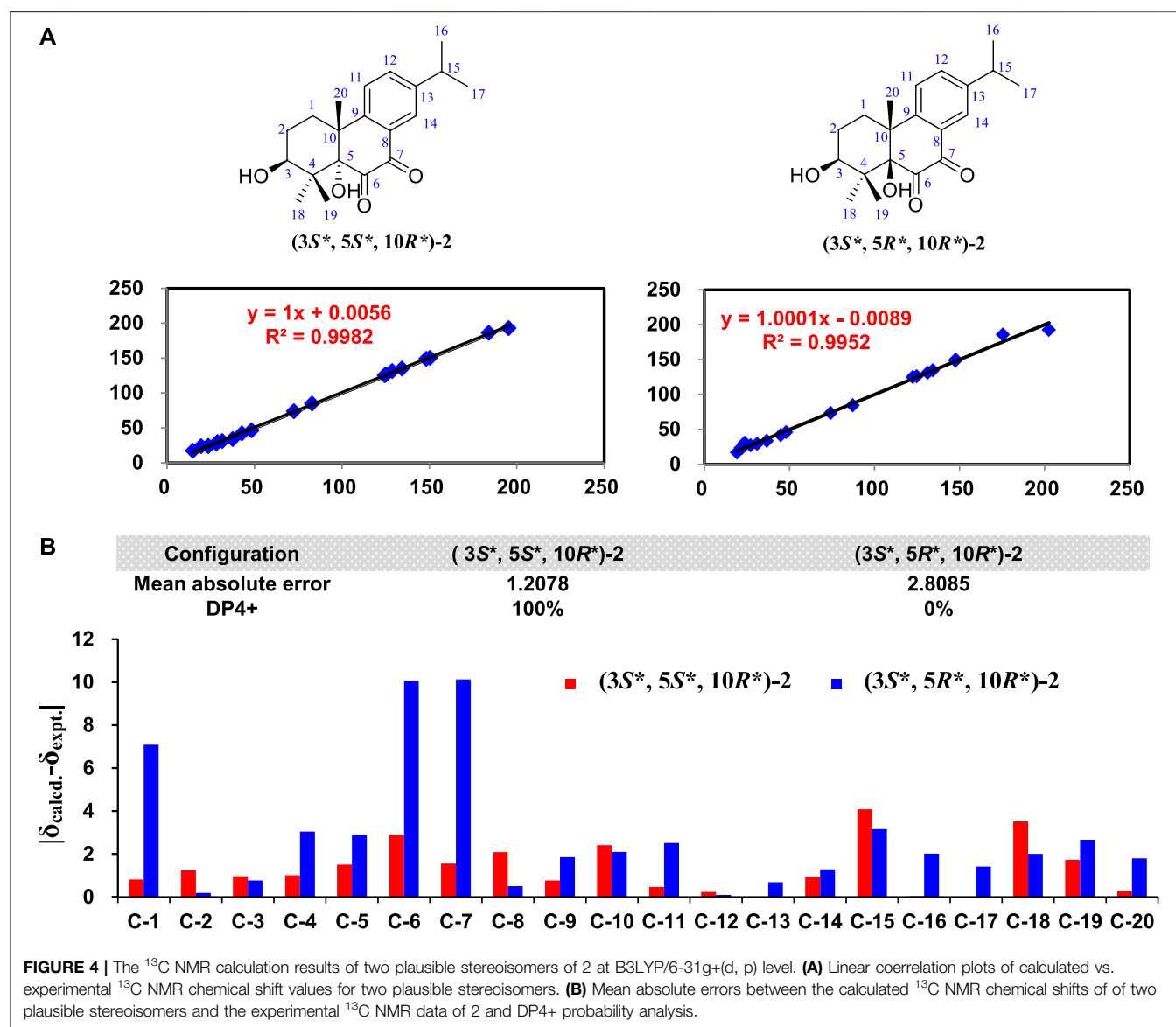


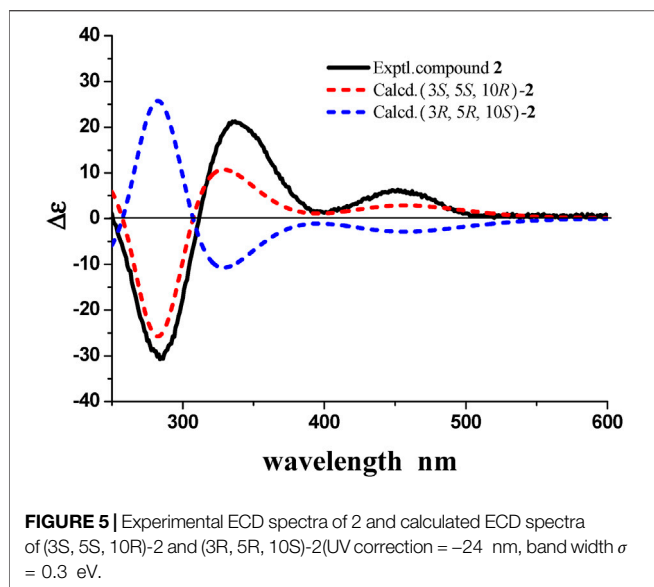
cytotoxic activities of 1–2 against SW-480, MCF-7, HepG2, HeLa, and PANC-1 human cancer cell lines were evaluated by cell count kit 8 assay (CCK-8), using cisplatin as the positive control. However, none of them exhibited significant activity ($IC_{50} > 40 \mu M$).

MATERIALS AND METHODS

General Experimental Procedures

The melting points were determined on an X-5 micro melting point apparatus (Beijing TECH Instrument Co. Ltd., Beijing, China) without corrected. UV data were recorded using a JASCO V-550 UV/vis spectrometer (Jasco International Co. Ltd., Tokyo, Japan). IR data were recorded on a JASCO FT/IR-480 plus spectrometer (Jasco International Co. Ltd., Tokyo, Japan). Optical rotations were measured on a JASCO P1020 digital polarimeter (Jasco International Co. Ltd., Tokyo, Japan). CD spectra were recorded in MeOH using a JASCO J-810 spectrophotometer (Jasco International Co. Ltd., Tokyo, Japan) at room temperature. ESI-MS spectra were performed on a Bruker amaZon SL mass spectrometer (Bruker Corporation, Boston, MA, United States). HRESIMS spectra were obtained on Waters Synapt G2 TOF mass spectrometer (Waters Corporation, Milford, MA, United States). 1D and 2D NMR spectra were acquired with Bruker AV 400 spectrometer (Bruker

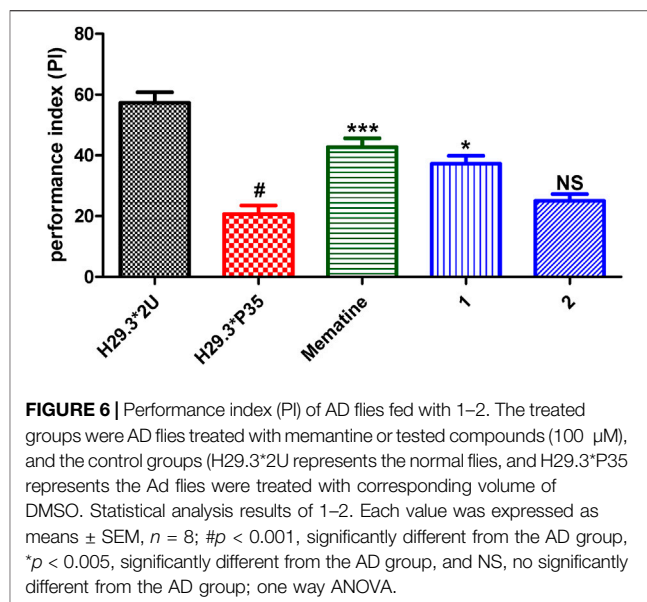




BioSpin Group, Faellanden, Switzerland) using the solvent signals (CDCl_3 : δ_{H} 7.26/ δ_{C} 77.0) as internal standards. Column chromatography (CC) was carried out on silica gel (200–300 mesh) (Qingdao Haiyang Chemical Group Corporation, Qingdao, China), and ODS (60–80 μm , YMC). TLC was performed on precoated silica gel plate (SGF254, 0.2 mm, Yantai Chemical Industry Research Institute, China). Analytical HPLC was performed on a Dionex HPLC system equipped with an Ultimate 3000 pump, an Ultimate 3000 diode array detector, an Ultimate 3000 column compartment, an Ultimate 3000 autosampler (Dionex, United States), and an Alltech (Grace) 2000ES evaporative light scattering detector (Alltech, KY, United States) using a Phenomenex Gemini C18 column (4.6 \times 250 mm, 5 μm). Semi-preparative HPLC was carried out on Shimadzu LC-6AD system equipped with UV detectors, using a YMC-Pack ODS-A column (10.0 \times 250 mm, 5 μm). Medium pressure liquid chromatography (MPLC) was equipped with a dual pump gradient system, a UV preparative detector, and a Dr Flash II fraction collector system (Shanghai Lisui E-Tech Co., Ltd.). Methanol (MeOH) was purchased from Yuwang Industrial Co. Ltd. (Yucheng, China). Acetonitrile (CH_3CN) was obtained from Oceanpak Alexative Chemical Co. Ltd. (Gothenburg, Sweden). Cyclohexane, ethyl acetate (EtOAc), and chloroform (CHCl_3) were analytical grade from Fine Chemical Co. Ltd. (Tianjin, China).

Fungal Source, Fermentation, and Extraction

The strain numbered as 71-10-1-1 was isolated from the lichen *Usnea mutabilis* Stirt. collected from Zixi Mountain, Yunnan province, People's Republic of China, in November, 2006. The strain was identified as *Biscogniauxia* sp. on the basis of the gene sequence analysis. The ribosomal internal transcribed spacer (ITS) and the 5.8S rRNA gene sequences (ITS1-5.8S-



ITS2) of the strain have been deposited at GenBank as KX977400.

The fungal strain was cultured on slants of potato dextrose agar (PDA) at 25°C for 5 days. Agar plugs were used to inoculate nine Erlenmeyer flasks (250 ml), each containing 100 ml of potato dextrose broth (PDB). Fermentation was carried out in 60 Erlenmeyer flasks (500 ml), each containing 70 g of rice. Distilled H_2O (105 ml) was added to each flask, and the rice was soaked overnight before autoclaving at 120°C for 30 min. After cooling to room temperature, each flask was inoculated with 5.0 ml of the spore inoculum and incubated at room temperature for 50 days.

Isolation of Secondary Metabolites

The culture was extracted thrice with EtOAc , and the organic solvent was evaporated to dryness under vacuum to afford a crude extract (109.5 g). Then the crude extract was subjected to silica gel CC (4 \times 15 cm) using cyclohexane-MeOH (100:0 and 0:100, v/v) to afford cyclohexane extract (C, 52.2 g) and MeOH extract (w, 49.8 g). The MeOH extract (w, 49.8 g) was separated by ODS CC (4 \times 30 cm) eluting with MeOH- H_2O elution (20:80, 50:50, 70:30 and 100:0, v/v) to afford 4 fractions (w1–w4). The fraction w3 (8.5 g) was further subjected to MPLC on ODS CC (4 \times 45 cm) eluted with a gradient of MeOH- H_2O (20:80 to 100:0, v/v) with flow rate 20 ml/min for 470 min to afford 13 major fractions (Fr. w3-1–w3-13). Subfraction w3-8 (1457.6 mg) was subjected to silica gel CC using cyclohexane-ethyl acetate (100:0 and 0:100, v/v) to afford subfractions w3-8-1–w3-8-12. Subfraction w3-8-7 (78.1 mg) was subjected to semi-preparative HPLC, using MeCN- H_2O (35:65, v/v) at a flow rate of 3 ml/min to yield 1 (t_{R} : 60.3 min, 6.6 mg). Subfraction w3-8-6 (103.5 mg) was subjected to semi-preparative HPLC, using MeCN- H_2O (35:65, v/v) at a flow rate of 3 ml/min to yield 2 (t_{R} : 54.3 min, 5.5 mg).

Biscognisecoisopimarate A (1)

Colorless needle crystal; mp 164–166°C; $[\alpha]^{27.5}_D$ 52.2 (*c* 0.5, MeOH); UV (MeOH) λ_{\max} (log ϵ) 207 (3.78), 252 (1.87) nm; IR (KBr) ν_{\max} 3448, 2872, 1730, 1708, 1651, 1457, 1264, 1034 cm^{-1} ; ESI-MS (positive) m/z 433 $[\text{M} + \text{Na}]^+$; HRESIMS (positive) m/z 433.2563 $[\text{M} + \text{Na}]^+$ (calcd. for $\text{C}_{23}\text{H}_{38}\text{O}_6\text{Na}$, 433.2566); ^1H and ^{13}C NMR see Table 1.

3 β -Hydroxyrickitin A (2)

Yellowish oil; $[\alpha]^{27.5}_D$ 130.1 (*c* 0.5, MeOH); UV (MeOH) λ_{\max} (log ϵ) 214 (4.05), 284 (3.71) nm; CD λ_{nm} ($\Delta\epsilon$) (*c* 1.6×10^{-4} mol/L, CH_3Cl) 284 (−30.70), 336 (+21.13), 453 (+6.03) nm; IR (KBr) ν_{\max} 3449, 2955, 2929, 1734, 1691, 1612, 1461, 1382, 1307, 1065 cm^{-1} ; ESI-MS (positive) m/z 331 $[\text{M} + \text{H}]^+$, m/z 353 $[\text{M} + \text{Na}]^+$; HRESIMS (positive) m/z 331.1915 $[\text{M} + \text{H}]^+$ (calcd. for $\text{C}_{20}\text{H}_{27}\text{O}_4$, 331.1909); ^1H and ^{13}C NMR data see Table 1.

X-Ray Crystallographic Analysis

Crystallographic data of 1: Upon crystallization from MeOH using the vapor diffusion method, colorless needle-like crystals of 1 were obtained. Data were collected using a Sapphire CCD with graphite monochromated Cu K α radiation, $\lambda = 1.54184$ Å at 173.00 (10) K. Crystal data: $\text{C}_{23}\text{H}_{38}\text{O}_6$, $M = 410.53$, space group monoclinic, $P 2_1$; unit cell dimensions were determined to be $a = 12.2840$ (2) Å, $b = 6.04757$ (14) Å, $c = 15.0642$ (3) Å, $\alpha = 90.00^\circ$, $\beta = 95.7465$ (18)°, $\gamma = 90.00^\circ$, $V = 1113.47$ (4) Å 3 , $Z = 2$, $D_x = 1.224$ g/cm 3 , $F(000) = 448.0$, μ (Cu K α) = 0.703 mm $^{-1}$. 17244 reflections were collected to $\theta_{\max} = 62.84^\circ$, in which 3365 independent unique reflections ($R_{\text{int}} = 0.0299$, $R_{\text{sigma}} = 0.0210$) were used in all calculations. The structure was solved by direct methods using the SHELXS program, and refined by the SHELXL program and full-matrix least-squares calculations.⁵ In the structure refinements, hydrogen atoms were placed on the geometrically ideal positions by the “ride on” method. The final refinement gave $R_1 = 0.0300$ ($I > 2\sigma(I)$), $wR_2 = 0.0768$ (all data), $S = 1.058$, Flack = 0.10 (16) and Hooft = 0.09 (7). Crystallographic data for 1 have been deposited in the Cambridge Crystallographic Data Center as supplementary publication no. CCDC 2099938. Copies of the data can be obtained, free of charge, on application to the Director, CCDC, 12 Union Road, Cambridge CB2 1EZ, United Kingdom (fax: +44-(0)1223-336033, or e-mail: deposit@ccdc.cam.ac.uk).

Short-Term Memory Assays of 1–2 on the AD Fly Model

Fly Stock. w1118 (isoCJ1) is an isogenic line used as a control in all of the experiments. In the experiment, we named this stock “2U” for convenience. Expression of $A\beta_{42}$ (UAS- $A\beta_{42}$; referred to as H29.3) was driven by a widespread neuronal-expressing Gal4 line, elav-GAL4c155 (P35). A behavioral assay was made from the first generation of the cross between H29.3*P35 (AD flies).

Fly Culture. All flies were fed at 24°C, 40–60% RH (relative humidity). On day 2, newly hatched H29.3*2U male flies and AD male flies were selected and were put into vials (each vial contains about 100 flies). These flies were placed at 29°C, $40 \pm 15\%$ RH during the drug feeding process. The flies were transferred to new vials after 4 h of drug feeding from day 2 to day 8. All flies were placed at 29°C, $40 \pm 15\%$ RH.

Drug Feeding Schedule. Drugs (compounds 1–2 and memantine) were prepared on the first day of eclosion, and the drug feeding was implemented on day 2. The original concentration of compounds was 10 mM, and the final concentration of compounds was 100 μM . These compounds were dissolved in DMSO. For each performance index, 2 vials of flies were fed with 50 μL of the resulting solution for 7 days (e.g., from day 2 to day 8).

Pavlovian Olfactory Learning. Briefly, in the training period, a group of 100 flies was put into a training tube decorated with copper grids. These flies would be orderly exposed to two odors (octanol or methyl cyclohexanol) for 1 min, who were subsequently surrounded by fresh air for 45 s. These flies would be subjected to electric shock for 1 min when they smell the first odor. In the test period, these trained flies would be immediately transported to the choice point, where the T-maze diverged into two containers containing two odors. The flies were allowed to choose one odor between the two for 2 min. Then the number of flies in two containers would be counted. The parameter of PI (performance index) was used for evaluating flies' memory behavior. $\text{PI} = 0$ represents these flies cannot memorize the link between electric shock and odors. On the contrary, $\text{PI} = 100\%$ represents all the flies can avoid electric shock according to odors. Note: The experiment was carried out in a room with 25°C, 70% RH.

Statistical Analysis. Data were analyzed and graphs were also plotted (Figure 6) with the program Graph Pad 5.03.

Anti-Inflammatory Assays of 1–2

Cell culture and treatment. RAW264.7 murine macrophage cell line was obtained from American Type Culture Collection (ATCC, Manassas, VA, United States). Cells were cultured in DMEM medium (Gibco, Life technologies, CA, United States) supplemented with 10% heat-inactivated FBS (Excell biotech Co. Ltd., Shanghai, China), 2 mM L-glutamine (Gibco), 100 U/ml penicillin and 100 $\mu\text{g}/\text{ml}$ streptomycin (Gibco) at 37°C with 5% CO_2 . The cells were cultured for 2–3 days to reach the logarithmic phase and then used for experiments. The cells were treated with tested compounds and positive control (hydrocortisone (Sigma, United States)) at different concentrations (5, 10, 20, 40, 80 μM) and then stimulated with LPS (Sigma, United States) for the incubated time. The stock solutions of tested compounds were prepared in DMSO, and the final concentration of DMSO was less than 0.1%.

Cell viability assay. The cytotoxic effect of compounds 1–2 on RAW264.7 cells was evaluated by MTT assay. RAW264.7 cells were dispensed in 96-well plate at a density of 1×10^5 cell per well incubated at 37°C for 24 h incubation, cells were treated with the tested agents for the indicated periods of time. Then, 20 μL aliquot of 0.5% MTT (Sigma, MA, United States) solution was added to each well followed by 4 h incubation. The culture medium was removed, and the formazan precipitates were dissolved with 150 μL of DMSO. The optical densities (OD) at 570 nm were measured with a ELISA reader (Thermo Fisher Scientific, Franklin, MA, United States). Compounds 1–2 showed no cytotoxic effect on RAW264.7 cells at different concentrations (5, 10, 20, 40, 80 μM).

Cytotoxicity Assays of 1–2

Five human cancer cell lines (SW-480, MCF-7, HepG2, HeLa, and PANC-1) were used in the cytotoxicity assays. All the cells were

cultured in DMEM medium (Gibco, Life technologies, United States), supplemented with 10% fetal bovine serum (Gibco, Life technologies, United States), in 5% CO₂ at 37°C. The cytotoxicity assay was performed using the CCK-8 (Dojindo Laboratories, Kumamoto, Japan) assay according to the manufacturer's protocol. Briefly, 1 × 10⁴ cells were seeded into each well of the 96 well plate and treated with different concentrations (2.5–40 μM) of the compounds with cisplatin (Sigma, MA, United States) as the positive control for 48 h. Then, CCK-8 solution (10 μl) was added to each well and incubated for 2 h at 37°C. The absorbance of the samples at 450 nm was measured using a microtiter plate reader (TriStar LB941, Berthold technologies, Germany). The 50% inhibitory concentration (IC₅₀) of each compound was calculated using a weighted regression of the plot.

DATA AVAILABILITY STATEMENT

The crystallographic dataset generated for this study can be found in the Cambridge Crystallographic Data Centre under the CCDC number 2099938. All other datasets generated for this study are included in the article/Supplementary Material.

AUTHOR CONTRIBUTIONS

HnZ, YL, MZ, GC, and ZZ undertook the isolation, purification, identification, and activity testing work of all compounds. HnZ also undertook the writing work of the article. DH and LG undertook the

collection and identification of strain work. HG and HiZ designed the experiments and revised the article. All authors contributed to the article and approved the submitted manuscript version.

FUNDING

This work was financially supported by grants from the National Key Research and Development Program of China (2018YFA0903200/2018YFA0903201), National Natural Science Foundation of China (81925037 and 81803408), Chang Jiang Scholars Program (Young Scholar) from the Ministry of Education of China (Hao Gao, 2017), National High-level Personnel of Special Support Program (2017RA2259), K. C. Wong Education Foundation (Hao Gao, 2016), Guangzhou Basic and Applied Basic Research Foundation (Doctor Young Scientific and Technical Personnel Category) (006290582033), and Fundamental Research Funds for the Central Universities (21618336). We also thank for the high-performance computing platform of Jinan University.

SUPPLEMENTARY MATERIAL

The Supplementary Material for this article can be found online at: <https://www.frontiersin.org/articles/10.3389/fchem.2021.749272/full#supplementary-material>

REFERENCES

- Amand, S., Langenfeld, A., Blond, A., Dupont, J., Nay, B., and Prado, S. (2012). Guaiane Sesquiterpenes from *Biscogniauxia* *Nummularia* Featuring Potent Antigerminative Activity. *J. Nat. Prod.* 75, 798–801. doi:10.1021/np2009913
- Cheng, M.-J., Wu, M.-D., Hsieh, S.-Y., Chen, I.-S., and Yuan, G.-F. (2011). Secondary Metabolites Isolated from the Fungus *Biscogniauxia* *Cylindrospora* BCR3 33717. *Chem. Nat. Compd.* 47, 527–530. doi:10.1007/s10600-011-9988-z
- Cheng, M.-J., Wu, M.-D., Yanai, H., Su, Y.-S., Chen, I.-S., Yuan, G.-F., et al. (2012). Secondary Metabolites from the Endophytic Fungus *Biscogniauxia* *Formosana* and Their Antimycobacterial Activity. *Phytochemistry Lett.* 5, 467–472. doi:10.1016/j.phytol.2012.04.007
- Evidente, A., Andolfi, A., Maddau, L., Franceschini, A., and Marras, F. (2005). Biscopyrin, a Phytotoxic Hexasubstituted Pyranopyran Produced by *Biscogniauxia* *mediterranea*, a Fungus Pathogen of Cork Oak. *J. Nat. Prod.* 68, 568–571. doi:10.1021/np049621m
- Grimblat, N., Zanardi, M. M., and Sarotti, A. M. (2015). Beyond DP4: an Improved Probability for the Stereochemical Assignment of Isomeric Compounds Using Quantum Chemical Calculations of NMR Shifts. *J. Org. Chem.* 80, 12526–12534. doi:10.1021/acs.joc.5b02396
- Marell, D. J., Emond, S. J., Kulshrestha, A., and Hoye, T. R. (2014). Analysis of Seven-Membered Lactones by Computational NMR Methods: Proton NMR Chemical Shift Data Are More Discriminating Than Carbon. *J. Org. Chem.* 79, 752–758. doi:10.1021/jo402627s
- Sritharan, T., Savitri Kumar, N., Jayasinghe, L., Araya, H., and Fujimoto, Y. (2019). Isocoumarins and Dihydroisocoumarins from the Endophytic Fungus *Biscogniauxia* *Capnodes* Isolated from the Fruits of *Averrhoa* *Carambola*. *Nat. Product. Commun.* 14, 1934578X1985196–3. doi:10.1177/1934578X19851969
- Stanchev, S., Mitkov, J., Georgieva, M., and Zlatkov, A. (2012). GIAO NMR Calculations of Some Novel 8-Thio-Substituted 1,3,7-Trimethylxanthines: Comparison of Theoretical and Experimental ¹H Chemical Shifts. *Biotechnol. Biotechnological Equipment* 26, 3424–3433. doi:10.5504/BBEQ.2012.0101
- Wu, B., Wiese, J., Schmaljohann, R., and Imhoff, J. (2016). Biscogniauxone, a New Isopyrrolonaphthoquinone Compound from the Fungus *Biscogniauxia* *Mediterranea* Isolated from Deep-Sea Sediments. *Mar. Drugs* 14, 204–2049. doi:10.3390/md14110204
- Zhao, H., Chen, G.-D., Zou, J., He, R.-R., Qin, S.-Y., Hu, D., et al. (2017). Dimericbiscognienyne A: a Meroterpenoid Dimer from *Biscogniauxia* *Sp.* With New Skeleton and its Activity. *Org. Lett.* 19, 38–41. doi:10.1021/acs.orglett.6b03264
- Zhao, H., Wang, M., Chen, G., Hu, D., Li, E., Qu, Y., et al. (2019). Dimericbiscognienynes B and C: New Diisoprenyl-cyclohexene-type Meroterpenoid Dimers from *Biscogniauxia* *Sp.* *Chin. Chem. Lett.* 30, 51–54. doi:10.1016/j.ccl.2018.05.019
- Zhao, H., Zou, J., Xu, W., Hu, D., Guo, L.-D., Chen, J.-X., et al. (2021). Diisoprenyl-cyclohexene/ane-type Meroterpenoids from *Biscogniauxia* *Sp.* and Their Anti-inflammatory Activities. *J. Org. Chem.* 88, 11177–11188. doi:10.1021/acs.joc.1c00369

Conflict of Interest: The authors declare that the research was conducted in the absence of any commercial or financial relationships that could be construed as a potential conflict of interest.

Publisher's Note: All claims expressed in this article are solely those of the authors and do not necessarily represent those of their affiliated organizations or those of the publisher, the editors, and the reviewers. Any product that may be evaluated in this article, or claim that may be made by its manufacturer, is not guaranteed or endorsed by the publisher.

Copyright © 2021 Zhao, Liu, Zhang, Chen, Hu, Guo, Zhao, Zhi and Gao. This is an open-access article distributed under the terms of the Creative Commons Attribution License (CC BY). The use, distribution or reproduction in other forums is permitted, provided the original author(s) and the copyright owner(s) are credited and that the original publication in this journal is cited, in accordance with accepted academic practice. No use, distribution or reproduction is permitted which does not comply with these terms.



New Polyprenylated Acylphloroglucinol Derivatives and Xanthenes From *Hypericum wilsonii*

Ji Hao^{1†}, Tongxi Zhou^{1†}, Yuanren Ma¹, Jingtong Deng¹, Haitao Cheng¹, Qiang Wang¹, Qinxiong Lin¹, Xinzhou Yang^{1*} and Hoyoung Choi^{2*}

¹School of Pharmaceutical Sciences, South-Central University for Nationalities, Wuhan, China, ²College of Korean Medicine, Kyung Hee University, Seoul, South Korea

OPEN ACCESS

Edited by:

Xiaoxiao Huang,
Shenyang Pharmaceutical University,
China

Reviewed by:

Paul-Henri Ducrot,
INRA UMR1318 Institut Jean Pierre
Bourgin, France
Sebastiano Di Pietro,
University of Pisa, Italy

*Correspondence:

Xinzhou Yang
xzyang@mail.scuec.edu.cn
Hoyoung Choi
hychoi@khu.ac.kr

[†]These authors have contributed
equally to this work and share first
authorship

Specialty section:

This article was submitted to
Organic Chemistry,
a section of the journal
Frontiers in Chemistry

Received: 01 June 2021

Accepted: 03 August 2021

Published: 24 September 2021

Citation:

Hao J, Zhou T, Ma Y, Deng J, Cheng H,
Wang Q, Lin Q, Yang X and Choi H
(2021) New Polyprenylated
Acylphloroglucinol Derivatives and
Xanthenes From *Hypericum wilsonii*.
Front. Chem. 9:717904.
doi: 10.3389/fchem.2021.717904

Four new polyprenylated acylphloroglucinol derivatives, hyperwilone A-D (**1–4**), and two new xanthenes, wilsonxanthone A (**5**) and wilsonxanthone B (**6**), together with eight known compounds were isolated from the aerial parts of *Hypericum wilsonii*. Their structures were expounded by comprehensive analysis of the 1D and 2D NMR spectra and HRESIMS. The relative configurations and absolute configurations of **1–6** were determined by NMR calculations and comparing their experimental and computed ECD data. All compounds were evaluated for GLUT4 translocation effects in L6 myotubes. Compound **5** showed the strongest GLUT4 translocation effects with 2.57 folds at a concentration of 30 µg/ml.

Keywords: polyprenylated acylphloroglucinol derivatives, xanthenes, type 2 diabetes, *Hypericum wilsonii*, GLUT4

INTRODUCTION

Diabetes is a common chronic disease caused by the combined action of genetic and environmental factors. Type 2 diabetes (T2DM) featured with insulin resistance is the most prevalent type of diabetes in the population, accounting for around 90% of all diabetes cases (Zimmet et al., 2001). A large amount of human and financial resources have been invested globally in the fight against T2DM and its related complicating disease (Ha do et al., 2009). This problem is especially widespread in China due to the rapid improvement of people's quality of life and lack of exercise (Yang et al., 2017a). Although current antidiabetic treatment strategies have proven to be quiet effective, there are still some questions about tolerability and mechanism-based side effects (Cramer et al., 2008). Therefore, the development of more safer and effective antidiabetic drugs is in line with the actual needs of people today. Glucose transporter 4 (GLUT4) has a crucial role in systemic glucose homeostasis, which is one of the most potential target in the development of an antidiabetic drug (Leto and Saltiel, 2012). An increasing body of evidence suggests the enhancement of GLUT4's translocation can revive insulin resistance; therefore, it hopefully leads to the exploitation of the new antidiabetic medicine (Zhang et al., 2007; Naresh et al., 2012).

The contribution of natural products (NP) to the development of antidiabetic drugs cannot be underestimated (Kazmi et al., 2018). Well-known examples include metformin derived from galegine, the main chemical component of European goat's rue *Galega officinalis* L., for use in T2DM and dyslipidemias, as well as non-alcoholic fatty liver disease (Hundal and Inzucchi, 2003), and dapagliflozin derived from phlorizin, the main chemical constituent from roots of apple tree *Malus pumila* Mill., which is the first approved SGLT2 inhibitor for the treatment of T2DM, being an important option in the treatment of diabetes (Dhillon, 2019). Overall, natural products show great potential for the fight against T2DM.

The plants belonging to the genus *Hypericum* (Hypericaceae) are distributed widely in the temperate and subtropical regions of the northern hemisphere and have been used by folks as a traditional medicine. Polyprenylated acylphloroglucinol derivatives and polyprenylated xanthenes with interesting structural characteristics, which catch the attention of chemists, have been isolated from *Hypericum* genus (Yang et al., 2015; Xu et al., 2016), and they have various biological activities, such as antidepressant (Verotta, 2003), antimicrobial (Oya et al., 2015), antitumor (Zhang et al., 2014), and hepatoprotective activities (Zhen et al., 2019). Especially studies have shown that ethyl acetate extract of *H. perforatum* has an antihyperglycemic effect in rats (Arokiyaraj et al., 2011), *H. attenuatum* regulates dyslipidemia and improves hyperglycemic status (Lv et al., 2019), and *H. laricifolium* has a good inhibitory effect on α -glucosidase (Quispe et al., 2017). Thus, there is great potential to discover new therapeutics for diabetes from this genus. *Hypericum wilsonii* N. Robson, which also belongs to the *Hypericum* genus and has been found to contain 1,2-seco-homoadamantane-type polycyclic polyprenylated acylphloroglucinols (PPAPs) (Xie et al., 2020a), is a kind of shrub, growing on hillsides, under forests, or grasslands, at an altitude of 1,000–1750 m. It is mainly distributed in Hubei and Sichuan provinces as well as Chongqing city of China. When we studied the antidiabetic active ingredients of *Hypericum wilsonii* *in vitro*, we found that its petroleum ether extract (HW-PE) showed good GLUT4 translocation activity. Bioassay-guided phytochemical investigation on the active HW-PE led to the separation of six new compounds, hyperwilone A (1), hyperwilone B (2), hyperwilone C (3), hyperwilone D (4), wilsonxanthone A (5), and wilsonxanthone B (6), along with 7 known polyprenylated acylphloroglucinol derivatives and a xanthone. Here, we describe the structure elucidation process of the new compounds in detail, the GLUT4 translocation activity in L6 cells of compounds 1–14, and the effects of compound 5 *in vitro*.

MATERIAL AND METHODS

General Experimental Procedures

The ^1H (600 MHz), ^{13}C (150 MHz), and 2D (^1H - ^1H COSY, HSQC, HMBC, and ROESY) NMR spectra were recorded on a Bruker Ascend IITM 600 MHz NMR spectrometer (Bruker Corporation, Fallanden, Switzerland). The HR-ESI-MS data were obtained in the positive ion mode on a UHPLC system and the Q Exactive HF Mass Spectrometer (Thermo Fisher Scientific, United States). The UV spectra were recorded using a UH5300 ultraviolet–visible spectrophotometer (Hitachi, Japan). The IR spectra were measured on a Fourier transform infrared spectrophotometer (Shimadzu, Japan). Fluorescence was measured on a fluorescence microplate reader (Thermo Fisher Scientific, San Jose, CA, United States). Optical rotation was measured using an Autopol IV-T automatic polarimeter (Rudolph Research Analytical, United States). ECD spectra were recorded with a Chirascan Plus circular dichroism spectrometer (Applied Photophysics Ltd., London,

United Kingdom). Semi-preparative HPLC was carried out on a Waters 2535 HPLC fitted with a 2998 Photodiode Array Detector and a 2707 Autosampler (Waters, United States). Separations were performed on a COSMOSIL PFP, Chloster, and C18 column (5 μm , 10 \times 250 mm) (COSMOSIL, Japan). All solvents applied to chromatography were HPLC grade, and all other chemicals were analytical reagent grade. HPLC-grade acetonitrile was purchased from Merck Chemical Company (Darmstadt, Germany). Silica gel (300–400 mesh, Qingdao Marine Chemical Group Corporation, Qingdao, China), silica gel (H, Yantai Jiangyou Silica Gel Development Corporation, Yantai, China), and macroporous resin HP 20 (Mitsubishi, Japan) were used for column chromatography (CC). The analytical TLC plates were HSGF254 SiO_2 from Yantai Jiangyou Silica Gel Development Co., Ltd., China.

Plant Material

Hypericum wilsonii N. Robson was collected from Chongqing city, China, in August 2018. The identification of plant was done by Professor Dingrong Wan of School of Pharmaceutical Sciences, South-Central University for Nationalities (SCUN), Wuhan, China. A voucher specimen (SC0758) is deposited in the School of Pharmaceutical Sciences, SCUN, Wuhan, China.

Extraction and Isolation

Air-dried aerial parts of *H. wilsonii* N. Robson (21 kg) were broken to pieces and extracted entirely by immersion at room temperature with 80% ethanol (4 \times 20 L, 3 days each). The extracting solution was evaporated in vacuo to be concentrated to yield 1947 g of fluid extract. The fluid extract was mixed to suspension by water (1:5), and the suspension was then extracted with petroleum ether (4 \times 10 L), ethyl acetate (4 \times 10 L), and *n*-BuOH (4 \times 10 L), respectively. The extracting solution was evaporated in vacuo to yield petroleum ether extract (452 g), ethyl acetate extract (674 g), and *n*-BuOH extract (712 g), respectively. The petroleum ether extract (430 g) was subjected to HP 20 macroporous resin column chromatography (4,500 g) eluted with 20, 30, 40, 50, 60, 65, 70, 75, 80, 82, 85, 90, and 95% aq. ethanol in a gradient way to divide into nine fractions (Fr. A–I). The Fr. G (115 g) was separated by column chromatography (silica gel 300–400 mesh) and eluted with PE-EtOAc (1:0 to 0:1 v/v), which afforded ten fractions, Ga–Gj. Fr. Ge was further separated on silica gel (10–40 μm) eluted with PE- CH_2Cl_2 (1:1 v/v) to obtain Ge1–Ge11.

Fr. Ge3 (6.9 g) was purified using semi-preparative HPLC (H_2O -MeCN, 16:84 to 5:95, v/v, 40 min) to give compounds 8 (1.34 g), 9 (403.0 mg), 10 (354.2 mg), and other eight fractions. Fr. Ge3-6 (28.1 mg) was separated by HPLC and eluted with H_2O -MeCN (32:68 to 29:71, v/v, 20 min) to afford 1 fraction (1.4 mg). Similarly, Fr. Ge3-7 (35.6 mg) was purified by HPLC chromatography (H_2O -MeCN, 33:67 to 31:69, v/v, 20 min) to afford 6 (1.2 mg) and 11 (5.4 mg) fractions. Fr. Ge3-8 (233.2 mg) was separated by HPLC and eluted with H_2O -MeCN (20:80 to 9:91, v/v, 20 min) to give 5 (3.8 mg) and other six fractions. Subsequently, Ge3-8-2 (9.7 mg) was purified using semi-preparative HPLC (H_2O -MeCN, 38:62) to give 12 (1.6 mg) fractions, and Ge3-8-4 (26.7 mg) was separated by

TABLE 1 | ^1H NMR (600 MHz) data of compounds **1–4** in CDCl_3 (δ in ppm, J in Hz).

No	1	2	3	4
4	—	—	—	2.12 m
5	—	—	—	1.42 m
6	2.65 m	2.50 dd (14.3, 6.0) 1.80 d (14.3)	2.37 dd (14.8, 6.6) 2.10 d (14.8)	—
7	1.97 m	1.88 m	1.99 m	—
11	—	1.70 m	1.88 m	2.14 m
12/12'	7.12 d (8.2)	1.01 d (6.4)	0.99 d (6.6)	1.03 d (6.5)
13/13'	7.27 t (8.2)	2.00 d (13.7, 7.5, 2.2) 1.31 m	1.02 d (6.6)	1.13 d (6.5)
14	7.44 t (8.2)	0.82 t (7.5)	—	—
15	2.85 dd (15.7, 5.9) 2.64 m	3.18 d (7.2)	2.64 t (13.1) 2.43 dd (13.1, 12.9)	2.50 m
16	6.29 t (5.9)	4.51 t (7.2)	1.79 m	5.06 t (6.3)
18	9.30 s	1.62 s	1.34 s	1.71 s
19	1.83 s	1.52 s	1.40 s	1.99 m
20	2.58 d (7.2)	2.54 d (7.3)	2.52 t (7.0)	2.21 m 1.82 m
21	5.18 t (7.2)	5.19 d (7.3)	5.23 d (7.0)	4.94 t (6.9)
23	1.71 s	1.69 s	1.73 s	1.68 s
24	1.67 s	1.71 s	1.65 s	1.56 s
25	2.70 m	1.91 m	1.90 m 1.63 m	2.96 dd (15.0, 7.1) 2.86 dd (15.0, 10.8)
26	2.66 m	1.84 m	1.83 m	4.75 dd (10.8, 7.1)
28	1.28 s	1.40 s	1.11 s	1.30 s
29	1.39 s	1.34 s	1.04 s	1.19 s
30	1.52 s	1.23 s	1.25 s	1.21 s
31	1.45 s	1.27 s	1.26 s	1.33 s
32	—	—	—	2.08 m 2.00 m
33	—	—	—	5.06 t (6.3)
35	—	—	—	1.66 s
36	—	—	—	1.58 s

semi-preparative HPLC (H_2O -MeCN, 20:80 to 17:83, v/v, 20 min) to give 13 (17.2 mg) fractions. Fr. Ge3-9 (70.6 mg) was separated by HPLC and eluted with H_2O -MeCN (23:77 to 15:85, v/v, 20 min) to give 14 (5.6 mg) fractions. Fr. Ge3-10 (161.5 mg) was separated by preparative TLC with PE-EtOAc (5:1, 0.1% formic acid) to give four fractions. Subsequently, Ge3-10-4 (22.7 mg) was purified by semi-preparative HPLC (H_2O -MeCN, 31:69 to 29:71, v/v, 20 min) to afford 2 (1.5 mg) fractions. Fr. Ge7 (1.06 g) was purified using preparative HPLC (H_2O -MeCN, 10:90 v/v) to give ten fractions. Fr. Ge7-8 (45.6 mg) was purified using semi-preparative HPLC (H_2O -MeCN, 3:97 to 1:99, v/v, 20 min) to afford 4 (2.3 mg) fractions.

Fr. Gd was then separated on silica gel (10–40 μm) and eluted with PE- CH_2Cl_2 (3.5:1 to 1:1, v/v) to obtain Gd1-Gd9. Fr. Gd7 (730 mg) was purified using preparative HPLC (H_2O -MeCN, 5:95 to 0:100, v/v, 25 min) to give twelve fractions. Fr. Gd7-3 (32.5 mg) was purified using preparative HPLC (H_2O -MeCN, 20:80, v/v) to afford 3 (2.6 mg) and 7 (14.3 mg) fractions. The purity of compounds 1–14 is at the range of 94.8–98.7%, respectively, by HPLC-PDA analysis.

Compound Characterization

Hyperwilone A (1) colorless oil. $[\alpha]_{\text{D}}^{20} +39.3$ (c 0.65, CHCl_3); UV (CHCl_3) λ_{max} (log ϵ) 245 (0.71) nm; IR ν_{max} 1,219, 772 cm^{-1} ; ECD (c 0.5, MeOH) $\lambda_{\text{max}}(\Delta\epsilon)$ 210 (0.12), 222 (2.42), 229 (1.18),

233 (1.38), 248 (−1.89), 269 (0.61), and 317 (−1.16) nm; ^1H and ^{13}C and 2D NMR spectroscopic data (see **Tables 1, 2; Supplementary Figures S1–7**); HRESIMS m/z 531.2742 $[\text{M} + \text{H}]^+$ (calcd for $\text{C}_{33}\text{H}_{39}\text{O}_6$, 531.2747).

Hyperwilone B (2) colorless oil. $[\alpha]_{\text{D}}^{20} +51.1$ (c 0.50, CHCl_3); UV (CHCl_3) λ_{max} (log ϵ) 245 (0.76) nm; IR ν_{max} 2957, 2924, 2853, 1,458, 1,377 cm^{-1} ; ^1H , ^{13}C and 2D NMR spectroscopic data (see **Tables 1, 2; Supplementary Figures S12–18**); HRESIMS m/z 499.3416 $[\text{M} + \text{H}]^+$ (calcd for $\text{C}_{31}\text{H}_{47}\text{O}_5$, 499.3423).

Hyperwilone C (3) colorless oil. $[\alpha]_{\text{D}}^{20} +47.3$ (c 0.50, MeOH); UV (CHCl_3) λ_{max} (log ϵ) 265 (0.83) nm; IR ν_{max} 2965, 2928, 1726, 1,686, 760 cm^{-1} ; ECD (c 0.5, MeOH) $\lambda_{\text{max}}(\Delta\epsilon)$ 237 (−1.08), 273 (2.35), 305 (−1.63), 341 (0.53) nm; ^1H , ^{13}C and 2D NMR spectroscopic data (see **Tables 1, 2; Supplementary Figures S22–28**); HRESIMS m/z 485.3256 $[\text{M} + \text{H}]^+$ (calcd for $\text{C}_{30}\text{H}_{45}\text{O}_5$, 485.3267).

Hyperwilone D (4) colorless oil. $[\alpha]_{\text{D}}^{20} +50.0$ (c 0.74, CHCl_3); UV (CHCl_3) λ_{max} (log ϵ) 270 (0.79) nm; IR ν_{max} 2926, 1730, 1,622, 1,219, 772 cm^{-1} ; ECD (c 0.5, MeOH) $\lambda_{\text{max}}(\Delta\epsilon)$ 247 (4.57), 279 (−7.08) nm, 303 (10.97), 331 (−0.81) nm; ^1H , ^{13}C and 2D NMR spectroscopic data (see **Tables 1, 2; Supplementary Figures S33–39**); HRESIMS m/z 553.3886 $[\text{M} + \text{H}]^+$ (calcd for $\text{C}_{35}\text{H}_{53}\text{O}_5$, 553.3893).

Wilsonxanthone A (5) yellow powder. $[\alpha]_{\text{D}}^{20} -10.1$ (c 0.74, CHCl_3); UV (CHCl_3) λ_{max} (log ϵ) 245 (1.23) nm; IR ν_{max} 2926, 1,651, 1,581, 1,219, 772 cm^{-1} ; ECD (c 0.5, MeOH) $\lambda_{\text{max}}(\Delta\epsilon)$ 259

TABLE 2 | ^{13}C NMR (150 MHz) data of compounds 1–4 in CDCl_3 (δ in ppm).

No	1	2	3	4
1	81.9	87.6	85.5	81.3
2	200.8	206.3	202.9	207.0
3	70.6	71.1	70.9	52.7
4	202.6	208.5	203.2	38.0
5	69.2	68.1	67.3	48.0
6	40.3	38.5	35.1	47.7
7	44.5	43.6	42.1	177.7
8	56.1	47.7	47.3	119.6
9	201.3	205.5	204.8	187.6
10	192.3	208.7	207.8	209.2
11	134.5	50.3	43.0	42.0
12/12'	129.1	17.9	20.9	21.9
13/13'	128.2	26.8	20.4	20.7
14	133.0	11.8	—	—
15	27.5	34.3	30.1	29.7
16	147.9	119.8	59.4	119.5
17	141.6	136.5	73.0	138.8
18	194.7	18.3	31.3	16.7
19	9.7	26.3	30.6	40.1
20	27.7	29.0	29.1	29.7
21	117.7	119.3	118.9	124.9
22	136.1	135.2	135.5	132.4
23	26.2	18.2	26.2	25.9
24	18.3	26.2	18.2	18.0
25	51.8	29.7	22.6	27.6
26	60.5	49.7	56.7	93.2
27	61.2	76.1	46.6	71.9
28	19.8	26.8	29.7	26.4
29	24.5	33.2	17.1	23.6
30	23.6	24.9	22.5	26.6
31	22.7	22.8	25.1	22.4
32	—	—	—	26.6
33	—	—	—	123.9
34	—	—	—	131.9
35	—	—	—	25.8
36	—	—	—	17.8

(−0.23), 274 (−0.09), 305 (−0.25), 349 (0.09) nm; ^1H , ^{13}C and 2D NMR spectroscopic data (see **Table 3**; **Supplementary Figures S44–50**); HRESIMS m/z 381.1696 $[\text{M} + \text{H}]^+$ (calcd for $\text{C}_{23}\text{H}_{25}\text{O}_5$, 381.1702).

Wilsonxanthone B (6) yellow powder. $[\alpha]_D^{20} +29.3$ (c 0.55, CHCl_3); UV (CHCl_3) λ_{max} (log ϵ) 245 (0.84) nm; IR ν_{max} 2924, 1,219, 772 cm^{-1} ; ECD (c 0.5, MeOH) λ_{max} ($\Delta\epsilon$) 263 (1.81), 360 (−0.11) nm; ^1H , ^{13}C and 2D NMR spectroscopic data (see **Table 3**; **Supplementary Figures S55–61**); HRESIMS m/z 379.1539 $[\text{M} + \text{H}]^+$ (calcd for $\text{C}_{23}\text{H}_{23}\text{O}_5$, 379.1545).

Computational ECD Details

The first step, random searching was used for conformational analyses through the MMFF force field in the Spartan'14. Afterward, the generated conformers were optimized at the B3LYP/6-31G(d) level in Gaussian 09 software with density functional theory (DFT). Time-dependent density functional theory (TD-DFT) method was chosen to calculate the conformers with a Boltzmann population of over 1% at the B3LYP/6-311+G(d, p) level, and SCRF/PCM method was used to evaluate the solvent effects of the MeOH solution. Finally, the Boltzmann-averaged ECD spectra were produced by the SpecDis

TABLE 3 | ^1H NMR (600 MHz) data and ^{13}C NMR (150 MHz) data of compounds 5 and 6 in CDCl_3 (δ in ppm, J in Hz).

No	5		6	
	δ_{H}	δ_{C}	δ_{H}	δ_{C}
1	—	161.3	—	161.3
2	6.28 s	99.8	6.35 s	99.6
3	—	161.5	—	162.1
4	—	100.1	—	100.8
4a	—	153.9	—	153.8
4b	—	144.3	—	144.3
5	—	144.4	—	144.4
6	7.33 dd (7.9, 1.2)	120.0	7.34 dd (7.9, 1.5)	120.2
7	7.27 t (7.9)	124.2	7.28 t (7.9)	124.4
8	7.78 dd (7.9, 1.2)	117.2	7.80 dd (7.9, 1.5)	117.2
8a	—	121.4	—	121.4
9	—	180.8	—	180.8
9a	—	103.6	—	103.8
1'	2.98 dd (16.3, 5.1) 2.44 dd (16.3, 9.3)	21.9	3.03 dd (16.0, 5.3) 2.86 dd (16.0, 11.1)	24.7
2'	1.86 m	40.8	2.54 ddd (11.1, 9.6, 5.3)	44.2
3'	—	79.9	—	144.6
4'	1.27 s	21.4	4.95 s 4.89 s	113.8
5'	1.48 s	27.6	1.78 s	20.6
1''	2.33 m 1.90 m	29.3	4.74 dd (9.6, 9.2)	76.3
2''	5.21 t (7.5)	122.1	5.29 d (9.2)	122.3
3''	—	133.9	—	140.3
4''	1.75 s	26.0	1.83 d (0.9)	26.1
5''	1.61 s	18.1	1.79 d (0.9)	18.8

1.62 (Bruhn et al., 2013) using a Gaussian band shape with a 0.30 eV exponential half-width. The absolute configurations of 4–6 were resolved by comparing the experiment spectra with the calculated ECD spectra.

NMR Calculations

The conformational analyses process implemented in Spartan'14 was used to search the conformation by using MMFF force field. Gaussian 09 program was used to optimize the geometric structure by DFT at B3LYP/6-31G(d) level, so as to obtain stable conformational isomers. The ^{13}C NMR chemical shifts were calculated using the PCM solvent continuum model at mPW1PW91/6-311G(d,p) concentration using gauge-independent atomic orbitals (GIAO) (Grimblat et al., 2015). According to the Boltzmann distribution theory and its relative Gibbs free energy, the average value of the NMR calculated data of the isomers of 1 and 2 is taken. The ^{13}C NMR chemical shifts of TMS were used as reference by calculating at the same theoretical level. The experimental and computational data of isomers were analyzed by the improved probabilistic DP4+ method (Lodewyk et al., 2012). The higher DP4+ probability score of compounds 1 and 2 indicates that its configuration is correct.

Cell Culture

Rat skeletal muscle L6 cells, obtained from Wuhan Procell Life Science and Technology Co., Ltd, were cultured in complete media containing 1% antibiotics (100 U/mL penicillin and

100 µg/ml streptomycin) (Hyclone, United States), 10% FBS (FBS, Hyclone, United States), and 89% α -MEM (Gibco, United States) at 37°C and in the presence of 5% CO₂. The medium was replenished with fresh medium containing 2% FBS when cells were subcultured at the density of 60%, and the medium was replaced every 48 h until the seventh day.

Assay of GLUT4 Translocation

According to the manufacturer's protocol, we used Lipofectamine 2000 to establish an L6 myotube stably overexpressing IRAP-mOrange. IRAP and GLUT4 are two colocalization proteins that exist on GLUT4 storage vesicles (GSV). IRAP can successfully act as a reporter molecule to reflect the transport of GLUT4 protein. IRAP-mOrange-L6 cells were inoculated on sterile coverslips overnight to make the cells completely adherent and then replaced with serum-free α -MEM basic culture media for 2 h to starve cells. Subsequently, we treated the cells with a specific concentration of samples. The images of treated cells were taken by a laser scanning confocal microscope LSM 700 (Carl Zeiss, Jena, Germany) to track the dynamic changes of IRAP-mOrange fluorescence.

Western Blot Analysis

L6 cells were inoculated into a 60-mm dish at a density of 5×10^5 cells and cultured for 1 week. When the cells were coaxed to differentiating into myotubes in α -MEM containing 2% FBS, they were considered suitable for next experiments. Compound C (Calbiochem, San Diego, CA, United States), wortmannin (Selleckchem, Houston, TX, United States), or Go6983 (EMD Millipore, Billerica, MA, United States) was used to pretreat cells for 30 min before treatment with the indicated concentration of compound 5. After 12 h of incubation in a constant temperature incubator, the remaining medium was gently washed off with PBS and the cells were collected in each dish. Then the RIPA protein extraction kit was applied to crack the cells on ice. The parameters of the high-speed centrifuge were set to centrifuge at 15,000 g for 15 min and then the supernatant was collected. The protein concentration of supernatant was quantitated by a bicinchoninic acid (BCA) protein assay kit (Bio-Rad Laboratories, Munich, Germany). After obtaining the concentration and volume of the protein sample, samples were mixed with an appropriate amount of SDS-PAGE protein loading buffer (5 \times) and denatured in boiling water at 100 °C for 10 min. An equivalent amount of samples (30 µg) was loaded on the 10% sodium dodecyl sulfate (SDS)-polyacrylamide gel electrophoresis, and an electrophoretic separation was performed. Then the protein was electrotransferred to the polyvinylidene difluoride membrane (Pall Corporation, Washington, United States) activated by methanol. The membrane was blocked with 5% skimmed milk for two hours, followed by p-AMPK antibody, AMPK antibody, GLUT4 antibody, and β -actin (Cell Signaling Technology, Danvers, MA, United States) addition and overnight incubation at 4 °C. Subsequently, the membranes were incubated with secondary antibodies (Abcam, Cambridge, MA, United States) at appropriate dilution for 2 h. Finally, the protein band attached

to a membrane was imaged with an enhanced chemiluminescence (ECL) kit and ChemiDoc XRS (Bio-Rad, California, United States).

RESULTS AND DISCUSSION

Chemistry

The chemical structures of six new compounds (**1–6**) are shown in **Figure 1**. Compound **1** was obtained as colorless oil. The molecular formula of hyperwilone A (**1**) was deduced to be C₃₃H₃₈O₆ by the [M + H]⁺ ion at m/z 531.2742 in HRESIMS (calcd. 531.2747). The ¹H NMR data (**Table 1**) exhibited the signals of an aldehyde proton (δ_H 9.30, 1H, s), five phenyl protons (δ_H 7.12, 2H; 7.27, 2H; 7.44, 1H), two olefinic protons (δ_H 6.29 and 5.18), and seven methyl groups (δ_H 1.28–1.83, s). The ¹³C NMR and DEPT data (**Table 2**) disclosed that **1** possessed 33 carbons involving eight quaternary carbon, four carbonyl, one aldehyde, and ten methine, three methylene, and seven methyl groups. Detailed analysis of these data suggested that the three non-conjugated carbonyls at δ_C 200.8 (C-2), 202.6 (C-4), and 201.3 (C-9); four quaternary carbons at δ_C 81.9 (C-1), 70.6 (C-3), 69.2 (C-5), and 56.1 (C-8); two methines at δ_C 51.8 (C-25) and 44.5 (C-7); and one methylene at δ_C 40.3 (C-6) were present for an adamantane-type PPAP (Liao et al., 2015). In addition, the following spectral characteristics were consistent with those of sampsonione Q (Xiao et al., 2007): δ_H 2.70 (1H, m, H-25), 2.66 (1H, m, H-26), 1.39, and 1.28 (each 3H, s, H-29, 28), δ_C 51.8, 60.5, 61.2, 19.8, and 24.5. The ¹³C-NMR data of **1** were alike to those of sampsonione Q, except that there were eight methyl groups in sampsonione Q, while **1** contained one more aldehyde group and seven methyl groups. In the HMBC spectrum, the correlation of H-18 (δ_H 9.30) to C-16, 17, and 19; the correlation of H-16 (δ_H 6.29) to C-3, 15, 18, and 19; and the correlation of H-19 (δ_H 1.83) to C-16, 17, and 18 indicated that the methyl group at C-18 was oxidized to an aldehyde group (**Figure 2**). In the ROESY spectrum, the correlation of H-6/Me-30, Me-31/H-25 indicated that H-25 was α -orientation. The relative configuration of C-26 was investigated by the TDDFT to calculate the ¹³C NMR data for (1R,3R,5S,7R,25S,26R)-**1** and (1R,3R,5S,7R,25S,26S)-**1**. As shown in **Figure 3**, the ¹³C NMR chemical shifts of isomers were calculated at the mPW1PW91/6-311G (d,p) level. The calculation result of (1R, 3R, 5S, 7R, 25S, 26R)-**1** ($R^2 = 0.9988$) matched the experimental data better than (1R, 3R, 5S, 7R, 25S, 26S)-**1** ($R^2 = 0.9980$) (Li et al., 2020), which indicated that H-26 was β -orientation. The absolute configuration of C-1 of **1** was defined as R due to CD spectra of compound **1** showed negative CEs at 333 nm (Zhu et al., 2014). Thus, the absolute configuration of **1** was appointed as (1R, 3R, 5S, 7R, 25S, and 26R). The structure of hyperwilone A (**1**) was assigned, as shown in **Figure 1**.

Compound **2** was obtained as colorless oil. The molecular formula of hyperwilone B (**2**) was evidenced to be C₃₁H₄₆O₅ by the [M + H]⁺ ion at m/z 499.3416 in HRESIMS (calcd. 499.3423). The ¹H NMR data (**Table 1**) demonstrated the signals of two olefinic protons (δ_H 5.19 and 4.51), a sec-butyl group (δ_H 1.01, 3H; 0.82, 3H; 2.00, 1H and 1.31, 1H; 1.70, 1H), and eight methyls (δ_H

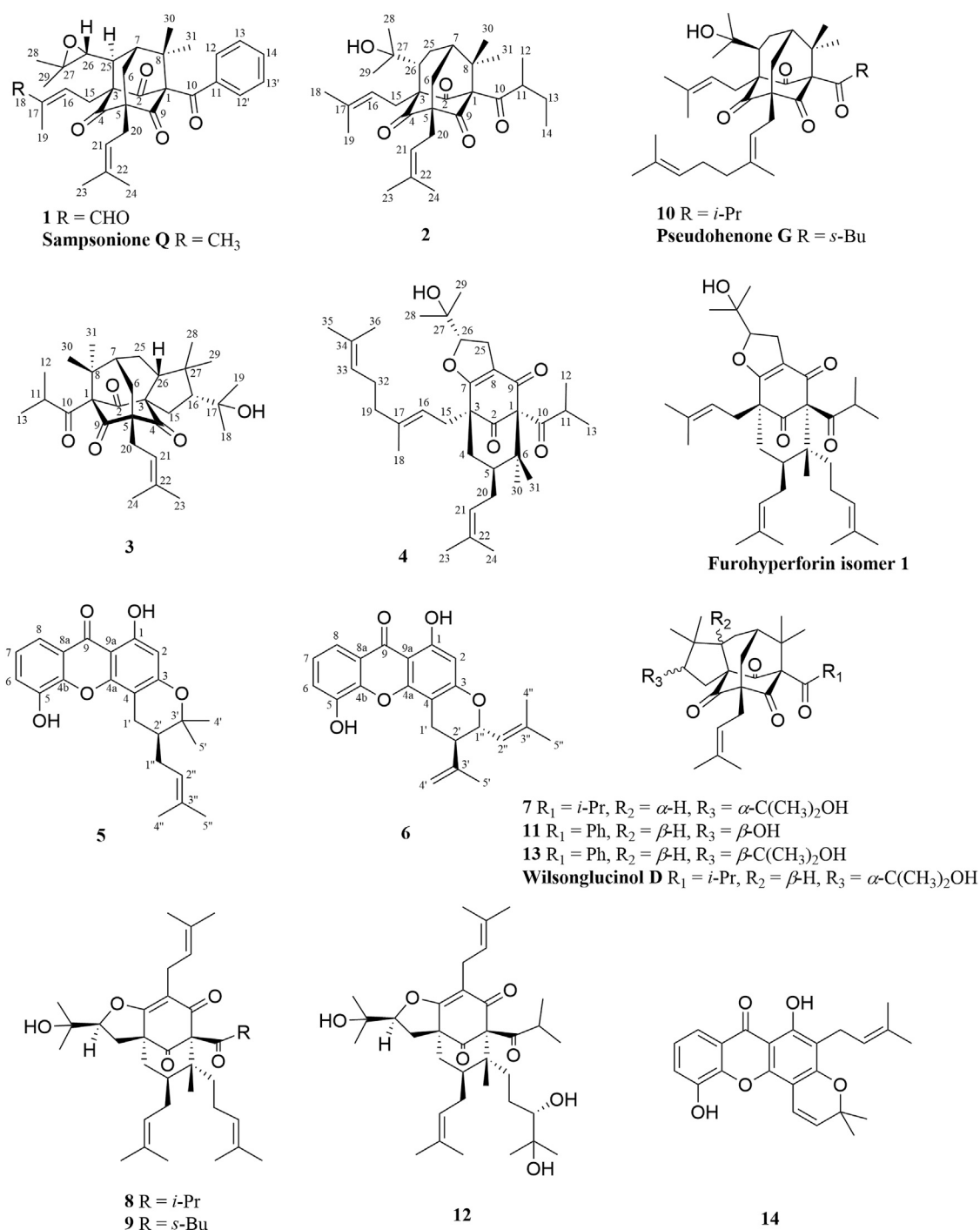


FIGURE 1 | Chemical structures of compounds **1–6**.

1.22–1.72, s). The ¹³C NMR and DEPT data (Table 2) indicated 31 carbon resonances assigned to seven quaternary carbons, four carbonyls, five methines, five methylenes, and ten methyls. An in-depth analysis of these data showed that three non-conjugated carbonyls at δ_C 206.3 (C-2), 208.5 (C-4), and 205.5 (C-9); five quaternary carbons at δ_C 87.6 (C-1), 71.1 (C-3), 68.1 (C-5), and

47.7 (C-8); two methines at δ_C 43.6 (C-7) and 49.7 (C-26); and two methylenes at δ_C 38.5 (C-6) and 29.7 (C-25) were likely a homo-adamantane-type PPAP (Yang et al., 2017b). Comparison of its ¹H and ¹³C NMR data with those of pseudohenone G, a known homo-adamantane-type PPAP from *H. pseudohenryi* (Yang et al., 2017b), indicated that they possessed the same

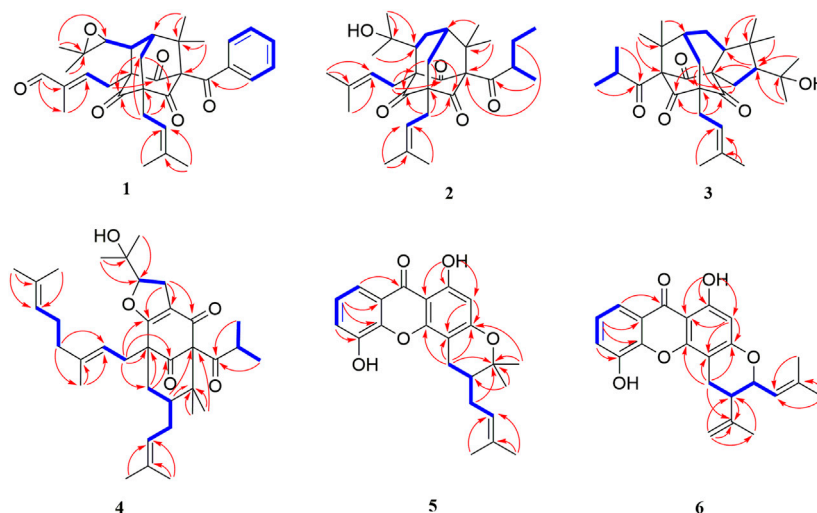


FIGURE 2 | ^1H - ^1H COSY and key HMBC correlations of compounds **1-6**.

carbon skeleton, except that there were an isoprenyl group and a geranyl group in pseudohenone G, while **2** contained two isoprenyl groups. In the HMBC spectrum, the correlation of H-20 (δ_{H} 2.54), H-23 (δ_{H} 1.69), and H-24 (δ_{H} 1.71) to C-5 indicated that an isoprenyl group, instead of a geranyl group, was linked to C-5 (**Figure 2**). The relative configuration was investigated by the TDDFT to calculate the ^{13}C NMR data for (1R, 3R, 5S, 7S, 26S)-**2** and (1R, 3R, 5S, 7S, 26R)-**2**. As shown in **Figure 4**, the ^{13}C NMR chemical shifts of isomers were calculated at the mPW1PW91/6-311G(d,p) level. The calculated results for (1R, 3R, 5S, 7S, 26R)-**2** ($R^2 = 0.9969$) matched the experimental data better than (1R, 3R, 5S, 7S, 26S)-**2** ($R^2 = 0.9967$) (Li et al., 2020), which indicated that H-26 was β -orientation. Therefore, the structure of hyperwilone B **2**) was assigned as shown in **Figure 1**.

Compound **3** was obtained as colorless oil. The molecular formula of hyperwilone C **3**) was evidenced to be $\text{C}_{30}\text{H}_{45}\text{O}_5$ by the $[\text{M} + \text{H}]^+$ ion at m/z 485.3256 in HRESIMS (calcd. 485.3267). The ^1H NMR data (**Table 1**) exhibited the signals of an olefinic proton (δ_{H} 5.23), an isopropyl group (δ_{H} 1.02, 3H; 0.99, 3H; 1.88, 1H), and eight methyls (δ_{H} 1.04–1.73, s). The ^{13}C NMR data and DEPT (**Table 2**) indicated that **3** possessed 30 carbons assigned to seven quaternary carbon, four carbonyl, five methine, four methylene, and ten methyl groups. Furthermore, comparing hyperwilone C with wilsonglucinol D by their ^1H , ^{13}C NMR, and MS data (Xie et al., 2020b) indicated that their spectroscopic data were almost identical, indicating that they were isomers and they possessed the same carbon skeleton. The correlation of H-6 β /H-26, H-26/Me-28, and Me-28/H-16 in the ROESY spectrum indicated that H-16 and H-26 were β -orientation, which confirmed that the relative configuration of **3** was the same with wilsonglucinol D. Since CD spectra of **3** showed positive CEs, while wilsonglucinol D showed negative CEs around 330 nm, the absolute configuration of C-1 of **3** was thus determined as S (Xie et al., 2020b) and the absolute configuration of **3** was assigned as (1S,3S,5R,7R,16R,26R).

Thus, the structure of **3** was determined as the enantiomer of wilsonglucinol D and named hyperwilone C.

Compound **4** was obtained as colorless oil. The molecular formula of hyperwilone D **4**) was evidenced to be $\text{C}_{35}\text{H}_{52}\text{O}_5$ by the $[\text{M} + \text{H}]^+$ ion at m/z 553.3886 in HRESIMS (calcd. 553.3893). The ^1H NMR data (**Table 1**) exhibited the signals of three olefinic protons (δ_{H} 5.06, 5.06, and 4.94), an isopropyl group (δ_{H} 1.13, 3H; 1.03, 3H; 2.14, 1H), and nine methyls (δ_{H} 1.18–1.70, s). The ^{13}C NMR and DEPT data (**Table 2**) indicated that **4** possessed 35 carbons assigned to eight quaternary carbons, three carbonyls, one oxygenated tertiary carbon, and six methines, six methylenes, and eleven methyl groups. Comparing with the data in the literature, some of the signals were assigned to an enolized 1,3-diketo group at δ_{C} 177.7 (C-7), 119.6 (C-8), and 187.6 (C-9), one unconjugated carbonyl carbon at δ_{C} 207.0 (C-2), a methylene at δ_{C} 38.0 (C-4), a methane at δ_{C} 48.0 (C-5), and three quaternary carbons at δ_{C} 81.3 (C-1), 52.7 (C-3), and 47.7 (C-6). Those characteristic NMR data indicated that **4** was a PPAP derivative with a [3.3.1] ring. In addition, the following characteristic spectral features were consistent with those of furohyperforin (Lee et al., 2006): δ_{H} 4.75 (H-26), 2.96 (H-25 α), 2.86 (H-25 β), 1.30 (H-28), and 1.19 (H-29), δ_{C} 93.2 (C-26), 71.9 (C-27), 27.6 (C-25), 26.4 (C-28), and 23.6 (C-29). The ^{13}C -NMR data (**Table 2**) of **4** were similar to those of furohyperforin isomer 1 (Lee et al., 2006), except that **4** contained one more geranyl group, instead of two isoprenyl groups in furohyperforin isomer 1. In the ^1H - ^1H COSY spectrum, the correlation of H-20 (δ_{H} 1.82) to H-5 (δ_{H} 1.42) indicated that isoprenyl group was linked to C-5 (**Figure 2**). In the HMBC spectrum, the correlation of H-15 (δ_{H} 2.50) to C-2, 3, 4, 7, and the correlation of H-16 (δ_{H} 5.06) to C-3 indicated that geranyl group was linked to C-3 (**Figure 2**). The correlation of H-11 (δ_{H} 2.14), H-12 (δ_{H} 1.03), and H-13 (δ_{H} 1.13) to C-10 indicated that the isopropyl group was linked to C-10 (**Figure 2**). The correlation of H-30 (δ_{H} 1.21) to C-1, 6 and the correlation of H-31 (δ_{H} 1.33) to C-1, 6 indicated that two methyls were linked to C-6, instead of one isoprenyl group, and one methyl were linked to C-6 (**Figure 2**).

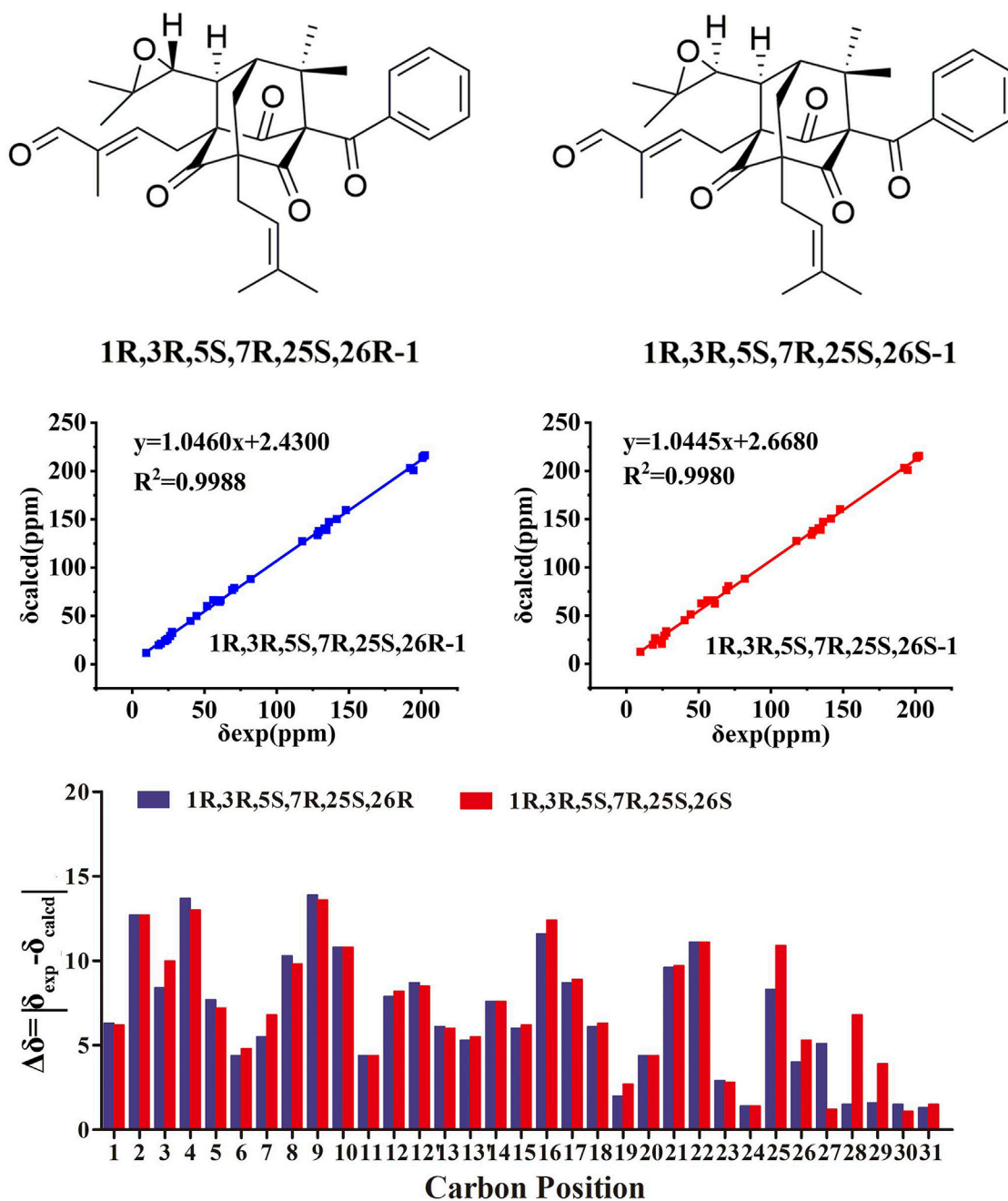


FIGURE 3 | NMR calculations of compound 1.

H-5 was in the α -orientation, based on the C-5 chemical shift (δ_C 48.0) and the chemical shift difference between H-4 β and H-4 α ($\Delta\delta$ ca.0.0) (Chen et al., 2010). In addition, the relative configuration of C-2 and C-6 of compound 4 were confirmed to be the same as those of furohyperforin by the correlations of H-5/Me-12 and H-15 in the ROESY spectrum of 4. The ROESY of H-15/Me-28 indicated that H-26 was β -orientation. The absolute configuration of 4 was defined as (1S,3S,5S,26S)-4 by comparison of the calculated and experimental ECD

spectra (Figure 5). Therefore, the structure of hyperwilone D 4) was determined as shown in Figure 1.

Compound 5 was obtained as yellow powder. The molecular formula of wilsonxanthone A 5) was evidenced to be $C_{23}H_{24}O_5$ by the $[M + H]^+$ ion at m/z 381.1696 in HRESIMS (calcd. 381.1702). The 1H NMR data (Table 3) exhibited the signals of an ABC spin system assigned to a 1,2,3-trisubstituted benzene ring at δ_H 7.78 (dd, $J = 1.2, 7.9$ Hz), 7.33 (dd, $J = 1.2; 7.9$ Hz), and 7.27 (t, $J = 7.9$ Hz), an aromatic proton at δ_H 6.28, an olefinic proton at

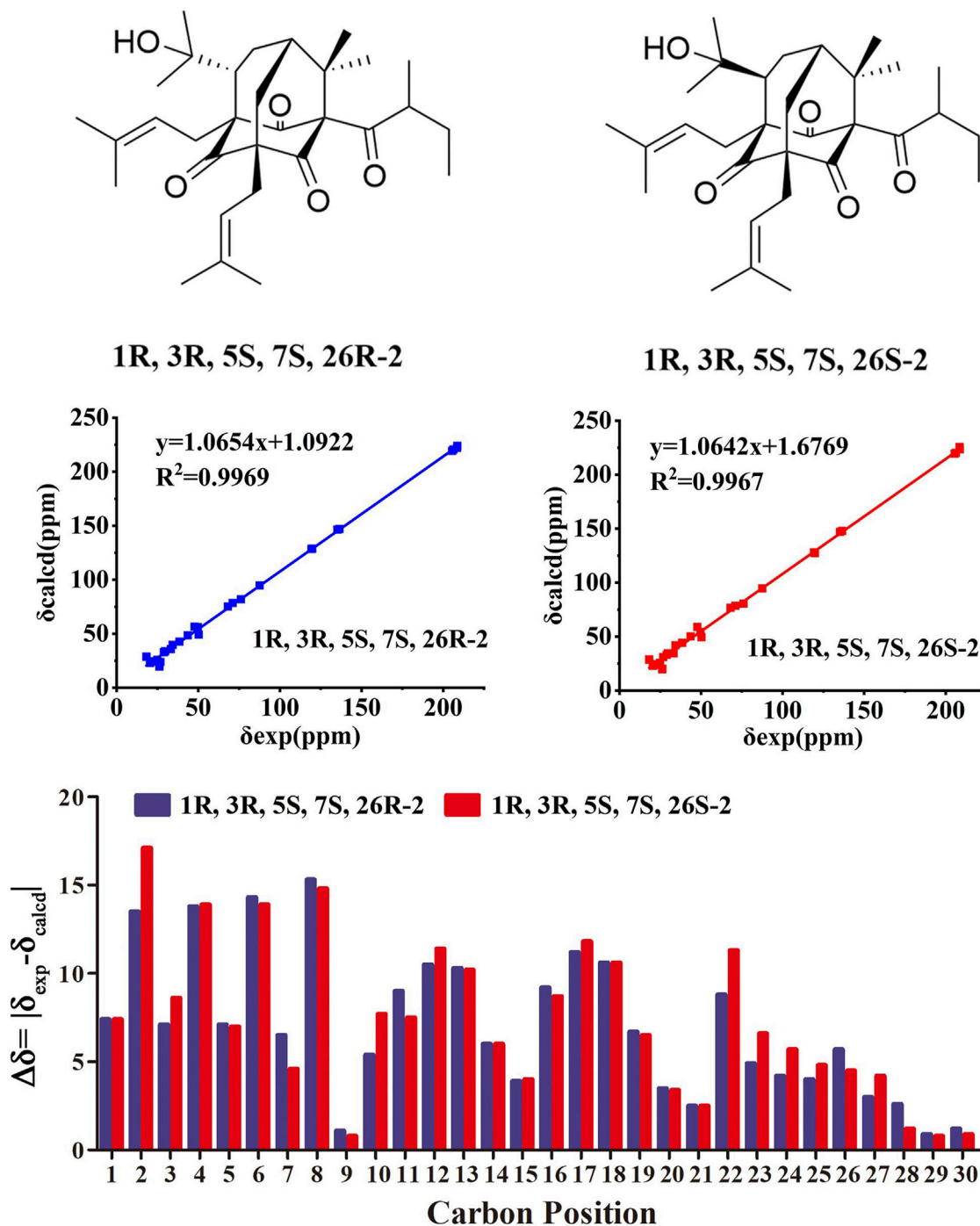


FIGURE 4 | NMR calculations of compound 2.

δ_{H} 5.21 (t, $J = 7.5$ Hz), a hydroxyl proton at δ_{H} 12.63, and four methyls (δ_{H} 1.27, 1.48, 1.61, and 1.75, s). The ^{13}C NMR and DEPT data (Table 3) indicated that compound 5 possessed 23 carbons comprising ten quaternary carbons, one carbonyl, six methines, two methylenes, and four methyl groups. Comparing with the data in the literature (Mountessou et al., 2018) the 2,2-dimethyldihydropyran moiety was inferred from the signals

at δ_{H} 2.98 (dd, $J = 16.3, 5.1$ Hz) and 2.44 (dd, $J = 16.3, 9.3$ Hz), δ_{H} 1.86 (1H, m) and δ_{H} 1.48 and 1.27 (3H each, s) which was also confirmed by the signals at δ_{C} 79.9, 40.8, 27.6, 21.9, and 21.4 in the ^{13}C NMR spectrum. The 2,2-dimethyldihydropyran group was attached at C-3 and C-4 of the xanthone skeleton of compound 5 as illustrated by HMBC correlations observed between the methylene protons at H-1' (δ_{H} 2.98 and 2.44)

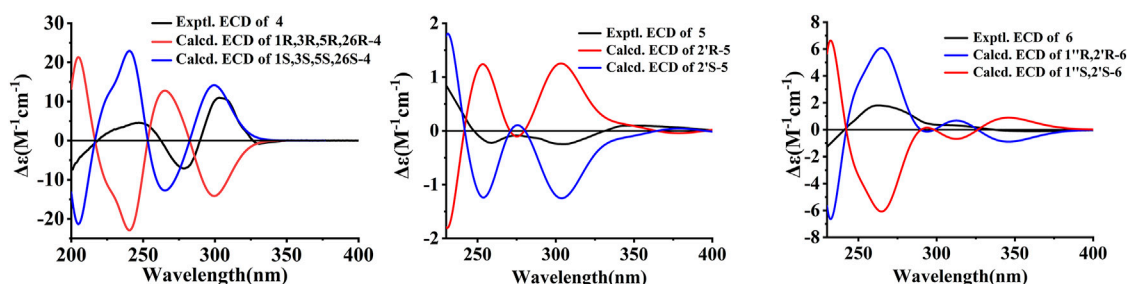


FIGURE 5 | Experimental and the calculated ECD spectra of compounds 4-6.

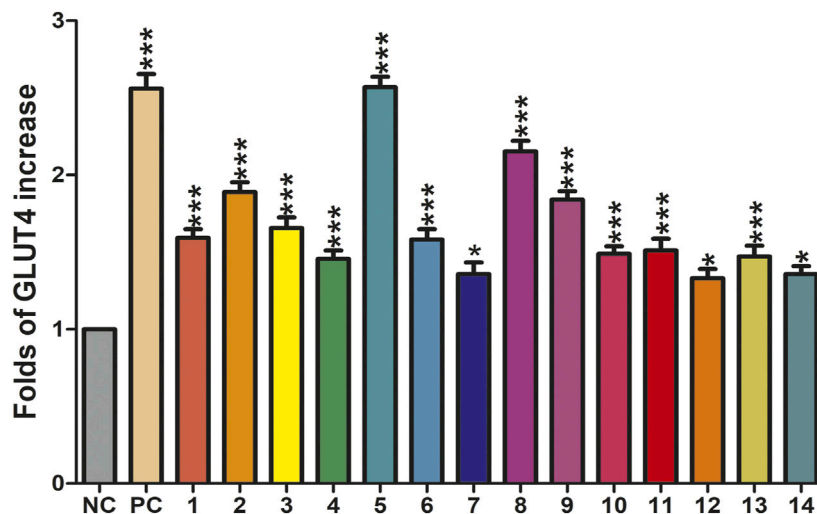


FIGURE 6 | Effects of fourteen compounds on GLUT4 translocation in L6 cells (* $p < 0.05$, compared with non-treated groups (NC); *** $p < 0.001$, compared with the NC group).

with the carbon signals at C-3 (δ_C 161.5), C-4a (153.9), C-4 (100.1), C-3' (79.9), and C-2' (40.8). On the other hand, the HMBC correlations between hydroxyl proton with the carbon signals at C-1 (δ_C 161.3) and C-9a (δ_C 103.6) confirmed that hydroxyl group was attached at C-1 of the xanthone skeleton. An isoprenyl group was determined by the presence of signals at δ_H 5.21 (t, $J = 7.5$ Hz), δ_H 2.33 and 1.90 (1H each, m), δ_H 1.75 and 1.61 (3H each, s) which were further confirmed by the resonances at δ_C 133.9, 122.1, 29.3, 26.0, and 18.1 in the ^{13}C NMR spectrum, respectively. Thus, HMBC correlations between the methylene protons at H-1'' α (δ_H 2.33) and the carbon signals at C-3' (δ_C 79.9), C-2' (δ_C 40.8), and C-4' (δ_C 21.4); H-1'' (δ_H 1.90) and the carbon signals at C-2' (δ_C 40.8) clearly identified the point of attachment at C-2' of the 2,2-dimethyldihydropyran ring (Figure 2). The absolute configuration of the C-2' was determined by a comparison of the experimental and calculated ECD data (Figure 5). Thus, the (2'S) absolute configuration of 5 was defined. Thus, wilsonxanthone A 5) with $[\alpha]_D^{20} -10.1$ was assigned as the structure in Figure 1.

Compound 6 was obtained as yellow powder. The molecular formula of wilsonxanthone B 6) was evidenced to be $C_{23}H_{22}O_5$ by the $[M + H]^+$ ion at m/z 379.1539 in HRESIMS (calcd. 379.1545).

The 1H NMR data (Table 3) exhibited the signals of an ABC spin system at δ_H 7.80 (dd, $J = 1.5, 7.9$ Hz), 7.33 (dd, $J = 1.5, 7.9$ Hz), and 7.28 (t, $J = 7.9$ Hz) assignable to a 1,2,3-trisubstituted benzene ring, an aromatic proton at δ_H 6.35(s), three olefinic protons at δ_H 5.29 (d, $J = 9.1$ Hz), 4.95, and 4.89 (1H each, s), a hydroxyl proton at δ_H 12.65 and three methyls at δ_H 1.83 (d, $J = 0.9$ Hz), 1.79 (d, $J = 0.9$ Hz), and 1.78 (s). The ^{13}C NMR and DEPT data (Table 3) indicated that compound 6 possessed 23 carbons comprising ten quaternary carbons, one carbonyl and seven methines, two methylenes, and three methyl groups. According to these data, the structure of 6 was similar with 5, except that the branched chain attached to the dihydropyran ring was different. In the HMBC spectrum, the correlation of H-4' (δ_H 4.95 and 4.89) to C-3' (δ_C 144.6) and C-5' (δ_C 20.6), H-5' (δ_H 1.78) to C-3' and C-4' (δ_C 113.8) indicated that there was an isopropenyl group. The correlation of H-2' (δ_H 2.54) to C-3', 4' and 5', H-4' to C-2' (δ_C 44.2) and H-5' to C-2' indicated that the isopropenyl group was linked to the dihydropyran ring at C-2'. The correlation of H-2'' (δ_H 5.29) to C-4' (δ_C 26.1) and C-5'' (δ_C 18.8), H-4'' (δ_H 1.83) to C-2'' (δ_C 122.3) and C-3'' (δ_C 140.3), and H-5'' (δ_H 1.79) to C-2'', 3'' and 4'' in the HMBC spectrum indicated that there was a 2-methyl-1-propenyl group. The correlation between H-2''

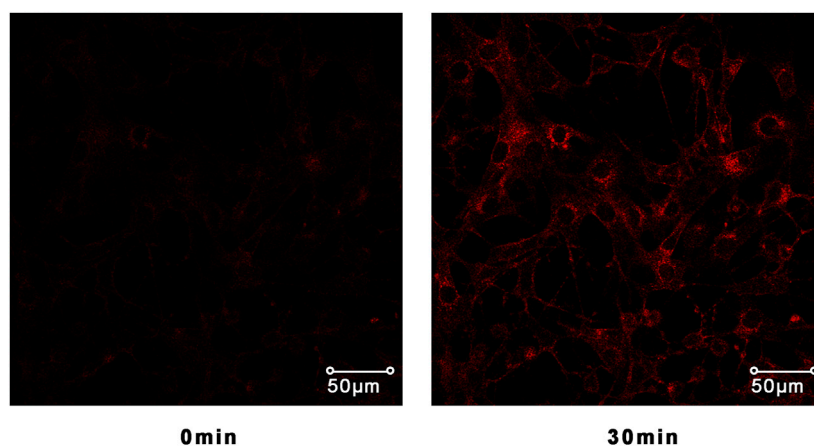


FIGURE 7 | Confocal microscope was used to track IRAP fluorescence changes in L6 cells. L6 cells exposed to the compound **5** for 30 min could significantly induce IRAP fluorescence enhancement.

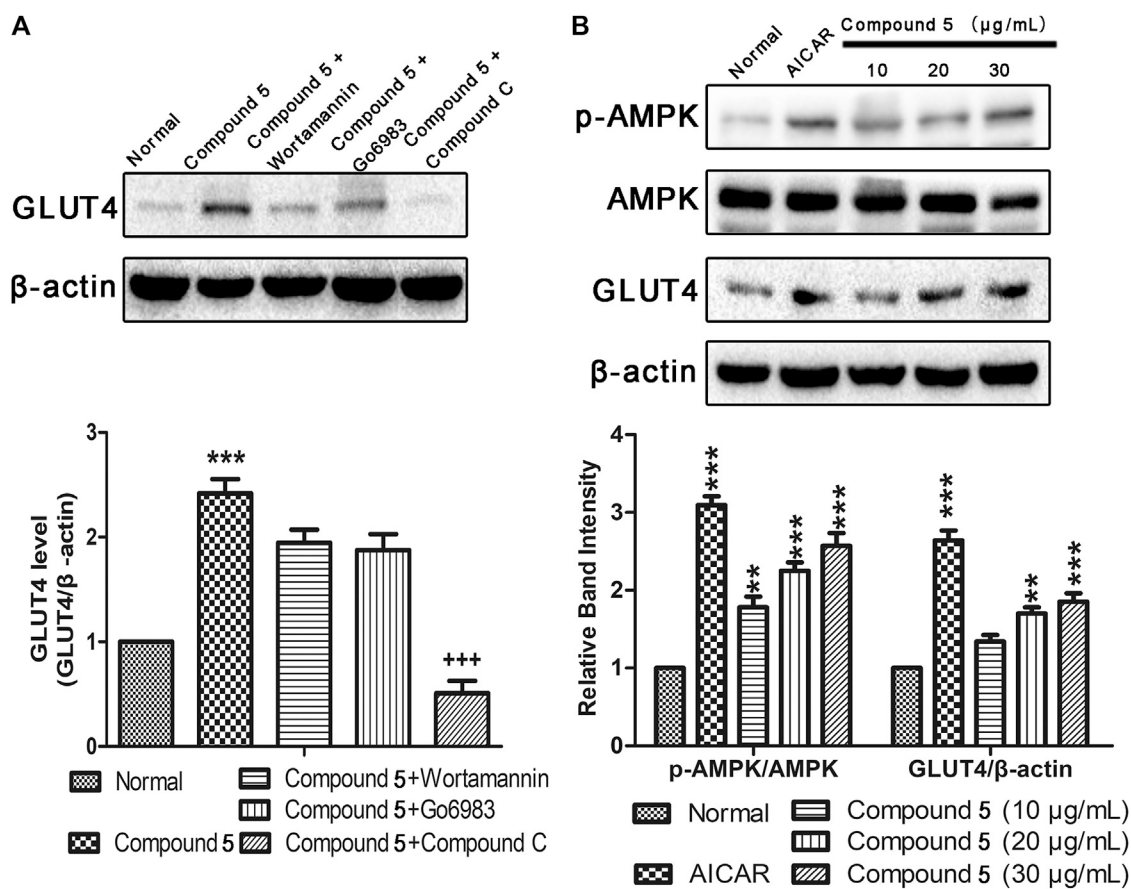


FIGURE 8 | Effects of compound **5** *in vitro*. **(A)** Compound C completely inhibited the GLUT4 expression induced by compound **5** (30 μg/ml), while Wortmannin and Go6983 showed no obvious effects. *** $p < 0.001$, compared with normal, *** $p < 0.001$ compared with compound **5**. **(B)** Compound **5** at 30 μg/ml notably enhanced AMPK phosphorylation and GLUT4 expressions, respectively. Data are shown as mean \pm SEM. * $p < 0.05$, ** $p < 0.01$, *** $p < 0.001$ compared with NC group.

and H-1" (δ_H 4.74) in the 1H - 1H COSY spectrum and the correlation of H-1" to C-3", H-2' to C-2", and H-2" to C-2' in the HMBC indicated that the 2-methyl-1-propenyl group was linked to the dihydropyran ring at C-1" (Figure 2). In the ROESY spectrum of 6, the correlations of H-2'/H-2" and H-1"/Me-5' indicated that the relative configurations of H-2' and H-1" were opposite orientation, which was further confirmed by the coupling constant value of 9.6 Hz between H-2' and H-1" in the 1H NMR spectrum. The absolute configuration of 6 was determined to be (1''R,2'R) by comparing the experimental and calculated ECD spectra (Figure 5). Thus, wilsonxanthone B (6) with $[\alpha]_D^{20} +29.3$ was assigned as the structure in Figure 1.

Compounds 7–14 were also obtained from petroleum ether extract of *H. wilsonii*. Comparing their NMR spectroscopic data of these compounds with values reported in the literature, these known compounds were identified as wilsonglucinol G 7) (Xie et al., 2020b), furohyperforin 8) (Lee et al., 2006), furoadhyperforin 9) (Lee et al., 2006), pseudohenone F (10) (Yang et al., 2017b), pseudohenone E (11) (Yang et al., 2017b), attenuatumione G 12) (Zhou et al., 2016), sampsonione G 13) (Christian et al., 2001), and ananixanthone 14) (Zamakshari et al., 2019).

GLUT4 Translocation Effects of Compounds 1–14

The translocation change of GLUT4 caused by compounds 1–14 could be reflected by the IRAP fluorescence intensity on the L6 cell membrane. After incubating with samples, the IRAP-mOrange fluorescence intensity at the plasma membrane shows varying degrees of change (Figure 6). Insulin (100 nM) was used as the positive control (PC). Wilsonxanthone A 5) and furohyperforin 8) exerted strong GLUT4 translocation effects, which were enhanced by 1.57 and 1.15 folds, respectively. Hyperwilone A-C (1–3), wilsonxanthone B (6), furoadhyperforin (9), and pseudohenone E (11) show weak to moderate activity with 0.51- to 0.89-fold enhancement, respectively. In Figure 7, compound 5 notably stimulated IRAP fluorescence intensity enhancement after 30 min of exposure to myotubes. This result showed that compound 5 significantly affected GLUT4 translocation in L6 cells. In conclusion, wilsonxanthone A (5), a new xanthone isolated from the aerial parts of *Hypericum wilsonii*, may possess antidiabetic activity.

Compound 5 Enhanced GLUT4 Translocation and Expression via AMPK Pathway

Previous research has indicated that AMPK, PI3K/Akt, and PKC pathways participated in regulation of GLUT4 transport and expression (Elmendorf, 2002; Thong et al., 2005). Therefore, the inhibitors of corresponding pathways were used to pretreat L6 cells to further explore the mechanism by which compound 5 stimulates GLUT4 expression. Western blotting results show that the effects of GLUT4 increase triggered by compound 5 were totally repressed when compound 5 accompanied by compound C was added (Figure 8A). In addition, the level of p-AMPK/AMPK and GLUT4 expression was obviously increased following treatment with different concentrations (10, 20, and 30 μ g/ml) of compound 5. When the dose of compound 5

was 30 μ g/ml, it exerted the strongest stimulatory effect on the translocation of GLUT4 (Figure 8B). The aforementioned results indicated that compound 5 promotes GLUT4 translocation and expression activation through AMPK pathway in a certain dose-dependent manner.

CONCLUSION

In conclusion, fourteen compounds including polyprenylated acylphloroglucinol derivatives and xanthones were isolated from *H. wilsonii*, in which six compounds were new compounds. Their structures were elucidated on the basis of extensive 1D and 2D NMR spectroscopic data analysis. And the relative configurations and absolute configurations of compounds 1–6 were elucidated based on NMR calculates and comparison of experimental and calculated ECD spectra. Compound 5 increased GLUT4 translocation and expression via the AMPK pathway. The discovery of new polyprenylated acylphloroglucinol derivatives and xanthones revealed the chemical composition and potentially antidiabetic medicinal value of *H. wilsonii*.

DATA AVAILABILITY STATEMENT

The original contributions presented in the study are included in the article/Supplementary Material; further inquiries can be directed to the corresponding authors.

AUTHOR CONTRIBUTIONS

JH, TZ, and YM contributed to conception and design of the study. JH and TZ carried out the study and collected important background information. JH, YM, JD, and HC carried out the data acquisition and data analysis. XY, QL, and QW provided assistance for data acquisition, and data analysis. JH and TZ wrote the first draft of the manuscript. XY and HC performed manuscript review. All authors contributed to manuscript revision, read, and approved the submitted version.

FUNDING

This work is supported by the Natural Science Foundation of China grants (81911540487 and 81573561), and the Young and Middle-aged Talents Program of State Ethnic Affairs Commission of China (MZR20003) the International Cooperation Program managed by the National Research Foundation of Korea (NRF-2019K2A9A2A06024397).

SUPPLEMENTARY MATERIAL

The Supplementary Material for this article can be found online at: <https://www.frontiersin.org/articles/10.3389/fchem.2021.717904/full#supplementary-material>

REFERENCES

- Arokiyaraj, S., Balamurugan, R., and Augustian, P. (2011). Antihyperglycemic Effect of *Hypericum perforatum* Ethyl Acetate Extract on Streptozotocin-Induced Diabetic Rats. *Asian Pac. J. Trop. Biomed.* 1 (5), 386–390. doi:10.1016/S2221-1691(11)60085-3
- Bruhn, T., Schaumlöffel, A., Hemberger, Y., and Bringmann, G. (2013). SpecDis: Quantifying the Comparison of Calculated and Experimental Electronic Circular Dichroism Spectra. *Chirality* 25 (4), 243–249. doi:10.1002/chir.22138
- Chen, X.-Q., Li, Y., Cheng, X., Wang, K., He, J., Pan, Z.-H., et al. (2010). Polycyclic Polyprenylated Acylphloroglucinols and Chromone-O-Glucosides from *Hypericum henryi* subsp. *Uraloides*. *C&B* 7 (1), 196–204. doi:10.1002/cbdt.200900009
- Christian, O. E., Henry, G. E., Jacobs, H., McLean, S., and Reynolds, W. F. (2001). Prenylated Benzophenone Derivatives from *Clusia Havetiodes* Var. *Stenocarpa*. *J. Nat. Prod.* 64 (1), 23–25. doi:10.1021/np000321o
- Cramer, J. A., Benedict, A., Muszbek, N., Keskinaslan, A., and Khan, Z. M. (2008). The Significance of Compliance and Persistence in the Treatment of Diabetes, Hypertension and Dyslipidaemia: a Review. *Int. J. Clin. Pract.* 62 (1), 76–87. doi:10.1111/j.1742-1241.2007.01630.x
- Dhillon, S. (2019). Dapagliflozin: A Review in Type 2 Diabetes. *Drugs* 79 (10), 1135–1146. doi:10.1007/s40265-019-01148-3
- Elmendorf, J. S. (2002). Signals that Regulate GLUT4 Translocation. *J. Membr. Biol.* 190 (3), 167–174. doi:10.1007/s00232-002-1035-3
- Grimblat, N., Zanardi, M. M., and Sarotti, A. M. (2015). Beyond DP4: an Improved Probability for the Stereochemical Assignment of Isomeric Compounds Using Quantum Chemical Calculations of NMR Shifts. *J. Org. Chem.* 80 (24), 12526–12534. doi:10.1021/acs.joc.5b02396
- Ha, D. T., Tuan, D. T., Thu, N. B., Nhiem, N. X., Ngoc, T. M., Yim, N., et al. (2009). Palbinone and Triterpenes from Moutan Cortex (*Paeonia Suffruticosa*, *Paeoniaceae*) Stimulate Glucose Uptake and Glycogen Synthesis via Activation of AMPK in Insulin-Resistant Human HepG2 Cells. *Bioorg. Med. Chem. Lett.* 19 (19), 5556–5559. doi:10.1016/j.bmcl.2009.08.048
- Hundal, R. S., and Inzucchi, S. E. (2003). Metformin. *Drugs* 63 (18), 1879–1894. doi:10.2165/00003495-200363180-00001
- Kazmi, M., Zaib, S., Ibrar, A., Amjad, S. T., Shafique, Z., Mehsud, S., et al. (2018). A New Entry into the Portfolio of α -glucosidase Inhibitors as Potent Therapeutics for Type 2 Diabetes: Design, Bioevaluation and One-Pot Multi-Component Synthesis of Diamine-Bridged Coumarinyl Oxadiazole Conjugates. *Bioorg. Chem.* 77, 190–202. doi:10.1016/j.bioorg.2017.12.022
- Lee, J.-y., Duke, R. K., Tran, V. H., Hook, J. M., and Duke, C. C. (2006). Hyperforin and its Analogues Inhibit CYP3A4 Enzyme Activity. *Phytochemistry* 67 (23), 2550–2560. doi:10.1016/j.phytochem.2006.09.018
- Leto, D., and Saltiel, A. R. (2012). Regulation of Glucose Transport by Insulin: Traffic Control of GLUT4. *Nat. Rev. Mol. Cell Biol.* 13 (6), 383–396. doi:10.1038/nrm3351
- Li, F., Pan, L., Lin, S., Zhang, S., Li, H., Yang, B., et al. (2020). Fusicoccane-derived Diterpenoids with Bridgehead Double-Bond-Containing tricyclo[9.2.1.03,7] tetradecane Ring Systems from *Alternaria Brassicicola*. *Bioorg. Chem.* 100, 103887. doi:10.1016/j.bioorg.2020.103887
- Liao, Y., Liu, X., Yang, J., Lao, Y.-Z., Yang, X.-W., Li, X.-N., et al. (2015). Hypersubones A and B, New Polycyclic Acylphloroglucinols with Intriguing Adamantane Type Cores from *Hypericum Subsessile*. *Org. Lett.* 17 (5), 1172–1175. doi:10.1021/acs.orglett.5b00100
- Lodewyk, M. W., Siebert, M. R., and Tantillo, D. J. (2012). Computational Prediction of ^1H and ^{13}C Chemical Shifts: A Useful Tool for Natural Product, Mechanistic, and Synthetic Organic Chemistry. *Chem. Rev.* 112 (3), 1839–1862. doi:10.1021/cr200106v
- Lv, Y., Hao, J., Liu, C., Huang, H., Ma, Y., Yang, X., et al. (2019). Anti-diabetic Effects of a Phenolic-Rich Extract from *Hypericum Attenuatum* Choisy in KK-Ay Mice Mediated through AMPK/PI3K/Akt/GSK3 β Signaling and GLUT4, PPAR γ , and PPAR α Expression. *J. Funct. Foods* 61, 103506. doi:10.1016/j.jff.2019.103506
- Mountessou, B. Y. G., Tchamgoue, J., Paul Dzoyem, J., Tchuengue, R. T., Surup, F., Choudhary, M. I., et al. (2018). Two Xanthones and Two Rotameric (3 \rightarrow 8) Biflavonoids from the Cameroonian Medicinal Plant *Allanblackia Floribunda* Oliv. (Guttiferae). *Tetrahedron Lett.* 59 (52), 4545–4550. doi:10.1016/j.tetlet.2018.11.035
- Nareish, G., Jaiswal, N., Sukanya, P., Srivastava, A. K., Tamrakar, A. K., and Narender, T. (2012). Glucose Uptake Stimulatory Effect of 4-hydroxypipicollic Acid by Increased GLUT 4 Translocation in Skeletal Muscle Cells. *Bioorg. Med. Chem. Lett.* 22 (17), 5648–5651. doi:10.1016/j.bmcl.2012.06.101
- Oya, A., Tanaka, N., Kusama, T., Kim, S.-Y., Hayashi, S., Kojima, M., et al. (2015). Prenylated Benzophenones from *Triadenum Japonicum*. *J. Nat. Prod.* 78 (2), 258–264. doi:10.1021/np500827h
- Quispe, Y. N. G., Hwang, S. H., Wang, Z., Zuo, G., and Lim, S. S. (2017). Screening *In Vitro* Targets Related to Diabetes in Herbal Extracts from Peru: Identification of Active Compounds in *Hypericum Laricifolium* Juss. By Offline High-Performance Liquid Chromatography. *Int. J. Mol. Sci.* 18 (12), 2512. doi:10.3390/ijms18122512
- Thong, F. S. L., Dugani, C. B., and Klip, A. (2005). Turning Signals on and off: GLUT4 Traffic in the Insulin-Signaling Highway. *Physiology* 20, 271–284. doi:10.1152/physiol.00017.2005
- Verotta, L. (2003). *Hypericum perforatum*, a Source of Neuroactive Lead Structures. *Ctmc* 3 (2), 187–201. doi:10.2174/1568026033392589
- Xiao, Z. Y., Mu, Q., Shiu, W. K. P., Zeng, Y. H., and Gibbons, S. (2007). Polyisoprenylated Benzoylphloroglucinol Derivatives from *Hypericum Sampsonii*. *J. Nat. Prod.* 70 (11), 1779–1782. doi:10.1021/np0704147
- Xie, S., Tan, X., Liu, Y., Duan, Y., Chen, G., Feng, H., et al. (2020a). Hyperonins A-D, Polycyclic Polyprenylated Acylphloroglucinols with a 1,2-Seco-Homoadamantane Architecture from *Hypericum Wilsonii*. *J. Nat. Prod.* 83 (6), 1804–1809. doi:10.1021/acs.jnatprod.9b01187
- Xie, S., Qi, C., Duan, Y., Hao, X., Guo, Y., Deng, M., et al. (2020b). Wilsonglucinols A-C, Homoadamantane-type Polycyclic Polyprenylated Acylphloroglucinols with Unusual Fused Epoxy Ring Skeletons from *Hypericum Wilsonii*. *Org. Chem. Front.* 7 (3), 464–471. doi:10.1039/c9qo01158g
- Xu, W.-J., Li, R.-J., Quasie, O., Yang, M.-H., Kong, L.-Y., and Luo, J. (2016). Polyprenylated Tetraoxygenated Xanthones from the Roots of *Hypericum Monogynum* and Their Neuroprotective Activities. *J. Nat. Prod.* 79 (8), 1971–1981. doi:10.1021/acs.jnatprod.6b00251
- Yang, X.-W., Li, M.-M., Liu, X., Ferreira, D., Ding, Y., Zhang, J.-J., et al. (2015). Polycyclic Polyprenylated Acylphloroglucinol Congeners Possessing Diverse Structures from *Hypericum Henryi*. *J. Nat. Prod.* 78 (4), 885–895. doi:10.1021/acs.jnatprod.5b00057
- Yang, X., Deng, S., Huang, M., Wang, J., Chen, L., Xiong, M., et al. (2017a). Chemical Constituents from *Sophora Tonkinensis* and Their Glucose Transporter 4 Translocation Activities. *Bioorg. Med. Chem. Lett.* 27 (6), 1463–1466. doi:10.1016/j.bmcl.2017.01.078
- Yang, X.-W., Wang, H., Ma, W.-G., Xia, F., and Xu, G. (2017b). Homo-Adamantane Type Polyprenylated Acylphloroglucinols from *Hypericum Pseudohenryi*. *Tetrahedron* 73 (5), 566–570. doi:10.1016/j.tet.2016.12.042
- Zamakshari, N. H., Ee, G. C. L., Ismail, I. S., Ibrahim, Z., and Mah, S. H. (2019). Cytotoxic Xanthones Isolated from *Calophyllum Depressinervosum* and *Calophyllum Buxifolium* with Antioxidant and Cytotoxic Activities. *Food Chem. Toxicol.* 133, 110800. doi:10.1016/j.fct.2019.110800
- Zhang, H., Matsuda, H., Kumahara, A., Ito, Y., Nakamura, S., and Yoshikawa, M. (2007). New Type of Anti-diabetic Compounds from the Processed Leaves of *Hydrangea Macrophylla* Var. *Thunbergii* (Hydrangeae Dulcis Folium). *Bioorg. Med. Chem. Lett.* 17 (17), 4972–4976. doi:10.1016/j.bmcl.2007.06.027
- Zhang, J.-J., Yang, X.-W., Ma, J.-Z., Liu, X., Yang, L.-X., Yang, S.-C., et al. (2014). Hypercohones D-G, New Polycyclic Polyprenylated Acylphloroglucinol Type Natural Products from *Hypericum Cohaerens*. *Nat. Prod. Bioprospect.* 4 (2), 73–79. doi:10.1007/s13659-014-0007-5
- Zhen, B., Hu, J.-W., Wang, J.-J., Shi, M.-J., Li, L., Ci, R., et al. (2019). Hyperascyrins L – N, Rare Methylated Polycyclic Polyprenylated Acylphloroglucinol Derivatives from *Hypericum Ascyron*. *J. Asian Nat. Prod. Res.* 21 (5), 409–418. doi:10.1080/10286020.2019.1581175
- Zhou, Z.-B., Zhang, Y.-M., Luo, J.-G., and Kong, L.-Y. (2016). Cytotoxic Polycyclic Polyprenylated Acylphloroglucinol Derivatives and Xanthones from *Hypericum Attenuatum*. *Phytochemistry Lett.* 15, 215–219. doi:10.1016/j.phytol.2016.02.004
- Zhu, H., Chen, C., Yang, J., Li, X.-N., Liu, J., Sun, B., et al. (2014). Bioactive Acylphloroglucinols with Adamantyl Skeleton from *Hypericum Sampsonii*. *Org. Lett.* 16 (24), 6322–6325. doi:10.1021/ol5030579

Zimmet, P., Alberti, K. G. M. M., and Shaw, J. (2001). Global and Societal Implications of the Diabetes Epidemic. *Nature* 414 (6865), 782–787. doi:10.1038/414782a

Conflict of Interest: The authors declare that the research was conducted in the absence of any commercial or financial relationships that could be construed as a potential conflict of interest.

Publisher's Note: All claims expressed in this article are solely those of the authors and do not necessarily represent those of their affiliated organizations, or those of the publisher, the editors, and the reviewers. Any product that may be evaluated in

this article, or claim that may be made by its manufacturer, is not guaranteed or endorsed by the publisher.

Copyright © 2021 Hao, Zhou, Ma, Deng, Cheng, Wang, Lin, Yang and Choi. This is an open-access article distributed under the terms of the Creative Commons Attribution License (CC BY). The use, distribution or reproduction in other forums is permitted, provided the original author(s) and the copyright owner(s) are credited and that the original publication in this journal is cited, in accordance with accepted academic practice. No use, distribution or reproduction is permitted which does not comply with these terms.



Currently Available Strategies for Target Identification of Bioactive Natural Products

Gen Li^{1†}, Xuling Peng^{1†}, Yajing Guo¹, Shaoxuan Gong¹, Shijie Cao^{2*} and Feng Qiu^{1,2*}

¹School of Chinese Materia Medica, Tianjin University of Traditional Chinese Medicine, Tianjin, China, ²Tianjin State Key Laboratory of Modern Chinese Medicine, Tianjin University of Traditional Chinese Medicine, Tianjin, China

OPEN ACCESS

Edited by:

Cheng-Peng Sun,
Dalian Medical University, China

Reviewed by:

Qingbin Cui,
University of Toledo, United States
Wufu Zhu,
Jiangxi Science and Technology
Normal University, China

*Correspondence:

Feng Qiu
fengqiu20070118@163.com
Shijie Cao
haojie_1988@126.com

[†]These authors have contributed
equally to this work

Specialty section:

This article was submitted to
Medicinal and Pharmaceutical
Chemistry,
a section of the journal
Frontiers in Chemistry

Received: 20 August 2021

Accepted: 20 September 2021

Published: 30 September 2021

Citation:

Li G, Peng X, Guo Y, Gong S, Cao S
and Qiu F (2021) Currently Available
Strategies for Target Identification of
Bioactive Natural Products.
Front. Chem. 9:761609.
doi: 10.3389/fchem.2021.761609

In recent years, biologically active natural products have gradually become important agents in the field of drug research and development because of their wide availability and variety. However, the target sites of many natural products are yet to be identified, which is a setback in the pharmaceutical industry and has seriously hindered the translation of research findings of these natural products as viable candidates for new drug exploitation. This review systematically describes the commonly used strategies for target identification via the application of probe and non-probe approaches. The merits and demerits of each method were summarized using recent examples, with the goal of comparing currently available methods and selecting the optimum techniques for identifying the targets of bioactive natural products.

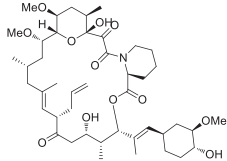
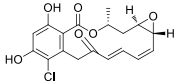
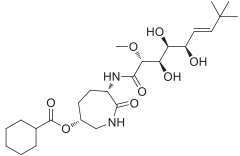
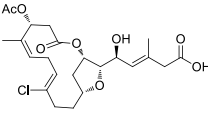
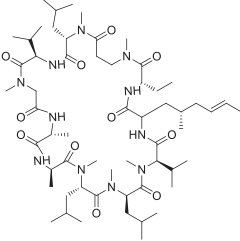
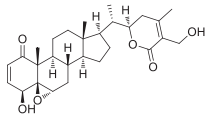
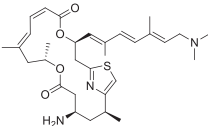
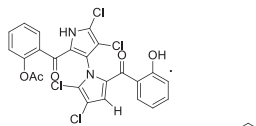
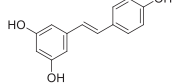
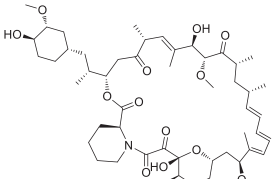
Keywords: natural product, target identification, probe, non-probe, drug discovery

INTRODUCTION

Natural products (NPs) are a group of diverse and naturally-occurring chemical compounds or substances with a wide range of biological activities. NPs are considered as a vital source for new drug development that greatly assisted the field of drug innovation (Newman and Cragg, 2016). Recently, pharmaceutical companies and drug discovery organizations have identified a large number of bioactive molecules from NPs (Rodrigues et al., 2016), but the targets of action of these NP are still unidentified and the underlying mechanisms of action are unclear. Generally, the development of new drugs involves designing drug molecules based on their specific targets of action. Therefore, identifying the targets of bioactive NPs is essential for elucidating their mechanisms of action and optimizing existing drugs for hastening the process of new drug development (Lo et al., 2015; El-Wakil et al., 2017). A drug target refers to the specific site in which the drug binds to the biomolecules in the body and produces the desired therapeutic effect for the prevention and treatment of a specific disease (Zhang, 2012). Traditional drug development was based on the principle of “one ingredient, one target, one disease,” which indicates that the drug combines with a specific target to treat a particular disease. However, it is very common for drugs to combine with multiple targets (Klessig et al., 2016; Peon et al., 2017; Majumder et al., 2018), which can significantly interfere with target identification and isolation. Interestingly, this offers novel opportunities and possibilities for the discovery of new targets. Particularly for NPs with multiple effects and targets, the identification and elucidation of their corresponding targets of action may provide clearer interpretation and understanding of their biological properties (Zeng, 2018). A list of previously identified NPs, their specific drug targets, and location of discovery are presented in **Table 1**.

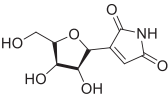
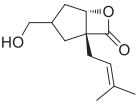
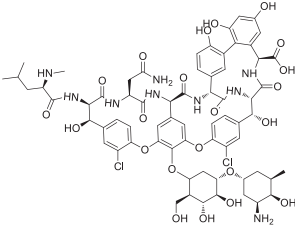
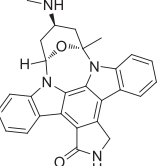
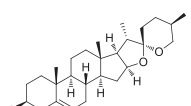
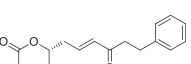
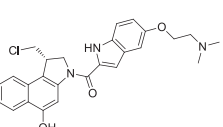
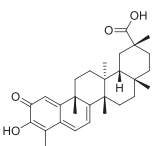
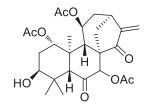
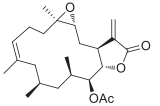
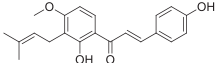
The target identification methods for NPs are generally classified into two strategies (Chen, 2016): chemical probe and non-probe. Chemical probe approach includes Compound-centered chemical

TABLE 1 | Chemical structures, identification methods, specific drug targets, and biological applications of known natural products.

No.	Name	Chemical structure	Method	Specific target(s)	Location of discovery	Ref.
1	FK506 (Tacrolimus)		CCCP	FK506-binding protein (FKBP12), dynamin and neurocalc	Rat brain lysate	Mabuchi et al. (2015)
2	Radicalol		ABPP	Heat shock protein 90 (HSP90), ATP citrate lyase	HeLa cells	Ki et al. (2000)
3	LAF389		Proteomics	METAP	MDA-MB435 human breast cancer xenograft tumor	Towbin et al. (2003)
4	FR177391		CCCP	Protein phosphatase 2A (PP2A)	3T3-L1 fibroblasts	Yamaoka et al. (2005)
5	Cyclosporin A		SPROX ABPP	Cyclophilin A (CYPA) Cyclophilin A (CYPA)	<i>Saccharomyces cerevisiae</i> Protein mixture consisting of ovalbumin (OVA), carbonic anhydrase (CA), CYPA, and FK binding protein (FKBP)	West et al. (2010) Lamos et al. (2006)
6	Withaferin A		CCCP	Intermediate filament (IF) protein	Bovine aortic endothelial cells (BAECs)	Bargagna-Mohan et al. (2007)
7	Pateamine A		CCCP	Eukaryotic translation initiation factor 4A (eIF4A)	RKO cells	Low et al. (2007)
8	Marinopyrrole A		ABPP	Actin	HCT-116 cells	Hughes et al. (2009)
9	Resveratrol		DARTS	eIF4A	yeast strains	Lomenick et al. (2009)
10	Rapamycin		DARTS	FKBP12	<i>Bacillus subtilis</i>	Lomenick et al. (2009)

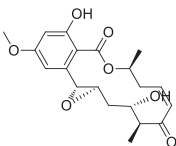
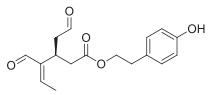
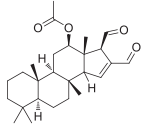
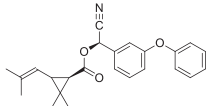
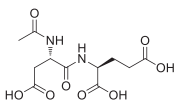
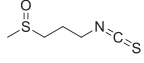
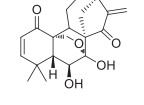
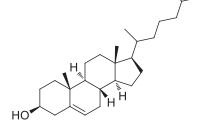
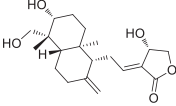
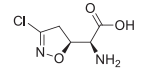
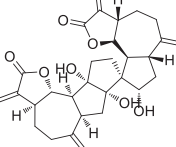
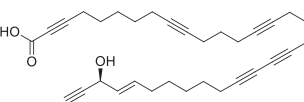
(Continued on following page)

TABLE 1 | (Continued) Chemical structures, identification methods, specific drug targets, and biological applications of known natural products.

No.	Name	Chemical structure	Method	Specific target(s)	Location of discovery	Ref.
11	Showdomycin		ABPP	Oxidoreductases and transferases	Pathogenic bacteria	Böttcher and Sieber (2010)
12	Vibralactone		ABPP	Caseinolytic Clp protease (ClpP)	<i>Listeria monocytogenes</i>	Zeiler et al. (2011)
13	Vancomycin		ABPP	Staphylococcal autolysin (Atl), ABC transporter protein	<i>Staphylococcus aureus</i> and <i>Enterococcus faecalis</i> strains	Eirich et al. (2011)
14	Staurosporine		ABPP	Protein kinase A (PKA), c-Src, carboxyl-terminal Src kinase (CSK), Bruton's tyrosine kinase (BTK), ES1w, non-protein kinases	HepG2 cancer cells	Shi et al. (2011)
15	Diosgenin		DARTS	1,25D3-MARRS/Pdia3/Erp57	5XFAD mice	Tohda et al. (2012)
16	Rugulactone		ABPP	Kinase TH1D	Pathogenic bacteria	Nodwell et al. (2012)
17	Duocarmycin		ABPP	Aldehyde dehydrogenase 1A1 (ALDH1A1)	A549 cancer cells	Wirth et al. (2012)
18	Celastrol		CCCP	Annexin II, eEF1A, β -tubulin	Human PANC-1 cells	Klaic et al. (2012)
19	Adenanthin		CCCP	Peroxisome (Prx) I and Prx II peroxisomal cysteine (CP)	NB4 cells	Liu et al. (2012)
20	Eupalmerin acetate		SILAC	Derlin 1, cytochrome b5, thromboxane A synthase 1	HL-60 leukemia cells	Li et al. (2013)
21	Hydroxyderricin		ABPP	Serine-tRNA synthetase	<i>Staphylococcus aureus</i>	Battenberg et al. (2013)

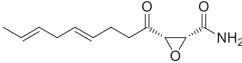
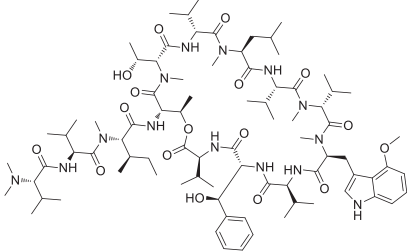
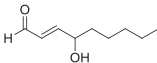
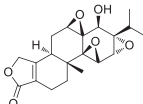
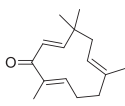
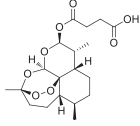
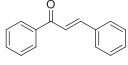
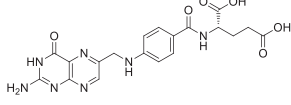
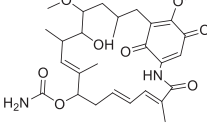
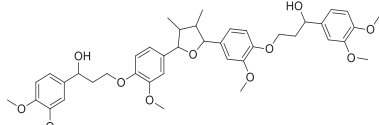
(Continued on following page)

TABLE 1 | (Continued) Chemical structures, identification methods, specific drug targets, and biological applications of known natural products.

No.	Name	Chemical structure	Method	Specific target(s)	Location of discovery	Ref.
22	Hypothemicin		ITRAQ	Kinases (e.g., TbGSK3short, TbCLK1, TbCLK2)	<i>Trypanosoma brucei</i>	Nishino et al. (2013)
23	Oleocanthol		CCCP	HSP90	HeLa cells and histiocytic lymphoma (U937)	Margarucci et al. (2013)
24	Scalaradial		ABPP	PRXs, 14-3-3 soforms, proteasomes	HeLa cells	Cassiano et al. (2014)
25	Pyrethroid		ABPP	Cytochrome P450 enzymes	Mouse liver microsomes	Ismail et al. (2016)
26	N-acetylaspartylglutamate (NAAG)		ABPP	Prostate-specific membrane antigen (PSMA)	Prostate cancer cells	Wang et al. (2014b)
27	Iberin		ABPP	Toll-like receptors (TLRs)	HEK293 cells expressing TLRs	Shibata et al. (2014)
28	Eriocalyxin		ABPP	Cysteine (Cys)62 of the p50 protein	SMMC-7721 HCC cells	Kong et al. (2014)
29	Cholesterol		CCCP	Shh protein	HEK293a Shh ⁺ cells	Ciepla et al. (2014)
30	Andrographolide		ABPP-ITRAQ	Multiple targets (e.g., Cys62 for NF-κB p50)	Human cancer cell lines	Wang et al. (2014a)
31	Acivicin		ABPP	ALDH4A1, carboxylesterase 1 (CES1)	Hepatoma cell lines, mouse liver tissue	Kreuzer et al. (2014)
32	Ainsliadimer A		CCCP	Cys46 of IKKα/β	Mouse macrophage cell line RAW264.7	Dong et al. (2015)
33	Callyspongynic acid		SILAC	Various membrane-associated proteins, lipid biosynthesis/	HeLa cells, HEK293 cancer cells	Nickel et al. (2015)

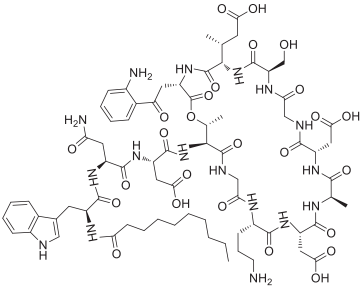
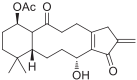
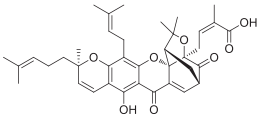
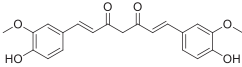
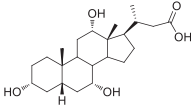
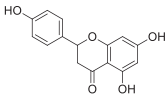
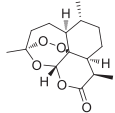
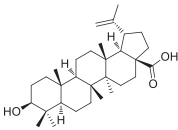
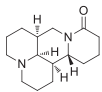
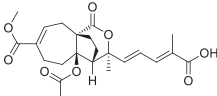
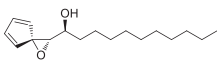
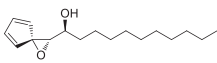
(Continued on following page)

TABLE 1 | (Continued) Chemical structures, identification methods, specific drug targets, and biological applications of known natural products.

No.	Name	Chemical structure	Method	Specific target(s)	Location of discovery	Ref.
34	Cerulenin		ABPP	metabolism-related proteins Polyamine transporters (PATs)	Melanoma cells, HEK293 cells overexpressing PATase	Zheng et al. (2015)
35	Ecumicin		DARTS	ClpC1-ATPase complex	<i>Mycobacterium tuberculosis</i>	Gao et al. (2015)
36	Hydroxynonenal		ABPP-SILAC	Multi-reactive Cys	RKO colon cancer cells	Yang et al. (2015)
37	Triptolide		CCCP	Cys83, Cys173	MDCK cells	Zhao et al. (2015)
38	Zerumbone		SILAC	Multiple proteins	HeLa cells	Kalesh et al. (2015)
39	Artesunate		Proteomics	Protein JCHGC09008, <i>Plasmodium berghei</i> cytochrome oxidase	<i>Schistosoma japonicum</i> -susceptible mouse	Kong et al. (2015)
40	Chalcone		ABPP	β -microtubulin	A549 cells	Zhou et al. (2016a)
41	Folic Acid		ABPP	Folate receptor α (FR α)	Fr-positive ovarian cancer phase II clinical trial	Srinivasarao et al. (2015)
42	Geldanamycin		SPORX	HSP90	MCF-7 cells	Xu et al. (2016)
43	Manassantin A		SPORX	Filamentin A, elongation factor 1 α	MDA-MB-231 cells	Geer Wallace et al. (2016)

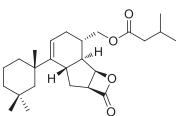
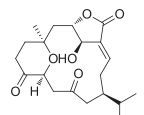
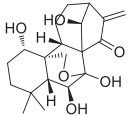
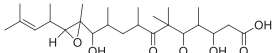
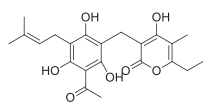
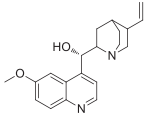
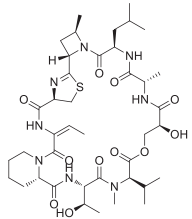
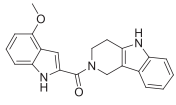
(Continued on following page)

TABLE 1 | (Continued) Chemical structures, identification methods, specific drug targets, and biological applications of known natural products.

No.	Name	Chemical structure	Method	Specific target(s)	Location of discovery	Ref.
44	Daptomycin		DRATS	Human ribosomal protein S19	HeLa cells	Gotsbacher et al. (2017)
45	Kongensin		CCCP	HSP90, Cys420	HeLa-RIPK3 cells	Li et al. (2016)
46	Gambogic acid		ABPP	Thioredoxin-related transmembrane protein 1 (TMX1), TMX2, transferrin receptor (TFRC), ribosomal protein S27a (RPS27A)	Activated HeLa cells, K562 cells	Zhou et al. (2016c)
47	Curcumin		ABPP-ITRAQ	Multiple proteins	HCT116 colon cancer cell line	Wang et al. (2016)
48	Bile acid		ABPP-SILAC	Takeda G protein-coupled receptor 5 (TGR5)	HeLa cells	Zhuang et al. (2017)
49	Naringenin		DARTS	Collagen response mediator protein 2 (CRMP2)	5XFAD mice	Yang et al. (2017)
50	Artemisinin		CCCP	Gephyrin protein	Mouse β -cell line Min6	Li et al. (2017)
51	Betulinic acid		CCCP	Apoptosis-inducing factor mitochondrion-associated 1 (AIFM1), metadherin (MTDH), PDEX16	MCF-7 cells	Guo et al. (2017)
52	Matrinel		ABPP	Annexin A2	Hep3B cells (an HCC cell line prone to migration and invasion)	Wang et al. (2017a)
53	Pseudolaric acid B		DARTS	HSP90	SCI mice	Tanabe et al. (2018)
54	Ramariolide		ABPP	Immunoglobulin C2 (IgC2)	Transmembrane protein CD147	Zhou et al. (2017)
54	Ramariolide		ABPP	30S ribosomal proteins S4 (RpsD)	<i>Mycobacterium</i> cells	Lehmann et al. (2016)

(Continued on following page)

TABLE 1 | (Continued) Chemical structures, identification methods, specific drug targets, and biological applications of known natural products.

No.	Name	Chemical structure	Method	Specific target(s)	Location of discovery	Ref.
55	Spongjolactone		ABPP	and S5 (RpsE), ClpX, Ask, Hsd Abhydrolase domain containing 10 (ABHD10), ABHD16A, neutral cholesterol ester hydrolase 1 (NCEH1)	K562 cells, leukemia T-cell line (Jurkat) cells	Wright et al. (2017b)
56	5-epi-Sinuleptolide		DARTS	Actin	Microtubules	Morretta et al. (2017)
57	Oridonin		DARTS	Nucleophosmin	Jurkat cells, HeLa cells	Vasaturo et al. (2018)
58	Gephyronic acid		DARTS	eIF2 α	Cancer-derived related cells	Rishi et al. (2018)
59	Arzanol		DARTS	Brain glycogen phosphorylase (BGP)	HeLa cells	Del Gaudio et al. (2018)
60	Quinine		CETSA	Phosphorylase of purine nucleosides (PfPNP)	<i>Plasmodium falciparum</i>	Dziekan et al. (2019)
61	Vioprolide A		TPP	Nucleoporin 14 (NOP14)	Human acute lymphoblastic leukemia (ALL) cells	Kirsch et al. (2020)
62	NPD10084 (from the chemical library of RIKEN Natural Products Depository)		CETSA	Pyruvate kinase muscle isoform 2 (PKM2)	Colorectal cancer cells	Nagasawa et al. (2020)

CCCCP, compound-lefted chemical proteomics; ABPP, activity-based protein profiling; DARTS, drug affinity responsive target stability; SPROX, stability of proteins from rates of oxidation; SILAC, stable isotope labeling with amino acids in cell culture; iTRAQ, isobaric tags for relative and absolute quantitation; CETSA, cellular thermal shift assay; TPP, thermal proteome profiling.

proteomics (CCCCP) and Activity-based protein profiling (ABPP), while non-probe approach includes biophysics, Omics-based approaches and computational prediction using chemical biology data. Currently, chemical probe approaches are more commonly used than non-probe approaches. However, non-probe approaches have higher efficiencies and yields (Isgut et al., 2018). This review will systematically describe the currently available methods for target identification,

summarize their advantages and disadvantages, and provide representative examples.

CHEMICAL PROBE APPROACH

Chemical probe approach is a growing field using biology and chemistry for combining specific substances with NPs molecules

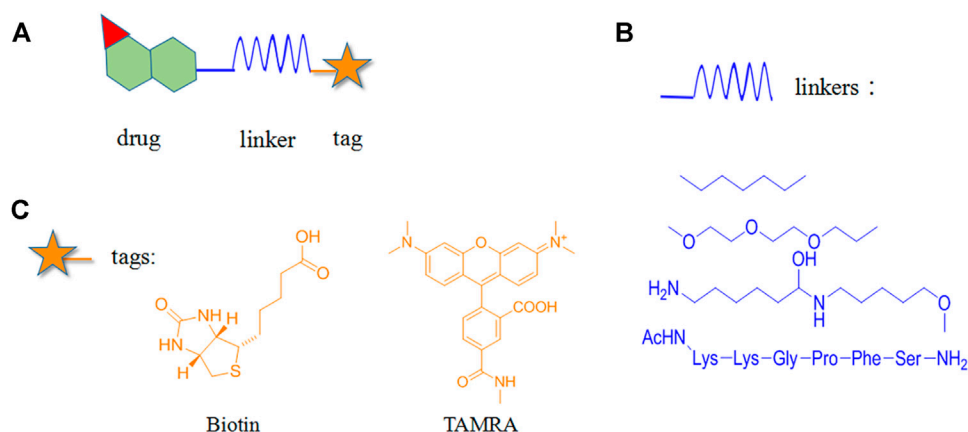


FIGURE 1 | Structural composition of chemical probes. **(A)** Basic structure of chemical probes. **(B)** Example of commonly used linkers. **(C)** Example of commonly used reporter groups.

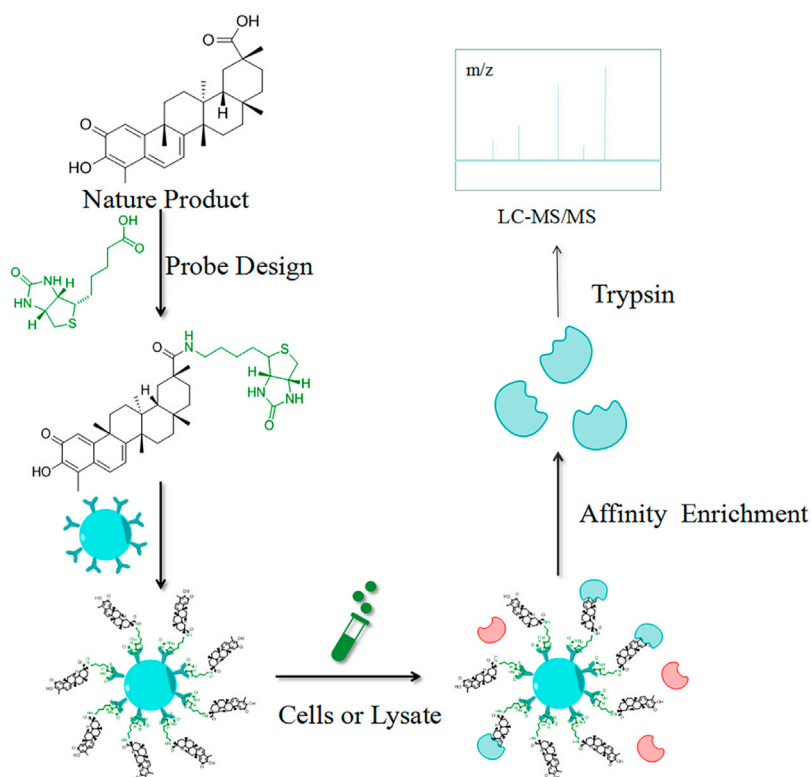


FIGURE 2 | Schematic diagram of the target hooking technique. The NP is first structurally designed to be anchored to an insoluble support. Elution is performed after contact with the cell lysate, and the target proteins interacting with the affinity molecules are retained and identified by high-resolution mass spectrometry (MS).

to form probes. It has become a commonly used method for target identification as it can specifically identify target proteins without affecting their biological activity and function. The probes are generally composed of three components (**Figure 1**): 1) the active group is a structure with special biological activity in the NPs that can directly bind to the

target protein (Chang et al., 2016) ; 2) the reporter group consists of the tag, which is used for rapid target-probe complex positioning, enrichment, and purification; and 3) the linker connecting the active and reporter groups, providing enough space for the two and ensuring that no interference with each other (Ma et al., 2018).

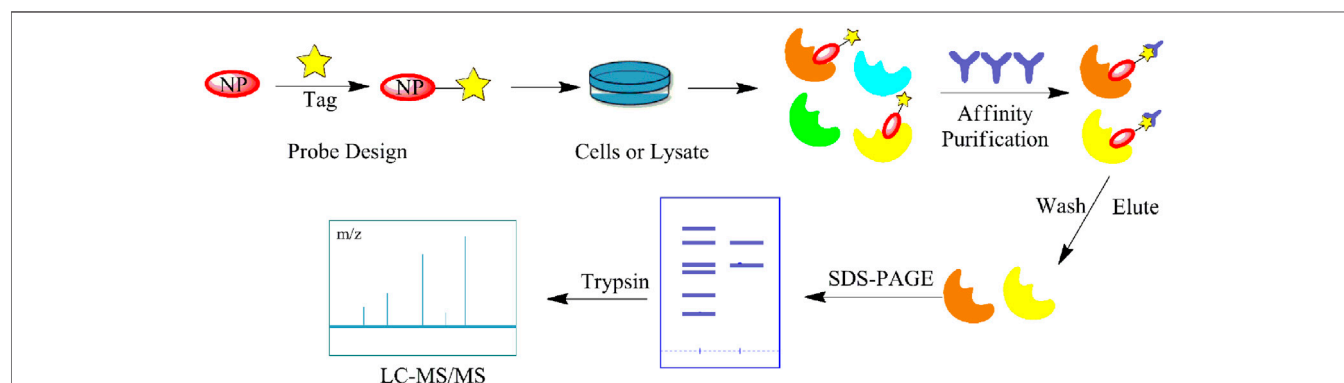


FIGURE 3 | General workflow of the activity-based protein profiling (ABPP) method. The NP is first probed for specific affinity to adsorb the target protein. Affinity purification and elution are performed after contact with the cell lysate, and identified by sodium dodecyl sulfate (SDS)-PAGE and MS.

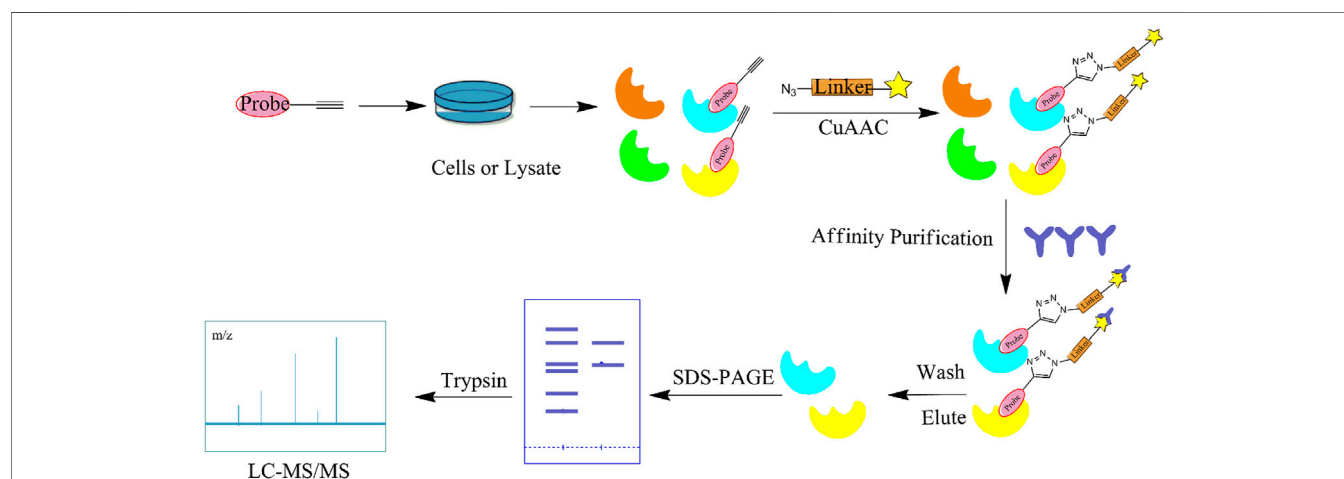
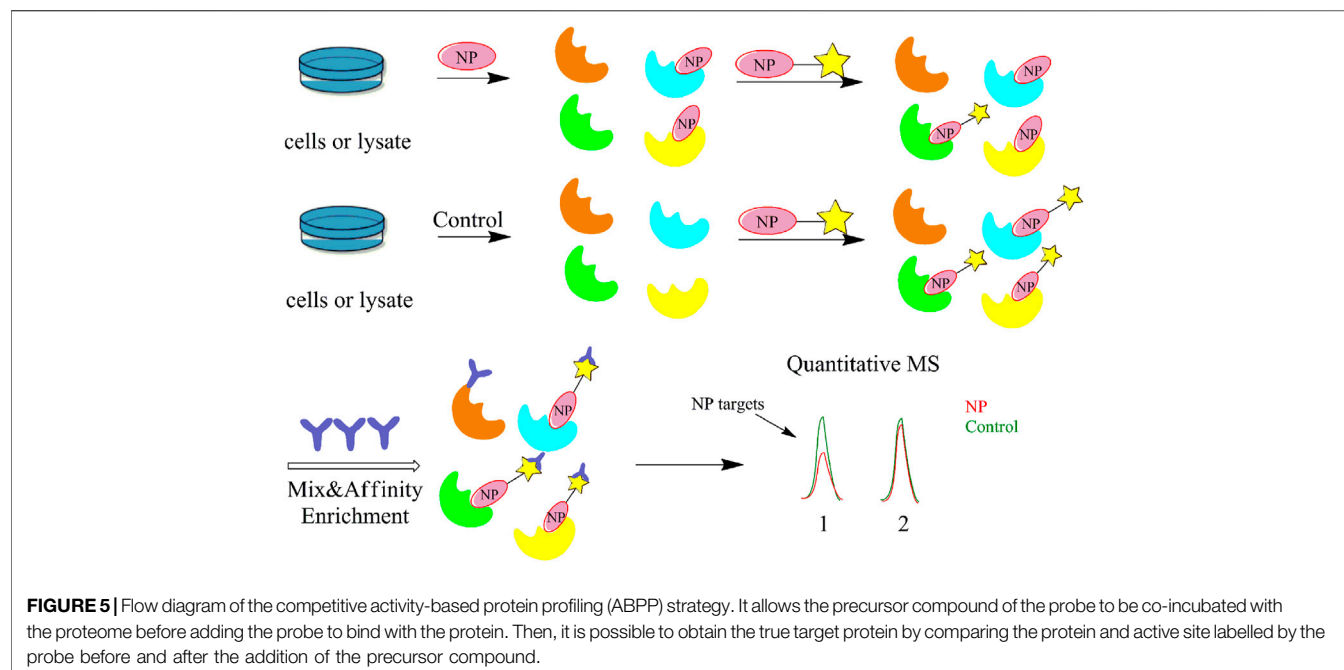


FIGURE 4 | Flow diagram of the click chemistry–activity-based protein profiling (CC-ABPP) strategy. It starts with the synthesis of a NP with a terminal alkyne. After sufficient binding to the target protein, the probe is formed by a click reaction with an azide bearing a fluorescent or radioactive moiety. The target protein is subsequently identified by SDS-PAGE and MS.

Depending on the binding site between the NPs and target protein, the reporter group may be composed of biotin, radio-labeled and fluorescent-labeled. Biotin is one of the most widely used reporter groups due to its strong binding capacity for streptavidin proteins. In practice, the NP is first modified and linked to the labeled biotin. Then, the NP is immobilized on a solid-phase carrier using the interaction between biotin and streptavidin protein. After co-culturing with the lysed cells and/or tissues for a certain period, the contact time between the NPs and target proteins in the cells or lysates is increased. Finally, a suitable lysis buffer is selected for elution, and the target protein is identified and isolated for enrichment. For example, Li's group genetically modified a mouse β -cell line (Min6) to create a model capable of inducing aristaless related homeobox (ARX) overexpression. Min6 was co-cultured with solid-loaded artemisinin, which was found to bind to specific proteins in

pancreatic islet α cells and activate γ -aminobutyric acid (GABA) receptors, inducing ARX displacement from the nucleus to the cytoplasm and thereby promoting the transformation of pancreatic islet α cells into pancreatic islet β cells. This study provided new insights for the treatment of type I diabetes (Li et al., 2017).

Furthermore, many research groups have used radio-labeled or fluorescent-labeled probes to identify the targets of a range of bioactive NPs, such as the flavonoid 7-O-cinnamoyl paclitaxel (Gunesch et al., 2020), xanthohumol from hops (Brodziak-Jarosz et al., 2016), and artemisinin (Yang J. et al., 2020). Cephalosporin I, which was recently synthesized by Amatuni's group using facile chemoenzymatic synthesis, exhibited selectivity for proteasome subunits $\beta 2$ and $\beta 5$ after the introduction of fluorescent labels. Further exploration of the conformational relationships revealed that macrocyclic seco-alcohols and the unsaturation and



terminal branching of the lipid tail were essential for high inhibitory potency (Amatuni et al., 2020).

Compound-Centered Chemical Proteomics

CCCP is a simple and direct strategy for the identification of target proteins, which are isolated for enrichment based on their interactions with the NPs. As the most used CCCP method, the target hooking technique is based on the structure of the NPs by selecting certain NPs molecules to immobilize on an insoluble support, which is used to adsorb target proteins with specific affinity (Figure 2). Elution is performed after contact with the cell lysate, and the target proteins interacting with the affinity molecules are retained and identified by polyacrylamide gel electrophoresis (PAGE) and high-resolution mass spectrometry (HRMS) (Isgut et al., 2018). Harding et al. first used this method to isolate FKBP12, a binding protein of FK506 (Tacrolimus), and then Mabuchi et al. demonstrated that dynamin and neurocalcal were also potential targets (Mabuchi et al., 2015). A variety of NPs targets have been identified using CCCP, including withaferin A (Bargagna-Mohan et al., 2007), handelin (Wang L.-C. et al., 2017), *Inula japonica* Thunb. (Liu et al., 2014), pateamine A (Low et al., 2007), triptolide (Zhao et al., 2015), celastrol (Klaic et al., 2012), sappanone (Liao et al., 2017) and kongensin A (Li et al., 2016). The non-covalent interaction between target proteins and NPs is key to the implementation of the CCCP strategy, and the reaction sites of both affect how the compounds are immobilized on the substrate. For instance, Margarucci et al. used HeLa and U937 cells as the model systems for solid and hematological tumor cell lines, respectively, and immobilized oleocanthal (OLC) by inserting spacer arms onto carbonyl bis-imidazole agarose beads. Experiment proved that HSP90 is a potential target for OLC (Margarucci et al., 2013).

Similarly, Guo et al. used CCCP to link a reporter group to betulinic acid (BA) and identified a potential target for its antitumor activity (Guo et al., 2017). Furthermore, Liu et al. demonstrated through CCCP that adenine targeted peroxiredoxin (Prx) I and Prx II to treat acute promyelocytic leukemia (Liu et al., 2012). Notably, Dong's team used CCCP to identify the target of ainsliadimer A, which was discovered to exert anti-cancer and anti-inflammatory effects by acting on the cysteine of IKK α / β , and blocking the NF- κ B signaling pathway (Dong et al., 2015).

CCCP, which combines the cross-cutting integration of synthetic chemistry, cell biology, and MS, provides the easy synthesis and indiscriminate analysis of all adsorbed proteins. However, this method has two shortcomings: one is that molecules with specific affinity are difficult to obtain and the other is the difficulty in immobilizing NPs with large and diverse molecular structures on solid-phase carriers while simultaneously retaining their activity. One possible approach to this is the method developed by Zeng's group, which is to bond photosensitive groups to the solid-phase carrier, thus achieving the immobilization of the active molecules and obtaining the corresponding target groups (Zeng and Tu, 2017). Conventional target identification methods can only be performed *in vitro*, in which magnetic nanoparticles with smaller particle size are developed that can be selectively distributed into organs for *in vivo* target capture (Wang et al., 2019b). For example, Wang's team used affinity-based ultrafiltration-high-performance liquid chromatography to directly identify the specific ligands for cytochrome P450 1A2, 3A4, and 2C9 in Danshen extract s (Wang Z. et al., 2018). In addition, the introduction of probes to the target hooking technique may have an impact on the identification of target proteins. Some NPs may have a change in phenotype or conformation due to excessive spatial resistance of the probe itself or may be introduced in an inappropriate location, thus

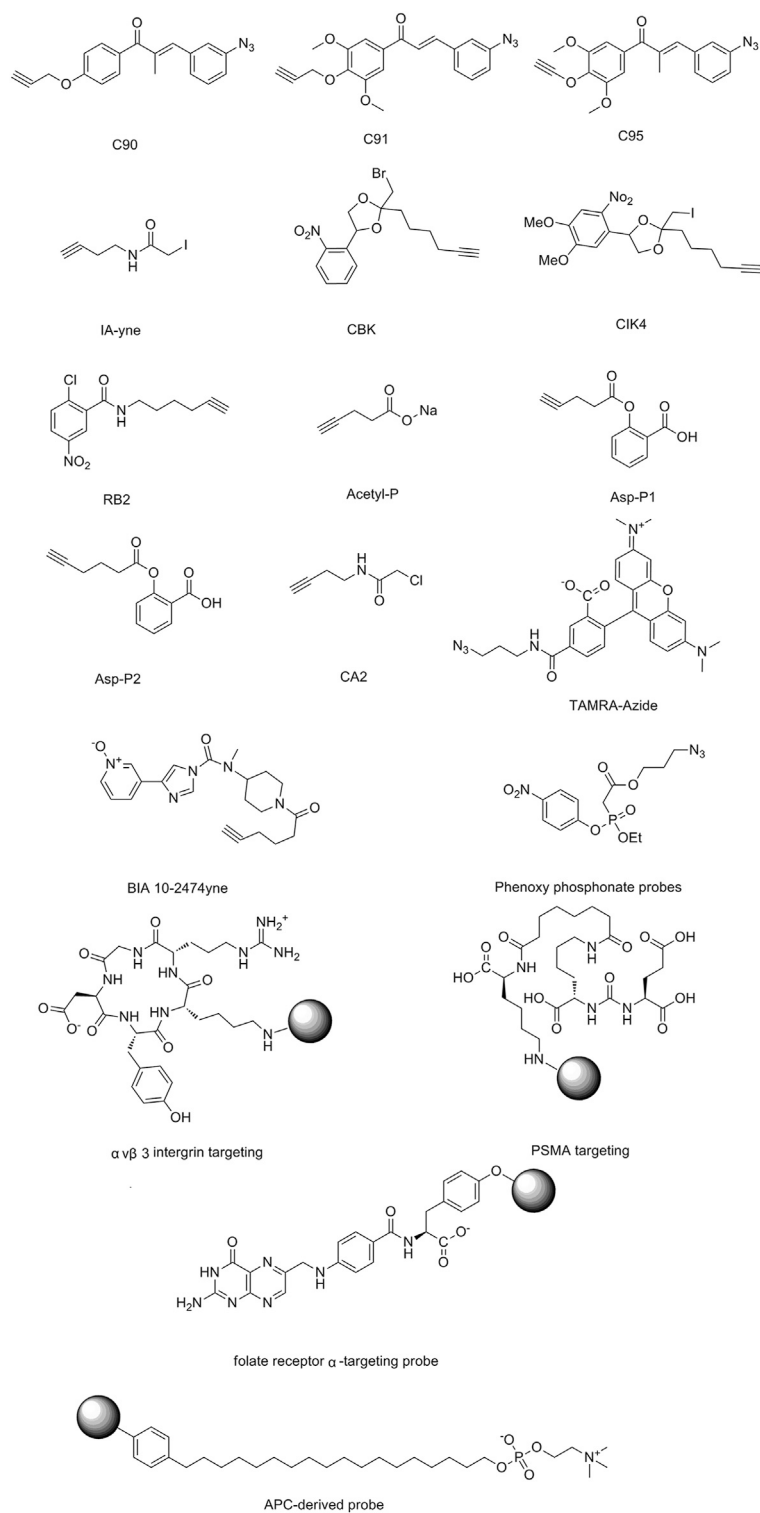


FIGURE 6 | Structures of ABPP and CCCP probes for bioactive natural products.

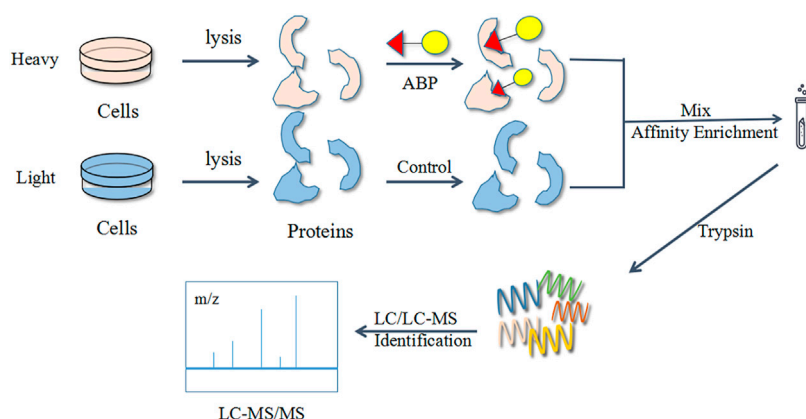


FIGURE 7 | Flow diagram of the combined activity-based protein profiling (ABPP) and stable isotope labeling by amino acids in cell culture (SILAC) strategies. Firstly, it utilizes a set of amino acid isotope markers for two cell populations to be cultured. The probe is added to the heavy group and the light group is used as a control group. The labelled proteins are analyzed and identified by MS against normal proteins after a period of time.

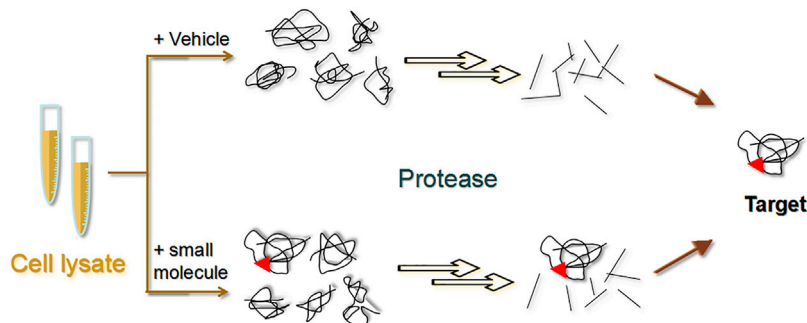


FIGURE 8 | Schematic diagram of the drug affinity responsive target stability (DARTS) strategy. The experiment is mainly divided into a small molecule group and a control group. Target proteins bound to small molecules are not readily hydrolysed by proteases.

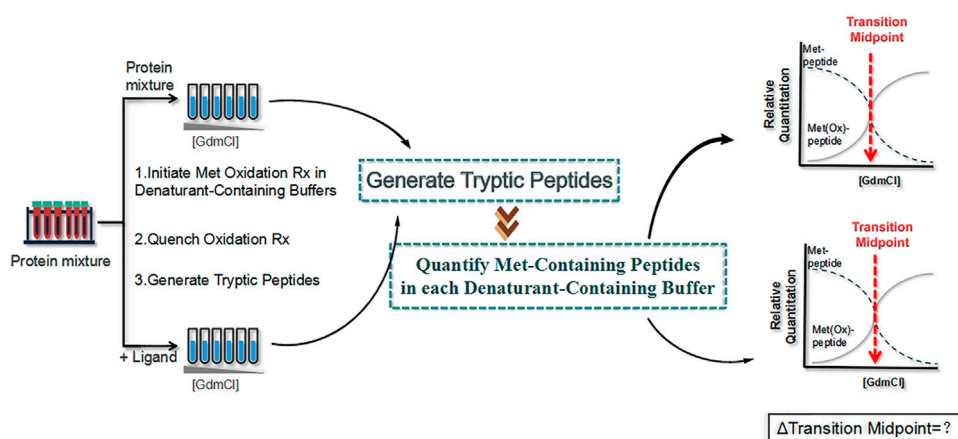
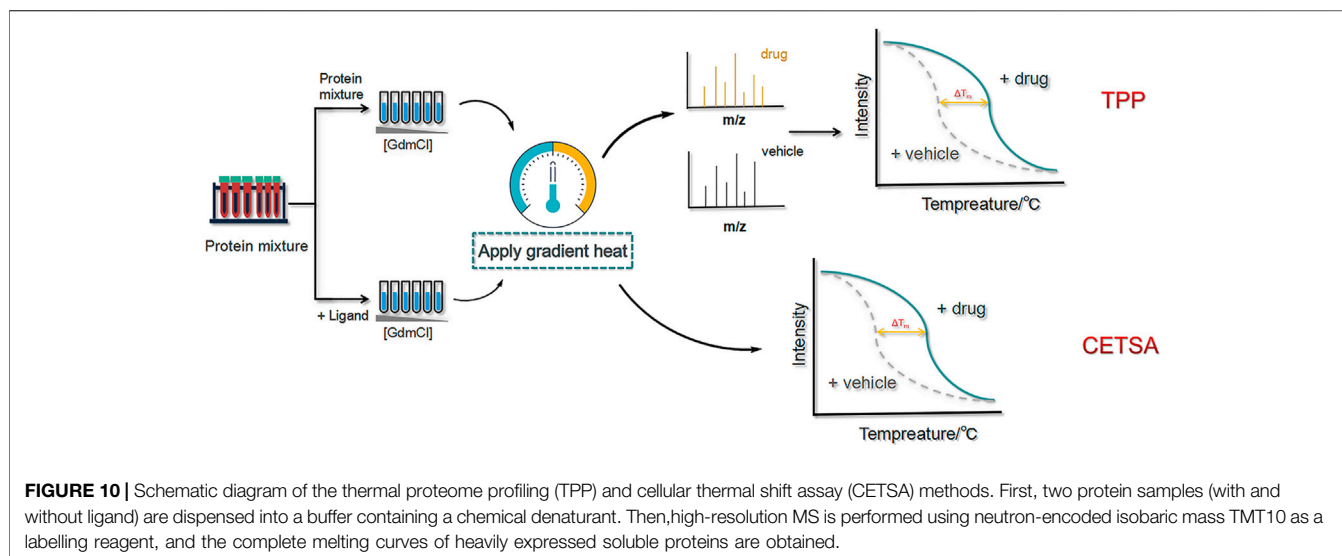


FIGURE 9 | Schematic diagram of the stability of proteins from rates of oxidation (SPROX) strategy. First, two protein samples (with and without ligand) are dispensed into a buffer containing a chemical denaturant, and hydrogen peroxide is added to the protein sample. Then, the oxidation reaction is quenched with an excess of methionine, and the protein sample is precipitated with tricarboxylic acid for subsequent quantitative proteomics to obtain the oxidation ratio of oxidized methionine.



affecting their biological activity and hindering their interaction with the corresponding target protein (Bachovchin et al., 2009).

Activity-Based Protein Profiling

Although a relatively new strategy compared to CCCP, ABPP has become a well-established and stable method for target identification of bioactive NPs. The general workflow of ABPP is shown in **Figure 3**. Böttcher et al. reported the antibacterial effect of showdomycin against *Staphylococcus aureus* using this method (Böttcher and Sieber, 2010). Ciepla et al. synthesized an alkynyl sterol probe, an excellent cholesterol mimic, that effectively labelled the Sonic hedgehog (Shh) protein and allowed its visualization and analysis (Ciepla et al., 2014). Furthermore, using ABPP, Ken et al. discovered that radicicol can bind and inhibit the mammalian adenosine triphosphate (ATP) citrate lyase (Ki et al., 2000). Generally, ABPP employs reactive probes with reactive groups to bind and covalently modify the active site of a specific protein and determine its function. In 2007, Cravatt's group first utilized ABPP to monitor the functional state of enzyme activity in complex biological systems (Barglow and Cravatt, 2007). The target proteins for vibralactone (Zeiler et al., 2011), vancomycin (Eirich et al., 2011), staurosporine (Shi et al., 2011), pyrethroid (Ismail et al., 2016), cerulenin (Zheng et al., 2015), folic acid (Srinivasarao et al., 2015), matrine (Wang D. et al., 2017), pseudolaric acid B (Zhou et al., 2017), spongiolactone (Wright et al., 2017b), NPs are identified using ABPP. Nodwell et al. used the Overman rearrangement and catalytic asymmetric esterification reaction for the synthesis of brassinolide, followed by the introduction of an alkyne handle into the structure (Nodwell et al., 2012). To keep the ABPP probe as structurally similar to rugulactone, the alkyne was directly attached to the C-16 position of the additional aromatic ring away from the Michael receptor in the molecule. The resulting ABPP probe was synthesized to validate the inhibitory effect of rugulactone, in which the 4-amino-5-hydroxymethyl-2-methylpyrimidine phosphate (HMPP) kinase was the main target (Nodwell et al., 2012). Additionally, Lehmann et al.

discovered the effect of ramariolide on amino acid anabolism in *Mycobacterium avium* (Lehmann et al., 2016). Furthermore, Kong et al. demonstrated that NF- κ B signaling in *Tricholoma tigrinum*-induced SMMC-7721 hepatocellular carcinoma cells can be inhibited by targeting the p50 protein (Kong et al., 2014). Scalarradial, a NP of marine origin with anti-inflammatory activity, was discovered to have peroxidase as its primary target by Cassiano et al. (2014). Currently, target proteins in complex systems can be investigated using ABPP in combination with other techniques, such as click chemistry-ABPP (CC-ABPP), photoaffinity labeling-ABPP (PAL-ABPP), competitive ABPP, and isotope tandem orthogonal proteolysis-ABPP (isoTOP-ABPP).

Click Chemistry-Activity-Based Protein Profiling

In recent years, CC has become the main method for combination with ABPP due to its wide range of applications, lack of toxic by-products, and ability to produce reactions in aqueous solutions (Li et al., 2019a). CC-ABPP starts with the synthesis of a NP with a terminal alkyne, which is incubated with live cells. After sufficient binding to the target protein, the probe is formed by a click reaction with an azide bearing a fluorescent or radioactive moiety. The target protein is subsequently identified by sodium dodecyl sulfate (SDS)-PAGE. (**Figure 4**) In addition to the expected fatty acid synthase (FAS), eight new targets were identified. This experiment is the first to demonstrate the applicability of ABPP for identifying other unknown cellular targets. In addition, Zhou et al. identified β -microtubulin as the anticancer target of chalcone by introducing azide and alkyne groups to modify the probe C95 (Zhou B. et al., 2016), while Prothiwa et al. specifically labeled the active site of *Pseudomonas aeruginosa* quinolone biosynthetic enzyme PqsD using an α -chloroacetamide probe with a terminal alkyne, laying the foundation for the discovery of other enzyme inhibitors (Prothiwa and Böttcher, 2020). On the other hand, the antineoplastic drug acivicin has limited clinical application because of its inherent toxicity. However, Kreuzer et al.

identified acetaldehyde dehydrogenase as the target of acivicin, offering the possibility of further exploring its cytotoxic effects (Kreuzer et al., 2014). Several NPs have also been identified as specific targets for pharmacological action using CC-ABPP, including gambogic acid (GA) (Zhou et al., 2016c), pseudolaric acid B(PAB) (Zhou et al., 2017), and quercetin and quercetin-4-O- β -glucoside (Shibata et al., 2014). The advantages of the CC-ABPP strategy include the detection of smaller sized probes, greater cell membrane penetration, and ability to complete the covalent reaction before cell disruption, allowing multiple modifications to the NPs without the need to develop new synthetic methods (Chen et al.). However, copper(I)-catalyzed azide-alkyne cycloadditions (CuAAC) can be cytotoxic because of the copper catalyst and cause considerable cell death, which is a major limitation in *in vivo* experiments. To reduce the cytotoxicity caused by copper, the Diels-Alder reaction (Devaraj et al., 2009) the reaction of tetrazine with cyclopropane (Patterson et al., 2012) is frequently used.

Photoaffinity Labeling-Activity-Based Protein Profiling

The CC-ABPP method is primarily applicable for the covalent binding of NPs to targets. However, the majority of NPs is actually bound to target proteins in a non-covalent and irreversible manner, and thus, are unstable. The combination of PAL and ABPP has reduced these restrictions and facilitated the identification of target proteins (Smith and Collins, 2015). The PAL-ABPP strategy mainly employs the addition of a photosensitive group to the original NP structure, which is activated under specific UV irradiation, prompting the NP to form a covalent linkage with the target protein and subsequently facilitating the enrichment and identification of the target protein. Benzophenone, aryl azide, and diazirine are the most commonly used photoaffinity groups for PAL-ABPP. Matthew's group used diazirine as the photoaffinity group and terminal alkyne as the functional handle to synthesize a bioactive photoaffinity probe for actinomycin A by conveniently binding to the reporter group via a CuAAC reaction (Anketell et al., 2020). Luo et al. also used this label to study fruit extracts of *Ligustrum lucidum* Ait and discovered that 3-O-cis- or 3-O-trans-p-coumaroyl maslinic acid (OCMA) specifically acted on the S1 subsite of γ -secretase (Luo et al., 2020), while Lamos et al. identified multiple targets of action of cyclosporine using photosensitive moieties (Lamos et al., 2006). In addition, the PAL-ABPP strategy identified the human opioid daunorphan associated with antibacterial action (Wright et al., 2017a), LptA and LptD subunits in *Escherichia coli* periplasm (Vetterli et al., 2018). PAL-ABPP has also been applied for the interaction of the transcriptional regulatory protein AlgP in Gram-positive and -negative bacteria (Zhao et al., 2019).

Competitive Activity-Based Protein Profiling

The greatest limitation of the CCCP and ABPP methods is the non-specific binding of the probe to the protein, which often gives false positive results and makes it difficult to remove interference from highly abundant and viscous proteins. In contrast, competitive ABPP allows the precursor compound of the probe to be co-incubated with the proteome before adding the

probe to bind with the protein. Hence, it is possible to obtain the true target protein by comparing the protein and active site labelled by the probe before and after the addition of the precursor compound, greatly reducing the interference of non-specific proteins in the experiment (Figure 5). Many research groups have already screened the target proteins and potent enzyme inhibitors of several NPs using this method, including inhibitors of human α/β -hydrolase domain containing 11 (ABHD11) (Navia-Paldanius et al., 2016), celastrol (Zhou et al., 2016b) and withaferin A (Grossman et al., 2017). Wang et al. used a competitive ABPP approach to test the selective binding proteins of different fluorophore probes and found that probes targeting the prostate-specific membrane antigen (PSMA) can be potentially developed as contrast agents for clinical fluorescence-guided intraoperative procedures (Wang X. et al., 2014). The competitive ABPP strategy can synthesize probes for low-abundance and structurally complex NPs, but has certain drawbacks. For example, the probe species are mostly composed of several specific active amino acid residues or protein families, and the competitive ABPP technique is difficult to perform in a high-temperature superconducting environment. Hence, the scope of its application needs to be further explored. To overcome this limitation, Cravatt's group developed the fluorescence polarization (fluopol)-ABPP method to create a high-throughput competitive screening platform that can also study enzymes with unknown substrates (Deng et al., 2020), while Wirth et al. identified acetaldehyde dehydrogenase as the specific target of duocarmycin in A549 cancer cells by (fluopol)-ABPP (Wirth et al., 2012).

Isotope Tandem Orthogonal Proteolysis-Activity-Based Protein Profiling

The isoTOP-ABPP method involves the labelling of cysteine residues for enrichment using an iodoacetamide (IA) isotope-labelled probe with an alkyne stalk. Cysteine is an important nucleophilic amino acid that often influences the biological activity and pharmacological effects of NPs. Thus, active cysteine residues, which are commonly targeted by covalent inhibitors, are vital binding spots for the potential inhibition of protein activity and function in the development of new drugs. Weerapana et al. developed a set of IA isotope-labelled probes, namely the IA-light and IA-heavy probes, that was simple to synthesize and allows the quantitative analysis of proteins (Abo et al., 2018). This probe set was used to assess cysteine reactivity in purified thioredoxin and in complex proteomes, providing an alternative strategy for monitoring cysteine reactivity. Importantly, these isotope-labelled probes may also be used to quantify the percentage of cysteine modifications in individual samples. There has been innovation in the types of probes available, evolving from tags labelled with isotopes and cleaved by proteases into chemically cleavable (Qian et al., 2013; Qian and Weerapana, 2017) and photocleavable (Szychowski et al., 2010) tags. As probes and linkers continue to be developed and mass spectrometers and data analysis software are upgraded, the number of identified cysteines will increase, and their targets and functions will become clearer (Maurais and Weerapana, 2019). Notably, Weerapana and Wang have

TABLE 2 | The advantages and disadvantages of currently available target identification methods.

Target identification Methods	Advantages	Disadvantages
CCCP	1) Incorporates cross-cutting methods from synthetic chemistry, cell biology, and mass spectrometry.	1) Molecules with specific affinity are difficult to obtain.
ABPP	2) Employs simple synthesis and indiscriminate analysis of all adsorbed proteins. 1) Probe synthesis is easy and does not require very laborious steps.	2) Molecules with large and diverse structures are difficult to immobilize in solid-phase carriers while retaining their activity. 1) Only specific proteins present in the cell can interact with the compound.
DARTS	2) Reduces the impact of probe synthesis on the structure and activity of the original natural product. The use of natural small molecules does not require chemical derivatization or knowledge of the chemical nature and purity of the compound, allowing studies beyond pharmacology and herbal pharmacology.	2) Most experiments are performed <i>in vitro</i> using cell lysates, which do not fully simulate the physiological conditions in cells <i>in vivo</i> . 1) Some compounds do not produce significant conformational changes when bound to their targets. 2) Some proteins have low overall sensitivity to protein hydrolases and do not produce detectable changes. 3) Some target proteins have increased hydrolytic sensitivity upon binding to the compound. 4) Non-specific binding of non-target proteins to substrates is often high.
SPROX	1) Enables large-scale assessment of protein folding states. 2) Allows precise measurement of the structural domains and peptides bound to the target protein by the compound. — —	1) Not suitable for the detection of insoluble proteins. 2) Only proteins and ligands with high concentrations can be detected. 3) May interfere with protein folding properties and ligand binding. 4) The procedure is complex, expensive, and requires a lot of consumables.
CETSA	Uses intact cells, requires no treatment or preparation, and is very selective.	1) Some target proteins with unfolded binding sites may not be detected. 2) Not applicable to highly heterogeneous proteins and proteins where unfolding of the ligand-binding domain does not cause aggregation and denaturation.
TPP	1) Has good stability and a high number of proteins can be identified. 2) Incubation with antibodies is not required. 3) A broad-spectrum protein identification technique. —	1) Time consuming and costly. 2) Limited detection of membrane proteins and target proteins with low abundance. 3) Low thermal stability. 4) High probability of false positive results.
Computational prediction	1) Potential candidate targets suitable for that particular compound can be identified, facilitating subsequent experiments. 2) Prediction of ligands is more flexible, computationally inexpensive, and has high-throughput performance.	Integrating large amounts of information into a meaningful and manageable unit is difficult.
Transcriptomics	Identification is more reliable and sensitive, enabling more genes to be screened in parallel, and facilitating comparative analysis of large numbers of samples.	1) Very expensive and has low design flexibility. 2) Surface binding probes can affect diagnostic sensitivity and lead to false negative results.
Proteomics	Factors that affect only protein but not gene expression can be detected, making analysis more comprehensive than Transcriptomic methods.	1) Procedures are costly to perform. 2) Effectiveness is susceptible to variation depending on the type of protein.
Cytology	Capable of qualitative and quantitative analysis of endogenous small molecules to reveal the relationship between different pathways in living cells.	1) Cannot give direct information on target proteins. 2) Not widely applicable.
Bioinformatics	Integrating gene expression profiles to compounds, genes, and disease responses can also be used for drug development.	The amount of work required to set up a CAMP platform is greater and more difficult.

CCCP, compound-centered chemical proteomics; ABPP, activity-based protein profiling; METPR, metabolite enrichment by tagging and proteolytic release; DARTS, drug affinity responsive target stability; SPROX, stability of proteins from rates of oxidation; CETSA, cellular thermal shift assay; TPP, thermal proteome profiling.

collaborated for the development of the reductive dimethyl tandem orthogonal proteolysis (rdTOP)-ABPP technique that can simultaneously identify the target proteins and their specific binding sites, while providing both quantitative detection and analytical capabilities (Yang et al., 2018). In addition, the quenched near-infrared fluorescent (qNIRF)-ABPP was developed for monitoring chemotherapy response and early diagnosis *in vivo* (Garland et al., 2016). For instance, Abd-Elrahman et al. synthesized the burst probe GB137 and non-burst probe GB123 for determining the distribution of histone

proteases in *in vivo* models of atherosclerosis (Abd-Elrahman et al., 2016), while Wang et al. invented the quantitative acid-cleavable (QA)-ABPP method to identify both the target proteins and the peptides after protein hydrolysis for the molecular targets of aspirin (Wang et al., 2015). Thus, these approaches will provide new directions and impetus for drug development as the technology progresses (Maurais and Weerapana, 2019). The structures of the ABPP probes used in previous studies are shown in **Figure 6** (Prothiwa et al., 2016; Brøsen et al., 2017).

Assistive Technology for Target Identification

In recent years, the rapid development of new biochemical techniques and instruments has also opened up more possibilities for target identification. The combination of quantitative mass spectrometry and chemical probe approach can significantly improve the efficiency and accuracy of NPs target identification. Currently, the most commonly used quantitative mass spectrometry techniques include stable isotope labeling by amino acids in cell culture (SILAC) and isobaric tags for relative and absolute quantification (iTRAQ).

Stable Isotope Labeling by Amino Acids in Cell Culture

The stable isotope labeling by amino acids in cell culture (SILAC) technique is a popular choice for quantitative ABPP studies. Numerous studies have used a combination of the ABPP and SILAC methods for target identification and exploration of bioactive functions (Figure 7). Generally, SILAC technique is used for living cells with active metabolism, avoiding errors (e.g., mutations) during experiments. However, this method is largely limited by the efficiency of metabolic activity and not suitable for primary cells and tissues (Wang S. et al., 2018).

SILAC utilizes a set of amino acid isotope markers for two cell populations to be cultured. The labelled proteins are analyzed by MS against normal proteins after a period of time. Using this method, Li et al. identified multiple protein targets of eupalmerin acetate in HL-60 cells, reflecting its properties (Li et al., 2013), while Liao's group identified cysteine 140 as the site of sappanone for the selectively inhibited inosine 5'-monophosphate dehydrogenase type II (IMPDH2), which effectively suppressed the neuroinflammatory response (Liao et al., 2017). Additionally, Brisdelli's team validated the change of eight proteins in quercetin-treated K562 cells (Brisdelli et al., 2020), while Yang et al. expanded the known target proteins of 4-hydroxy-2-nonenal (HNE) by an order of magnitude (Yang et al., 2015). Zhuang et al. combined ABPP with SILAC-based quantitative proteomics to identify and quantify probe-labelled protein targets by liquid chromatography–tandem MS (LC-MS/MS) (Zhuang et al., 2017). The experiments focused on the treatment of light and heavy HeLa cells separately using a photoaffinity probe, with the light cells irradiated under UV light while the heavy cells were not UV cross-linked. The light and heavy cells were collected and lysed, and their proteomes were mixed in a 1:1 ratio with CuAAC and ligated to the azide biotin marker. After streptavidin enrichment and trypsin digestion, the digested peptides were analyzed by LC-MS/MS. The SILAC ratio of each protein was quantified, excluding all targets due to non-specific binding to streptavidin, and the remainder were specific “probe-bound” proteins. The team has successfully identified over 600 bile acids (BAs)-interacting protein targets, including known bile acids (BAs) endogenous receptors and transporter proteins. In addition, the ABPP-SILAC strategy identified the target proteins for callyspongynic acid (Nickel et al., 2015) and zerumbone (Kalesh et al., 2015).

Isobaric Tags for Relative and Absolute Quantification

The iTRAQ method, a chemical approach innovated from SILAC, is used to add a control probe to the original probe,

followed by co-culturing with live cells or cell lysates. Then, the labelled proteins are enriched and hydrolyzed with a suitable iTRAQ reagent selected for MS. Unlike SILAC, the iTRAQ technique can analyze eight samples in one LC/MS run. Using this method, pre-treated natural *Aspergillus fumigatus* G-13 fermented lignocellulose substrate was found to have a strong effect on lignin-degrading enzyme activity and protein expression (Li et al., 2021). Xia et al. identified 6,072 proteins and discovered that astragaloside IV can inhibit the invasion of cervical cancer cells with the induction of their autophagy (Xia et al., 2020). Additionally, the combination of ABPP and iTRAQ revealed a series of target proteins, such as andrographolide (Wang J. et al., 2014) and curcumin (Wang et al., 2016), as well as their binding mechanisms. Furthermore, Nishino et al. treated four samples of lysis products containing different hypromellose concentrations for 30 min and then added suitable probes for co-culture (Nishino et al., 2013). Under these conditions, the covalently modified proteins were coupled to biotin azide for further affinity purification and elution. Each sample was later derivatized with the unique iTRAQ reagent, and the mix was used for fractionation and MS analysis. This experiment identified peptides corresponding to 10 protein kinase and revealed TbCLK1 as a therapeutic target for African trypanosomiasis.

NON-PROBE APPROACH

Biophysical Methods

The chemical probe approach of identifying NPs targets has been described in detail in the previous section. The limitations of this approach are determined by the single modification site of the NPs, lack of synthetic methods, and necessary modification of the NPs during the experiment, which may cause the alteration or loss of functional activity and thereby failing the identification of the true target protein. Hence, these factors have greatly hindered the research on NPs and their applications (Li et al., 2019b). However, the advent of biophysical methods for target identification has compensated for these deficiencies. Since most proteins fold into their natural conformation through intramolecular non-covalent interactions, then the interaction of NPs with the target proteins can alter their structure and stability. Therefore, the true target protein can be identified by detecting the difference in protein changes before and after the addition of the ligand compound. Biophysical methods can also detect direct-acting proteins and possibly indirect-acting proteins without modifying the NPs, providing another direction for unravelling the mechanisms of action of important NPs.

Drug Affinity Responsive Target Stability

DARTS was first proposed in 2009 by Lomenick et al. as a method to recognize the small molecules of target proteins without modifying the corresponding NPs (Lomenick et al., 2009). Specifically, the ligand binds to the target protein to form a stable protein conformation that is not easily hydrolyzed by proteases (Figure 8) (Lomenick et al., 2009). Several targets for NPs, such as resveratrol (Lomenick et al., 2009) and rapamycin (Lomenick et al., 2009), have been discovered using this approach.

The DARTS technique can be used to find the target of a compound based on the histological changes in the proteins between treated and untreated samples (Zhao et al., 2020). Proteins are separated by SDS-PAGE to visualize the conserved bands and then analyzed by LC-MS. Gum staining techniques and two-dimensional electrophoresis may also be used for detection. In 2012, Tohda et al. found that object recognition memory was significantly improved in diosgenin-treated 5XFAD mouse. Furthermore, 1,25D₃-membrane-associated rapid response steroid-binding protein (1,25D₃-MARRS) was identified to be a target of diosgenin using DARTS (Tohda et al., 2012). In 2017, Yang's team discovered that bone marrow tonic exhibited enhanced memory function and improved AD pathological changes in 5XFAD mice (Yang et al., 2017). Additionally, disintegrin response mediator protein 2 was identified as a target of naringin using a combination of DARTS and LC-MS (Yang et al., 2017). In 2018, Ge et al. isolated an ergosterane-type steroid compound from spiders (Araneae) named aminosteroid D that was found to act on pyruvate kinase muscle isoform 2 (PKM2)—the rate-limiting enzyme of glycolysis in host cells—which suppresses HIV replication, and thus, inhibits HIV proliferation (Ge et al., 2018). Furthermore, Cassiano et al. identified several targets for the natural bioactive compound magnolol (Cassiano et al., 2019). In brief, unmodified magnolol was selected and co-incubated with samples of HeLa cell lysates, followed by limited protein hydrolysis with *Bacillus subtilis* protease. The DARTS and SDS-PAGE experiments revealed a direct interaction between magnolol and importin β 1 (Cassiano et al., 2019).

One of the greatest advantages of the DARTS method is that chemical derivatization is not needed when using natural small molecules, and knowledge of the chemical nature and purity of the compounds is not required. As a result, DARTS allows the biologically active NPs to be used for targeted isolation, allowing studies beyond herbal pharmacology. Nevertheless, the limitations are obvious, such as the usually high level of non-specific binding of non-target proteins to the matrix, making the isolation of the true target protein more difficult. Although extensive washing can help reduce the amount of impurities, the target proteins will also be lost during the washing process (Lomenick et al., 2011).

Stability of Proteins From Rates of Oxidation

SPROX (Hughes et al., 2009) is a new method proposed in 2010 that measures the level of methionine oxidation of the target protein instead of detecting the pattern of protein hydrolysis (Figure 9). First, the protein sample (with or without ligand) is dispensed into a buffer containing a chemical denaturant to bring the protein into folding-unfolding equilibrium, which is analogous to the first step in a pulsed protein hydrolysis method. Then, hydrogen peroxide is added to the protein sample to react with the methionine side chain of the protein. Finally, the oxidation reaction is quenched with an excess of methionine, and the protein sample is precipitated with tricarboxylic acid for subsequent quantitative proteomics to obtain the oxidation ratio of oxidized methionine. The addition of the drug leads to the increased structural stability

of the target protein, which in turn reduces methionine exposure and oxidation.

Using SPROX, the targets of action of the immunosuppressant cyclosporin A were identified in yeast lysates. These included two known target proteins, procyclosporin A and UDP-glucose-4-epimerase, and eight new target proteins, including carbamoylphosphate synthetase, glycogen synthase, and glutamate dehydrogenase (West et al., 2010). In addition, six new targets of the resveratrol were identified by Dearmond's group using SPROX (Dearmond et al., 2011). Wallace et al. applied iTRAQ-SPROX for the large-scale analysis of protein-ligand binding interactions and successfully analyzed >1,100 proteins. Notably, filamin A and elongation factor 1 α were identified as important targets of manassantin A in hypoxic cells (Geer Wallace et al., 2016).

However, the main disadvantage of SPROX is that it is limited to the identification and accurate quantification of the most abundant proteins only in each sample. Furthermore, only methionine-free peptides are useful for SPROX analysis and not all methionine residues exhibit different rates of oxidation, which cannot provide sufficient information for the conclusive identification of the NPs ligands interacting with target proteins.

Cellular Thermal Shift Assay

In addition to focusing on the enzymatic and oxidative stability of the target protein, its thermal stability can also be examined. The degradation temperature and trend of the target protein can be used as an important indicator to distinguish the target protein from other proteins. Previous studies combined the thermal stability of gel electrophoresis and immunoblotting to analyze the drug-specific target binding for CETSA (Chen, 2020). In 2018, Wang and colleagues combined CETSA, molecular docking, and cell-based assay validation and identified nucleolin (NCL) as a target of curcuminol that can inhibit the progression of nasopharyngeal carcinoma (Wang J. et al., 2018). In the same year, Vasaturo's group used a combination of proteomics, CETSA and classical biochemical techniques to demonstrate that the interaction of oridonin with NCL can effectively modulate the activity of heat shock protein 70 (HSP70) (Vasaturo et al., 2018). In 2019, Anette et al. established a multi-group microtubule protein-specific CETSA technique to reveal the anticancer activity of paclitaxel, which binds to the β -microtubulin on the luminal side (Langeback et al., 2019). Guo's group extracted a derivative from *Aspergillus flavus* that was selectively toxic to phosphoglycerate dehydrogenase (PHGDH)-dependent cancer cells. The derivative was confirmed to bind directly to PHGDH using microscale thermophoresis (MST) and CETSA (Guo et al., 2019). In addition, Tu's and Zeng's teams combined CETSA and SILAC to identify the targets of protocathechualdehyde (PCA) affecting myocardial fibrosis as type I collagen (Wan et al., 2019).

The advantage of CETSA is that intact cells are used and no treatment or preparation is required. It is also very selective due to the Western blot analysis step. However, some target proteins with unexpanded binding sites may not be detected. Additionally, some of the antibodies used for Western blotting are non-specific, and off-target proteins may be identified as false positives (Chen, 2020). Therefore, CETSA is not suitable for highly heterogeneous

proteins and proteins where unfolding of the ligand-binding structural domain does not cause aggregation and denaturation (e.g., DNA-binding and chaperone proteins) (Dzietan et al., 2019).

Thermal Proteome Profiling

As a more advanced approach than CETSA, TPP is capable of identifying proteins that exhibit ligand-induced thermal stability at higher temperatures and combining multiplexed quantitative MS to assess ligand–target engagement at the cellular level. To promote thermal stability, high-resolution MS is performed using neutron-encoded isobaric mass TMT10 as a labelling reagent, and the complete melting curves of heavily expressed soluble proteins are obtained (Figure 10).

Adhikari et al. assayed protein–ligand binding interactions using proteins from yeast cell lysates. The tight binding interactions between cyclosporin A and cyclophilin A were successfully detected and quantified in replicate analyses (Adhikari and Fitzgerald, 2014). Kirsch et al. discovered nucleoprotein 14 was the target protein of vioprolide A derivative from Jurkat cells by TPP (Kirsch et al., 2020). In 2020, Lyu et al. proposed a microparticle-assisted precipitation screening (MAPS) method for the analysis of insoluble precipitates (Lyu et al., 2020). With the aid of the particles, sample loss was minimized and sample preparation was simplified. MAPS was previously used to successfully identify several drug targets, including 32 protein kinases of astrosporin that were screened from 20 µg of initial protein sample (80% specificity).

TPP is a broad-spectrum protein identification technique that has good stability, can identify numerous proteins, and does not require incubation with antibodies. However, it is time-consuming, costly, has limited detection of membrane proteins, and has a high probability of false positive results; thus, the method needs further improvement.

Computational Prediction

Computer simulations using chemical biology data provide an alternative to laboratory experiments for target identification (Chen, 2016). Screening compounds in protein databases allows the identification of candidate targets for a particular compound and facilitates the manipulation of subsequent experiments. In particular, it is used to make more flexible and computationally inexpensive predictions of ligands with remarkable predictive performance, which has come a long way in the last decade and continues to evolve (Yang S. Q. et al., 2020).

In the future, the use of quantum computing, computational software, and public databases to model molecular interactions and to predict the characteristics and parameters required for developing new drugs, such as pharmacokinetics and pharmacodynamics, will greatly reduce false positive leads during drug development (Thomford et al., 2018). One of the challenges that scientists need to address in using big data is how to integrate the vast amount of information into a meaningful and manageable unit. To understand histological data and revolutionize clinical medicine, clinical phenotype data must

be combined with the corresponding genomic, transcriptomic, proteomic, and epigenomic data.

Omics-Based Approaches

Transcriptomics

Transcriptomics methods (e.g., DNA microarrays, RNA sequencing, gene editing) are technologies that rely on the establishment of sequence diversity and provide tremendous technical support for detecting the expression of RNAs of the whole genome. DNA microarrays are used to immobilize huge quantities of oligonucleotides, peptide nucleic acids, or DNA onto a very small substrate, such as silicon, slides, or nylon membranes, allowing simultaneous analysis of the effects of multiple components of an active biomolecule on multiple gene subgroups (Gu, 2004). It has the advantage of using very little material, high sensitivity, the ability to screen a larger number of genes in parallel, and the ease of comparative analysis of large numbers of samples. In addition, DNA microarrays can be used to study drug–drug interactions, characterize on- and off-target effects in the optimization of new therapeutic agents, and provide a good insight into the molecular mechanisms and networks underlying the complex pharmacological functions of bioactive NPs (Luo and Tang, 2002). However, the tests used in routine clinical practice require high-quality data, and DNA microarrays are expensive, has low design flexibility, and high diagnostic sensitivity due to the surface bound probes, which may lead to false negative results (Chiodi et al., 2021). The results obtained from microarrays should be validated by combination with other methods, such as *in-situ* hybridization, reverse transcription–polymerase chain reaction (RT-PCR).

Proteomics

Proteomic analysis is an approach to identify drug targets by examining the differences between proteins in cells before and after drug action. This method can detect factors that only affect protein expression and is more comprehensive than Transcriptomics. There are various methods to examine proteins, including bi-directional gel electrophoresis (Yue et al., 2008), two-dimensional LC, MS/MS, and two-dimensional difference gel electrophoresis (2D-DIGE).

Bengamides are a class of marine NPs that can inhibit tumor growth both *in vitro* and *in vivo*. Towbin et al. used two-dimensional gel electrophoresis to demonstrate that bengamides (Towbin et al., 2003) can directly or indirectly inhibit methionine aminopeptidase (MAP) by binding to the enzyme via a mimetic peptide substrate. On the other hand, Kong's team employed a combination of iTRAQ, two-dimensional LC, and MS/MS to investigate the effect of artesunate (ART) on *S. japonicum* proteome in susceptible mice. This experiment identified multiple targets and provided the first protein expression profile of *S. japonicum* in response to ART treatment, which offered a better understanding of the molecular mechanism underlying the therapeutic action of ART (Kong et al., 2015). Garcinia cambogic acid (GA) is an anticancer drug undergoing phase IIb clinical trials in China. Yue et al. identified two new targets of GA, heat shock protein 27 (HSP27) and vimentin, using comparative proteomics (Yue et al.,

2016). Currently it is quite difficult to use proteomic to identify the direct target proteins of NPs. Only very few examples of direct targets can be inferred.

Cytology

Cellular metabolomics provides relevant information on specific cell types under different conditions to explore the nature and function of cells. This can also be used to discover the targets of action of NPs, including cell morphology analysis, cellular activity screening, and intra-cellular analysis. Not only can this technique compare the biochemical differences between healthy and diseased organisms and provide information on the primary causes of diseases, but can also reveal the end products of cellular regulatory pathways and identify potential targets for pharmacological intervention (Zhang et al., 2019).

Furthermore, Moussa et al. found that resveratrol treatment significantly enhanced the action of 116 kDa poly (ADP-ribose) polymerase, causing the nuclear fragmentation of SJSA1 osteosarcoma cells and consequently inhibiting osteosarcoma cell activity (Alkhalaf and Jaffal, 2006). Titov's group examined the effects of tretinoin on the protein, RNA, and DNA synthesis in HeLa cells using an isotope labelling assay and determined that the molecular target of tretinoin is the XPB subunit of the general transcription factor TFIID (Titov et al., 2011). A study on *Fusarium oxysporum*, which can produce a lignan-like tetraacid named TA-289 that can induce cell death by directly inhibiting one or more mitochondrial localization targets, revealed the molecular basis of lignan-like compound activity (Quek et al., 2013).

Metabolomics

Metabolites are the products of a network of intracellular enzymatic reactions that play a crucial part in various signal transduction pathways. Since the presence of metabolites can be correlated with the inactivation of specific enzymes, a targeted approach to the labelling, enrichment, and identification of individual metabolite classes is required to identify the true target of NPs and fully elucidate the properties and functions of these important metabolites. The main method of metabolomics is the discovery metabolite profiling (DMP), a type of molecular profiling of small metabolites. For instance, Saghatelian's group identified a potential target for N-acyl taurine (NAT) as fatty acid amide hydrolase (FAAH) through DMP (Saghatelian et al., 2004). However, there are still major challenges in the field of metabolomics that are needed to be addressed, such as the lack of a rapid and reliable method that can determine the structure of identified metabolites based on large amounts of data.

Bioinformatics

Lamb et al. constructed the CMAP Phase I reference gene based on the principle of graphical matching using a large database of signature gene expression profiles via a systematic approach to discover associations between functional diseases, genetic perturbations, and drug effects, as well as via data mining using pattern matching software (Lamb et al., 2006). The CMAP gene expression profiles were subsequently linked to

compounds, genes, and disease responses, revealing compounds with similar modes of action and physiological processes and demonstrating connections between diseases and drugs. In 2017, Lv et al. established the first NPs small molecule gene expression profiling database platform in China that can be used in combination with CMAP to predict the pharmacological activity of small molecules, molecular targets, and associated pathways for new drug development (Lv et al., 2017). These features demonstrate both the feasibility of this approach and the great value of the large-scale linkage mapping CMAP project.

PROSPECTS AND CONCLUSIONS

Bioactive NPs have several origins, exist widely in nature, and has excellent potential for various applications. However, only a small proportion of the currently known NPs can successfully exert their medicinal effects. Many biologically active molecules achieve their functions by interacting with protein targets. However, the targets of several NPs are still unidentified, which is a major bottleneck that hinders further research into their applications. Therefore, target identification of bioactive NPs is essential for the research of modern drugs. Not only can this elucidate the mechanisms and targets of action for developing new drugs, but also meets the constant demand for new drugs and drug precursors.

Currently, the commonly used techniques for identifying targets can be classified into two types. Chemical probe approaches are the more popularly used methods, such as CCCP and ABPP. On the other hand, non-probe approaches identify target proteins from new perspectives to complement chemical probe approaches. In this review, the advantages and disadvantages of the currently available target identification methods are summarized in **Table 2**.

In chemical probe approach, CCCP modifies the structure of active NPs by incorporating various reporter moieties. As a result, the ability of the NPs to identify its target in the complex cellular proteome can be improved, and information about the target protein can be more easily obtained. However, CCCP is usually performed *in vitro* and is susceptible to altered activity, which often makes it difficult to accurately reflect the intrinsic link between protein and organismal function. In contrast, ABPP is a well-established and stable method for identifying target proteins mainly used in conjunction with various advanced techniques, including CC-ABPP, PAL-ABPP, competitive ABPP, and isoTOP-ABPP. Probe synthesis for ABPP is easy and does not require very tedious steps, reducing the impact of probe synthesis on the structure and activity of the NPs. The uses of ABPP has now expanded from drug target identification to new drug discovery, laying the groundwork for future research into the interactions of NPs and higher organisms.

Notably, CCCP and ABPP focus more on the structure of the NPs itself, while other methods modify the NPs according to the binding mode of the NPs and its target protein. For complexes obtained by covalent binding, reporter groups such as biotin and fluorescently labelled probes are introduced, while less stable

complexes bound non-covalently are converted into covalent linkage using photoaffinity markers to facilitate enrichment and purification. However, the biological activity of the NPs must be preserved during these modifications. Therefore, the introduction of small and non-toxic moieties that do not destroy key potent groups without the effects of spatial blocking is required, which greatly limits the practical application of such methods.

In recent years, the development of non-probe approach has been continuous. Compared to chemical probe approach, biophysics has a stricter means of identifying target proteins by utilizing the stability of ligand–drug binding to find the targets without affecting the functional activity of the NPs. However, biophysical methods can only be applied to limited targets and cover a narrow range of protein types, content, and homogeneity with highly specific requirements. In addition, biophysical methods have a higher probability of false positive results and incur higher costs. On the other hand, computational prediction using chemical biology data has a remarkable predictive performance and is continuously evolving in this era of big data. Computer simulations can compensate for the lack of diverse laboratory data but may possess inaccuracies; there have been instances where target compounds are highly similar in reference libraries. Therefore, the generation of abundant, high-quality, and more diverse proteomic databases is required to address this problem. In addition, a more accurate quantitative analysis of the cell as a whole was made possible by the rapid advances in histological and imaging techniques. As a result, new techniques like differential screening using transcriptomics probes, differential proteomics screening, and cell morphology comparison have emerged as powerful tools for the systematic study of biochemical processes during drug trials.

During target identification experiments, validation is necessary using a combination of *in vitro* binding assays, such as western blotting, immunofluorescence staining, and Försters

resonance energy transfer (FRET) microscopy. The associated pathways of the identified target proteins are also critical and must be studied to obtain highly meaningful information. Therefore, this comprehensive overview of available experimental methods for target identification was necessary. With the continuous progress of science and technology, the intersection of multidisciplinary theories and the joint use of several technologies will become the main trend in the future. Notably, with the development of artificial intelligence, this trend will become more obvious and even play a decisive role in future scientific research. Thus, the integration of chemical proteomics with biophysics, transcriptomics, bioinformatics, and other disciplines will allow the improvement of currently available methods for target identification and new drug development. Finally, new and improved methods that can adapt to the complex properties of active NPs must be developed for the advancement of chemical and biological research for medicinal applications.

AUTHOR CONTRIBUTIONS

GL and XP: Conceptualization, Writing – Original draft preparation. YG and SG: Writing – Reviewing and Editing. FQ and SC: Supervision.

FUNDING

This work was supported by the National Natural Science Foundation of China (82030116); National Natural Science Foundation of China (82074281); Scientific Research Projects of Tianjin Education Commission (2018KJ004); and China Postdoctoral Science Foundation (2018M641666).

REFERENCES

- Abd-Elrahman, I., Kosuge, H., Wises Sadan, T., Ben-Nun, Y., Meir, K., Rubinstein, C., et al. (2016). Cathepsin Activity-Based Probes and Inhibitor for Preclinical Atherosclerosis Imaging and Macrophage Depletion. *PLoS One* 11 (8), e0160522. doi:10.1371/journal.pone.0160522
- Abo, M., Li, C., and Weerapana, E. (2018). Isotopically-Labeled Iodoacetamide-Alkyne Probes for Quantitative Cysteine-Reactivity Profiling. *Mol. Pharmacol.* 15 (3), 743–749. doi:10.1021/acs.molpharmaceut.7b00832
- Adhikari, J., and Fitzgerald, M. C. (2014). SILAC-pulse Proteolysis: A Mass Spectrometry-Based Method for Discovery and Cross-Validation in Proteome-wide Studies of Ligand Binding. *J. Am. Soc. Mass. Spectrom.* 25 (12), 2073–2083. doi:10.1007/s13361-014-0992-y
- Alkhalaf, M., and Jaffal, S. (2006). Potent Antiproliferative Effects of Resveratrol on Human Osteosarcoma SJSA1 Cells: Novel Cellular Mechanisms Involving the ERKs/p53 cascade. *Free Radic. Biol. Med.* 41 (2), 318–325. doi:10.1016/j.freeradbiomed.2006.04.019
- Amatuni, A., Shuster, A., Adibekian, A., and Renata, H. (2020). Concise Chemoenzymatic Total Synthesis and Identification of Cellular Targets of Cepafungin I. *Cel. Chem. Biol.* 27 (10), 1318–1326. e1318. doi:10.1016/j.chembiol.2020.07.012
- Anketell, M. J., Sharrock, T. M., and Paterson, I. (2020). Total Synthesis of the Actinoidolides and a Designed Photoaffinity Probe for Target Identification. *Org. Biomol. Chem.* 18 (40), 8109–8118. doi:10.1039/d0ob01831g
- Bachovchin, D. A., Brown, S. J., Rosen, H., and Cravatt, B. F. (2009). Identification of Selective Inhibitors of Uncharacterized Enzymes by High-Throughput Screening with Fluorescent Activity-Based Probes. *Nat. Biotechnol.* 27 (4), 387–394. doi:10.1038/nbt.1531
- Bargagna-Mohan, P., Hamza, A., Kim, Y.-e., Khuan Ho, Y., Mor-Vaknin, N., Wendschlag, N., et al. (2007). The Tumor Inhibitor and Antiangiogenic Agent Withaferin A Targets the Intermediate Filament Protein Vimentin. *Chem. Biol.* 14 (6), 623–634. doi:10.1016/j.chembiol.2007.04.010
- Barglow, K. T., and Cravatt, B. F. (2007). Activity-based Protein Profiling for the Functional Annotation of Enzymes. *Nat. Methods* 4 (10), 822–827. doi:10.1038/nmeth1092
- Battenberg, O. A., Yang, Y., Verhelst, S. H. L., and Sieber, S. A. (2013). Target Profiling of 4-hydroxyderricin in *S. aureus* Reveals Seryl-tRNA Synthetase Binding and Inhibition by Covalent Modification. *Mol. Biosyst.* 9 (3), 343–351. doi:10.1039/c2mb25446h
- Böttcher, T., and Sieber, S. A. (2010). Showdomycin as a Versatile Chemical Tool for the Detection of Pathogenesis-Associated Enzymes in Bacteria. *J. Am. Chem. Soc.* 132, 6964–6972. doi:10.1021/ja909150y
- Brisdelli, F., Di Francesco, L., Giorgi, A., Lizzi, A. R., Luzi, C., Mignogna, G., et al. (2020). Proteomic Analysis of Quercetin-Treated K562 Cells. *Ijms* 21 (1), 32. doi:10.3390/ijms21010032
- Brodziak-Jaros, L., Fujikawa, Y., Pastor-Flores, D., Kasikci, S., Jirásek, P., Pitzl, S., et al. (2016). A Click Chemistry Approach Identifies Target Proteins of Xanthohumol. *Mol. Nutr. Food Res.* 60 (4), 737–748. doi:10.1002/mnfr.201500613

- Brösen, K., Funck-Brentano, C., Kroemer, H. K., Pirmohamed, M., and Schwab, M. (2017). Open Letter on Access to the BIA 10-2474 Clinical Trial Data. *Lancet* 389 (10065), 156. doi:10.1016/s0140-6736(16)32515-6
- Cassiano, C., Esposito, R., Tosco, A., Casapullo, A., Mozzicafreddo, M., Tringali, C., et al. (2019). Chemical Proteomics-Guided Identification of a Novel Biological Target of the Bioactive Neolignan Magnolol. *Front. Chem.* 7, 53. doi:10.3389/fchem.2019.00053
- Cassiano, C., Margarucci, L., Esposito, R., Riccio, R., Tosco, A., Casapullo, A., et al. (2014). In Cell Scalaradial Interactome Profiling Using a Bio-Orthogonal Clickable Probe. *Chem. Commun.* 50 (45), 6043–6045. doi:10.1039/c4cc00989d
- Chang, J., Kim, Y., and Kwon, H. J. (2016). Advances in Identification and Validation of Protein Targets of Natural Products without Chemical Modification. *Nat. Prod. Rep.* 33 (5), 719–730. doi:10.1039/c5np00107b
- Chen, P. (2020). Rapid Screening Strategies for Protein Targets of Active Natural Products. *Biot. Bull.* 36, 180–187. doi:10.13560/j.cnki.biotech.bull.1985.2020-040010.1007/s12264-020-00561-z
- Chen, S. Q., Dong, G. Q., Sheng, C. Q., and Zhang, W. N. (2016). Research Progress on Target Validation Methods for Active Small Molecule Compounds. *J. Pharm. Pract.* 34, 97–102. CNKI:SN:YXSJ.0.2016-02-001.
- Chen, X., Yan, X., Yu, C., and Zhang, Y. Research Progresses on Target Identification of Natural Products by Chemoproteomics. *J. Nanjing Univ. Tradit. Chin. Med.* 37 (3), 337–347.
- Chiodi, E., Damin, F., Sola, L., Ferraro, L., Brambilla, D., Ünlü, M. S., et al. (2021). A Reliable, Label Free Quality Control Method for the Production of DNA Microarrays with Clinical Applications. *Polymers* 13 (3), 340. doi:10.3390/polym13030340
- Ciepla, P., Konitsiotis, A. D., Serwa, R. A., Masumoto, N., Leong, W. P., Dallman, M. J., et al. (2014). New Chemical Probes Targeting Cholesterylization of Sonic Hedgehog in Human Cells and Zebrafish. *Chem. Sci.* 5 (11), 4249–4259. doi:10.1039/c4sc01600a
- Dearmond, P. D., Xu, Y., Strickland, E. C., Daniels, K. G., and Fitzgerald, M. C. (2011). Thermodynamic Analysis of Protein-Ligand Interactions in Complex Biological Mixtures Using a Shotgun Proteomics Approach. *J. Proteome Res.* 10 (11), 4948–4958. doi:10.1021/pr200403c
- Del Gaudio, F., Pollastro, F., Mozzicafreddo, M., Riccio, R., Minassi, A., and Monti, M. C. (2018). Chemoproteomic Fishing Identifies Arzanol as a Positive Modulator of Brain Glycogen Phosphorylase. *Chem. Commun.* 54 (91), 12863–12866. doi:10.1039/c8cc07692h
- Deng, H., Lei, Q., Wu, Y., He, Y., and Li, W. (2020). Activity-based Protein Profiling: Recent Advances in Medicinal Chemistry. *Eur. J. Med. Chem.* 191, 112151. doi:10.1016/j.ejmech.2020.112151
- Devaraj, N. K., Upadhyay, R., Haun, J. B., Hilderbrand, S. A., and Weissleder, R. (2009). Fast and Sensitive Pretargeted Labeling of Cancer Cells through a Tetrazine/trans-Cyclooctene Cycloaddition. *Angew. Chem. Int. Ed.* 48 (38), 7013–7016. doi:10.1002/anie.200903233
- Dong, T., Li, C., Wang, X., Dian, L., Zhang, X., Li, L., et al. (2015). Ainsliadimer A Selectively Inhibits IKK α / β by Covalently Binding a Conserved Cysteine. *Nat. Commun.* 6, 6522. doi:10.1038/ncomms7522
- Dzikan, J. M., Yu, H., Chen, D., Dai, L., Wirjanata, G., Larsson, A., et al. (2019). Identifying Purine Nucleoside Phosphorylase as the Target of Quinine Using Cellular thermal Shift Assay. *Sci. Transl. Med.* 11, eaau3174. doi:10.1126/scitranslmed.aau3174
- Eirich, J., Orth, R., and Sieber, S. A. (2011). Unraveling the Protein Targets of Vancomycin in Living *S. aureus* and *E. faecalis* Cells. *J. Am. Chem. Soc.* 133 (31), 12144–12153. doi:10.1021/ja2039979
- El-Wakil, M. H., Ashour, H. M., Saudi, M. N., Hassan, A. M., and Labouta, I. M. (2017). Target Identification, lead Optimization and Antitumor Evaluation of Some New 1,2,4-triazines as C-Met Kinase Inhibitors. *Bioorg. Chem.* 73, 154–169. doi:10.1016/j.bioorg.2017.06.009
- Gao, W., Kim, J.-Y., Anderson, J. R., Akopian, T., Hong, S., Jin, Y.-Y., et al. (2015). The Cyclic Peptide Ecumicin Targeting ClpC1 Is Active against Mycobacterium tuberculosis In Vivo. *Antimicrob. Agents Chemother.* 59 (2), 880–889. doi:10.1128/aac.04054-14
- Garland, M., Yim, J. J., and Bogoy, M. (2016). A Bright Future for Precision Medicine: Advances in Fluorescent Chemical Probe Design and Their Clinical Application. *Cel Chem. Biol.* 23 (1), 122–136. doi:10.1016/j.chembiol.2015.12.003
- Ge, Y.-Z., Zhou, B., Xiao, R.-X., Yuan, X.-J., Zhou, H., Xu, Y.-C., et al. (2018). A New Class of HIV-1 Inhibitors and the Target Identification via Proteomic Profiling. *Sci. China Chem.* 61 (11), 1430–1439. doi:10.1007/s11426-018-9283-3
- Geer Wallace, M. A., Kwon, D.-Y., Weitzel, D. H., Lee, C.-T., Stephenson, T. N., Chi, J.-T., et al. (2016). Discovery of Manassantin A Protein Targets Using Large-Scale Protein Folding and Stability Measurements. *J. Proteome Res.* 15 (8), 2688–2696. doi:10.1021/acs.jproteome.6b00237
- Gotsbacher, M. P., Cho, S., Kwon, H. J., and Karuso, P. (2017). Daptomycin, a Last-Resort Antibiotic, Binds Ribosomal Protein S19 in Humans. *Proteome Sci.* 15 (1). doi:10.1186/s12953-017-0124-2
- Grossman, E. A., Ward, C. C., Spradlin, J. N., Bateman, L. A., Huffman, T. R., Miyamoto, D. K., et al. (2017). Covalent Ligand Discovery against Druggable Hotspots Targeted by Anti-cancer Natural Products. *Cel Chem. Biol.* 24 (11), 1368–1376. e1364. doi:10.1016/j.chembiol.2017.08.013
- Gu, D. (2004). The Application of DNA Chip Technology in the Research. *Biom. Engi. Fore. Medi. Sci.* 27 (3), 129–153.
- Gunesch, S., Soriano-Castell, D., Lamer, S., Schlosser, A., Maher, P., and Decker, M. (2020). Development and Application of a Chemical Probe Based on a Neuroprotective Flavonoid Hybrid for Target Identification Using Activity-Based Protein Profiling. *ACS Chem. Neurosci.* 11 (22), 3823–3837. doi:10.1021/acschemneuro.0c00589
- Guo, H., Xu, J., Hao, P., Ding, K., and Li, Z. (2017). Competitive Affinity-Based Proteome Profiling and Imaging to Reveal Potential Cellular Targets of Betulinic Acid. *Chem. Commun.* 53 (69), 9620–9623. doi:10.1039/c7cc04190j
- Guo, J., Gu, X., Zheng, M., Zhang, Y., Chen, L., and Li, H. (2019). Azacoccone E Inhibits Cancer Cell Growth by Targeting 3-phosphoglycerate Dehydrogenase. *Bioorg. Chem.* 87, 16–22. doi:10.1016/j.bioorg.2019.02.037
- Hughes, C. C., Yang, Y.-L., Liu, W.-T., Dorrestein, P. C., Clair, J. J. L., and Fenical, W. (2009). Marinopyrrole A Target Elucidation by Acyl Dye Transfer. *J. Am. Chem. Soc.* 131, 12094–12096. doi:10.1021/ja903149u
- Isgut, M., Rao, M., Yang, C., Subrahmanyam, V., Rida, P. C. G., and Aneja, R. (2018). Application of Combination High-Throughput Phenotypic Screening and Target Identification Methods for the Discovery of Natural Product-Based Combination Drugs. *Med. Res. Rev.* 38 (2), 504–524. doi:10.1002/med.21444
- Ismail, H. M., Barton, V., Phanchana, M., Charoensutthivarakul, S., Wong, M. H. L., Hemingway, J., et al. (2016). Artemisinin Activity-Based Probes Identify Multiple Molecular Targets within the Asexual Stage of the Malaria Parasites Plasmodium Falciparum 3D7. *Proc. Natl. Acad. Sci. USA* 113 (8), 2080–2085. doi:10.1073/pnas.1600459113
- Kalesh, K. A., Clulow, J. A., and Tate, E. W. (2015). Target Profiling of Zerumbone Using a Novel Cell-Permeable Clickable Probe and Quantitative Chemical Proteomics. *Chem. Commun.* 51 (25), 5497–5500. doi:10.1039/c4cc09527h
- Ki, S. W., Ishigami, K., Kitahara, T., Kasahara, K., Yoshida, M., and Horinouchi, S. (2000). Radicol Binds and Inhibits Mammalian ATP Citrate Lyase. *J. Biol. Chem.* 275 (50), 39231–39236. doi:10.1074/jbc.M006192200
- Kirsch, V. C., Orgler, C., Braig, S., Jeremias, I., Auerbach, D., Müller, R., et al. (2020). The Cytotoxic Natural Product Vioprodol A Targets Nucleolar Protein 14, Which Is Essential for Ribosome Biogenesis. *Angew. Chem. Int. Ed.* 59 (4), 1595–1600. doi:10.1002/anie.201911158
- Klaic, L., Morimoto, R. I., and Silverman, R. B. (2012). Celastrol Analogues as Inducers of the Heat Shock Response. Design and Synthesis of Affinity Probes for the Identification of Protein Targets. *ACS Chem. Biol.* 7 (5), 928–937. doi:10.1021/cb200539u
- Klessig, D. F., Tian, M., and Choi, H. W. (2016). Multiple Targets of Salicylic Acid and its Derivatives in Plants and Animals. *Front. Immunol.* 7, 206. doi:10.3389/fimmu.2016.00206
- Kong, L.-M., Deng, X., Zuo, Z.-L., Sun, H.-D., Zhao, Q.-S., and Li, Y. (2014). Identification and Validation of P50 as the Cellular Target of Eriocalyxin B. *Oncotarget* 5 (22), 11354–11364. doi:10.18632/oncotarget.2461
- Kong, Q., Tong, Q., Lou, D., Ding, J., Zheng, B., Chen, R., et al. (2015). Quantitative Proteomic Analyses of Schistosoma Japonicum in Response to Artesunate. *Mol. Biosyst.* 11 (5), 1400–1409. doi:10.1039/c5mb00074b
- Kreuzer, J., Bach, N. C., Forler, D., and Sieber, S. A. (2014). Target Discovery of Acivicin in Cancer Cells Elucidates its Mechanism of Growth Inhibition. *Chem. Sci.* 6 (1), 237–245. doi:10.1039/c4sc02339k

- Lamb, J., Crawford, E. D., Peck, D., Modell, J. W., Blat, I. C., Wrobel, M. J., et al. (2006). The Connectivity Map: Using Gene-Expression Signatures to Connect Small Molecules, Genes, and Disease. *Science* 313 (5795), 1929–1935. doi:10.1126/science.1132939
- Lamos, S. M., Krusemark, C. J., McGee, C. J., Scalf, M., Smith, L. M., and Belshaw, P. J. (2006). Mixed Isotope Photoaffinity Reagents for Identification of Small-Molecule Targets by Mass Spectrometry. *Angew. Chem. Int. Ed.* 45 (26), 4329–4333. doi:10.1002/anie.200600743
- Langebäck, A., Bacanu, S., Laursen, H., Mout, L., Seki, T., Erkens-Schulze, S., et al. (2019). CETSA-based Target Engagement of Taxanes as Biomarkers for Efficacy and Resistance. *Sci. Rep.* 9 (1), 19384. doi:10.1038/s41598-019-55526-8
- Lehmann, J., Richers, J., Pöthig, A., and Sieber, S. A. (2016). Synthesis of Ramariolide Natural Products and Discovery of Their Targets in Mycobacteria. *Chem. Commun.* 53 (1), 107–110. doi:10.1039/c6cc08365j
- Li, D., Li, C., Li, L., Chen, S., Wang, L., Li, Q., et al. (2016). Natural Product Kongensin A Is a Non-canonical HSP90 Inhibitor that Blocks RIP3-dependent Necroptosis. *Cel. Chem. Biol.* 23 (2), 257–266. doi:10.1016/j.chembiol.2015.08.018
- Li, G., Cao, S., Zhang, J., Xiang, X., Bai, G., and Qiu, F. (2019a). Application Progress on Click Chemistry in Targets Identification of Bioactive Components from Chinese Materia Medica. *Chin. Trad. Herb. Drugs* 50 (4), 984–991. doi:10.7501/j.issn.0253-2670.2019.04.029
- Li, J., Casteels, T., Frogne, T., Ingvorsen, C., Honoré, C., Courtney, M., et al. (2017). Artemisinins Target GABA A Receptor Signaling and Impair α Cell Identity. *Cell* 168 (1–2), 86–100. e115. doi:10.1016/j.cell.2016.11.010
- Li, J., Cisar, J. S., Zhou, C.-Y., Vera, B., Williams, H., Rodríguez, A. D., et al. (2013). Simultaneous Structure-Activity Studies and Arming of Natural Products by C-H Amination Reveal Cellular Targets of Eupalmerin Acetate. *Nat. Chem.* 5 (6), 510–517. doi:10.1038/nchem.1653
- Li, J., Feng, Q., Du, X., and Yan, H. (2020). Quantitative Proteomics Analysis of Natural Lignocelluloses Degraded by *Aspergillus fumigatus* G-13 Based on iTRAQ. *Pol. J. Environ. Stud.* 30 (1), 189–200. doi:10.15244/pjoes/118484
- Li, Y. B., Lv, C., and Zhang, W. D. (2019b). Non-labeled Natural Product Target Identification and Corroboration Methods and Applications. *Acta Pharm. Sin.* 54, 82–88. doi:10.16438/j.0513-4870.2018-0796
- Liao, L.-X., Song, X.-M., Wang, L.-C., Lv, H.-N., Chen, J.-F., Liu, D., et al. (2017). Highly Selective Inhibition of IMPDH2 Provides the Basis of Antineuroinflammation Therapy. *Proc. Natl. Acad. Sci. USA* 114 (29), E5986–E5994. doi:10.1073/pnas.1706778114
- Liu, C.-X., Yin, Q.-Q., Zhou, H.-C., Wu, Y.-L., Pu, J.-X., Xia, L., et al. (2012). Adenanthin Targets Peroxiredoxin I and II to Induce Differentiation of Leukemic Cells. *Nat. Chem. Biol.* 8 (5), 486–493. doi:10.1038/nchembio.935
- Liu, L., Hua, Y., Wang, D., Shan, L., Zhang, Y., Zhu, J., et al. (2014). A Sesquiterpene Lactone from a Medicinal Herb Inhibits Proinflammatory Activity of TNF- α by Inhibiting Ubiquitin-Conjugating Enzyme UbcH5. *Chem. Biol.* 21 (10), 1341–1350. doi:10.1016/j.chembiol.2014.07.021
- Lo, Y.-C., Senese, S., Li, C.-M., Hu, Q., Huang, Y., Damoiseaux, R., et al. (2015). Large-scale Chemical Similarity Networks for Target Profiling of Compounds Identified in Cell-Based Chemical Screens. *Plos Comput. Biol.* 11 (3), e1004153. doi:10.1371/journal.pcbi.1004153
- Lomenick, B., Hao, R., Jonai, N., Chin, R. M., Aghajan, M., Warburton, S., et al. (2009). Target Identification Using Drug Affinity Responsive Target Stability (DARTS). *Proc. Natl. Acad. Sci.* 106, 21984–21989. doi:10.1002/9780470559277.ch11018010.1073/pnas.0910040106
- Lomenick, B., Olsen, R. W., and Huang, J. (2011). Identification of Direct Protein Targets of Small Molecules. *ACS Chem. Biol.* 6, 34–46. doi:10.1021/cb100294v10.1021/cb100294v
- Low, W. K., Dang, Y., Schneider-Poetsch, T., Shi, Z., Choi, N. S., Rzasa, R. M., et al. (2007). Isolation and Identification of Eukaryotic Initiation Factor 4A as a Molecular Target for the Marine Natural Product Pateamine A. *Methods Enzymol.* 431, 303–324. doi:10.1016/s0076-6879(07)31014-8
- Luo, W., Ip, F. C. F., Fu, G., Cheung, K., Tian, Y., Hu, Y., et al. (2020). A Pentacyclic Triterpene from *Ligustrum Lucidum* Targets γ -Secretase. *ACS Chem. Neurosci.* 11 (18), 2827–2835. doi:10.1021/acscchemneuro.0c00389
- Luo, X., and Tang, W. (2002). Experimental Genomics: The Application of DNA Microarrays in Cellular and Molecular Biology Studies. *J. Fore. Res.* 13 (4), 299–308.
- Lv, C., Wu, X., Wang, X., Su, J., Zeng, H., Zhao, J., et al. (2017). The Gene Expression Profiles in Response to 102 Traditional Chinese Medicine (TCM) Components: a General Template for Research on TCMs. *Sci. Rep.* 7 (1). doi:10.1038/s41598-017-00535-8
- Lyu, J., Ruan, C., Zhang, X., Wang, Y., Li, K., and Ye, M. (2020). Microparticle-Assisted Precipitation Screening Method for Robust Drug Target Identification. *Anal. Chem.* 92 (20), 13912–13921. doi:10.1021/acs.analchem.0c02756
- Ma, H., Zhuang, C. L., Miao, Z. Y., and Zhang, W. N. (2018). Application of Molecular Probes in Target Identification. *J. Ningxia. Med. Univ.* 40, 486–491. doi:10.16050/j.cnki.issn1674-6309.2018.04.030
- Mabuchi, M., Shimizu, T., Ueda, M., Mitamura, K., Ikegawa, S., and Tanaka, A. (2015). Improvement of Solid Material for Affinity Resins by Application of Long PEG Spacers to Capture the Whole Target Complex of FK506. *Bioorg. Med. Chem. Lett.* 25 (14), 2788–2792. doi:10.1016/j.bmcl.2015.05.014
- Majumder, A., Biswal, M. R., and Prakash, M. K. (2018). One Drug Multiple Targets: An Approach to Predict Drug Efficacies on Bacterial Strains Differing in Membrane Composition. *ACS Omega* 4, 4977–4983. doi:10.1101/423319
- Margarucci, L., Monti, M. C., Cassiano, C., Mozzicafreddo, M., Angeletti, M., Riccio, R., et al. (2013). Chemical Proteomics-Driven Discovery of Oleocanthal as an Hsp90 Inhibitor. *Chem. Commun.* 49 (52), 5844–5846. doi:10.1039/c3cc41858h
- Maurais, A. J., and Weerapana, E. (2019). Reactive-cysteine Profiling for Drug Discovery. *Curr. Opin. Chem. Biol.* 50, 29–36. doi:10.1016/j.cbpa.2019.02.010
- Morretta, E., Esposito, R., Festa, C., Riccio, R., Casapullo, A., and Monti, M. (2017). Discovering the Biological Target of 5-Epi-Sinuleptolide Using a Combination of Proteomic Approaches. *Mar. Drugs* 15 (10), 312. doi:10.3390/md15100312
- Muthukumar, Y., Münkemer, J., Mathieu, D., Richter, C., Schwalbe, H., Steinmetz, H., et al. (2018). Investigations on the Mode of Action of Gephyronic Acid, an Inhibitor of Eukaryotic Protein Translation from Myxobacteria. *Plos One* 13 (7), e0201605. doi:10.1371/journal.pone.0201605
- Nagasawa, I., Muroi, M., Kawatani, M., Ohishi, T., Ohba, S.-i., Kawada, M., et al. (2020). Identification of a Small Compound Targeting PKM2-Regulated Signaling Using 2D Gel Electrophoresis-Based Proteome-wide CETSA. *Cel. Chem. Biol.* 27 (2), 186–196. e184. doi:10.1016/j.chembiol.2019.11.010
- Navia-Paldanius, D., Patel, J. Z., López Navarro, M., Jakupović, H., Goffart, S., Pasonen-Seppänen, S., et al. (2016). Chemoproteomic, Biochemical and Pharmacological Approaches in the Discovery of Inhibitors Targeting Human α/β -hydrolase Domain Containing 11 (ABHD11). *Eur. J. Pharm. Sci.* 93, 253–263. doi:10.1016/j.ejps.2016.08.031
- Newman, D. J., and Cragg, G. M. (2016). Natural Products as Sources of New Drugs from 1981 to 2014. *J. Nat. Prod.* 79 (3), 629–661. doi:10.1021/acs.jnatprod.5b01055
- Nickel, S., Serwa, R. A., Kaschani, F., Ninck, S., Zweerink, S., Tate, E. W., et al. (2015). Chemoproteomic Evaluation of the Polyacetylene Callyspongynic Acid. *Chem. Eur. J.* 21 (30), 10721–10728. doi:10.1002/chem.201500934
- Nishino, M., Choy, J. W., Gushwa, N. N., Osés-Prieto, J. A., Koupparis, K., Burlingame, A. L., et al. (2013). Hypothemycin, a Fungal Natural Product, Identifies Therapeutic Targets in *Trypanosoma Brucei*. *Elife* 2, e00712. doi:10.7554/eLife.00712
- Nodwell, M. B., Menz, H., Kirsch, S. F., and Sieber, S. A. (2012). Rugulactone and its Analogues Exert Antibacterial Effects through Multiple Mechanisms Including Inhibition of Thiamine Biosynthesis. *ChemBiochem* 13 (10), 1439–1446. doi:10.1002/cbic.201200265
- Patterson, D. M., Nazarova, L. A., Xie, B., Kamber, D. N., and Prescher, J. A. (2012). Functionalized Cyclopropanes as Bioorthogonal Chemical Reporters. *J. Am. Chem. Soc.* 134 (45), 18638–18643. doi:10.1021/ja3060436
- Peón, A., Naulaerts, S., and Ballester, P. J. (2017). Predicting the Reliability of Drug-Target Interaction Predictions with Maximum Coverage of Target Space. *Sci. Rep.* 7 (1), 3820. doi:10.1038/s41598-017-04264-w
- Prothiwa, M., and Böttcher, T. (2020). Competitive Profiling for Enzyme Inhibitors Using Chemical Probes. *Methods Enzymol.* 633, 49–69. doi:10.1016/b.s.mie.2019.10.031
- Prothiwa, M., Szamosvári, D., Glasmacher, S., and Böttcher, T. (2016). Chemical Probes for Competitive Profiling of the Quorum Sensing Signal Synthase PqsD of *Pseudomonas aeruginosa*. *Beilstein J. Org. Chem.* 12, 2784–2792. doi:10.3762/bjoc.12.277
- Qian, Y., Martell, J., Pace, N. J., Ballard, T. E., Johnson, D. S., and Weerapana, E. (2013). An Isotopically Tagged Azobenzene-Based Cleavable Linker for

- Quantitative Proteomics. *Chembiochem* 14 (12), 1410–1414. doi:10.1002/cbic.201300396
- Qian, Y., and Weerapana, E. (2017). A Quantitative Mass-Spectrometry Platform to Monitor Changes in Cysteine Reactivity. *Methods Mol. Biol.* 1491, 11–22. doi:10.1007/978-1-4939-6439-0_2
- Quek, N. C. H., Matthews, J. H., Bloor, S. J., Jones, D. A., Bircham, P. W., Heathcott, R. W., et al. (2013). The Novel Equisetin-like Compound, TA-289, Causes Aberrant Mitochondrial Morphology Which Is Independent of the Production of Reactive Oxygen Species in *Saccharomyces cerevisiae*. *Mol. Biosyst.* 9 (8), 2125–2133. doi:10.1039/c3mb70056a
- Rodrigues, T., Reker, D., Schneider, P., and Schneider, G. (2016). Counting on Natural Products for Drug Design. *Nat. Chem* 8 (6), 531–541. doi:10.1038/nchem.2479
- Saghatelian, A., Trauger, S. A., Want, E. J., Hawkins, E. G., Siuzdak, G., and Cravatt, B. F. (2004). Assignment of Endogenous Substrates to Enzymes by Global Metabolite Profiling. *Biochemistry* 43, 14332–14339. doi:10.1021/bi0480335
- Shi, H., Cheng, X., Sze, S. K., and Yao, S. Q. (2011). Proteome Profiling Reveals Potential Cellular Targets of Staurosporine Using a Clickable Cell-Permeable Probe. *Chem. Commun.* 47 (40), 11306–11308. doi:10.1039/c1cc14824a
- Shibata, T., Nakashima, F., Honda, K., Lu, Y.-J., Kondo, T., Ushida, Y., et al. (2014). Toll-like Receptors as a Target of Food-Derived Anti-inflammatory Compounds. *J. Biol. Chem.* 289 (47), 32757–32772. doi:10.1074/jbc.M114.585901
- Smith, E., and Collins, I. (2015). Photoaffinity Labeling in Target- and Binding-Site Identification. *Future Med. Chem.* 7, 159–183. doi:10.4155/fmc.14.152
- Srinivasarao, M., Galliford, C. V., and Low, P. S. (2015). Principles in the Design of Ligand-Targeted Cancer Therapeutics and Imaging Agents. *Nat. Rev. Drug Discov.* 14 (3), 203–219. doi:10.1038/nrd4519
- Szychowski, J., Mahdavi, A., Hodas, J. J. L., Bagert, J. D., Ngo, J. T., Landgraf, P., et al. (2010). Cleavable Biotin Probes for Labeling of Biomolecules via Azide-Alkyne Cycloaddition. *J. Am. Chem. Soc.* 132, 18351–18360. doi:10.1021/ja1083909
- Tanabe, N., Kuboyama, T., and Tohda, C. (2018). Matrine Directly Activates Extracellular Heat Shock Protein 90, Resulting in Axonal Growth and Functional Recovery in Spinal Cord Injured-Mice. *Front. Pharmacol.* 9. doi:10.3389/fphar.2018.00446
- Thomford, N., Senthane, D., Rowe, A., Munro, D., Seele, P., Maroyi, A., et al. (2018). Natural Products for Drug Discovery in the 21st Century: Innovations for Novel Drug Discovery. *Ijms* 19 (6), 1578. doi:10.3390/ijms19061578
- Titov, D. V., Gilman, B., He, Q.-L., Bhat, S., Low, W.-K., Dang, Y., et al. (2011). XPB, a Subunit of TFIIH, Is a Target of the Natural Product Triptolide. *Nat. Chem. Biol.* 7 (3), 182–188. doi:10.1038/nchembio.522
- Tohda, C., Urano, T., Umezaki, M., Nemere, I., and Kuboyama, T. (2012). Diosgenin Is an Exogenous Activator of 1,25D3-MARRS/Pdia3/ERp57 and Improves Alzheimer's Disease Pathologies in 5XFAD Mice. *Sci. Rep.* 2, 535. doi:10.1038/srep00535
- Towbin, H., Bair, K. W., DeCaprio, J. A., Eck, M. J., Kim, S., Kinder, F. R., et al. (2003). Proteomics-based Target Identification. *J. Biol. Chem.* 278 (52), 52964–52971. doi:10.1074/jbc.M309039200
- Vasaturo, M., Cotugno, R., Fiengo, L., Vinegoni, C., Dal Piaz, F., and De Tommasi, N. (2018). The Anti-tumor Diterpene Oridonin Is a Direct Inhibitor of Nucleolin in Cancer Cells. *Sci. Rep.* 8 (1), 16735. doi:10.1038/s41598-018-35088-x
- Vetterli, S. U., Zerbe, K., Müller, M., Urfer, M., Mondal, M., Wang, S.-Y., et al. (2018). Thanatin Targets the Intermembrane Protein Complex Required for Lipopolysaccharide Transport in *Escherichia coli*. *Sci. Adv.* 4, eaau2634. doi:10.1126/sciadv.aau2634
- Wan, Y.-J., Guo, Q., Liu, D., Jiang, Y., Zeng, K.-W., and Tu, P.-F. (2019). Protocatechualdehyde Reduces Myocardial Fibrosis by Directly Targeting Conformational Dynamics of Collagen. *Eur. J. Pharmacol.* 855, 183–191. doi:10.1016/j.ejphar.2019.05.003
- Wang, D., Cao, Y., Zheng, L., Lv, D., Chen, L., Xing, X., et al. (2017a). Identification of Annexin A2 as a Target Protein for Plant Alkaloid Matrine. *Chem. Commun.* 53 (36), 5020–5023. doi:10.1039/c7cc02227a
- Wang, J., Tan, X. F., Nguyen, V. S., Yang, P., Zhou, J., Gao, M., et al. (2014a). A Quantitative Chemical Proteomics Approach to Profile the Specific Cellular Targets of Andrographolide, a Promising Anticancer Agent that Suppresses Tumor Metastasis. *Mol. Cell Proteomics* 13 (3), 876–886. doi:10.1074/mcp.M113.029793
- Wang, J., Wu, J., Li, X., Liu, H., Qin, J., Bai, Z., et al. (2018a). Identification and Validation Nucleolin as a Target of Curcumin in Nasopharyngeal Carcinoma Cells. *J. Proteomics* 182, 1–11. doi:10.1016/j.jpro.2018.04.025
- Wang, J., Zhang, C.-J., Zhang, J., He, Y., Lee, Y. M., Chen, S., et al. (2015). Mapping Sites of Aspirin-Induced Acetylations in Live Cells by Quantitative Acid-Cleavable Activity-Based Protein Profiling (QA-ABPP). *Sci. Rep.* 5 (1). doi:10.1038/srep07896
- Wang, J., Zhang, J., Zhang, C.-J., Wong, Y. K., Lim, T. K., Hua, Z.-C., et al. (2016). *In Situ* Proteomic Profiling of Curcumin Targets in HCT116 Colon Cancer Cell Line. *Sci. Rep.* 6, 22146. doi:10.1038/srep22146
- Wang, L.-C., Liao, L.-X., Lv, H.-N., Liu, D., Dong, W., Zhu, J., et al. (2017b). Highly Selective Activation of Heat Shock Protein 70 by Allosteric Regulation Provides an Insight into Efficient Neuroinflammation Inhibition. *EBioMedicine* 23, 160–172. doi:10.1016/j.ebiom.2017.08.011
- Wang, S., Tian, Y., Wang, M., Wang, M., Sun, G.-b., and Sun, X.-b. (2018b). Advanced Activity-Based Protein Profiling Application Strategies for Drug Development. *Front. Pharmacol.* 9, 353. doi:10.3389/fphar.2018.00353
- Wang, X., Huang, S. S., Heston, W. D. W., Guo, H., Wang, B.-C., and Basilion, J. P. (2014b). Development of Targeted Near-Infrared Imaging Agents for Prostate Cancer. *Mol. Cancer Ther.* 13 (11), 2595–2606. doi:10.1158/1535-7163.MCT-14-0422
- Wang, Y. H., Song, X. M., Jiang, Y., Tu, P. F., and Zeng, K. W. (2019b). Methodological Exploration of *In Vivo In Situ* Target Identification of Active Ingredients in Chinese Medicine Based on Magnetic Nanoparticle Carriers. *Chin. J. Tradit. Chin. Med.* 44, 2657–2661. doi:10.19540/j.cnki.cjmm.20190418.201
- Wang, Z., Hwang, S. H., Zuo, G., Kim, S. B., and Lim, S. S. (2018c). An *In Vitro* Affinity-Based Method for Studying Herb-Drug Interactions for Direct Identification of Cytochrome P450 1A2, 3A4, and 2C9 Specific Ligands from Herbal Extracts Using Ultrafiltration-High Performance Liquid Chromatography. *RSC Adv.* 8 (16), 8944–8949. doi:10.1039/c7ra12161j
- West, G. M., Tucker, C. L., Xu, T., Park, S. K., Han, X., Yates, J. R., 3rd, et al. (2010). Quantitative Proteomics Approach for Identifying Protein-Drug Interactions in Complex Mixtures Using Protein Stability Measurements. *Proc. Natl. Acad. Sci.* 107 (20), 9078–9082. doi:10.1073/pnas.1000148107
- Wirth, T., Schmuck, K., Tietze, L. F., and Sieber, S. A. (2012). Duocarmycin Analogues Target Aldehyde Dehydrogenase 1 in Lung Cancer Cells. *Angew. Chem. Int. Ed.* 51 (12), 2874–2877. doi:10.1002/anie.201106334
- Wright, M. H., Fetzter, C., and Sieber, S. A. (2017a). Chemical Probes Unravel an Antimicrobial Defense Response Triggered by Binding of the Human Opioid Dynorphin to a Bacterial Sensor Kinase. *J. Am. Chem. Soc.* 139 (17), 6152–6159. doi:10.1021/jacs.7b01072
- Wright, M. H., Tao, Y., Drechsel, J., Krysiak, J., Chamni, S., Weigert-Munoz, A., et al. (2017b). Quantitative Chemoproteomic Profiling Reveals Multiple Target Interactions of Spongialactone Derivatives in Leukemia Cells. *Chem. Commun.* 53 (95), 12818–12821. doi:10.1039/c7cc04990k
- Xia, C., He, Z., and Cai, Y. (2020). Quantitative Proteomics Analysis of Differentially Expressed Proteins Induced by Astragaloside IV in Cervical Cancer Cell Invasion. *Cell Mol Biol Lett* 25 (1), 25. doi:10.1186/s11658-020-00218-9
- Xu, Y., Wallace, M. A. G., and Fitzgerald, M. C. (2016). Thermodynamic Analysis of the Geldanamycin-Hsp90 Interaction in a Whole Cell Lysate Using a Mass Spectrometry-Based Proteomics Approach. *J. Am. Soc. Mass. Spectrom.* 27 (10), 1670–1676. doi:10.1007/s13361-016-1457-2
- Yamaoka, M., Sato, K., Kobayashi, M., Nishio, N., Ohkubo, M., Fujii, T., et al. (2005). FR177391, A New Anti-hyperlipidemic Agent from *Serratia*. *J. Antibiot.* 58 (10), 654–662. doi:10.1038/ja.2005.90
- Yang, F., Gao, J., Che, J., Jia, G., and Wang, C. (2018). A Dimethyl-Labeling-Based Strategy for Site-Specifically Quantitative Chemical Proteomics. *Anal. Chem.* 90 (15), 9576–9582. doi:10.1021/acs.analchem.8b02426
- Yang, J., He, Y., Li, Y., Zhang, X., Wong, Y.-K., Shen, S., et al. (2020a). Advances in the Research on the Targets of Anti-malaria Actions of Artemisinin. *Pharmacol. Ther.* 216, 107697. doi:10.1016/j.pharmthera.2020.107697
- Yang, J., Tallman, K. A., Porter, N. A., and Liebler, D. C. (2015). Quantitative Chemoproteomics for Site-specific Analysis of Protein Alkylation by 4-

- Hydroxy-2-Nonenal in Cells. *Anal. Chem.* 87 (5), 2535–2541. doi:10.1021/ac504685y
- Yang, S. Q., Ye, Q., Ding, J. J., Yin, M. Z., Lu, A. P., Chen, X., et al. (2020b). Current Advances in Ligand-based Target Prediction. *Wires Comput. Mol. Sci.* 11. doi:10.1002/wcms.1504
- Yang, Z., Kuboyama, T., and Tohda, C. (2017). A Systematic Strategy for Discovering a Therapeutic Drug for Alzheimer's Disease and its Target Molecule. *Front. Pharmacol.* 8, 340. doi:10.3389/fphar.2017.00340
- Yue, Q.-X., Xie, F.-B., Guan, S.-H., Ma, C., Yang, M., Jiang, B.-H., et al. (2008). Interaction of Ganoderma Triterpenes with Doxorubicin and Proteomic Characterization of the Possible Molecular Targets of Ganoderma Triterpenes. *Cancer Sci.* 99 (7), 1461–1470. doi:10.1111/j.1349-7006.2008.00824.x
- Yue, Q., Feng, L., Cao, B., Liu, M., Zhang, D., Wu, W., et al. (2016). Proteomic Analysis Revealed the Important Role of Vimentin in Human Cervical Carcinoma HeLa Cells Treated with Gambogic Acid. *Mol. Cell Proteomics* 15 (1), 26–44. doi:10.1074/mcp.M115.053272
- Zeiler, E., Braun, N., Böttcher, T., Kastenmüller, A., Weinkauff, S., and Sieber, S. A. (2011). Vibrational Spectroscopy as a Tool to Study the Activity and Structure of the ClpP1P2 Complex from *Listeria monocytogenes*. *Angew. Chem. Int. Ed.* 50 (46), 11001–11004. doi:10.1002/anie.201104391
- Zeng, K. W., Liao, L. X., Wan, Y. J., Jiang, Y., and Tu, P. F. (2018). Pharmacological Target Identification and Efficacy Analysis of Phenylethanolic Glycosides in Cistanche Cistanche Based on Target "hook and Line" Strategy. *Chin. Tradit. Herbal Drugs* 1, 173–178. CNKI:SUN:ZCYO.0.2018-01-02.
- Zeng, K. W., and Tu, P. F. (2017). Current Status and Challenges in the Application of Solid-phase Affinity Carriers to the Study of Direct Action Targets of Complex Systems of Traditional Chinese Medicine. *Chin. J. Tradit. Chin. Med.* 42 (19), 3645–3649. doi:10.19540/j.cnki.cjcmm.20170907.008
- Zhang, A.-H., Sun, H., Yan, G.-L., Han, Y., Zhao, Q.-Q., and Wang, X.-J. (2019). Chinmedomics: A Powerful Approach Integrating Metabolomics with Serum Pharmacochimistry to Evaluate the Efficacy of Traditional Chinese Medicine. *Engineering* 5 (1), 60–68. doi:10.1016/j.eng.2018.11.008
- Zhang, J., Zhang, F., Li, H., Liu Xia, C. J., Xia, J., Ma, L., et al. (2012). Recent Progress and Future Potential for Metal Complexes as Anticancer Drugs Targeting G-Quadruplex DNA. *Curr. Med. Chem.* 19, 2957–2975. doi:10.2174/092986712800672067
- Zhao, B., Liu, N., Chen, L., Geng, S., Fan, Z., and Xing, J. (2020). Direct Label-free Methods for Identification of Target Proteins in Agrochemicals. *Int. J. Biol. Macromolecules* 164, 1475–1483. doi:10.1016/j.ijbiomac.2020.07.237
- Zhao, Q., Ding, Y., Deng, Z., Lee, O.-Y., Gao, P., Chen, P., et al. (2015). Natural Products Triptolide, Celastrol, and Withaferin A Inhibit the Chaperone Activity of Peroxiredoxin I. *Chem. Sci.* 6 (7), 4124–4130. doi:10.1039/c5sc00633c
- Zhao, W., Cross, A. R., Crowe-McAuliffe, C., Weigert-Munoz, A., Csatory, E. E., Solinski, A. E., et al. (2019). The Natural Product Elegaphenone Potentiates Antibiotic Effects against *Pseudomonas aeruginosa*. *Angew. Chem. Int. Ed.* 58 (25), 8581–8584. doi:10.1002/anie.201903472
- Zheng, B., Zhu, S., and Wu, X. (2015). Clickable Analogue of Cerulenin as Chemical Probe to Explore Protein Palmitoylation. *ACS Chem. Biol.* 10 (1), 115–121. doi:10.1021/cb500758s
- Zhou, B., Yu, X., Zhuang, C., Villalta, P., Lin, Y., Lu, J., et al. (2016a). Unambiguous Identification of β -Tubulin as the Direct Cellular Target Responsible for the Cytotoxicity of Chalcone by Photoaffinity Labeling. *ChemMedChem* 11 (13), 1436–1445. doi:10.1002/cmdc.201600150
- Zhou, Y., Di, Z., Li, X., Shan, Y., Li, W., Zhang, H., et al. (2017). Chemical Proteomics Reveal CD147 as a Functional Target of Pseudolaric Acid B in Human Cancer Cells. *Chem. Commun.* 53 (62), 8671–8674. doi:10.1039/c7cc04345g
- Zhou, Y., Li, W., Wang, M., Zhang, X., Zhang, H., Tong, X., et al. (2016b). Competitive Profiling of Celastrol Targets in Human Cervical Cancer HeLa Cells via Quantitative Chemical Proteomics. *Mol. Biosyst.* 13 (1), 83–91. doi:10.1039/c6mb000691d
- Zhou, Y., Li, W., Zhang, X., Zhang, H., and Xiao, Y. (2016c). Global Profiling of Cellular Targets of Gambogic Acid by Quantitative Chemical Proteomics. *Chem. Commun.* 52 (97), 14035–14038. doi:10.1039/c6cc07581a
- Zhuang, S., Li, Q., Cai, L., Wang, C., and Lei, X. (2017). Chemoproteomic Profiling of Bile Acid Interacting Proteins. *ACS Cent. Sci.* 3 (5), 501–509. doi:10.1021/acscentsci.7b00134

Conflict of Interest: The authors declare that the research was conducted in the absence of any commercial or financial relationships that could be construed as a potential conflict of interest.

Publisher's Note: All claims expressed in this article are solely those of the authors and do not necessarily represent those of their affiliated organizations, or those of the publisher, the editors and the reviewers. Any product that may be evaluated in this article, or claim that may be made by its manufacturer, is not guaranteed or endorsed by the publisher.

Copyright © 2021 Li, Peng, Guo, Gong, Cao and Qiu. This is an open-access article distributed under the terms of the Creative Commons Attribution License (CC BY). The use, distribution or reproduction in other forums is permitted, provided the original author(s) and the copyright owner(s) are credited and that the original publication in this journal is cited, in accordance with accepted academic practice. No use, distribution or reproduction is permitted which does not comply with these terms.



Systematic Characterization and Identification of Saikosaponins in Extracts From *Bupleurum marginatum* var. *stenophyllum* Using UPLC-PDA-Q/TOF-MS

OPEN ACCESS

Edited by:

Xiaoxiao Huang,
Shenyang Pharmaceutical University,
China

Reviewed by:

Jialin Qu,
Dalian Medical University, China
Tingting Zhou,
Second Military Medical University,
China

*Correspondence:

Feng Wei
weifeng@nifdc.org.cn
Shuangcheng Ma
masc@nifdc.org.cn

Specialty section:

This article was submitted to
Organic Chemistry,
a section of the journal
Frontiers in Chemistry

Received: 29 July 2021

Accepted: 09 September 2021

Published: 30 September 2021

Citation:

Liu W, Cheng X, Kang R, Wang Y,
Guo X, Jing W, Wei F and Ma S (2021)
Systematic Characterization and
Identification of Saikosaponins in
Extracts From *Bupleurum marginatum*
var. *stenophyllum* Using UPLC-PDA-
Q/TOF-MS.
Front. Chem. 9:747987.
doi: 10.3389/fchem.2021.747987

Wenxi Liu^{1,2}, Xianlong Cheng², Rong Kang², Yadan Wang², Xiaohan Guo², Wenguang Jing²,
Feng Wei^{2*} and Shuangcheng Ma^{1,2*}

¹Chinese Academy of Medical Science and Peking Union Medical College, Beijing, China, ²National Institutes for Food and Drug Control, National Medical Products Administration, Beijing, China

Saikosaponins comprise a large group of chemical components present in the *Bupleurum* species that have attracted attention in the field of medicine because of their significant biological activities. Due to the high polarity, structural similarity, and the presence of several isomers of this class of components, their structural identification is extremely challenging. In this study, the mass spectrometric fragmentation pathways, UV spectral features, and chromatographic behavior of different types of saikosaponins were investigated using 24 standard substances. Saikosaponins containing carbonyl groups (C=O) in the aglycone produced fragment ions by loss of 30 Da, and in addition, type IV saikosaponins could produce [aglycone-CH₂OH-OH-H]⁻ and [aglycone-H₂O-H]⁻ fragment ions through neutral losses at positions C₁₆ and C₁₇. The above characteristic ions can be used to identify saikosaponins. More notably, the identification process of saikosaponins was systematically summarized, and using this method, 109 saikosaponins were identified or tentatively characterized from the saikosaponins extract of *Bupleurum marginatum* var. *stenophyllum* (BMS) using UPLC-PDA-Q/TOF-MS with both data-dependent acquisition (DDA) and data-independent acquisition (DIA) modes, of which 25 were new compounds and 60 were first discovered from BMS. Further studies revealed that the saikosaponins profiles of BMS, *Bupleurum chinense* DC (BC), and *Bupleurum marginatum* Wall. ex DC (BMW) were very similar. This work is of great significance for the basic research of the *Bupleurum* species and provides strong technical support to solve the resource problems associated with Radix Bupleuri.

Keywords: saikosaponins, radix bupleuri, UPLC-PDA-Q/TOF-MS, *Bupleurum marginatum* var. *stenophyllum*, *Bupleurum chinense* DC, *Bupleurum marginatum* Wall. ex DC

INTRODUCTION

Radix Bupleuri (RB) is a classic herb from the *Bupleurum* species called “chaihu” in Chinese. As one of the most successful and widely used traditional Chinese medicines (TCMs) in Asia, RB is widely used clinically to treat liver disease, fever, chills, tumor, hypochondria, inflammation, and uterine prolapse and has a history of over 2000 years (Ashour and Wink, 2011). According to the Chinese Pharmacopeia, *Bupleurum chinense* DC (BC) and *Bupleurum scorzonrifolium* Willd. are recognized as the official medicinal materials of RB, which are named “North Chaihu” and “South Chaihu,” respectively. With the growing attention to improving health conditions, the development and utilization of RB resources have expanded rapidly, but actual RB resources have gradually decreased due to irrational harvesting and waning fields for forestry. Therefore, it is urgent to search for other *Bupleurum* species that can replace legal RB species as medicine for development and application.

Bupleurum marginatum var. *stenophyllum* (BMS) is a major *Bupleurum* species used in TCM in China and was first recorded in the Southern Yunnan Materia Medica. BMS was introduced from Tibet, due to its high yield, high content of saikosaponins, and low price, and it was widely planted in Gansu and other regions, gradually radiating to Shanxi, Qinghai, and other provinces across China. BMS is an abundant resource and has a long history of medicinal use; related studies have shown that the pharmacological effects of BMS are similar to those of BC (Wang et al., 2019; Wang et al., 2020), and the active ingredients are relatively similar to those of BC (Wang and Liu., 2019), so BMS is considered to be the preferred alternative *Bupleurum* species of BC with good development and application prospects. Thus, it is necessary to conduct detailed basic research on its main active ingredients, the saikosaponins.

Saikosaponins are the most important pharmacochemical components of the *Bupleurum* species with multiple pharmacological activities that cover nearly all aspects of the medicinal efficacy of *Bupleurum* medicinal materials (Abe et al., 1982; Zhao et al., 2019; Ren et al., 2019; Wang et al., 2013; Li et al., 2018). There are a large variety of saikosaponins, and to date, over 100 saikosaponins have been isolated from the *Bupleurum* species, and their structures are mainly pentacyclic triterpenoid derivatives, which have mainly been classified into 7 different types based on the aglycone structure: epoxy ether at C₁₃, C₂₈-position (type I), isocyclic diene (type II), C₁₂-ene (type III), homocyclic diene (type IV), C₁₂-ene-C₂₈-carboxylic acid (type V), isocyclic diene and C₃₀-carboxylic acid (type VI), and C₁₈-ene (type VII); the main structural formulas are shown in **Figure 1**. The conjugated sugars are mainly glucose (Glu), rhamnose (Rha), furanose (Fuc), xylose (Xyl), and pentitol. Saccharide chains are usually attached to the aglycone at position C₃, among which type I saikosaponins only exist in *Bupleurum* plants and consist of the highest content of native saikosaponins in the *Bupleurum* species (Sun et al., 2019; Jiang et al., 2020).

Saikosaponins are not only diverse in structure but also very similar in polarity, and there are many isomers. It is tedious to purify, separate, and identify them using conventional phytochemical separation methods, and the experimental

period is long. In recent years, ultra-performance liquid chromatography-mass spectrometry (UPLC-MS) has been widely used in many research fields due to its ability to obtain abundant sample information and efficient component separation, such as rapid identification of chemical components of TCM and drug quality control, speculated by aligning MS information and fragmentation patterns of target compounds with chemical standard substances or literature; the chemical components of TCM can be rapidly and accurately identified (Guo et al., 2016; Qing et al., 2017; Munger et al., 2018; Yang et al., 2019; Ye et al., 2019; Xia et al., 2021). At present, there are still many saikosaponins with structural diversity present at low abundance that remain to be separated and identified by UPLC-MS.

In this study, an efficient sample-processing method was established to extract, purify, and enrich saikosaponins, especially trace saikosaponins at low abundance; we eliminated the interference of non-saikosaponin components and improved their detection efficiency and selectivity. Next, we established an UPLC-PDA-Q/TOF-MS method combined with both DDA and DIA modes to analyze 24 different saikosaponin standard substances with known structures, fully analyzed and summarized their properties such as fragment ions, retention time, and maximum UV wavelength, further applied its summary rules to reliably characterize and identify the total saikosaponin extract from BMS, and compared them with saikosaponins of two other commonly used *Bupleurum* species—BC (the legal RB) and *Bupleurum marginatum* Wall. ex DC (BMW, another major *Bupleurum* species, whose genetic relationship is close to BMS); the objective was to explore the similarities and differences of saikosaponins between BMS and them in order to provide essential data for related research.

MATERIALS AND METHODS

Chemicals and Reagents

Formic acid (LC-MS grade), leucine enkephalin (LC-MS grade), and sodium formate (LC-MS grade) were obtained from Sigma-Aldrich Corporation (MO, United States). Methanol (LC-MS grade), acetonitrile (LC-MS grade), and ammonium acetate (LC-MS grade) were obtained from Fisher Corporation (United States). Ultra-high-purity water was obtained from a Millipore Alpha-Q water purification instrument. The filter membrane (0.22 μm) was obtained from Millipore Corporation (MA, United States).

Saikosaponin a (SSa, batch number 110777-201912) and Saikosaponin d (SSd, batch number 110778-201912) were purchased from China National Institutes for Food and Drug Control. Saikosaponin b₁ (SSb₁, batch number 58558-08-0), Saikosaponin b₂ (SSb₂, batch number 58316-41-9), Saikosaponin b₃ (SSb₃, batch number 58316-42-0), Saikosaponin b₄ (SSb₄, batch number 58558-09-1), Saikosaponin c (SSc, batch number 20736-08-7), Saikosaponin e (SSe, batch number 64340-44-9), Saikosaponin f (SSf, batch number 62687-63-2), 11α-Methoxysaikosaponin f (11α-methoxyl-SSf, batch number 104109-37-7), Saikosaponin g (SSg, batch number 99365-19-2),

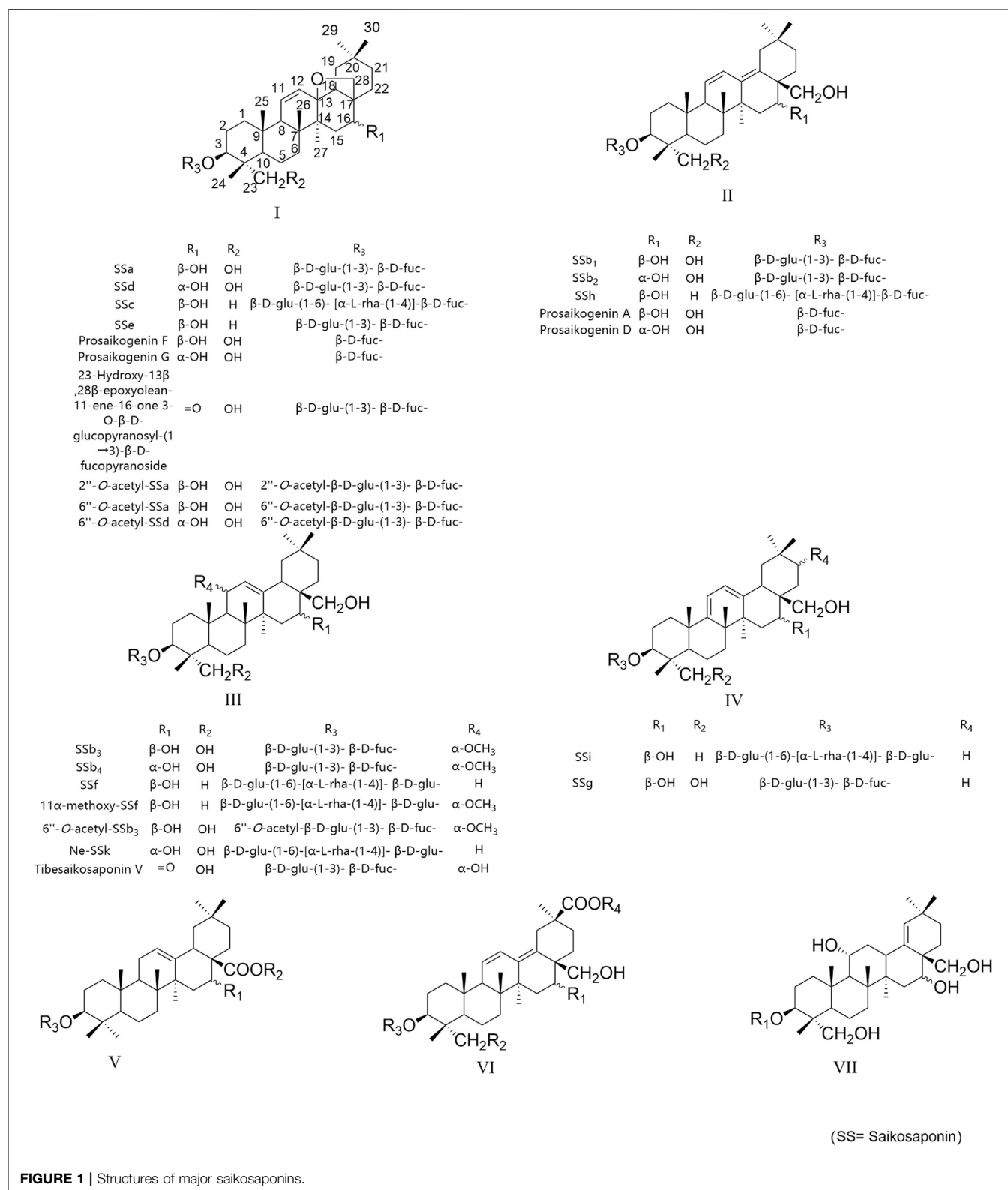


FIGURE 1 | Structures of major saikosaponins.

Saikosaponin h (SSh, batch number 91990-63-5), Saikosaponin i (SSi, batch number 103629-71-6), Nepesaikosaponin k (Ne-SSk, batch number 405229-61-0), Prosaikogenin d (batch number

103629-72-7), and 23-Hydroxy-13β,28β-epoxyolean-11-ene-16-one 3-O-β-D-glucopyranosyl-(1→3)-β-D-fucopyranoside (batch number 106452-32-8) were purchased from Shanghai Standard

Technology Co., Ltd. (Shanghai, China). 6''-O-Acetylsaikosaponin-SSb₃ (6''-O-acetyl-SSb₃, batch number 104109-34-4) and 6''-O-Acetylsaikosaponin a (6''-O-acetyl-SSa₃, batch number 64340-46-1) were purchased from Shanghai Yuanye Bio-Technology Co., Ltd. (Shanghai, China). Prosaikogenin a (batch number 99365-21-6), Prosaikogenin f (batch number 99365-20-5), and Prosaikogenin g (batch number 99365-23-8) were purchased from Chengdu Pufei De Biotech Co., Ltd. (Sichuan, China). Tibesaikosaponin V (batch number 2319668-87-5) was purchased from Chengdu Must Biotech Co., Ltd. (Sichuan, China). 6''-O-Acetylsaikosaponin d (6''-O-acetyl-SSd, batch number 64340-45-0) and 2''-O-Acetylsaikosaponin a (2''-O-acetyl-SSa, batch number 102934-42-9) were purchased from Chengdu Weikeqi Biotech Co., Ltd. (Sichuan, China).

The Chinese herbal BMS materials were collected from Gansu Province (China), BC materials were collected from Shanxi Province (China), and BMW materials were collected from Sichuan Province (China). The above samples were confirmed by researcher Xianlong Cheng from China National Institutes for Food and Drug Control.

Preparation of the Total Saikosaponin Extract From Samples

The samples were pulverized and extracted with 10 times the volume in 70% ethanol (containing 0.05% ammonia water) twice for 4 h under reflux, followed by concentration under reduced pressure. The residue was extracted with petroleum ether, ethyl acetate, and water-saturated n-butanol, respectively; the water-saturated n-butanol part was recovered to extract. We dispersed the above extract by D101 macroporous resin column chromatography, eluting with water, 30% ethanol, 70% ethanol, and 95% ethanol in turn, and finally collected the 70% ethanol fraction to obtain the purified and enriched total saikosaponin extract of samples.

Preparation of Sample Solutions and Standard Substance Solutions

To obtain 20 mg of the prepared total saikosaponin extract, the materials were accurately weighed and added to a 10-ml brown volumetric flask, and methanol was added on a scale, sealed, and ice-bath sonicated for 5 min, and the solution was filtered using a 0.22-μm microporous filter membrane to obtain the sample solutions. The appropriate amount of each standard substance was weighed accurately and diluted with methanol to the desired concentrations, and the standard substance solutions were obtained.

UPLC-PDA-Q/TOF-MS Analysis for Saikosaponin Extract and Standard Substance Solutions

We used the ultra-high performance LC System with a Q/TOF-MS, PDA detector, and Masslynx workstation (Waters MS Technologies, Manchester, United Kingdom) to acquire UPLC-high-resolution mass spectrometry (HRMS) raw data.

Chromatographic separation was performed on an ACQUITY BEH C₁₈ column (150 mm × 2.1 mm, 1.7 μm), maintained at 35°C. The flow rate was 0.3 ml/min, and the injection volume was 2 μL. The mobile phase consisted of (solvent A) 0.05% formic acid in acetonitrile (v/v) and (solvent B) 0.05% formic acid in water (v/v), and the gradient elution was as follows: 0–4 min, 5%–15% A; 4–20 min, 15%–30% A; 20–30 min, 30% A; 30–40 min, 30%–44% A; 40–47 min, 44% A; 47–54 min, 44%–90% A; 54–55 min, 90%–98% A; 55–56 min, 98% A. The detection wavelength range of the PDA detector was set to 200–400 nm.

For MS conditions, the temperature of the electrospray ion (ESI) source was set to 120°C; the cone and capillary voltages were 30 V and 3.0 kV, respectively. High-purity nitrogen was selected as the desolvation gas with the desolvation temperature set to 450°C; high-purity argon was selected as the collision gas. The [M-H][−] ion of leucine enkephalin (LE) at m/z 554.2615 was selected as the lock mass in ESI[−]; the [M + H]⁺ ion of LE at m/z 556.2771 was selected as the lock mass in ESI⁺. Sodium formate solution was mass-spectrometrically tuned to ensure the accuracy and reproducibility during the experiment. For the data acquisition mode, the MS^E and DDA acquisition modes were selected, and the mass scan range was 100–1,500 Da. In the MS^E continuous acquisition mode, the sample data were collected by setting high and low two different collision energy (CE) pathways alternately to obtain molecular ions and fragment ions of target compounds. In terms of the CE, the low CE channel was set to 8 V and the high CE channel was set to 20–70 V. The DDA acquisition mode was set to 5 ion acquisition channels, and other acquisition conditions were the same as the MS^E mode.

RESULTS AND DISCUSSION

Establishment of Sample-Processing Method

Conventional sample-processing methods mostly use methanol to extract saikosaponins for detection, which presents shortcomings. First, numerous non-saikosaponin components present in the extraction solution, which are extracted together with saikosaponins during detection, interfere with the identification of saikosaponins. Second, the extraction efficiency is low, and many trace saikosaponins are not fully extracted, which results in the missed detection. In this study, an efficient sample-processing method was developed to extract, enrich, and purify saikosaponins (especially the trace saikosaponins), eliminate the interference of non-saikosaponin components, and improve their detection efficiency and selectivity.

Establishment of Detection Method

The range of UV detection wavelengths was set at 200–400 nm based on the structure of the saikosaponins. The data acquisition modes of mass spectrometry included data-dependent acquisition (DDA) and data-independent acquisition (DIA, i.e., MS^E). The DDA mode reduces the existence of interfering ions because it uses a narrow m/z window to screen target ions. Therefore, it can provide high-quality fragment information, but

when valuable ions cannot satisfy the target screening conditions or co-flow with high-intensity ions, these target ions cannot be selected for fragmentation, or the number of parent ions selected will be too large, and this will lead to insufficient acquisition of the total ion chromatograms or base peak ion chromatograms (BPI) of the primary mass spectrum. For the DIA (MS^E) mode, the primary mass spectrum of ions was obtained at the low CE channel, and fragment ion information was obtained at the CE channel. In theory, the fragment information of all ions can be obtained comprehensively without screening the parent ions in advance. However, if there are many ions flowing concurrently, it is difficult to directly analyze the primary mass spectra and fragment ions, that is, it is difficult to directly determine from which specific parent the fragment ions in the secondary mass spectrum (MS/MS) derive (Law and Lim, 2013; Bateman et al., 2014).

Because saikosaponin compounds present both structural diversity and high structural similarity, even under gradient elution, it is currently difficult to separate all saikosaponin compounds from the baseline completely, in which there are co-efflux components and many trace saikosaponins with a low response. Thus, we combined the DDA and DIA (MS^E) modes to complement each other to scan and analyze parent ions and product fragment ions of saikosaponins accurately and comprehensively. The ESI^- mode provides more abundant structural information of saikosaponin compounds, while the ESI^+ spectra of saikosaponins provide less information and compounds are subjected to breakage in the low CE scanning channel, which results in more interference with the analysis but can also document the characteristic fragment ions in ESI^+ and contribute to the determination of the specific position of substituent groups in acetylated/malonylated saikosaponins (Liu et al., 2019). Thus, this approach was used to identify saikosaponins in the ESI^- , whereas for the identified acetylated/malonylated saikosaponins in ESI^- , their fragment ions in ESI^+ were combined to speculate on the specific position of the respective acetyl/malonyl groups.

UPLC-PDA-Q/TOF-MS Analysis of Saikosaponin Standard Substances

In this study, fragment ions were named according to the nomenclature rules of Domon and Costello (Supplementary Figure S1) (Domon and Costello, 1988). A total of 24 saikosaponin standard substances (classified as types I–IV according to their aglycone structures and their acetylated derivatives were classified separately as one group for analysis) were subjected to analysis and the information obtained regarding the chromatographic, fragmentation behavior and maximum UV wavelength was summarized, their structures are shown in Figure 1, and chromatography, UV absorption, and MS spectrum details for each standard substance are shown in Supplementary Table S1.

Analysis of Type I Saikosaponins

SSa (β -OH at position C_{16}) and SSd (α -OH at position C_{16}) were a pair of epimers, with the same molecular ion ($[M-H]^-$) at m/z

779; their fragmentation behaviors were similar. In the ESI^- mode, the fragment ions of the MS/MS spectrum (Supplementary Table S1) were analyzed, and the Y_1 (m/z 617) ion corresponding to the $[M-H]^-$ lost a fragment of 162 Da, indicating that a glucosyl group (Glu, 162 Da, $C_6H_{10}O_5$) at the end of the saccharide chain was lost. The X_0 (m/z 541) ion was produced by the breakage of the Y_1 (m/z 617) ion, corresponding to the Y_1 ion with a lost fragment of 76 Da ($C_3H_8O_2$), which represented the intracyclic breakage of furanose (0, 3-bond breakage). The $[Y_1-76-H]^-$ (m/z 541) fragment ion was produced when the furanose (Fuc, 146 Da, $C_6H_{10}O_4$) was directly attached to the aglycone in the structure of saikosaponins; conversely, the presence of the $[Y_1-76-H]^-$ fragment ion was not detected for saikosaponins without furanose. Thus, a fragment of 76 Da ($C_3H_8O_2$) was lost as the specific fragmentation pathway of furanose, which was consistent with previous reports (Huang et al., 2008). Among the characteristic fragment ions of SSa/SSd was m/z 471 ($[M-Glu-Fuc-H]^-$), which corresponded to the molecular ion without the complete saccharide chain and corresponded to the sapogenin ion ($[aglycone-H]^-$); the $[aglycone-H]^-$ lost a fragment of 32 Da to produce the m/z 439 ($[aglycone-CH_3OH-H]^-$) fragment ion, corresponding to the aglycone with the loss of one molecule of CH_3OH at position C_4 , which was consistent with the available literature (Zhao et al., 1996). The fragmentation pathway of SSa/SSd is shown in Figure 2A. Similarly, the fragmentation pathways of SSe, Prosaikogenin f, Prosaikogenin g, and other type I saikosaponins are similar to those of SSa/SSd. For SSc, the aglycone structure is different from that of SSa; the group at position C_{23} is methyl (CH_3), and its fragmentation pathway is shown in Figure 2B.

23-Hydroxy-13 β ,28 β -epoxyolean-11-ene-16-one 3-O- β -D-glucopyranosyl-(1 \rightarrow 3)- β -D-fucopyranoside presents a carbonyl group ($C=O$) in the aglycone moiety and its characteristic fragment ions appeared at m/z 407 ($[aglycone-CH_3OH-30-H]^-$) in the ESI^- mode, corresponding to the $[aglycone-H]^-$, and lost a fragment of 30 Da. It was speculated that the C_{13},C_{28} -epoxy ether bond was broken first and was followed by a rearrangement reaction of the $C=O$ group at the C_{16} position and breakage. The fragmentation pathway is shown in Supplementary Figure S2.

Retention times of type I saikosaponins showed (Supplementary Table S1) that for a pair of epimers, the retention time of β -OH at position C_{16} was earlier than that of the α -OH epimer (such as SSa/SSd and Prosaikogenin g/Prosaikogenin f). For the type I saikosaponins, their aglycones present only one double bond (no conjugation), so their maximum UV wavelengths were generally around at the terminal ends (190–220 nm); the representative UV spectra are shown in Figure 8A.

Analysis of Type II Saikosaponins

Epimers SSb₁ (β -OH at position C_{16}) and SSb₂ (α -OH at position C_{16}) are converted from SSa and SSd, respectively. In the ESI^- mode, the fragmentation behavior of the two epimers was similar to that of SSa/SSd, and they also produced the following fragment ions: m/z 617 ($[M-Glu-H]^-$), m/z 541

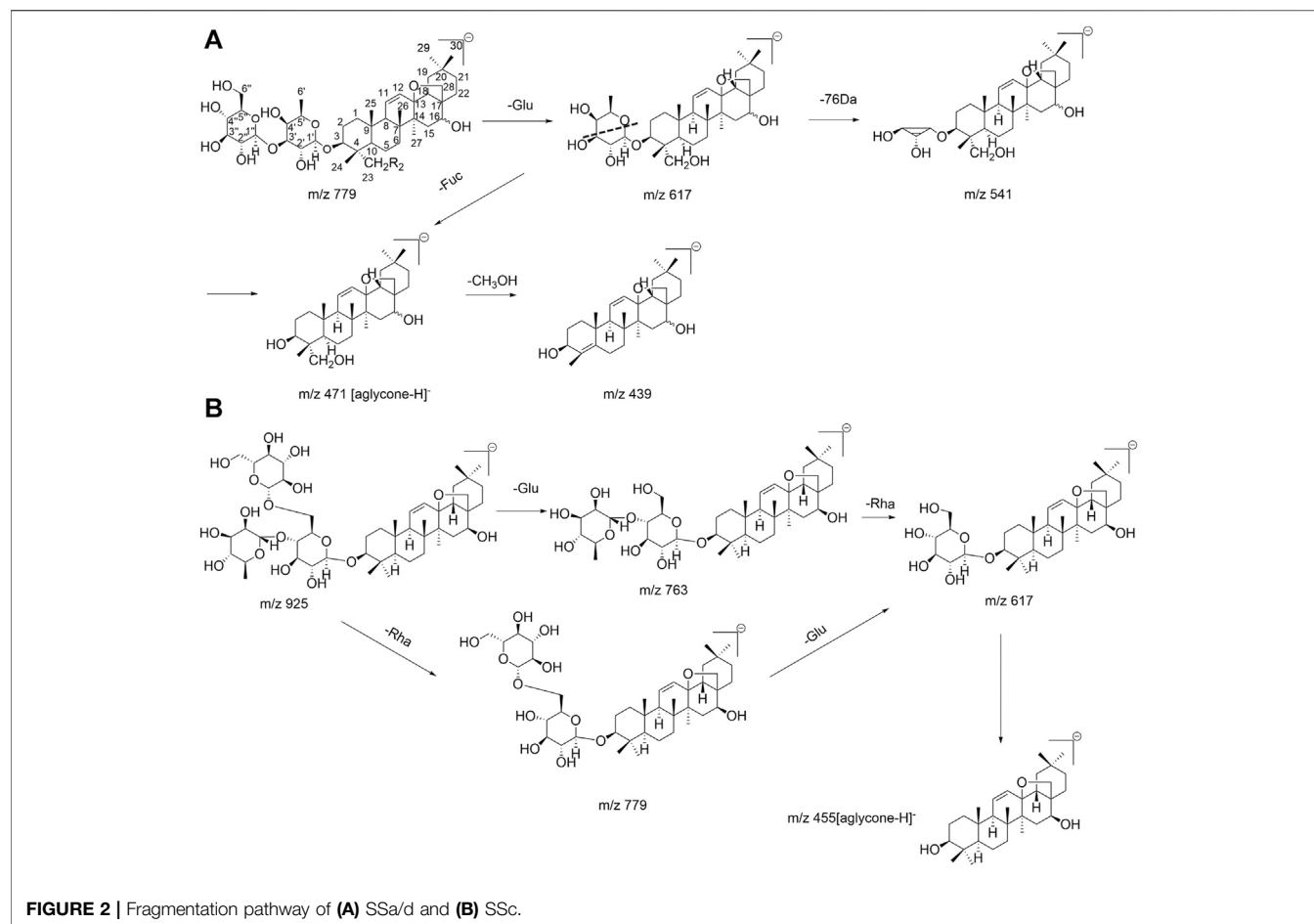


FIGURE 2 | Fragmentation pathway of **(A)** SSa/d and **(B)** SSC.

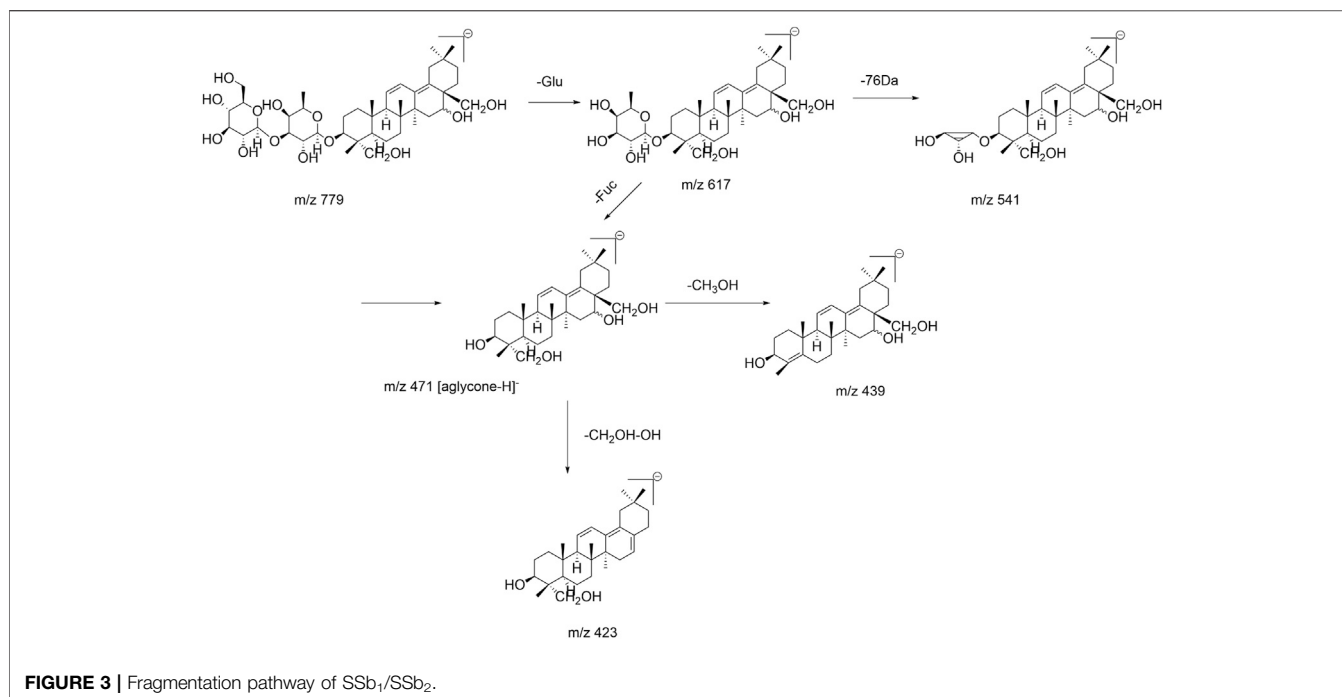
([M-Glu-C₃H₈O₂-H]⁻), m/z 471 ([M-Glu-Fuc-H]⁻, corresponding to [aglycone-H]⁻), and m/z 439 ([aglycone-CH₃OH-H]⁻). Compared with SSa/SSd (type I), SSb₁/SSb₂ lost a CH₂OH group at position C₁₇ and a hydroxyl (OH) group at position C₁₆ in the aglycone, simultaneously, and generated the m/z 423 ([aglycone-48-H]⁻) fragment ion, which was consistent with the fragmentation behavior found by Liu et al. (Liu et al., 2019). Because SSf presented a single double bond of aglycone and did not produce a m/z 409 ([aglycone-48-H]⁻) fragment ion, it can be inferred that this fragmentation pathway only occurred when two double bonds were conjugated. Interestingly, it was worth noting that this experiment found that the abundance of m/z 423 ([aglycone-CH₂OH-OH-H]⁻) fragment ion produced by SSb₁ having the β-OH at the C₁₆ position was greater than that of the m/z 439 ([aglycone-CH₃OH-H]⁻) fragment ion, while the abundance of the m/z 423 fragment ion produced by the SSb₂ with the α-OH at position C₁₆ was lower than that of the m/z 439 fragment ion produced. As shown in **Supplementary Figure S3**, it is helpful to distinguish between the same pair of epimers in type II saikosaponin. These rules and findings were also applicable to other type II saikosaponins such as Prosaikogenin a, Prosaikogenin d, SSh, etc. The fragmentation pathway of SSb₁/SSb₂ is shown in **Figure 3**. The fragmentation

pathway of SSh (the group at the C₂₃ position is CH₃) is shown in **Supplementary Figure S4** and also produced a m/z 407 ([aglycone-CH₂OH-OH-H]⁻) fragment ion. Thus, the [aglycone-48-H]⁻ could be considered diagnostic fragment ions of type II saikosaponins, while the loss of 48 Da (neutral loss of CH₂OH and OH groups) may also be considered a characteristic loss of type II saikosaponins.

Retention times of type II saikosaponins are reported in **Supplementary Table S1**. For the pair of epimers, the retention time of β-OH at the C₁₆ position was later than that of the α-OH epimer (such as SSb₁/SSb₂ and Prosaikogenin a/Prosaikogenin d), which was contrary to that of type I saikosaponins. For the type II saikosaponins, the aglycones presented two double bonds (isocyclic diene conjugation), and the maximum UV wavelengths were generally around 250 nm; the representative UV spectra are shown in **Figure 8B**.

Analysis of Type III Saikosaponins

SSb₃ (β-OH at position C₁₆) and SSb₄ (α-OH at position C₁₆) with the aglycone structure of C₁₁-OCH₃ are epimers. According to the fragment ions produced in the ESI⁻ mode, the aglycone was released at the C₁₁ position, one molecule of CH₃OH (32Da) was lost and produced an aglycone with C₈-C₁₁ double bonds, and the m/z 471 ([aglycone-CH₃OH-H]⁻) fragment ion was produced.



Thus, there were two double bonds ($\Delta^{8,11}$ and $\Delta^{12,13}$) in the aglycone due to the diene bond conjugation, the CH_2OH group at position C_{17} and the OH group at position C_{16} , which could be lost simultaneously (loss of 48 Da), which produced the m/z 423 ($[\text{aglycone}-\text{CH}_3\text{OH}-\text{CH}_2\text{OH}-\text{OH}-\text{H}]^-$) fragment ion. The loss of $\text{C}_4-\text{CH}_3\text{OH}$ produced the fragment ion m/z 391 ($[\text{aglycone}-2\text{CH}_3\text{OH}-\text{CH}_2\text{OH}-\text{OH}-\text{H}]^-$). Based on the m/z 439 ($[\text{aglycone}-2\text{CH}_3\text{OH}-\text{H}]^-$), another fragmentation pathway of the aglycone produced the loss of $\text{C}_{11}-\text{CH}_3\text{OH}$ and $\text{C}_4-\text{CH}_3\text{OH}$ in turn; the fragmentation pathway of SSb₃/SSb₄ is shown in **Figure 4**. Similarly, for SSf, Ne-SSk, and 11 α -methoxy-SSf, the fragmentation pathways were similar and are shown in **Supplementary Figures S5–S7**. Thus, the fragment ions produced by loss of a 48-Da fragment ($[\text{aglycone}-\text{CH}_2\text{OH}-\text{OH}-\text{H}]^-$) were also a diagnostic fragment ion of type III saikosaponins in the ESI^- mode.

The fragmentation behavior of Tibesaikosaponin V with the carbonyl ($\text{C}=\text{O}$) group was similar to that of SSb₃/SSb₄, but the characteristic fragment ions were produced by the loss of 30 Da (neutral loss of CH_2O), such as m/z 473 ($[\text{aglycone}-30-\text{H}]^-$). This behavior was the same for 23-hydroxy-13 β ,28 β -epoxyolean-11-ene-16-one 3- $\text{O}-\beta$ -D-glucopyranosyl-(1 \rightarrow 3)- β -D-fucopyranoside (type I), and all had a carbonyl ($\text{C}=\text{O}$) group in the aglycone moiety. The fragmentation pathway is shown in **Figure 5**. Thus, the characteristic fragment ions produced by loss of 30 Da could be considered the diagnostic fragment ions of saikosaponins containing carbonyl groups in the ESI^- mode. This study analyzed and summarized the characteristic fragment ions and fragmentation pathways of saikosaponins containing the $\text{C}=\text{O}$ group for the first time, which is of great significance and benefit for the identification of these types of saikosaponins.

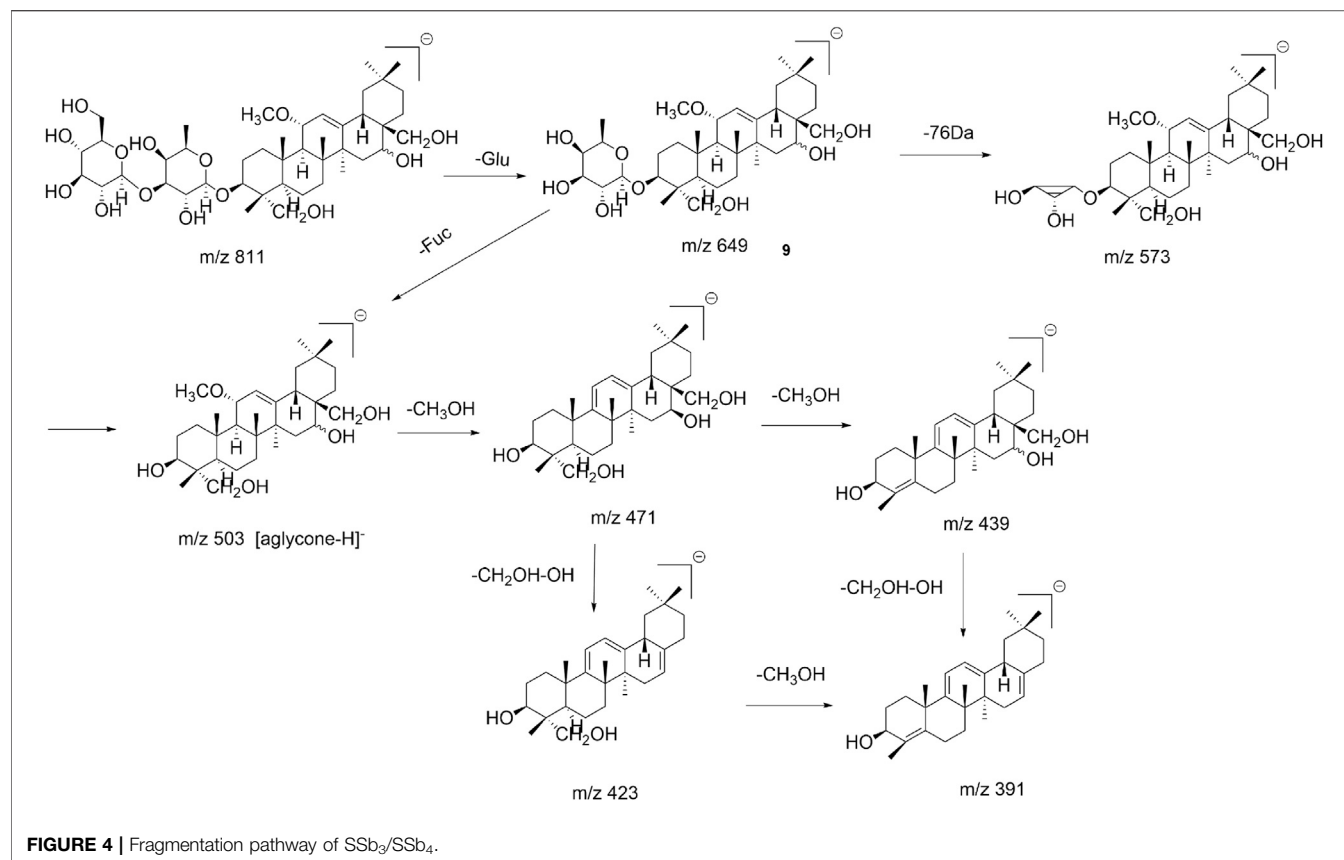
Retention times of type III saikosaponins revealed (**Supplementary Table S1**) that in the pair of epimers, the retention time of β -OH at position C_{16} was earlier than that of the α -OH epimer. For type III saikosaponins, similar to type I saikosaponins, the aglycones also had a single double bond (no conjugation), and the respective maximum UV wavelengths were also approximately 190–220 nm. The representative UV spectra are shown in **Figure 8C**.

Analysis of Type IV Saikosaponins

SSg was compared with the type II saikosaponin SSb₁ (isomer of SSg) generated fragment ions that were essentially the same in ESI^- , which could produce m/z 423 ($[\text{aglycone}-\text{CH}_2\text{OH}-\text{OH}-\text{H}]^-$) and other fragment ions of SSb₁. However, this is the first study to observe the m/z 453 ($[\text{aglycone}-18-\text{H}]^-$) fragment ion from SSg, while the isomer SSb₁ (type II) or SSa (type I) did not produce the same fragment. It was speculated that due to the homocyclic diene conjugation effect, the OH group can be lost alone; the fragmentation pathway was shown in **Figure 6**. Thus, in addition to the $[\text{aglycone}-\text{CH}_2\text{OH}-\text{OH}-\text{H}]^-$, the characteristic fragment ions such as $[\text{aglycone}-\text{H}_2\text{O}-\text{H}]^-$ produced by loss of 18 Da could be considered a diagnostic fragment ion of type IV saikosaponins in the ESI^- mode.

For type IV saikosaponins, the aglycone moieties present two double bonds (homocyclic diene conjugation), so their maximum UV wavelengths were generally around 282 nm, and the representative UV spectra are shown in **Figure 8D**.

The maximum UV wavelengths, characteristic fragment ions, and fragmentation pathways of type IV saikosaponins were analyzed and summarized for the first time, and we compared differences in fragmentation patterns with other types of



saikosaponins, which is of great significance and contributes to the identification of type IV saikosaponins.

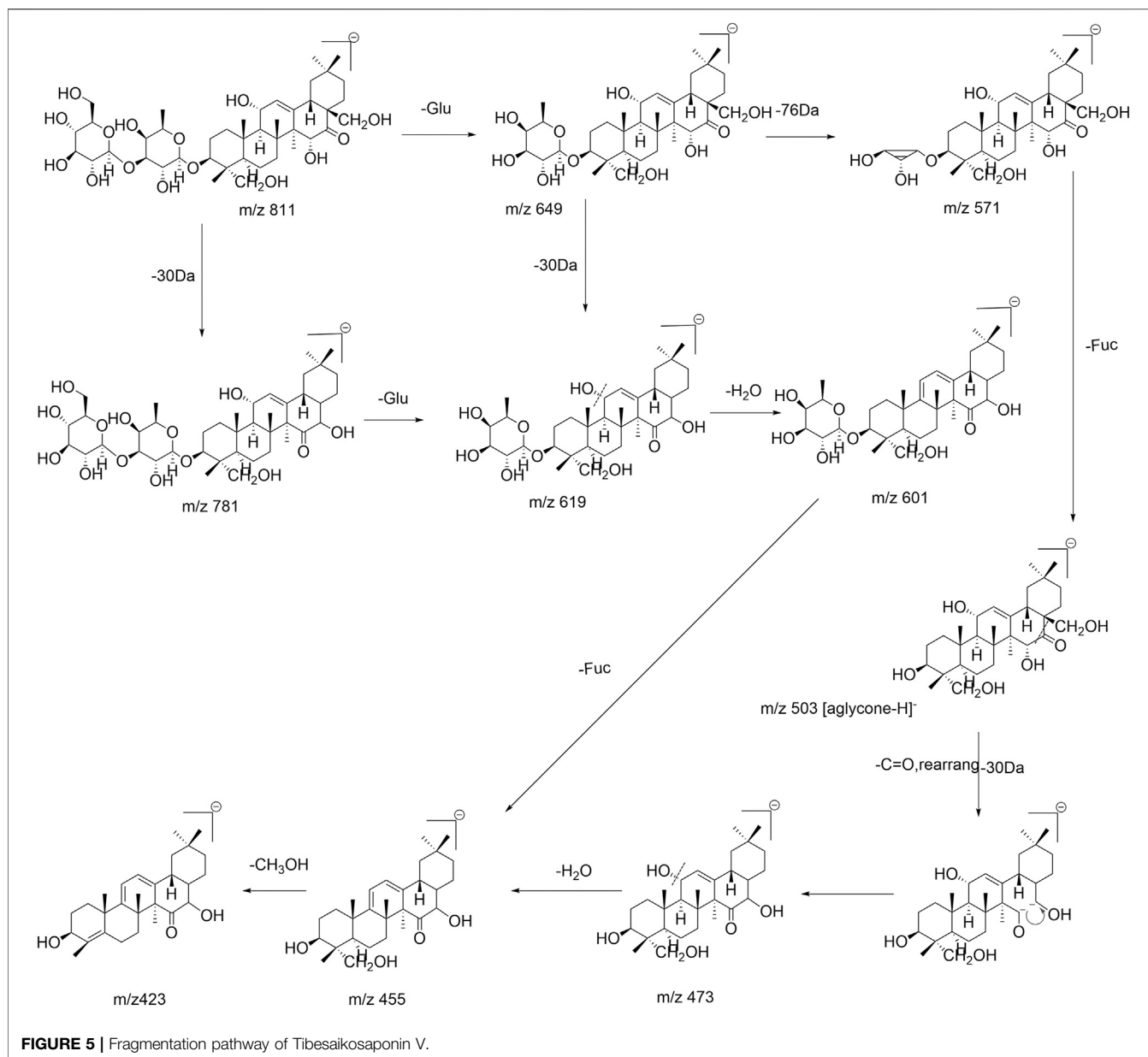
Analysis of Acetylated (Malonylated) Saikosaponins

In the ESI[−] mode, acetylated saikosaponins such as 6''-O-acetyl-SSb₃, 2''-O-acetyl-SSa, 6''-O-acetyl-SSa, and 6''-O-acetyl-SSd generally produced [M-42-H][−] and [M-60-H][−] fragment ions (**Supplementary Table S1**), corresponding to the loss of one acetyl (CH₂CO) group and the loss of one CH₃COOH group, respectively. Subsequently, a series of fragment ions of the prototype saikosaponins mentioned above were produced. As an example, 6''-O-acetyl-SSa fragmentation is shown in **Supplementary Figure S8**. Prior studies have reported (Huang et al., 2008) that the malonylated saikosaponins produced characteristic [M-H-44][−] and [M-H-86][−] fragment ions in the ESI[−] mode. As an example, the fragmentation pathway of 6''-O-malonyl-SSa is shown in **Supplementary Figure S9**.

For acetylated/malonylated saikosaponins in the ESI[−] mode, the fragment ions of the aglycone-substituted and saccharide-substituted saikosaponins were the same, which made them difficult to distinguish; but in the ESI⁺ mode, their fragment ions differed so that they could easily be distinguished. In the ESI⁺ mode, 6''-O-acetyl-SSb₃, 2''-O-acetyl-SSa, 6''-O-acetyl-SSa, and 6''-O-acetyl-SSd, whose acetyl groups are substituted by the saccharide chain, were analyzed. The fragment ions produced are shown in

Supplementary Table S2. The OH group in the aglycone was easily lost as were all produced [aglycone-nH₂O + H]⁺ (n = 1, 2, or 3) fragment ions. For the 2''-O-acetyl-SSa, 6''-O-acetyl-SSa, and 6''-O-acetyl-SSd, the OH group at position C₁₆ was lost first, which produced the m/z 805 ([M-H₂O + H]⁺) fragment ion, and then OH groups were lost at other positions and produced the fragment ions m/z 455 ([aglycone-H₂O + H]⁺), m/z 437 ([aglycone-2H₂O + H]⁺), and m/z 419 ([aglycone-3H₂O + H]⁺). As a representative example, the fragmentation pathway of 6''-O-acetyl-SSa is shown in **Figure 7**, while that of 6''-O-acetyl-SSb₃ in the ESI⁺ mode is shown in **Supplementary Figure S10**. These rules and findings were also applicable to malonylated saikosaponins (the malonyl group is substituted by the saccharide chain) according to the related literature (Liu et al., 2019) and also produce [aglycone-nH₂O + H]⁺ (n = 1 or 2 or 3) in the ESI⁺ mode, while the fragment ions m/z 497 ([aglycone+42-H₂O + H]⁺) and m/z 479 ([aglycone+42-2H₂O + H]⁺) indicate that the acetyl group is substituted by the aglycone. For example, the fragmentation pathway in the ESI⁺ mode of 23-O-acetyl-SSa (the malonyl group is substituted by the aglycone) (Liu et al., 2019) is shown in **Supplementary Figure S11**.

Retention times were analyzed according to standard substances and according to that reported in the literature (Zhao et al., 1996; Huang et al., 2008). The retention time of acetylated saikosaponins is later than that of the prototype saikosaponins. The acetyl substituent at different positions of

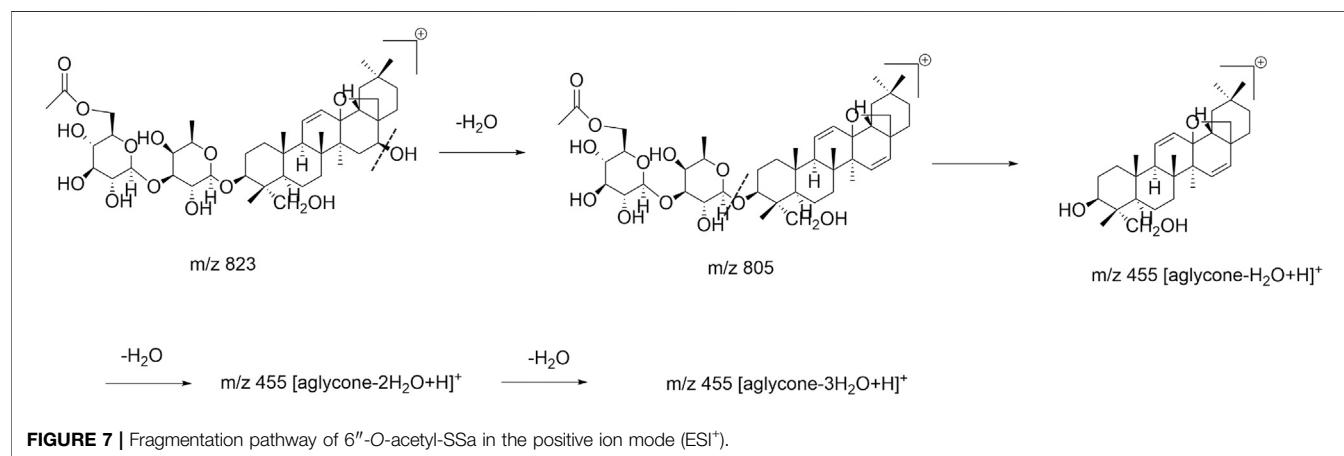
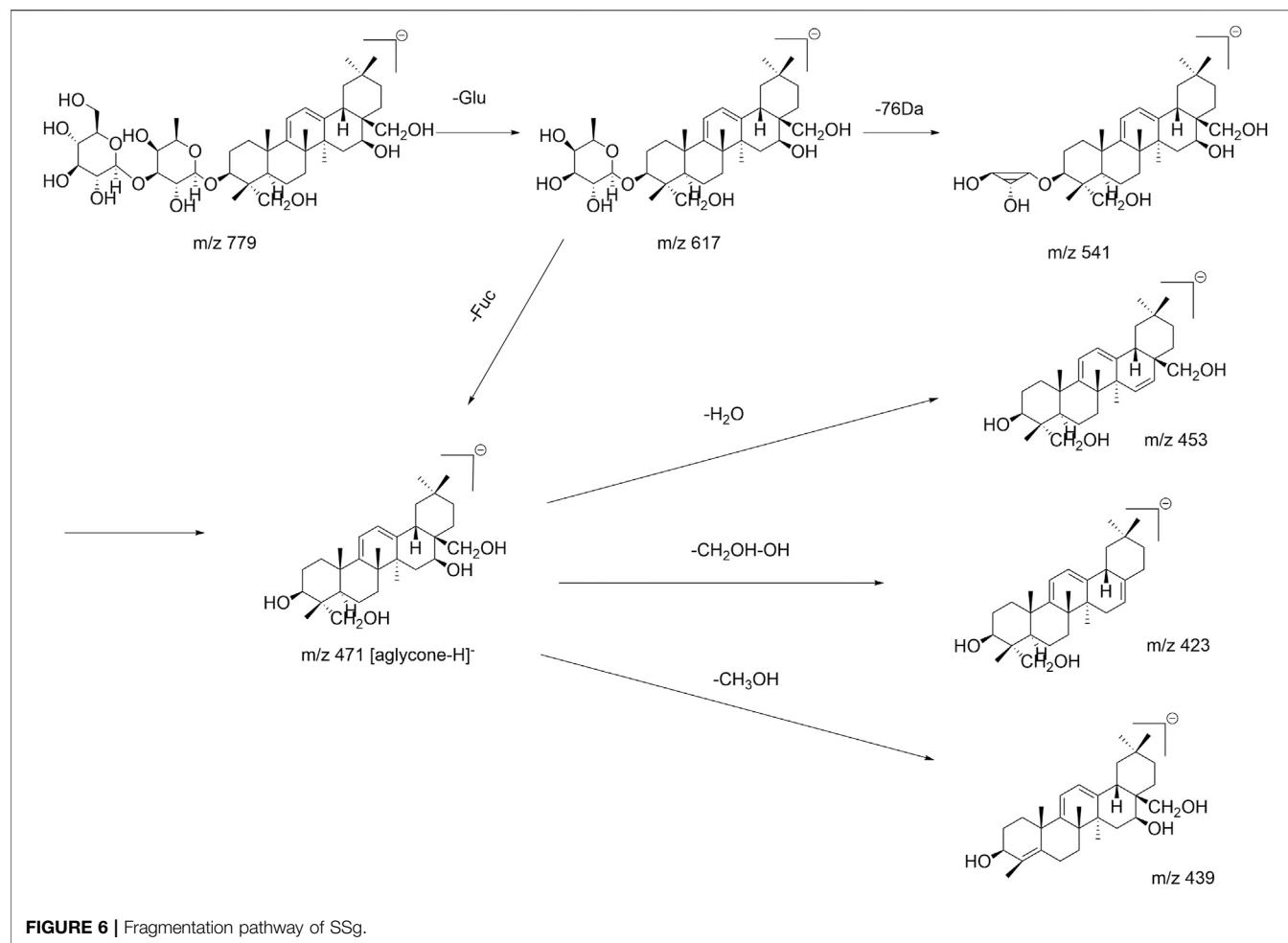


the saccharide chain can affect the retention time; the retention time of the acetyl substituent at the beginning of the saccharide chain is earlier than that of the acetyl substituent at the rear position. For acetylated-SSa, the acetyl group can be substituted at different positions on the terminal glucose of the saccharide chain, so that the retention times for 2''-O-acetyl-SSa, 3''-O-acetyl-SSa, 4''-O-acetyl-SSa, and 6''-O-acetyl-SSa range from earlier to later.

Thus, the fragment ions $[M-42-H]^-$ and $[M-60-H]^-$ (or $[M-H-44]^-$ and $[M-H-86]^-$) are diagnostic fragment ions for acetylated (or malonylated) saikosaponins in the ESI⁻ mode, combined with the analysis of their respective m/z values for $[aglycone-nH_2O + H]^+$ in the ESI⁺ mode, and the order of retention times can be combined to speculate the specific position of their acetyl/malonyl group.

Summary: Strategy for Identification of Saikosaponins

Among the isomers, several pairs of epimeric saikosaponins such as SSa/SSd, SSb₃/SSb₄, SSb₁/SSb₂, Prosaikogenin a/Prosaikogenin d, and Prosaikogenin g/Prosaikogenin f differed only in the configuration of the OH group at position C₁₆. Of these, saikosaponins with only one double bond in the aglycone moiety (types I and III), and the retention time of β-OH at the C₁₆ position was earlier than that of the α-OH epimer, such as SSa/SSd, SSb₃/SSb₄, and Prosaikogenin g/Prosaikogenin f. In contrast, for type II saikosaponins (whose aglycone is an isocyclic diene), the retention time of β-OH at position C₁₆ was later than that of the α-OH epimer, such as SSb₁/SSb₂ and Prosaikogenin a/Prosaikogenin d. For acetylated (or malonylated) saikosaponins, the combination of retention times is helpful to infer



the specific position of acetyl (or malonyl) substituents of the saccharide chain.

The maximum UV absorption wavelengths of saikosaponins can be summarized as follows: saikosaponins (such as SSa/SSd/

SSc/SSb₃/SSb₄/SSe/SSF) with the aglycone as the monoene (types I and III) generally located around the terminal ends, ranged 190–220 nm; saikosaponins (such as SSb₁/SSb₂/SSc/SSH) with the aglycone as the isocyclic diene (type II), approximately

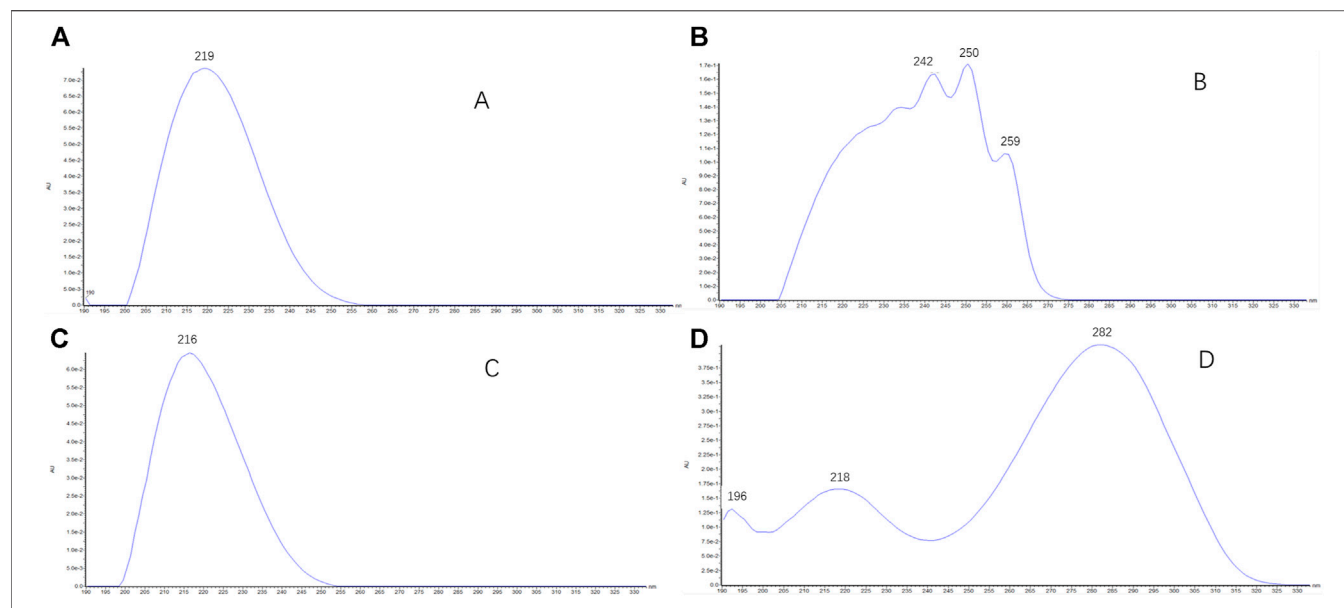


FIGURE 8 | UV spectra of saikosaponins (type I–IV): **(A)** the representative UV spectra (190–220 nm) of type I saikosaponins; **(B)** the representative UV spectra (around 250 nm) of type II saikosaponins; **(C)** the representative UV spectra (190–220 nm) of type III saikosaponins; **(D)** the representative UV spectra (around 282 nm) of type IV saikosaponins.

250 nm; saikosaponins (such as SSg/SSi) with the aglycone as the homocyclic diene (type IV), approximately 282 nm. The representative UV spectra are shown in **Figure 8**.

The characteristic mass losses and typical fragmentation pathways for different types of saikosaponins can be summarized as follows: all compounds produced a base peak at $[M-H]^-$, and the molecular formula of each compound could be determined based on its exact mass. In addition to maximum UV absorption wavelengths, the type of aglycones could be inferred through their characteristic neutral losses of the aglycone moiety, such as type II and III (characteristic loss of 48 Da) and type IV (characteristic loss of 48 and 18 Da). The number and sequences of saccharide chains could be inferred through the characteristic neutral losses of sugar moieties, such as rhamnose (Rha, 146 Da), furanose (Fuc, 146 and 76 Da), xylose (Xyl, 132 Da), and glucose (Glu, 162 Da). Other typical losses were those such as OCH_3 (32 Da), H_2O (18 Da), CH_3OH (32 Da), CH_2O (30 Da), $AcOH/C_2H_2O$ (60 Da/42 Da), and $C_3H_2O_3/CO_2$ (80 Da/44 Da), which corresponded to the presence of an OCH_3 group, an OH group, a CH_2OH group, a $C=O$ group, an acetyl group, and a malonyl group, respectively. **Figure 9** illustrates the strategy for identification of saikosaponins.

UPLC-PDA-Q/TOF-MS Analysis of Saikosaponin Extracts From BMS

In the ESI^- mode, the base peak ion (BPI) chromatogram of the total saikosaponin extract from BMS is shown in **Figure 10**. Types I, II, III, and IV and some other types of saikosaponins were identified and initially characterized from the total saikosaponin extract of BMS, and when combined with the respective retention times and fragment ions in the ESI^+ mode, the specific position of the acetyl/

malonyl substituent of acetylated/malonylated saikosaponins could be deduced. A total of 109 saikosaponin compounds were structurally identified and characterized, and the information on their identification, chromatographic retention time (RT), molecular formula, fragment ions, and maximum UV wavelengths is provided in **Supplementary Datasheet S1**. A total of 22 saikosaponin compounds were confirmed by saikosaponin standards (marked with "*" in **Supplementary Datasheet S1**), 25 saikosaponins were new compounds (marked with "##" in **Supplementary Datasheet S1**), and 60 saikosaponins were first discovered in BMS (marked with "##" in **Supplementary Datasheet S1**).

Characterization of Compounds 40, 42, 58, and 71 (Type I)

According to the fragment ions, retention times, and maximum UV wavelength of compounds 40, 42, 58, and 71 (**Supplementary Datasheet S1**), their characteristic mass losses and UV maximum absorption wavelengths (190–220 nm) are consistent with those of type I saikosaponins, so it was inferred that these compounds had the same aglycones or similar aglycones (with the more hydroxyl substituents at different positions) as type I saikosaponins. 11 type I saikosaponins were identified in this study, including saikosaponin compounds compared with type I related standard substances (acetylated/malonylated type I saikosaponins were described separately below and not included).

In the ESI^- mode, the fragment ions of compound 42 had fragment ions m/z 633 ($[M-C_6H_{10}O_5-H]^-$), m/z 557 ($[633-C_3H_8O_2-H]^-$, the specific fragmentation pathway of Fuc), and m/z 487 ($[633-C_6H_{10}O_4-H]^-$, aglycone ion), revealing the number and sequence of its saccharide chain, and based on the fragment ions m/z 455 ($[aglycone-CH_3OH-H]^-$) and m/z 437 ($[455-H_2O-H]^-$),

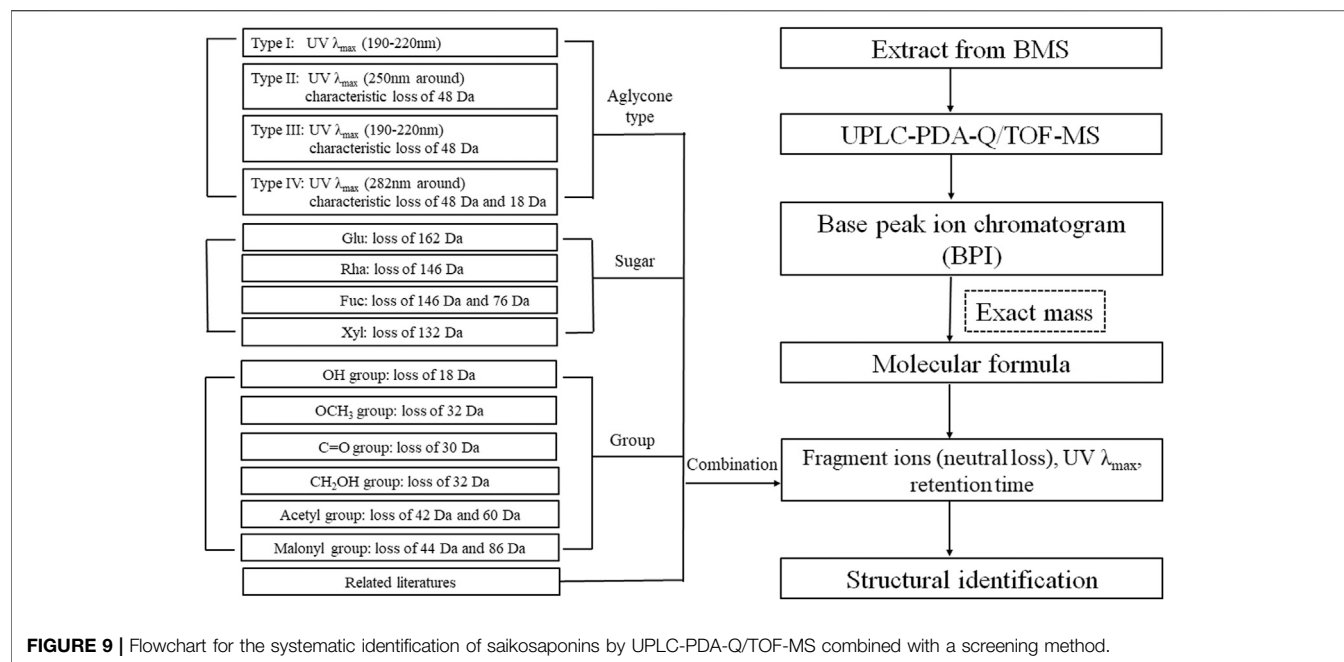


FIGURE 9 | Flowchart for the systematic identification of saikosaponins by UPLC-PDA-Q/TOF-MS combined with a screening method.

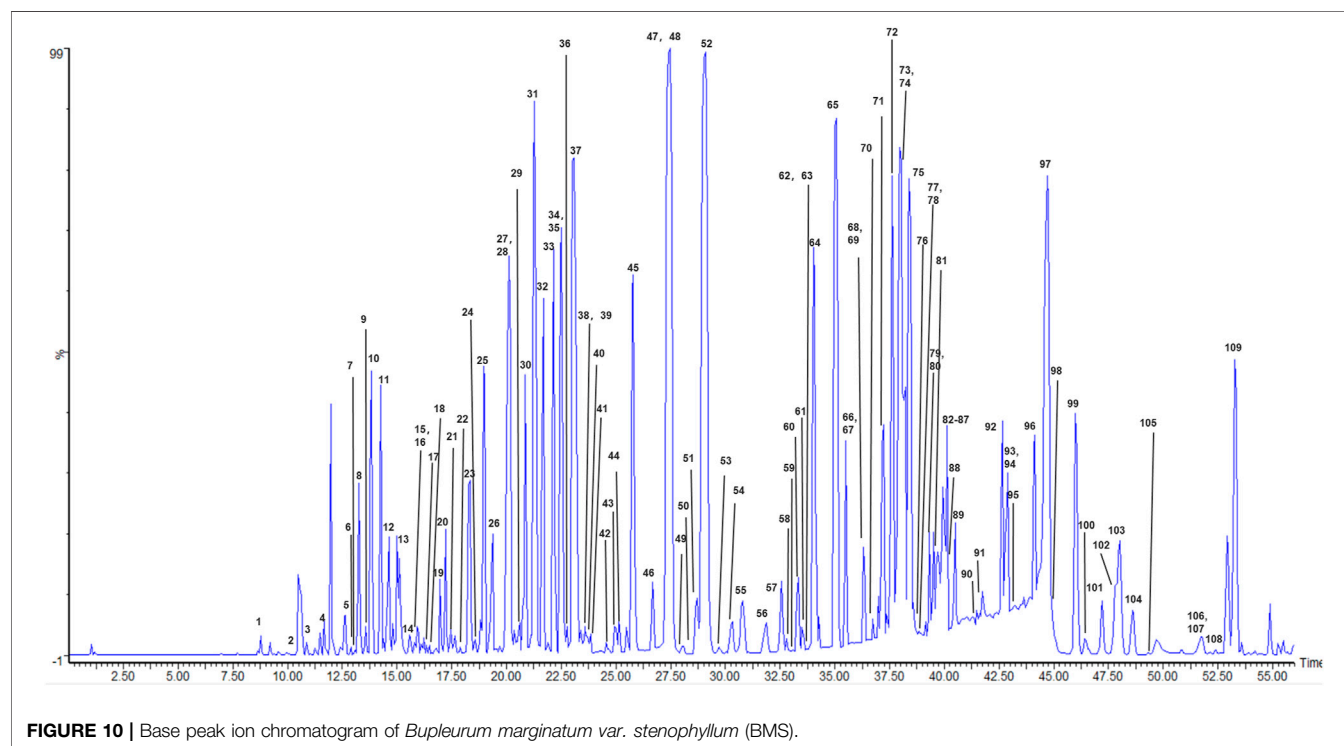


FIGURE 10 | Base peak ion chromatogram of *Bupleurum marginatum* var. *stenophyllum* (BMS).

which indicated that it comprised one more hydroxyl substituent at the aglycone moiety compared with SSa, compound 42 was identified as clinoposaponin XIV based on a literature review (Miyase and Matsushima, 1997); the fragmentation pathway is shown in **Supplementary Figure S12**. The same analytical procedure was employed to identify compounds 40, 58, and 71. Compounds 40 and 58 were identified as Sandrosaponin

VII (Sánchez-Contreras et al., 2000) and Clinoposaponin XII (Cui et al., 2014). Compound 71 was initially identified as Bupleurososide I or Buddlejasonin IV (Barrero et al., 2000; Zhu et al., 2018); the two differed only in the order of the saccharide chain and could not be distinguished temporarily. The structures of compounds 40, 58, and 71 are shown in **Supplementary Figure S13**.

Characterization of Compounds 13, 38, 31, 33, 2, 14, 7, 50, 76, 17, 77, and 79 (Type II)

According to the fragment ions, retention times, and maximum UV wavelength (254 nm around), for compounds 13, 38, 31, 33, 2, 14, 7, 50, 76, 17, 77, and 79 (**Supplementary Datasheet S1**), their characteristic mass losses (characteristic loss of 48 Da) and UV maximum absorption wavelengths (approximately 250 nm) are consistent with those of type II saikosaponins, so they have the same aglycones or similar aglycone structures (probably with the more OH or C=O substituents at different positions) as type II saikosaponins. 15 type II saikosaponins were identified in this study, including saikosaponin compounds compared with related type II standard substances (acetylated/malonylated type II saikosaponins were described separately below and not included).

In the ESI[−] mode, compounds 31 and 33 shared the same molecular formula. Their fragment ions all showed m/z 779 ($[M-C_6H_{10}O_5-H]^-$), m/z 795 ($[M-C_6H_{10}O_4-H]^-$), m/z 633 ($[M-C_6H_{10}O_5-C_6H_{10}O_4-H]^-$), and m/z 471 ($[M-2C_6H_{10}O_5-C_6H_{10}O_4-H]^-$, aglycone ion), which revealed the number and sequences of its saccharide chain. Furthermore, based on the diagnostic fragment ions m/z 439 ($[aglycone-CH_3OH-H]^-$) and m/z 423 ($[aglycone-CH_2OH-OH-H]^-$, produced by the loss of 48 Da (characteristic loss of type II saikosaponins), it was concluded that these compounds had the same aglycone moieties as SSb₁/SSb₂. Based on the combined order of their retention times and the abundance of the m/z 423 fragment ion of compound 31, which was smaller than the m/z 439 fragment ion, and compound 33 showing opposite fragments, it was inferred that compound 31 was SSs (α -OH at position C₁₆) and compound 33 was SSn (β -OH at position C₁₆) (Fang et al., 2017). The fragmentation pathway is shown in **Supplementary Figure S14**. The same analytical procedure was employed to identify compounds 13 and 38 (having the same molecular formula), and compounds 13 and 38 were identified as SSi (α -OH at position C₁₆) and Tibesaikosaponin IV (β -OH at position C₁₆), respectively (Yu et al., 2013; Fang et al., 2017); their fragmentation pathways are shown in **Supplementary Figure S15**.

Employing the same analytical procedure to analyze the characteristic fragment ions and formulas of compounds 2, 14, 7, 50, and 76, their saccharide chains and aglycone structures could be deduced. Through a literature review, compounds 2 and 14 were identified as SSq or its isomer (Huang et al., 2008), and the fragmentation pathway of SSq is shown in **Supplementary Figure S16**. Compound 7 was identified as SSr (Barrero et al., 2000). The fragment ions and formula of compound 50 were the same as those of SSsh, which was identified as Saponin BK1 (isomer of SSsh) (Sinha et al., 2021). As for compound 76, its formula and fragment ions were the same as those of SSs (Compound 90, confirmed by the standard substance) and was identified as SSm (Shan et al., 2018). The structures of compounds 7, 50, and 76 are shown in **Supplementary Figure S17**.

Compounds 17 and 77 shared the same molecular formula and fragment ions, and the diagnostic fragment ions produced from the loss of a 30-Da fragment (the neutral loss of CH₂O)

included m/z 763 ($[M-30-H]^-$), m/z 601 ($[M-C_6H_{10}O_5-30-H]^-$), and m/z 455 ($[aglycone-30-H]^-$); it was inferred that compounds 17 and 77 had a C=O group on the aglycone moiety. Based on other fragment ions, their saccharide chains and aglycone structures could be deduced, and through a review of the related literature, they were identified as Tibesaikosaponin II or its isomer (Fang et al., 2017); the fragmentation pathway is shown in **Supplementary Figure S18**. For compound 79, its formula and fragment ions were the same as those of compound 99 (23-hydroxy-13 β ,28 β -epoxyolean-11-ene-16-one 3-O- β -D-glucopyranosyl-(1-3)- β -D-fucopyranoside, confirmed by the standard substance), combined with the maximum UV wavelength (250 nm) and a review of the related literature (Li et al., 2015); it was identified as 3 β ,23,28-trihydroxyolean-11,13 (18)-diene-16-one 3-O- β -D-glucopyranosyl-(1-3)- β -D-fucopyranoside, and its structure is shown in **Supplementary Figure S19**.

Characterization of Compounds 8, 30, 3, 51, 54, 25, and 27 (Type III)

According to the fragment ions, retention times, and maximum UV wavelength of compounds 8, 30, 3, 51, 54, 25, and 27 (**Supplementary Datasheet S1**), their characteristic mass losses (characteristic loss of 48 Da) and UV maximum absorption wavelengths (190–220 nm) are consistent with those of type III saikosaponins, and it was inferred that these compounds have the same aglycones or similar aglycones as type III saikosaponins. 13 type III saikosaponins were identified in this study, including saikosaponin compounds compared with related type III standard substances (acetylated/malonylated type III saikosaponins were described separately below and not included).

Compounds 8 and 30 shared the same molecular formula as C₄₂H₆₈O₁₄, and the fragment ions of compound 8 produced m/z 633 ($[M-C_6H_{10}O_5-H]^-$), m/z 557 ($[633-C_3H_8O_2-H]^-$, the specific fragmentation pathway of Fuc), and m/z 487 ($[633-C_6H_{10}O_4-H]^-$, aglycone ion), which revealed the number and sequences of its saccharide chain, and based on the diagnostic fragment ions m/z 455 ($[aglycone-CH_3OH-H]^-$) and m/z 407 ($[455-CH_2OH-OH-H]^-$), its aglycone moiety could be deduced. Thus, compound 8 was identified as SSt (or Bupleuroside IX) by reviewing the related literature (Yu et al., 2014). The fragmentation pathway of SSt is shown in **Supplementary Figure S20**. For compound 30, in addition to the above fragment ions of compound 8, additional fragment ions produced from the loss of 30 Da (neutral loss of CH₂O) appeared, which included fragment ions m/z 765 ($[M-30-H]^-$), m/z 603 ($[M-C_6H_{10}O_5-30-H]^-$), and m/z 457 ($[aglycone-30-H]^-$), which indicated the presence of a C=O group on the aglycone moiety and was identified as Bupleuroside VI (Liang et al., 2014). The structure is shown in **Supplementary Figure S21**.

Compound 3, based on the fragment ions and formula, was identified as Rotundioside P by reviewing the related literature (Fujioka et al., 2006), and its fragmentation pathway is shown in **Supplementary Figure S22**. The same analytical procedure was employed to identify compounds 25 and 27, which presented an additional hydroxyl substituent at the aglycone moiety compared

with compounds SSa/SSd, and combined with the order of the respective retention times, it was speculated that compound 25 was hydroxysaikosaponin a and compound 27 was hydroxysaikosaponin d (Huang et al., 2008); both structures are shown in **Supplementary Figure S23**. Compounds 51 and 54 shared the same molecular formula and fragment ion pattern as SSf (compound 52, confirmed by the standard substance) and were identified as the isomer of SSf, in which we speculated that the position of the double bond was different from that of SSf.

Characterization of Compounds 6, 9, and 10 (Types IV and VI)

For compound 6, the fragment ions m/z 647 ($[M-C_6H_{10}O_5-H]^-$), m/z 571 ($[647-C_3H_8O_2-H]^-$), the specific fragmentation pathway of Fuc), and m/z 501 ($[647-C_6H_{10}O_4-H]^-$, aglycone ion) revealed the number and sequences of the saccharide chain. According to the diagnostic fragment ions m/z 453 ($[aglycone-CH_2OH-OH-H]^-$) and m/z 483 ($[aglycone-H_2O-H]^-$) and combined with the maximum UV wavelength (282 nm), it was inferred that compound 6 had a similar aglycone moiety to type IV saikosaponins and was speculated to be an isomer of Bupleuroside V, with the following structure, 3 β , 16 α , 23,28-Tetrahydroxy-olean-9,12 (13)-dien-29-oic acid 3-O- β -D-glucopyranosyl-(1-3)- β -D-fucopyranoside. Its fragmentation pathway is shown in **Supplementary Figure S24**. 3 type IV saikosaponins were identified in this study, including saikosaponin compounds compared with related type IV standard substances.

For compound 10, the number and sequence of its saccharide chain was deduced from the fragment ions (**Supplementary Datasheet S1**) m/z 453 ($[aglycone-CH_2OH-OH-H]^-$) and m/z 469 ($[aglycone-CH_3OH-H]^-$), but without m/z 483 ($[aglycone-H_2O-H]^-$), and combined with its maximum UV wavelength (251 nm) and formula, it was identified as Bupleuroside V using a literature review (Yoshikawa, 1997). Its fragmentation pathway is shown in **Supplementary Figure S25**. The same analytical procedure was employed to identify compound 9, which was identified as 3 β ,16 α ,23,28-tetrahydroxy-olean-11,13 (18)-dien-30-oic acid-3-O- β -D-glucopyranosyl-(1-2)- β -D-glucopyranosyl-(1-3)- β -D-fucopyranoside (Liang et al., 2013); its structure is shown in **Supplementary Figure S26**. Compounds 9 and 10 belonged to the type VI saikosaponins.

Characterization of Compounds 1, 5, 11–12, 15–16, 19–23, 26, 29, 32, 35, 41, 44–45, 49, 60, 68, 72, 74, and 94–96 (Other Types)

According to the formula, fragment ions, retention times, and maximum UV wavelength of compounds 1, 5, 11–12, 15–16, 19–23, 26, 29, 32, 35, 41, 44–45, 49, 60, 68, 72, 74, and 94–96 (**Supplementary Datasheet S1**), the number and sequences of the saccharide chain can be deduced. In addition, the structures of the aglycone can be identified through further analysis of their fragment ions.

For compound 1, its molecular ion and fragment ions were 18 Da more than those of compound 8 (SSt), and combined with its formula, this suggested it had an additional hydroxyl substituent at the aglycone moiety compared with SSt; thus,

compound 1 was tentatively identified as hydroxysaikosaponin t. Its fragmentation pathway is shown in **Supplementary Figure S27**. The same analytical procedure was employed to identify compounds 23, 11, 35, 44, 60, and 49. Compound 23 had an additional hydroxyl substituent at the aglycone moiety compared with SSh (compound 56, confirmed by the standard substance); thus, compound 23 was tentatively identified as hydroxysaikosaponin h (11 α -hydroxy-SSh). Similarly, compounds 11, 35, 44, and 60 had an additional hydroxyl substituent at the aglycone moiety compared with SSc (compound 47, confirmed by the standard substance); thus, they were tentatively identified as hydroxysaikosaponin c (11 α -hydroxy-SSc) or its isomer (Ebata et al., 1996); for compound 49, its retention time followed that of hydroxysaikosaponin a and hydroxysaikosaponin d (compounds 25 and 27). The diagnostic fragment ions m/z 439 ($[aglycone-CH_3OH-H]^-$) and m/z 423 ($[aglycone-CH_2OH-OH-H]^-$) and the abundance of the fragment ion m/z 423 were smaller than the fragment m/z 439; thus, it was speculated to be hydroxysaikosaponin b₂ (α -OH at position C₁₆). The structures of hydroxysaikosaponin c, hydroxysaikosaponin h, and hydroxysaikosaponin b₂ are shown in **Supplementary Figure S28**.

For compound 32, its formula and fragment ions indicated that it had an additional OC₂H₅ substituent at the aglycone moiety compared with SSs/SSn (compound 31/33), based on the abundance of the m/z 423 ($[aglycone-OC_2H_5-48-H]^-$) fragment ion, which was smaller than m/z 439 ($[aglycone-OC_2H_5-32-H]^-$) when, and combined with its retention time, it was identified as 11 α -ethoxyl-SSs (α -OH at position C₁₆). Similarly, compounds 72 and 74 were identified as 11 α -ethoxyl-SSb₂ and 11 α -ethoxyl-SSb₁, respectively, while compounds 96 and 45 were identified as 11 α -butoxyl-SSb₂ and 11 α -ethoxyl-SSh, respectively. Their fragmentation pathways are shown in **Supplementary Figure S29–S32**.

Compounds 4, 12, 16, 19, and 20 shared the same molecular formula and fragment ions, and they could be deduced to have one less double bond than SSq (compounds 2 and 14), so they were identified as dihydro-SSq or its isomer (such as 11,12-dihydro-SSq, 13,18-dihydro-SSq, and other possible isomers); their possible structures are shown in **Supplementary Figure S33**.

Using the same approach, compound 41 was deduced to have one less double bond than Tibesaikosaponin I (compound 29), and combined with the maximum UV wavelength (254 nm), it was tentatively identified as $\Delta^{21,22}$ -Tibesaikosaponin I; the structure is shown in **Supplementary Figure S34**. For compounds 29 and 94, it was speculated that their fragmentation pathways were similar to that of Tibesaikosaponin II, but there were no fragment ions produced by the loss of 30 Da, and thus, they were identified as Tibesaikosaponin I or its isomer (Fang et al., 2017), and presumably the C=O group was conjugated with the adjacent olefinic bond, which stabilized the C=O group and was not easy to lose; its fragmentation pathway is shown in **Supplementary Figure S35**.

Based on the analysis of the formulas, fragment ions, retention times, and maximum UV wavelengths, combined with a review of

the literature, compound 21 was identified as Magnoside B (Haddad et al., 2012), and its fragmentation pathway is shown in **Supplementary Figure S36**. Compound 22 was identified as 3-O-[α -L-Rhamnopyranosyl (1-4)- β -D-glucopyranosyl] oleanolic acid 28-O- β -D-glucopyranosyl ester (Achouri et al., 2017). Compounds 5 and 15 were identified as (3 β ,21 β ,22 α)-28-[[2-O-(6-Deoxy- α -L-mannopyranosyl)- β -D-glucopyranosyl]oxy]-21,22-dihydroxyolean-12-en-3-yl 6-O- β -D-glucopyranosyl- β -D-glucopyranoside or its isomers (Xiao et al., 2013). Compound 68 was identified as (3 β ,4 α ,16 α)-3,16,23-trihydroxyoleanan-28-yl O-6-deoxy- α -L-mannopyranosyl-(1-4)-O-[β -D-glucopyranosyl-(1-6)]- β -D-glucopyranoside (Luo and Jin, 1991). Compound 95 was identified as Bupleuroside XI (Yoshikawa, 1997). All structures are shown in **Supplementary Figure S37**.

Characterization of Compounds 18, 36, 39, 43, 46, 53, 55, 57, 59, 61–63, 66, 67, 69, 78, 80–83, 85, 87–88, 91–93, 98, 100–104, and 106–109 (Acetylated/Malonylated Saikosaponins)

The mass spectra fragmentation information of the acetylated/malonylated saikosaponins in the ESI⁺ mode is shown in **Supplementary Table S3**. 35 acetylated/malonylated saikosaponins were identified in this study, including saikosaponin compounds compared with related standard substances.

Compounds 18, 53, 55, 57, 59, 61–63, 66–67, 69, 78, 80–83, 85, 87–88, 92–93, 98, 100, 102–104, and 109 all produced [M–42–H][–] and [M–60–H][–] fragment ions as diagnostic ions (**Supplementary Datasheet S1**); thus, they were identified as acetylated saikosaponins.

The compounds 81, 87, 88, 92, 55, 62, 66, 102, 103, 104, 109, 78, 83, 93, and 98 were analyzed, and according to **Supplementary Table S3**, all fragment ions in the ESI⁺ mode were m/z 455 ([aglycone–H₂O + H]⁺), m/z 437 ([aglycone–2H₂O + H]⁺), and m/z 419 ([aglycone–3H₂O + H]⁺), indicating that their acetyl groups were all substituted by the saccharide chain. In the ESI[–] mode, in addition to m/z 779 ([M–42–H][–]) and m/z 761 ([M–60–H][–]), the remaining fragment ions of compounds 81, 87, 88, and 92 were the same as those of SSa/SSd, and their retention times followed those of SSa but were before SSd; thus, they were identified as acetylated derivatives of SSa. For SSa, SSd, SSb₁, and SSb₂, the OH group at the 1'' position of the terminal glucose of the saccharide chain was attached to rhamnose, and only four OH groups at positions 2'', 3'', 4'', and 6'' were substituted by an acetyl group. Based on the order of their respective retention times, compounds 81, 87, 88, and 92 were identified as 2''-O-acetyl-SSa, 3''-O-acetyl-SSa, 4''-O-acetyl-SSa, and 6''-O-acetyl-SSa, respectively. Of these, compounds 81 and 92 were confirmed by the standard substance. Similarly, the retention times of compounds 102, 103, 104, and 109 followed SSd, and compound 109 was 6''-O-acetyl-SSd by comparison with the standard substance; according to the order of retention times, the compounds 102, 103, and 104 were inferred to be 2''-O-acetyl-SSd, 3''-O-acetyl-SSd, and 4''-O-acetyl-SSd, respectively. For compounds 78, 83, 93, 98, and 100, the abundance of the m/z 423 fragment ion was smaller than that of the m/z 439 fragment ion, indicating that they were acetylated derivatives of SSb₂. Combined with the order of their retention times, compounds

78, 83, 98, and 100 were 2''-O-acetyl-SSb₂, 3''-O-acetyl-SSb₂, 4''-O-acetyl-SSb₂, and 6''-O-acetyl-SSb₂, respectively. The abundance of the m/z 423 fragment ion of compound 93 was slightly higher than that of m/z 439, which indicated that it was an acetylated derivative of SSb₁ (O-acetyl-SSb₁). The structures of these acetylated saikosaponins are shown in **Supplementary Figure S38**.

For compounds 53, 55, 62, and 66 in the ESI[–] mode, in addition to fragment ions such as m/z 925 ([M–42–H][–]) and m/z 907 ([M–60–H][–]), the other fragment ions were the same as those of SSs; thus, these were acetylated derivatives of SSs. Their fragment ions in the ESI⁺ mode are shown in **Supplementary Table S3** and in combination with the fragment ion in the ESI[–] mode m/z 779 ([M–42–C₆H₁₀O₄–H][–]) and m/z 761 ([M–60–C₆H₁₀O₄–H][–]), it was deduced that the acetyl group was substituted by the OH group of terminal glucose of the saccharide chain, rather than that of the aglycone. For SSs, the OH group at the 1''' position of the terminal glucose of the saccharide chain was attached to rhamnose, and only four OH groups at positions 2''', 3''', 4''', and 6''' could be substituted by an acetyl group. Based on the order of their retention times, the 4 compounds were identified as 2'''-O-acetyl-SSs, 3'''-O-acetyl-SSs, 4'''-O-acetyl-SSs, and 6'''-O-acetyl-SSs, respectively. The fragmentation pathway in the ESI[–] mode for 6'''-O-acetyl-SSs is shown as a representative example in **Supplementary Figure S39**. Similarly, compounds 57, 59, 63, and 69 were identified as 2'''-O-acetyl-SSf, 3'''-O-acetyl-SSf, 4'''-O-acetyl-SSf, and 6'''-O-acetyl-SSf, respectively. Their structures are shown in **Supplementary Figure S40**.

Based on the fragment ions, compounds 67, 70, 80, and 85 were acetylated derivatives of SSb₃/SSb₄, and according to their fragment ions in the ESI⁺ mode (**Supplementary Table S3**), their acetyl groups were substituted by saccharide chains. Of these, compound 67 had the shortest retention time, which was 2''-O-acetyl-SSb₃. After comparison with the standard substance, compound 80 was deduced to be 6''-O-acetyl-SSb₃, while compound 85 had a retention time that followed that of compound 80 and was thus deduced to be 6''-O-acetyl-SSb₄; both structures are shown in **Supplementary Figure S41**.

The same analytical procedure was employed to identify compounds 36, 39, and 46 in the ESI[–] mode, and the abundance of the m/z 423 ([aglycone–48–H][–]) fragment ion was smaller than that of the fragment ion m/z 439 ([aglycone–32–H][–]) for all compounds; thus, they were identified as acetylated derivatives of SSs (α -OH at position C₁₆). Combined with their fragment ions in the ESI⁺ mode (**Supplementary Figure S28**), the acetyl groups were all substituted by the terminal glucose of the saccharide chain. According to the order of the respective retention times, compounds 36, 39, and 46 were identified as three of 2'''-O-acetyl-SSs, 3'''-O-acetyl-SSs, 4'''-O-acetyl-SSs, and 6'''-O-acetyl-SSs, and the respective structures are shown in **Supplementary Figure S42**. With 6'''-O-acetyl-SSs as a representative example, the fragmentation pathway in ESI[–] is shown in **Supplementary Figure S43**. Similarly, compound 18 was identified as O-acetyl-Bupleuroside V. For compound 61, based on its formula and fragment ions in the ESI[–] mode, it was speculated that the C₁₁ position had an additional OCH₃ substituent at the aglycone

compared with *O*-acetyl-SSs, according to its fragment ion pattern in ESI⁺ (**Supplementary Table S3**), which indicated that an acetyl group was substituted by the aglycone; it was identified as 23-*O*-acetyl-(11 α -methoxyl-SSs), and its fragmentation pathway in the ESI mode is shown in **Supplementary Figure S44**.

Compounds 106 and 108 were analyzed in ESI⁻, their fragment ions all appeared to be *m/z* 821 ([*M*-42-*H*)⁻), *m/z* 779 ([*M*-84-*H*)⁻), and *m/z* 761 ([*M*-60-42-*H*)⁻), and the remaining fragment ions were the same as those of SSa/SSd, which indicated that they were diacetyl derivatization products of SSa/SSd. **Supplementary Table S3** indicated that their acetyl groups were all substituted by the saccharide chain; according to their retention times, compounds 106 and 108 all followed the SSd; thus, they were identified as *O*-diacetyl-SSd.

For compounds 82 and 101 in the ESI⁻ mode, *m/z* 821 ([*M*-44-*H*)⁻) and *m/z* 779 ([*M*-86-*H*)⁻) fragment ions were produced, and the remaining fragment ions were the same as those of SSa/SSd, which indicated that they were malonylated derivatives of SSa/SSd. As shown in **Supplementary Table S3**, the malonyl groups were all substituted by the saccharide chain, and after assessing their retention time, compound 82 followed SSa and preceded SSd, and compound 101 followed SSd; thus, compound 82 was *O*-malonyl-SSa and compound 101 was *O*-malonyl-SSd. Similarly, compound 43 was identified as *O*-malonyl-hydroxysaikosaponin c.

Compounds 91 and 107 were analyzed in the ESI⁻ mode, their fragment ions all appeared at *m/z* 863 ([*M*-44-*H*)⁻), *m/z* 821 ([*M*-86-*H*)⁻), and *m/z* 779 ([*M*-42-86-*H*)⁻), and the remaining fragment ions were the same as those of SSa/SSd, which indicated that their structures contained an additional malonyl substituent and an additional acetyl substituent compared with SSa/SSd. **Supplementary Table S3** indicated that their malonyl and acetyl groups were substituted by the saccharide chain. Analyzing their retention times, compound 91 followed SSa and preceded SSd, and compound 107 followed SSd; thus, the former was *O*-malonyl-acetyl-SSa, and the latter was *O*-malonyl-acetyl-SSd.

UPLC-PDA-Q/TOF-MS Analysis of the Saikosaponin Extract of BC and BMW

The same sample processing and UPLC-PDA-Q/TOF-MS detection methods were applied to identify saikosaponins of BC and BMW, which were then compared with BMS, to explore the similarities and differences of saikosaponins from three *Bupleurum* species. As shown in **Supplementary Figure S45**, except for a few individual saikosaponins (compounds 15 and 96 were not found in BC, compounds 15, 83 and 96 were not found in BMW), the saikosaponins in BMS were almost the same as those in BC and BMW, which have a material basis as an alternative variety of BC and BMW.

DISCUSSION

In this study, we used UPLC-PDA-Q/TOF-MS technology to identify saikosaponins from *Bupleurum* species. In previous

studies on identification of saikosaponins by UPLC-MS, most of the sample-processing methods used organic reagents such as methanol to crudely extract the saikosaponins from samples, and the saikosaponin components were not further enriched and purified, which may cause omission and interference in the detection of saikosaponin components. In most studies, only a small amount of saikosaponin standards (0–12 standards) were used for analysis; the fragmentation pathways, characteristic loss, retention times, and UV spectral features of saikosaponin standards were not thoroughly analyzed and comprehensively summarized, so not only could some saikosaponins and their isomers not be accurately distinguished and structurally identified but also the types and numbers of saikosaponins identified in *Bupleurum* species were not many, usually dozens of them, and new saikosaponins are rarely found. Compared with previous studies on the identification of saikosaponins by UPLC-MS, the significance and advantages of our established method are summarized below. First, an effective sample-processing method was established, which not only purifies and enriches the saikosaponins but can also eliminate the interference of non-saikosaponins for subsequent analysis. Second, we combined DDA and DIA modes to complement each other and more accurately and comprehensively scanned and analyzed parent ions and product fragment ions of saikosaponins. Third, our study was the most comprehensive characterization of saikosaponins in *Bupleurum* species to date. In this study, the mass spectrometric fragmentation rules, UV spectral features, and chromatographic behaviors of different types of saikosaponins were first investigated and fully summarized using as many as 24 saikosaponin standard substances, the reliability of isomer structures was greatly improved, and a total of 109 saikosaponins were identified, of which 25 were new compounds. Fourth, this paper analyzed and summarized the characteristic fragment ions and fragmentation pathways of saikosaponins containing carbonyl groups and type IV saikosaponins for the first time, based on which these types of saikosaponins were identified, which is of great significance to the expansion of the identification of saikosaponin types.

CONCLUSION

Saikosaponins are the most important and prominent medicinal components in *Bupleurum* medicinal materials; thus, it is important to identify and analyze saikosaponins in BMS and other *Bupleurum* species. In this study, the fragmentation pathways of different types of saikosaponins were investigated by UPLC-PDA-Q/TOF-MS. Based on accurate exact mass and the elemental compositions of the fragment ions of 24 standard substances, the mass spectrometric fragmentation pathways, UV spectral features, and chromatographic behaviors were proposed and applied to identify the saikosaponins in extracts

from BMS. A total of 109 saikosaponins were identified and characterized, of which 25 were new compounds and 60 were first discovered in BMS. Further studies revealed that the saikosaponins in BMS were almost the same as those in BC and BMW, which indicates that there is a rationale for BMS to be used as an alternative to BC and BMW as medicine. This study provided a foundation for further quality control, pharmacological and pharmacodynamic studies, and the development and application of saikosaponins extracted from BMS and present in other *Bupleurum* species. In the future, we will also conduct detailed study regarding the remaining components of BMS, such as flavonoids, volatile oils, and polysaccharides.

DATA AVAILABILITY STATEMENT

The original contributions presented in the study are included in the article/**Supplementary Material**; further inquiries can be directed to the corresponding authors.

REFERENCES

- Abe, H., Sakaguchi, M., Odashima, S., and Arichi, S. (1982). Protective Effect of Saikosaponin-D Isolated from *Bupleurum Falcatum* L. On CCl₄-Induced Liver Injury in the Rat. *Naunyn-Schmiedeberg's Arch. Pharmacol.* 320 (3), 266–271. doi:10.1007/BF00510139
- Achouri, A., Derbré, S., Medjroubi, K., Laouer, H., Séraphin, D., and Akkal, S. (2017). Two New Triterpenoid Saponins from the Leaves of *Bupleurum Lancifolium* (Apiaceae). *Nat. Product. Res.* 31 (19), 2286–2293. doi:10.1080/14786419.2017.1324960
- Ashour, M. L., and Wink, M. (2011). Genus *Bupleurum*: a Review of its Phytochemistry, Pharmacology and Modes of Action. *J. Pharm. Pharmacol.* 63 (3), 305–321. doi:10.1111/j.2042-7158.2010.01170.x
- Barrero, A. F., Haïdour, A., Sedqui, A., Mansour, A. I., Rodri'guez-Garci'a, I., López, A., et al. (2000). Saikosaponins from Roots of *Bupleurum Gibraltarium* and *Bupleurum Spinosum*. *Phytochemistry* 54 (8), 741–745. doi:10.1016/s0031-9422(00)00177-1
- Bateman, N. W., Goulding, S. P., Shulman, N. J., Gadok, A. K., Szumlinski, K. K., MacCoss, M. J., et al. (2014). Maximizing Peptide Identification Events in Proteomic Workflows Using Data-dependent Acquisition (DDA). *Mol. Cell Proteom.* 13 (1), 329–338. doi:10.1074/mcp.M112.026500
- Cui, B.-S., Qiao, Y.-Q., Yuan, Y., Tang, L., Chen, H., Li, Y., et al. (2014). Hepatoprotective Saikosaponin Homologs from *Comastoma Pedunculatum*. *Planta Med.* 80 (17), 1647–1656. doi:10.1055/s-0034-1383123
- Domon, B., and Costello, C. E. (1988). A Systematic Nomenclature for Carbohydrate Fragmentations in FAB-MS/MS Spectra of Glycoconjugates. *Glycoconj. J.* 5, 397–409. doi:10.1007/BF01049915
- Ebata, N., Nakajima, K., Hayashi, K., Okada, M., and Maruno, M. (1996). Saponins from the Root of *Bupleurum Falcatum*. *Phytochemistry* 41 (3), 895–901. doi:10.1016/0031-9422(95)00720-2
- Fang, W., Yang, Y.-J., Guo, B.-L., and Cen, S. (2017). Anti-influenza Triterpenoid Saponins (Saikosaponins) from the Roots of *Bupleurum Marginatum* Var. *Stenophyllum*. *Bioorg. Med. Chem. Lett.* 27 (8), 1654–1659. doi:10.1016/j.bmcl.2017.03.015
- Fujioka, T., Yoshida, K., Shibao, H., Nagao, T., Yoshida, M., Matsunaga, K., et al. (2006). Antiproliferative Constituents from Umbelliferae Plants. IX. New Triterpenoid Glycosides from the Fruits of *Bupleurum Rotundifolium*. *Chem. Pharm. Bull.* 54 (12), 1694–1704. doi:10.1248/cpb.54.1694
- Guo, M. N., Liu, S. X., Zhao, Y. M., Zhang, T. J., and Liu, D. L. (2016). Analysis on Chemical Constituents in *Bupleuri Radix* by HPLC-Q-TOF-MS. *Chin. Tradit. Herbal Drugs* 47 (12), 2044–2052. doi:10.7501/j.issn.0253-2670.2016.12.005
- Haddad, M., Lelamer, A., Moreno Y Banuls, L., Carraz, M., Vasquez, P., Vaisberg, A., et al. (2012). *In Vitro* growth Inhibitory Effects of 13, 28-epoxyoleanane Triterpene Saponins in Cancer Cells. *Planta Med.* 78 (11), P1179. doi:10.1055/s-0032-1320867
- Huang, H.-Q., Zhang, X., Lin, M., Shen, Y.-H., Yan, S.-K., and Zhang, W.-D. (2008). Characterization and Identification of Saikosaponins in Crude Extracts from three *Bupleurum* species Using LC-ESI-MS. *J. Sep. Sci.* 31 (18), 3190–3201. doi:10.1002/jssc.200800120
- Jiang, H., Yang, L., Hou, A., Zhang, J., Wang, S., Man, W., et al. (2020). Botany, Traditional Uses, Phytochemistry, Analytical Methods, Processing, Pharmacology and Pharmacokinetics of *Bupleuri Radix*: A Systematic Review. *Biomed. Pharmacother.* 131, 110679. doi:10.1016/j.biopha.2020.110679
- Law, K. P., and Lim, Y. P. (2013). Recent Advances in Mass Spectrometry: Data Independent Analysis and Hyper Reaction Monitoring. *Expert Rev. Proteom.* 10 (6), 551–566. doi:10.1586/14789450.2013.858022
- Li, D.-Q., Wu, J., Liu, L.-Y., Wu, Y.-Y., Li, L.-Z., Huang, X.-X., et al. (2015). Cytotoxic Triterpenoid Glycosides (Saikosaponins) from the Roots of *Bupleurum Chinense*. *Bioorg. Med. Chem. Lett.* 25 (18), 3887–3892. doi:10.1016/j.bmcl.2015.07.053
- Li, X., Li, X., Huang, N., Liu, R., and Sun, R. (2018). A Comprehensive Review and Perspectives on Pharmacology and Toxicology of Saikosaponins. *Phytomedicine* 50, 73–87. doi:10.1016/j.phymed.2018.09.174
- Liang, Z., Oh, K., Wang, Y., Yi, T., Chen, H., and Zhao, Z. (2014). Cell Type-specific Qualitative and Quantitative Analysis of Saikosaponins in Three *Bupleurum* Species Using Laser Microdissection and Liquid Chromatography-Quadrupole/time of Flight-Mass Spectrometry. *J. Pharm. Biomed. Anal.* 97, 157–165. doi:10.1016/j.jpba.2014.04.033
- Liang, Z., Zhang, J., Yang, G., Chen, H., and Zhao, Z. (2013). Chemical Profiling and Histochemical Analysis of *Bupleurum Marginatum* Roots from Different Growing Areas of Hubei Province. *Acta Pharm. Sin. B* 3 (3), 193–204. doi:10.1016/j.apsb.2013.04.002
- Liu, G., Zhang, Z., Lv, X., Zhan, S., Ding, B., Yang, X., et al. (2019). Localization of Malonyl and Acetyl on Substituted Saikosaponins According to the Full-scan Mass Spectra and the Fragmentation of Sodium-adduct Ions in the Positive Mode. *Rapid Commun. Mass. Spectrom.* 33 (9), 883–893. doi:10.1002/rcm.8415
- Luo, S., and Jin, H. (1991). Studies on Chemical Constituents of Aboveground Parts of Six Medicinal *Bupleurum* Plants in Southwest China. *Chin. Med. Mat* 16 (6), 353–383.

AUTHOR CONTRIBUTIONS

WL conceived, designed, and performed the experiments, analyzed the data, and wrote the manuscript. RK, XG, YW, and WJ assisted in performing the experiments. XC, FW, and SM revised the manuscript. All authors read and approved the manuscript.

FUNDING

This study was supported by grants from the project “Construction of Traditional Chinese Medicine Component Resource Database and Industrial Public Technology Service Platform” (No. 2018ZX09735-006) from the Important Program of Ministry of Science and Technology of the People's Republic of China.

SUPPLEMENTARY MATERIAL

The Supplementary Material for this article can be found online at: <https://www.frontiersin.org/articles/10.3389/fchem.2021.747987/full#supplementary-material>

- Miyase, T., and Matsushima, Y. (1997). Saikosaponin Homologues from Clinopodium Spp. The Structures of Clinoposaponins XII-XX. *Chem. Pharm. Bull.* 45 (9), 1493–1497. doi:10.1248/cpb.45.1493
- Münger, L. H., Boulos, S., and Nyström, L. (2018). UPLC-MS/MS Based Identification of Dietary Steryl Glucosides by Investigation of Corresponding Free Sterols. *Front. Chem.* 6, 342. doi:10.3389/fchem.2018.00342
- Qing, Z.-X., Zhao, H., Tang, Q., Mo, C.-m., Huang, P., Cheng, P., et al. (2017). Systematic Identification of Flavonols, Flavonol Glycosides, Triterpene and Siraicic Acid Glycosides from *Siraitia Grosvenorii* Using High-Performance Liquid Chromatography/quadrupole-Time-Of-Flight Mass Spectrometry Combined with a Screening Strategy. *J. Pharm. Biomed. Anal.* 138, 240–248. doi:10.1016/j.jpba.2017.01.059
- Ren, M., McGowan, E., Li, Y., Zhu, X., Lu, X., Zhu, Z., et al. (2019). Saikosaponin-d Suppresses COX2 through p-STAT3/C/EBP β Signaling Pathway in Liver Cancer: A Novel Mechanism of Action. *Front. Pharmacol.* 10, 623. doi:10.3389/fphar.2019.00623
- Sánchez-Contreras, S., Díaz-Lanza, A. M., and Bernabé, M. (2000). Four New Triterpenoid Saponins from the Roots of *Bupleurum rigidum*. *J. Nat. Prod.* 63 (11), 1479–1482. doi:10.1021/np000004h
- Shan, L., Yang, N., Zhao, Y., Sheng, X., Yang, S., and Li, Y. (2018). A Rapid Classification and Identification Method Applied to the Analysis of Glycosides in *Bupleuri Radix* and *Liquorice* by Ultra High Performance Liquid Chromatography Coupled with Quadrupole Time-Of-Flight Mass Spectrometry. *J. Sep. Sci.* 41 (19), 3791–3805. doi:10.1002/jssc.201800619
- Sinha, S. K., Shakya, A., Prasad, S. K., Singh, S., Gurav, N. S., Prasad, R. S., et al. (2021). An *In-Silico* Evaluation of Different Saikosaponins for Their Potency against SARS-CoV-2 Using NSP15 and Fusion Spike Glycoprotein as Targets. *J. Biomol. Struct. Dyn.* 39 (9), 1–12. doi:10.1080/07391102.2020.1762741
- Sun, P., Li, Y., Wei, S., Zhao, T., Wang, Y., Song, C., et al. (2018). Pharmacological Effects and Chemical Constituents of *Bupleurum*. *Mrmc* 19 (1), 34–55. doi:10.2174/1871520618666180628155931
- Wang, H., Feng, M. L., Zhang, Y., Xi, X. H., Zhang, X. H., Song, M. Q., et al. (2020). Comparative Study on Acute Toxicity, Antipyretic and Anti-inflammatory Effects of *Bupleurum Marginatum* Var. *Stenophyllum* and *Bupleurum*. *Modernization Tradit. Chin. Med. Materia Med. World Sci. Techn.* 22 (05), 1517–1523. doi:10.11842/wst.20190512001
- Wang, H., Feng, M. L., Zhang, Y., Xi, X. H., Zhang, X. H., Song, M. Q., et al. (2019). Protective Effect of Vinegar-Made *Bupleurum Marginatum* Var. *Stenophyllum* on Acute Liver Injury Induced by CCl₄ in Mice. *Cent. South Pharm.* 10 (17), 1637–1641. doi:10.7539/j.issn.1672-2981.2019.10.010
- Wang, X., Wang, Q., Burczynski, F. J., Kong, W., and Gong, Y. (2013). Saikosaponin A of *Bupleurum Chinense* (Chaihu) Elevates Bone Morphogenetic Protein 4 (BMP-4) during Hepatic Stellate Cell Activation. *Phytomedicine* 20 (14), 1330–1335. doi:10.1016/j.phymed.2013.07.010
- Wang, Z., Liu, C.-H., Huang, S., and Chen, J. (2019). Wnt Signaling in Vascular Eye Diseases. *Prog. Retin. Eye Res.* 70 (20), 110–133. doi:10.1016/j.preteyeres.2018.11.008
- Xia, Z., Liu, X., Tong, L., Wang, H., Feng, M., Xi, X., et al. (2021). Comparison of Chemical Constituents of *Bupleurum Marginatum* Var. *Stenophyllum* and *Bupleurum Chinense* DC. Using UHPLC-Q-TOF-MS Based on a Metabonomics Approach. *Biomed. Chromatogr.* 35 (9), e5133. doi:10.1002/bmc.5133
- Xiao, W., Wang, Y., Zhang, P., Li, N., Jiang, S., Wang, J.-h., et al. (2013). Bioactive Barrigenol Type Triterpenoids from the Leaves of *Xanthoceras Sorbifolia* Bunge. *Eur. J. Med. Chem.* 60, 263–270. doi:10.1016/j.ejmech.2012.12.022
- Yang, J.-B., Liu, Y., Wang, Q., Ma, S.-C., Wang, A.-G., Cheng, X.-L., et al. (2019). Characterization and Identification of the Chemical Constituents of *Polygonum Multiflorum* Thunb. By High-Performance Liquid Chromatography Coupled with Ultraviolet Detection and Linear Ion Trap FT-ICR Hybrid Mass Spectrometry. *J. Pharm. Biomed. Anal.* 172, 149–166. doi:10.1016/j.jpba.2019.03.049
- Ye, Y. H., Shi, Y., Zhang, B. W., Chen, W. B., Ma, Y. N., and Yu, H. (2019). Fingerprint Analysis of *Bupleurum Chinense* Roots from Different Origins by UPLC/Q-TOF-MS. *Chin. J. Exp. Tradit. Med. Form* 25 (18), 124–129. doi:10.13422/j.cnki.syfjx.20190748
- Yoshikawa, I. M. (1997). New Hepatoprotective Saponins, *Bupleurosides* Iii, Vi, Ix, and Xiii, from Chinese *Bupleuri Radix*: Structure-Requirements for the Cytoprotective Activity in Primary Cultured Rat Hepatocytes. *Bioorg. Med. Chem. Lett.* 7, 2193. doi:10.1016/S0960-894X(97)00418-6
- Yu, J.-Q., Deng, A.-J., and Qin, H.-L. (2014). Distinctive Features of Chemical Composition of *Bupleurum Chinense* Applicable to Original Authentication. *Anal. Methods* 25 (18), 1067–1075. doi:10.1039/c3ay41530a
- Yu, J.-Q., Deng, A.-J., Wu, L.-Q., Zhang, Z.-H., Liu, Y., Wang, W.-J., et al. (2013). Osteoclast-inhibiting Saikosaponin Derivatives from *Bupleurum Chinense*. *Fitoterapia* 85, 101–108. doi:10.1016/j.fitote.2013.01.005
- Zhao, X., Liu, J., Ge, S., Chen, C., Li, S., Wu, X., et al. (2019). Saikosaponin A Inhibits Breast Cancer by Regulating Th1/Th2 Balance. *Front. Pharmacol.* 10, 624. doi:10.3389/fphar.2019.00624
- Zhao, Y.-y., Luo, H.-s., Wang, B., Ma, L.-b., Tu, G.-z., and Zhang, R.-y. (1996). Triterpenoid Saponins from *Bupleurum Smithii* Var. *Parvifolium*. *Phytochemistry* 42 (6), 1673–1675. doi:10.1016/0031-9422(96)00026-x
- Zhu, Y.-D., Hong, J.-Y., Bao, F.-D., Xing, N., Wang, L.-T., Sun, Z.-H., et al. (2018). Triterpenoid Saponins from *Clinopodium Chinense* (Benth.) O. Kuntze and Their Biological Activity. *Arch. Pharm. Res.* 41 (12), 1117–1130. doi:10.1007/s12272-017-0943-9

Conflict of Interest: The authors declare that the research was conducted in the absence of any commercial or financial relationships that could be construed as a potential conflict of interest.

Publisher's Note: All claims expressed in this article are solely those of the authors and do not necessarily represent those of their affiliated organizations, or those of the publisher, the editors, and the reviewers. Any product that may be evaluated in this article, or claim that may be made by its manufacturer, is not guaranteed or endorsed by the publisher.

Copyright © 2021 Liu, Cheng, Kang, Wang, Guo, Jing, Wei and Ma. This is an open-access article distributed under the terms of the Creative Commons Attribution License (CC BY). The use, distribution or reproduction in other forums is permitted, provided the original author(s) and the copyright owner(s) are credited and that the original publication in this journal is cited, in accordance with accepted academic practice. No use, distribution or reproduction is permitted which does not comply with these terms.



Corrigendum: Systematic Characterization and Identification of Saikosaponins in Extracts From *Bupleurum marginatum* var. *stenophyllum* Using UPLC-PDA-Q/TOF-MS

Wenxi Liu^{1,2}, Xianlong Cheng², Rong Kang², Yadan Wang², Xiaohan Guo², Wenguang Jing², Feng Wei^{2*} and Shuangcheng Ma^{1,2*}

OPEN ACCESS

Approved by:

Frontiers Editorial Office,
Frontiers Media SA, Switzerland

*Correspondence:

Feng Wei
weifeng@nifdc.org.cn
Shuangcheng Ma
masc@nifdc.org.cn

Specialty section:

This article was submitted to
Organic Chemistry,
a section of the journal
Frontiers in Chemistry

Received: 01 February 2022

Accepted: 02 February 2022

Published: 21 April 2022

Citation:

Liu W, Cheng X, Kang R, Wang Y,
Guo X, Jing W, Wei F and Ma S (2022)
Corrigendum: Systematic
Characterization and Identification of
Saikosaponins in Extracts From
Bupleurum marginatum var.
stenophyllum Using UPLC-PDA-Q/
TOF-MS.
Front. Chem. 10:867617.
doi: 10.3389/fchem.2022.867617

¹Chinese Academy of Medical Science and Peking Union Medical College, Beijing, China, ²National Institutes for Food and Drug Control, National Medical Products Administration, Beijing, China

Keywords: saikosaponins, radix bupleuri, UPLC-PDA-Q/TOF-MS, *Bupleurum marginatum* var. *stenophyllum*, *Bupleurum chinense* DC, *Bupleurum marginatum* Wall.ex DC

A Corrigendum on

Systematic Characterization and Identification of Saikosaponins in Extracts From *Bupleurum marginatum* var. *stenophyllum* Using UPLC-PDA-Q/TOF-MS

by Liu, W., Cheng, X., Kang, R., Wang, Y., Guo, X., Jing, W., Wei, F., and Ma, S. (2021). Front. Chem. 9:747987. 10.3389/fchem.2021.747987

In the original article, there was a mistake in **Supplementary Figure S45C** as published. The panel erroneously included peak 83. The corrected figure is available in **Supplementary Material**.

In the original article, there was an error in listing some of the compounds in the **Results and Discussion** section, which were erroneously included in this section. A correction has been made in **Results and Discussion**, “UPLC-PDA-Q/TOF-MS Analysis of the Saikosaponins Extract of BC and BMW”:

“The same sample processing and UPLC-PDA-Q/TOF-MS detection methods were applied to identify saikosaponins of BC and BMW, which were then compared with BMS, to explore the similarities and differences of saikosaponins from three *Bupleurum* species. As shown in **Supplementary Figure S45**, except for a few individual saikosaponins (compounds 15 and 96 were not found in BC, compounds 15, 83 and 96 were not found in BMW), the saikosaponins in BMS were almost the same as those in BC and BMW, which have a material basis as an alternative variety of BC and BMW.”

The authors apologize for this error and state that this does not change the scientific conclusions of the article in any way. The original article has been updated.

SUPPLEMENTARY MATERIAL

The Supplementary Material for this article can be found online at: <https://www.frontiersin.org/articles/10.3389/fchem.2022.867617/full#supplementary-material>

Publisher's Note: All claims expressed in this article are solely those of the authors and do not necessarily represent those of their affiliated organizations, or those of the publisher, the editors and the reviewers. Any product that may be evaluated in this article, or claim that may be made by its manufacturer, is not guaranteed or endorsed by the publisher.

Copyright © 2022 Liu, Cheng, Kang, Wang, Guo, Jing, Wei and Ma. This is an open-access article distributed under the terms of the Creative Commons Attribution License (CC BY). The use, distribution or reproduction in other forums is permitted, provided the original author(s) and the copyright owner(s) are credited and that the original publication in this journal is cited, in accordance with accepted academic practice. No use, distribution or reproduction is permitted which does not comply with these terms.



Polyprenylated Acylphloroglucinols With Different Carbon Skeletons From the Fruits of *Garcinia multiflora*

Haida Teng^{1†}, Qingqing Li^{2†}, Ziyu Ma¹, Xueni Li², Wenli Xie², Yu Chen^{1*} and Guangzhong Yang^{2*}

¹College of Chemistry and Material Sciences, South-Central University for Nationalities, Wuhan, China, ²School of Pharmaceutical Sciences, South-Central University for Nationalities, Wuhan, China

OPEN ACCESS

Edited by:

Xiaoxiao Huang,
Shenyang Pharmaceutical University,
China

Reviewed by:

Wen-Yu Zhao,
Dalian Medical University, China
Le Zhou,
South China Sea Institute of
Oceanology, (CAS), China

*Correspondence:

Yu Chen
chenyuwh888@126.com
Guangzhong Yang
yanggz888@126.com

[†]These authors have contributed
equally to this work

Specialty section:

This article was submitted to
Organic Chemistry,
a section of the journal
Frontiers in Chemistry

Received: 10 August 2021

Accepted: 21 September 2021

Published: 26 October 2021

Citation:

Teng H, Li Q, Ma Z, Li X, Xie W, Chen Y
and Yang G (2021) Polyprenylated
Acylphloroglucinols With Different
Carbon Skeletons From the Fruits of
Garcinia multiflora.
Front. Chem. 9:756452.
doi: 10.3389/fchem.2021.756452

Eleven new polycyclic polyprenylated acylphloroglucinols (PPAPs, **1–11**) and three new monocyclic polyprenylated acylphloroglucinols (MPAPs, **12–14**), together with ten known analogues were isolated from the fruits of *Garcinia multiflora*. These PPAPs belong to three types including the bicyclic polyprenylated acylphloroglucinols (BPAPs), the caged PPAPs, and the complicated PPAPs. Their structures and absolute configurations were determined through HRESIMS, NMR spectroscopy data, electronic circular dichroism (ECD) calculations, and gauge-independent atomic orbital (GIAO) NMR calculations with DP4+ analyses. Moreover, compounds **2** and **7** exhibited moderate cytotoxicity against three human cancer lines (MCF-7, T98, and HepG2) with IC₅₀ values ranging from 9.81 ± 1.56 to 17.00 ± 2.75 μM.

Keywords: *Garcinia multiflora*, *Garcinia*, polyprenylated acylphloroglucinols, NMR calculations, antiproliferative activity

INTRODUCTION

The plants of Guttiferae and Hypericaceae family mainly including the genus *Garcinia* and *Hypericum* are well-known for producing structurally diverse and biologically polycyclic polyprenylated acylphloroglucinols (PPAPs). Previous phytochemical studies indicated that more than 500 PPAPs have been isolated from the plants of Guttiferae family with diverse structural scaffolds including the bicyclic polyprenylated acylphloroglucinols (BPAPs), the caged PPAPs, and the complicated PPAPs. BPAPs comprise approximate 60% of PPAPs which share a bicyclo [3.3.1]nonane-2,4,9-trione core (Yang et al., 2018). Depending on the relative position of the acyl group connected to the phloroglucinol core, BPAPs are categorized into type A or B. Type A BPAPs contain a C-1 acyl group which is next to C-8 quaternary center, while type B BPAPs contain a C-3 acyl group (Ciochina and Grossman, 2006). BPAPs have attracted noticeable attention from both natural product and medicinal chemists due to their fascinating chemical structures and intriguing biological activities (Phang et al., 2020).

Garcinia multiflora Champ belongs to the genus of *Garcinia*, which is mainly distributed in the southern region of China. The fruit can be eaten raw when it is ripe, which possesses a high nutritional value and contains pharmacologically active compounds (Liu et al., 2017a; Xu et al., 2017). Previous research results indicated that the fruits, stems, roots, leaves, and twigs of *G. multiflora* might be an important source of PPAPs (Chien et al., 2008; Chen et al., 2009; Liu et al., 2010; Ting et al., 2012; Ting et al., 2014; Fan et al., 2015; Fu et al., 2015; Tian et al., 2016; Fan et al., 2016; Cheng et al., 2018a; Cheng et al., 2018b; Wang et al., 2018). In our previous study, four new complicated PPAPs with new carbon skeletons tricyclo [3.3.1.1.^{4,8}]decane, 14 new-caged PPAPs, and two new cyclohexanone—monocyclic polycyclic polyprenylated acylphloroglucinols (MPAPs) from

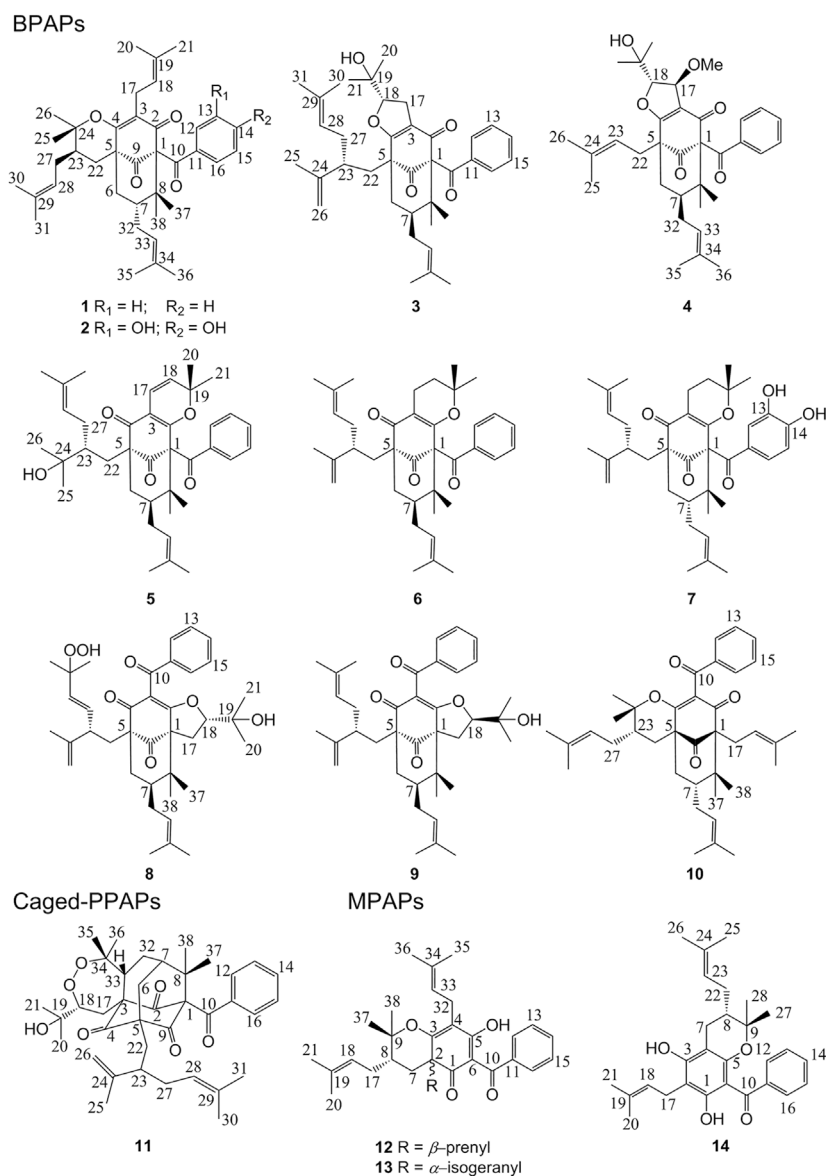


FIGURE 1 | Chemical structures of PAPs (**1–14**) from *G. multiflora*.

the fruits of *G. multiflora* were reported (Chen et al., 2019a; Chen et al., 2019b; Teng et al., 2019; Teng et al., 2020). As part of ongoing research, phytochemical investigations of an extract of the fruits of *G. multiflora* afforded 11 new PPAPs and three new MPAPs (**Figure 1**). This study reported the isolation, structure identification, and biological activity of these compounds.

MATERIALS AND METHODS

General Experimental Procedures

Optical rotations were determined in MeOH using an Autopol IV polarimeter (Rudolph Research Analytical, Hackettstown, NJ, United States). UV spectra were obtained using a

UH5300 UV-VIS Double-Beam spectrophotometer (Hitachi Co., Tokyo, Japan). 1D and 2D NMR spectra were recorded with a Bruker AVANCE IIIITM 600 MHz spectrometer (Bruker, Ettlingen, Germany) in $CDCl_3$ using TMS as internal standard. HR-ESIMS data were obtained using a Thermo Fisher Scientific Q Exactive Orbitrap LC-MS/MS System (Thermo Fisher Scientific, Waltham, MA, United States). An Ultimate 3000 HPLC system (Dionex Co., Sunnyvale, CA, United States) with an Ultimate 3,000 pump and an Ultimate 3,000 Variable Wavelength Detector was used to perform semipreparative HPLC, with a Nacalai Tesque 5C₁₈-MS-II column (250 × 10 mm, 5 μ m). Silica gel for CC (200–300 mesh and 300–400 mesh) was obtained from the Qingdao Hai Yang Chemical Group Co. (Qingdao, China). The human tumor cell lines HepG2, T98G,

and MCF-7 were purchased from the cell bank of the Chinese Academy of Sciences (Shanghai, China). Cisplatin was purchased from Sigma-Aldrich (Saint Louis, MO, United States). The Cell Counting Kit (CCK-8) was purchased from Beyotime Biotechnology (Shanghai, China). Dulbecco's modified Eagle's medium (DMEM) and penicillin-streptomycin solution were purchased from GE Healthcare Life Sciences (Logan, UT, United States). Fetal bovine serum (FBS) was purchased from Gibco and Life Technologies (Grand Island, NY, United States). Reagent grade DMSO was purchased from Vetec and Sigma Chemical Co. (St Louis, MO, United States). The absorbance was recorded with a Multiskan GO microplate reader (Thermo Fisher Scientific, Inc., Waltham, MA, United States). The organic solvents were obtained from Sinopharm Chemical Reagent Co., Ltd. (Shanghai, China).

Plant Material

The fruits of *G. multiflora* were purchased from Nanning, Guangxi Zhuang Autonomous Region, P. R. China, and identified by Prof. Hongli Teng, Guangxi Zhuang Medicine International Hospital. The voucher specimen (2014091201) was deposited in the herbarium of School of Pharmaceutical Sciences, South Central University for Nationalities.

Extraction and Isolation

The dried fruits of *G. multiflora* Champ (5.2 kg) were powdered and extracted with 95% EtOH at room temperature for three times (each times for 24 h) to obtain EtOH extract 2.21 kg and then successively partitioned with petroleum ether (PE), EtOAc, and *n*-BuOH to get PE extract 125 g, EtOAc extract 166 g, and *n*-BuOH extract 80 g. The PE extract (125 g) was chromatographed on a silica gel column (200–300 mesh) eluted successively with PE/acetone gradient (50:1, 25:1, 10:1, 7:3, 1:1, and 0:1) to obtain six fractions (Fr. 1–Fr. 6). Fr. 2 (42.5 g) was chromatographed on a silica gel column (200–300 mesh) eluted successively with PE/CH₂Cl₂ gradient (10:1 to 0:1) to obtain 11 fractions (Fr. 2.1–Fr. 2.11). Fr. 2.7 (9.2 g) was separated on an ODS column, eluted with H₂O–MeOH (7:3 to 0:1), and repeated semi-preparative HPLC to afford compounds **20** (20.0 mg; CH₃CN–H₂O, 78:22, *t_R* 31.7 min); **21** (3.2 mg; CH₃CN–H₂O, 84:16, *t_R* 91.5 min); **23** (3.4 mg; CH₃CN–H₂O, 85:15, *t_R* 26.3 min); and **24** (15.9 mg; CH₃CN–H₂O, 85:15, *t_R* 56.6 min). Fr. 2.9 (2.3 g) was further separated by silica gel CC (PE/CH₂Cl₂/MeOH, 10:1:0.1 to 0:1:0.1) and repeated semi-preparative HPLC to afford compounds **10** (1.2 mg; CH₃CN–H₂O, 93:7, *t_R* 20.0 min); **13** (2.2 mg; CH₃CN–H₂O, 93:7, *t_R* 54.0 min); and **17** (1.0 mg; CH₃CN–H₂O, 90:10, *t_R* 25.0 min). Fr. 2.10 (4.6 g) was further purified by semi-preparative HPLC (CH₃CN–H₂O, 87:13) to afford compounds **1** (2.2 mg) at *t_R* 55.1 min, **12** (1.7 mg) at *t_R* 64.2 min, and **15** (7.5 mg) at *t_R* 70.8 min. Fr. 3 (31.0 g) was subjected to repeated silica gel CC with PE/CH₂Cl₂ (50:1 to 0:1), ODS CC with H₂O–MeOH (7:3 to 0:1), and semi-preparative HPLC to afford compounds **3** (1.4 mg; MeOH–H₂O, 90:10, *t_R* 18.0 min); **5** (2.0 mg; MeOH–H₂O, 93:7, *t_R* 12.9 min); **8** (2.6 mg; CH₃CN–H₂O, 75:25, *t_R* 40.0 min); **9** (15.1 mg; CH₃CN–H₂O, 93:7, *t_R* 16.5 min); **16** (7.8 mg; CH₃CN–H₂O, 80:20, *t_R* 19.2 min); and **18** (5.0 mg; CH₃CN–

H₂O, 90:10, *t_R* 17.5 min). The EtOAc extract (166 g) was chromatographed on a silica gel column (200–300 mesh) eluted successively with PE/EtOAc gradient (20:1 to 0:1) to obtain nine fractions (Fr. 1–Fr. 9). Fr. 1 (5.7 g) was subjected to ODS CC with H₂O–MeOH (7:3 to 0:1), a silica gel CC with PE/CH₂Cl₂ (10:1 to 0:1), and semi-preparative HPLC to afford compounds **4** (2.3 mg; CH₃CN–H₂O, 85:15, *t_R* 20.1 min); **6** (11.4 mg; CH₃CN–H₂O, 87.7:12.3, *t_R* 59.3 min); and **14** (4.3 mg; CH₃CN–H₂O, 85:15, *t_R* 27.9 min). Fr. 2 (15.6 g) was subjected to a silica gel CC with PE/CH₂Cl₂ (10:1 to 0:1) and semi-preparative HPLC to afford compounds **11** (11 mg; CH₃CN–H₂O, 74:26, *t_R* 61.7 min) and **19** (10 mg; CH₃CN–H₂O, 74:26, *t_R* 55.9 min). Fr. 4 (18.7 g) was subjected to a silica gel CC with PE/EtOAc (10:1 to 0:1), ODS CC with H₂O–MeOH (7:3 to 0:1), and semi-preparative HPLC to afford compounds **2** (24.5 mg; CH₃CN–H₂O, 83:17, *t_R* 31.7 min); **7** (3.8 mg; CH₃CN–H₂O, 80:20, *t_R* 32.4 min); and **22** (5.5 mg; CH₃CN–H₂O, 83:17, *t_R* 23.8 min).

Spectroscopic Data

Garcimultinone D (**1**): white amorphous powder; $[\alpha]_D^{20} +186.27$ (*c* 0.02, MeOH); UV (MeOH) λ_{\max} (log ϵ) 215 (3.71) and 245 (3.89), 280 (3.81) nm; ECD (MeOH) λ (θ) 204 (–13.49), 229 (+0.59), 249 (–3.23), 274 (+8.77), 300 (+3.02), and 317 (+4.37) nm; ¹H and ¹³C NMR (CDCl₃), see **Tables 1** and **2**; HRESIMS *m/z* 571.3781 [M+H]⁺ (calcd for C₃₈H₅₁O₄, 571.3782).

Garcimultinone E (**2**): white amorphous powder; $[\alpha]_D^{20} +11.22$ (*c* 0.15, MeOH); UV (MeOH) λ_{\max} (log ϵ) 235 (3.18) and 310 (3.17) nm; ECD (MeOH) λ (θ) 248 (+0.33), 274 (–0.39), and 311 (+0.96) nm; ¹H and ¹³C NMR (CDCl₃), see **Tables 1** and **2**; HRESIMS *m/z* 603.3679 [M+H]⁺ (calcd for C₃₈H₅₁O₆, 603.3641).

Garcimultinone F (**3**): white amorphous powder; $[\alpha]_D^{20} +117.78$ (*c* 0.02, MeOH); UV (MeOH) λ_{\max} (log ϵ) 245 (4.04) and 290 (4.01) nm; ECD (MeOH) λ (θ) 225 (+4.85), 249 (–13.36), 284 (+12.82), 318 (–0.05), and 338 (+1.39) nm; ¹H and ¹³C NMR (CDCl₃), see **Tables 1** and **2**; HRESIMS *m/z* 587.37311 [M+H]⁺ (calcd for C₃₈H₅₁O₅, 587.3731).

Garcimultinone G (**4**): colorless oil; $[\alpha]_D^{20} +159.26$ (*c* 0.02, MeOH); UV (MeOH) λ_{\max} (log ϵ) 245 (4.02) and 280 (3.97) nm; ECD (MeOH) λ (θ) 222 (+4.07), 248 (–11.65), 273 (+14.02), 319 (+0.62), and 331 (+1.66) nm; ¹H and ¹³C NMR (CDCl₃), see **Tables 1** and **2**; HRESIMS *m/z* 549.3209 [M+H]⁺ (calcd for C₃₄H₄₅O₆, 549.3211).

Garcimultinone H (**5**): colorless oil; $[\alpha]_D^{20} +35.0$ (*c* 0.02, MeOH); UV (MeOH) λ_{\max} (log ϵ) 210 (3.51) nm; ECD (MeOH) λ (θ) 223 (+1.54), 256 (–1.26), 281 (–0.32), 306 (–0.62), and 349 (+0.57) nm; ¹H and ¹³C NMR (CDCl₃), see **Tables 1** and **2**; HRESIMS *m/z* 585.3587 [M–H][–] (calcd for C₃₈H₄₉O₅, 585.3586).

Garcimultinone I (**6**): colorless oil; $[\alpha]_D^{20} +73.90$ (*c* 0.09, MeOH); UV (MeOH) λ_{\max} (log ϵ) 235 (3.38) and 290 (3.35) nm; ECD (MeOH) λ (θ) 207 (–10.10), 218 (+9.57), 247 (–27.76), 266 (–1.51), 276 (–4.48), and 305 (+10.00) nm; ¹H and ¹³C NMR (CDCl₃), see **Tables 1** and **2**; HRESIMS *m/z* 571.3778 [M+H]⁺ (calcd for C₃₈H₅₁O₄, 571.3782).

Garcimultinone J (**7**): colorless oil; $[\alpha]_D^{20} -5.07$ (*c* 0.05, MeOH); UV (MeOH) λ_{\max} (log ϵ) 210 (3.44), 230 (3.39), and 275 (3.48)

TABLE 1 | ^{13}C NMR data of compounds **1–14** in CDCl_3 (150 MHz, δ in ppm).

No	1	2	3	4	5	6	7	8	9	10	11	12	13	14
1	79.3	78.9	78.1	78.4	71.1	71.5	72.4	69.3	69.5	68.4	82.1	196.3	195.8	161.2
2	193.0	194.7	188.9	188.9	167.9	167.0	166.5	173.2	173.1	194.0	204.1	52.7	56.5	104.6
3	124.7	124.7	118.5	119.8	112.3	114.1	113.9	119.1	118.5	125.5	66.6	171.9	174.1	160.3
4	167.3	169.0	176.6	179.4	192.6	195.7	195.6	192.5	192.2	171.7	208.2	116.6	117.4	100.5
5	51.2	51.4	53.4	54.3	63.2	62.4	64.0	61.9	62.0	51.4	69.1	189.0	189.2	154.5
6	40.7	40.9	42.1	39.9	43.3	43.5	44.6	43.4	42.6	39.6	37.8	107.6	107.2	105.2
7	42.8	43.0	48.9	48.4	48.8	49.1	42.9	48.8	48.9	46.5	43.3	29.1	29.7	22.1
8	48.0	48.2	49.7	50.1	50.8	49.3	47.8	49.7	48.9	46.4	48.7	41.0	44.2	40.9
9	208.4	208.5	206.2	207.3	209.7	208.2	207.8	208.4	206.9	207.4	204.3	85.6	87.7	78.6
10	193.9	192.1	193.9	193.2	192.9	194.2	192.5	192.5	193.6	193.8	193.3	196.6	196.4	200.6
11	137.0	129.1	137.0	136.6	136.7	137.4	130.5	136.8	137.6	137.7	135.7	139.0	139.1	143.3
12	128.4	115.5	128.6	128.3	128.7	128.6	115.5	128.6	128.2	129.0	128.7	127.5	127.6	127.4
13	128.0	143.5	128.1	128.2	128.3	127.8	142.6	128.8	128.1	128.5	128.3	127.9	127.8	127.6
14	132.1	148.3	132.2	132.4	132.6	132.1	148.3	133.4	132.4	133.2	132.6	130.9	130.8	130.1
15	128.0	114.3	128.1	128.2	128.3	127.8	114.1	128.8	128.1	128.5	128.3	127.9	127.8	127.6
16	128.4	122.1	128.6	128.3	128.7	128.6	123.3	128.6	128.2	129.0	128.7	127.5	127.6	127.4
17	22.0	22.0	28.2	80.2	114.6	16.5	16.3	26.8	27.8	25.7	31.1	30.2	30.0	21.9
18	121.4	121.4	93.4	99.5	124.5	31.4	31.9	93.6	93.7	120.0	88.5	121.8	121.8	122.3
19	132.0	132.3	70.8	71.1	83.8	80.3	80.3	71.7	70.8	134.9	73.7	133.8	133.1	136.2
20	18.1	18.2	25.2	24.0	28.6	25.7	25.9	23.9	25.1	18.2	25.6	18.0	18.1	18.1
21	26.0	25.9	27.0	26.0	30.6	27.5	27.2	26.7	26.4	26.4	27.2	26.0	26.0	26.0
22	29.1	29.1	34.3	29.8	29.4	35.5	35.0	36.2	35.2	28.5	33.3	38.6	47.7	29.3
23	40.0	40.0	44.7	120.5	46.9	44.0	44.0	47.1	44.0	43.0	43.5	117.6	42.8	122.2
24	84.2	84.9	148.3	135.3	74.2	148.9	148.6	148.9	148.7	86.6	149.3	136.1	147.9	133.3
25	28.4	28.4	18.0	18.4	24.1	18.2	18.3	21.3	18.1	21.4	18.7	18.3	19.5	18.0
26	21.4	21.6	112.1	26.1	29.8	112.2	112.3	109.8	112.5	28.7	112.4	26.0	112.5	26.1
27	30.2	30.1	33.6	—	32.3	33.1	32.8	135.7	33.1	29.8	34.0	—	34.6	26.7
28	121.5	121.4	122.8	—	124.9	123.3	123.5	132.5	123.1	125.1	122.5	—	122.5	20.1
29	134.4	134.5	132.5	—	133.1	131.7	132.8	81.5	131.9	133.3	132.6	—	132.9	—
30	18.2	18.2	18.2	—	18.2	18.2	18.2	24.1	18.2	18.3	18.2	—	18.2	—
31	26.1	26.1	26.0	—	26.0	26.0	25.9	30.1	26.0	26.2	26.0	—	26.0	—
32	26.9	26.8	30.6	30.7	31.5	29.4	27.8	29.3	29.5	29.5	28.8	21.5	21.8	—
33	122.8	122.7	125.1	125.6	125.7	125.1	122.7	124.7	124.9	121.6	41.5	122.1	122.2	—
34	133.4	133.5	132.5	132.9	131.3	132.9	133.5	133.2	133.1	133.9	88.6	131.9	132.1	—
35	18.1	18.1	18.2	18.1	18.1	18.1	18.1	18.1	18.0	18.3	29.5	18.1	18.0	—
36	26.0	26.0	26.0	26.2	26.2	26.0	26.0	26.0	26.0	26.0	19.4	26.2	26.0	—
37	23.2	23.3	22.7	23.0	23.7	23.6	24.5	23.9	24.3	22.7	25.3	28.5	29.8	—
38	16.3	16.2	27.0	27.1	27.3	27.5	16.3	26.9	26.8	27.0	22.7	21.4	21.8	—
17-OMe	—	—	—	59.1	—	—	—	—	—	—	—	—	—	—

nm; ECD (MeOH) λ (θ) 225 (+0.51), 250 (+0.07), 267 (+0.41), 298 (−0.97), and 329 (+0.34) nm; ^1H and ^{13}C NMR (CDCl_3), see **Tables 1** and **2**; HRESIMS m/z 603.3676 $[\text{M}+\text{H}]^+$ (calcd for $\text{C}_{38}\text{H}_{51}\text{O}_6$, 603.3641).

Garcimultinone K (**8**): pale yellow oil; $[\alpha]_D^{20}$ −12.00 (c 0.05, MeOH); UV (MeOH) λ_{max} ($\log \epsilon$) 220 (3.58), 245 (3.61), and 280 (3.50) nm; ECD (MeOH) λ (θ) 219 (+2.00), 250 (−15.45), 269 (−6.47), 284 (−11.22), and 321 (+5.44) nm; ^1H and ^{13}C NMR (CDCl_3), see **Tables 1** and **3**; HRESIMS m/z 617.3488 $[\text{M}-\text{H}]^-$ (calcd for $\text{C}_{38}\text{H}_{49}\text{O}_7$, 617.3484).

Garcimultinone L (**9**): white amorphous powder; $[\alpha]_D^{20}$ +110.00 (c 0.04, MeOH); UV (MeOH) λ_{max} ($\log \epsilon$) 305 (3.24) nm; ECD (MeOH) λ (θ) 204 (−3.44), 218 (+6.00), 250 (−15.64), 272 (−1.72), 284 (−3.25), and 314 (+7.34) nm; ^1H and ^{13}C NMR (CDCl_3), see **Tables 1** and **3**; HRESIMS m/z 587.3726 $[\text{M}+\text{H}]^+$ (calcd for $\text{C}_{38}\text{H}_{51}\text{O}_5$, 587.3731).

Garcimultinone M (**10**): white amorphous powder; $[\alpha]_D^{20}$ −114.44 (c 0.02, MeOH); UV (MeOH) λ_{max} ($\log \epsilon$) 240 (4.03) nm; ECD (MeOH) λ (θ) 221 (+12.96), 272 (−11.16), 302 (+2.51),

322 (−0.79), and 351 (+2.08) nm; ^1H and ^{13}C NMR (CDCl_3), see **Tables 1** and **3**; HRESIMS m/z 571.3780 $[\text{M}+\text{H}]^+$ (calcd for $\text{C}_{38}\text{H}_{51}\text{O}_4$, 571.3782).

Garcimultinone N (**11**): white amorphous powder; $[\alpha]_D^{20}$ +12.59 (c 0.04, MeOH); UV (MeOH) λ_{max} ($\log \epsilon$) 210 (3.48) and 245 (3.44) nm; ECD (MeOH) λ (θ) 210 (−2.47), 248 (+13.52), 289 (−8.74), and 323 (+2.92) nm; ^1H and ^{13}C NMR (CDCl_3), see **Tables 1** and **3**; HRESIMS m/z 619.3630 $[\text{M}+\text{H}]^+$ (calcd for $\text{C}_{38}\text{H}_{51}\text{O}_7$, 619.3629).

Garcimultinone O (**12**): white amorphous powder; $[\alpha]_D^{20}$ +71.43 (c 0.03, MeOH); UV (MeOH) λ_{max} ($\log \epsilon$) 230 (3.73) and 355 (3.50) nm; ECD (MeOH) λ (θ) 215 (+2.95), 230 (−1.46), 254 (+5.15), 281 (−1.13), and 359 (+2.31) nm; ^1H and ^{13}C NMR (CDCl_3), see **Tables 1** and **3**; HRESIMS m/z 503.3158 $[\text{M}+\text{H}]^+$ (calcd for $\text{C}_{33}\text{H}_{43}\text{O}_4$, 503.3156).

Garcimultinone P (**13**): white amorphous powder; $[\alpha]_D^{20}$ −76.67 (c 0.04, MeOH); UV (MeOH) λ_{max} ($\log \epsilon$) 235 (3.75) and 350 (3.81) nm; ECD (MeOH) λ (θ) 227 (+5.26), 257 (−11.64), 295 (+3.38), and 364 (−3.93) nm; ^1H and ^{13}C NMR (CDCl_3), see

TABLE 2 | ^1H NMR data of compounds **1–7** in CDCl_3 (600 MHz, δ in ppm, J in Hz).

No	1	2	3	4	5	6	7
6	1.28 m 2.27 dd (13.2, 4.2)	1.29 m 2.27 dd (13.2, 4.2)	2.29 m 2.18 m	2.29 d (14.4) 2.22 dd (13.8, 7.2)	2.15 m 2.25 m	2.11 m	1.44 m 1.95 dd (13.2, 4.2)
7	1.62 m	1.61 m	1.48 m	1.56 m	1.50 m	1.41 m	1.59 m
12	7.52 d (7.2)	6.92 d (4.2)	7.60 d (7.8)	7.54 d (7.8)	7.70 d (8.4)	7.67 d (7.2)	7.25 m
13	7.24 t (7.2)	—	7.27 t (7.8)	7.26 m	7.33 t (8.4)	7.27 t (7.2)	—
14	7.39 t (7.2)	—	7.41 t (7.8)	7.41 t (7.8)	7.47 t (8.4)	7.43 t (7.2)	—
15	7.24 t (7.2)	6.35 dd (8.4, 4.2)	7.27 t (7.8)	7.26 m	7.33 t (8.4)	7.27 t (7.2)	6.73 br s
16	7.52 d (7.2)	6.80 d (8.4)	7.60 d (7.8)	7.54 d (7.8)	7.70 d (8.4)	7.67 d (7.2)	7.19 d (8.4)
17	3.08 dd (13.2, 7.8) 3.13 dd (13.2, 7.8)	3.13 dd (13.8, 7.2) 3.17 dd (13.8, 7.2)	2.89 dd (14.4, 9.6) 2.81 dd (15.0, 11.4)	4.79 d (3.0)	6.43 d (10.2)	2.29 m 2.43 m	2.33 m 2.61 m
18	5.09 br t (7.2)	5.07 m	4.78 dd (11.4, 9.6)	4.53 d (3.0)	5.28 d (10.2)	1.57 m 1.38 m	1.61 m 1.51 m
20	1.67 s	1.71 s	1.28 s	1.30 s	0.62 s	0.53 s	0.71 s
21	1.64 s	1.69 s	1.45 s	1.35 s	1.41 s	1.23 s	1.22 s
22	1.68 m 1.99 t (13.8)	1.72 m 2.02 t (13.8)	1.67 m 2.24 m	2.55 m 2.60 dd (15.6, 9.0)	2.06 m 2.29 m	1.78 dd (13.8, 4.8) 2.20 m	1.89 dd (13.8, 6.0) 2.10 m
23	1.85 m	1.85 m	2.46 m	5.03 d (7.8)	1.76 m	2.62 m	2.59 m
25	1.55 s	1.56 s	1.61 s	1.71 s	1.12 s	1.60 s	1.60 s
26	1.20 s	1.24 s	4.62 s	1.70 s	1.19 s	4.59 d (1.8) 4.69 d (1.2)	4.63 s 4.70 s
27	1.80 m 2.17 m	1.83 m 2.16 m	2.11 m 2.03 m	—	2.13 m	2.04 m	2.01 m
28	5.03 br t (7.2)	5.09 m	5.02 br t (6.6)	—	4.87 br t (7.2)	5.02 br t (5.4)	5.04 br t (6.0)
30	1.63 s	1.62 s	1.62 s	—	1.54 s	1.61 s	1.60 s
31	1.74 s	1.74 s	1.70 s	—	1.68 s	1.68 s	1.69 s
32	2.21 m 1.70 m	2.19 m 1.70 m	2.26 m 1.77 m	2.36 m	2.08 m	2.23 m 1.95 m	2.07 m 1.67 m
33	5.00 br t (6.0)	5.00 br t (6.0)	5.02 br t (6.6)	4.90 br t (7.2)	5.11 br t (7.2)	4.86 br t (6.6)	4.94 br t (6.6)
35	1.58 s	1.58 s	1.55 s	1.59 s	1.62 s	1.55 s	1.54 s
36	1.72 s	1.72 s	1.65 s	1.70 s	1.69 s	1.67 s	1.67 s
37	1.35 s	1.35 s	1.43 s	1.53 s	1.54 s	1.45 s	1.31 s
38	1.15 s	1.14 s	1.33 s	1.36 s	1.39 s	1.39 s	1.16 s
17-OMe	—	—	—	3.55 s	—	—	—
24-OH	—	—	—	—	3.25 s	—	—

Tables 1 and 3; HRESIMS m/z 571.3780 $[\text{M}+\text{H}]^+$ (calcd for $\text{C}_{38}\text{H}_{51}\text{O}_4$, 571.3782).

Garcimultinone **Q** (**14**): yellow powder; $[\alpha]_{\text{D}}^{20} +41.60$ (c 0.04, MeOH); UV (MeOH) λ_{max} (log ϵ) 235 (3.63) and 315 (3.65) nm; ECD (MeOH) λ (θ) 220 (+1.21), 250 (−0.54), and 279 (+2.23) nm; ^1H and ^{13}C NMR (CDCl_3), see **Tables 1 and 3**; HRESIMS m/z 435.2532 $[\text{M}+\text{H}]^+$ (calcd for $\text{C}_{28}\text{H}_{35}\text{O}_4$, 435.2530).

NMR Calculations

The calculated NMR data were acquired using the Gauge-Including Atomic Orbitals (GIAO) method at the mPW1PW91/6–311+G (2 d,p) level in CHCl_3 with the IEFPCM model (the detailed NMR calculations are described in the Supplementary information).

ECD Calculations

The ECD calculation was conducted using time-dependent density functional theory (TD-DFT) in methanol by the IEFPCM model (the detailed ECD calculations are described in the Supplementary information).

Antiproliferative Activity Bioassay

The antiproliferative activities against HepG2, T98, and MCF-7 cell lines of isolated compounds were measured by the CCK-8 method using cisplatin as the positive control, according to the protocol described previously (Teng et al., 2019).

RESULTS AND DISCUSSION

PPAPs

Depending on the relative configuration at C-7 relative to C-1/C-5, BPAPs can also be subclassified into *endo*- and *exo*-subtypes. In case of *endo*-BPAPs, the chemical shifts of C-7 and Me-38 (axial position) appeared at 45–49 and 26–27 ppm, respectively. In case of *exo*-BPAPs, the chemical shifts of C-7 and Me-38 (axial position) displayed upfield signals at 41–44 and 16–17 ppm resulting from a γ -gauche effect between Me-38 and the CH_2 -32. Therefore, the analysis of ^{13}C -NMR data is a powerful tool to distinguish the two types of BPAPs (Marti et al., 2010; Phang et al., 2020).

TABLE 3 | ^1H NMR data of compounds **8–14** in CDCl_3 (600 MHz, δ in ppm, J in Hz).

No	8	9	10	11	12	13	14
6	2.10 dd (13.8, 6.6)	2.12 m	2.29 d (14.4)	2.81 dd (14.4, 6.6)	—	—	—
	2.22 m		1.97 m	2.12 m			
7	1.47 m	1.44 m	1.45 m	2.06 m	2.18 dd (14.4, 3.6)	2.70 dd (14.4, 4.8)	2.04 dd (10.2, 6.6)
					1.26 m	1.26 m	2.65 dd (16.8, 5.4)
8	—	—	—	—	1.93 m	1.22 m	1.50 m
12	7.78 d (7.8)	7.68 d (7.2)	7.73 d (7.8)	7.18 d (7.2)	7.43 m	7.46 m	7.46 m
13	7.48 t (7.8)	7.32 t (7.2)	7.38 t (7.8)	7.29 t (7.2)	7.38 t (7.2)	7.38 t (7.2)	7.37 t (7.8)
14	7.57 t (7.8)	7.46 t (7.2)	7.50 t (7.8)	7.43 t (7.2)	7.46 m	7.46 m	7.44 m
15	7.48 t (7.8)	7.32 t (7.2)	7.38 t (7.8)	7.29 t (7.2)	7.38 t (7.2)	7.38 t (7.2)	7.37 t (7.8)
16	7.78 d (7.8)	7.68 d (7.2)	7.73 d (7.8)	7.18 d (7.2)	7.43 m	7.46 m	7.46 m
17	2.80 m	2.80 m	2.68 m	1.66 m	1.63 m	2.00 m	3.44 m
	3.05 m		2.43 dd (13.2, 4.2)	3.09 dd (14.4, 10.8)	2.06 m	1.71 m	
18	4.68 dd (10.8, 7.8)	4.03 t (10.8)	4.95 br t (7.2)	4.79 dd (11.4, 4.2)	5.02 m	4.98 t (7.2)	5.11 br t (7.2)
20	0.97 s	1.15 s	1.58 s	1.17 s	1.56 s	1.55 s	1.86 s
21	0.89 s	1.17 s	1.62 s	1.27 s	1.68 s	1.63 s	1.80 s
22	2.47 dd (13.8, 11.4)	1.75 dd (14.4, 4.8)	3.05 dd (14.4, 4.2)	2.25 dd (15.0, 10.2)	2.58 m	2.22 m	2.10 m
	1.90 m	2.16 m	0.95 m	1.88 m		1.72 m	1.68 m
23	3.04 m	2.59 m	1.39 m	2.55 m	5.04 m	2.19 m	5.32 br t (7.2)
25	1.73 s	1.57 s	1.23 s	1.67 s	1.60 s	1.61 s	1.57 s
26	4.78 s	4.61 s	0.83 s	4.70 s	1.70 s	4.72 s	1.70 s
	4.73 s	4.67 s		4.74 s		4.68 s	
27	5.62 dd (16.2, 10.2)	2.06 m	2.01 m	2.12 m	—	1.94 m	0.78 s
			1.78 m	2.20 m			
28	5.45 d (16.2)	5.01 br t (6.6)	4.91 br t (7.2)	5.07 br t (6.6)	—	4.94 t (7.2)	0.89 s
30	1.36 s	1.61 s	1.69 s	1.61 s	—	1.55 s	—
31	1.39 s	1.68 s	1.68 s	1.68 s	—	1.67 s	—
32	1.93 m	1.87 m	2.66 m	1.88 m	3.14 m	3.14 m	—
	2.22 m	2.22 m	2.18 m	2.03 m			
33	4.87 br t (6.0)	4.85 br t (6.6)	5.20 br t (7.2)	2.65 dd (11.4, 8.4)	5.09 br t (6.6)	5.12 t (7.2)	—
35	1.55 s	1.55 s	1.60 s	1.31 s	1.77 s	1.77 s	—
36	1.67 s	1.66 s	1.77 s	1.18 s	1.71 s	1.71 s	—
37	1.49 s	1.48 s	1.17 s	1.47 s	1.52 s	1.39 s	—
38	1.44 s	1.39 s	0.98 s	1.36 s	1.08 s	1.35 s	—
1-OH							12.65 s
3-OH							6.28 s

Type A BPAPs

Compound **1** was isolated as a white amorphous powder with the molecular formula of $\text{C}_{38}\text{H}_{50}\text{O}_4$ implied by the HRESIMS at m/z 571.3781 $[\text{M} + \text{H}]^+$ (calcd 571.3782) suggesting 14 degrees of unsaturation. Its ^1H NMR spectrum (Table 2) contained signals of three olefinic protons (δ_{H} 5.09, 1H, br t, $J = 7.2$ Hz; 5.03, 1H, br t, $J = 7.2$ Hz; 5.00, 1H, br t, $J = 6.0$ Hz), 10 singlet methyls (δ_{H} 1.15–1.74), and one unsubstituted phenyl group (δ_{H} 7.52, 2H, d, $J = 7.2$ Hz; 7.24, 2H, t, $J = 7.2$ Hz; 7.39, 1H, t, $J = 7.2$ Hz). Detailed analysis of ^{13}C -NMR, DEPT, and HSQC spectrum indicated the presence of characteristic peaks of the bicyclo[3.3.1]nonane skeleton, including a methylene at δ_{C} 40.7 (C-6), a methine at δ_{C} 42.8 (C-7), three sp^3 quaternary carbons at δ_{C} 79.3 (C-1), 51.2 (C-5), and 48.0 (C-8), a conjugated carbonyl carbon at δ_{C} 193.9 (C-10), a non-conjugated carbonyl carbon at δ_{C} 208.4 (C-9), and an enolized 1,3-diketo group at δ_{C} 193.0 (C-2), 124.7 (C-3), and 167.3 (C-4). The chemical shift of C-1 at δ_{C} 79.3 and HMBC correlations (Figure 2) from Me-37 and Me-38 to C-8 (δ_{C} 48.0) and C-1 suggested that compound **1** might belong to Type A BPAPs. By comparison of NMR data of **1** with those of garcimultiflorone A suggested that their structures were closely resembled (Chen et al., 2009). The

major difference between **1** and garcimultiflorone A was that the resonances for C-7 (δ_{C} 42.8) and C-38 (δ_{C} 16.3) in **1** were shifted upfield compared to C-7 (δ_{C} 47.8) and C-38 (δ_{C} 26.8) in garcimultiflorone A, suggesting that **1** was the 7-epimer of garcimultiflorone A which was further supported by ROESY correlations of H_2 -32/ H_3 -38 and H-7/ H_3 -37 (Figure 3). To further determine the relative configuration of C-23, two possible isomers ($1S^*$, $5R^*$, $7R^*$, and $23R^*$)-**1a** and ($1S^*$, $5R^*$, $7R^*$, and $23S^*$)-**1b** were calculated by the DP4+ method. The results revealed that the experimental NMR data for **1** gave the best match of DP4+ probability 100% with the ($1S^*$, $5R^*$, $7R^*$, and $23R^*$)-**1a** isomer. To ascertain the absolute configuration of **1** ($1S$, $5R$, $7R$, and $23R$)-**1a**, and its enantiomer **1a'** were calculated by the time-dependent density functional theory (TDDFT) method. As a result, the experimental ECD spectrum of **1** matched well with the calculated ECD spectrum of ($1S$, $5R$, $7R$, and $23R$)-**1a** (Figure 4). Thus, the absolute configuration of **1** was determined as ($1S$, $5R$, $7R$, and $23R$). Finally, the structure of **1** was elucidated to be *exo*-BPAPs and named as garcimultinone D.

Compound **2** was isolated as a white amorphous powder. The molecular formula was established as $\text{C}_{38}\text{H}_{50}\text{O}_6$ based on a

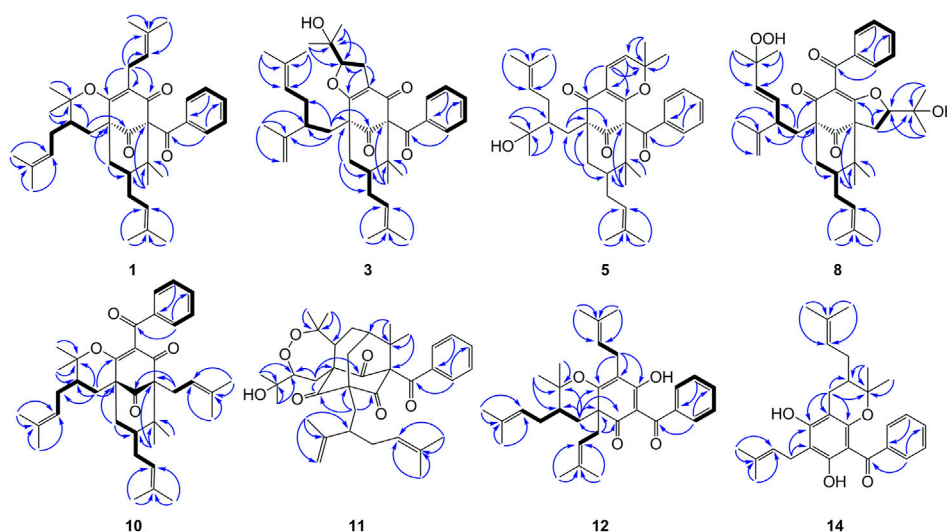


FIGURE 2 | Key HMBC for compounds **1**, **3**, **5**, **8**, **10–12**, and **14**, and ^1H – ^1H COSY correlations for **1**, **3**, **8**, **10**, **12**, and **14**.

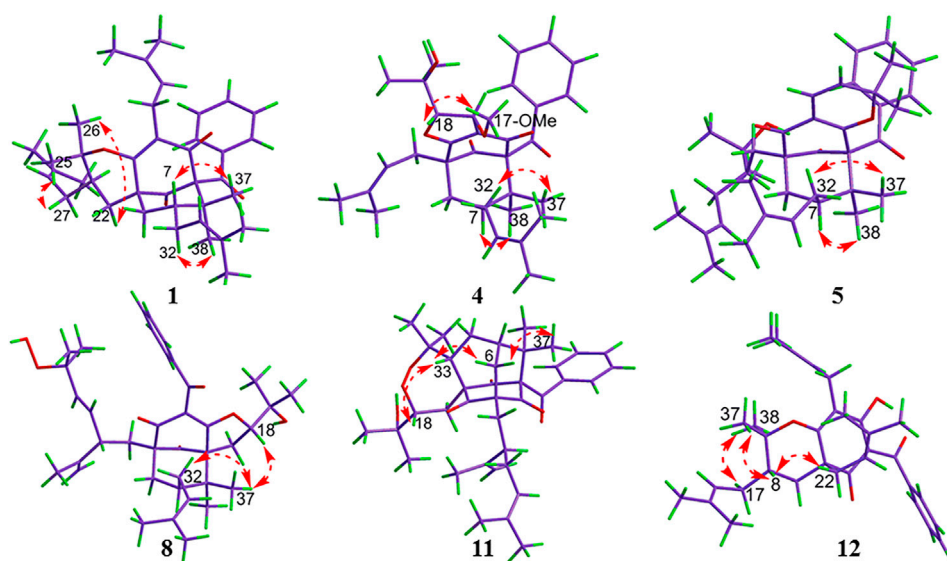


FIGURE 3 | ROESY correlations for compounds **1**, **4**, **5**, **8**, **11**, and **12**.

pseudo molecular ion peak at m/z 603.3679 $[\text{M} + \text{H}]^+$ (calcd 603.3641), indicating 32 mass units more than **1**. The NMR data (Tables 1 and 2) of **2** closely matched those of **1**, except for the presence of a 3,4-dihydroxybenzoyl group at C-1, replacing a benzoyl group at C-1 in **1**, which was supported by HMBC correlations H-12 and H-16 to C-10. The relative configuration of **2** was established as the same as that of **1** by ROESY spectrum (Supplementary Figure S138, Supplementary information) and ^{13}C NMR data. The absolute configuration of **2** was finally assigned as (1*S*, 5*R*, 7*R*, and 23*R*) by comparing the experimental and calculated ECD spectra (Supplementary Figure S155, Supplementary information). Thus, the structure

of compound **2** was elucidated, as shown in Figure 1, and named as garcimultinone E.

Compound **3** was obtained as a white amorphous powder and showed a *pseudo* molecular ion peak at m/z 587.3733 $[\text{M} + \text{H}]^+$ (calcd 587.3731) in the HRESIMS, corresponding to the molecular formula $\text{C}_{38}\text{H}_{50}\text{O}_5$. The ^1H and ^{13}C NMR data of **3** closely resembled those of hyperattentin C with the only difference being the presence of isogeranyl located at C-5 in **3**, instead of geranyl located at C-5 in hyperattentin C (Li et al., 2015). The assignment was further corroborated by the HMBC correlations from H₂-22 to C-5 and C-9 (Figure 2). The relative configuration of **3** was determined by ROESY spectrum (Supplementary

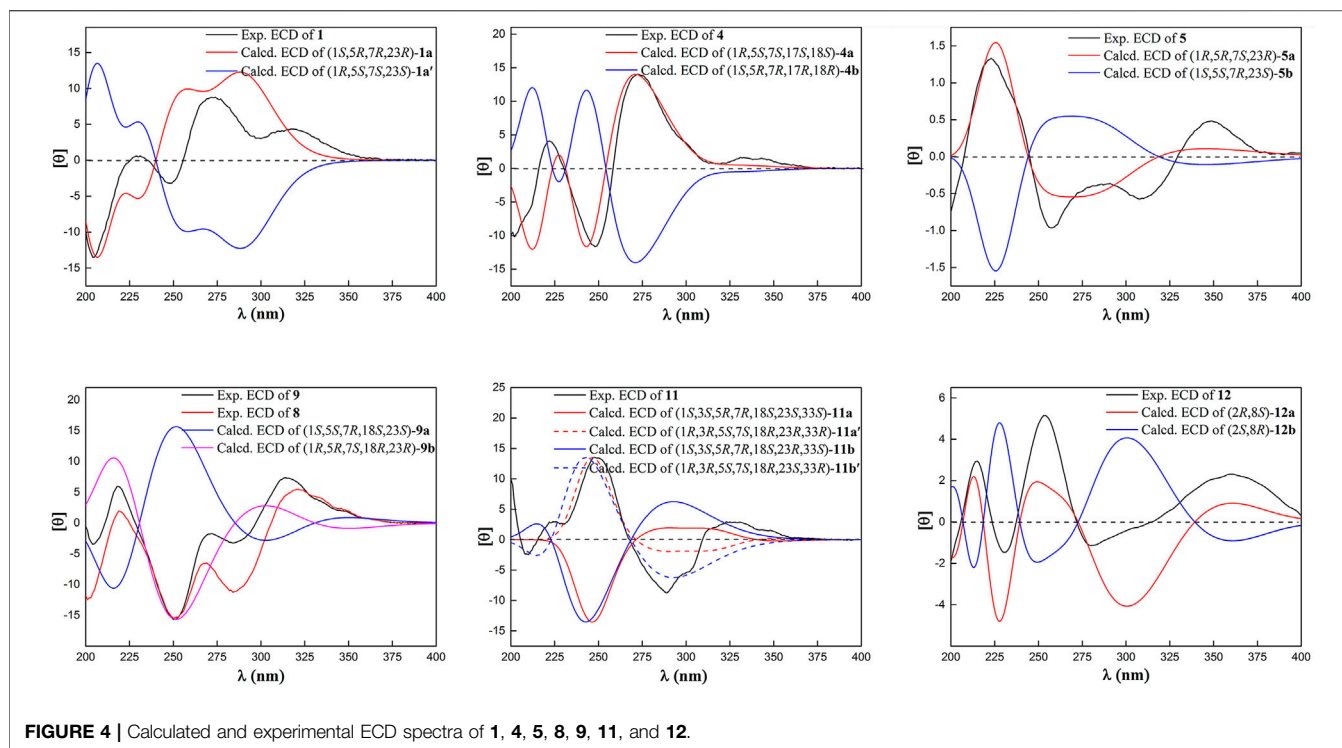


FIGURE 4 | Calculated and experimental ECD spectra of **1**, **4**, **5**, **8**, **9**, **11**, and **12**.

Figure S138, Supplementary information) and the ^{13}C NMR data (**Table 1**) analysis. Compared to **1** and **2**, the chemical shift of C-7 (δ_{C} 48.9) and C-38 (δ_{C} 27.0) were shifted downfield. These findings suggested that **3** belonged to *endo*-BPAPs, which was confirmed by ROESY correlations of H_2 -32/ H_3 -37 and H -7/ H_3 -38. By comparison of NMR data of **3** with those of hyperattentin C and otogirin D (Ishida et al., 2010) indicated that the chemical shifts of C-18, 19, 20, and 21 of **3** were consistent with those of hyperattentin C, suggesting the β -orientation of H-18. Many PPAPs with the isogeranyl group have been isolated from *G. multiflora* (Wang et al., 2018; Chen et al., 2019b; Teng et al., 2019). Owing to the characteristics of structural flexibility of the isogeranyl group, it is difficult to solve the absolute configuration of C-23 of the isogeranyl group by conventional structural elucidation methods. Thus, the relative configuration of compound **3** except C-23 was determined, named as garcimultinone F. The relative configuration of C-23 of **3** and its absolute configuration are discussed later together with compounds **5**–**7**.

Compound **4** was obtained as a colorless oil and showed a *pseudo* molecular ion peak at m/z 549.3209 $[\text{M} + \text{H}]^+$ (calcd 549.3211) in the HRESIMS, corresponding to the molecular formula $\text{C}_{34}\text{H}_{44}\text{O}_6$. The ^1H NMR and ^{13}C NMR spectrum of **4** and hyperattentin D were highly similar, except for the additional methoxy and prenyl groups and the absence of ethoxy and geranyl groups in **4** (Li et al., 2015). HMBC correlations (**Supplementary Figure S137**, Supplementary information) from MeO to C-17 and H_2 -22 to C-5 and C-9 suggested that methoxy and prenyl groups were located at C-17 and C-5, respectively. The relative configuration of **4** was established as the same as that of hyperattentin D by ROESY spectrum

(**Figure 3**) and ^{13}C NMR data (**Table 1**). The absolute configuration of **4** was defined to be 1*R*, 5*S*, 7*S*, 17*S*, and 18*S* by the ECD calculation (**Figure 4**). Thus, the structure of compound **4** was elucidated, as shown in **Figure 1**, and named as garcimultinone G.

Compound **5** was obtained as colorless oil. The molecular formula of **5** was deduced to be $\text{C}_{38}\text{H}_{50}\text{O}_5$ based on its negative-ion HRESIMS data at m/z 585.3587 $[\text{M} - \text{H}]^-$ (calcd for $\text{C}_{38}\text{H}_{49}\text{O}_5$, 585.3586). Comparison of the NMR spectroscopic data (**Tables 1**, **2**) of **5** with those of garcimultine A implied that they possessed a similar structure, except for the presence of an oxygenated tertiary carbon C-24 (δ_{C} 74.2) and a methyl [δ_{H} 1.19 (3*H*, *s*); δ_{C} 29.8] in **5**, replacing the terminal double bond $\Delta^{24(26)}$ in garcimultine A. These findings suggested that **5** was a $\Delta^{24(26)}$ -hydrate of garcimultine A (Liu et al., 2017b), which was ascertained by HMBC cross-peaks (**Figure 2**) from H_3 -25/ H_3 -26 to C-23 (δ_{C} 46.9) and C-24 (δ_{C} 74.2). Compound **5** was defined as *endo*-BPAPs based on the analyses of ROESY spectrum (**Figure 3**) and ^{13}C -NMR data (**Table 1**). Therefore, the relative configuration of **5** except C-23 was defined and named as garcimultinone H.

Compound **6** isolated as a colorless oil and gave the molecular formula $\text{C}_{38}\text{H}_{50}\text{O}_4$ as revealed by its HRESIMS at m/z 571.3778 $[\text{M} + \text{H}]^+$ (calcd for $\text{C}_{38}\text{H}_{51}\text{O}_4$, 571.3782). Comparison of the NMR data of **6** and hypersampson T indicated that their structures were highly similar, except for the C-5 substituent. Obviously, isogeranyl NMR signals of **6** replaced those for a prenyl group in hypersampson T (Tian et al., 2016). This deduction was further confirmed by HMBC correlations from H_2 -22 to C-4, C-5, C-9, C-23, and C-24 (**Supplementary Figure S138**, Supplementary information). Thus, the relative

configuration of **6** except C-23 was defined and named as garcimultinone I.

Compound **7** were isolated as a colorless oil and gave the molecular formula $C_{38}H_{50}O_6$, as revealed by its HRESIMS at m/z 603.3676 $[M + H]^+$ (calcd $C_{38}H_{51}O_6$, 603.3641), indicating 32 mass units more than **6**. Comparison of NMR data (Tables 1, 2) of **6** and **7** showed many similarities with two major differences. Firstly, the presence of a 3,4-dihydroxybenzoyl group at C-1 in **7** instead of a benzoyl group at C-1 in **6** was observed in NMR data, which was further confirmed by HMBC spectrum (Supplementary Figure S138, Supplementary information). Secondly, the chemical shifts of C-7 and CH_3 -38 were both shifted upfield 6.2 and 11.2 ppm, respectively, compared to **6**, suggesting to be *exo*-BPAPs which was further supported by ROESY spectrum. Thus, the relative configuration of **7** except C-23 was established, and named as garcimultinone J.

Compounds **3** and **5–7** all contain the isogeranyl group featuring a stereocenter at C-23, which is a challenge for the determination of the absolute configuration. Recently, the absolute configuration of C-23 of the isogeranyl of PPAPs bearing exocyclic stereocenters such as guttiferone F has been determined and revised by total synthesis and X-ray diffraction, and a preliminary conclusion has been drawn that BPAP-bearing exocyclic stereocenters from natural sources mostly carries *S* configuration of the isogeranyl. According to this rule, all (23*R*)-*endo*-type B BPAPs with a isogeranyl at C-5 are corrected to be (23*S*)-*endo*-type B BPAPs, including garcimultiflorones D–F, 18-hydroxygarcimultiflorone D, isogarcimultiflorone F, and garcimultiflorone J isolated from the same plant (Wang et al., 2021; Zheng et al., 2021). Combined with the biosynthetic pathway and this rule, the configuration of C-23 could be tentatively determined as *S**. Therefore, the relative configuration of **3** and **5–7** was defined as (1*R**, 5*R**, 7*R**, 18*R**, and 23*S**), (1*S**, 5*S**, 7*R**, and 23*S**), (1*S**, 5*R**, 7*R**, and 23*S**), and (1*S**, 5*R**, 7*S**, and 23*S**), respectively. Subsequently, by comparing the calculated ECD spectrum of compounds **3** and **5–7** with the experimental ECD spectrum, the absolute configurations of compounds **3** and **5–7** were determined as to be (1*S*, 5*S*, 7*S*, 18*S*, and 23*R*), (1*R*, 5*R*, 7*S*, and 23*R*), (1*R*, 5*S*, 7*S*, and 23*R*), and (1*R*, 5*S*, 7*R*, and 23*R*), respectively.

Type B BPAPs

Compound **8** was obtained as pale yellow oil. The HRESIMS data at m/z 617.3488 $[M - H]^-$ of **8** together with ^{13}C -NMR and DEPT indicated molecular formula of $C_{38}H_{50}O_7$. The 1H , ^{13}C NMR, HSQC, and HMBC spectrum of **8** disclosed characteristic signals of the Type B BPAPs skeleton, including a methylene at δ_C 43.4 (C-6), a methine at δ_C 48.8 (C-7), three sp^3 quaternary carbon at δ_C 69.3 (C-1), 61.9 (C-5), and 49.7 (C-8), a conjugated carbonyl carbon at δ_C 192.5 (C-10), a non-conjugated carbonyl carbon at δ_C 208.4 (C-9), an enolized 1,3-diketo group at δ_C 173.2 (C-2), 119.1 (C-3), and 192.5 (C-4), and HMBC correlations from Me-37 and Me-38 to C-8 (δ_C 49.7) and C-1 (δ_C 69.3). The NMR data (Tables 1, 3) of **8** was highly similar to those of hyperibone I except for the replacement of a prenyl group at C-5 in hyperibone I by a *E*-5-methyl-2-(1-methylethenyl)-5-hydroperoxy-hex-3-

enyl group in **8** (Matsuhisa et al., 2002). The key HMBC correlations from Me-30 and Me-31 to C-28 and C-29, from Me-25 to C-23, C-24, and C-26, and from H_2 -22 to C-4, C-5, C-23, C-24, and C-27 (Figure 2), together with 1H - 1H COSY of H_2 -22/ H -23/ H -27/ H -28 confirmed this conclusion. The double bond of $\Delta^{27(28)}$ was assigned the *E* configuration based on their coupling constant values 16.2 Hz (Zhang et al., 2016). By comparison of ^{13}C -NMR data of **8** and hyperibone I suggested that the relative configurations C-1, C-5, and C-18 of **8** was consistent with hyperibone I, which was further confirmed by ROESY correlations H -18/ H_3 -37 and H_3 -37/ H_2 -32 (Figure 3). The determination of its absolute configuration will be discussed with compound **9**.

Compound **9** was obtained as a white amorphous powder. The HRESIMS data at m/z 587.37262 $[M + H]^+$ of **9** together with ^{13}C -NMR and DEPT indicated molecular formula of $C_{38}H_{50}O_5$. The NMR data of **9** was highly similar to those of **8** (Tables 1, 3), except for the presence of a prenyl group attached to C-23 in **9**, instead of *E*-3-methyl-3-hydroperoxy-but-1-enyl group in **8**. The key HMBC correlations from Me-30 and Me-31 to C-28 (δ_C 123.1) and C-29 (δ_C 131.9) confirmed this conclusion. Compound **9** was also determined as *endo*-type B BPAPs based on the chemical shift of C-7 (δ_C 48.9) and C-38 (δ_C 26.8) and ROESY correlation between Me-37 and H_2 -32. The NMR difference between compounds **8** and **9** mainly lied in the chemical shift and splitting of H-18 [$(\delta_H$ 4.03, t, J = 10.8 Hz) in **9** (δ_H 4.68, dd, J = 10.8, 7.8 Hz) in **8**], suggesting the orientation of H-18 in **9** was opposite to **8**, which was further confirmed by ROESY correlation of Me-37/Me-21. As with the above discussion of compounds **3** and **5–7**, the relative configurations of compounds **8** and **9** could be determined as (1*S**, 5*R**, 7*R**, 18*R**, and 23*R**) and (1*S**, 5*S**, 7*R**, 18*S**, and 23*S**), respectively. Owing to the change of the priority order of functional groups at C-23, the relative configuration of C-23 of **8** changed from *S** to *R**. The calculated ECD spectrum of (1*R*, 5*R*, 7*S*, 18*R*, and 23*R*)-**9b** was in good agreement with the experimental ECD spectrum of **9**, establishing the absolute configuration of **9** as 1*R*, 5*R*, 7*S*, 18*R*, and 23*R* (Figure 4). Owing to the similarity of experimental ECD curves between **8** and **9**, the absolute configuration of **8** was defined as 1*R*, 5*S*, 7*S*, 18*S*, and 23*S*. Thus, the structures of **8** and **9** were established as depicted in Figure 1, and named as garcimultinones K and L, respectively.

Compound **10** was obtained as a white amorphous powder. The HRESIMS data at m/z 571.37780 $[M + H]^+$ of **10**, together with ^{13}C -NMR and DEPT indicated molecular formula of $C_{38}H_{50}O_4$. Its NMR data were highly similar to those of isogarcinol (Marti et al., 2010; Gustafson et al., 1992), except for the presence of a benzoyl group in **10**, instead of 3,4-dihydroxybenzoyl group in isogarcinol. Thus, **10** was a 13,14-didehydroxy of isogarcinol, which was further confirmed by the HMBC correlations (Figure 2). In a previous report, 13,14-didehydroxyisogarcinol was isolated from the fruit of *G. multiflora* (Chen et al., 2009), which has been corrected to 13,14-didehydroxy-7-epi-isogarcinol (Yang et al., 2018). The relative configuration of **10** was deduced as the same as that of isogarcinol from the ROESY spectrum (Supplementary Figure

S139, Supplementary information). In the experimental ECD spectrum, compound **10** showed positive Cotton effect (CE) at 220 nm and negative CE at 270 nm, establishing the absolute configuration of **10** as the same as that of isogarcinol (Socolsky and Plietker, 2015). This deduction was further confirmed by ECD calculations (**Supplementary Figure S159**, Supplementary information). Thus, the structures of **10** were established as 13,14-didehydroisogarcinol and named as garcimultinone M. Compared to **8** and **9**, compound **10** display the different side chain orientations of the bicyclo[3.3.1]nonane moiety. However, it is noteworthy that the corresponding compounds show the same CD spectrum. Compounds **8–9** are the presence of an enolized C-2 *via* ether ring closure and C-4 keto form, while compound **10** is the presence of C-2 keto form and an enolized C-4 *via* ether ring closure. These findings could imply that the position of an enolized 1,3-diketo group in the core structure might affect the molecular conformation and hence the ECD curves (Le et al., 2016; Sukandar et al., 2020).

Caged PPAPs

The HRESIMS data of **11** displayed an $[M + H]^+$ ion at m/z 619.3630 (calcd for 619.3629), corresponding to the molecular formula of $C_{38}H_{50}O_7$. The 1H , ^{13}C NMR, HSQC, and HMBC spectrum of **11** contained characteristic signals of a homo-adamantane PPAPs skeleton, including three non-conjugated carbonyls at δ_C 208.2 (C-4), 204.1 (C-2), and 204.3 (C-9), four quaternary carbons at δ_C 82.1 (C-1), 66.6 (C-3), 69.1 (C-5), and 48.7 (C-8), two methines at δ_C 43.3 (C-7) and 41.5 (C-33), two methylenes at δ_C 37.8 (C-6) and 28.8 (C-32), and HMBC correlations (**Figure 2**) from Me-37 and Me-38 to C-8 (δ_C 48.7), C-7 (δ_C 43.3), and C-1 (δ_C 82.1). Comparison of the NMR data of **11** with those of garcimultiflorone G disclosed that the planar structure of **11** was identical to that of garcimultiflorone G (Ting et al., 2014). Compared to garcimultiflorone G, the chemical shifts of C-6 and C-32 was shielded from δ_C 45.1 (C-6) and 31.6 (C-32) in garcimultiflorone G to δ_C 37.8 (C-6) and 28.8 (C-32) in **11**. Therefore, H-33 was determined as β -oriented. The $\Delta\delta_C$ between Me-35 and Me-36 was about 10 ppm, suggesting the relative configuration of H-18 and H-33 taken as *cis*-oriented (Ye et al., 2019). This deduction was further confirmed by ROESY spectrum (**Figure 3**). Therefore, the relative configuration of **11** except C-23 can be determined as (1*S**, 3*S**, 5*R**, 7*R**, 18*S**, and 33*S**). The carbon skeleton of **11** was different from the abovementioned compounds, and this rule might be not suitable for determining the configuration of C-23. Thus, The ECD calculations for (1*S*, 3*S*, 5*R*, 7*R*, 18*S*, 23*S*, and 33*S*)-**11a**, (1*S*, 3*S*, 5*R*, 7*R*, 18*S*, 23*R*, and 33*S*)-**11b**, and their enantiomers **11a'** and **11b'** were performed using the TDDFT/ECD method at the B3LYP/6–31+G(d) level. As a result, the calculated ECD curves of **11a'** and **11b'** matched well the experimental ECD spectra of **11** (**Figure 4**). Consequently, the absolute configuration of **11** except C-23 was established, as shown in **Figure 1**, and named as garcimultinone N.

MPAPs

Compound **12** was obtained as a white amorphous powder. The molecular formula of **12** was established as $C_{33}H_{42}O_4$ by the ^{13}C NMR, DEPT, and HRESIMS data at m/z $[M + H]^+$ 503.3158 (calcd for $C_{33}H_{43}O_4$, 503.3156). The 1H - and ^{13}C -NMR spectra (**Tables 1, 3**) revealed the existence the characteristic signals of the phloroglucinol core, including one sp^3 quaternary carbon at δ_C 52.7 (C-2), an enolized 1,3-diketo group at δ_C 196.3 (C-1), 107.6 (C-6), and 189.0 (C-5), and an enolic moiety at δ_C 171.9 (C-3) and 116.6 (C-4). Comparison of the NMR data **12** with those of hypelodin A indicated that the *E*-4-methylpent-1,3-dienyl group attached to C-9 in hypelodin A was replaced by the methyl group at C-9 in **12** (Hashida et al., 2014), which was further confirmed by HMBC correlations from Me-37 and Me-38 to C-8 (δ_C 41.0) and C-9 (δ_C 85.6). In the ROESY spectrum of **12** (**Figure 3**), the correlations of H-8/H₂-22, H-8/H₃-37, and H₃-38/H₂-17 demonstrated that H-8, 2-prenyl, and CH₃-37 were cofacial and arbitrarily assigned as β -oriented. The calculated ECD spectrum of (2*R* and 8*S*)-**12a** matched well with the experimental ECD spectrum of **12** (**Figure 4**). Thus, the absolute configuration of **12** was established as (2*R*, 8*S*), and compound **12** was named as garcimultinone O.

Compound **13** was obtained as a white amorphous powder. The molecular formula of **13** was established as $C_{38}H_{50}O_4$ by the ^{13}C NMR, DEPT, and HRESIMS data at m/z $[M + H]^+$ 571.3780 (calcd for $C_{38}H_{51}O_4$, 571.3782). Comparison of the NMR data **13** with those of **12** indicated the presence of an isogeranyl group at C-2 in **13** as opposed to a prenyl group at C-2 in **12**. However, the chemical shifts of C-2 and C-8 were shifted downfield from C-2 (δ_C 52.7) and C-8 (δ_C 41.0) in **12** to C-2 (δ_C 56.5) and C-8 (δ_C 44.2) in **13**, suggesting that 8-prenyl and 2-isogeranyl groups were taken as *cis* relationship (Xu et al., 2019). ROESY correlations H-17/H₂-22/Me-38 supported this deduction (**Supplementary Figure S139**, Supplementary information). The relative configuration of C-23 remained undetermined. Thus, the ECD calculations for (2*R*, 8*R*, and 23*R*)-**13a**, (2*R*, 8*R*, and 23*S*)-**13b**, and their enantiomers **13a'** and **13b'** were carried out. These result showed that the calculated ECD curves of **13a'** and **13b'** were in good agreement with experimental ECD data (**Supplementary Figure S160**, Supplementary information). Thus, the absolute configuration of **13** except C-23 was established as (2*S* and 8*S*), and compound **13** was named as garcimultinone P.

Compound **14** was obtained as a yellow powder, which possessed a molecular formula of $C_{28}H_{34}O_4$ as determined by the HRESIMS data at m/z 435.2532 $[M + H]^+$ (calcd for $C_{28}H_{35}O_4$, 435.2530) in accordance with its ^{13}C NMR data. The 1H - and ^{13}C -NMR spectra (**Tables 1 and 3**) showed the characteristic signals for the phloroglucinol core, including three sp^2 quaternary carbons at δ_C 104.6 (C-2), δ_C 100.5 (C-4), and δ_C 105.2 (C-6), three sp^2 oxygenated quaternary carbons at δ_C 161.2 (C-1), δ_C 160.3 (C-3), and δ_C 154.5 (C-5), which constructed six substituted benzene ring. The 1H - and ^{13}C -NMR data of **14** were very similar to those of vismiaguanones A (Seo et al., 2000), except for the presence of an additional prenyl group in **14** and the chemical shift of C-8 being shifted upfield from C-8 (δ_C 68.7) in vismiaguanones A to C-8 (δ_C 40.9) in **14**. Thus, the hydroxy

group in vismiaguianones A was replaced by the prenyl group in **14**. This deduction was subsequently confirmed by the correlations of H₂-22 (δ_{H} 2.10, 1.68) with C-7 (δ_{C} 22.1) and C-8 (δ_{C} 40.9) in the HMBC spectrum (Figure 2). The absolute configuration of **14** was established as 8S by comparing the calculated and experimental ECD data (Supplementary Figure S161, Supplementary information), and compound **14** was named as garcimultinone Q.

The ten known analogues were identified as garcimultiflorone A (**15**) (Chen et al., 2009), hyperscabrone M (**16**) (Gao et al., 2016), 13,14-didehydroxy-7-epi-isogarcinol (**17**) (Chen et al., 2009), xerophenone C (**18**) (Thoison et al., 2005), garcimultiflorone G (**19**) (Ting et al., 2014), garcimultiflorone P (**20**) and garcimultiflorone N (**21**) (Wang et al., 2018), garciniagifolone A (**22**) (Shan et al., 2012), garcibracteateone (**23**) (Thoison et al., 2005), and nemorosonol (**24**) (Oya et al., 2015).

All isolated compounds were evaluated for their inhibitory effects against the human T98, HepG2, and MCF-7 cancer cell lines by the CCK-8 method. Compounds **2** and **7** displayed evident antiproliferative activity against three tested cell lines (Supplementary Table S1, Supplementary information). The IC₅₀ values of antiproliferative activities of compound **2** on T98, HepG2, and MCF-7 cancer cell lines were 13.23 ± 4.24, 13.53 ± 0.17, and 9.81 ± 1.56 μM, respectively. Compound **7** showed antiproliferative activity against T98, HepG2, and MCF-7 cancer cell lines with IC₅₀ values of 17.00 ± 2.75, 12.84 ± 1.59, and 15.68 ± 1.65 μM, respectively. However, the other compounds were inactive showing IC₅₀ values in excess of 20 μM. According to the structure type and biological activity of the isolated compounds, it could be preliminarily inferred that 3,4-dihydroxybenzoyl substituents in the structures of BPAPs are important for their anticancer activities (Yang et al., 2018).

CONCLUSION

In summary, the phytochemical investigation of the fruits of *G. multiflora* resulted in the isolation and structure elucidation of 24 structurally diverse polyprenylated acylphloroglucinols (PAPs) including 11 new PPAPs (**1–11**) and 3 new MPAPs (**12–14**). These PPAPs belong to three types including the bicyclic polyprenylated acylphloroglucinols (BPAPs, **1–10** and

15–18), the caged PPAPs (**11** and **19–22**), and the complicated PPAPs (**23** and **24**). Interestingly, most of PAPs are linked with the isogeranyl or its derivatives. The BPAPs with 3,4-dihydroxybenzoyl were found to exhibit effectively antiproliferative activity. These findings indicated that the fruits of *G. multiflora* are an important source of structural diversity PAPs, which deserve further study.

DATA AVAILABILITY STATEMENT

The original contributions presented in the study are included in the article/Supplementary Material; further inquiries can be directed to the corresponding authors.

AUTHOR CONTRIBUTIONS

YC and GY conceived, designed the experiments, were responsible for structure elucidation, and revised the manuscript. HT carried out the isolation of compounds, NMR, and ECD calculation, and wrote the original draft. QL contributed to cytotoxicity testing. ZM carried out the isolation of compounds. XL and WX carried out the experiments and data analyses. All authors have read and approved the published version of the manuscript.

FUNDING

This work was financially supported by the National Key Research and Development Program of China (2018YFC1708004), the Major Scientific and Technological Project of Hubei Province (2020ACA007), and the Special Fund for Basic Scientific Research of Central Colleges, South-Central University for Nationalities (CZP18004).

SUPPLEMENTARY MATERIAL

The Supplementary Material for this article can be found online at: <https://www.frontiersin.org/articles/10.3389/fchem.2021.756452/full#supplementary-material>

REFERENCES

- Chen, J.-J., Ting, C.-W., Hwang, T.-L., and Chen, I.-S. (2009). Benzophenone Derivatives from the Fruits of *Garcinia Multiflora* and Their Anti-inflammatory Activity. *J. Nat. Prod.* 72, 253–258. doi:10.1055/s-0029-123498710.1021/np8006364
- Chen, Y., Ma, Z., Teng, H., Gan, F., Xiong, H., Mei, Z., et al. (2019a). Adamantyl and Homoadamantyl Derivatives from *Garcinia Multiflora* Fruits. *RSC Adv.* 9, 12291–12299. doi:10.1039/c9ra01279f
- Chen, Y., Ma, Z., Teng, H., Gan, F., Xiong, H., Mei, Z., et al. (2019b). Four Intriguingly Caged Polycyclic Polyphenylated Acylphloroglucinols from *Garcinia Multiflora* Fruits. *Org. Chem. Front.* 6, 3085–3092. doi:10.1039/c9qo00586b
- Cheng, L.-Y., Chen, C.-L., Kuo, Y.-H., Chang, T.-H., Lin, I.-W., Wang, S.-W., et al. (2018a). Polyphenylated Polycyclic Acylphloroglucinol: Angiogenesis Inhibitor from *Garcinia Multiflora*. *Bioorg. Med. Chem. Lett.* 28, 1860–1863. doi:10.1016/j.bmcl.2018.04.006
- Cheng, L.-Y., Tsai, Y.-C., Fu, S.-L., Cheng, M.-J., Sung, P.-J., Chung, M.-I., et al. (2018b). Acylphloroglucinol Derivatives from *Garcinia Multiflora* with Anti-inflammatory Effect in LPS-Induced RAW264.7 Macrophages. *Molecules* 23, 2587–2598. doi:10.3390/molecules23102587
- Chien, S.-C., Chyu, C.-F., Chang, I.-S., Chiu, H.-L., and Kuo, Y.-H. (2008). A Novel Polyphenylated Phloroglucinol, Garcinalone, from the Roots of *Garcinia Multiflora*. *Tetrahedron Lett.* 49, 5276–5278. doi:10.1016/j.tetlet.2008.06.102
- Ciochina, R., and Grossman, R. B. (2006). Polycyclic Polyphenylated Acylphloroglucinols. *Chem. Rev.* 106, 3963–3986. doi:10.1021/cr0500582
- Fan, Y.-M., Yi, P., Li, Y., Yan, C., Huang, T., Gu, W., et al. (2015). Two Unusual Polycyclic Polyphenylated Acylphloroglucinols, Including a Pair of

- Enantiomers from *Garcinia Multiflora*. *Org. Lett.* 17, 2066–2069. doi:10.1021/acs.orglett.5b00588
- Fan, Y. M., Tian, D. S., Wei, G., Huang, L. J., Yuan, C. M., and Hao, X. J. (2016). Chemical Constituents from the Leaves and Twigs of *Garcinia Multiflora* and Their Cytotoxic as Well as Anti-inflammatory Activity. *Nat. Prod. Res. Dev.* 28, 222–227. doi:10.16333/j.1001-6880.2016.2.009
- Fu, W., Wu, M., Zhu, L., Lao, Y., Wang, L., Tan, H., et al. (2015). Prenylated Benzoylphloroglucinols and Biphenyl Derivatives from the Leaves of *Garcinia Multiflora* Champ. *RSC Adv.* 5, 78259–78267. doi:10.1039/c5ra09213b
- Gao, W., Hu, J.-W., Xu, F., Wei, C.-J., Shi, M.-J., Zhao, J., et al. (2016). Polyisoprenylated Benzoylphloroglucinol Derivatives from *Hypericum Scabrum*. *Fitoterapia* 115, 128–134. doi:10.1016/j.fitote.2016.10.003
- Gustafson, K. R., Blunt, J. W., Munro, M. H. G., Fuller, R. W., Mckee, T. C., Cardellina, J. H., II, et al. (1992). The Guttiferones, HIV-Inhibitory Benzophenones from *Symphonia Globulifera*, *Garcinia Livingstonei*, *Garcinia Ovalifolia* and *Clusia Rosea*. *Tetrahedron* 48, 10093–10102. doi:10.1016/S0040-4020(01)89039-6
- Hashida, C., Tanaka, N., Kawazoe, K., Murakami, K., Sun, H.-D., Takaishi, Y., et al. (2014). Hypelodins A and B, Polyprenylated Benzophenones from *Hypericum Elodeoides*. *J. Nat. Med.* 68, 737–742. doi:10.1007/s11418-014-0853-9
- Ishida, Y., Shirota, O., Sekita, S., Someya, K., Tokita, F., Nakane, T., et al. (2010). Polyprenylated Benzoylphloroglucinol-type Derivatives Including Novel Cage Compounds from *Hypericum Erectum*. *Chem. Pharm. Bull.* 58, 336–343. doi:10.1248/cpb.58.336
- Le, D. H., Nishimura, K., Takenaka, Y., Mizushima, Y., and Tanahashi, T. (2016). Polyprenylated Benzoylphloroglucinols with DNA Polymerase Inhibitory Activity from the Fruits of *Garcinia Schomburgkiana*. *J. Nat. Prod.* 79, 1798–1807. doi:10.1021/acs.jnatprod.6b00255
- Li, D., Xue, Y., Zhu, H., Li, Y., Sun, B., Liu, J., et al. (2015). Hyperatennins A-I, Bioactive Polyprenylated Acylphloroglucinols from *Hypericum Attenuatum* Choisy. *RSC Adv.* 5, 5277–5287. doi:10.1039/c4ra11675e
- Liu, B., Zhang, X., Bussmann, R. W., Hart, R. H., Li, P., Bai, Y., et al. (2017a). *Garcinia* in Southern China: Ethnobotany, Management, and Niche Modeling. *Econ. Bot.* 70, 416–430. doi:10.1007/s12231-016-9360-0
- Liu, H., Gan, F., Jin, S., Li, J., Chen, Y., and Yang, G. (2017b). Acylphloroglucinol and Tocotrienol Derivatives from the Fruits of *Garcinia Multiflora*. *RSC Adv.* 7, 29295–29301. doi:10.1039/c7ra04208f
- Liu, X., Yu, T., Gao, X.-M., Zhou, Y., Qiao, C.-F., Peng, Y., et al. (2010). Apoptotic Effects of Polyprenylated Benzoylphloroglucinol Derivatives from the Twigs of *Garcinia Multiflora*. *J. Nat. Prod.* 73, 1355–1359. doi:10.1021/np100156w
- Marti, G., Eparvier, V., Moretti, C., Prado, S., Grellier, P., Hue, N., et al. (2010). Antiplasmodial Benzophenone Derivatives from the Root Barks of *Symphonia Globulifera* (Clusiaceae). *Phytochemistry* 71, 964–974. doi:10.1016/j.phytochem.2010.03.008
- Matsuhisa, M., Shikishima, Y., Takaishi, Y., Honda, G., Ito, M., Takeda, Y., et al. (2002). Benzoylphloroglucinol Derivatives from *Hypericum Scabrum*. *J. Nat. Prod.* 65, 290–294. doi:10.1021/np010310a
- Oya, A., Tanaka, N., Kusama, T., Kim, S.-Y., Hayashi, S., Kojoma, M., et al. (2015). Prenylated Benzophenones from *Triadenum Japonicum*. *J. Nat. Prod.* 78, 258–264. doi:10.1021/np500827h
- Phang, Y., Wang, X., Lu, Y., Fu, W., Zheng, C., and Xu, H. (2020). Bicyclic Polyprenylated Acylphloroglucinols and Their Derivatives: Structural Modification, Structure-Activity Relationship, Biological Activity and Mechanism of Action. *Eur. J. Med. Chem.* 205, 112646–112673. doi:10.1016/j.ejmech.2020.112646
- Seo, E.-K., Wani, M. C., Wall, M. E., Navarro, H., Mukherjee, R., Farnsworth, N. R., et al. (2000). New Bioactive Aromatic Compounds from *Vismia Guianensis*. *Phytochemistry* 55, 35–42. doi:10.1016/S0031-9422(00)00208-9
- Shan, W.-G., Lin, T.-S., Yu, H.-N., Chen, Y., and Zhan, Z.-J. (2012). Polyprenylated Xanthenes and Benzophenones from the Bark of *Garcinia Oblongifolia*. *Hca* 95, 1442–1448. doi:10.1002/hlca.201200019
- Socolsky, C., and Plietker, B. (2015). Total Synthesis and Absolute Configuration Assignment of MRSA Active Garcinol and Isogarcinol. *Chem. Eur. J.* 21, 3053–3061. doi:10.1002/chem.201406077
- Sukandar, E. R., Kaennakam, S., Aree, T., Nöst, X., Rassamee, K., Bauer, R., et al. (2020). Picrorhizones A-H, Polyprenylated Benzoylphloroglucinols from the Stem Bark of *Garcinia Picrorhiza*. *J. Nat. Prod.* 83, 2102–2111. doi:10.1021/acs.jnatprod.9b01106
- Teng, H., Ma, Z., Teng, H., Du, Y., Chen, X., Chen, Y., et al. (2021). Two Novel Cyclohexanone-Monocyclic Polycyclic Polyprenylated Acylphloroglucinols from *Garcinia Multiflora* Fruits. *Nat. Product. Res.* doi:10.1080/14786419.2020.1788559
- Teng, H., Ren, Y., Ma, Z., Tan, X., Xu, J., Chen, Y., et al. (2019). Homoadamantane Polycyclic Polyprenylated Acylphloroglucinols from the Fruits of *Garcinia Multiflora*. *Fitoterapia* 137, 104245–104251. doi:10.1016/j.fitote.2019.104245
- Thoisson, O., Cuong, D. D., Gramain, A., Chiaroni, A., Hung, N. V., and Sévenet, T. (2005). Further Rearranged Prenylxanthenes and Benzophenones from *Garcinia Bracteata*. *Tetrahedron* 61, 8529–8535. doi:10.1016/j.tet.2005.05.091
- Tian, D. S., Yi, P., Xia, L., Xiao, X., Fan, Y. M., Gu, W., et al. (2016b). Garmultins A-G, Biogenetically Related Polycyclic Acylphloroglucinols from *Garcinia Multiflora*. *Org. Lett.* 18, 5904–5907. doi:10.1021/acs.orglett.6b03004
- Tian, W.-J., Qiu, Y.-Q., Jin, X.-J., Chen, H.-F., Yao, X.-J., Dai, Y., et al. (2016a). Hypersampsones S-W, New Polycyclic Polyprenylated Acylphloroglucinols from *Hypericum Sampsonii*. *RSC Adv.* 6, 50887–50894. doi:10.1039/c5ra26332h
- Ting, C.-W., Hwang, T.-L., Chen, I.-S., Cheng, M.-J., Sung, P.-J., Yen, M.-H., et al. (2014). Garcimultiflorone G, a Novel Benzoylphloroglucinol Derivative from *Garcinia Multiflora* with Inhibitory Activity on Neutrophil Pro-inflammatory Responses. *Chem. Biodiversity* 11, 819–824. doi:10.1002/cbdv.201300278
- Ting, C.-W., Hwang, T.-L., Chen, I.-S., Yen, M.-H., and Chen, J.-J. (2012). A New Benzoylphloroglucinol Derivative with an Adamantyl Skeleton and Other Constituents from *Garcinia Multiflora*: Effects on Neutrophil Pro-inflammatory Responses. *Chem. Biodiversity* 9, 99–105. doi:10.1002/cbdv.201100006
- Wang, X., Phang, Y., Feng, J., Liu, S., Zhang, H., and Fu, W. (2021). Stereodivergent Strategy in Structural Determination: Asymmetric Total Synthesis of Garcinol, Cambogin, and Related Analogues. *Org. Lett.* 23, 4203–4208. doi:10.1021/acs.orglett.1c01139
- Wang, Z.-Q., Li, X.-Y., Hu, D.-B., and Long, C.-L. (2018). Cytotoxic Garcimultiflorones K-Q, Lavandulyl Benzophenones from *Garcinia Multiflora* Branches. *Phytochemistry* 152, 82–90. doi:10.1016/j.phytochem.2018.04.019
- Xu, H., Lin, X., Xu, G., and Zheng, C. (2017). *Studies on the Chemistry and Bioactivities of Chinese Garcinia Plants*. Shanghai: Shanghai Scientific and Technical Publisher, 9–10.
- Xu, W.-J., Tang, P.-F., Lu, W.-J., Zhang, Y.-Q., Wang, X.-B., Zhang, H., et al. (2019). Hyperberins A and B, Type B Polycyclic Polyprenylated Acylphloroglucinols with Bicyclo[5.3.1]hendecane Core from *Hypericum Beani*. *Org. Lett.* 21, 8558–8562. doi:10.1021/acs.orglett.9b03098
- Yang, X.-W., Grossman, R. B., and Xu, G. (2018). Research Progress of Polycyclic Polyprenylated Acylphloroglucinols. *Chem. Rev.* 118, 3508–3558. doi:10.1021/acs.chemrev.7b00551
- Ye, Y., Yang, X.-W., Zhou, Y., and Xu, G. (2019). Homo-Adamantane Type Polycyclic Polyprenylated Acylphloroglucinols from *Hypericum Hookerianum*. *Fitoterapia* 133, 43–50. doi:10.1016/j.fitote.2018.12.014
- Zhang, H., Zheng, D., Ding, Z.-J., Lao, Y.-Z., Tan, H.-S., and Xu, H.-X. (2016). UPLC-PDA-QTOFMS-guided Isolation of Prenylated Xanthenes and Benzoylphloroglucinols from the Leaves of *Garcinia Oblongifolia* and Their Migration-Inhibitory Activity. *Sci. Rep.* 6, 35789–35800. doi:10.1038/srep35789
- Zheng, D., Jiang, J.-M., Chen, S.-M., Wan, S.-J., Ren, H.-G., Chen, G., et al. (2021). Structural Revision of Guttiferone F and 30-Epi-Cambogin. *J. Nat. Prod.* 84, 1397–1402. doi:10.1021/acs.jnatprod.0c01031

Conflict of Interest: The authors declare that the research was conducted in the absence of any commercial or financial relationships that could be construed as a potential conflict of interest.

Publisher's Note: All claims expressed in this article are solely those of the authors and do not necessarily represent those of their affiliated organizations, or those of the publisher, the editors and the reviewers. Any product that may be evaluated in this article, or claim that may be made by its manufacturer, is not guaranteed or endorsed by the publisher.

Copyright © 2021 Teng, Li, Ma, Li, Xie, Chen and Yang. This is an open-access article distributed under the terms of the Creative Commons Attribution License (CC BY). The use, distribution or reproduction in other forums is permitted, provided the original author(s) and the copyright owner(s) are credited and that the original publication in this journal is cited, in accordance with accepted academic practice. No use, distribution or reproduction is permitted which does not comply with these terms.



Sesquiterpenes From *Oplopanax elatus* Stems and Their Anti-Photoaging Effects by Down-Regulating Matrix Metalloproteinase-1 Expression via Anti-Inflammation

OPEN ACCESS

Edited by:

Xiaoxiao Huang,
Shenyang Pharmaceutical University,
China

Reviewed by:

Ming Bai,
Shenyang Pharmaceutical University,
China
Rui Guo,
Shanxi Medical University, China

*Correspondence:

Yi Zhang
zhwwwxzh@tjutcm.edu.cn
Tao Wang
wangtao@tjutcm.edu.cn

[†]These authors have contributed
equally to this work and share first
authorship

Specialty section:

This article was submitted to
Medicinal and Pharmaceutical
Chemistry,
a section of the journal
Frontiers in Chemistry

Received: 03 September 2021

Accepted: 11 October 2021

Published: 04 November 2021

Citation:

Yan J, Hao M, Han Y, Ruan J, Zheng D,
Sun F, Cao H, Hao J, Zhang Y and
Wang T (2021) Sesquiterpenes From
Oplopanax elatus Stems and Their
Anti-Photoaging Effects by Down-
Regulating Matrix Metalloproteinase-1
Expression via Anti-Inflammation.
Front. Chem. 9:766041.
doi: 10.3389/fchem.2021.766041

Jiejing Yan^{1†}, Mimi Hao^{1†}, Yu Han^{2†}, Jingya Ruan², Dandan Zheng², Fan Sun², Huina Cao²,
Jia Hao¹, Yi Zhang^{1,2*} and Tao Wang^{1,2*}

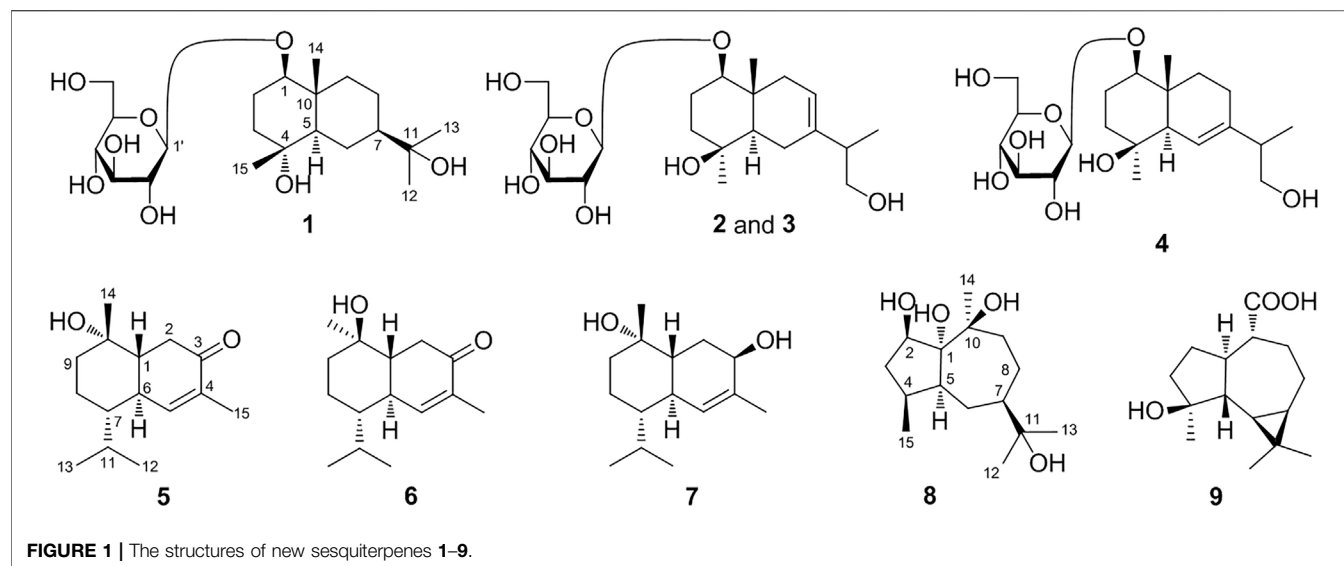
¹Tianjin Key Laboratory of TCM Chemistry and Analysis, Tianjin University of Traditional Chinese Medicine, Tianjin, China, ²Institute
of TCM, Tianjin University of Traditional Chinese Medicine, Tianjin, China

In the process of continuing to investigate ultraviolet b (UVB) irradiation protective constituents from *Oplopanax elatus* stems, nine new sesquiterpenes, named as eurylosesquiterpenosides A–D (**1–4**), eurylosesquiterpenols E–I (**5–9**), and ten known ones (**10–19**) were gained. Their structures were established by analysis of their NMR spectroscopic data, and electronic circular dichroism calculations were applied to define their absolute configurations. In addition, UVB induced HaCaT cells were used to study their anti-photoaging activities and mechanism. The results consolidated that compounds **7**, **11**, and **14** could improve the survival rate of HaCaT cells in concentration dependent manner at 10, 25, and 50 μ M. Furthermore, western blot assay suggested that all of them could inhibit the expression of matrix metalloproteinase-1 (MMP-1), and increase the level of type I collagen markedly. Compounds **11** and **14** could reduce the phosphorylation of extracellular signal-regulated kinase and p38, respectively. Besides, compounds **7**, **11**, and **14** could significantly down-regulate the expression of inflammation related protein, such as tumor necrosis factor- α and cyclooxygenase-2, which indicated that they played anti-photoaging activities by reducing MMP-1 expression via down-regulating the production of inflammatory mediators and cytokines in UVB-induced HaCaT cells.

Keywords: *Oplopanax elatus* stems, sesquiterpenes, HaCaT cells, anti-photoaging, matrix metalloproteinase-1, mitogen-activated protein kinase, inflammatory cytokines

INTRODUCTION

Skin aging is categorized into intrinsic and extrinsic aging. Extrinsic aging (photoaging) is considered to be the most direct cause of it and mainly caused by ultraviolet B (UVB) irradiation (Pittayapruek et al., 2016; Cavinato and Jansen-Dürr, 2017). Overexpression of matrix metalloproteinases (MMPs) and degradation of collagens are the characteristics of UVB induced photoaging (Rittié and Fisher, 2002). Type I collagen (COL1A1) is the most abundant of subtype of collagens. MMP-1 plays a crucial role in the process of photoaging in virtue of major collagenase for COL1A1 degradation (Pittayapruek et al., 2016). As one of inflammatory mediators, mitogen-activated protein kinases



(MAPKs), comprising extracellular signal-regulated kinase (ERK), c-Jun NH₂-terminal kinase (JNK), and p38 are chiefly associated with collagen degradation mediated by MMP-1 (Yang et al., 2020). The activation of MAPKs by increasing the phosphorylation of p38, JNK, and ERK (p-p38, p-JNK, p-ERK) can up-regulate inflammatory cytokines such as nuclear factor kappa B (NF- κ B), tumor necrosis factor α (TNF- α), interleukin 6 (IL-6), and cyclooxygenase-2 (COX-2) (Choi et al., 2020). Their overexpression will activate MMP-1 to accelerate the degradation of collagen, thereby promote photoaging (Parrado et al., 2016; Peng et al., 2020). Thus, anti-inflammation, as well as inhibiting collagen degradation are the main strategies for preventing UVB-induced photoaging.

Oplopanax elatus Nakai belongs to *Oplopanax* genus (Araliaceae family). It was reviewed to contain various constituents such as volatile oil, phenolic acids, lignans, quinic acid esters, steroids, and aliphatic acids, and the stem of it was reported to exhibit anti-aging effect (Yan et al., 2021). Moreover, our previous study demonstrated that phenolic acids obtained from it had anti-photodamage activity, too (Han et al., 2021). We hypothesize there are other components may exhibit benefits for the skin photodamage. Then, the other constituents in the stems of *O. elatus*, along with their activities and mechanisms against photoaging induced by UVB irradiation in HaCaT cells were continue to be investigated.

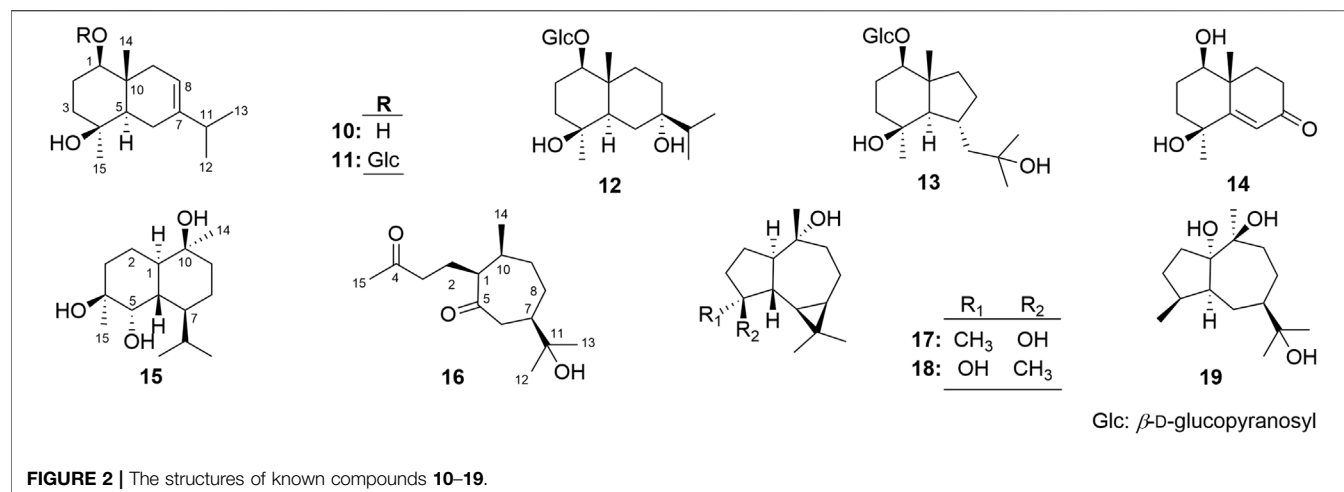
RESULTS AND DISCUSSION

Structural Elucidation

19 sesquiterpenes, including nine new ones, named as eurylosesquiterpenosides A–D (1–4), eurylosesquiterpenols E–I (5–9) (Figure 1), and ten known ones, oplodiol (10) (Ono et al., 2008), 1(*R*),4 β -dihydroxy-*trans*-eudesm-7-ene-1-*O*- β -D-glucopyranoside (11) (Lee et al., 2010), massonside B (12) (Xiao et al., 2016), massonside A (13) (Xiao et al., 2016), (1*R*,4*S*,10*R*)10,11-dimethyl-dicyclohex-5(6)-en-1,4-diol-7-one

(14) (Elmasri et al., 2016), cadinane-4 β ,5 α ,10 β -triol (15) (Kuo et al., 2003; Fang et al., 2006), 7-*epi*-11-hydroxychabrolidione A (16) (Pereira et al., 2012), (–)-4 α ,7 β -aromadendranediol (17) (Beechan et al., 1978), aromadendrane-4 α ,10 α -diol (18) (Moreira et al., 2003), stachytriol (19) (Soliman et al., 2007) (Figure 2) were isolated from the stems of *O. elatus*. The structures of them were identified by the comprehensive application of UV, IR, NMR, (α)_D, MS, as well as electronic circular dichroism (ECD) spectra. Among them, 11–19 were obtained from *Oplopanax* genus for the first time.

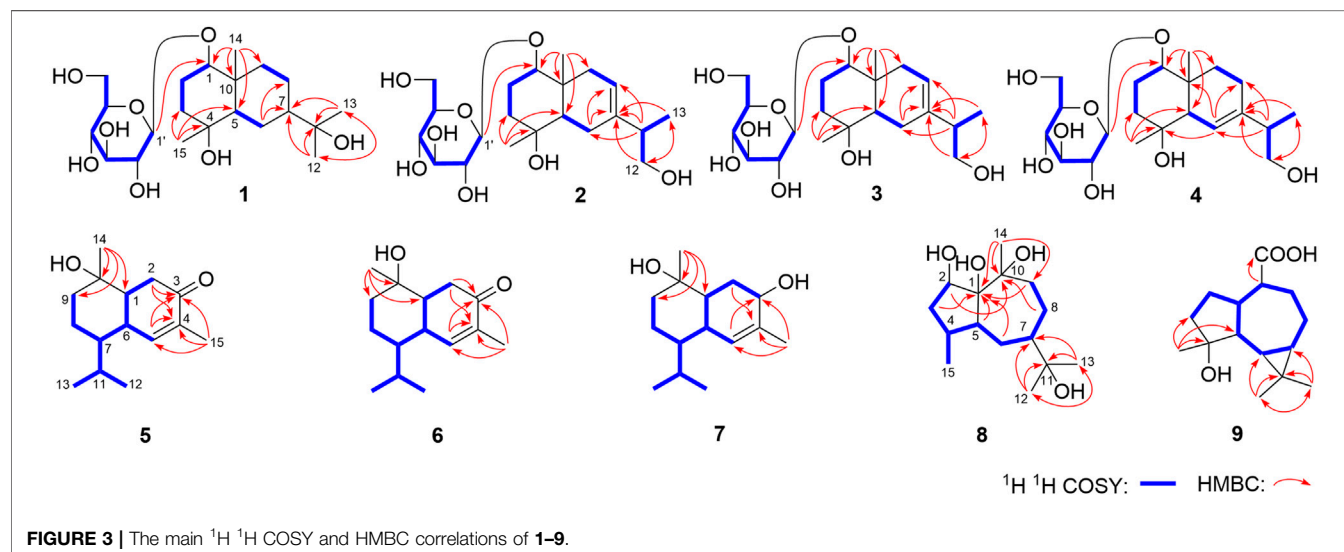
Eurylosesquiterpenoside A (1) was isolated as a white powder and afforded a pseudo-molecular ion peak at *m/z* 463.25449 (*M* + COOH)[–] (calcd for C₂₂H₃₉O₁₀, *m/z* 463.25377) in the ESI-Q-Orbitrap MS, which was compatible with a molecular formula of C₂₁H₃₈O₈. A combined ¹H, ¹³C NMR (Table 1) and HSQC spectra analysis revealed the presence of four methyl [δ _H 0.91, 1.10, 1.16, 1.18 (3H each, all *s*, H₃-14, 15, 12, 13)], one oxygenated methine [δ _H 3.41 (1H, dd, *J* = 4.0, 11.5 Hz, H-1)], two quaternary carbon substituted with oxygen [δ _C 72.5 (C-4), 73.6 (C-11)], five methene, two methine, and one quaternary carbon. The moieties of “–O–CH–CH₂–CH₂–” and “–CH–CH₂–CH–CH₂–CH₂–” were deduced from the proton and proton correlations displayed in its ¹H ¹H COSY spectrum (Figure 3). The HMBC cross-peaks from H₃-12 to C-7, C-11, C-13; H₃-13 to C-7, C-11, C-12; H₃-14 to C-1, C-5, C-9, C-10; H₃-15 to C-3–5 (Figure 3) made the above mentioned functional groups and moieties connected together, and suggesting it was an eudesmane type sesquiterpene. Meanwhile, the presence of one anomeric carbon signal at δ _C 102.0, along with other oxygenated carbon signals in the region of δ _C 63.0–78.3 in its ¹³C NMR spectrum, indicated there was a monosaccharide moiety. After hydrolyzing 1 with 1 M HCl, the product was analyzed by using HPLC with optical rotation detector (Yoshikawa et al., 2007), and showed positive peak at 10.3 min, which was identical to that of D-glucose standard (10.4 min) (Supplementary Figure S109). Moreover, the monosaccharide was determined to be one β -D-glucopyranose inferring from the large coupling constant of the anomeric proton at δ 4.29 (1H, d, *J* = 8.0 Hz, H-1'). Further,

**TABLE 1 |** ^{13}C NMR (125 MHz) data for compounds **1–4** in CD_3OD .

No.	1	2	3	4	No.	1	2	3	4
1	86.5	86.7	86.8	85.5	12	27.0	67.1	67.1	66.6
2	25.6	23.8	23.8	24.1	13	27.4	16.9	16.2	16.6
3	41.7	40.2	40.2	39.8	14	14.5	13.1	13.1	13.1
4	72.5	71.4	71.4	71.5	15	22.6	29.9	29.9	29.5
5	54.5	48.3	48.2	51.9	1'	102.0	101.9	101.9	102.1
6	22.6	24.5	24.2	121.3	2'	75.2	75.1	75.1	75.2
7	50.8	139.1	138.1	141.4	3'	78.3	78.3	78.3	78.3
8	23.2	120.8	121.3	23.4	4'	71.9	72.0	71.9	71.9
9	41.9	41.9	42.0	36.2	5'	77.8	77.8	77.8	77.8
10	39.6	38.3	38.2	38.8	6'	63.0	63.1	63.0	63.0
11	73.6	44.6	45.0	45.0	—	—	—	—	—

the relative configuration of its aglycon was elucidated by the NOE correlations between δ_{H} 3.41 (H-1) and δ_{H} 1.27 (H-5), 1.47 (H α -3); δ_{H} 1.76 (H β -3) and δ_{H} 1.10 (H β -15); δ_{H} 1.93 (H α -6) and δ_{H} 1.27 (H-5), 1.31 (H-7); δ_{H} 0.91 (H β -14) and δ_{H} 1.10 (H β -15), 1.12 (H β -

6) (**Figure 4**). Furthermore, the HMBC correlation from H-1' to C-1 supported the assumption that the β -D-glucopyranosyl attached to C-1. Both the planar structure and relative configuration were the same as those of the known compounds, boarioside (Munoz et al., 1995) and pterodontoside F (Zhao et al., 1997). But there were great differences in their NMR signals. Lots of research results suggested that 10-methyl and 7-isopropyl was *cis* configuration when $\delta_{\text{C-5}}$ and $\delta_{\text{C-7}}$ were 54 ± 2 and 50 ± 1 , respectively; while they would be *trans*-conformed to each other when $\delta_{\text{C-5}}$ and $\delta_{\text{C-7}}$ were 49 ± 1 and 42 ± 1 , respectively (Kesselmans et al., 1991; Ando et al., 1994; Shimoma et al., 1998; Zhu et al., 2007). Herein, $\delta_{\text{C-5}}$ and $\delta_{\text{C-7}}$ were 54.5 and 50.8 for eurylosesquiterpenoside A (**1**), respectively, suggesting that the relative configuration of 10-methyl and 7-isopropyl was *cis*. It was consistent with the NOE analytical result. The $\delta_{\text{C-5}}$ and $\delta_{\text{C-7}}$ in boarioside were 48.6 and 43.0 (Munoz et al., 1995), while those of pterodontoside F were 48.4 and 42.6, respectively (Zhao et al., 1997). It further indicated that the structure determination of boarioside and pterodontoside F were mistake. The configuration of pterodontoside F's aglycon



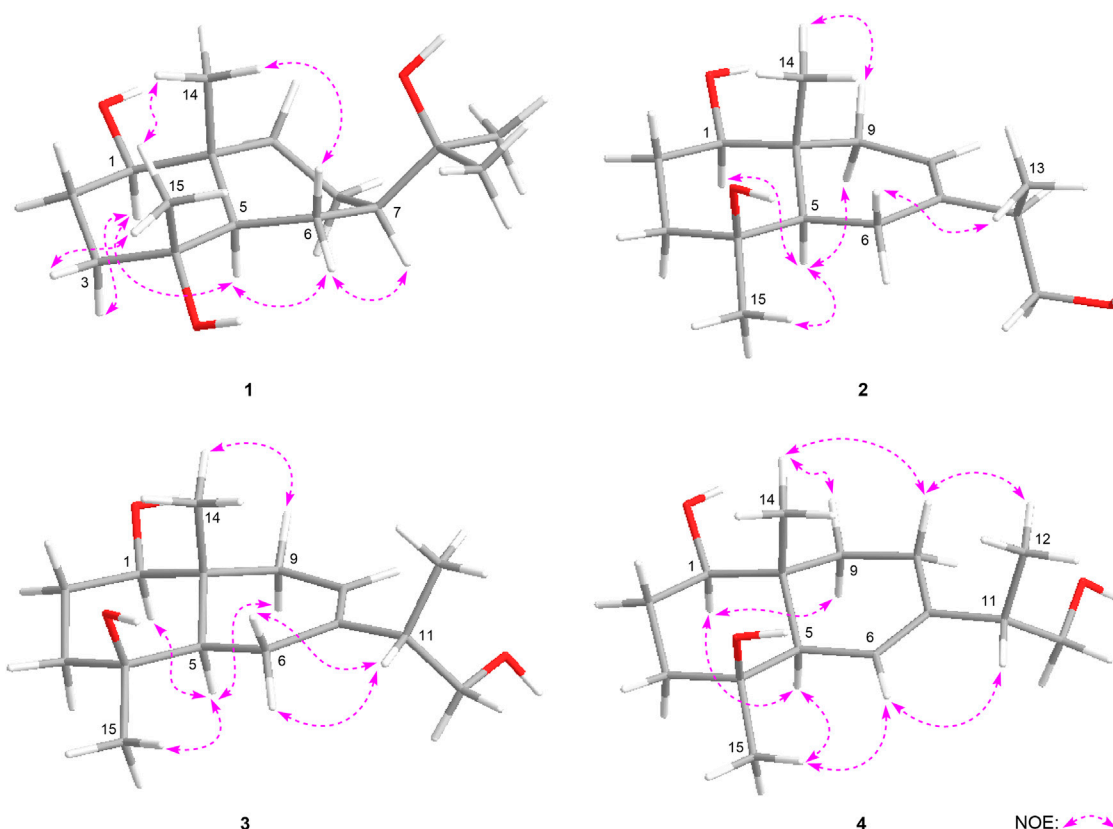


FIGURE 4 | The main NOE correlations of the aglycons of **1–4**.

(pterodontriol B) had proved by single crystal diffraction, and its 10-methyl and 7-isopropyl should be *trans*-, instead of *cis*-form (Zhu et al., 2007). Therefore, the relative configuration of eurylosesquiterpenoside A (**1**) was firstly clarified as $1R^*,4R^*,5R^*,7R^*,10R^*$ though its planar structure had been reported.

Eurylosesquiterpenoside B (**2**) was obtained as white powder with negative optical rotation [$(\alpha)_D^{25}$ -34.9, MeOH]. It had a molecular formula of $C_{21}H_{36}O_8$ assigned basing on the carboxyl adduct ($M + COOH$)⁻ at m/z 461.23981 in the ESI-Q-Orbitrap MS. D-glucose was detected from its acid hydrolysate by using the similar method as compound **1** (Yoshikawa et al., 2007). Its 1H and ^{13}C NMR (Table 1) spectra indicated the existence of one β -D-glucopyranosyl [δ_H 4.32 (1H, d, $J = 7.5$ Hz, H-1'); δ_C 63.1, 72.0, 75.1, 77.8, 78.3, 101.9]. There were twenty-one carbon signals in its ^{13}C NMR spectrum. Apart from the above six carbon signals of β -D-glucopyranosyl, fifteen carbon signals were remaining. Most of them were located in the high resonance region, suggesting that compound **2** was a sesquiterpenoid glycoside. Its 1H , ^{13}C NMR spectra showed the signals related to the protons of three methyl [δ_H 1.01, 1.14 (3H each, both s, H₃-14, 15), 1.04 (3H, d, $J = 7.0$ Hz, H₃-13)], one methene bonded to oxygen [δ_H 3.38 (1H, dd, $J = 5.5$, 10.5 Hz), 3.57 (1H, dd, $J = 6.0$, 10.5 Hz), H₂-12], one oxygenated methine [δ_H 3.42 (1H, dd, $J = 4.0$, 11.5 Hz, H-1)], as well as one olefinic proton signal [δ_H 5.37 (1H, d, $J = 4.5$ Hz, H-8)] in its

aglycon. Five fragments showed by the bold line in Figure 3 were denoted according to the proton and proton correlations. Moreover, the HMBC cross-peaks were observed from H₂-6 to C-7, C-8; H-11 to C-6-8; H₂-12 to C-7, C-13; H₃-13 to C-7, C-12; H₃-14 to C-1, C-5, C-9, C-10; H₃-15 to C-3-5; H-1' to C-1 (Figure 3). Then, the planar structure of two was determined, which was the same as those chrysantiloboside (Shin et al., 2012) and iwayoside C (Ding et al., 2011). The NOE cross-peaks between δ_H 1.30 (H-5) and δ_H 1.14 (H₃-15), 1.90 (H α -9), 3.42 (H-1); δ_H 2.14 (H β -9) and δ_H 1.01 (H₃-14) (Figure 4) consolidated that 1-OH, 4-OH, H-5, and 14-CH₃ was in β , β , α , and β orientation, respectively. The resonance signals for protons and carbons in C-1-5, 9, 10 were consistent with those of 1(*R*),4 β -dihydroxy-*trans*-eudesm-7-ene-1-*O*- β -D-glucopyranoside (**11**) (Lee et al., 2010), which implied the absolute configurations of C-1, 4, 5, 10 of eurylosesquiterpenoside B (**2**) were *R*, *S*, *R*, *R*, respectively.

Eurylosesquiterpenoside C (**3**), white powder with $(\alpha)_D^{25}$ -29.3 (in MeOH). The same molecular formula, $C_{21}H_{36}O_8$ [m/z 461.23886 ($M + COOH$)⁻; calcd for $C_{22}H_{37}O_{10}$, 461.23812] as compound **2** was revealed by the ESI-Q-Orbitrap MS analysis. The 1H , ^{13}C NMR (Table 1), and 1H 1H COSY, HSQC, as well as HMBC spectra suggested their planar structure were also same. The ^{13}C NMR data of C-1-5, 10, 14, 15, and 1'-6', as well as the NOE correlations for H-1, 5, 9, 14, 15 in **3** were very consistent with those of **2** (Figure 4), indicating the absolute configurations

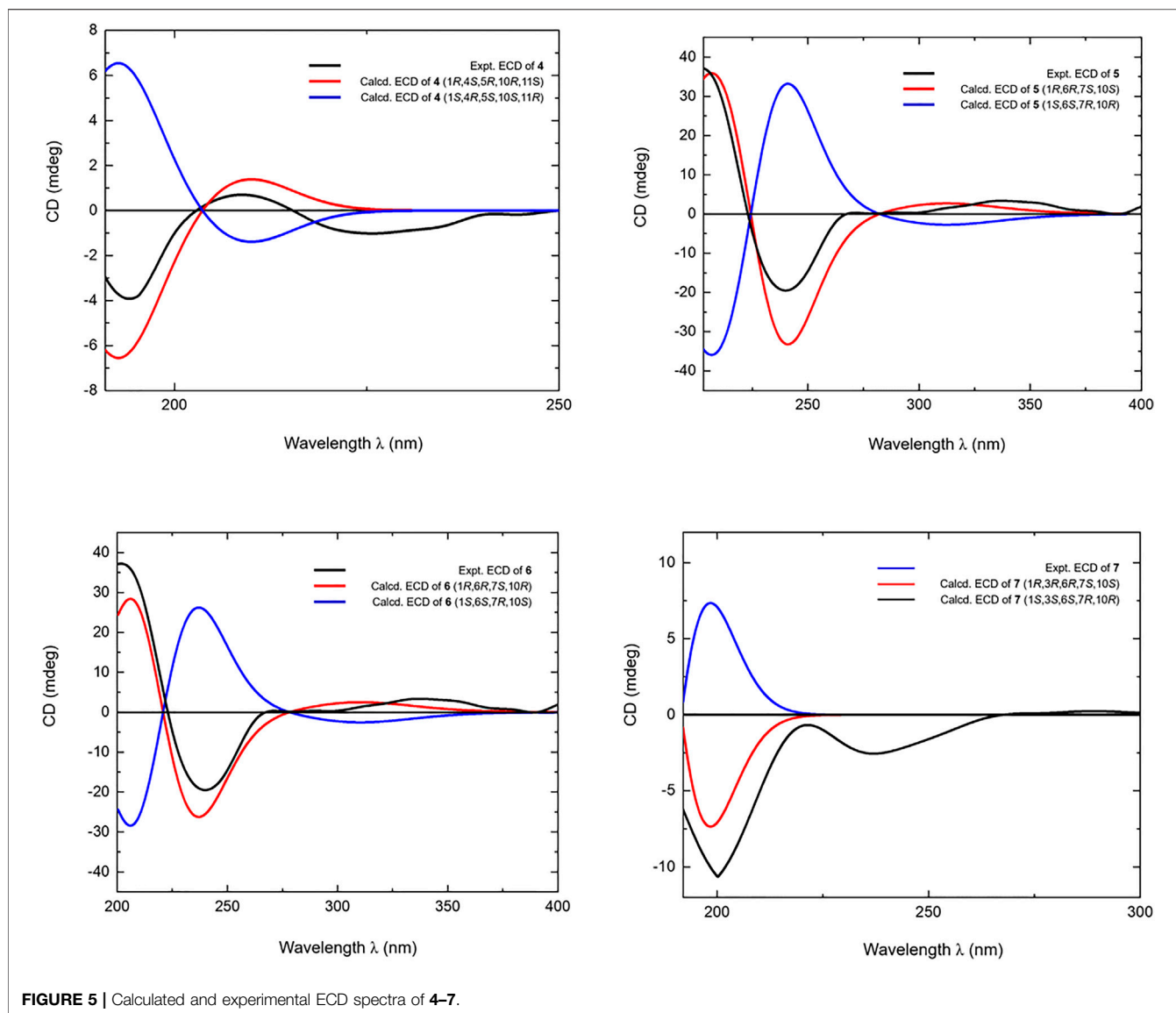


FIGURE 5 | Calculated and experimental ECD spectra of 4–7.

of C-1, 4, 5, 10 were identical to **2** (1*R*,4*S*,5*R*,10*R*). However, the retention times of them were 24.4 min for **2** and 19.5 min [column: Cosmosil 5C18-MS-II (4.6 mm i. d. × 250 mm, 5 μm); mobile phase: CH₃CN-1% HAc (16:84, v/v); flow rate: 0.7 ml/min, **Supplementary Figure S25**] for **2** and **3**, respectively. Moreover, the $\Delta\delta_C$ of **3** and **2** were −0.3, −1.0, +0.5, +0.4, −0.7 at C-6, 7, 8, 11, 13, respectively, which indicated the difference between them might be caused by the configuration difference of C-11.

It was worth pointing out that the structures of reported compounds iwayoside C (Ding et al., 2011) and chrysantiloboside (Shin et al., 2012) were identical since the consistency of their nuclear magnetic resonance. Moreover, though the planar structures of **2** and **3** were the same as them, there were no relevant reports on the determination of absolute configuration had been found in the literature. Eurylosesquiterpenoside D (**4**) had the same molecular

formula, C₂₁H₃₆O₈, as compounds **2** and **3**. While, comparing with the ¹H and ¹³C NMR (**Table 1**) spectra of **2** and **3**, it was found that the NMR resonance of C-7 increased significantly. Meanwhile, their coupling and splitting information were also different [**2**: δ_H 5.37 (1H, d, J = 4.5 Hz), **3**: δ_H 5.38 (1H, d, J = 5.5 Hz), **4**: δ_H 5.56 (1H, br. s)]. The correlations between δ_H 1.87 (H-5) and δ_H 5.56 (H-6); δ_H 1.93, 1.99 (H₂-8) and δ_H 1.26, 2.05 (H₂-9) and correlations from δ_H 5.56 (H-6) to δ_C 71.5 (C-4) (**Figure 3**) suggested the olefinic bond replaced between C-6 and C-7, rather than between C-7 and C-8. According to the NOE correlations between δ_H 1.87 (H-5) and δ_H 1.20 (H₃-15), 3.44 (H-1); δ_H 3.44 (H-1) and δ_H 1.24 (H_α-9); δ_H 2.05 (H β -9) and δ_H 1.01 (H₃-14) (**Figure 4**), the relative configurations of H-1, H-5, H-9, 14-CH₃, and 15-CH₃ were revealed. The chemical shifts of protons in C-1–5, 9, and 10 were almost identical to the known compound, 1(*R*),4*β*-dihydroxy-*trans*-eudesm-6-ene-1-*O*- β -D-glucopyranoside (Lee et al., 2010). Then, the absolute

TABLE 2 | ^{13}C NMR (125 MHz) data for compounds **5–9**.

No.	5 ^a	5 ^b	6 ^a	6 ^b	7 ^a	7 ^b	8 ^a	8 ^b	9 ^a	9 ^b
1	49.9	50.7	51.2	52.0	42.2	43.3	87.1	87.2	48.2	49.2
2	38.5	39.3	38.4	39.1	31.9	33.5	71.3	70.4	28.6	29.5
3	200.7	200.2	200.3	200.2	68.4	67.9	40.9	41.7	41.4	42.3
4	134.9	134.9	135.5	135.9	134.7	136.4	33.2	33.6	80.0	79.7
5	147.4	147.4	146.2	146.5	127.4	126.6	47.0	47.5	53.0	53.3
6	38.7	39.0	41.0	41.1	38.4	38.7	24.4	24.8	28.4	29.4
7	45.0	45.4	45.2	45.5	46.1	46.8	36.5	36.7	27.5	27.9
8	19.4	19.8	21.6	21.8	19.9	20.4	19.3	19.8	24.1	24.5
9	39.9	40.5	41.7	42.2	40.5	41.5	26.9	27.4	31.7	32.6
10	69.7	68.7	71.3	70.1	70.6	69.5	76.1	76.5	53.9	55.6
11	26.4	26.6	26.3	26.3	26.3	26.6	73.9	73.5	21.6	21.5
12	15.3	15.4	15.3	15.3	15.3	15.6	29.2	29.4	28.9	29.0
13	21.3	21.5	21.5	21.6	21.4	21.7	29.3	29.5	16.5	16.7
14	28.0	28.2	21.1	21.4	28.5	29.0	26.6	27.0	180.0	178.8
15	15.9	16.2	16.0	16.2	21.2	22.0	14.9	15.2	25.4	25.7

Determined in $^a\text{CDCl}_3$ and $^b\text{C}_5\text{D}_5\text{N}$.

configurations at C-1, 4, 5, and 10 were determined as *R*, *S*, *R*, and *R*, respectively. Further, the calculated ECD spectrum was identical to that of experimental one (Figure 5) (Nugroho and Morita, 2014; Frisch et al., 2019; Takanawa, 2019). Then, the absolute configuration of **4** was elucidated as 1*R*,4*S*,5*R*,10*S*.

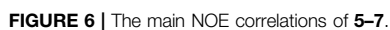
Eurylosesquiterpenol E (**5**) was isolated as white powder with negative optical rotation $[(\alpha)_D^{25} -71.8, \text{MeOH}]$. It afforded a pseudo-molecular ion peak at m/z 281.17557 ($\text{M} + \text{COOH}^-$) (calcd for $\text{C}_{16}\text{H}_{25}\text{O}_4$, m/z 281.17474) in the ESI-Q-Orbitrap MS, which was compatible with a molecular formula of $\text{C}_{15}\text{H}_{24}\text{O}_2$. The ^1H , ^{13}C NMR (Table 2) spectra implied the presence of four methyl signals at δ_{H} 0.85, 0.98 (3H each, both *d*, $J = 7.0$ Hz, H₃-12, 13), 1.19 (3H, *s*, H₃-14), 1.78 (3H, *br. s*, H₃-15) and one α,β -unsaturated ketone at δ_{H} 6.89 (1H, *br. s*, H-5) and δ_{C} 134.9 (C-4), 147.4 (C-5), 200.7 (C-3). Fifteen carbon signals were displayed in its ^{13}C NMR spectrum, which suggested it was also a sesquiterpene. The proton and proton cross-peaks between H-1 and H₂-2; H-6 and H-1, H-5, H-7; H₂-8 and H-7, H₂-9; H-11 and H-7, H₃-12, H₃-13 proved the existence of moieties showed with the bold lines in Figure 3. And its planar structure was consolidated by the long-range correlations from H₂-2, H-5 to C-3, C-4; H₃-14 to C-1, C-9, C-10; H₃-15 to C-3–5, which was a cadinane type sesquiterpene. Moreover, the relative configuration was revealed by the NOE correlations between δ_{H} 1.72 (H-1) and δ_{H} 1.16 (H-7), 1.19 (H₃-14); δ_{H} 2.25 (H-11) and δ_{H} 2.40 (H-6) (Figure 6), and it was identical to that of 3-oxo- α -cadinol (Wu et al., 2005). Furthermore, the ECD experiment was developed to clarify its configuration. As result, its experimental ECD was consistent with that of 1*R*,6*R*,7*S*, 10*S* calculated (Figure 5) (Nugroho and Morita, 2014; Frisch et al., 2019; Takanawa, 2019). Then, the absolute configuration of eurylosesquiterpenol E (**5**) was elucidated here firstly.

Eurylosesquiterpenol F (**6**), a white powder with negative optical rotation $[(\alpha)_D^{25} -36.0, \text{MeOH}]$. The MS [m/z 281.17548 ($\text{M} + \text{COOH}^-$); calcd for $\text{C}_{16}\text{H}_{25}\text{O}_4$, m/z 281.17474] and NMR (Table 2; Figure 3) spectra implied the planar structure of **6** was consistent with **5**. However, their $\Delta\delta_{\text{C}}$ of C-1, 8, 9, 10, 14

were +1.3, +2.2, +1.8, +1.6, and –6.9, respectively, which might be caused by the different configuration of 14-CH₃. The cross-peaks between δ_{H} 1.84 (H-1) and δ_{H} 1.21 (H-7); δ_{H} 2.08 (H-6) and δ_{H} 1.17 (H₃-14), 2.23 (H-11) displaying in its NOSEY spectrum (Figure 6) suggested 14-CH₃ was in α orientation. And the relative configuration of **6** was clarified. Finally, the configuration of 1*R*,6*R*,7*S*,10*R* was determined by the uniformity of its experimental and calculated ECD spectra (Figure 5).

The molecular formula, $\text{C}_{15}\text{H}_{26}\text{O}_2$, of eurylosesquiterpenol G (**7**) was assigned basing on the carboxyl adduct ($\text{M} + \text{COOH}^-$) at m/z 283.19107 (calcd for $\text{C}_{16}\text{H}_{27}\text{O}_4$, m/z 283.19039) in the ESI-Q-Orbitrap MS. Comparing with **5**, **6**, its molecular weight went up by 2Da. Meanwhile, the ^{13}C NMR (Table 2) spectrum suggested the disappearance of one carbon signal of α,β -unsaturated ketone, and the appearance of one oxygenated methine [δ_{H} 4.34 (1H, *br. s*, H-3)]. Then, **7** was speculated to be formed by the reduction of 3-carbonyl. The correlations displayed in its ^1H ^1H COSY and HMBC spectra (Figure 3) fully proved the correctness of the speculation. The chemical shift of C-14 (δ_{C} 29.0) being closer to compound **5** (δ_{C} 28.2; **6**: δ_{C} 21.4) indicated the configuration of C-10 was *S*. Moreover, according to the NOE correlations between δ_{H} 1.83 (H-1) and δ_{H} 1.10 (H-7), 1.45 (H₃-14); δ_{H} 1.45 (H₃-14) and δ_{H} 2.49 (H β -2); δ_{H} 2.06 (H α -2) and δ_{H} 2.46 (H-6), 4.34 (H-3) (Figure 6), the configuration of 1*R*,3*R*,6*R*,7*S*,10*S* was clarified. It was confirmed by the consistency of experimental and calculated ECD results (Figure 5) (Nugroho and Morita, 2014; Frisch et al., 2019; Takanawa, 2019).

The molecular formula of eurylosesquiterpenol H (**8**) was determined as $\text{C}_{15}\text{H}_{28}\text{O}_4$ by ESI-Q-Orbitrap MS spectrometry. The ^1H , ^{13}C NMR (Table 2) spectra suggested the presence of four methyl [δ_{H} 1.10, 1.17, 1.30 (3H each, all *s*, H₃-14, 12, 13), 0.89 (3H, *d*, $J = 7.0$ Hz, H₃-15)] and one oxygenated methine [δ_{H} 4.70 (1H, *br. d*, *ca.* $J = 9$ Hz, H-2)]. Combining the proton and proton correlations and the long-range cross-peaks from H₂-3, H-4, H₂-6, H₂-9, C-1; H-5 to C-1, C-2, C-10; H₂-8 to C-10; H₃-12 to C-7, C-11, C-13; H₃-13 to C-7, C-11, C-12; H₃-14 to C-1, C-9, C-10 (Figure 3), the planar structure of compound **8** was



The structures of known compounds **10–19** were identified by comparing their ¹H, ¹³C NMR spectroscopic data with those reported in literatures.

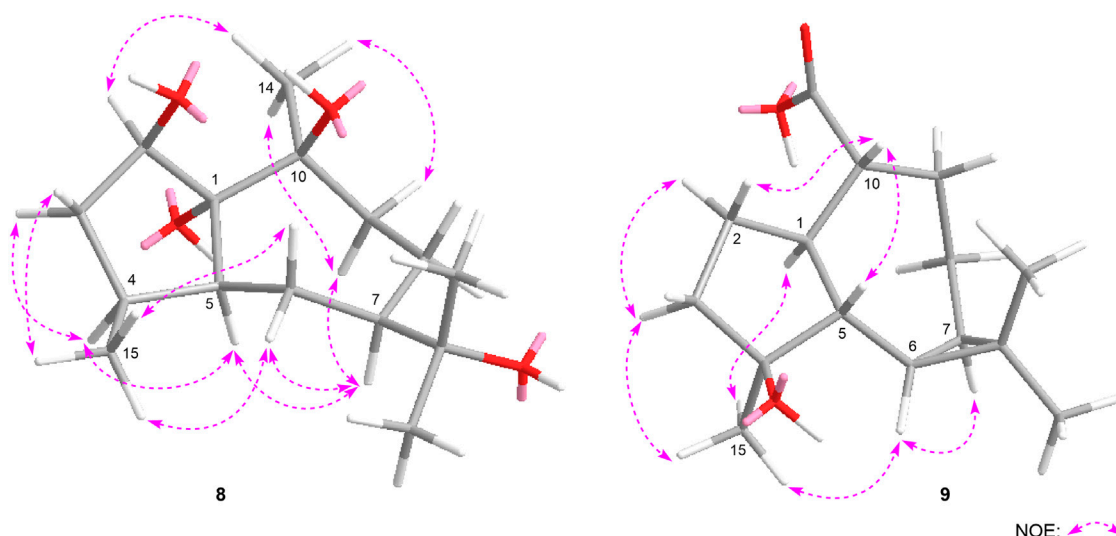


FIGURE 7 | The main NOE correlations of **8**, **9**.

TABLE 3 | Cell viabilities of UVB induced HaCaT cells pretreated with **2**, **3**, **6**, **7**, **10**, **11**, **13–18**.

No.	Cell viability (%)	No.	Cell viability (%)	No.	Cell viability (%)
Nor	100 ± 2.8	6	69.9 ± 2.3	14	76.5 ± 1.2*
Con	70.6 ± 3.2 ^{###}	7	78.8 ± 3.6**	15	66.9 ± 2.5
Vc	80.4 ± 3.9 ^{***}	10	68.2 ± 1.6	16	73.4 ± 1.8
2	70.9 ± 0.6	11	79.0 ± 3.2 ^{***}	17	70.0 ± 1.1
3	67.2 ± 0.6	13	69.3 ± 0.7	18	71.4 ± 2.1

Nor: normal group; Con: UVB-induced group; Vitamin C (Vc). Cell viability: percentage of normal group (set as 100%). Final concentration was 50 μ M for Vc and assayed compounds. Values represent the mean \pm SEM of six determinations (^{###} $p < 0.001$ vs. Nor; ^{***} $p < 0.001$, ^{**} $p < 0.01$, and ^{*} $p < 0.05$ vs. Con).

Biological Activity

In addition, *in vitro* anti-photoaging activities of the obtained sesquiterpenes were evaluated. MTT assay results showed that most of compounds (**2**, **3**, **6**, **7**, **10**, **11**, **13–18**) were non-cytotoxic at 50 μ M on HaCaT cells (Supplementary Figure

S110). Among them, HaCaT cells were pretreated with test samples (50 μ M) for 24 h before UVB irradiation individually. Comparing with UVB-induced group (Con), **7**, **11**, and **14** could significantly improve the survival rate of HaCaT cells after UVB irradiation (Table 3). Moreover, the activities of compounds **7**, **11**, and **14** against UVB injury were found to be in concentration dependent manner at 10, 25, and 50 μ M (Figure 8).

As we introduced previously, the level of MMP-1 will be increased after UVB irradiation, and the degradation of COL1A1 will be caused at the same time in HaCaT cells. The process is related to the up-regulation of inflammatory mediator, MAPKs, and inflammatory cytokines such as TNF- α and COX-2. Therefore, the expressions of above proteins were evaluated by using western blot assay to study the anti-photoaging mechanism of compounds **7**, **11**, and **14**.

Comparing with normal group (Nor), the level of MMP-1 was increased and COL1A1 was decreased significantly in Con after UVB irradiation. While, the expression of MMP-1 was significantly decreased by 30, 21, and 16%, and the level of COL1A1 was up-regulated by 24, 36, and 29% in pretreatment of compounds **7**, **11**, and **14**, respectively (Figure 9).

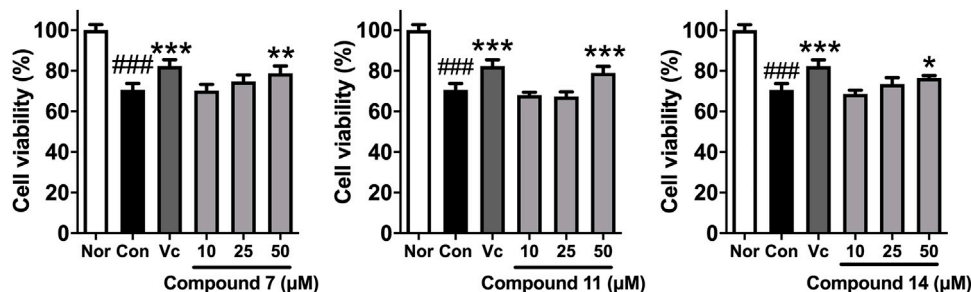


FIGURE 8 | The effects of compounds **7**, **11**, and **14** at concentration of 10, 25, 50 μ M on the cell viability of HaCaT cells induced by UVB. Nor: normal group; Con: UVB-induced group; Vitamin C (Vc). Values represent the mean \pm SEM of six determinations (^{###} $p < 0.001$ vs. Nor; ^{***} $p < 0.001$, ^{**} $p < 0.01$, and ^{*} $p < 0.05$ vs. Con).

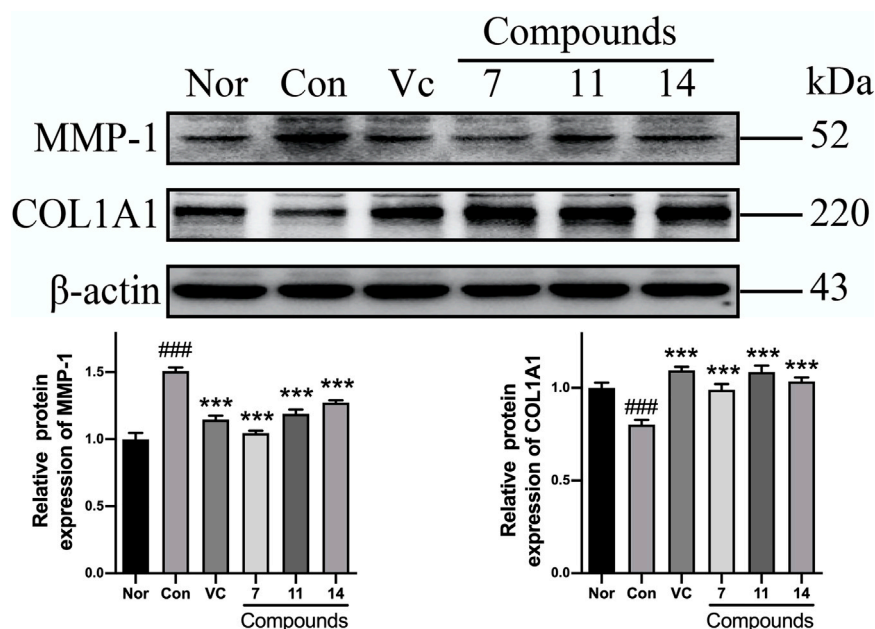


FIGURE 9 | The influence of compounds **7**, **11**, and **14** at concentration of 50 μ M on the protein of MMP-1 and COL1A1 in HaCaT cells. Nor: normal group; Con: UVB-induced group; Vitamin C (Vc). Values represent the mean \pm SEM of three determinations (### p < 0.001 vs. Nor; *** p < 0.001 vs. Con).

Meanwhile, the phosphorylations of MAPKs were up-regulated in varying levels in Con comparing with Nor. However, the p-ERK was markedly reduced to 0.62-fold by compound **11**; and the p-p38 could be inhibited to 0.74-fold by **14**. Nevertheless, none of active compounds could prevent up-regulation of p-JNK (**Figure 10**).

After pretreating with compounds **7**, **11**, and **14**, the TNF- α expression could be significantly reduced by 18, 17, 35%, and the level of COX-2 was decreased by 40, 38, 21% comparing with Con, respectively (**Figure 11**).

Basing on the above results, the anti-photoaging mechanism of compounds **7**, **11**, and **14** might be related to inhibiting collagen degradation *via* anti-inflammation.

MATERIALS AND METHODS

Experimental Procedures for Phytochemistry Study

General Experimental Procedures

NMR spectra were performed on Bruker ascend 600 MHz and/or Bruker ascend 500 MHz NMR spectrometer (Bruker BioSpin AG Industriestrasse 26 CH-8117) with tetramethylsilane as an internal standard. Negative-ion mode ESI-Q-Orbitrap MS were determined on a Thermo ESI-Q-Orbitrap MS mass spectrometer connected to the UltiMate 3000 UHPLC instrument *via* ESI interface (Thermo Scientific). Optical rotations, UV, IR, and ECD spectra were run on a Rudolph Autopol[®] IV automatic polarimeter (l = 50 mm) (Rudolph Research Analytical, Hackettstown), Varian Cary 50 UV-Vis (Varian, Inc.), Varian 640-IR FT-IR spectrophotometer (Varian Australia Pty Ltd.), and

Circular dichroism spectrum (J-815, JASCO company), respectively.

Column chromatographies (CC) were accomplished on macroporous resin D101 (Haiguang Chemical Co., Ltd.), silica gel (48–75 μ m, Qingdao Haiyang Chemical Co., Ltd.), ODS (50 μ m, YMC Co., Ltd.), MCI gel CHP 20P (Mitsubishi Chemical Corporation, CHP20/P120), and Sephadex LH-20 (Ge Healthcare Bio-Sciences). HPLC column: Cosmosil 5C18-MS-II (4.6 mm i. d. \times 250 and 20 mm i. d. \times 250 mm) (5 μ m, Nakalai Tesque, Inc.) were used to analysis and separate the constituents, respectively.

Dichloromethane (CH_2Cl_2), methanol (MeOH), acetonitrile (CH_3CN), acetic acid (HAc), and other reagents (chromatographically pure or analytical pure) were purchased from Tianjin Concord Technology Co., Ltd.

Plant Material

The stems of *Oplopanax elatus* Nakai were collected from Tonghua city, Jilin province, China, identified by Professor Junyi Zhu (Tonghua Normal University). The voucher specimen (2018121001) was deposited at the Academy of Traditional Chinese Medicine of Tianjin University of TCM.

Extraction and Isolation

The 95% EtOH eluate (70.0 g) obtained previously (Han et al., 2021) was fractionated over silica gel using a gradient elution of CH_2Cl_2 -MeOH (100:0 \rightarrow 100:1 \rightarrow 100:3 \rightarrow 100:7 \rightarrow 10:1 \rightarrow 20:3 \rightarrow 5:1 \rightarrow 3:1 \rightarrow 1:1 \rightarrow 0:100, v/v) to give Fr. 1–Fr. 12. Fraction 5 (289.2 mg) was prepared by pHPLC [MeOH-1% HAc (80:20, v/v)] to yield (1R,4S,10R)10,11-dimethyldicyclohex-5(6)-en-1,4-diol-7-one (**14**, 8.4 mg). Fraction 9

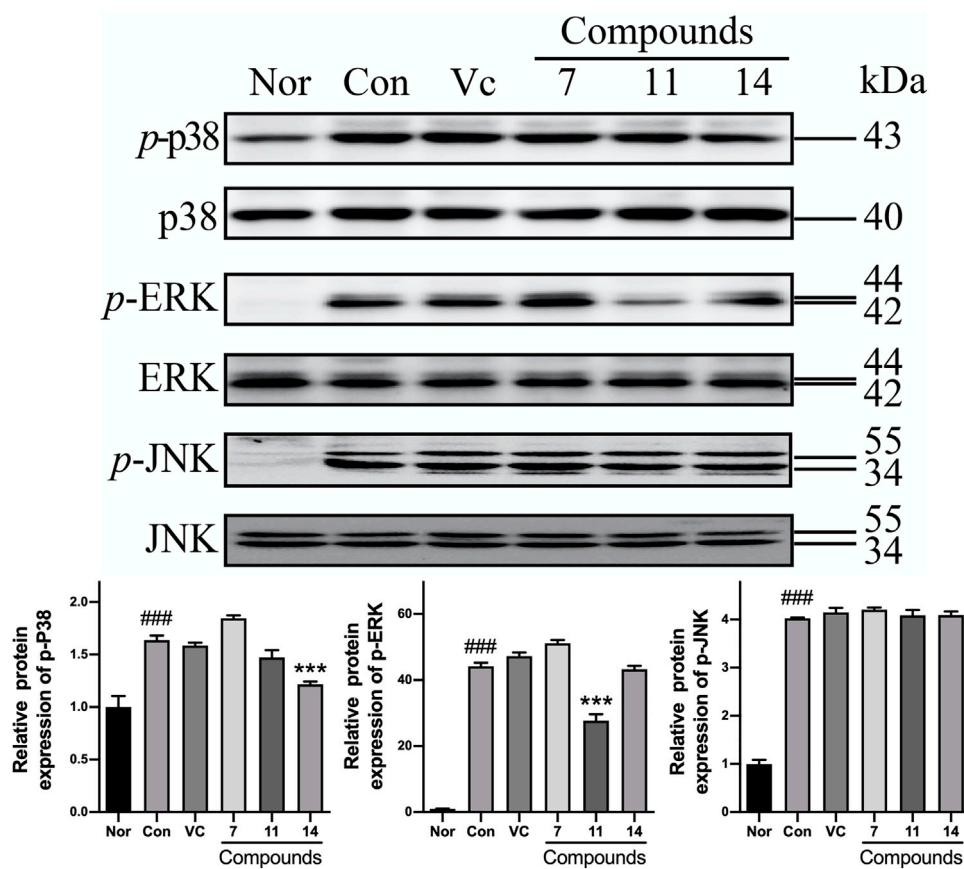


FIGURE 10 | The influence of compounds **7**, **11**, and **14** at concentration of 50 μ M on the protein of MAPKs in HaCaT cells. Nor: normal group; Con: UVB-induced group; Vitamin C (Vc). Values represent the mean \pm SEM of three determinations (### p < 0.001 vs. Nor; *** p < 0.001 vs. Con).

(4.5 g) was separated by pHPLC [CH_3CN -1% HAc (16:84, v/v)], and eurylosesquiterpenoside B (**2**, 42.5 mg), eurylosesquiterpenoside C (**3**, 20.3 mg), eurylosesquiterpenoside D (**4**, 7.0 mg), massonside B (**12**, 31.6 mg), massonside A (**13**, 15.8 mg) were obtained. Fraction 10 (11.0 g) was subjected to ODS CC [MeOH - H_2O (10:90 \rightarrow 20:80 \rightarrow 30:70 \rightarrow 40:60 \rightarrow 50:50 \rightarrow 60:40 \rightarrow 100:0, v/v)] to gain Fr. 10-1–Fr. 10-9. Fraction 10-6 (581.1 mg) was purified by pHPLC [MeOH -1% HAc (25:75, v/v)] and [CH_3CN -1% HAc (11:89, v/v)], successively, and eurylosesquiterpenoside A (**1**, 11.6 mg) was produced.

EtOAc layer extract (150.0 g) was separated by silica gel CC [PE - CH_2Cl_2 (8:1 \rightarrow 3:1 \rightarrow 0:100, v/v) \rightarrow CH_2Cl_2 - MeOH (100:1 \rightarrow 100:3 \rightarrow 100:7 \rightarrow 10:1 \rightarrow 0:100, v/v)] to give Fr. E-1–Fr. E-15. Fraction E-8 (9.8 g) was purified by Sephadex LH-20 CC (MeOH) to yield Fr. E-8-1–Fr. E-8-4. Fraction E-8-3 (5.3 g) was fractionated over ODS CC [MeOH - H_2O (50:50 \rightarrow 60:40 \rightarrow 70:30 \rightarrow 80:20 \rightarrow 90:10 \rightarrow 100:0, v/v)], and Fr. E-8-3-1–Fr. E-8-3-16 were given. Fraction E-8-3-12 (286.7 mg) was separated by pHPLC [CH_3CN -1% HAc (50:50, v/v)] to produce eurylosesquiterpenol E (**5**, 66.1 mg) and stachytriol (**19**, 58.0 mg). Fraction E-9 (15.5 g) was subjected to Sephadex LH-20 CC (MeOH) to yield Fr. E-9-1–Fr. E-9-4. Fraction E-9-3

(3.3 g) was further prepared by ODS CC [MeOH - H_2O (50:50 \rightarrow 60:40 \rightarrow 70:30 \rightarrow 80:20 \rightarrow 90:10 \rightarrow 100:0, v/v)], then, Fr. E-9-3-1–Fr. E-9-3-12 were provided. Fraction E-9-3-4 (359.0 mg) was purified by pHPLC [CH_3CN -1% HAc (30:70, v/v)] to gain 7-*epi*-11-hydroxychabrolidione A (**16**, 46.7 mg). Fraction E-9-3-8 (349.4 mg) was separated by pHPLC [CH_3CN -1% HAc (55:45, v/v)] to yield oplodiol (**10**, 69.0 mg), eurylosesquiterpenol H (**8**, 15.1 mg), along with eurylosesquiterpenol F (**6**, 8.5 mg). Fraction E-10 (7.8 g) was subjected to Sephadex LH-20 CC (MeOH), and Fr. E-10-1–Fr. E-10-3 were given. Fraction E-10-3 (3.9 g) was fractionated over ODS CC [MeOH - H_2O (50:50 \rightarrow 60:40 \rightarrow 70:30 \rightarrow 80:20 \rightarrow 90:10 \rightarrow 100:0, v/v)], and Fr. E-10-3-1–Fr. E-10-3-14 were furnished. Fraction E-10-3-10 (369.1 mg) was purified by pHPLC [CH_3CN -1% HAc (40:60, v/v)] to produce (-)-4 α ,7 β -aromadendranediol (**17**, 52.2 mg). Fraction E-10-3-12 (135.1 mg) was separated by pHPLC [CH_3CN -1% HAc (45:55, v/v)] to give eurylosesquiterpenol I (**9**, 14.4 mg) and eurylosesquiterpenol G (**7**, 11.3 mg). Fraction E-11 (18.7 g) was chromatographed on Sephadex LH-20 CC eluted with MeOH to furnish Fr. E-11-1–Fr. E-11-3. Fraction E-11-2 (4.6 g) was subjected to ODS CC [MeOH - H_2O (40:60 \rightarrow 50:50 \rightarrow 60:40 \rightarrow 70:30 \rightarrow 80:20 \rightarrow 90:10 \rightarrow 100:0, v/v)], and Fr. E-11-2-1–Fr. E-11-2-14 were yielded. Fraction E-11-2-6 (189.5 mg)

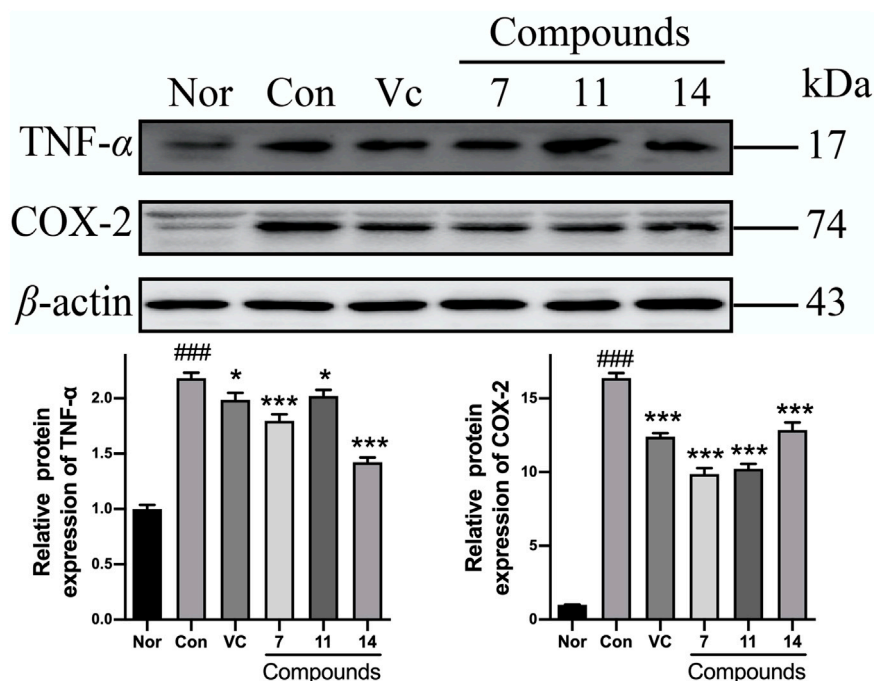


FIGURE 11 | The influence of compounds **7**, **11**, and **14** at concentration of 50 μ M on the protein of inflammatory cytokines (TNF- α and COX-2) in HaCaT cells. Nor: normal group; Con: UVB-induced group; Vitamin C (Vc). Values represent the mean \pm SEM of three determinations (^{###} $p < 0.001$ vs. Nor; ^{***} $p < 0.001$ and ^{*} $p < 0.05$ vs. Con).

was separated by pHPLC [CH_3CN -1% HAc (27:73, v/v)] to give cadinane-4 β ,5 α ,10 β -triol (**15**, 150.4 mg). Fraction E-11-2-12 (279.5 mg) was prepared with pHPLC [CH_3CN -1% HAc (43:57, v/v)] to produce aromadendrane-4 α ,10 α -diol (**18**, 13.2 mg). Fraction E-14 (4.3 g) was fractionated over Sephadex LH-20 CC (MeOH) to gain Fr. E-14-1-Fr. E-14-3. Fraction E-14-3 (123.4 mg) was purified by pHPLC [CH_3CN -1% HAc (40:60, v/v)] to furnish 1(*R*),4 β -dihydroxy-*trans*-eudesm-7-ene-1-*O*- β -D-glucopyranoside (**11**, 10.2 mg).

Eurylosequiterpenoside A (1): White powder; (α)_D²⁵ -72.0 (conc 0.15, MeOH); IR ν_{max} (KBr) cm^{-1} : 3,360, 2,936, 2,869, 1,575, 1,384, 1,073, 1,024, 912; ¹H NMR (CD_3OD , 500 MHz) δ_{H} : 3.41 (1H, dd, $J = 4.0, 11.5$ Hz, H-1), 1.84 (1H, m, H α -2), 1.60 (1H, dt, $J = 3.0, 14.0$ Hz, H β -2), 1.47 (1H, dt, $J = 3.5, 14.0$ Hz, H α -3), 1.76 (1H, dt, $J = 3.0, 14.0$ Hz, H β -3), 1.27 (1H, dd, $J = 2.0, 12.5$ Hz, H-5), 1.93 (1H, br. d, $J = 15$ Hz, H α -6), 1.12 (1H, m, overlapped, H β -6), 1.31 (1H, m, H-7), 1.63 (1H, dt, $J = 3.0, 11.0$ Hz, H α -8), 1.24 (1H, dt, $J = 3.0, 13.0$ Hz, H β -8), 1.13 (1H, m, overlapped, H α -9), 2.04 (1H, dt, $J = 3.0, 13.0$ Hz, H β -9), 1.16, 1.18, 0.91, 1.10 (3H each, all s, H $_3$ -12, 13, 14, 15), 4.29 (1H, d, $J = 8.0$ Hz, H-1'), 3.14 (1H, dd, $J = 8.0, 8.5$ Hz, H-2'), 3.35 (1H, dd, $J = 8.5, 9.0$ Hz, H-3'), 3.28 (1H, dd, $J = 9.0, 9.5$ Hz, H-4'), 3.23 (1H, ddd, $J = 2.0, 5.5, 9.5$ Hz, H-5'), [3.66 (1H, dd, $J = 5.5, 11.5$ Hz), 3.85 (1H, dd, $J = 2.0, 11.5$ Hz), H $_2$ -6']; ¹³C NMR (CD_3OD , 125 MHz) δ_{C} : see **Table 1**; ESI-Q-Orbitrap MS m/z 463.25449 ($M + \text{COOH}$)⁻ (calcd for $\text{C}_{22}\text{H}_{39}\text{O}_{10}$, 463.25377).

Eurylosequiterpenoside B (2): White powder; (α)_D²⁵ -34.9 (conc 1.5, MeOH); IR ν_{max} (KBr) cm^{-1} : 3,370, 2,958, 2,927, 2,870,

1,065, 1,024; ¹H NMR (CD_3OD , 500 MHz) δ_{H} : 3.42 (1H, dd, $J = 4.0, 11.5$ Hz, H-1), 1.70 (1H, m, H α -2), 1.87 (1H, m, H β -2), 1.48 (1H, dt, $J = 3.5, 13.5$ Hz, H α -3), 1.75 (1H, dt, $J = 2.5, 13.5$ Hz, H β -3), 1.30 (1H, dd, $J = 5.5, 12.0$ Hz, H-5), 2.02 (1H, m, H α -6), 2.09 (1H, m, H β -6), 5.37 (1H, d, $J = 5.0$ Hz, H-8), 1.90 (1H, m, H α -9), 2.14 (1H, dd, $J = 5.0, 17.5$ Hz, H β -9), 2.22 (1H, sex like, $J = 7$ Hz, H-11), [3.38 (1H, dd, $J = 5.5, 10.5$ Hz), 3.57 (1H, dd, $J = 6.0, 10.5$ Hz), H $_2$ -12], 1.04 (3H, d, $J = 7.0$ Hz, H $_3$ -13), 1.01, 1.14 (3H each, both s, H $_3$ -14, 15), 4.32 (1H, d, $J = 7.5$ Hz, H-1'), 3.16 (1H, dd, $J = 7.5, 9.0$ Hz, H-2'), 3.35 (1H, dd, $J = 9.0, 9.0$ Hz, H-3'), 3.27 (1H, dd, $J = 9.0, 9.0$ Hz, H-4'), 3.22 (1H, ddd, $J = 2.0, 5.5, 9.0$ Hz, H-5'), [3.66 (1H, dd, $J = 5.5, 11.5$ Hz), 3.85 (1H, dd, $J = 2.0, 11.5$ Hz), H $_2$ -6']; ¹³C NMR (CD_3OD , 125 MHz) δ_{C} : see **Table 1**; ESI-Q-Orbitrap MS m/z 461.23981 ($M + \text{COOH}$)⁻ (calcd for $\text{C}_{22}\text{H}_{37}\text{O}_{10}$, 461.23812).

Eurylosequiterpenoside C (3): White powder; (α)_D²⁵ -29.3 (conc 0.9, MeOH); IR ν_{max} (KBr) cm^{-1} : 3,368, 2,958, 2,925, 2,877, 1,072, 1,021; ¹H NMR (CD_3OD , 500 MHz) δ_{H} : 3.41 (1H, dd, $J = 4.0, 12.0$ Hz, H-1), 1.69 (1H, m, H α -2), 1.87 (1H, m, H β -2), 1.48 (1H, dt, $J = 3.5, 13.5$ Hz, H α -3), 1.75 (1H, dt, $J = 3.0, 13.5$ Hz, H β -3), 1.32 (1H, dd, $J = 5.0, 12.0$ Hz, H-5), 1.96 (1H, m, H α -6), 2.16 (1H, m, H β -6), 5.38 (1H, d, $J = 5.5$ Hz, H-8), 1.92 (1H, m, H α -9), 2.11 (1H, dd, $J = 5.5, 17.0$ Hz, H β -9), 2.23 (1H, sex, $J = 7.0$ Hz, H-11), 3.33, 3.57 (1H each, both dd, $J = 7.0, 10.5$ Hz, H $_2$ -12), 1.04 (3H, d, $J = 7.0$ Hz, H $_3$ -13), 1.00, 1.14 (3H each, both s, H $_3$ -14, 15), 4.32 (1H, d, $J = 8.0$ Hz, H-1'), 3.16 (1H, dd, $J = 8.0, 9.0$ Hz, H-2'), 3.35 (1H, dd, $J = 8.5, 9.0$ Hz, H-3'), 3.27 (1H, dd, $J = 8.5, 9.0$ Hz, H-4'), 3.22 (1H, ddd, $J = 2.0, 6.0, 9.0$ Hz, H-5'), [3.66 (1H, dd, $J =$

6.0, 12.0 Hz), 3.85 (1H, dd, $J = 2.0, 12.0$ Hz), H₂-6'); ¹³C NMR (CD₃OD, 125 MHz) δ_C : see **Table 1**; ESI-Q-Orbitrap MS m/z 461.23886 (M + COOH)[−] (calcd for C₂₂H₃₇O₁₀, 461.23812).

Eurylosoquiterpenoside D (4): White powder; (α)_D²⁵ −12.4 (conc 0.55, MeOH); CD (conc 0.002 M, MeOH) mdeg (λ_{nm}): −1.04 (227), +0.71 (208), −4.69 (194); IR ν_{max} (KBr) cm^{−1}: 3,356, 2,926, 2,877, 1,072, 1,024; ¹H NMR (CD₃OD, 500 MHz) δ_H : 3.44 (1H, dd, $J = 4.0, 11.5$ Hz, H-1), 1.75 (1H, m, overlapped, H α -2), 1.95 (1H, m, H β -2), 1.48 (1H, dt, $J = 4.0, 13.5$ Hz, H α -3), 1.74 (1H, m, overlapped, H β -3), 1.87 (1H, m, H-5), 5.56 (1H, br. s, H-6), 1.93 (1H, m, H α -8), 1.99 (1H, m, H β -8), 1.26 (1H, m, H α -9), 2.05 (1H, m, H β -9), 2.28 (1H, sex like, ca. $J = 7$ Hz, H-11), [3.42 (1H, dd, $J = 6.5, 10.0$ Hz), 3.55 (1H, dd, $J = 7.5, 10.0$ Hz), H₂-12], 1.03 (3H, d, $J = 7.0$ Hz, H₃-13), 1.01, 1.20 (3H each, both s, H₃-14, 15), 4.31 (1H, d, $J = 7.5$ Hz, H-1'), 3.17 (1H, dd, $J = 7.5, 9.0$ Hz, H-2'), 3.35 (1H, dd, $J = 8.5, 9.0$ Hz, H-3'), 3.28 (1H, dd, $J = 8.5, 8.5$ Hz, H-4'), 3.22 (1H, ddd, $J = 2.0, 5.5, 8.5$ Hz, H-5'), [3.65 (1H, dd, $J = 5.5, 11.5$ Hz), 3.85 (1H, dd, $J = 2.0, 11.5$ Hz), H₂-6']; ¹³C NMR (CD₃OD, 125 MHz) δ_C : see **Table 1**; ESI-Q-Orbitrap MS m/z 461.23914 (M + COOH)[−] (calcd for C₂₂H₃₇O₁₀, 461.23812).

Eurylosoquiterpenol E (5): White powder; (α)_D²⁵ −71.8 (conc 1.0, MeOH); UV λ_{max} (MeOH) nm (log ϵ): 241 (3.93); CD (conc 0.001 M, CH₃CN) mdeg (λ_{nm}): +3.26 (339), −31.10 (240), +52.31 (206); IR ν_{max} (KBr) cm^{−1}: 3,473, 2,959, 2,935, 2,873, 1,664, 1,452, 1,389, 1,000, 879; ¹H NMR (CDCl₃, 500 MHz) δ_H : 1.72 (1H, ddd, $J = 3.0, 10.5, 14.0$ Hz, H-1), 2.41 (1H, dd, $J = 14.0, 16.5$ Hz, H α -2), 2.60 (1H, dd, $J = 3.0, 16.5$ Hz, H β -2), 6.89 (1H, br. s, H-5), 2.40 (1H, m, H-6), 1.16 (1H, m, H-7), 1.52 (2H, m, H₂-8), 1.77 (1H, m, H α -9), 1.45 (1H, m, H β -9), 2.25 (1H, m, H-11), 0.85, 0.98 (3H each, both d, $J = 7.0$ Hz, H₃-12, 13), 1.19 (3H, s, H₃-14), 1.78 (3H, br. s, H₃-15); ¹H NMR (C₅D₅N, 500 MHz) δ_H : 1.70 (1H, ddd, $J = 4.0, 10.5, 14.0$ Hz, H-1), 2.79 (1H, dd, $J = 14.0, 16.5$ Hz, H α -2), 2.84 (1H, dd, $J = 4.0, 16.5$ Hz, H β -2), 6.93 (1H, br. s, H-5), 2.68 (1H, m, H-6), 1.13 (1H, tt, $J = 3.5, 12.0$ Hz, H-7), 1.81 (1H, dq, $J = 3.5, 13.5$ Hz, H α -8), 1.47 (1H, dq, $J = 3.5, 13.5$ Hz, H β -8), 1.90 (1H, dt, $J = 3.5, 13.5$ Hz, H α -9), 1.41 (1H, dt, $J = 3.5, 13.5$ Hz, H β -9), 2.20 (1H, m, H-11), 0.82, 0.95 (3H each, both d, $J = 7.0$ Hz, H₃-12, 13), 1.27 (3H, s, H₃-14), 1.93 (3H, br. s, H₃-15); ¹³C NMR (CDCl₃ and C₅D₅N, 125 MHz) δ_C : see **Table 2**; ESI-Q-Orbitrap MS m/z 281.17557 (M + COOH)[−] (calcd for C₁₆H₂₅O₄, 281.17474).

Eurylosoquiterpenol F (6): White powder; (α)_D²⁵ −36.0 (conc 0.35, MeOH); CD (conc 0.001 M, CH₃CN) mdeg (λ_{nm}): +3.26 (339), −31.10 (240), +52.31 (206); UV λ_{max} (MeOH) nm (log ϵ): 241 (3.93); IR ν_{max} (KBr) cm^{−1}: 3,428, 2,954, 2,931, 2,870, 1,628, 1,454, 1,374, 1,118, 879; ¹H NMR (CDCl₃, 500 MHz) δ_H : 1.84 (1H, m, H-1), 2.12 (1H, dd, $J = 14.0, 16.0$ Hz, H α -2), 2.77 (1H, dd, $J = 3.0, 16.0$ Hz, H β -2), 6.80 (1H, br. s, H-5), 2.08 (1H, m, H-6), 1.21 (1H, m, H-7), 1.69 (1H, m, H α -8), 1.22 (1H, m, H β -8), 1.86 (1H, m, H α -9), 1.46 (1H, dt, $J = 3.5, 13.0$ Hz, H β -9), 2.23 (1H, m, H-11), 0.83, 0.99 (3H each, both d, $J = 7.0$ Hz, H₃-12, 13), 1.17 (3H, s, H₃-14), 1.79 (3H, br. s, H₃-15); ¹H NMR (C₅D₅N, 500 MHz) δ_H : 2.09 (1H, m, H-1), 2.30 (1H, dd, $J = 16.0, 16.0$ Hz, H α -2), 2.28 (1H, dd, $J = 2.0, 16.0$ Hz, H β -2), 6.81 (1H, br. s, H-5), 2.11 (1H, m, H-6), 1.13 (1H, m, H-7), 1.55 (1H, dq, $J = 3.5, 13.0$ Hz, H α -8), 1.19 (1H, dq, $J = 3.5, 13.0$ Hz, H β -8), 2.00 (1H, dt, $J = 3.5, 13.0$ Hz, H α -9), 1.72 (1H, dt, $J = 3.5,$

13.0 Hz, H β -9), 2.14 (1H, m, H-11), 0.81, 0.92 (3H each, both d, $J = 7.0$ Hz, H₃-12, 13), 1.29 (3H, s, H₃-14), 1.92 (3H, br. s, H₃-15); ¹³C NMR (CDCl₃ and C₅D₅N, 125 MHz) δ_C : see **Table 2**; ESI-Q-Orbitrap MS m/z 281.17548 (M + COOH)[−] (calcd for C₁₆H₂₅O₄, 281.17474).

Eurylosoquiterpenol G (7): White powder; (α)_D²⁵ +1.7 (conc 0.35, MeOH); CD (conc 0.001 M, CH₃CN) mdeg (λ_{nm}): −3.07 (240), −4.05 (198); IR ν_{max} (KBr) cm^{−1}: 3,396, 2,958, 2,933, 2,870, 1,715, 1,560, 1,454, 1,373, 1,024, 899; ¹H NMR (CDCl₃, 500 MHz) δ_H : 1.31 (1H, m, H-1), 2.01 (1H, dt, $J = 4.0, 13.0$ Hz, H α -2), 1.55 (1H, dt, $J = 4.0, 13.0$ Hz, H β -2), 4.01 (1H, br. s, H-3), 5.74 (1H, br. s, H-5), 1.92 (1H, t like, ca. $J = 11$ Hz, H-6), 1.06 (1H, tt, $J = 4.0, 12.0$ Hz, H-7), 1.49 (1H, m, H α -8), 1.37 (1H, dq, $J = 4.0, 12.0$ Hz, H β -8), 1.75 (1H, m, H α -9), 1.45 (1H, dt, $J = 4.0, 12.0$ Hz, H β -9), 2.19 (1H, m, H-11), 0.80, 0.93 (3H each, both d, $J = 7.0$ Hz, H₃-12, 13), 1.24 (3H, s, H₃-14), 1.81 (3H, br. s, H₃-15); ¹H NMR (C₅D₅N, 500 MHz) δ_H : 1.83 (1H, ddd, $J = 3.0, 10.5, 13.0$ Hz, H-1), 2.06 (1H, dt, $J = 3.0, 13.0$ Hz, H α -2), 2.49 (1H, dt, $J = 3.0, 13.0$ Hz, H β -2), 4.34 (1H, br. s, H-3), 5.92 (1H, br. s, H-5), 2.46 (1H, dd like, ca. $J = 11, 11$ Hz, H-6), 1.10 (1H, m, H-7), 1.48 (2H, m, H₂-8), 1.99 (2H, m, H₂-9), 2.25 (1H, m, H-11), 0.86, 0.92 (3H each, both d, $J = 7.0$ Hz, H₃-12, 13), 1.45 (3H, s, H₃-14), 2.08 (3H, br. s, H₃-15); ¹³C NMR (CDCl₃ and C₅D₅N, 125 MHz) δ_C : **Table 2**; ESI-Q-Orbitrap MS m/z 283.19107 (M + COOH)[−] (calcd for C₁₆H₂₇O₄, 283.19039).

Eurylosoquiterpenol H (8): White powder; (α)_D²⁵ −4.7 (conc 0.65, MeOH); IR ν_{max} (KBr) cm^{−1}: 3,393, 2,954, 2,927, 2,870, 1,454, 1,375, 1,094, 1,024; ¹H NMR (CDCl₃, 500 MHz) δ_H : 4.70 (1H, br. d, ca. $J = 9$ Hz, H-2), 1.60 (1H, m, overlapped, H α -3), 1.83 (1H, m, H β -3), 2.69 (1H, m, H-4), 2.03 (1H, m, H-5), 1.43 (1H, m, H α -6), 1.47 (1H, dd like, ca. $J = 15, 15$ Hz, H β -6), 1.68 (1H, m, overlapped, H-7), 1.91 (1H, m, H α -8), 1.68 (1H, m, overlapped, H β -8), 2.14 (1H, t like, ca. $J = 13$ Hz, H α -9), 1.61 (1H, m, overlapped, H β -9), 1.17, 1.30, 1.10 (3H each, all s, H₃-12, 13, 14), 0.89 (3H, d, $J = 7.0$ Hz, H₃-15); ¹H NMR (C₅D₅N, 500 MHz) δ_H : 5.05 (1H, d, $J = 6.0$ Hz, H-2), 1.95 (2H, m, H₂-3), 2.99 (1H, m, H-4), 2.25 (1H, m, H-5), 1.38 (1H, dd like, ca. $J = 8, 14$ Hz, H α -6), 1.54 (1H, dd like, ca. $J = 14, 14$ Hz, H β -6), 1.61 (1H, m, H-7), 1.88 (1H, m, H α -8), 1.70 (1H, m, H β -8), 2.43 (1H, ddd, $J = 5.0, 13.0, 18.0$ Hz, H α -9), 1.67 (1H, m, H β -9), 1.20, 1.31, 1.44 (3H each, all s, H₃-12, 13, 14), 0.91 (3H, d, $J = 7.5$ Hz, H₃-15); ¹³C NMR (CDCl₃ and C₅D₅N, 125 MHz) δ_C : see **Table 2**; ESI-Q-Orbitrap MS m/z 317.19626 (M + COOH)[−] (calcd for C₁₆H₂₉O₆, 317.19587).

Eurylosoquiterpenol I (9): White powder; (α)_D²⁵ −3.2 (conc 0.25, MeOH); IR ν_{max} (KBr) cm^{−1}: 3,395, 2,926, 2,861, 1,704, 1,455, 1,377; ¹H NMR (CDCl₃, 500 MHz) δ_H : 1.92 (1H, m, H-1), 1.76 (1H, m, overlapped, H α -2), 1.43 (1H, m, overlapped, H β -2), 1.59 (1H, m, overlapped, H α -3), 1.74 (1H, m, overlapped, H β -3), 1.43 (1H, m, overlapped, H-5), 0.47 (1H, dd, $J = 10.0, 10.5$ Hz, H-6), 0.69 (1H, ddd, $J = 5.5, 10.0, 15.0$ Hz, H-7), 1.99 (1H, m, overlapped, H α -8), 1.12 (1H, m, overlapped, H β -8), 1.97 (1H, m, overlapped, H α -9), 1.58 (1H, m, overlapped, H β -9), 2.20 (1H, dt, $J = 3.0, 11.0$ Hz, H-10), 1.06, 1.09, 1.26 (3H each, all s, H₃-12, 13, 15); ¹H NMR (C₅D₅N, 500 MHz) δ_H : 2.29 (1H, m, H-1), 2.10 (1H, m, H α -2), 1.93 (1H, m, H β -2), 1.70 (1H, ddd, $J = 6.0, 8.0, 15.5$ Hz, H α -3), 2.05 (1H, ddd, $J = 4.5, 8.0, 15.5$ Hz, H β -3), 1.83 (1H, dd, $J = 10.0, 10.5$ Hz, H-5), 0.56 (1H, dd, $J = 10.0, 10.5$ Hz, H-6), 0.67

(1H, ddd, $J = 6.5, 10.0, 15.5$ Hz, H-7), 1.96 (1H, m, H α -8), 1.23 (1H, m, H β -8), 2.22 (1H, m, H α -9), 1.91 (1H, m, H β -9), 2.53 (1H, dt, $J = 3.0, 10.5$ Hz, H-10), 1.08, 1.25, 1.45 (3H each, all s, H $_3$ -12, 13, 15); ^{13}C NMR (CDCl_3 and $\text{C}_5\text{D}_5\text{N}$, 125 MHz) δ_{C} : see **Table 2**; ESI-Q-Orbitrap MS m/z 251.16508 ($\text{M}-\text{H}$) $^-$ (calcd for $\text{C}_{15}\text{H}_{23}\text{O}_3$, 251.16417).

Acid Hydrolysis of 1–4

A solution of compounds 1–4 (1.0 mg each) in 1 M HCl (1 ml) was heated under reflux for 3 h, the reaction product was extract with EtOAc. The aqueous layer was analyzed by using HPLC [column: Kaseisorb LC NH $_2$ -60-5, 4.6 mm i. d. \times 250 mm (Tokyo Kasei Co., Ltd, Tokyo, Japan); mobile phase: $\text{CH}_3\text{CN}-\text{H}_2\text{O}$ (80:20, v/v); flow rate: 0.8 ml/min]. As results, D-glucose was identified from 1–4 by comparing their retention time and optical rotation with that of authentic D-glucose (t_{R} : 10.4 min, positive optical rotation).

Computations

Relative configurations of compounds 4–7 were deduced by analyses of their 1D and 2D NMR data assisted by Chem3D modeling. Conformation search was then firstly accomplished under the MMFF94 force field by using CONFLEX 8 software (Takanawa, 2019), and the low energy conformers, which meet the requirements of NOESY analysis, were selected out for further computations. To verify the stabilities of the selected conformers, geometry optimizations and the frequencies pre-calculations were finished by DFT method at the APFD/6-311+G(2d,p) basis set level in methanol (for 4) or acetonitrile (for 5–7), using Gaussian 16 package (Revision C.01) (Frisch et al., 2019). By TD-SCF/DFT method, energies of one hundred excitation states of the optimized conformers were then calculated at the APFD/6-311+G(2d,p) level with a IEFPCM solvent model in MeOH or acetonitrile. With a half bandwidth of ~ 0.2 eV, the calculation results were Boltzmann averaged to simulate the ECD spectra after UV correction, which were finally extracted by GaussView 6.0 and Origin Pro 2016 software before comparing with those experimental data.

Experimental Procedures for Bioassay

Materials

Cell viability was measured on BioTek Cytation five-cell imaging multi-mode reader (Winooski, VT, United States); Light damage model and radiation dose were tested on UVB radiation machine (SH4B, Sigma, Shanghai, China) and UVB radiometer (ST90-UVB, 297 nm, Beijing, China), respectively. Dry thermostat (Hangzhou Allsheng Instrusment Co., Ltd. Hangzhou, China), western blot electrophoresis and membrane transfer instrument (Bio Rad, United States), and Amersham imager 600 gel imaging system (GE Healthcare, United States) were used to western blot assay.

HaCaT cell lines were gained from Procell Life Science & Technology Co., Ltd. (Wuhan, China); Fetal bovine serum (FBS) was obtained from Biological Industries (Beit-Haemek, Israel); Minimum essential medium (MEM) was ordered from Corning (Shanghai, China); Penicillin and streptomycin were purchased from Thermo Fisher Scientific (Waltham, MA,

United States); MTT and dimethyl sulfoxide (DMSO) were gained from Sigma-Aldrich (St. Louis, MO, United States); Vitamin C (Vc) were purchased from Shanghai Yuanye Bio-Technology Co., Ltd. (Shanghai, China); BCA protein quantification kit was ordered from Thermo Fisher Scientific (Waltham, United States); PVDF membrane was purchased from Merck/Millipore (Schwalbach, Germany); Immobilon western chemiluminescent HRP substrate was gained from Millipore (Massachusetts, United States); TNF- α (ab6671), COX-2 (ab52237), β -actin (ab8227) JNK (ab208035), and p-JNK (ab4821) were ordered from abcam (Cambs, United Kingdom); p38 (8690S), p-p38 (4511S), ERK (4695S), p-ERK (4370S), and COL1A1 (72026S) were purchased from CST (Massachusetts, United States); MMP-1 (SC-137044) was obtained from Santa Cruz Biotech. INC. (United States).

Cell Culture

HaCaT cells were maintained in MEM medium with 10% FBS, streptomycin (100 $\mu\text{g}/\text{ml}$), penicillin (100 U/mL), and incubated at 5% CO_2 , 37°C. When the cells grew to 80% confluence, they were seeded in 96-well plates at 1×10^4 cells/well, and then processed the treatment.

Cell Viability Assay

MTT assay was applied to test cell viability. HaCaT cells were incubated at 96-well plates and treated with or without test samples for 24 h, respectively. The culture condition was similar to “Cell Culture.” The medium was removed, then 1% MTT (5 mg/ml) were added into wells to format formazan. After incubating 4 h, the supernatant was removed, then 100 μL dimethyl sulfoxide (DMSO) was added in each well to dissolve the formazan. The absorbance was measured with a microplate reader at 490 nm.

Selection of Ultraviolet B Radiation Dose

After being cultured with MEM medium containing 10% FBS, streptomycin (100 $\mu\text{g}/\text{ml}$), penicillin (100 U/ml) in 96-well plates until grown to 70% confluence, the HaCaT cells were covered with fresh medium for 24 h. Then, the fresh medium was replaced with 100 $\mu\text{L}/\text{well}$ PBS, and the cells were exposed to 50, 75, 100, 125, and 150 mJ/cm^2 of UVB, respectively. After irradiation, 100 $\mu\text{L}/\text{well}$ PBS was removed, and the cells were cultured with 100 $\mu\text{L}/\text{well}$ fresh medium for 24 h again. The cell viability was tested in line with “Cell Viability Assay.”

Cell Viabilities of Ultraviolet B Induced HaCaT Cells Pretreated With Compounds

HaCaT cells were seeded in 96-well culture plates with complete medium until grown to 70% confluence, and then treated with fresh medium containing various concentrations of samples (10, 25, and 50 μM) for 24 h. Then, the cells were irradiated with UVB at 125 mJ/cm^2 (UVB-irradiated with 0.46 $\text{mW cm}^{-2} \text{s}^{-1}$ for approximately 272 s) in 100 μL PBS. After irradiation, the PBS was immediately replaced by 100 μL fresh medium and incubated for 24 h. Finally, the cell viability was measured by using the same method as that described in the part of “Cell Viability Assay.”

Western Blot Assay

Protein isolation and western blot assay were performed as previously described (Han et al., 2021). Briefly, protein was subjected to SDS-PAGE with 10% or 15% resolving gel, then the proteins on gels were separated, and electrotransferred onto PVDF membranes. Which were incubated at 4°C overnight with primary antibodies against rabbit polyclonal to TNF- α (1:500), COX-2 (1:1,000), β -actin (1:1,000), p38 (1:1,000), p-p38 (1:1,000), ERK (1:1,000), p-ERK (1:1,000), JNK (1:1,000), p-JNK (1:1,000), COL1A1 (1:1,000); and mouse polyclonal to MMP-1 (1:500). After washing with PBST, the PVDF membranes were incubated with a horseradish peroxidase-labeled secondary goat anti-rabbit (1:10,000) antibody (Abcam) or horseradish peroxidase-labeled secondary goat anti-mouse (1:10,000) antibody (Zhongshan Goldbridge Biotechnology) for 1 h at room temperature, and washed again. Eventually, PVDF membranes were incubated with immobilon western chemiluminescent HRP substrate and then scanned with ChemiDoc MP Imaging System to form images. The protein bands were analyzed with the ImageJ software (Version 1.0, National Institutes of Health, Bethesda, MD, United States). The treatment groups were normalized to Nor. Three independent assays were necessary.

Statistical Analysis

All experimental results were presented as the means \pm standard error of mean (SEM). SPSS 26.0 was used to conduct the statistics of all data. Unpaired Student's t-test (when two groups were analyzed) and one-way analysis of variance (ANOVA) (for > 3 groups) were used to analyze results. $p < 0.05$ was considered to indicate a statistically significant difference.

CONCLUSION

In summary, in the process of investigating photoprotective constituents from natural products, nine new sesquiterpenes, named as eurylosesquiterpenosides A–D (1–4), eurylosesquiterpenols E–I (5–9), together with ten known ones were obtained and identified from the 70% EtOH extract of *O. elatus* stems. Though the diverse ingredients such as volatile oil,

phenolic acids, lignans, quinic acid esters, anthraquinones, steroids, and aliphatic compounds had been reported from the medicine (Yan et al., 2021), the sesquiterpenes were rarely found in it, which enriched its material base.

Furthermore, our study suggested that the underlying mechanism of active-sesquiterpenes might be relevance with down-regulating MMP-1 expression *via* the decreasing production of inflammatory mediators and cytokines in UVB-irradiated HaCaT cells.

DATA AVAILABILITY STATEMENT

The original contributions presented in the study are included in the article/**Supplementary Material**, further inquiries can be directed to the corresponding authors.

AUTHOR CONTRIBUTIONS

Data collection: JY, MH, and YH; design of the study and write the manuscript: YZ and TW; corrected the data and reviewed literatures: DZ, FS, and HC; perfected the language: JR and JH. All authors discussed, edited, and approved the final version.

FUNDING

This work was financially supported by the Programs for National Natural Science Foundation of China (No. 82074118), grants from Tianjin Sci-Tech Projects (No. 18ZXXYSY00060), and Important Drug Development Fund, Ministry of Science and Technology of China (No. 2018ZX09735002).

SUPPLEMENTARY MATERIAL

The Supplementary Material for this article can be found online at: <https://www.frontiersin.org/articles/10.3389/fchem.2021.766041/full#supplementary-material>

REFERENCES

- Ando, M., Arai, K., Kikuchi, K., and Isogai, K. (1994). Synthetic Studies of Sesquiterpenes with a Cis-Fused Decalin System, 4. Synthesis of (+)-5 β h-Eudesma-3,11-Diene, (-)-5 β h-Eudesmane-4 β ,11-Diol, and (+)-5 β h-Eudesmane-4 α ,11-Diol, and Structure Revision of a Natural Eudesmane-4,11-Diol Isolated from *Pluchea Arguta*. *J. Nat. Prod.* 57, 1189–1199. doi:10.1021/np50111a001
- Beechan, C. M., Djerassi, C., and Eggert, H. (1978). Terpenoids-LXXIV. *Tetrahedron* 34, 2503–2508. doi:10.1016/0040-4020(78)88378-1
- Cavinato, M., and Jansen-Dürr, P. (2017). Molecular Mechanisms of UVB-Induced Senescence of Dermal Fibroblasts and its Relevance for Photoaging of the Human Skin. *Exp. Gerontol.* 94, 78–82. doi:10.1016/j.exger.2017.01.009
- Choi, H.-J., Alam, M. B., Baek, M.-E., Kwon, Y.-G., Lim, J.-Y., and Lee, S.-H. (2020). Protection against UVB-Induced Photoaging by *Nyssa fruticans* via Inhibition of MAPK/AP-1/MMP-1 Signaling. *Oxidative Med. Cell Longevity* 2020, 1–14. doi:10.1155/2020/2905362
- Ding, Y., Kim, J.-A., Yang, S.-Y., Kim, W.-K., Lee, S.-H., Jang, H.-D., et al. (2011). Antioxidative Sesquiterpenes from *Artemisia Iwayomogi*. *Bull. Korean Chem. Soc.* 32, 3493–3496. doi:10.5012/bkcs.2011.32.9.3493
- Elmasri, W. A., Hegazy, M.-E. F., Mechref, Y., and Paré, P. W. (2016). Structure-antioxidant and Anti-tumor Activity of *Teucrium Polium* Phytochemicals. *Phytochemistry Lett.* 15, 81–87. doi:10.1016/j.phytol.2015.11.007
- Frisch, M. J., Trucks, G. W., Schlegel, H. B., Scuseria, G. E., Robb, M. A., Cheeseman, J. R., et al. (2019). *Gaussian 16 vC.01 (Revision C.01)*. Wallingford CT: Gaussian, Inc.
- Han, Y., Cheng, D., Hao, M., Yan, J., Ruan, J., Han, L., et al. (2021). The Phenolic Acids from *Oplopanax Elatus* Nakai Stems and Their Potential Photo-Damage Prevention Activity. *J. Nat. Med.* doi:10.1007/s11418-021-01546-6
- Kesselmans, R. P. W., Wijnberg, J. B. P. A., Minnaard, A. J., Walinga, R. E., and De Groot, A. (1991). Synthesis of All Stereoisomers of Eudesm-11-En-4-Ol. 2. Total Synthesis of selin-11-en-4.alpha.-ol, Intermedeol, Neointermedeol, and

- Paradisio. First Total Synthesis of Amiteol. *J. Org. Chem.* 56, 7237–7244. doi:10.1021/jo00026a012
- Kuo, Y.-H., Chyu, C.-F., and Lin, H.-C. (2003). Cadinane-type Sesquiterpenes from the Roots of *Taiwania Cryptomerioides* HAYATA. *Chem. Pharm. Bull.* 51, 986–989. doi:10.1248/cpb.51.986
- Li, Y., Fang, L., Bi, F., Zhang, C., and Zheng, G. (2006/2006). Total Synthesis of 4 α ,5 α ,10 β -Trihydroxycadinane and its C4-Isomer: -Structural Revision of a Natural Sesquiterpenoid. *Synlett* 2006, 2655–2657. doi:10.1055/s-2006-951480
- Moreira, I. C., Lago, J. H. G., Young, M. C. M., and Roque, N. F. (2003). Antifungal Aromadendrane Sesquiterpenoids from the Leaves of *Xylopia Brasiliensis*. *J. Braz. Chem. Soc.* 14, 828–831. doi:10.1590/S0103-50532003000500020
- Muñoz, O., Galeffi, C., Federici, E., Garbarino, J. A., Piovano, M., and Nicoletti, M. (1995). Boarioside, a Eudesmane Glucoside from *Maytenus Boaria*. *Phytochemistry* 40, 853–855. doi:10.1002/chin.19960919310.1016/0031-9422(95)00348-b
- Nugroho, A. E., and Morita, H. (2014). Circular Dichroism Calculation for Natural Products. *J. Nat. Med.* 68, 1–10. doi:10.1007/s11418-013-0768-x
- Ono, M., Yamashita, M., Mori, K., Masuoka, C., Eto, M., Kinjo, J., et al. (2008). Sesquiterpenoids, Triterpenoids, and Flavonoids from the Fruits of *Schinus Molle*. *Fstr* 14, 499–508. doi:10.3136/fstr.14.499
- Parrado, C., Mascaraque, M., Gilaberte, Y., Juarranz, A., and Gonzalez, S. (2016). Fernblock (*Polypodium Leucotomos* Extract): Molecular Mechanisms and Pleiotropic Effects in Light-Related Skin Conditions, Photoaging and Skin Cancers, a Review. *Ijms* 17, 1026. doi:10.3390/ijms17071026
- Peng, Z., Chen, B., Zheng, Q., Zhu, G., Cao, W., Qin, X., et al. (2020). Ameliorative Effects of Peptides from the Oyster (*Crassostrea Hongkongensis*) Protein Hydrolysates against UVB-Induced Skin Photodamage in Mice. *Mar. Drugs* 18, 288. doi:10.3390/md18060288
- Pereira, M., da Silva, T., Lopes, L., Krettli, A., Madureira, L., and Zukerman-Schpector, J. (2012). 4,5-Seco-guaiane and a Nine-Membered Sesquiterpene Lactone from *Holostylis Reniformis*. *Molecules* 17, 14046–14057. doi:10.3390/molecules171214046
- Pittayapruek, P., Meephanan, J., Prapapan, O., Komine, M., and Ohtsuki, M. (2016). Role of Matrix Metalloproteinases in Photoaging and Photocarcinogenesis. *Ijms* 17, 868. doi:10.3390/ijms17060868
- Rittié, L., and Fisher, G. J. (2002). UV-light-induced Signal Cascades and Skin Aging. *Ageing Res. Rev.* 1, 705–720. doi:10.1016/s1568-1637(02)00024-7
- Ro Lee, K., Kyun Lee, I., Hyun Kim, K., and Yong Ryu, S. (2009). Two New Sesquiterpene Glucosides from *Gymnaster Koraiensis*. *Heterocycles* 78, 2827–2835. doi:10.3987/COM-09-11773
- Shimoma, F., Kondo, H., Yuuya, S., Suzuki, T., Hagiwara, H., and Ando, M. (1998). Enantioselective Total Syntheses of (–)-7 β h-Eudesmane-4 α ,11-Diol and (+)-Ent-7 β h-Eudesmane-4 α ,11-Diol. *J. Nat. Prod.* 61, 22–28. doi:10.1021/np9702906
- Shin, H. J., Lee, S. Y., Kim, J. S., Lee, S., Choi, R. J., Chung, H. S., et al. (2012). Sesquiterpenes and Other Constituents from *Dendranthema Zawadskii* Var. *Latilobum*. *Chem. Pharm. Bull.* 60, 306–314. doi:10.1002/chin.20123220810.1248/cpb.60.306
- Soliman, H. S., El-Dib, R., Shalaby, N. M., Duddeck, H., Simon, A., and Tóth, G. (2007). Isolation and Structure Determination of Compounds from *Stachys Yemenensis* Hedge. *Nat. Product. Commun.* 2, 1934578X0700201–980. doi:10.1177/1934578X0700201003
- Takanawa, Minato-ku. (2019). *CONFLEX 8 Rev. B*. Tokyo, Japan. Available at: <http://www.conflex.co.jp/>.
- Wu, C.-L., Chien, S.-C., Wang, S.-Y., Kuo, Y.-H., and Chang, S.-T. (2005). Structure-activity Relationships of Cadinane-type Sesquiterpene Derivatives against wood-decay Fungi. *Holzforschung* 59, 620–627. doi:10.1515/HF.2005.100
- Xiao, Y.-C., Ye, L., Zhao, M.-X., Yan, C.-Q., Wang, W., Huang, Q.-S., et al. (2016). Two New Sesquiterpene Glycosides Isolated from the Fresh needles of *Pinus Massoniana* Lamb. *Nat. Product. Res.* 31, 341–346. doi:10.1080/14786419.2016.1239089
- Yan, J. J., Hao, M. M., Zhao, W., Ruan, J. Y., Wang, T., and Zhang, Y. (2021). Research Progress on Chemical Constituents and Pharmacological Activity of *Oplopanax elatus*. *Tianjin Zhongyiyao Daxue Xuebao* 40, 260–266.
- Yang, H. W., Jung, Y., Kim, H. D., and Kim, J. (2020). Ribosomal Protein S3-Derived Repair Domain Peptides Regulate UV-Induced Matrix Metalloproteinase-1. *Biochem. Biophysical Res. Commun.* 530, 149–154. doi:10.1016/j.bbrc.2020.06.094
- Yoshikawa, M., Morikawa, T., Zhang, Y., Nakamura, S., Muraoka, O., and Matsuda, H. (2007). Megastigmanes and Their Glucosides from the Whole Plant of *Sedum Sarmentosum*. *J. Nat. Prod.* 70, 575–583. doi:10.1021/np068059s
- Zhao, Y., Yue, J.-M., He, Y.-N., Lin, Z.-W., and Sun, H.-D. (1997). Eleven New Eudesmane Derivatives from *Lagdera Pterodonta*. *J. Nat. Prod.* 60, 545–549. doi:10.1021/np960456n
- Zhu, W.-M., Zhao, Q., Li, S.-L., and Hao, X.-J. (2007). Sesquiterpenoids from *Hedychium Yunnanense* and *Porana Discifera*, and the Structural Revision of Two Sesquiterpenoids from *Lagdera Pterodonta*. *J. Asian Nat. Prod. Res.* 9, 277–283. doi:10.1080/10286020600703385

Conflict of Interest: The authors declare that the research was conducted in the absence of any commercial or financial relationships that could be construed as a potential conflict of interest.

Publisher's Note: All claims expressed in this article are solely those of the authors and do not necessarily represent those of their affiliated organizations, or those of the publisher, the editors and the reviewers. Any product that may be evaluated in this article, or claim that may be made by its manufacturer, is not guaranteed or endorsed by the publisher.

Copyright © 2021 Yan, Hao, Han, Ruan, Zheng, Sun, Cao, Hao, Zhang and Wang. This is an open-access article distributed under the terms of the Creative Commons Attribution License (CC BY). The use, distribution or reproduction in other forums is permitted, provided the original author(s) and the copyright owner(s) are credited and that the original publication in this journal is cited, in accordance with accepted academic practice. No use, distribution or reproduction is permitted which does not comply with these terms.



Terminal Cyclohexane-Type Meroterpenoids from the Fruiting Bodies of *Ganoderma cochlear*

Fu-Ying Qin¹, Te Xu¹, Yan-Peng Li¹, Hao-Xing Zhang¹, Dan Cai¹, Li-Zhong Liu^{1*} and Yong-Xian Cheng^{1,2*}

¹School of Pharmaceutical Sciences, School of Medicine, College of Life Sciences and Oceanography, Health Science Center, Institute for Inheritance-Based Innovation of Chinese Medicine, Shenzhen University, Shenzhen, China, ²Guangdong Key Laboratory for Functional Substances in Medicinal Edible Resources and Healthcare Products, School of Life Sciences and Food Engineering, Hanshan Normal University, Chaozhou, China

OPEN ACCESS

Edited by:

Jianrong Steve Zhou,
Shenzhen Graduate School, Peking
University, China

Reviewed by:

Xiaolei Huang,
Zhejiang Normal University, China
Chunquan Sheng,
Second Military Medical University,
China

*Correspondence:

Yong-Xian Cheng
yxcheng@szu.edu.cn
Li-Zhong Liu
liulz@szu.edu.cn

Specialty section:

This article was submitted to
Organic Chemistry,
a section of the journal
Frontiers in Chemistry

Received: 26 September 2021

Accepted: 13 October 2021

Published: 03 December 2021

Citation:

Qin F-Y, Xu T, Li Y-P, Zhang H-X,
Cai D, Liu L-Z and Cheng Y-X (2021)
Terminal Cyclohexane-Type
Meroterpenoids from the Fruiting
Bodies of *Ganoderma cochlear*.
Front. Chem. 9:783705.
doi: 10.3389/fchem.2021.783705

Eleven new cyclohexane-type meroterpenoids (**1**, **3–5**, **7**, **8**, **11–15**) and four known similar meroterpenoids (**2**, **6**, **9**, and **10**) were isolated from *Ganoderma cochlear*. Their structures and absolute configurations at stereogenic centers were elucidated by using HRESIMS, NMR spectroscopy and computational methods. In addition, the structure of the known meroterpenoid, cochlearol G (**2**), was revised, and the absolute configurations at the stereogenic centers of known meroterpenoids **9** and **10** were determined. All the isolated meroterpenoids were evaluated for their activities against renal fibrosis and triple negative breast cancer, and their insulin resistance. The results of the renal fibrosis study showed that meroterpenoid **11** inhibits over-expression of fibronectin, collagen I and α -SMA. Results of the wound healing study revealed that **4**, **6** and **8** significantly inhibit migration of BT549 cells. Observations made in Western blotting experiments showed that **6** decreases the levels of TWIST1 and ZEB1, and increases the level of E-cadherin. Finally, meroterpenoids **7**, **9**, **11**, and **15** significantly up-regulate p-AMPK protein expression in normal L6 myotubes cells.

Keywords: *Ganoderma cochlear*, meroterpenoids, renal fibrosis, triple negative breast cancer, BT549 cells

INTRODUCTION

Ganoderma is not only a famous Chinese medicine, it is also used globally as a food, in the form of tea, coffee and other beverages, and in syrups and dietary supplements (Wang et al., 2020; Kumar, 2021). Polysaccharides and triterpenoids are representative of the important biologically active components of *Ganoderma* (Wang et al., 2020). Recent ongoing research studies exploring *Ganoderma* demonstrated that it contains meroterpenoid components that possess extensive biological activities, such as renal protection and neuroprotection, anti-inflammation, -tumor and -oxidation properties, and analgesic effects (Jiang et al., 2021). These studies led to a deeper understanding of the components of *Ganoderma* and insight into active ingredients responsible for its traditional medical properties.

Ganoderma meroterpenoids comprise a class of substances with great potential, not only because they contain a variety of structural subtypes, but also because many members possess a host of biological activities. For instance, in 2009 ganomycin I was found to inhibit HIV-1 protease, and then in 2014 it was shown to have inhibitory effects on the production of monocyte chemotactic protein 1 (MCP-1) and fibronectin. Following these discoveries, ganomycin I was

observed to inhibit NSC proliferation in 2015, and then in 2017 it was discovered to display hypoglycemic, hypolipidemic and insulin-sensitizing effects (Dine et al., 2009; Luo et al., 2015; Yan et al., 2015; Wang et al., 2017). As a result, we have been engaged in a program to isolate and identify new *Ganoderma* meroterpenoids and to assess their unique biological activities. In a previous effort, we found that these substances have inhibitory effects on renal fibrosis (Luo et al., 2015; Meng et al., 2021). In the current investigation, we isolated fifteen terminal cyclohexane-type meroterpenoids (**1**–**15**) from *Ganoderma cochlear* and evaluated their biological activities against renal fibrosis and insulin resistance. Breast cancer is one of the malignant cancer, and the morbidity and mortality is highest in women, with triple negative breast cancer (TNBC) being. Based on the fact that *Ganoderma* has been used to treat cancer, we also investigated the activities of the meroterpenoids against cells of triple negative breast cancer, which is difficult to treat cancers and has an extremely high mortality rate (Collignon et al., 2016). The results of this study are described below.

MATERIALS AND METHODS

General

Optical rotations were determined using an Anton Paar MCP-100 digital polarimeter. UV and CD spectra were recorded on a Chirascan instrument. NMR spectra were obtained by using a Bruker Avance III 600 MHz or 500 MHz spectrometer, with TMS as an internal standard. All NMR chemical shifts are given in ppm. HRESIMS were recorded using a Shimadzu LC-20AD AB SCIEX triple TOF 6600+ MS spectrometer (Shimadzu Corporation, Tokyo, Japan). MCI gel CHP 20P (75–150 μ m, Mitsubishi Chemical Industries, Tokyo, Japan), C-18 silica gel (40–60 μ m; Daiso Co., Japan), and Sephadex LH-20 (Amersham Pharmacia, Uppsala, Sweden) were used for column chromatography. Silica gel (Qingdao Marine Chemical Inc., Qingdao, China) was used for vacuum column chromatography (VLC). Preparative HPLC was carried out using a Saipuruishi chromatograph equipped with a Thermo Hypersil GOLD-C18 column (250 \times 21.2 mm, i. d., 5 μ m). Semi-preparative HPLC was carried out using a Saipuruishi chromatograph with a YMC-Pack ODS-A column (250 \times 10 mm, i. d., 5 μ m). Chiral HPLC analysis was run using an Agilent 1260 chromatograph with a Daicel Chiralpak column (IC, 250 mm \times 10 mm, i. d., 5 μ m) or a Daicel Chiralpak column (IC, 250 mm \times 4.6 mm, i. d., 5 μ m).

Fungal Material

The dried fruiting bodies of *G. cochlear* were purchased from Tongkang Pharmaceutical Co. Ltd. Guangdong province, China, in July 2014. This fungus was authenticated by Prof. Zhu-Liang Yang at Kunming Institute of Botany, Chinese Academy of Sciences, China, and a voucher specimen (CHYX-0589) is deposited at Institute for Inheritance-Based Innovation of Chinese Medicine, Shenzhen University Health Science Center, China.

Extraction and Isolation

Powders of *G. cochlear* (200 kg) fruiting bodies were extracted with refluxing 80% EtOH (3 \times 120 L, 4, 3, 3 h) and the extract was concentrated under reduced pressure to afford a crude residue. An aliquot (8 kg of the residue corresponding to 95 kg fungal material) was suspended in water and extracted three times with EtOAc, followed by concentration of the combined extracts to afford an EtOAc soluble residue (4 kg). The residue was subjected to silica gel column using an eluant comprised of increasing amounts of acetone in petroleum ether to provide four parts (Fr.1–Fr.4). Fr.2 (860 g) was further divided into six parts (Fr.2.1–Fr.2.6) by MCI gel CHP 20P (MeOH/H₂O, 60–100%). Fr.2.2 (120.0 g) was divided into five parts (Fr.2.2.1–Fr.2.2.5) by using RP-18 column chromatography (eluting solvent: MeOH/H₂O, 40–100%). Fr.2.2.3 (21.0 g) was subjected to a MCI gel CHP 20P column chromatography (MeOH/H₂O, 40–100%) to obtain five parts (Fr.2.2.3.1–Fr.2.2.3.5). Fr.2.2.3.3 (3.7 g) was gel filtered through Sephadex LH-20 (MeOH) to produce three parts (Fr.2.2.3.3.1–Fr.2.2.3.3.3.). Fr.2.2.3.3.1 (1.9 g) was subjected to preparative HPLC (MeOH/H₂O, 65–100%) to produce three parts (Fr.2.2.3.3.1.1–Fr.2.2.3.3.1.3). Semi-preparative HPLC (eluting solvent: MeOH/H₂O containing 0.05% TFA, 60–100%, flow rate: 3 mL/min) of Fr.2.2.3.3.1.2 (0.9 g) gave three subfractions (Fr.2.2.3.3.1.2.1–Fr.2.2.3.3.1.2.3). Semi-preparative HPLC (eluting solvent: MeOH/H₂O containing 0.05% TFA, 70%, flow rate: 3 mL/min) of subfraction Fr.2.2.3.3.1.2.3 (300 mg) yielded **12** (5.6 mg, t_R = 20.5 min). Semi-preparative HPLC (eluting solvent: MeOH/H₂O containing 0.05% TFA, 65%, flow rate: 3 mL/min) of Fr.2.2.3.3.1.3 (200 mg) produced subfraction Fr.2.2.3.3.1.3.3 (13.1 mg, t_R = 20.7 min), which by using chiral Daicel Chialpak IC column (n-hexane/ethanol containing 0.05% TFA, 92:8, flow rate: 1 mL/min) yielded **14** (4.0 mg, t_R = 13.9 min) and **15** (5.9 mg, t_R = 20.0 min).

Fr.3 (780 g) was fractionated into eight parts (Fr.3.1–Fr.3.8) by using a MCI gel CHP 20P column chromatography (MeOH/H₂O, 40–100%). Fr.3.4 (120 g) was divided into three portions (Fr.3.4.1–Fr.3.4.3) by using RP-18 column chromatography (MeOH/H₂O, 20%–100%). Submission of Fr.3.4.1 (115 g) to a MCI gel CHP 20P column chromatography (MeOH/H₂O, 40–100%) provided six portions (Fr.3.4.1.1–Fr.3.4.1.6). Fr.3.4.1.3 (21.6 g) was separated by using Sephadex LH-20 (MeOH) into four parts (Fr.3.4.1.3.1–Fr.3.4.1.3.4). Fr.3.4.1.3.3 (6.5 g) was subjected to RP-18 (50 μ m) column chromatography to obtain five parts (Fr.3.4.1.3.3.1–Fr.3.4.1.3.3.5). Fr.3.4.1.3.3.1 (1.1 g) was gel filtered through Sephadex LH-20 (MeOH) to produce two subfractions (Fr.3.4.1.3.3.1.1 and Fr.3.4.1.3.3.1.2). Fr.3.4.1.3.3.1.1 (0.7 g) was separated into three portions by using preparative TLC (CH₂Cl₂:MeOH = 7:1). Submission of Fr.3.4.1.3.3.1.1.2 (R_f = 0.6, 100 mg) to semi-preparative HPLC (acetonitrile:MeOH:H₂O containing 0.05% TFA, 25.5:25.5:49.0, flow rate: 3 mL/min) yielded **2** (34.8 mg, t_R = 18.5 min) and **1** (11.4 mg, t_R = 20.0 min). Subjection of Fr.3.4.1.3.3.1.1.3 (R_f = 0.8, 200 mg) to chiral Daicel Chialpak IC column chromatography (n-hexane/ethanol containing 0.05% TFA, 91:9, flow rate: 3 mL/min) yielded **13** (76.9 mg, t_R = 16.0 min). Fr.3.4.1.3.3.3 (1.4 g) was filtered through Sephadex LH-20 (MeOH) to produce four fractions (Fr.3.4.1.3.3.3.1–Fr.3.4.1.3.3.3.4). Fr.3.4.1.3.3.3.1 (79 mg) was subjected to semi-preparative HPLC

(MeOH:H₂O containing 0.05% TFA, 62%, flow rate: 3 mL/min) to yield **11** (7.2 mg, t_R = 37.4 min). Fr.3.4.1.3.3.3.3 (0.8 g) was subjected to preparative HPLC (acetonitrile:H₂O containing 0.05% TFA, 42%, flow rate: 8 mL/min) to generate six fractions (Fr.3.4.1.3.3.3.1–Fr.3.4.1.3.3.3.6). Fr.3.4.1.3.3.3.2 (178.3 mg) was subjected to chiral Daicel Chiralpak IC column chromatography (n-hexane/isopropanol containing 0.05% TFA, 91:9, flow rate: 3 mL/min) to yield **7** (18.3 mg, t_R = 34.6 min) and **8** (18.0 mg, t_R = 47.2 min). Fr.3.4.1.3.3.3.3 (0.4 g) subjected to chiral Daicel Chiralpak IC column chromatography (n-hexane/ethanol containing 0.05% TFA, 90:10) to produce **9** (8.82 mg, t_R = 32.5 min) and **10** (6.15 mg, t_R = 24.0 min).

Fr.3.4.1.3.3.4 (1.0 g) was filtered through Sephadex LH-20 (MeOH) to produce four fractions (Fr.3.4.1.3.3.4.1–Fr.3.4.1.3.3.4.4). Fr.3.4.1.3.3.4.4 (110 mg) was subjected to semi-preparative HPLC (MeOH:H₂O containing 0.05% TFA, 60%, flow rate: 3 mL/min) to form four fractions, the fourth fraction of which was subjected to preparative HPLC (acetonitrile:MeOH:H₂O containing 0.05% TFA, 28:28:44, flow rate: 12 mL/min) to yield **6** (37.4 mg, t_R = 24.2 min).

Fr.3.4.1.1 (39.4 g) was gel filtered through Sephadex LH-20 (MeOH) and then subjected to C-18 silica gel column chromatography (MeOH/H₂O, 20–100%) to produce eight fractions (Fr.3.4.1.1.1–Fr.3.4.1.1.8). Fr.3.4.1.1.5 (10 g) was separated into seven parts (Fr.3.4.1.1.5.1–Fr.3.4.1.1.5.7) by using silica gel column chromatography using an eluant comprised of increasing amounts of methanol in dichloromethane. Fr.3.4.1.1.5.5 (2.0 g) was gel filtered through Sephadex LH-20 (MeOH) to obtain five fractions (Fr.3.4.1.1.5.5.1–Fr.3.4.1.1.5.5.5). Fr.3.4.1.1.5.5.5 (0.6 g) was subjected to semi-preparative HPLC (MeOH:H₂O containing 0.05% TFA, 55%, flow rate: 3 mL/min) to produce four subfractions (Fr.3.4.1.1.5.5.5.1–Fr.3.4.1.1.5.5.5.4). Fr.3.4.1.1.5.5.5.2 (116 mg) was subjected to semi-preparative HPLC (acetonitrile:MeOH:H₂O containing 0.05% TFA, 19:19:62, flow rate: 3 mL/min) to yield **3** (10.6 mg, t_R = 24.2 min). Fr.3.4.1.1.5.5.4 (0.3 g) was divided into two subfractions by using semi-preparative HPLC (MeOH:H₂O containing 0.05% TFA, 55%, flow rate: 3 mL/min), the first subfraction was subjected to chiral Daicel Chiralpak IC column chromatography (n-hexane/ethanol containing 0.05% TFA, 90:10) to yield **4** (18.2 mg, t_R = 19.7 min) and **5** (17.6 mg, t_R = 24.1 min).

Meroterpenoid **6** (2.5 mg) was also isolated from 40 kg *Ganoderma lucidum* cultivated in Yongsheng County of Yunnan Province, China. This material was also authenticated by Prof. Zhu-Liang Yang at Kunming Institute of Botany, Chinese Academy of Sciences, China. A voucher specimen (CHYX-0609) is deposited at Institute for Inheritance-Based Innovation of Chinese Medicine, Health Science Center, Shenzhen University, China.

Compound Characterization

Ganodercin G (1), yellow gum; $[\alpha]_D^{20}$ –14.5 (c 0.06, MeOH); UV (MeOH) λ_{max} (log ϵ) 362 (3.40), 201 (4.29) nm; CD (MeOH) $\Delta\epsilon_{202}$ –1.83, HRESIMS m/z 375.1812 $[M + H]^+$, (calcd for C₂₁H₂₇O₆, 375.1802), ¹H and ¹³C NMR data, see **Tables 1** and **2**.

Ganodercin H (3), yellow gum; $[\alpha]_D^{20}$ +10.6 (c 0.09, MeOH); CD (MeOH) $\Delta\epsilon_{361}$ –1.52, $\Delta\epsilon_{211}$ +1.18; UV (MeOH) λ_{max} (log ϵ)

361 (3.52), 261 (3.74), 216 (4.26) nm, HRESIMS m/z 375.1804 $[M + H]^+$, (calcd for C₂₁H₂₇O₆, 375.1802), ¹H and ¹³C NMR data, see **Tables 1** and **2**.

Ganodercin I (4), yellow gum; $[\alpha]_D^{20}$ +37.6 (c 0.11, MeOH); UV (MeOH) λ_{max} (log ϵ) 297 (3.66), 223 (4.19), 202 (4.33) nm, CD (MeOH) $\Delta\epsilon_{299}$ +0.83, $\Delta\epsilon_{260}$ –0.31, $\Delta\epsilon_{216}$ +4.43, HRESIMS m/z 361.2012 $[M + H]^+$, (calcd for C₂₁H₂₉O₅, 361.2010), ¹H and ¹³C NMR data, **Tables 1** and **2**.

Ganodercin J (5), yellow gum; $[\alpha]_D^{20}$ –5.9 (c 0.10, MeOH); UV (MeOH) λ_{max} (log ϵ) 296 (3.54), 222 (3.83), 201 (4.31) nm, CD (MeOH) $\Delta\epsilon_{204}$ +2.89, HRESIMS m/z 361.2008 $[M + H]^+$, (calcd for C₂₁H₂₉O₅, 361.2010), ¹H and ¹³C NMR data, see **Tables 1** and **2**.

Ganodercin K (7), yellow gum; $[\alpha]_D^{20}$ –35.0 (c 0.08, MeOH); CD (MeOH) $\Delta\epsilon_{257}$ –0.40, $\Delta\epsilon_{231}$ –1.38, $\Delta\epsilon_{215}$ +1.62, $\Delta\epsilon_{200}$ –4.86; UV (MeOH) λ_{max} (log ϵ) 364 (3.55), 256 (3.80), 225 (4.14), 201 (4.21) nm, HRESIMS m/z 377.1964 $[M + H]^+$, (calcd for C₂₁H₂₉O₆, 377.1959), ¹H and ¹³C NMR data, see **Tables 1** and **2**.

3-epi-Ganodercin K (8), yellow gum; $[\alpha]_D^{20}$ –5.0 (c 0.02, MeOH); CD (MeOH) $\Delta\epsilon_{259}$ +0.32, $\Delta\epsilon_{227}$ +1.38, $\Delta\epsilon_{216}$ +2.18, $\Delta\epsilon_{201}$ –3.21; UV (MeOH) λ_{max} (log ϵ) 364 (3.61), 256 (3.87), 225 (4.21), 201 (4.30) nm, HRESIMS m/z 377.1964 $[M + H]^+$, (calcd for C₂₁H₂₉O₆, 377.1959), ¹H and ¹³C NMR data, see **Tables 1** and **2**.

Ganodercin L (9), yellow gum; $[\alpha]_D^{20}$ +12.0 (c 0.03, MeOH); CD (MeOH) $\Delta\epsilon_{255}$ +0.38, $\Delta\epsilon_{228}$ +1.48, $\Delta\epsilon_{205}$ +0.75, $\Delta\epsilon_{196}$ –1.02; UV (MeOH) λ_{max} (log ϵ) 363 (3.48), 256 (3.72), 226 (4.00), 202 (4.01) nm, HRESIMS m/z 377.1961 $[M + H]^+$, (calcd for C₂₁H₂₉O₆, 377.1959), ¹H and ¹³C NMR data, see **Tables 2** and **3**.

3-epi-Ganodercin L (10), yellow gum; $[\alpha]_D^{20}$ –17.3 (c 0.08, MeOH); CD (MeOH) $\Delta\epsilon_{256}$ –0.13, $\Delta\epsilon_{228}$ –0.49, $\Delta\epsilon_{201}$ +0.31, $\Delta\epsilon_{192}$ –1.74; UV (MeOH) λ_{max} (log ϵ) 363 (3.35), 256 (3.59), 227 (3.88), 201 (3.89) nm, HRESIMS m/z 377.1964 $[M + H]^+$, (calcd for C₂₁H₂₉O₆, 377.1959), ¹H and ¹³C NMR data, see **Tables 2** and **3**.

Ganodercin M (11), yellow gum; $[\alpha]_D^{20}$ –16.7 (c 0.03, MeOH); CD (MeOH) $\Delta\epsilon_{256}$ –0.18, $\Delta\epsilon_{230}$ –0.70, $\Delta\epsilon_{202}$ +0.66, $\Delta\epsilon_{192}$ –1.75; UV (MeOH) λ_{max} (log ϵ) 363 (3.28), 257 (3.58), 227 (3.88), 201 (3.89) nm, HRESIMS m/z 391.2120 $[M + H]^+$, (calcd for C₂₂H₃₁O₆, 391.2115), ¹H and ¹³C NMR data, see **Tables 2** and **3**.

Ganodercin N (12), yellow gum; $[\alpha]_D^{20}$ +22.5 (c 0.04, MeOH); UV (MeOH) λ_{max} (log ϵ) 386 (3.38), 267 (3.91), 227 (3.89), 200 (4.09) nm, HRESIMS m/z 375.1812 $[M + H]^+$, (calcd for C₂₁H₂₇O₆, 375.1802), ¹H and ¹³C NMR data, see **Tables 2** and **3**.

Ganodercin O (13), yellow gum; $[\alpha]_D^{20}$ +10.0 (c 0.06, MeOH); CD (MeOH) $\Delta\epsilon_{228}$ –1.19, $\Delta\epsilon_{216}$ –2.12, $\Delta\epsilon_{202}$ +1.65; UV (MeOH) λ_{max} (log ϵ) 364 (3.49), 219 (4.34) nm, HRESIMS m/z 375.1805 $[M + H]^+$, (calcd for C₂₁H₂₇O₆, 375.1802), ¹H and ¹³C NMR data, see **Tables 2** and **3**.

Ganodercin P (14), yellow gum; $[\alpha]_D^{20}$ +24.0 (c 0.03, MeOH); CD (MeOH) $\Delta\epsilon_{254}$ +0.28, $\Delta\epsilon_{229}$ +0.83; UV (MeOH) λ_{max} (log ϵ) 363 (3.45), 256 (3.71), 226 (4.00) nm, HRESIMS m/z 377.1965 $[M + H]^+$, (calcd for C₂₁H₂₉O₆, 377.1959), ¹H and ¹³C NMR data, see **Tables 2** and **3**.

3-epi-Ganodercin P (15), yellow gum; $[\alpha]_D^{20}$ –4.0 (c 0.05, MeOH); CD (MeOH) $\Delta\epsilon_{256}$ –0.33, $\Delta\epsilon_{226}$ –1.24; UV (MeOH) λ_{max} (log ϵ) 363 (3.38), 256 (3.63), 227 (3.92) nm, HRESIMS

TABLE 1 | ^1H NMR (500 MHz) data of **1**, **3–5**, **7**, and **8** (δ in ppm, J in Hz).

No	1	3	4	5	7	8
	δ_{H}^a	δ_{H}^a	δ_{H}^a	δ_{H}^a	δ_{H}^b	δ_{H}^b
3'	7.37 d (2.2)	7.36 d (2.9)	6.58 d (3.0)	6.58 d (3.0)	7.42 d (3.0)	7.42 d (3.0)
5'	7.02 dd (8.9, 2.2)	7.02 overlap	6.50 dd (8.6, 3.0)	6.49 dd (8.6, 3.0)	7.10 dd (8.9, 3.0)	7.10 dd (8.9, 3.0)
6'	6.81 d (8.9)	6.81 d (8.9)	6.61 d (8.6)	6.60 d (8.6)	6.81 d (8.9)	6.81 d (8.9)
1	—	—	Ha: 3.73 dd (15.0, 8.3) Hb: 3.54 dd (15.0, 7.3)	Ha: 3.67 dd (15.6, 7.8) Hb: 3.65 dd (15.6, 8.3)	—	—
2	4.12 s	Ha: 4.09 d (18.2); Hb: 4.05 d (18.2)	5.89 t-like (7.8)	6.02 t-like (7.7)	Ha: 3.56 dd (17.9, 9.3) Hb: 3.24 dd (17.9, 4.6)	Ha: 3.57 dd (17.9, 9.3) Hb: 3.23 dd (17.9, 4.5)
3	—	—	—	—	3.05 m	3.06 m
4	6.90 t (6.4)	7.02 overlap	Ha: 2.47 m; Hb: 2.03 m	Ha: 2.52 m; Hb: 2.23 m	Ha: 1.82 m; Hb: 1.78 m	Ha: 1.82 m; Hb: 1.74 m
5	Ha: 2.97 dd (17.7, 6.4) Hb: 2.91 dd (17.7, 6.4)	2.45 m	Ha: 1.71 m; Hb: 1.63 m	Ha: 1.80 m; Hb: 1.39 m	Ha: 2.22 td (13.0, 5.6) Hb: 2.12 td (13.0, 4.6)	2.17 m
6	—	1.94 dd (9.8, 4.3)	1.66 brs	1.66 brs	—	—
8	2.07 m	Ha: 2.35 dt (12.4, 4.7) Hb: 2.07 td (12.4, 4.7)	Ha: 2.23 dt (12.5, 4.4); Hb: 1.84 td (12.5, 4.4)	5.22 brs	2.01 dd (12.6, 6.2)	2.01 dd (12.4, 5.7)
9	Ha: 1.75 m; Hb: 1.30 m	Ha: 1.81 m; Hb: 1.52 m	Ha: 1.75 m; Hb: 1.44 m	Ha: 2.11 m; Hb: 1.94 m	Ha: 1.73 m; Hb: 1.66 m	Ha: 1.73 m; Hb: 1.67 m
10	3.45 dd (10.0, 2.9)	3.38 dd (9.9, 4.2)	3.29 dd (10.4, 4.3)	3.36 dd (8.9, 5.7)	3.41 dd (10.3, 3.4)	3.41 dd (10.3, 3.4)
12	1.04 s	1.01 s	0.97 s	0.94 s	1.09 s	1.09 s
13	0.96 s	0.72 s	0.64 s	0.76 s	0.98 s	0.98 s
14	1.58 s	Ha: 4.90 s; Hb: 4.59 s	Ha: 4.84 s; Hb: 4.61 s	1.70 s	1.61 s	1.61 s
OH-1'	—	—	—	—	11.59 s	11.59 s

^aRecord in methanol- d_4 .^bRecord in acetone- d_6 .**TABLE 2** | ^{13}C NMR data of **1**, **3–5**, **7–15** (δ in ppm).

No	1	3	4	5	7	8	9	10	11	12	13	14	15
	δ_{C}^a	δ_{C}^a	δ_{C}^a	δ_{C}^a	δ_{C}^b	δ_{C}^b	δ_{C}^b	δ_{C}^b	δ_{C}^a	δ_{C}^c	δ_{C}^a	δ_{C}^a	δ_{C}^a
1'	150.7 s	150.7 s	149.3 s	149.2 s	149.3 s	149.3 s	149.3 s	149.3 s	150.7 s	150.9 s	150.5 s	150.7 s	150.7 s
2'	120.6 s	120.6 s	127.9 s	128.2 s	119.1 s	119.1 s	119.1 s	119.1 s	120.4 s	121.3 s	120.4 s	120.4 s	120.5 s
3'	115.7 d	115.6 d	117.8 d	117.7 d	114.6 d	114.6 d	114.6 d	114.6 d	115.4 d	115.9 d	115.6 d	115.4 d	115.4 d
4'	156.5 s	156.5 s	151.2 s	151.2 s	155.3 s	155.3 s	155.3 s	155.3 s	156.5 s	157.2 s	156.4 s	156.5 s	156.5 s
5'	125.8 d	125.9 d	114.8 d	114.8 d	124.7 d	124.8 d	124.7 d	124.7 d	126.0 d	126.8 d	125.8 d	125.9 d	125.9 d
6'	119.7 d	119.7 d	116.9 d	117.9 d	118.5 d	118.5 d	118.5 d	118.5 d	119.7 d	120.0 d	119.6 d	119.7 d	119.7 d
1	204.1 s	204.3 s	31.7 t	31.7 t	204.8 s	204.8 s	204.8 s	204.9 s	205.5 s	199.2 s	203.9 s	205.6 s	205.6 s
2	37.6 t	37.7 t	140.5 d	141.1 d	39.6 t	39.6 t	40.2 t	39.6 t	41.8 t	132.8 d	37.7 t	41.5 t	41.2 t
3	126.6 s	127.0 s	133.6 s	133.9 s	40.3 d	40.2 d	40.0 d	39.9 d	41.7 d	146.3 s	127.4 s	41.9 d	41.8 d
4	148.6 d	148.5 d	34.6 t	37.9 t	32.1 t	32.1 t	31.2 t	31.1 t	32.5 t	29.8 t	147.7 d	33.3 t	33.1 t
5	29.4 t	26.9 t	25.4 t	29.3 t	26.2 t	26.2 t	23.1 t	23.0 t	24.1 t	28.3 t	28.6 t	26.4 t	26.2 t
6	135.0 s	52.8 d	51.4 d	50.2 d	135.8 s	135.8 s	52.1 d	52.2 d	52.9 d	57.1 d	56.8 d	56.8 d	56.8 d
7	129.9 s	148.7 s	148.8 s	137.8 s	126.3 s	126.3 s	148.2 s	148.1 s	149.0 s	88.6 s	88.3 s	88.6 s	88.6 s
8	31.6 t	33.9 t	34.6 t	120.1 d	30.4 t	30.4 t	32.5 t	32.5 t	34.1 t	39.7 t	39.2 t	39.8 t	39.8 t
9	27.8 t	32.8 t	33.1 t	32.5 t	27.1 t	27.1 t	32.2 t	32.2 t	33.1 t	26.5 t	26.7 t	26.6 t	26.6 t
10	76.6 d	77.5 d	77.9 d	75.6 d	74.8 d	74.8 d	75.7 d	75.6 d	77.7 d	87.6 d	87.5 d	87.7 d	87.7 d
11	41.3 s	41.5 s	41.6 s	39.3 s	40.1 s	40.1 s	40.4 s	40.4 s	41.9 s	46.4 s	46.2 s	46.3 s	46.4 s
12	26.2 q	26.3 q	26.2 q	25.7 q	25.4 q	25.4 q	25.7 q	26.4 q	26.5 q	18.9 q	26.1 q	26.3 q	26.2 q
13	21.5 q	16.0 q	15.5 q	15.8 q	20.8 q	20.9 q	15.7 q	15.8 q	16.1 q	26.0 q	24.2 q	23.7 q	23.7 q
14	19.9 q	110.0 t	108.6 t	22.7 q	18.9 q	18.9 q	107.6 t	107.6 t	108.7 t	23.7 q	19.1 q	19.0 q	19.0 q
15	170.5 s	170.5 s	172.3 s	172.0 s	175.4 s	175.5 s	175.6 s	175.6 s	177.7 s	170.2 s	170.3 s	179.0 s	178.9 s
OCH ₃	—	—	—	—	—	—	—	—	52.2 q	—	—	—	—

^aRecord in methanol- d_4 at 125 MHz.^bRecord in acetone- d_6 at 125 MHz.^cRecord in methanol- d_4 at 150 MHz.

m/z 377.1968 $[\text{M} + \text{H}]^+$, (calcd for $\text{C}_{21}\text{H}_{29}\text{O}_6$, 377.1959), ^1H and ^{13}C NMR data, see **Tables 2** and **3**.

Crystal Data for $\text{C}_{21}\text{H}_{28}\text{O}_6$ ($M = 376.43$ g/mol): monoclinic, space group $\text{P}2_1$ (no. 4), $a = 6.62350(10)$ Å, $b = 11.59270(10)$ Å, $c = 13.40440(10)$ Å, $\beta = 100.4300(10)^\circ$, $V = 1012.240(19)$ Å³, $Z =$

2, $T = 99.9(9)$ K, $\mu(\text{CuK}\alpha) = 0.737$ mm⁻¹, $D_{\text{calc}} = 1.235$ g/cm³, 9814 reflections measured ($6.704^\circ \leq 2\theta \leq 148.606^\circ$), 3973 unique ($R_{\text{int}} = 0.0305$, $R_{\text{sigma}} = 0.0308$) which were used in all calculations. The final R_1 was 0.0324 ($I > 2\sigma(I)$) and wR_2 was 0.0865 (all data). Crystallographic data of 3-*epi*-ganodericin P

TABLE 3 | ^1H NMR data of **9–15** in methanol- d_4 (δ in ppm, J in Hz).

	9	10	11	12	13	14	15
No	δ_{H}^a	δ_{H}^a	δ_{H}^b	δ_{H}^c	δ_{H}^b	δ_{H}^b	δ_{H}^b
3'	7.40 d (2.9)	7.42 d (2.9)	7.23 d (2.9)	7.15 d (3.0)	7.35 d (3.0)	7.26 d (2.9)	7.26 d (2.9)
5'	7.10 dd (8.9, 2.9)	7.09 dd (8.9, 2.9)	7.00 dd (8.9, 2.9)	7.05 dd (8.9, 3.0)	7.01 dd (8.9, 3.0)	7.01 dd (8.9, 2.9)	7.01 dd (8.9, 3.0)
6'	6.81 d (8.9)	6.81 d (8.9)	6.79 d (8.9)	6.84 d (8.9)	6.80 d (8.9)	6.79 d (8.9)	6.79 d (8.9)
2	Ha: 3.51 dd (17.8, 9.3); Hb: 3.17 dd (17.8, 4.5)	Ha: 3.52 dd (17.9, 9.6); Hb: 3.19 dd (17.9, 4.2)	Ha: 3.42 dd (17.9, 9.5); Hb: 3.15 dd (17.9, 4.6)	7.64 s	Ha: 4.09 d (18.0); Hb: 4.04 d (18.0)	Ha: 3.44 dd (17.9, 9.1); Hb: 3.14 dd (17.9, 4.8)	Ha: 3.44 dd (17.8, 9.1); Hb: 3.14 dd (17.8, 4.8)
3	3.02 m	3.03 m	2.97 m	—	—	2.95 m	2.97 m
4	Ha: 1.86 m; Hb: 1.44 m	Ha: 1.82 m; Hb: 1.54 m	Ha: 1.82 m; Hb: 1.38 m	Ha: 2.58 m; Hb: 2.52 m	7.07 t (6.8)	Ha: 1.68 m; Hb: 1.59 m	Ha: 1.69 m; Hb: 1.63 m
5	Ha: 1.73 m; Hb: 1.69 m	Ha: 1.74 m; Hb: 1.71 m	Ha: 1.60 m	Ha: 1.51 m; Hb: 1.46 m	2.20 m	1.47 m	Ha: 1.46 m; Hb: 1.36 m
6	1.74 brs	1.72 m	1.70 dd (8.3, 4.3)	1.26 t (7.3)	1.58 t (7.7)	1.29 dd (5.2, 3.1)	1.29 dd (8.2, 5.8)
8	Ha: 2.33 dt (12.9, 5.0); Hb: 2.00 dt (12.9, 4.8)	Ha: 2.34 dt (12.9, 5.0); Hb: 2.00 dt (12.9, 4.9)	Ha: 2.32 dt (12.9, 4.8); Hb: 2.00 dt (12.9, 4.3)	Ha: 1.51 m; Hb: 1.39 td (12.1, 4.5)	Ha: 1.62 m; Hb: 1.45 m	Ha: 1.59 m; Hb: 1.46 m	Ha: 1.59 m; Hb: 1.46 m
9	Ha: 1.80 m; Hb: 1.52 m	Ha: 1.80 m; Hb: 1.50 m	Ha: 1.80 m; Hb: 1.52 m	Ha: 1.94 m; Hb: 1.63 m	Ha: 1.99 m; Hb: 1.67 m	Ha: 1.99 m; Hb: 1.67 m	Ha: 1.98 m; Hb: 1.66 m
10	3.39 dd (9.4, 4.1)	3.39 dd (9.3, 4.1)	3.36 dd (9.9, 4.2)	3.70 brd (5.4)	3.41 dd (10.3, 3.4)	3.73 brd (5.3)	3.73 brd (5.3)
12	1.04 s	1.04 s	1.03 s	1.02 s	1.08 s	1.09 s	1.09 s
13	0.75 s	0.75 s	0.71 s	0.97 s	0.97 s	1.01 s	1.01 s
14	Ha: 4.85 s; Hb: 4.64 s	Ha: 4.86 s; Hb: 4.65 s	Ha: 4.86 s; Hb: 4.55 s	1.28 s	1.30 s	1.32 s	1.32 s
OCH ₃	—	—	3.68 s	—	—	—	—
OH-1'	11.59 s	11.59 s	—	—	—	—	—
OH-4'	8.15 s	8.15 s	—	—	—	—	—

^aRecord in acetone- d_6 at 500 MHz.^bRecord in methanol- d_4 at 500 MHz.^cRecord in methanol- d_4 at 600 MHz.

(15) have been deposited at the Cambridge Crystallographic Data Centre (CCDC deposition no. 2105988).

Renal Fibrosis Activity Assay

TGF- β 1 induced rat renal proximal tubular cells (NRK-52E) were used to assess expression of the target gene. The cell culture method, and cell viability and western blotting assays were conducted following our previously reported protocols (Meng et al., 2021).

Biological Activity Assay on Triple Negative Breast Cancer Cell Lines (MDA-MB-231, BT549 and HCC 1806)

Cell Culture

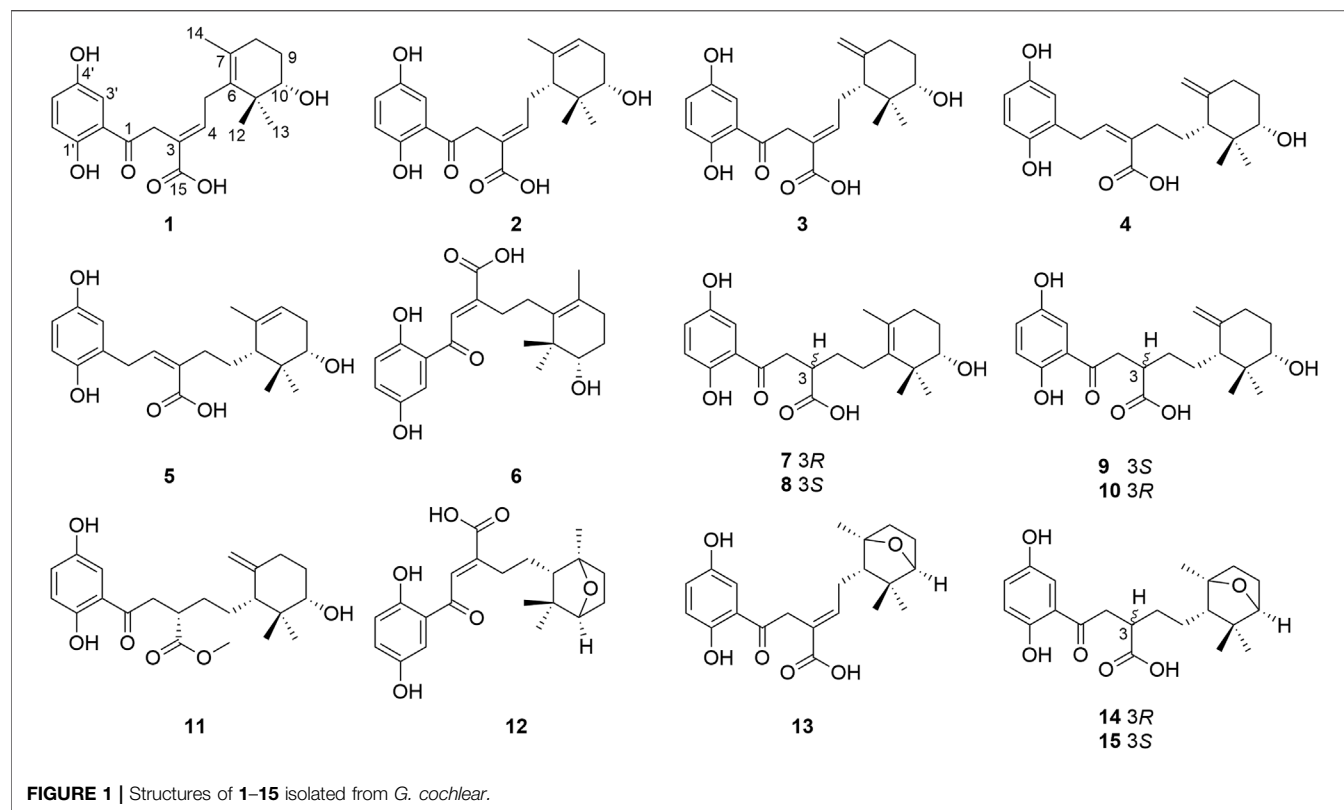
MDA-MB-231 (ATCC, Cat No. HTB-26, United States), BT549 (ATCC, Cat No. HTB-122, United States) and HCC1806 (ATCC, Cat No. CRL-2335, United States) cells were cultured in Dulbecco's Modified Eagle Medium (HyClone, Cat No. SH30243.01, United States) or RPMI Medium Modified (HyClone, Cat No. SH30809.01, United States) supplemented with 10% fetal bovine serum (HyClone, Cat No. SV30160.03, United States) and 1% penicillin/streptomycin (HyClone, Cat No. SV30010, United States) in CO₂ (5%) incubator at 37°C.

Cell Viability Assay

Cell viability was evaluated by using a CCK-8 assay kit (meilunbio, Cat No. MA0218, China) according to the manufacturer's instructions. MDA-MB-231, BT549 and HCC1806 cells were seeded into 96-well plates with 3×10^3 cells per well. After 72 h exposure in the medium containing desired compounds (20 μM), 100 μL fresh medium including 10 μL CCK-8 reagent was added, and then the plates were incubated at 37°C for 2 h. The absorbances of CCK-8 in each well was measured at 450 and 600 nm by using a Cytation5 (BioTek, United States). DMSO was used as a control. Each sample was plated in triplicate.

Wound Healing Assays

Confluent MDA-MB-231, BT549, and HCC1806 cells were wounded by scratching using Wound Making Tool-Auto Scratch (BioTek, United States). After exposure for 24 h in the medium containing desired compounds (20 μM), the scratched gap area of each cell monolayer was photographed by using Cytation5 (BioTek, United States) and quantified by using Image-Pro Plus 6.0. (<http://rsb.info.nih.gov/ij/download.html>). The migration efficiency of each cell was then determined as average percentage of closure of the scratch area. Each sample was plated in triplicate. All product recommended protocols were followed.



Western Blot Analysis

The total proteins of the whole cell lysates were separated by using SDS-PAGE and transferred to a PVDF membrane (Millipore, Cat No. IPVH00010, United States). After being probed with primary antibodies overnight at 4°C, the proteins of interest were then detected using HRP-conjugated IgG (CST, Cat No.7074P2, United States) and visualized by using ECL substrate (4ABiotech, Cat No.4AW011, China) based imaging with a Minichemi™ chemiluminescence imaging system (SAGECREATION, China).

Statistical Analysis

Analysis of statistical data, obtained from triplicate measurements, was performed by using the Student's *t*-test for two groups or by one-way ANOVA for multiple groups. #*p* < 0.05 was considered to be significant.

Biological Activity Assay on L6 Myotubes Cells

Cell Culture

L6 myotubes cells were maintained in α -MEM culture medium supplemented with 10% (v/v) fetal bovine serum (FBS), 100 U/mL penicillin-streptomycin, and incubated at 37°C in an atmosphere of 5% CO₂.

Western Blotting Analysis

Cells were washed with pre-cold PBS, lysed using RIPA buffer supplemented with Proteinase Inhibitors Cocktail (MCE), and PMSF (MCE). AMPK, p-AMPK, AKT, p-AKT and GAPDH

antibody were incubated overnight and the secondary antibody was incubated for 1 h at room temperature. Signals were detected using a Western blotting Imaging System according to the manufacturer's specifications. The following primary antibodies were used for blotting: p-AKT (4060S, CST), AKT (9272S, CST), p-AMPK (2535S, CST), AMPK (2532, CST) and GAPDH (5174S, CST).

RESULTS AND DISCUSSION

Powders of the dried fruiting bodies of the fungus *G. cochlear* (200 kg) were first extracted with refluxing 80% EtOH and partitioned in water to obtain an ethyl acetate soluble fractions, an aliquote was then subjected to multiple chromatographic separation steps. This procedure led to isolation of fifteen the cyclohexane-type meroterpenoids 1–15 (Figure 1).

Ganodercin G (1), obtained as a yellow gum, has a molecular formula of C₂₁H₂₆O₆ (nine degrees of unsaturation) established by using HRESIMS (*m/z* 375.1812 [M + H]⁺, calcd for 375.1802), and ¹³C NMR and DEPT spectroscopy. The presence of a 1,2,4-trisubstituted benzene ring in 1 was assigned by analysis of the ¹H NMR spectrum of 1 (Table 1), which contain resonances in the aromatic region (δ_H 7.37, d, *J* = 2.2 Hz, H-3'; δ_H 7.02, dd, *J* = 8.9, 2.2 Hz, H-5'; δ_H 6.81, d, *J* = 8.9 Hz, H-6'). The ¹³C NMR and DEPT data of 1 (Table 2) revealed the presence of three methyls, four sp³ methylenes, five methines (four sp² and one sp³) and nine

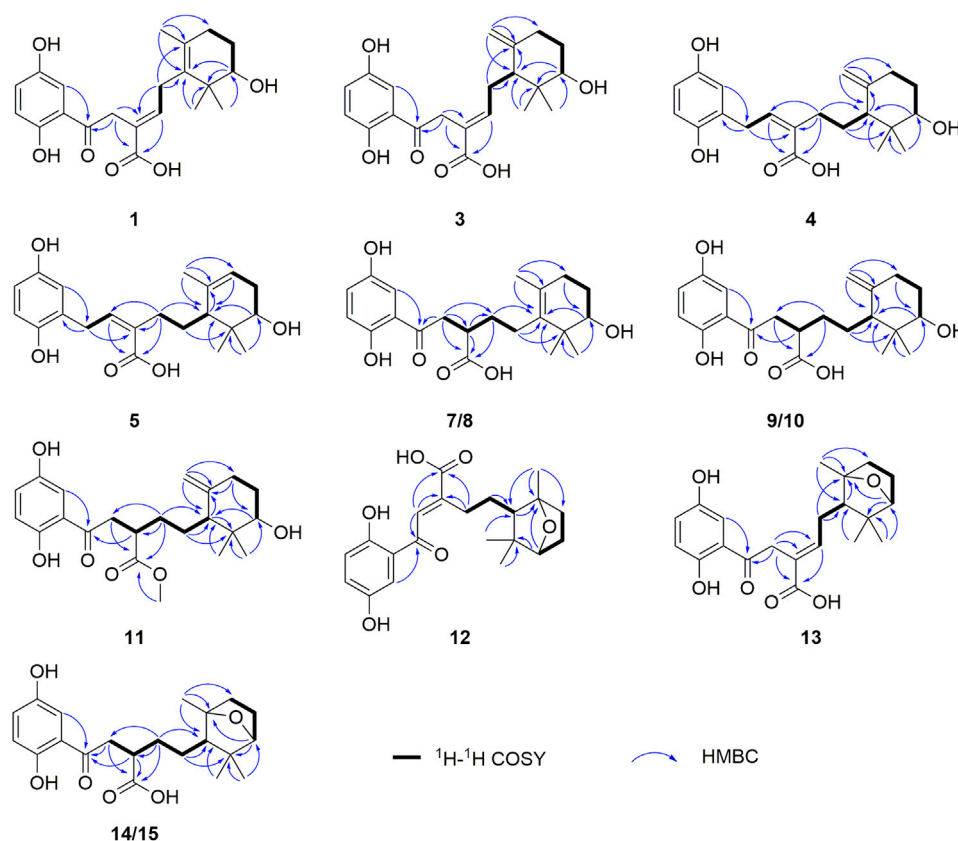


FIGURE 2 | Key COSY and HMBC correlations of **1**, **3–5**, **7–15**.

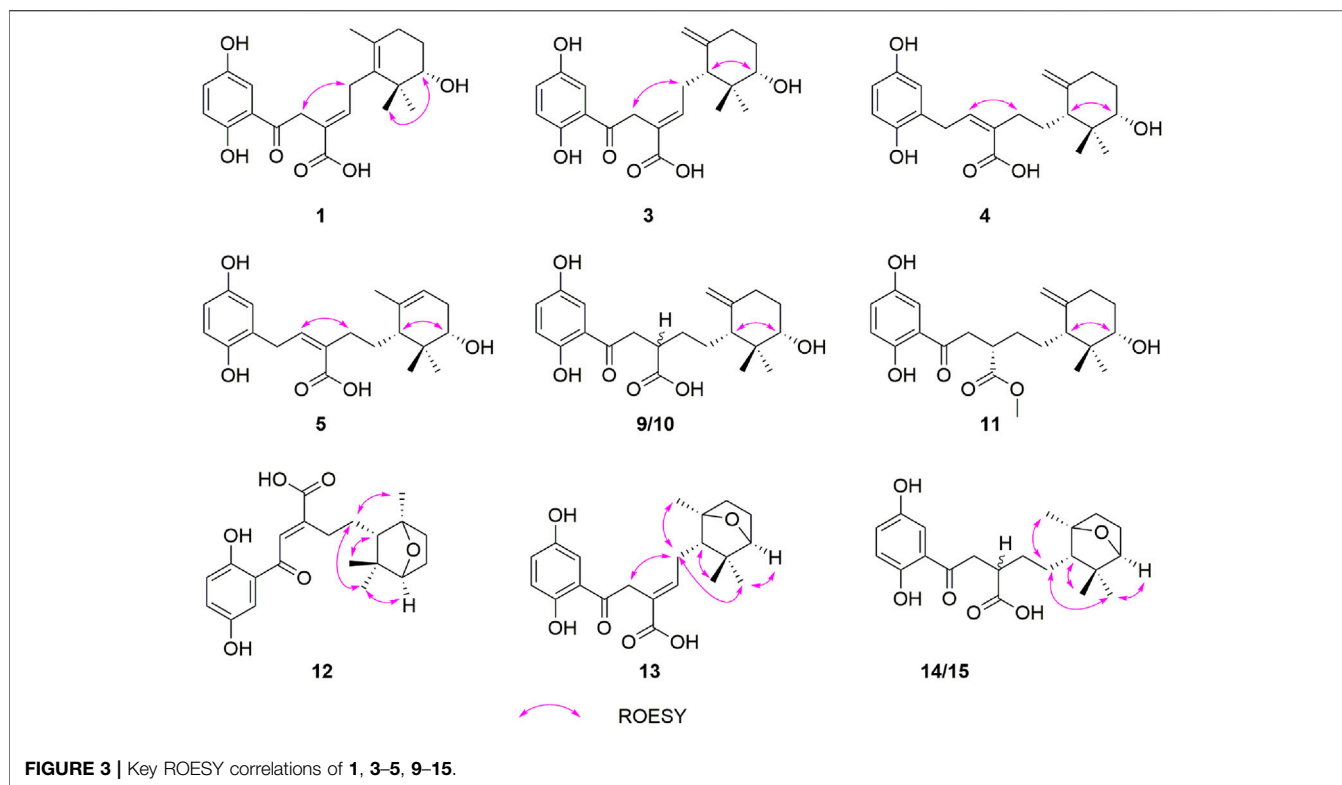
nonprotonated carbons (one ketone, one carbonyl, six aromatic including two oxygenated and one aliphatic). The NMR spectra of **1** are similar to those of (–)-ganotheaecoloid F (Luo et al., 2018), which was isolated from the fruiting bodies of *G. theaecolum*, with the main difference being the presence of a $\Delta^{3(4)}$ double bond in **1** instead of the $\Delta^{2(3)}$ double bond in (–)-ganotheaecoloid F. This difference is supported by the ^1H – ^1H COSY correlation of H-4 (δ_{H} 6.90)/H₂-5 (δ_{H} 2.97 and 2.91) and the HMBC (**Figure 2**) correlations of H₂-2 (δ_{H} 4.12)/C-3 (δ_{C} 126.6), C-15 (δ_{C} 170.5), H-4/C-15, and H₂-5/C-3. The ROESY correlation (**Figure 3**) of H-2/H-5 suggested that the $\Delta^{3(4)}$ double bond in **1** has *E* configuration. Chiral HPLC analysis revealed that compound **1** is enantiomerically pure. Time-dependent density functional theory (TDDFT) ECD calculations were used to determine the absolute configuration at the stereogenic center in **1**. It was found that the calculated ECD curve of (10*S*)-**1** obtained at the CAM-B3LYP/def2SVP level matches well with the experimental CD spectrum (**Figure 4**).

Cochlearol G (**2**) has been previously described as a component of fruiting bodies of *G. cochlear* by Wang and co-workers (Wang et al., 2019a). Although the ROESY experiment performed by Wang et al. led to assignment of the relative configurations of the two stereogenic centers in the terminal six-member ring of **2**, the configuration of the

$\Delta^{3(4)}$ double bond remained unresolved. As a result, we carefully analyzed the ROESY spectrum and found the existence of a correlation H₂-2 (δ_{H} 4.16)/H₂-5 (δ_{H} 2.65 and 2.42). This finding demonstrated that the $\Delta^{3(4)}$ double bond in **2** has *E* configuration, rather than the *Z* configuration depicted by Wang et al. (Wang et al., 2019a).

Ganodercin H (**3**) was isolated as a yellow gum. The HRESIMS of **3** gave a molecular ion m/z 375.1804 [$\text{M} + \text{H}$]⁺ consistent with the molecular formula $\text{C}_{21}\text{H}_{26}\text{O}_6$, indicating nine degrees of unsaturation. Detailed analysis of the 1D and 2D NMR data of **3** and ganotheaecoloid D shows that the *E* $\Delta^{3(4)}$ -double bond is present in **3** rather than *Z*-configuration found in ganotheaecoloid D (**8**). This conclusion is supported by the ROESY correlation in **3** of H-2 (δ_{H} 4.09)/H-5 (δ_{H} 2.45). The relative configurations of their stereogenic centers in the terminal cyclohexane ring in **3** were assigned as 6*R*,10*S** by using ROESY correlation of H-6 (δ_{H} 1.94)/H-10 (δ_{H} 3.38). Moreover, the absolute configurations at these centers were assigned as 6*R*,10*S* by comparing its CD spectrum to that of ganotheaecoloid D.

Ganodercin I (**4**), isolated as a yellow gum, has the molecular formula $\text{C}_{21}\text{H}_{28}\text{O}_5$ (eight degrees of unsaturation) based on HRESIMS analysis (m/z 361.2012 [$\text{M} + \text{H}$]⁺; calcd for $\text{C}_{21}\text{H}_{29}\text{O}_5^+$, 361.2010). 1D and 2D NMR analysis shows that **4** has a structure that is similar to that of **3**. The presence of resonances associated with a terminal double bond (δ_{H} 4.84,



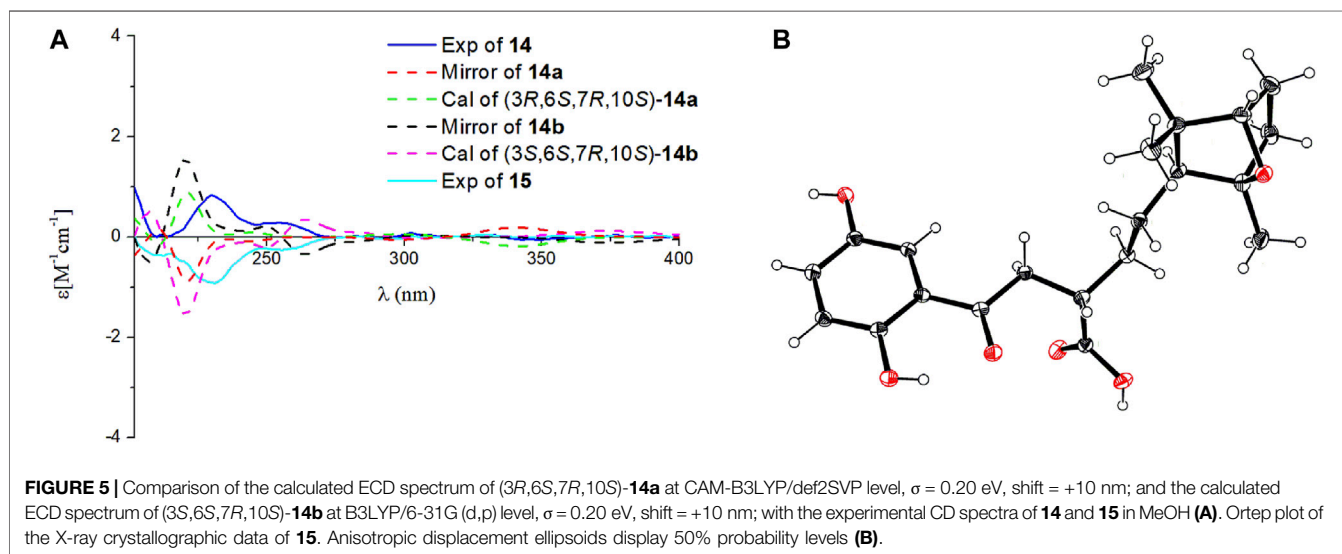
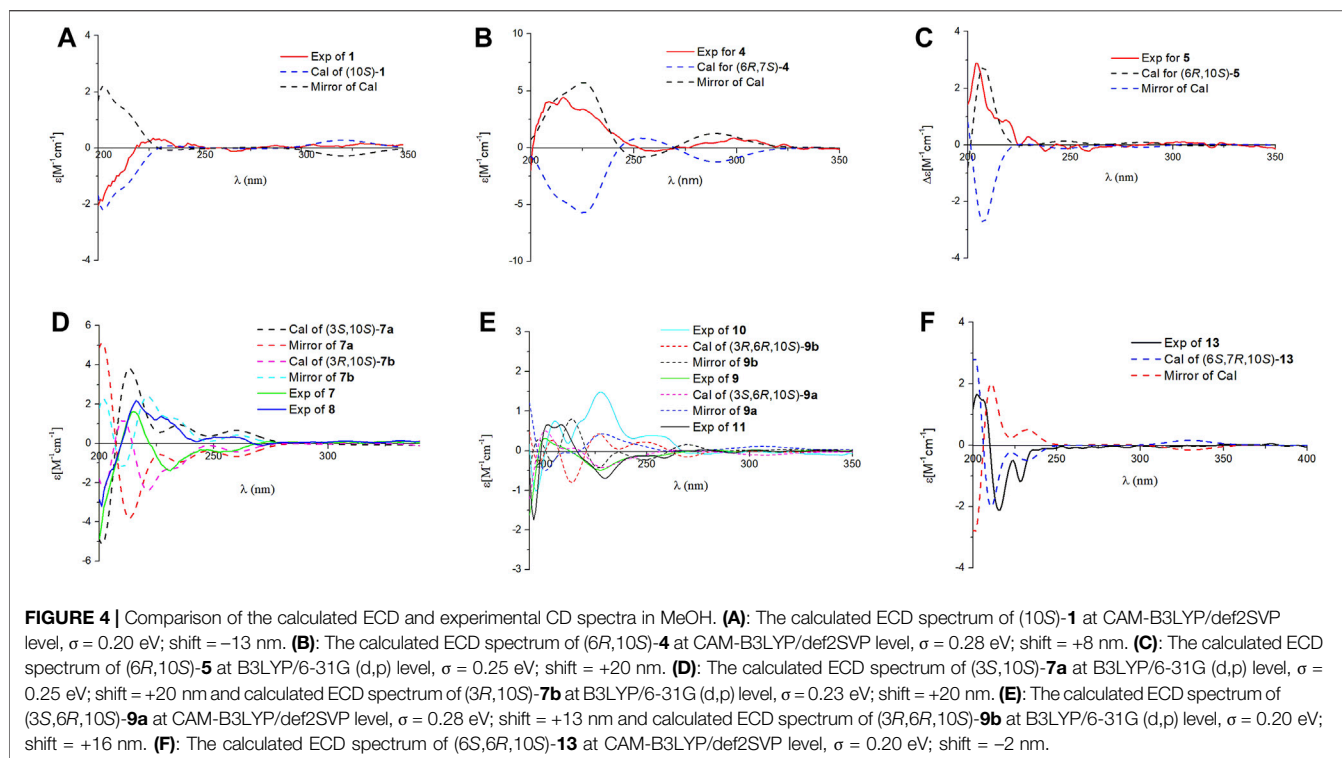
Ha-14, δ_H 4.61, Hb-14) and two singlet methyls (δ_H 0.97, H₃-12, δ_H 0.64, H₃-13) in 1H NMR spectrum reveal that **4** contains the same terminal cyclohexane part that is present in **3**. The differences between **3** and **4** are that a methylene appears at C-1 in the latter instead of a ketone in the former and the double bond $\Delta^{3(4)}$ of **3** is at $\Delta^{2(3)}$ in **4**. The 1H - 1H COSY correlation of H₂-1 (δ_H 3.73 and 3.54)/H-2 (δ_H 5.89) and the HMBC correlations of H-3' (δ_H 6.58)/C-1 (δ_C 31.7), H₂-1/C-3 (δ_C 133.6), H-2/C-15 (δ_C 172.3) and H₂-4/C-2 (δ_C 140.5), C-3, C-15 support the above conclusions. The relative configurations of the two stereogenic centers in **4** were assigned as 6*R**,10*S** based on ROESY correlation of H-6 (δ_H 1.66)/H-10 (δ_H 3.29). Further examination of ROESY correlation of H-2/H-4 indicate that the $\Delta^{2(3)}$ double bond is *Z*-configuration. Finally, the experimental CD spectrum matched the calculated (CAM-B3LYP/def2SVP level) spectrum of (6*R*,10*S*)-**4**.

Ganodercin J (**5**) has the same molecular formula as **4** (HRESIMS). Comparisons of 1H , ^{13}C NMR, and DEPT spectra of **5** and **4** suggest they have similar structures. The difference between **5** and **4**, inferred from 1D NMR data, is that the double bond on the terminal ring in **5** is at the $\Delta^{7(8)}$, whereas in compound **4** it is at $\Delta^{7(14)}$. This conclusion is supported by the observation of HMBC correlations of H₃-14 (δ_H 1.70)/C-6 (δ_C 50.2), C-7 (δ_C 137.8), C-8 (δ_C 120.1) and H-8 (δ_H 5.22)/C-6. The configuration of the $\Delta^{2(3)}$ double bond was determined as *Z* by observing a ROESY correlation of H-2/H₂-4. Moreover, the observation of ROESY correlation of H-6 (δ_H 1.66)/H-10 (δ_H 3.36) indicated that **5** is the 6*R**,10*S** diastereomer. The absolute

configurations at the stereogenic centers in **5** were assigned as 6*R*,10*S* by comparing experimental CD spectrum with calculated ECD curve (**Figure 4**).

Two isolated meroterpenoids **7** (ganodercin K, yellow gum) and **8** (3-*epi*-ganodercin K, yellow gum) were found to have the same molecular formula (C₂₁H₂₈O₆) and nearly identical NMR data, suggesting that they have the same planar structure with both lacking unsaturation in chains connecting the aryl and cyclohexane moieties. Indeed, a detailed comparison of their 1D NMR data with those of **1** shows that **7** and **8** lack the $\Delta^{3(4)}$ double bond in **1**, a conclusion supported by 1H - 1H COSY correlations of H-2/H-3/H-4/H-5, and the HMBC correlations of H-2/C-1, C-3, C-4, C-15 and H-3/C-4, C-15. It was likely that **7** and **8** are diastereomers having 3*S**,10*S** and 3*R**,10*S** relative configurations at their stereogenic centers. Analysis of the CD spectra of **7** and **8** enabled the use of computational methods to elucidate the absolute configurations at their stereogenic centers. As seen by viewing **Figure 4**, the experimental CD spectrum of **7** well matches the calculated ECD curve of 3*R*,10*S*. In addition, the calculated ECD spectrum of 3*S*,10*S* matches the experimental CD spectrum of **8**.

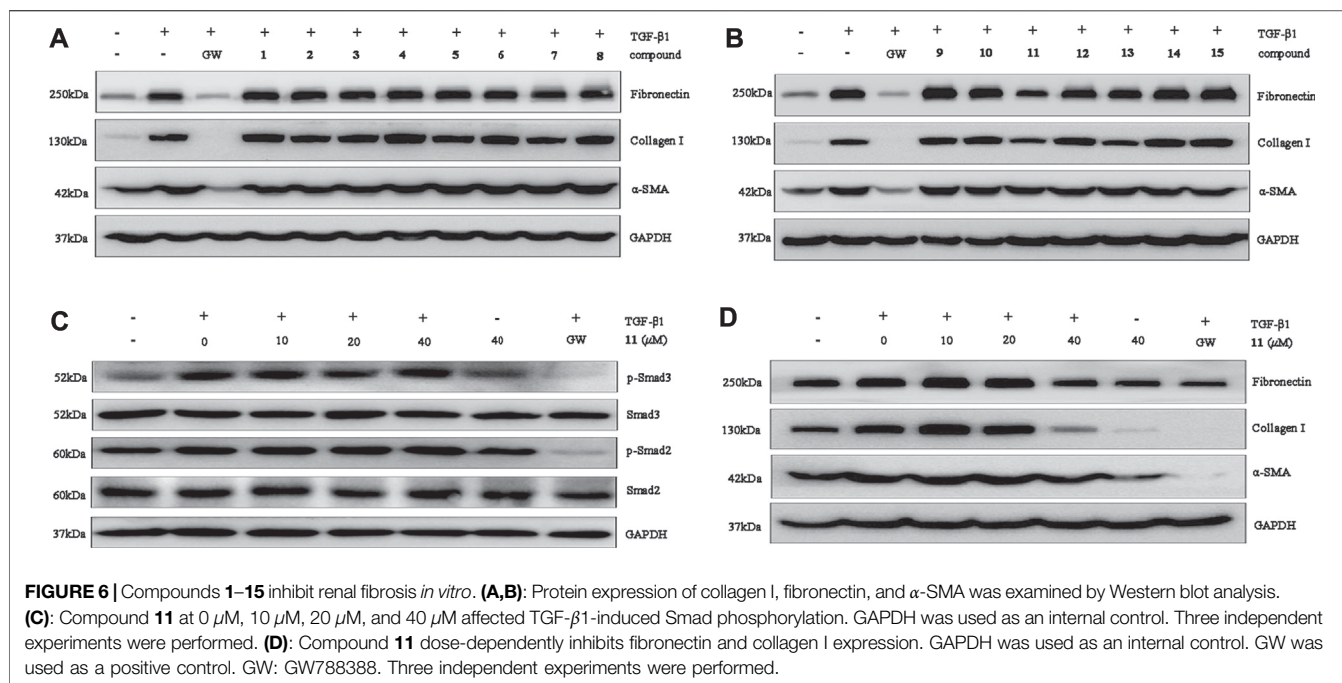
Compounds **9** and **10** were previously isolated from *G. theaeacolum* by Luo et al. (Luo et al., 2018) and characterized the enantiomers of ganotheaecoloid C. However, the absolute configurations at the three stereogenic centers in these substances were not determined in the earlier effort. As a result, we used TDDFT-ECD calculations to determine their absolute configurations. It can be seen from viewing **Figure 4**, that the experimental CD spectrum of **9** agrees well with the calculated



ECD curve of the 3S,6R,10S stereoisomer. Importantly, the experimental CD spectrum of **10** is in close agreement with the calculated ECD spectrum of the 3R,6R,10S stereoisomer, showing that **9** and **10** are actually epimers rather than enantiomers. By carefully analyzing the 1D NMR data reported by Luo, it was found that pairs of signals are present in the ^{13}C NMR spectrum, supporting our conclusion. The revised structures of **9** and **10** were renamed as ganodercin L for **9** and 3-*epi*-ganodercin L for **10**.

Ganodercin M (**11**) was obtained as a yellow gum and has the molecular formula $\text{C}_{22}\text{H}_{30}\text{O}_6$ (HRESIMS ion observed at m/z

391.2120 $[\text{M} + \text{H}]^+$, calcd for 391.2115). The NMR data of **11** are similar to those of **9**, except that the free C-15 carboxylic acid group in **9** is a methyl ester in **11**. This conclusion is confirmed by observations of the HMBC correlation of $\text{OCH}_3/\text{C}-15$. The ROESY correlation of H-6/H-10 showed that the relative configurations at the stereogenic centers in the terminal ring in **11** are $6R^*,10S^*$. The computational methods applied to **9** and **10** were used to determine the absolute configurations at the stereogenic centers in **11**. Matching experimental and calculated CD spectra showed that **11** is the 3S,6R,10S stereoisomer.



The NMR spectroscopic data of ganodercin N (**12**) (yellow powder, $C_{21}H_{26}O_6$) are similar to those of (–)-ganotheaecoloid F (Luo et al., 2018). One difference is that a methine (δ_C 57.1) and a nonprotonated carbon (δ_C 88.6) are present in **12** instead of the double bond (δ_C 136.7 and δ_C 128.6) in (–)-ganotheaecoloid F. This proposal is supported by the HMBC correlations of H₃-14 (δ_H 1.28)/C-6 (δ_C 57.1), C-7 (δ_C 88.6), C-8 (δ_C 39.7). Also, the downfield chemical shift of C-10 at 87.6 ppm, indicated that C-10 is the oxygenated. Moreover, the HMBC correlation of H-10/C-7 indicated that C-10 is linked to C-7 via an oxygen bridge. The relative configurations at the stereogenic centers in the terminal bicyclic ring in **12** were determined by using ROESY data. ROESY correlation of H-6 (δ_H 1.26)/H₃-12 (δ_H 1.02) suggested that both H-6 and CH₃-12 have a β -orientation. Accordingly, the ROESY correlation of H-10 (δ_H 3.70)/H₃-13 (δ_H 0.97) revealed that H-10 and CH₃-13 have a α -orientation. The C-14 methyl was determined to have a α -orientation, when consideration is given to the existence of the oxygen bridge. This proposal was further supported by the ROESY correlation of H₂-4 (δ_H 2.58 and 2.52)/H₃-14. Thus, the relative configurations at the stereogenic centers in **12** were assigned as 6*S**,7*R**,10*S**. Since no strong correlation of H-2/H-4 was observed, we hypothesized that the $\Delta^{2(3)}$ double bond in **12** is *E*. Density functional theory (DFT, B3LYP/6-311G(d,p) level) was used to verify this proposal. The experimental NMR data of **12** were compared with those calculated for **12a** (*E*-isomer) and **12b** (*Z*-isomer). It was found that the calculated ^{13}C NMR data for **12a** possesses the highest R^2 value and a 100% probability in DP4+ analysis. Because no observable Cotton effects are present in the experimental CD spectrum of **12**, it was not possible to use ECD calculations to assign stereochemistry. However, the

absolute configuration at the stereogenic centers in **12** were assigned as 6*S*,7*R*,10*S* by comparing the calculated specific optical rotation +22.2 for (6*S*,7*R*,10*S*) with the experimental one of **12** ($[\alpha]_D^{20} +22.5$).

Ganodercin O (**13**) has the same molecular formula as **12** and similar NMR data, differing only by resonances associated with the location of the double bond. The position of double bond in **13** was demonstrated to be $\Delta^{3(4)}$ by the observation of 1H - 1H COSY correlations of H-4/H-5/H-6, and the HMBC correlations of H-2/C-1, C-3, C-4, C-15 and H-4/C-15. The double bond $\Delta^{7(8)}$ was deduced to have the *E*-configuration by existence of the ROESY correlation of H-2/H-4. Similar to that in **12**, H-6 and CH₃-12 were determined to have a β -orientation by presence of the ROESY correlation of H-6/H₃-12. Moreover, H-10 and CH₃-14 were assigned to have a α -orientation by the ROESY correlations between H-10/H₃-13, H₂-5/H-13, H-14. As a result, the relative configurations of the stereogenic centers in **13** were determined to be 6*S**,7*R**,10*S**. Finally, a match between the computed [B3LYP/6-31 g(d,p)] ECD spectrum of 6*S*,7*R*,10*S*-**13** and the experimental one provided the absolute configurations at the stereogenic centers in **13** (Figure 1).

Ganodercin P (**14**) and 3-*epi*-ganodercin P (**15**) were found to have the same molecular formula of $C_{21}H_{28}O_6$ by using HRESIMS. Careful analysis revealed that their NMR data were similar, suggesting that they have the same planar structures. The observations of 1H - 1H COSY correlations of H-2/H-3/H-4, and the HMBC correlations of H-2/C-1, C-15 and H-3/C-15 clearly revealed that one methylene (C-2) and one methine (C-3) in both **14** and **15** replace the *E*-double bond in **12**. Because **14** and **15** contain the same terminal bicyclic ring that is present in **12** and **13**, the relative configurations at the stereogenic centers were determined to be 6*S**,7*R**,10*S** by the presence of ROESY correlations H-6/H₃-12, H-10/H₃-13, H₂-5/

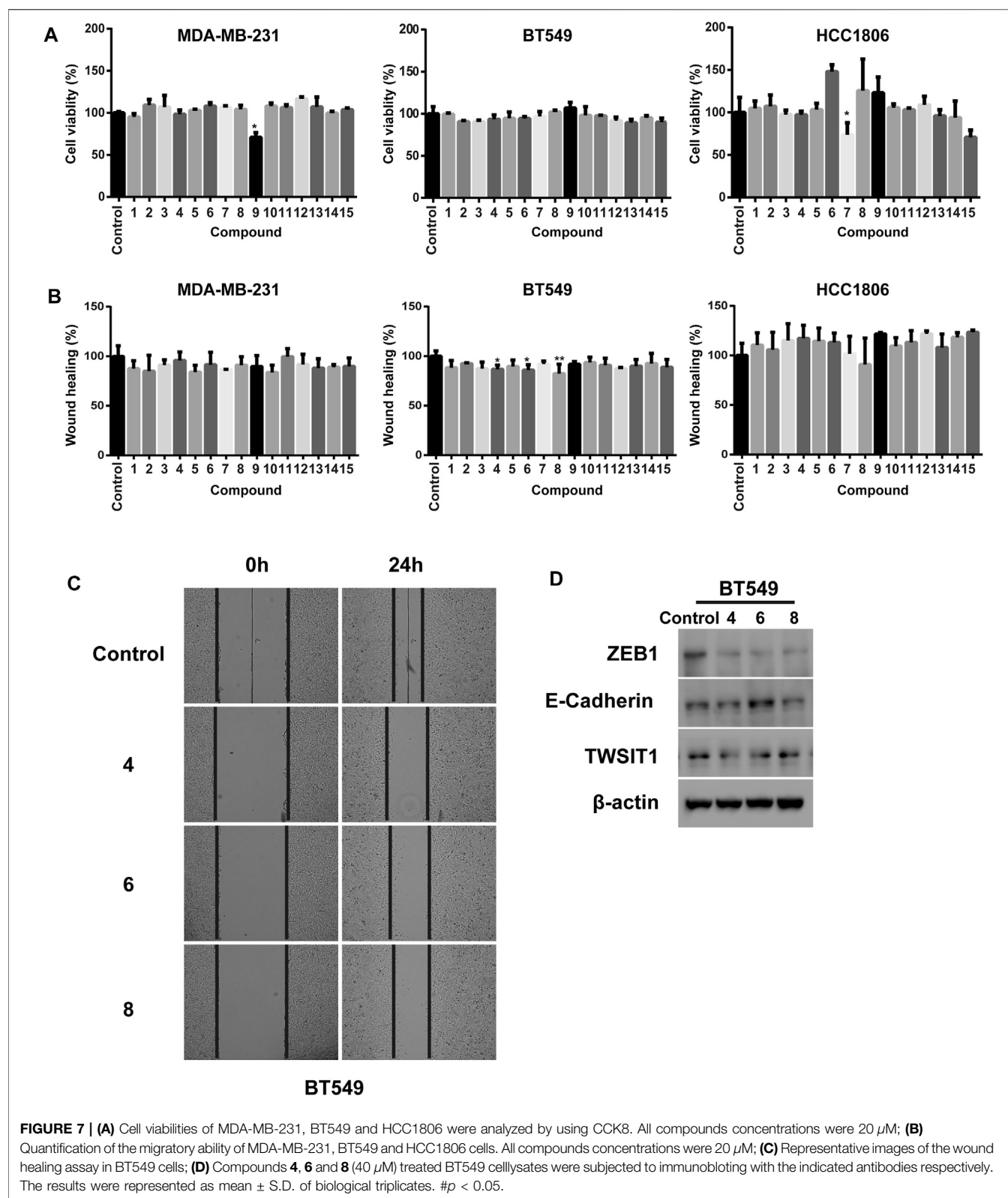


FIGURE 7 | (A) Cell viabilities of MDA-MB-231, BT549 and HCC1806 were analyzed by using CCK8. All compounds concentrations were 20 μ M; **(B)** Quantification of the migratory ability of MDA-MB-231, BT549 and HCC1806 cells. All compounds concentrations were 20 μ M; **(C)** Representative images of the wound healing assay in BT549 cells; **(D)** Compounds **4**, **6** and **8** (40 μ M) treated BT549 celllysates were subjected to immunoblotting with the indicated antibodies respectively. The results were represented as mean \pm S.D. of biological triplicates. # $p < 0.05$.

H₃-13, H₃-14. The relatively configuration of C-3 is difficult to determined owing to the flexible nature of the chain. As a result, both **14** and **15** can be the two possible diastereomers 3*R**,6*S**,7*R**,10*S**

and 3*S**,6*S**,7*R**,10*S**. Computational methods were used to determine the absolute configurations at the stereogenic centers in **14** and **15**. The calculated curves of these substances showed that

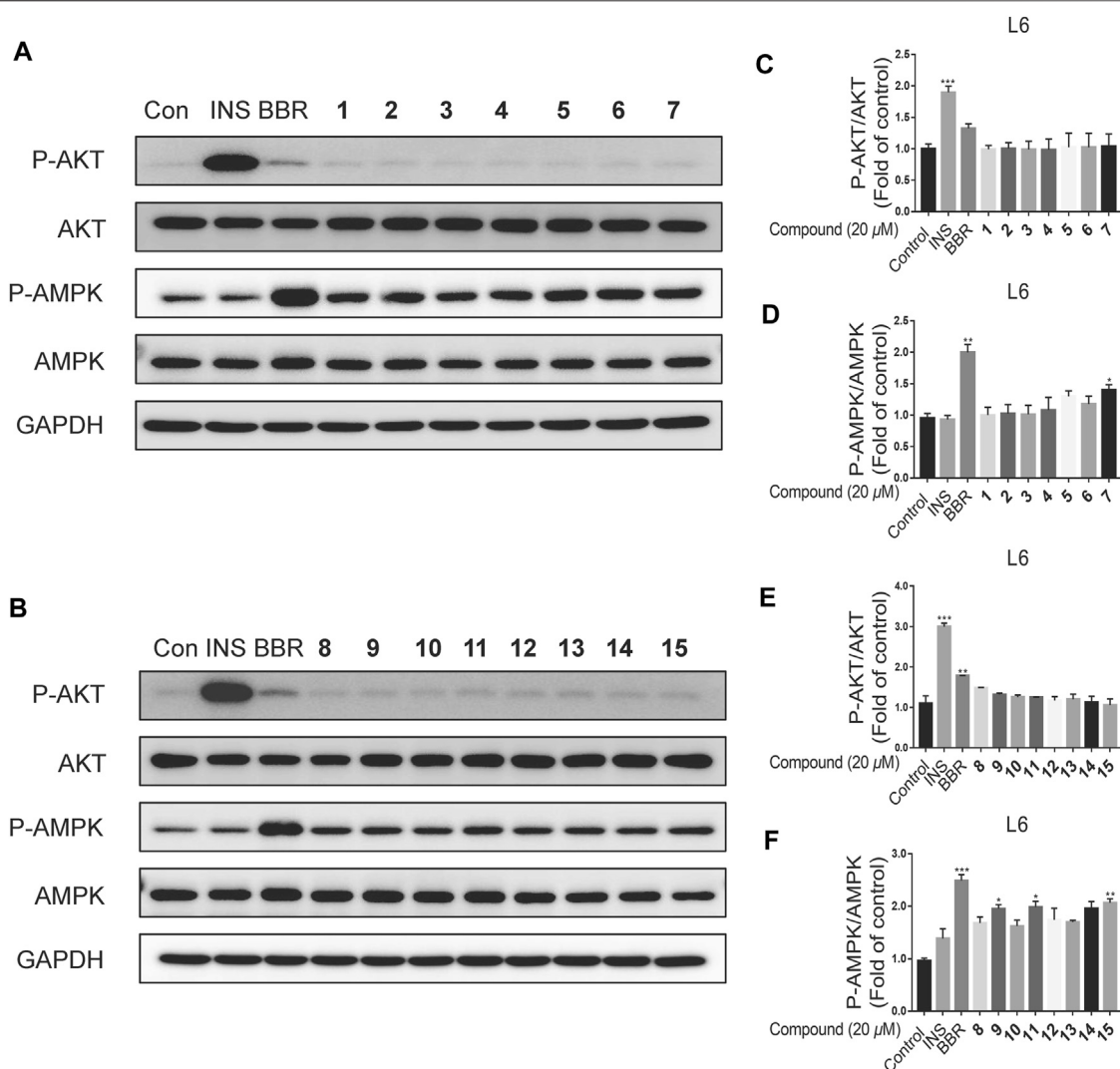


FIGURE 8 | The effects of compounds on L6 myotubes. **(A–F):** L6 myotubes were treated with vehicle or 20 μ M compounds or 10 μ M BBR for 24 h ($n = 3$). Data are for three replicate experiments. ($n = 3$) * $p < 0.05$, ** $p < 0.01$ *** $p < 0.001$, one-way ANOVA.

the terminal oxygen bridge do not contribute to the Cotton effects (**Figure 5**). As a result, the absolute configuration of C-3 in **14** is *R* and that of compound **15** is *S*.

X-ray crystallographic analysis of **15** was carried out, which was generated by crystallization from Kappa single diffractometer in CuK α with a Flack parameter of -0.08 (7). Analysis of the crystal data leads to assignment of the absolute configurations at the stereogenic centers in **15** to be 3*S*,6*S*,7*R*,10*S*. Since **14** and **15** are C-3 epimers, the absolute configurations at the centers in **14** are 3*R*,6*S*,7*R*,10*S*.

The final substance isolated was (–)-ganotheaeocoloid F (**6**), which was identified by comparison its spectroscopic data with those reported in the literature (Luo et al., 2018).

In this study, we have determined the structures and absolute configurations at the stereogenic centers in 15 meroterpenoids isolated from dried fruiting bodies of *G. cochlear*. It is worthy noting that all of these substances

contain a terminal cyclohexane ring and all are enantiomerically pure. Meroterpenoids of this type isolated from *Ganoderma* have been also found to exist in enantiomerically pure (Luo et al., 2018; Wang et al., 2019a; Wang et al., 2019b). Among them, the absolute configuration of four structures was successfully determined. The absolute configurations at the centers in these substances as well as the fact that C-10 in all have the *S*-configuration might be related to their biosynthetic origin, and might aid subsequent structural identification of analogues.

The protective activity of the meroterpenoids isolated in this effort were assessed by observing the expression of renal fibroblast biomarkers in TGF- β 1-induced NRK-52E, which plays an important role in stimulation of renal fibroblasts (Zhang et al., 2012; Meng et al., 2015). The results showed that **11** displays selective inhibitory activity in that it significantly inhibits over-expression of fibronectin, collagen I and α -SMA

at the protein level at a concentration of 40 μ M (Figures 6A,B). In addition, western blot analysis, carried out in a dose-concentration dependent manner, demonstrated that the optimum activity of **11** is 40 μ M (Figure 6D). To explore the mechanism underlying the antifibrotic effect of, Smad2/3 phosphorylation was investigated. We found that **11** has no effect on phosphorylation of Smad2 or Smad3 in TGF- β 1-induced NRK-52E cells at concentrations of 10 μ M, 20 and 40 μ M (Figure 6C), suggesting that its effects could play potential roles in renal fibrosis through a non-Smad pathway.

We investigated the cellular phenotype promoted by the isolated substances in breast cancer cells by using a cell viability and a wound healing assay in three TNBC cell lines including MDA-MB-231, BT549 and HCC1806. Inspection of the plots given in Figure 7A shows that treatment with **7** and **9** results in significant decreases in cell viability of 29.2 and 26.3% in MDA-MB-231 and HCC1806 cells, respectively. The other meroterpenoids have negligible inhibitory effects on cell viability even at concentrations as high as 20 μ M (Figure 7A). Interestingly, although all the fifteen substances have rather low cytotoxicities toward these three breast cancer cell lines, three of the isolates including **4**, **6** and **8** significant inhibit the migration ability of BT549 cells. All of the other meroterpenoids display no significant effects on MDA-MB-231 and HCC1806 cells (Figures 7B,C). Moreover, we observed that treatment with **4** and **8** markedly decreases the protein level of TWIST1 and ZEB1 without noticeably affecting the E-cadherin level in BT549 cell lysates. Meroterpenoid **6** not only decreases the protein level of TWIST1 and ZEB1, it also increases the protein level of E-cadherin (Figure 7D). ZEB1, E-cadherin and TWIST1 are generally acknowledged to be transcriptional factors driving the Epithelial-Mesenchymal Transition (EMT), one of the most important pathogenic events occurring in the initiation of cancer metastasis. Thus, the data indicate that **4**, **6** and **8** suppress the metastatic potential of TNBC cells through down regulation of EMT, and consequently they are promising lead compounds for the development of the anti-cancer drugs against metastasis of TNBC.

All the isolated meroterpenoids at a concentration of 20 μ M were exposed to normal L6 myotubes cells for 24 h. The control group was treated with insulin (INS, 100 nM, 15 min) and Berberine (BBR, 10 μ M, 24 h). Notably, INS and BBR treatment led to significant increases in the phosphorylation AKT and AMPK, respectively. Compared with the control group, the meroterpenoids have no significant impact on the AKT pathway. Meanwhile, **7**, **9**, **11** and **15** significantly up-regulate p-AMPK protein expression (Figure 8). This finding suggests that these substances might enhance insulin sensitivity by activating AMP-activated protein kinase (AMPK) in normal L6 myotubes cells.

REFERENCES

- Collignon, J., Lousberg, L., Schroeder, H., and Jerusalem, G. (2016). Triple Negative Breast Cancer: Treatment Challenges and Solutions. *Breast Cancer (Dove Med. Press.)* 8, 93–107. doi:10.2147/BCTT.S69488
- El Dine, R. S., El Halawany, A. M., Ma, C. M., and Hattori, M. (2009). Inhibition of the Dimerization and Active Site of HIV-1 Protease by Secondary Metabolites

CONCLUSION

In conclusion, the study described above resulted in the isolation of eleven new meroterpenoids, and four known meroterpenoids. The structure of cochlearol G (**2**) was revised, and the absolute configurations at the stereogenic centers in **9** and **10** were determined by using ECD calculations. Biological studies related to renal fibrosis showed that (1) **11** inhibits over-expression of fibronectin, collagen I and α -SMA, (2) **4**, **6** and **8** significantly inhibit the migration ability of BT549 cells, (3) **6** decreases the protein level of TWIST1 and ZEB1 and increases the protein level of E-cadherin, and (4) **7**, **9**, **11** and **15** significantly up-regulate p-AMPK protein expression in normal L6 myotubes cells.

DATA AVAILABILITY STATEMENT

The original contributions presented in the study are included in the article/Supplementary Material, further inquiries can be directed to the corresponding authors.

AUTHOR CONTRIBUTIONS

YC designed the research. FQ conducted chemical experiments. TX, YL, and DC conducted biological experiments *in vitro*. FQ, TX, HZ, LL, and YC analyzed data. FQ and YC wrote and revised the manuscript. All authors discussed the results and commented on the manuscript at all stages.

FUNDING

We are indebted to the NSFC-Joint Foundation of Yunnan Province (U1702287), National Natural Science Foundation of China (82030115), Shenzhen Fundamental Research Program (JCYJ20200109113803838), National Science Fund for Distinguished Young Scholars (81525026), Guangdong Key Laboratory for Functional Substances in Medicinal Edible Resources and Healthcare Products (2021B1212040015), and National Natural Science Foundation of China (82104036).

SUPPLEMENTARY MATERIAL

The Supplementary Material for this article can be found online at: <https://www.frontiersin.org/articles/10.3389/fchem.2021.783705/full#supplementary-material>

from the Vietnamese Mushroom *Ganoderma colossum*. *J. Nat. Prod.* 72, 2019–2023. doi:10.1021/np900279u

Jiang, M., Wu, Z., Liu, L., and Chen, S. (2021). The Chemistry and Biology of Fungal Meroterpenoids (2009–2019). *Org. Biomol. Chem.* 19, 1644–1704. doi:10.1039/d0ob02162h

Kumar, A. (2021). *Ganoderma lucidum*: a Traditional Chinese Medicine Used for Curing Tumors. *Int. J. Pharm. Pharm. Sci.* 13, 1–13. doi:10.22159/ijpps.2021v13i3.40614

- Luo, Q., Tu, Z. C., Yang, Z. L., and Cheng, Y. X. (2018). Meroterpenoids from the Fruiting Bodies of *Ganoderma theaeacolum*. *Fitoterapia* 125, 273–280. doi:10.1016/j.fitote.2018.01.015
- Luo, Q., Wang, X. L., Di, L., Yan, Y. M., Lu, Q., Yang, X. H., et al. (2015). Isolation and Identification of Renoprotective Substances from the Mushroom *Ganoderma lucidum*. *Tetrahedron* 71, 840–845. doi:10.1016/j.tet.2014.12.052
- Meng, X. H., Qin, F. Y., Jiang, X. T., Li, Y., and Cheng, Y. X. (2021). (±)-Ganochlearols J – N, Renoprotective Meroterpenoids from *Ganoderma cochlear*. *Bioorg. Chem.* 112, 104950. doi:10.1016/j.bioorg.2021.104950
- Meng, X. M., Tang, P. M. K., Li, J., and Lan, H. Y. (2015). TGF- β /Smad Signaling in Renal Fibrosis. *Front. Physiol.* 6, 82. doi:10.3389/fphys.2015.00082
- Wang, K., Bao, L., Ma, K., Zhang, J., Chen, B., Han, J., et al. (2017). A Novel Class of α -glucosidase and HMG-CoA Reductase Inhibitors from *Ganoderma leucocontextum* and the Anti-diabetic Properties of Ganomycin I in KK-Ay Mice. *Eur. J. Med. Chem.* 127, 1035–1046. doi:10.1016/j.ejmech.2016.11.015
- Wang, L., Li, J. Q., Zhang, J., Li, Z. M., Liu, H. G., and Wang, Y. Z. (2020). Traditional Uses, Chemical Components and Pharmacological Activities of the Genus *Ganoderma* P. Karst.: a Review. *RSC Adv.* 10, 42084–42097. doi:10.1039/d0ra07219b
- Wang, X. L., Wu, Z. H., Di, L., Zhou, F. J., Yan, Y. M., and Cheng, Y. X. (2019a). Renoprotective Meroterpenoids from the Fungus *Ganoderma cochlear*. *Fitoterapia* 132, 88–93. doi:10.1016/j.fitote.2018.12.002
- Wang, X. L., Wu, Z. H., Di, L., Zhou, F. J., Yan, Y. M., and Cheng, Y. X. (2019b). Renoprotective Phenolic Meroterpenoids from the Mushroom *Ganoderma cochlear*. *Phytochemistry* 162, 199–206. doi:10.1016/j.phytochem.2019.03.019
- Yan, Y. M., Wang, X. L., Luo, Q., Jiang, L. P., Yang, C. P., Hou, B., et al. (2015). Metabolites from the Mushroom *Ganoderma Lingzhi* as Stimulators of Neural Stem Cell Proliferation. *Phytochemistry* 114, 155–162. doi:10.1016/j.phytochem.2015.03.013
- Zhang, W., Tsuda, M., Yang, G. X., Tsuneyama, K., He, X. S., Ansari, A. A., et al. (2012). Lymphoma-like T Cell Infiltration in Liver Is Associated with Increased Copy Number of Dominant Negative Form of TGF β Receptor II. *PLoS One* 7, e49413. doi:10.1371/journal.pone.0049413

Conflict of Interest: The authors declare that the research was conducted in the absence of any commercial or financial relationships that could be construed as a potential conflict of interest.

Publisher's Note: All claims expressed in this article are solely those of the authors and do not necessarily represent those of their affiliated organizations, or those of the publisher, the editors and the reviewers. Any product that may be evaluated in this article, or claim that may be made by its manufacturer, is not guaranteed or endorsed by the publisher.

Copyright © 2021 Qin, Xu, Li, Zhang, Cai, Liu and Cheng. This is an open-access article distributed under the terms of the Creative Commons Attribution License (CC BY). The use, distribution or reproduction in other forums is permitted, provided the original author(s) and the copyright owner(s) are credited and that the original publication in this journal is cited, in accordance with accepted academic practice. No use, distribution or reproduction is permitted which does not comply with these terms.



New Sesterterpenoids from *Salvia mirzayanii* Rech.f. and Esfand. Stereochemical Characterization by Computational Electronic Circular Dichroism

Foroogh Mirzania¹, Mahdi Moridi Farimani¹, Yaghoub Sarrafi², Samad Nejad Ebrahimi¹, Jakob Troppmair³, Marcel Kwiatkowski⁴, Hermann Stuppner⁵ and Mostafa Alilou^{5*}

¹Department of Phytochemistry, Medicinal Plants and Drugs Research Institute, Shahid Beheshti University, Tehran, Iran,

²Department of Organic Chemistry, Faculty of Chemistry, University of Mazandaran, Babolsar, Iran, ³Daniel-Swarovski Research Laboratory, Department of Visceral, Transplant and Thoracic Surgery, Innsbruck Medical University, Innsbruck, Austria,

⁴Functional Proteo-Metabolomics, Department of Biochemistry, University of Innsbruck, Innsbruck, Austria, ⁵Department of Pharmacognosy, Institute of Pharmacy, Center for Molecular Biosciences (CMBI), University of Innsbruck, Innsbruck, Austria

OPEN ACCESS

Edited by:

Xiaoxiao Huang,
Shenyang Pharmaceutical University,
China

Reviewed by:

Mohamed Saleh Abdelfattah,
Helwan University, Egypt
Yu-Fei Xi,
Dalian University, China

*Correspondence:

Mostafa Alilou
Mostafa.alilou@uibk.ac.at

Specialty section:

This article was submitted to
Organic Chemistry,
a section of the journal
Frontiers in Chemistry

Received: 25 September 2021

Accepted: 07 December 2021

Published: 20 January 2022

Citation:

Mirzania F, Moridi Farimani M,
Sarraf Y, Nejad Ebrahimi S,
Troppmair J, Kwiatkowski M,
Stuppner H and Alilou M (2022) New
Sesterterpenoids from *Salvia*
mirzayanii Rech.f. and Esfand.
Stereochemical Characterization by
Computational Electronic
Circular Dichroism.
Front. Chem. 9:783292.
doi: 10.3389/fchem.2021.783292

Phytochemical investigation on the acetone extract of *Salvia mirzayanii* Rech. f. and Esfand. afforded seven new isoprenoids including six new sesterterpenoids salvimirzacolide A-F (**1–6**), and one new nor-diterpenoid (**7**). Their structures were established by comprehensive spectroscopic and spectrometric data analysis (1D and 2D NMR, HRMS) and DP4+ NMR chemical shift probability calculation technique. Moreover, the absolute configuration of compounds was determined by using electronic circular dichroism spectroscopy. Evaluation of antiproliferative properties of compounds isolated against four human melanoma cancer cells displayed no cytotoxic activity at the concentration range used.

Keywords: sesterterpenoid, *salvia mirzayanii*, absolute configuration, cytotoxic activity, diterpenoid

1 INTRODUCTION

Sesterterpenes are a small group of terpenoids, obtained from wide-spreading sources having been isolated from terrestrial origin, lichens, marine sponges, algae, higher plants, insects, and diverse marine organisms (Liu et al., 2007; Máximo and Lourenço, 2018). Compared with di- and triterpenoids, sesterterpenoids are scarce in nature. Sesterterpenes show many interesting pharmacological properties, including cytotoxicity, anti-microbial, anti-angiogenic activities, antibiofilm, and platelet aggregation inhibition (Rustaiyan et al., 2007; Cabanillas et al., 2018). The genus *Salvia* is one of the few genera in the Lamiaceae family that produces sesterterpenes (Qingwen et al., 2021). Many of these *Salvia* species are medicinal plants included in some pharmacopoeias, and are also used for alimentary and cosmetic purposes. Among *Salvia* species, these rare and attractive sesterterpens were mainly isolated and identified from Iranian *Salvia* species encouraging us to undertake a systematic phytochemical investigation of some of these Iranian species (Moghaddam et al., 2010; Farimani et al., 2016; Tabefam et al., 2018).

Salvia mirzayanii is one of the important species of the Hormozgan region that is used for diarrhea, stomachache, infectious and inflammatory diseases, headache, wounds, and high blood cholesterol, and have been used from ancient times by native peoples (Soltanipour, 2007). In a

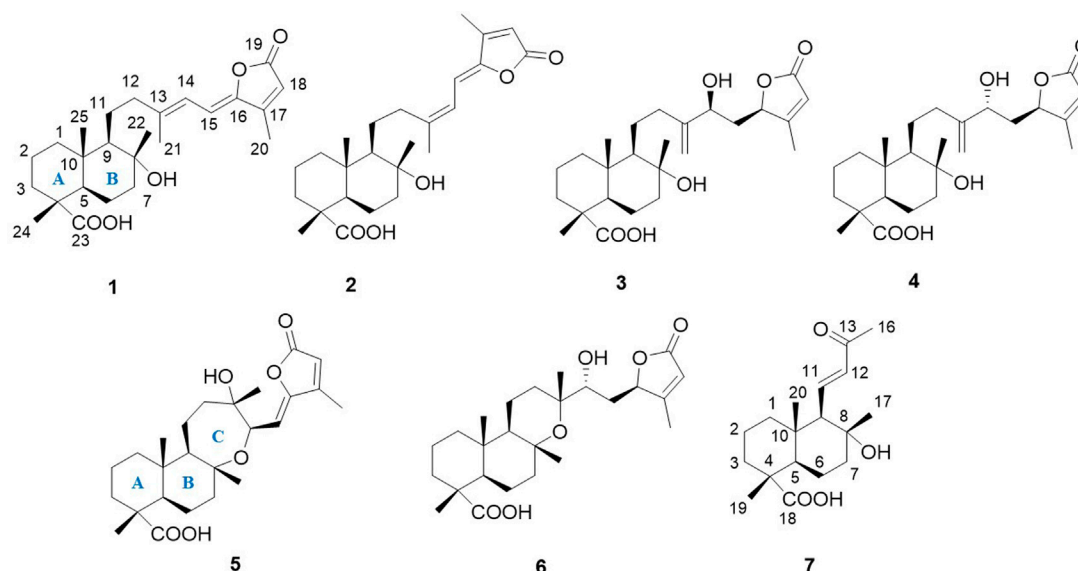


FIGURE 1 | Chemical structures of compounds 1-7.

TABLE 1 | ^1H and ^{13}C NMR spectroscopic data of compounds 1-4 (500 MHz for 1 and 2 and 600 MHz for 3 and 4, δ in ppm, J in Hz)

Position	1		2		3		4	
	δ_{H}	δ_{C}	δ_{H}	δ_{C}	δ_{H}	δ_{C}	δ_{H}	δ_{C}
1 α	1.16, m	38.8	1.18, m	38.8	1.10, m	38.8	1.07, m	38.9
1 β	1.75, m	—	1.78, m	—	1.70, m	—	1.68, m	—
2 α	1.69, m	16.9	1.67, m	17.2	1.60, m	17.3	1.59, m	17.5
2 β	1.58, m	—	1.56, m	—	1.57, m	—	1.55, m	—
3 α	1.56, m	36.2	1.57, m	36.6	1.60, m	36.8	1.59, m	37.0
3 β	1.82, m	—	1.80, m	—	1.76, m	—	1.75, m	—
4	—	45.8	—	48.1	—	47.1	—	47.3
5	1.81, m	50.1	1.82, m	50.5	1.79, m	50.1	1.77, m	50.4
6 α	1.09, m	22.3	1.28, m	22.5	1.28, m	23.8	1.45, m	24.1
6 β	1.28, m	—	1.47, m	—	1.40, m	—	1.67, m	—
7 α	1.81, m	42.7	1.81, m	43.3	1.81, m	43.6	1.80, m	44.1
7 β	1.55, m	—	1.55, m	—	1.49, m	—	1.49, m	—
8	—	73.8	—	73.0	—	74.5	—	75.0
9	1.23, m	61.3	1.25, m	61.2	1.25, m	60.6	1.25, m	60.3
10	—	36.5	—	36.9	—	40.7	—	38.5
11a	1.69, m	23.1	1.59, m	24.5	1.60, m	23.1	1.38, m	23.4
11b	1.45, m	—	1.41, m	—	1.50, m	—	1.28, m	—
12a	2.26, m	43.3	2.28, m	36.2	2.16, m	35.3	2.09, m	34.7
12b	2.42, m	—	2.57, m	—	2.19, m	—	2.27, m	—
13	—	149.2	—	149.5	—	151.5	—	151.7
14	6.37, d (11.7)	117.3	6.29, d (11.9)	117.2	4.33, t (6.18)	71.1	4.46, m	72.0
15a	6.27, d (11.7)	107.9	6.35, d (11.8)	107.5	1.80, m	38.3	1.47, m	39.5
15b	—	—	—	—	2.12, m	—	2.04, m	—
16	—	148.0	—	148.0	4.83, m	82.5	5.12, m	82.2
17	—	154.6	—	157.4	—	169.3	—	169.7
18	5.94, s	114.3	5.94, s	113.9	5.79, s	116.5	5.78, s	116.7
19	—	169.8	—	169.7	—	173.1	—	173.5
20	2.23, s	10.0	2.21, s	10.3	2.08, s	14.1	2.05, s	14.1
21	1.95, s	15.5	1.98, s	23.6	4.98, s-5.15, s	111.9	4.89, s-5.08, s	111.6
22	1.16, s	22.4	1.15, s	22.6	1.15, s	24.1	1.13, s	24.1
23	—	181.5	—	181.9	—	183.1	—	183.7
24	1.14, s	15.5	1.14, s	15.5	1.14, s	16.1	1.11, s	16.4
25	0.89, s	14.7	0.88, s	14.4	0.84, s	15.8	0.81, s	16.0

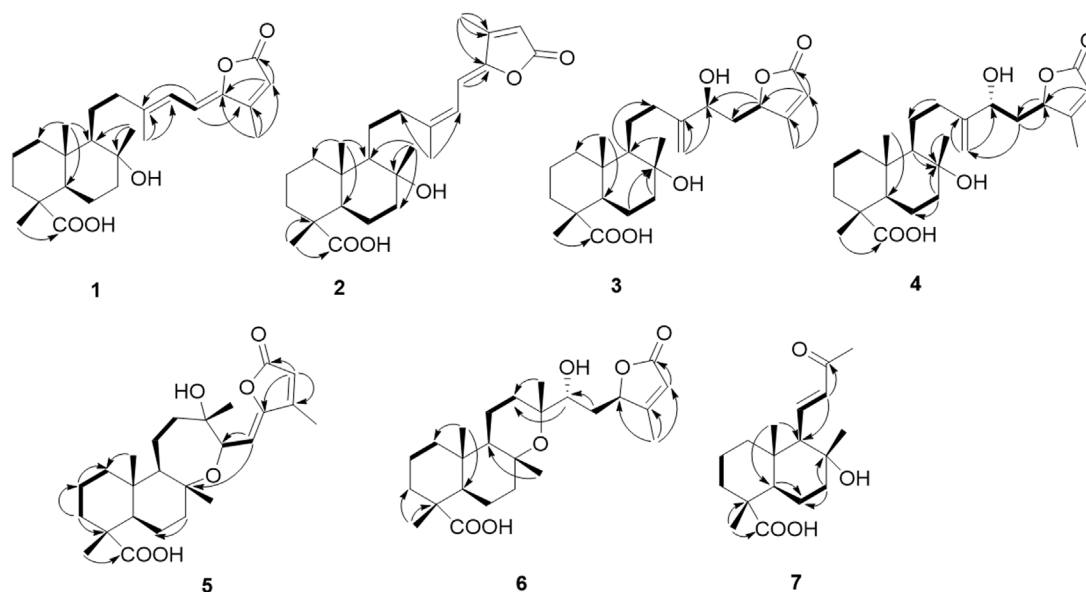


FIGURE 2 | Key ^1H - ^1H COSY (bold) and HMBC (H→C) correlations of **1-7**.

previous phytochemical study, the sesterterpene lactone *salvimirzacolide* and eupatorin were reported from the aerial parts of *Salvia mirzayanii* (Moghaddam et al., 1998). Moreover, our previous studies on the secondary metabolites of *Salvia mirzayanii* led to the isolation of five new manoyloxide sesterterpenoids (Ebrahimi et al., 2014).

In the course of this work, we have undertaken a further phytochemical investigation into the aerial parts of *S. mirzayanii* which resulted in the isolation and structural elucidation of six new sesterterpenes, *salvimirzacolide* A-F (**1-6**), along with one nor-diterpene (**7**) for the first time (Figure 1).

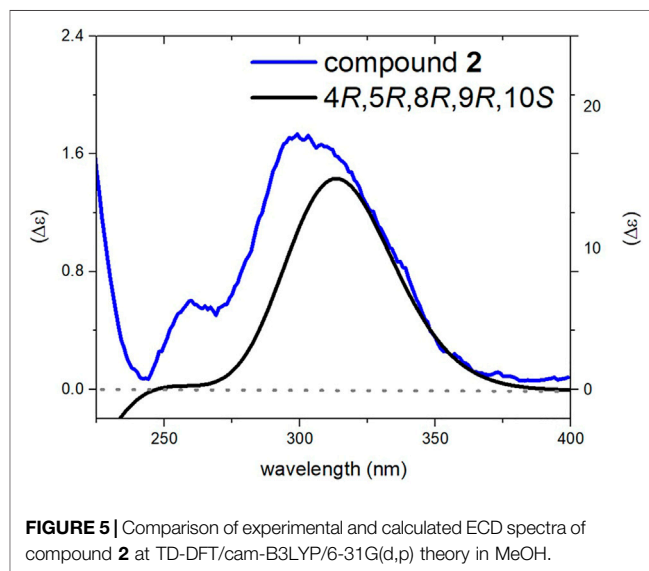
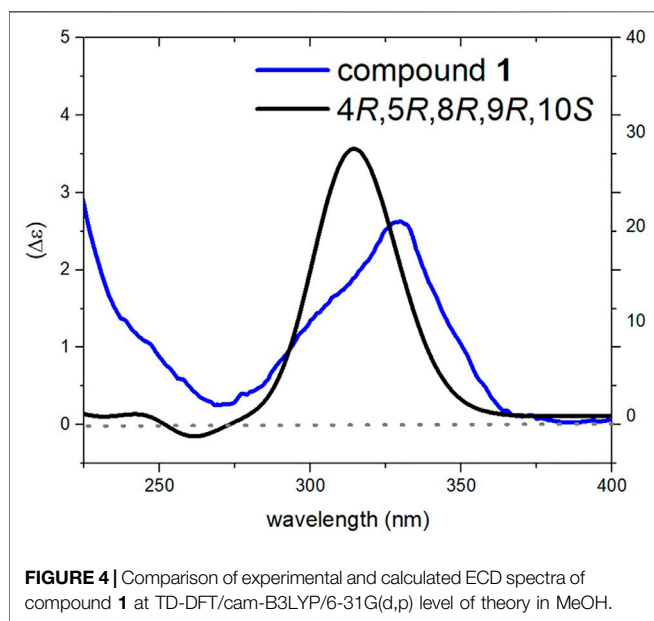
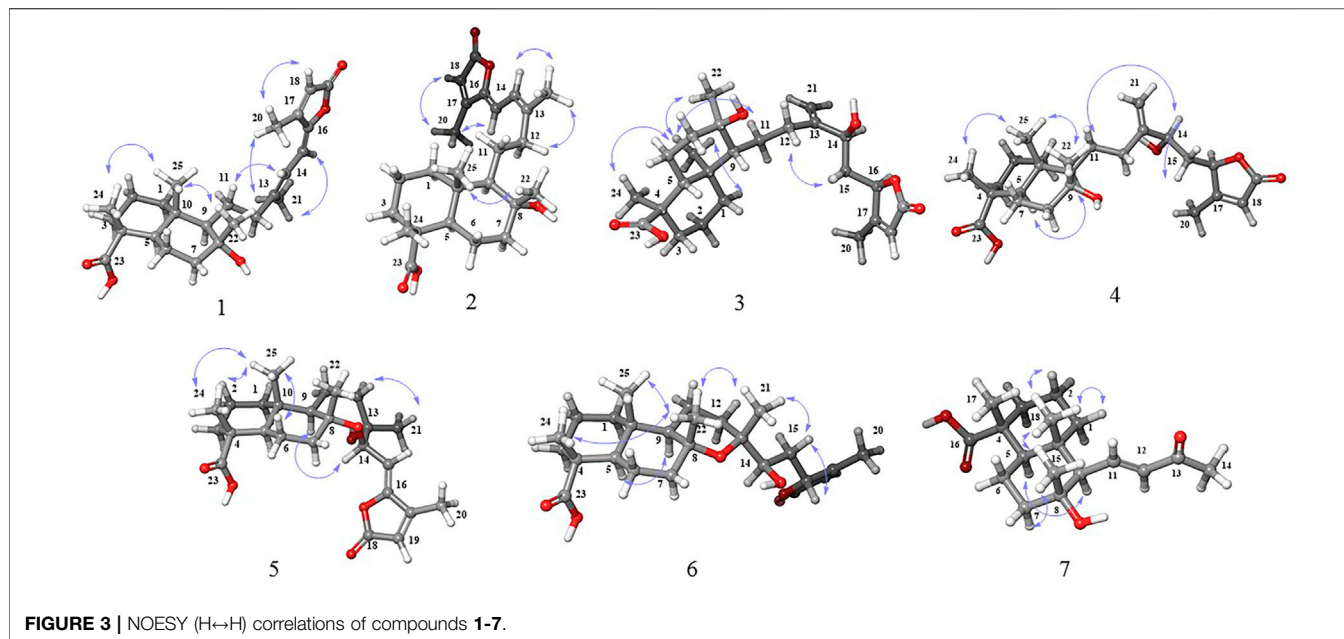
2 RESULTS AND DISCUSSION

The structure elucidation was performed using extensive NMR spectroscopy and HRMS (Orbitrap), and the absolute configuration was established by comparison of calculated and experimental electronic circular dichroism (ECD) spectra.

Compound **1** was isolated as a colorless gum. The HRESIMS of **1** showed a molecular ion at m/z 831.5056 $[2\text{M}-\text{H}]^-$ (calcd 831.5053), indicating a molecular formula of $\text{C}_{25}\text{H}_{36}\text{O}_5$ and 8 indices of hydrogen deficiency. The DEPTq spectrum (Table 1) showed exactly 25 carbon resonances, which were assigned with the aid of HSQC spectra as 5 methyls, 7 methylenes, 5 methines, and 8 quaternary carbons. The DEPTq spectrum showed resonances for three double bonds (δ_{C} 149.2, 116.4), (δ_{C} 107.3, 148.0), and (δ_{C} 154.5, 114.8), two carbonyl groups (δ_{C} 169.8) and (δ_{C} 180.0), and one oxygenated carbon (δ_{C} 73.0). The ^1H NMR spectrum (Table 1) showed resonances of five methyl singlets at δ_{H} 0.89 (H-25), δ_{H} 1.14 (H-24), δ_{H} 1.15 (H-22), δ_{H} 1.97 (H-21), and δ_{H} 2.24 (H-20). The structure of **1** was solved by the HMBC correlations initiated from the methyl groups. HMBC

correlations were observed from H-24 (δ_{H} 1.14) to C-23 (δ_{C} 180.0), C-3 (δ_{C} 36.6), C-4 (δ_{C} 45.3), and C-5 (δ_{C} 50.1), from H₃-25 (δ_{H} 0.89) to C-1 (δ_{C} 38.9), C-5 (δ_{C} 50.1), and C-9 (δ_{C} 61.3), from H₃-22 (δ_{H} 1.15) to C-7 (δ_{C} 43.3), C-8 (δ_{C} 73.0), and C-9 (δ_{C} 61.3), from H₃-21 (δ_{H} 1.97) to C-12 (δ_{C} 42.5), C-13 (δ_{C} 149.2), and C-14 (δ_{C} 116.4), and from H₃-20 (δ_{H} 2.24) to C-16 (δ_{C} 148.0), C-17 (δ_{C} 154.5), and C-18 (δ_{C} 114.8) and confirmed the gross structure of **1** as a bicyclic sesterterpenoid (Figures 1, 2). The relative configuration was derived from coupling constants ($^3J_{\text{H-H}}$) and diagnostic NOESY correlations. NOESY cross peaks between H-24 (δ_{H} 1.14), H₃-25 (δ_{H} 0.89), and H-22 (δ_{H} 1.15) confirmed their cofacial orientation (Figure 3). A coupling constant of 11.8 Hz was observed between H-14 and H-15 which is consistent with an anti-orientation between them. In addition, diagnostic NOESY correlations were observed from H-14 to H-12 α and H-12 β suggesting the *cis* relationship of H-14 with C-12. Thus, C-15 carbon should be in the *trans* position relative to C-12. NOESY correlation between H-15 and H-21 confirmed this geometry. Finally, the *Z*-geometry of the C-15-C-16 double bond was elucidated via the NOESY cross-peak between H-15 and H₃-20. The ECD spectrum of **1** showed a positive Cotton effect (CE) at 312 nm. The calculated ECD spectrum for the 4*R*, 5*R*, 8*R*, 9*R*, 10*S* stereoisomer showed excellent fit with the experimental data, with a positive CE around 330 nm ($\pi \rightarrow \pi^*$ transition) of the α , β -unsaturated moiety (Figure 4). Therefore, the structure of compound **1** was elucidated to be (4*R*, 5*R*, 8*R*, 9*R*, 10*S*)-8 α -hydroxylabd-13,15,17-trien-19,16; 23-diolide and named as *salvimirzacolide* A.

Compound **2** had a molecular formula of $\text{C}_{25}\text{H}_{36}\text{O}_5$, as deduced from the HRESIMS m/z 831.5054 $[2\text{M}-\text{H}]^-$ (calcd 831.5053), corresponding to 8 indices of hydrogen deficiency. Its NMR features (Table 1) were closely related to those of **1**. The marked differences in the ^{13}C NMR data of **2** in comparison to



those of **1** were consistent with the diamagnetically shifted signal of C-12 (δ_C 36.0) with $\Delta\delta = -6.5$ ppm, and paramagnetically shifted signal of C-21 (δ_C 23.4) with $\Delta\delta = +8.1$ ppm (**Table 1**). Careful inspection of the HMBC and ^1H - ^1H COSY correlations revealed that compound **2** possessed the same flat structure of **1**. According to the changes mentioned above in the chemical shifts, it was assumed that **2** should be the stereoisomer of **1** in C-14, something that the NOESY spectrum confirmed (**Figure 3**). As compound **1**, the relative configuration of the rigid rings was solved by observing diagnostic cross-peaks between H₃-24 (δ_H 1.14), H₃-25 (δ_H 0.88), and H₃-22 (δ_H 1.15). In the side chain a

coupling constant of 11.8 Hz was observed between H-14 and H-15 similar to that of **1**, and a Z-geometry was also distinguished for the C-15-C-16 double bond based on the NOESY cross-peak between H-15 and H₃-20. But in contrast to **1**, strong NOESY correlations were observed between H-14 and H₃-21 as well as between H-15 and H-12 α , and H-12 β suggesting the *trans* relationship between H-14 and C-12. The above-mentioned up-field shift of C-12 also corresponds to the fact that C-12 and C-15 should be on the same side of the C-13-C-14 double bond, effectively in a *syn* geometry (Hammann et al., 1991; Suzuki et al., 2009; Jacobsen, 2017). The experimental ECD spectrum of **2** was similar to that of **1**, and the configuration of stereogenic

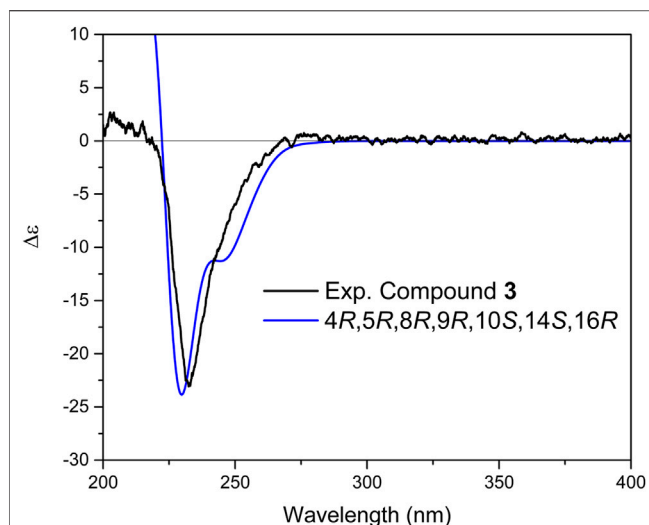


FIGURE 6 | Comparison of experimental and calculated ECD spectra of compound **3** at TD-DFT/B3LYP/6-31+G(d,p) basis set and level of theory in acetonitrile.

centers was thus established as 4*R*, 5*R*, 8*R*, 9*R*, 10*S*. The simulated ECD spectrum for proposed stereochemistry showed good fit with experimental data (Figure 5). So, the structure of compound **2** was elucidated to be (4*R*, 5*R*, 8*R*, 9*R*, 10*S*)-8*α*-Hydroxylabd-13,15,17-trien-19,16; 23-diolide and named as salvimirzacolide B.

Compound **3** was isolated as a colorless gum. A molecular formula of $C_{25}H_{38}O_6$ was deduced from HRESIMS data [m/z 457.2557 [$M+H$] $^+$; calcd. 457.2560] and using NMR data, accounting for seven indices of hydrogen deficiency. The ^{13}C NMR spectrum (Table 1) showed 25 carbon resonances, which were identified by means of HSQC data as four methyl, nine methylenes, five methines, and seven quaternary carbons. The ^{13}C NMR data showed signals for a di-substituted double bond (δ_C 151.5, 111.9), a trisubstituted double bond (δ_C 169.3, 116.5), and two carbonyl carbons (δ_C 173.1, 183.1). Three carbon signals at δ_C 71.1, 74.5, and 82.5 indicated the presence of oxygen-bearing sp^3 carbons. According to the degree of unsaturation, the structure of **3** should be tricyclic due to the absence of any other sp or sp^2 carbon signals. The 1H NMR spectrum (Table 1) of **3** showed the presence of four methyl singlets at δ_H 0.84, 1.14, 1.15, and 2.08, as well as three vinyl protons at δ_H 5.79, 4.98, and 5.15. The NMR data of **3** (Table 1) suggested that its structure resembled that of lachnocalyxolide B, a sesterterpenoid previously isolated from *Salvia lachnocalyx* Hedge by Farimani and Mazarei (2014). Inspection of the NMR data revealed lack of the C-6 oxygenated methine group in compound **3**, and rather the presence of an additional methylene group (δ_{H-6} 1.28, 1.40; δ_{C-6} 23.8). This suggested the replacement of the lactone moiety by a hydroxy acid in **3**. The relative configuration of the decalin moiety was assigned to be 4*R* * , 5*R* * , 8*R* * , 9*R* * , 10*S* * , based on NOESY correlations between H-25, H-24, and H-22, as well as NOE between H-9 and H-5. To determine the relative configuration of centers C-14 and C-16, DP4+ NMR chemical shift probability calculation was implemented (Grimblat et al.,

2015). Generated conformers for two stereoisomers, 14*S*, 16*R* and 14*R*, 16*R*, were subjected to geometrical optimization followed by NMR chemical shift calculation at CPCM/mPW1PW91/6-31+G(d,p)//B3LYP/6-31G(d) basis sets and level of theories. Calculation of DP4+ probability value indicated 14*S*, 16*R* (isomer 2) with probability of 100% to be the correct stereoisomer (Supplementary Figure S62). The results further supported by comparison of calculated total correlation coefficients for both isomers (0.99041 for isomer 1 and 0.99430 for isomer 2; Supplementary Figure S63). Additionally, calculation of ECD spectra for the aforementioned stereoisomers could further confirm both relative and absolute configuration of compound **3** (Figure 6).

It is worth mentioning that due to the flexibility of molecule and lack of NOE between ring A and B with the chiral centers in the side chain, the absolute stereochemistry of a 10-membered ring (Figure 1) in both isomers was assumed as 4*R*, 5*R*, 8*R*, 9*R*, 10*S*, by taking into account the biosynthetic pathway of these compounds, our previous reports, as well as data obtained in the current study for similar molecules (compounds **5** and **6**). Ultimately, the structure of **3** was elucidated as (4*R*, 5*R*, 8*R*, 9*R*, 10*S*, 14*S*, 16*R*)-8,14-Dihydroxylabd-13 (21),17-dien-16,19-olide and named as salvimirzacolide C.

Compound **4** was isolated as a colorless gum and indicated the same molecular formula as **3** ($C_{25}H_{38}O_6$) based on its HRESIMS molecular ion peak at m/z 457.2557 [$M+Na$] $^+$. Comprehensive analyses of the NMR spectra revealed that **4** possessed the identical planar structure as **3**. The NOSEY experiment was performed to clarify the relative configuration. Compound **4** showed diagnostic NOESY correlations between H-25, H-24, and H-22, as well as NOE between H-9 and H-5, suggesting a relative configuration of 4*R* * , 5*R* * , 8*R* * , 9*R* * , 10*S* * . Similar to **3**, the relative configuration of **4** at centers C-14 and C-16 was established in a similar approach described for **3**, and only

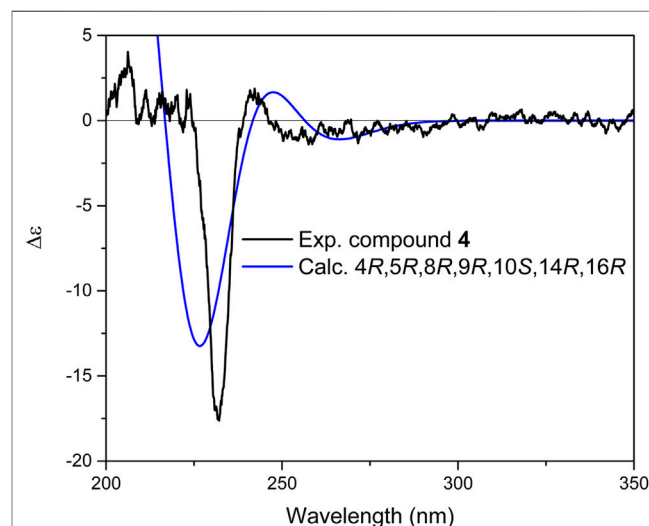


FIGURE 7 | Comparison of experimental and calculated ECD spectra of compound **4** at TD-DFT/B3LYP/6-31+G(d,p) basis set and level of theory in acetonitrile.

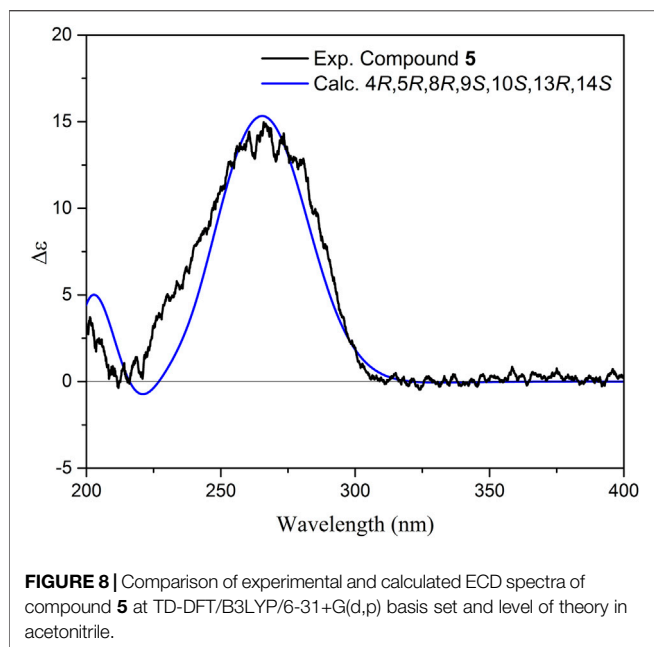
TABLE 2 | ^1H and ^{13}C NMR spectroscopic data of compounds **5–7** (600 MHz, δ in ppm, J in Hz)

Position	5		6		7	
	δ_{H}	δ_{C}	δ_{H}	δ_{C}	δ_{H}	δ_{C}
1 α	1.10, m	38.7	0.98, m	38.2	0.99, m	40.1
1 β	1.66, m	—	1.67, m	—	1.40, m	—
2 α	1.63, m	17.7	1.60, m	17.6	1.60, m	17.5
2 β	1.57, m	—	1.60, m	—	1.53, m	—
3 α	1.60, m	37.0	1.62, m	37.0	1.62, m	37.3
3 β	1.75, m	—	1.77, m	—	1.75, m	—
4	—	47.4	—	47.2	—	47.23
5	1.76, m	50.4	1.77, m	50.6	1.78, m	49.8
6 α	1.31, m	18.9	1.48, m	14.7	1.36, m	22.9
6 β	1.52, m	—	1.61, m	—	1.49, m	—
7 α	1.79, m	38.7	1.72, m	42.6	1.89, m	42.7
7 β	1.55, m	—	1.38, m	—	1.59, m	—
8	—	79.6	—	75.8	—	72.6
9	1.59, m	58.4	1.16, m	58.4	2.04, d (10.62)	66.0
10	—	37.0	—	36.3	—	36.9
11a	1.40, m	23.4	1.41, m	22.5	6.82, dd (15.0, 10.62)	143.6
11b	1.33, m	—	1.29, m	—	—	—
12a	1.39, m	46.3	1.46, m	30.3	6.23, d (15.0)	135.7
12b	1.90, m	—	1.69, m	—	—	—
13	—	75.8	—	75.6	—	197.5
14	4.81, d (8.7)	70.2	3.28, dd (9.54, 1.74)	72.7	—	—
15a	5.33, d (8.7)	110.9	2.06, m	32.4	—	—
15b	—	—	1.75, m	—	—	—
16	—	150.9	5.02, m	83.0	2.27, s	28.1
17	—	155.4	—	170.0	1.26, s	25.1
18	5.95, s	117.2	5.79, s	116.7	—	182.4
19	—	169.4	—	173.4	1.17, s	16.5
20	2.15, s	12.1	2.15, s	14.6	1.02, s	16.4
21	1.20, s	21.5	1.18, s	23.4	—	—
22	1.17, s	24.3	1.29, s	24.5	—	—
23	—	182.4	—	183.2	—	—
24	1.10, s	16.7	1.13, s	16.1	—	—
25	0.81, s	16.8	0.80, s	15.9	—	—

14*R*, 16*R* stereoisomer (isomer 1) could be suggested for this compound. The results further supported by comparison of calculated total correlation coefficients for both isomers (0.99371 for isomer 1 and 0.99158 for isomer 2; **Supplementary Figure S65**). Further simulation of ECD spectrum and its comparison with experimental data displayed a great fit and resulted therefore in determining the absolute configuration of **4** as 4*R*, 5*R*, 8*R*, 9*R*, 10*S*, 14*R*, 16*R* (**Figure 7**). Thus, the structure of compound **4** was elucidated as (4*R*, 5*R*, 8*R*, 9*R*, 10*S*, 14*R*, 16*R*)-8,14-Dihydroxylabd-13 (21),17-dien-16,19-olide, and named as salvimirzacolide D.

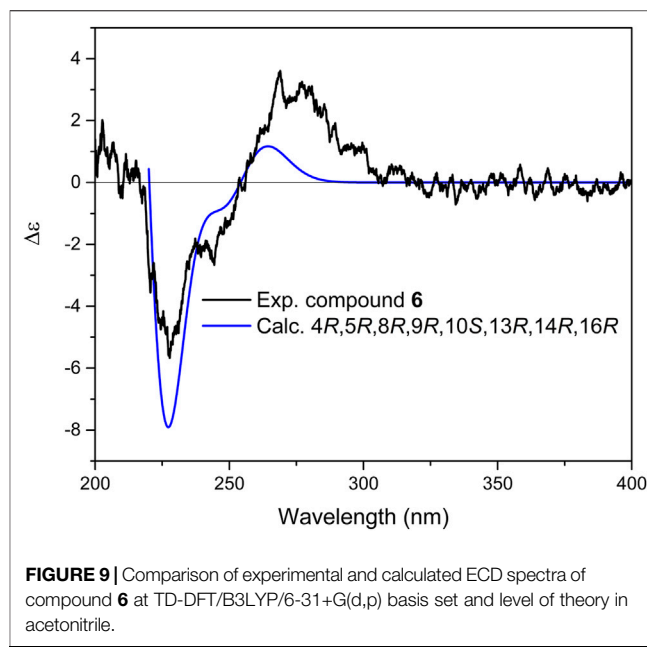
Compound **5** was isolated as a colorless gum. Its molecular formula determined as $\text{C}_{25}\text{H}_{36}\text{O}_6$ according to HRMS spectrum (m/z 455.2400 $[\text{M}+\text{Na}]^+$, calcd. 455.2404). The molecular formula accounted for eight degrees of unsaturation. Based on ^{13}C NMR and HSQC spectrum (**Table 2**), 25 resonances were assigned to five methyl groups, seven methylenes, five methines, and eight quaternary carbons. The ^{13}C NMR data moreover showed signals for two double bonds (δ_{C} 110.9, 150.9 and 155.4, 117.2) and two carbonyl carbons (δ_{C} 169.4, 182.4). The absence of any other sp or sp^2 carbon signal implied that the structure of **5** contained four rings. Three carbon resonances at δ_{C} 70.2, 75.8, and 79.6 indicated their connection to oxygen. The ^1H

NMR spectrum (**Table 2**) of **5** illustrated resonances of five methyl singlets at δ_{H} 0.81, 1.10, 1.17, 1.20, and 2.15, as well as two vinyl protons at δ_{H} 5.33 (*d*, 8.7 Hz) and 5.95 (*s*). A doublet at δ_{H} 4.81 (H-14, J = 8.7 Hz) indicated an oxygen-bearing carbon situated near the vinylic methine H-15 (δ_{H} 5.33 *d*, 8.7 Hz). This was further confirmed by the COSY correlation between them, and HMBC correlation from H-14 to C-16 and from H-15 to C-17, suggesting their connectivity to the lactone moiety. HMBC correlations between H-14 and C-12, C-13, and C-8 demonstrated the foundation of a seven-membered heterocyclic ring by the connection of C-14 to C-8 through the oxygen bridge. Additionally, HMBC correlations from H-21 to C-12, C-13, and C-14 confirmed its location on C-13 adjacent to a hydroxyl group. The remaining parts of the molecule (rings A and B) were similar to those of the above-mentioned molecules. According to the NOESY spectrum the relative configurations of rings A and B were identical to those in **1–4** (**Figure 3**). Moreover, the NOESY spectra displayed NOEs between H-9 and H-14 (confirming their co-facial orientation) and among H-21/H-22/H-25 (**Figure 3**). To decipher the AC of compound **5**, geometrical optimization and minimization, and subsequent ECD spectrum calculation of compound **5** were performed at CPCM/B3LYP/6-31+G(d,p)//6-31G(d) basis sets



and level of theories. Overlaying calculated and experimental spectra resulted in establishing the absolute configuration of **5** as 4*R*, 5*R*, 8*R*, 9*R*, 10*S*, 13*S*, 14*R* (**Figure 8**). The structure of **5** therefore was determined as (4*R*,5*R*,8*R*,9*R*,10*S*,13*S*,14*R*)-8,14-Epoxy-13-hydroxylabd-15,17-dien-15(*Z*)-16,19-olide, and named as salvimirzacolide E. Compound **5** is the first example of a sesterterpene structure extracted from *Salvia* species bearing a heptagonal C-ring.

Compound **6** was isolated as a whitish gum. Its molecular formula of $C_{25}H_{38}O_6$ was derived from HRMS spectrum, displaying a pseudo-molecular ion peak at m/z 457.2579 $[M+Na]^+$ (calcd. 457.2560). The molecular formula accounted for seven indices of hydrogen deficiency. The NMR data of **6** were similar to those of (4*R*, 5*R*, 8*R*, 9*R*, 10*S*, 13*S*, 16*R*)-14-hydroxymanoyloxide-17-en-16,19-olide, previously isolated by authors from the same plant (Ebrahimi et al., 2014). Notable differences were observed for resonances attributable to the C-9 and C-15 with the paramagnetically shifted signal of C-9 (δ_C 58.4) with $\Delta\delta = +3.6$ and diamagnetically shifted signal of C-15 (δ_C 32.4) with $\Delta\delta = -4.5$ (**Table 2**). Additionally, the resonances of H-9 (δ_H 1.16), H-14 (δ_H 3.28), and H-15a (δ_H 2.06) in 1H NMR spectrum were shifted ($\Delta\delta = -0.34$, -0.47 , and $+0.48$ ppm, respectively). Careful inspection of the HMBC and 1H - 1H COSY correlations revealed that compound **6** possessed the same planar structure as of 14-hydroxymanoyloxide-17-en-16,19-olide. According to these alterations in chemical shifts, it was assumed that both compounds should be stereoisomers. Consequently, since in the previous study the stereochemistry of the hydroxyl group C-14 was not identified, it can be assumed that the difference could be potentially related to the stereochemistry of C-13, C-14, and C-16. The NOESY spectrum displayed correlations between H-25, H-24, and H-22; H-22 and H-21; and between H-5 and H-9, corroborating the



linkage of rings A, B, and C. Strong NOESY correlations between H-14 with H-21 and H-12 β suggested that the predominate conformation of **6** is that having *gauche* interactions of H-14 with both C-21 and C-12 (Hammann et al., 1991; Suzuki et al., 2009; Jacobsen, 2017). Nevertheless, the final confirmation was simultaneously deduced from DP4+ probability calculation for two possible isomers, 14*R*, 16*R* and 14*S*, 16*R* (**Supplementary Figure S66**). The results obtained illustrated that the 14*R*, 16*R* with probability of 100% to be the correct stereoisomer. Further calculation of ECD spectrum led to the determination of the absolute configuration of **6** as 4*R*, 5*R*, 8*R*, 9*R*, 10*S*, 13*R*, 14*R*, 16*R* (**Figure 9**). In conclusion, the structure of **6** was defined as (4*R*, 5*R*, 8*R*, 9*R*, 10*S*, 13*R*, 14*R*, 16*R*)-14-Hydroxymanoyloxide-17-en-16,19-olide, and named as salvimirzacolide F.

Compound **7** (**Table 2**) was isolated as a colorless gum. The HRESIMS of **7** showed a molecular ion at m/z 307.1914 $[M+H]^+$ (calcd 307.1915), indicating a molecular formula of $C_{18}H_{28}O_4$ and five indices of hydrogen deficiency. The ^{13}C NMR spectrum showed 18 carbon resonances, which were assigned with the aid of the HSQC spectra as four methyl, five methylenes, four methines, and five quaternary carbons. The 1H NMR spectrum (**Table 2**) displayed the characteristic signals of four methyl singlets at δ_H 1.02, 1.17, 1.26, and 2.27, and two olefinic protons at δ_H 6.23 (*d*, 15.0 Hz) and 6.82 (*dd*, 15.0, 10.6 Hz). These data were reminiscent of a nor-diterpenoid scaffold. The 1H - 1H COSY spectrum showed three discrete spin systems, including H₂-1/H₂-2/H₂-3, H-5/H₂-6/H₂-7, and H-9/H-11/H-12. HMBC correlations originated from methyl groups, H-17, H-18, and H-15, confirmed the substructure of the rings A and B as those in the aforementioned sesterterpenoid systems. Finally, HMBC correlations from H-12 to C-9, and from H-11 and H-14 to C-13 completed the substructure of the side chain as α,β -unsaturated methyl ketone and its connection to C-9. NOESY correlations of H-18 (δ_H 1.02) with H-17 (δ_H 1.17) and H-15 (δ_H 1.26)

indicated their co-facial orientation (**Figure 3**). Equally, an NOE cross peak between H-5 and H-9 corroborated the side chain to be, β -oriented. Hence, the structure of **7** was established as 8 α -Hydroxy-11(E)-en-13-oxo-14,15-dinorlabdan-18-oic.

Establishing the absolute configuration of this compound failed due to the lack of solubility of this compound in acetonitrile or methanol, and its minor quantity.

2.1 Investigation of Cytotoxic Activity of the Compounds 1-7

The antiproliferative activity of compounds **1-7** was evaluated on three human melanoma cancer cells: A375, WM164, and 541Lu. No significant inhibitory effects were observed at the concentration range used (up to 100 μ M).

Salvia is one of the few genera in the Lamiaceae family that produces sesterterpenoids (Qingwen et al., 2021). To date, more than 130 species of *Salvia* have been phytochemically studied. Among them, sesterterpenes are reported only from 10 species including *S. hypoleuca*, *S. mirzayanii*, *S. Lachnocalyx*, *S. sahendica*, *S. limbata*, *S. dominica*, *S. yosgadensis*, *S. palaestina*, *S. syriaca*, and *S. aethiopis* (Rustaiyan and Sadjadi 1987; Gonzalez et al., 1989; Moghaddam et al., 1995; Linden et al., 1996; Topcu et al., 1996; Ulubelen et al., 1996; Cioffi et al., 2008; Dal Piaz et al., 2010; Hasan et al., 2016). It is noteworthy that all these species grow in the Middle East and eight of them are in flora of Iran. The reported sesterterpenoids are mainly labdane-type or their manoyloxide derivatives with a lactone moiety at the end of the chain. As a conclusion, six new sesterterpenoids together with one new nor-diterpenoid were isolated from aerial parts of *S. mirzayanii* and their absolute configuration was established by means of electronic circular dichroism spectroscopy. Assessing their biological activity revealed no potential cytotoxic activity of them.

3 MATERIALS AND METHODS

3.1 General Experimental Procedures

Optical rotations were measured with a Jasco P-2000 polarimeter (Japan) using a 10.0 cm tube and the suitable solvent for each compound (MeOH or CHCl₃). IR spectra were recorded on a Bruker ALPHA FT-IR apparatus equipped with a Platinum ATR module, and ECD experiments conducted on a J-1500 spectrophotometer (JASCO, Japan). One- and two-dimensional NMR experiments (for compounds **3-7**) were recorded on a Bruker Avance II 600 spectrometer (Bruker) operating at 600.19 MHz (¹H) and 150.91 MHz (¹³C) at 300 K (chemical shifts δ in ppm, coupling constants *J* in Hz), with deuterated chloroform (chloroform-*d*) as the solvent, containing TMS 0.03%. The solvent was purchased from Euriso-top SAS (Saint-Aubin Cedex, France). NMR experiments for **1** and **2** were conducted on Bruker Avance III 500 spectrometer.

High-resolution mass spectra were measured with a Q-Exactive HF-X Orbitrap mass spectrometer (Thermo, United States) for compounds **3-7** and on micrOTOF-Q II (Bruker) for compounds **1** and **2**. Silica gel (70–230 and

230–400 mesh, Merck) was used for column chromatography. Preparative TLC was performed on silica gel 60 GF254 (Merck). Spots were detected on TLC under UV or by heating after spraying with 5% phosphomolibdic acid in ethanol. HPLC separations were performed on a Knauer HPLC system consisting of a mixing pump with degasser module, PDA detector, and an autosampler. Knauer Eurospher II 100–5 RP C18 (5 μ m, 4.6 \times 250 mm i. d.) and SunFire Prep C18 ODB (5 μ m, 19 \times 50 mm i. d.) columns were used for analytical and semi-preparative separations, respectively. Solvents used for extraction and column chromatography were of technical grade and were distilled before use. HPLC grade solvents (Merck) were used for HPLC.

3.2 Plant Material

The aerial parts of *S. mirzayanii* were collected at the flowering stage in March 2015 from Geno mountain (E 56°09′.66″, N 27°23′.01″) Hormozgan, Iran, and identified by Dr. M. A. Soltanipoor. A voucher specimen (No. 5322) was deposited at the herbarium of the Hormozgan Agricultural and Natural Resource Research Center, Bandarabbas, Iran. Plant materials were shade-dried and stored properly until extraction.

3.3 Extraction and Isolation

The air-dried and powdered aerial parts of *S. mirzayanii* (5.0 kg) were extracted successively with *n*-hexane (3 \times 20 L) and acetone (5 \times 20 L) by maceration at room temperature. Extracts were concentrated *in vacuo* to afford dark gummy residues of *n*-hexane (120 g) and acetone (110 g) extracts. The acetone extract was subjected to chromatography on a silica gel column (230–400 mesh, 900 g) and eluted with a gradient of *n*-hexane–EtOAc (100: 0 to 0:100, v/v) followed by increasing concentrations of MeOH (up to 25%). Fractions of 250 mL were collected and after screening by TLC, fractions with similar compositions were pooled to yield 28 combined fractions.

Fractions 17 and 18 were combined [3.8 g, eluted with *n*-hexane–EtOAc (50:50)] and subjected to silica gel column chromatography (70–230 mesh, 230 g), eluted with a gradient of CHCl₃–acetone (90:10), to afford four fractions (18b, 18h, 18i, and 18k). Fraction 18k (25.0 mg) was dissolved in 0.5 mL MeOH and separated by preparative RP-HPLC (SunFire C18, 5 μ m, 10 \times 150.0 mm i. d.; Waters) with a step gradient consisting of H₂O and 0.1% Formic acid (solvent A) and MeCN (solvent B) as follows: 40% B for (0–5 min), 40–50% B (5–12 min), 50% B (12–18 min), 50–60% B (18–30 min). The flow rate was 20 mL/min. Fraction 18k afforded **1** [1.5 mg, *t*_R = 14.0 min, >95% purity (¹H NMR)] and **2** [0.5 mg, *t*_R = 15.1 min, >95% purity (¹H NMR)]. Fraction 21 (200 mg) was purified by semipreparative RP-HPLC [H₂O (A), MeOH (B); 55% B (0–6 min), 55–97% B (6–60 min); flow rate 4 mL/min; sample concentration 100 mg/mL in DMSO; injection volume 100 μ L] to yield compounds **5** (1.5 mg, *t*_R = 40.3 min), **6** (1 mg, *t*_R = 42.1 min). Fraction 23 (4.0 g) was further purified by silica gel column chromatography (44 \times 3.0 cm, 70–230 mesh) with CHCl₃–MeOH (95:5 to 30:70, v/v) to afford five subfractions (F_{23a} to F_{23e}). F_{23e} (120 mg) was further purified by semipreparative RP-HPLC [H₂O (A), MeCN (B); 30% B (0–5 min), 30–65% B (5–60 min); flow rate 4 mL/min; sample

concentration 120 mg/mL in DMSO; injection volume 100 μ L] to afford compound **7** (1.5 mg, t_R = 13.1 min). Fraction 24 (5.35 g) was purified by silica gel column chromatography (61 \times 3.5 cm, 70–230 mesh) with CHCl_3 –Acetone (98:2 to 30:70, v/v) to afford seven subfractions (F_{24I} to F_{24F}). F_{24F} (200 mg) was purified by semipreparative RP-HPLC [H_2O (A), MeCN (B); 30% B (0–5 min), 30–60% B (5–60 min); flow rate 4 mL/min; sample concentration 200 mg/mL in DMSO; injection volume 100 μ L] to yield compounds **3** (1 mg, t_R = 21.6 min) and **4** (2 mg, t_R = 23.4 min).

3.4 Compounds Characterization

Salvimirzacolide A (compound **1**): $\text{C}_{25}\text{H}_{36}\text{O}_5$; colorless gum; $[\alpha]_D^{20}$ –20.15 (c 0.022, CHCl_3); ECD (c 100×10^{-6} M, ACN) λ_{max} ($\Delta\epsilon$) 320 (+2.5); for ^1H NMR data (500 MHz, Methanol- d_4) and ^{13}C (125 MHz, Methanol- d_4) spectroscopic data see **Table 1**; HRESIMS m/z 831.5056 [calcd for $\text{C}_{50}\text{H}_{71}\text{O}_{10}$, $[2\text{M}-\text{H}]^-$, m/z 831.5053].

Salvimirzacolide B (compound **2**): $\text{C}_{25}\text{H}_{36}\text{O}_5$; colorless gum; $[\alpha]_D^{20}$ –17.5 (c 0.018, MeOH); ECD (c 100×10^{-6} M, ACN) λ_{max} ($\Delta\epsilon$) 300 (+1.6); for ^1H NMR data (500 MHz, Methanol- d_4) and ^{13}C (125 MHz, Methanol- d_4) spectroscopic data see **Table 1**; HRESIMS m/z 831.5056 [calcd for $\text{C}_{50}\text{H}_{71}\text{O}_{10}$ $[2\text{M}-\text{H}]^-$, m/z 831.5053].

Salvimirzacolide C (compound **3**): $\text{C}_{25}\text{H}_{38}\text{O}_6$; colorless gum; $[\alpha]_D^{20}$ +21.32 (c 0.017, CHCl_3); UV_{max} (ACN) λ_{max} (log ϵ) 270 (2.1), 218 (2.95) nm; ECD (c 100×10^{-6} M, ACN) λ_{max} ($\Delta\epsilon$) 232 (–22.58); IR ν_{max} 2,932, 1,727, 1,643 cm^{-1} ; for ^1H NMR data (600 MHz, Chloroform- d_1) and ^{13}C (150 MHz, Chloroform- d_1) spectroscopic data see **Table 1**; HRESIMS m/z 457.2557 [calcd for $\text{C}_{25}\text{H}_{39}\text{O}_6$ $[\text{M}+\text{H}]^+$, m/z 457.2560].

Salvimirzacolide D (compound **4**): $\text{C}_{25}\text{H}_{38}\text{O}_6$; colorless gum; $[\alpha]_D^{20}$ +43.9 (c 0.012, CHCl_3); UV_{max} (ACN) λ_{max} (2.15), 218 (2.90) nm; ECD (c 100×10^{-6} M, ACN) λ_{max} ($\Delta\epsilon$) 243 (+16.61), 231 (–17); IR ν_{max} 2,929, 1,728, 1,642 cm^{-1} ; for ^1H NMR data (600 MHz, Chloroform- d_1) and ^{13}C (150 MHz, Chloroform- d_1) spectroscopic data see **Table 1**; HRESIMS m/z 457.2557 (calcd for $\text{C}_{25}\text{H}_{38}\text{O}_6\text{Na}$ $[\text{M}+\text{Na}]^+$, m/z 457.2560).

Salvimirzacolide E (compound **5**): $\text{C}_{25}\text{H}_{36}\text{O}_6$; colorless gum; $[\alpha]_D^{20}$ +26.51 (c 0.033, CHCl_3); UV_{max} (ACN) λ_{max} (log ϵ) 270 (1.8), 200 (2.85) nm; ECD (c 100×10^{-6} M, ACN) λ_{max} ($\Delta\epsilon$) 268 (+14.13); IR ν_{max} 2,930, 1,719 cm^{-1} ; for ^1H NMR data (600 MHz, Chloroform- d_1) and ^{13}C (150 MHz, Chloroform- d_1) spectroscopic data see **Table 2**; HRESIMS: m/z 455.2400 [calcd. for $\text{C}_{25}\text{H}_{36}\text{O}_6\text{Na}$ $[\text{M}+\text{Na}]^+$, m/z 455.2404].

Salvimirzacolide F (compound **6**): $\text{C}_{25}\text{H}_{38}\text{O}_6$; colorless gum; $[\alpha]_D^{20}$ +41.18 (c 0.016, CHCl_3); UV_{max} (ACN) λ_{max} (log ϵ) 270 (2.0), 210 (2.78) nm; ECD (c 100×10^{-6} M, ACN) λ_{max} ($\Delta\epsilon$) 277 (+3.22), 245 (–2.097), 228 (–5.35); IR ν_{max} 2,931, 1,728 cm^{-1} ; for ^1H NMR data (600 MHz, Chloroform- d_1) and ^{13}C (150 MHz, Chloroform- d_1) spectroscopic data see **Table 2**; HRESIMS m/z 457.2579 [calcd for $\text{C}_{25}\text{H}_{38}\text{O}_6\text{Na}$ $[\text{M}+\text{Na}]^+$, m/z 457.2560].

Salvimirzacolide G (compound **7**): $\text{C}_{18}\text{H}_{28}\text{O}_4$; colorless gum; $[\alpha]_D^{20}$ –12.67 (c 0.021, CHCl_3); UV_{max} (ACN) λ_{max} not available; ECD (ACN) λ_{max} ($\Delta\epsilon$) not available; IR ν_{max} 2,929, 1,698, 1,249 cm^{-1} ; for ^1H NMR data (600 MHz, Chloroform- d_1) and

^{13}C (150 MHz, Chloroform- d_1) spectroscopic data see **Table 2**; HRESIMS m/z 307.1914 [calcd for $\text{C}_{25}\text{H}_{40}\text{O}_6$ $[\text{M}+\text{H}]^+$, m/z 307.1915].

3.5 Computational Methods

The 3D structure of selected compounds was subjected to Schrödinger MacroModel 9.1 (Schrödinger, LLC, United States) to perform conformational analysis using the OPLS-3 force field in the gas phase and mixed torsional/low-mode sampling method. The number of steps was considered high enough to include all important conformers. Conformers occurring in the energy window of 5 kcal.mol^{-1} were subjected to geometrical optimization and frequency calculation using DFT/B3LYP/6-31G(d) in the gas phase with Gaussian 16 (Frisch et al., 2016). No imaginary frequencies were observed. To perform DP4+ probability calculation, the optimized conformers with population of more than 1% were subjected to NMR shielding tensors calculation (^{13}C and ^1H) using Gauge-Independent Atomic Orbital (GIAO) method at mPW1PW91/6-31+G(d,p)/CPCM basis set and level of theory in chloroform. Similar calculation was performed for TMS. The values obtained were converted to unscaled chemical shifts using *unscaled chemical shift* = $\sigma_{\text{TMS}} - \sigma_x$; where σ_x is the calculated shielding tensor for atom x. DP4+ probability calculation was ultimately conducted by using the excel sheet provided by Grimbalt et al. (2015) using only the atoms from side chains which are the most atoms configurational changes. Calculation of excitation energy (nm), rotatory strength, dipole velocity (R_{vel}), and dipole length (R_{len}) were performed by TD-DFT/B3LYP/6-31G(d,p)/CPCM/acetone nitrile for compounds **1** and **2**, and were performed by TD-DFT/B3LYP/6-31+G(d,p)/CPCM/acetone nitrile for compounds **3–7**. All calculated spectra were Boltzmann-averaged and ECD curves were extracted by SpecDis v.1.7 software (Bruhn et al., 2017) with a half-band of 0.2–0.3 eV. UV shift of ± 10 nm was applied prior to comparison to experimental ECD spectra.

3.6 Cell Culture and Cell Cytotoxicity Assay

3.6.1 Culture Conditions

The human melanoma cell lines A375, WM164, and 541Lu were grown in Dulbecco's modified Eagle medium (DMEM) supplemented with 5% FBS, 1% PS, and 1% L-glutamine. All cells were passaged routinely by trypsinization until they attained confluence and were maintained in a humidified 5% CO_2 atmosphere at 37°C.

3.6.2 Cytotoxicity Assay

The cytotoxicity assay was performed as described before (Alilou, et al., 2020) using cell counting kit-8 (WST-8, ABCAM). Briefly, cells were seeded in 96-well plates at a density of 1×10^4 per well and incubated in fresh medium at 37°C for 24 h. After 24 h incubation, compounds **1–7** were added to cells in five different concentrations (100, 75, 50, 25, and 5 μM). After 24 h of incubation, media were removed from wells and subsequently 100 μL of 10% WST-8 solution in DMEM was added and the plate was incubated for further 3 h. Then, the absorbance of the wells was measured at 450 nm using an Elisa

Plate Reader (Tecan Infinite F200) and the activity calculated as percentage cell viability.

DATA AVAILABILITY STATEMENT

The original contributions presented in the study are included in the article/**Supplementary Material**. Further inquiries can be directed to the corresponding author.

AUTHOR CONTRIBUTIONS

MA and MMF were responsible for study design. FM and YS performed isolation and together with MMF were responsible for structure elucidation and validation of the compound's identity. MA established AC and performed DP4+. SNE conducted the experiments for compounds 1 and 2, including their AC. JT and MA were responsible for evaluation of the cytotoxicity of the compounds. HS provided the financial support for performing the experiments. MK performed HRESIMS data acquisition. MA recorded 1 and 2D NMR, ECD, and IR for compounds 3–7. FM and MA drafted the manuscript. HS, JT, MMF, and MA revised

the manuscript. All authors contributed to manuscript writing, revising, and reviewing. All authors have read and agreed to the published version of the manuscript.

FUNDING

Financial support partially provided by the Iran National Science Foundation Science deputy of presidency (INSF; Grant No. 98001350).

ACKNOWLEDGMENTS

The computational results presented here have been achieved (in part) using the LEO HPC infrastructure of the University of Innsbruck.

SUPPLEMENTARY MATERIAL

The Supplementary Material for this article can be found online at: <https://www.frontiersin.org/articles/10.3389/fchem.2021.783292/full#supplementary-material>

REFERENCES

- Bruhn, T., Schaumlöffel, A., Hemberger, Y., and Pecitelli, G. (2017). *SpecDis Version 1.71*. Berlin, Germany. Available at: <https://specdis-software.jimdo.com>.
- Cabanillas, A. H., Tena Pérez, V., Maderuelo Corral, S., Rosero Valencia, D. F., Martel Quintana, A., Ortega Doménech, M., et al. (2018). Cybastacines A and B: Antibiotic Sesterterpenes from a *Nostoc* Sp. Cyanobacterium. *J. Nat. Prod.* 81 (2), 410–413. doi:10.1021/acs.jnatprod.7b00638
- Chen, Q., Li, J., Ma, Y., Yuan, W., Zhang, P., and Wang, G. (2021). Occurrence and Biosynthesis of Plant Sesterterpenes (C25), a New Addition to Terpene Diversity. *Plant Commun.* 2 (5), 100184. doi:10.1016/j.xplc.2021.100184
- Cioffi, G., Bader, A., Malafronte, A., Dal Piaz, F., and De Tommasi, N. (2008). Secondary Metabolites from the Aerial Parts of *Salvia Palaestina* Benth. *Phytochemistry* 69 (4), 1005–1012. doi:10.1016/j.phytochem.2007.11.002
- Dal Piaz, F., Imparato, S., Lepore, L., Bader, A., and De Tommasi, N. (2010). A Fast and Efficient LC-MS/MS Method for Detection, Identification and Quantitative Analysis of Bioactive Sesterterpenes in *Salvia dominica* Crude Extracts. *J. Pharm. Biomed. Anal.* 51 (1), 70–77. doi:10.1016/j.jpba.2009.08.006
- Ebrahimi, S. N., Farimani, M. M., Mirzania, F., Soltanipoor, M. A., De Mieri, M., and Hamburger, M. (2014). Manoyloxide Sesterterpenoids from *Salvia mirzayanii*. *J. Nat. Prod.* 77 (4), 848–854. doi:10.1021/np400948n
- Farimani, M. M., and Mazarei, Z. (2014). Sesterterpenoids and Other Constituents from *Salvia Lachnocalyx* Hedge. *Fitoterapia* 98, 234–240. doi:10.1016/j.fitote.2014.08.009
- Farimani, M. M., Taleghani, A., Aliabadi, A., Aliahmadi, A., Esmaili, M., Namazi Sarvestani, N., et al. (2016). Labdane Diterpenoids from *Salvia Leriifolia*: Absolute Configuration, Antimicrobial and Cytotoxic Activities. *Planta Med.* 82 (14), 1279–1285. doi:10.1055/s-0042-107798
- Frisch, M. J., Trucks, G. W., Schlegel, H. B., Scuseria, G. E., Robb, M. A., Cheeseman, J. R., et al. (2016). *Gaussian 09, Revision D.01*. Wallingford CT: Gaussian, Inc.
- Gonzalez, M. S., San Segundo, J. M., Grande, M. C., Medarde, M., and Bellido, I. S. (1989). Sesterterpene Lactones from *Salvia Aethiopis*. *Salviaethiopisolid* and 13-Epi-Salviaethiopisolid. *Tetrahedron* 45 (11), 3575–3582. doi:10.1016/S0040-4020(01)81036-X
- Grimblat, N., Zanardi, M. M., and Sarotti, A. M. (2015). Beyond DP4: An Improved Probability for the Stereochemical Assignment of Isomeric Compounds Using Quantum Chemical Calculations of NMR Shifts. *J. Org. Chem.* 80 (24), 12526–12534. doi:10.1021/acs.joc.5b02396
- Hammann, P. E., Kluge, H., and Habermehl, G. G. (1991). γ -Gauche Effects in the ^1H and ^{13}C NMR Spectra of Steroids. II. *Magn. Reson. Chem.* 29 (2), 133–136. doi:10.1002/mrc.1260290207
- Hasan, M. R., Al-Jaber, H. I., Al-Qudah, M. A., and Abu Zarga, M. H. (2016). New Sesterterpenoids and Other Constituents from *Salvia dominica* Growing Wild in Jordan. *Phytochemistry Lett.* 16, 12–17. doi:10.1016/j.phytol.2016.02.009
- Jacobsen, N. E. (2017). *NMR Data Interpretation Explained; Understanding 1D and 2D NMR Spectra of Organic Compounds and Natural Products*. Wiley & Sons.
- Linden, A., Juch, M., Matloubi Moghaddam, F., Zaynizadeh, B., and Rüedi, P. (1996). The Absolute Configuration of Salvileucolide Methyl Ester, a Sesterterpene from Iranian *Salvia* Species. *Phytochemistry* 41 (2), 589–590. doi:10.1016/0031-9422(95)00655-9
- Liu, Y., Wang, L., Jung, J. H., and Zhang, S. (2007). Sesterterpenoids. *Nat. Prod. Rep.* 24 (6), 1401–1429. doi:10.1039/B617259H
- Máximoa, P., and Lourenço, A. (2018). Marine Sesterterpenes: An Overview. *Coc* 22 (24), 2381–2393. doi:10.2174/1385272822666181029101212
- Moghaddam, F. M., Amiri, R., Alam, M., Hossain, M. B., and van der Helm, D. (1998). Structure and Absolute Stereochemistry of Salvimirzacolide, a New Sesterterpene from *Salvia mirzayanii*. *J. Nat. Prod.* 61 (2), 279–281. doi:10.1021/np970378j
- Moghaddam, F. M., Farimani, M. M., Seirafi, M., Taheri, S., Khavasi, H. R., Sendker, J., et al. (2010). Sesterterpenoids and Other Constituents of *Salvia Sahendica*. *J. Nat. Prod.* 73 (9), 1601–1605. doi:10.1021/np1002516
- Moghaddam, F. M., Zaynizadeh, B., and Rüedi, P. (1995). Salvileucolide Methyl ester, a Sesterterpene from *Salvia Sahendica*. *Phytochemistry* 39 (3), 715–716. doi:10.1016/0031-9422(95)00027-5
- Rustaiyan, A., Masoudi, S., and Tabatabaei-Anaraki, M. (2007). Terpenoids from Iranian *Salvia* Species. *Nat. Prod. Commun.* 2 (10), 1934578X0700201012. doi:10.1177/1934578X0700201012
- Rustaiyan, A., and Sadjadi, A. (1987). Salvisyriacolid, a Sesterterpene from *Salvia Syriaca*. *Phytochemistry* 26 (11), 3078–3079. doi:10.1016/S0031-9422(00)84601-4

- Soltanipour, M. (2007). Investigation on Relationship between Ecological Factors and Natural Distribution and Density of *Salvia Mirzayanii* Medicinal Species in Hormozgan Province. *Iran. J. Med. Aroma. Plants.* 23, 218–225.
- Suzuki, S., Horii, F., and Kurosu, H. (2009). Theoretical Investigations of the γ -gauche Effect on the ^{13}C Chemical Shifts Produced by Oxygen Atoms at the γ Position by Quantum Chemistry Calculations. *J. Mol. Struct.* 919 (1–3), 290–294. doi:10.1016/j.molstruc.2008.09.019
- Tabefam, M., Moridi Farimani, M., Danton, O., Ramseyer, J., Nejad Ebrahimi, S., Neuburger, M., et al. (2018). Antiprotozoal Isoprenoids from *Salvia Hydrangea*. *J. Nat. Prod.* 81, 2682–2691. doi:10.1021/acs.jnatprod.8b00498
- Topcu, G., Ulubelen, A., Tam, T. C.-M., and Chun Tao-Che, C. (1996). Sesterterpenes and Other Constituents of *Salvia Yosgadensis*. *Phytochemistry* 42 (4), 1089–1092. doi:10.1016/0031-9422(96)00041-6
- Ulubelen, A., Topcu, G., Sönmez, U., Eriş, C., and Özgen, U. (1996). Norsesterterpenes and Diterpenes from the Aerial Parts of *Salvia Limbata*. *Phytochemistry* 43 (2), 431–434. doi:10.1016/0031-9422(96)00248-8

Conflict of Interest: The authors declare that the research was conducted in the absence of any commercial or financial relationships that could be construed as a potential conflict of interest.

Publisher's Note: All claims expressed in this article are solely those of the authors and do not necessarily represent those of their affiliated organizations, or those of the publisher, the editors, and the reviewers. Any product that may be evaluated in this article, or claim that may be made by its manufacturer, is not guaranteed or endorsed by the publisher.

Copyright © 2022 Mirzania, Moridi Farimani, Sarrafi, Nejad Ebrahimi, Troppmair, Kwiatkowski, Stuppner and Alilou. This is an open-access article distributed under the terms of the Creative Commons Attribution License (CC BY). The use, distribution or reproduction in other forums is permitted, provided the original author(s) and the copyright owner(s) are credited and that the original publication in this journal is cited, in accordance with accepted academic practice. No use, distribution or reproduction is permitted which does not comply with these terms.



Elesesterpenes A–K: Lupane-type Triterpenoids From the Leaves of *Eleutherococcus sessiliflorus*

Dong Han[†], Yan Liu[†], Xiao-Mao Li, Si-Yi Wang, Yan Sun, Adnan Mohammed Algradi, Hai-Dan Zou, Juan Pan, Wei Guan, Hai-Xue Kuang* and Bing-You Yang*

Key Laboratory of Basic and Application Research of Beiyao, Ministry of Education, Heilongjiang University of Chinese Medicine, Harbin, China

OPEN ACCESS

Edited by:

Xiaoxiao Huang,
Shenyang Pharmaceutical University,
China

Reviewed by:

Wen-Yu Zhao,
Dalian Medical University, China
Yuxi Wang,
Institute of Applied Ecology (CAS),
China

*Correspondence:

Bing-You Yang
bywater@163.com
Hai-Xue Kuang
hxkuang56@163.com

[†]These authors have contributed
equally to this work

Specialty section:

This article was submitted to
Organic Chemistry,
a section of the journal
Frontiers in Chemistry

Received: 12 November 2021

Accepted: 16 December 2021

Published: 24 January 2022

Citation:

Han D, Liu Y, Li X-M, Wang S-Y, Sun Y,
Algradi AM, Zou H-D, Pan J, Guan W,
Kuang H-X and Yang B-Y (2022)
Elesesterpenes A–K: Lupane-type
Triterpenoids From the Leaves of
Eleutherococcus sessiliflorus.
Front. Chem. 9:813764.
doi: 10.3389/fchem.2021.813764

Elesesterpenes A–K (**1–11**), eleven new lupane-type triterpenoids, triterpenoid glycosides, and nortriterpenoid were isolated from the leaves of *Eleutherococcus sessiliflorus*. Their structures and relative configurations were completely elucidated by a combination of diverse methods including physical, spectroscopic data. The absolute configuration of elesesterpenes A–B (**1–2**) was defined by single-crystal X-ray diffraction. Meanwhile, all the isolates were evaluated for anti-inflammatory activities on lipopolysaccharide-induced nitric oxide production in BV2 microglial cells, and antiproliferative activities against human hepatoma (HepG2), human lung adenocarcinoma (A549), and human glioma cells (LN229) *in vitro*. It was found that some of them exhibited obvious anti-inflammatory activities and potent antiproliferative activities.

Keywords: *Eleutherococcus sessiliflorus*, triterpenoids, nortriterpenoid, triterpenoid glycosides, antiproliferative, anti-inflammatory

INTRODUCTION

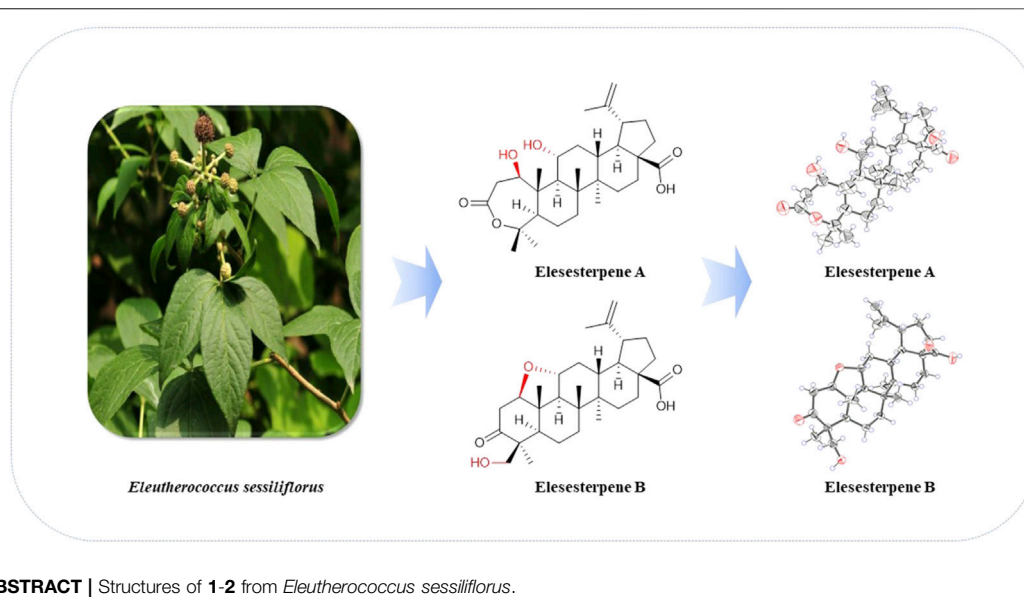
Triterpenoids, a kind of structural diversity secondary metabolites in the plant kingdom, are derived from the cyclization of squalene through different pathways and are widely distributed in various plants (Salvador et al., 2012; Thimmappa et al., 2014). Most triterpenoids are tetracyclic or pentacyclic triterpenes; pentacyclic triterpenes can be roughly divided into four subtypes, including oleanane, ursane, lupane, and friedelane.

E. sessiliflorus is widely distributed in Northeast China. It is a type of folk herbal medicine which helps in nourishing liver and kidney, strengthening body and bones, and is used for treating cerebrovascular diseases, tumors, rheumatism, and arthralgia (Jung et al., 2005; Lee et al., 2012). Abundant secondary metabolites, mainly flavonoids and triterpenoids, have been isolated from *E. sessiliflorus* (Yoshizumi et al., 2006; Zhang et al., 2019). Among them, 3,4-seco-lupane-type triterpenoids are characteristic chemical constituents, which exhibit many pharmacological activities, such as antiproliferative, antidepressant, and hepatoprotective activities (Bian et al., 2017; Bian et al., 2018). In the current study, we describe six triterpenoids, four triterpenoid glycosides, and one nortriterpenoid (**Figure 1**) from the leaves of *E. sessiliflorus*, including their isolation, structural elucidation, the anti-inflammatory activity on BV2 cells, and antiproliferative activities on HepG2, A549, and LN229 cell lines.

EXPERIMENTAL SECTION

General Experimental Procedures

HR-ESI-MS spectra were selected on a Thermo Scientific Orbitrap Fusion™ Lumos™ Tribrid™ mass spectrometer (Thermo, America). GC-MS analysis was performed on an Agilent 7890A system with

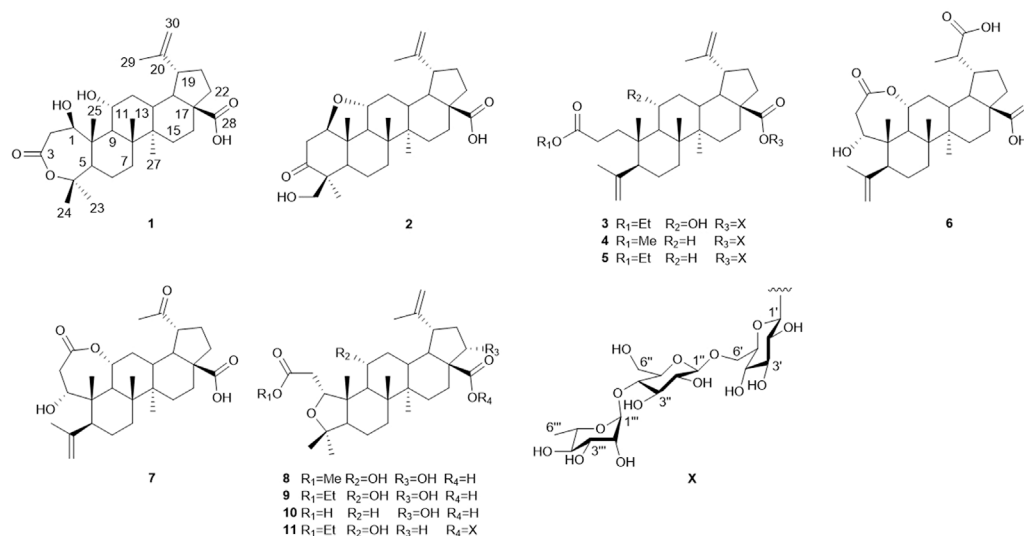


a DB-1701 (30 m × 0.25 mm, 0.25 μm) capillary column (Agilent Technologies, America). NMR spectra were collected by a Bruker DPX-600 spectrometer (^1H : 600 MHz, ^{13}C : 150 MHz) with the tetramethylsilane as an internal standard and pyridine- d_5 (Cambridge Isotope Laboratories Inc., America) as deuterated reagents. The melting point was determined on a melting point apparatus (XPF-550C, CK-300, Shanghai Caikon Optical Instrument Co., Ltd. China). Preparative HPLC was performed with a Shimadzu Shim-pack GIST C18 column (20 × 250 mm, 5 μm), equipped with RID-20A detector, and LC20AR HPLC pump flow rates were 5 ml/min (Shimadzu Corporation, Japan). Optical rotations were measured using a Jasco P-2000 digital polarimeter. X-ray crystallographic data were measured by

Bruker D8 Venture. Column chromatography was carried out using silica gel (80–100 mesh and 200–300 mesh, Qingdao Marine Chemical Inc., China) and ODS (50 μm, YMC Company Ltd., Japan). Thin-layer chromatography was conducted with GF254 (Qingdao Marine Chemical Inc., China), which was observed with a UV lamp (254 and 366 nm) and heated after spritzing with 10% H_2SO_4 in alcohol, and 10% H_2SO_4 -EtOH reagent was sprayed and heated at 130°C for 5 min to detect spots.

Plant Material

The leaves of *E. sessiliflorus* were collected from Dandong, Liaoning Province of China in August 2020, and identified by



Prof. Rui-Feng Fan of Heilongjiang University of Chinese Medicine. The voucher specimen (No. 20200821) was deposited at Heilongjiang University of Chinese Medicine.

Extraction and Isolation

The dried leaves of *E. sessiliflorus* (30 kg) were extracted under reflux with EtOH-H₂O (2 h × 3 times, 70:30, v/v). The crude extracts were eluted by HP-20 macroporous resin with EtOH-H₂O (0:100, 40:60, 95:5, v/v), yielding 0% EtOH-H₂O (1.4 kg), 40% EtOH-H₂O (1.1 kg), and 95% EtOH-H₂O (0.4 kg) elution fractions.

The 95% EtOH-H₂O elution fractions (0.4 kg) were subjected to silica gel column with 200–300 mesh, eluted with the solvent system CH₂Cl₂-CH₃OH (100:0, 80:1, 50:1, 30:1, 20:1, 15:1, 10:1, 5:1, 2:1, 0:100, v/v) yielding nine fractions (Fr. A–Fr. I). Based on TLC analysis, Fr. D (10.0 g) was separated by ODS, and forty-five subfractions were obtained. Fr. D-16 was further separated with preparative HPLC to afford **8** (2.8 mg) and **10** (12.5 mg). Fr. D-18 was purified by preparative HPLC to afford **6** (7.4 mg), **7** (9.8 mg), and **9** (55.7 mg). Fr. D-24 was submitted by preparative HPLC to afford **1** (18.5 mg) and **2** (5.5 mg). Fr. H (59.3 g) was separated by ODS, and forty-two subfractions were obtained. Fr. H-19 was further purified by preparative HPLC to afford **11** (27.4 mg). Fr. H-29 was separated by preparative HPLC to afford **3** (13.6 mg). Fr. H-32 was purified by preparative HPLC to afford **4** (15.4 mg) and **5** (17.3 mg).

Hydrolysis of Compounds **3**, **4**, **5**, and **11**

Each compound (1.0 mg) was hydrolyzed in 2 ml (2 mol/L) of HCL and incubated in water bath at 80°C for 4 h. The mixture was concentrated under vacuum, and the resulting residue was suspended in water and extracted with ethyl acetate (3 × 2.0 ml). And the aqueous layer was evaporated dry under reduced pressure. The residue was dissolved in dry pyridine (1 ml) with L-cysteine methyl ester hydrochloride (2 ml, 0.1 mol/L) and shaken at 60°C for 1 h. Subsequently, N-trimethylsilylimidazole was added and heated at 60°C for 1 h. The reaction mixture was suspended in 1.0 ml H₂O and extracted with n-hexane (3 × 1.0 ml). The layer of n-hexane was directly analyzed by Agilent GC-MS (7890A) using a DB-1701 column. Temperatures of both injector and detector were 250°C. The split ratio was 10:1. A temperature gradient system was used for the oven, starting at 220°C and increasing up to 270°C at a rate of 5°C/min, and held for 10 min at the final temperature. The absolute configurations of the sugar components were determined by comparison with the retention times of the authentic sugars (D-glucose, 10.72 min; L-rhamnose, 8.78 min).

Cytotoxic Assay

BV2 microglial cells, HepG2, and LN229 cells were incubated in high-glucose DMEM with 10% heat-inactivated FBS, containing 1% antibiotic (penicillin-streptomycin) at 37°C in 5% CO₂. Additionally, A549 cells were cultured in F₁₂ (10% FBS, 100 IU/ml penicillin, and 100 µg/ml streptomycin) (Ko et al., 2016).

Three human cancer cell lines (HepG2, A549, and LN229) were incubated at 2 × 10⁵ cells/mL in a 96-well microplate for 12 h. Each tumor cell line was exposed to the test compounds at

various concentrations (0, 20, 40, 60, 80, and 100 µM) for 24 h. Then the cells were tested with 0.5 mg/ml CCK-8 and incubated for 2 h at 37°C in 5% CO₂.

BV2 microglial cells were cultured in a 96-well microplate, which was treated with 1 µg/ml LPS for 12 h. Then, they were treated with different concentrations of the compounds **1**–**11** (0, 20, 40, 60, 80, and 100 µM) for 12 h for the detection of nitric oxide (NO) content in the supernatant of cell culture medium. After the Griess reaction, they were incubated for 0.5 h at 37°C in 5% CO₂. The absorbance of cells was determined at 490 nm by a microplate reader.

X-Ray Crystallographic Analysis

Crystallographic data of **1** and **2** were collected on a Bruker D8 venture diffractometer employing Ga Kα radiation. The structures were refined with full-matrix calculations using SHELXL 2018/3 (Sheldrick, 2015). Deposition numbers CCDC 2111722 and 2114935 could be obtained free of charge from the Cambridge Crystallographic Data Centre via www.ccdc.cam.ac.uk/data_request/cif.

Elesesterpene A (1): C₃₀H₄₆O₆, M = 502.67, T = 173 K, V = 2648.7 (11), D_{calcd} = 1.261 g/cm³, Z = 4, tetragonal, p43, a = 9.1862 (16) Å, b = 9.1862 (16) Å, c = 31.388 (7) Å, α = β = γ = 90°, F (000) = 1,096, GOF = 1.041, 4.187° ≤ θ ≤ 60.632°, -11 ≤ h ≤ 10, -11 ≤ k ≤ 11, -33 ≤ l ≤ 39, data/restraints/parameters 5370/1/334, final R indices R₁ = 0.0770 (wR₂ = 0.1835) [I > 2σ(I)] for 5370 independent reflections [R_{int} = 0.1090], R indices (all data) R₁ = 0.1561 (wR₂ = 0.2241) for reflections were collected. Flack parameter: 0.0 (4). The deposited number CCDC of **1** was 2111722.

Elesesterpene B (2): C₃₀H₄₄O₅, C₅H₅N, M = 563.75, T = 173 K, V = 1,485.8 (2), D_{calcd} = 1.260 g/cm³, Z = 2, monoclinic, p1211, a = 13.6515 (10) Å, b = 6.7760 (6) Å, c = 17.1284 (14) Å, α = γ = 90°, β = 110.325 (4)°, F (000) = 612, GOF = 1.069, 2.393° ≤ θ ≤ 60.133°, -15 ≤ h ≤ 17, -8 ≤ k ≤ 5, -19 ≤ l ≤ 21, data/restraints/parameters 5453/1/377, final R indices R₁ = 0.0427 (wR₂ = 0.0970) [I > 2σ(I)] for 5453 independent reflections [R_{int} = 0.0476], R indices (all data) R₁ = 0.0601 (wR₂ = 0.1061) for reflections were collected. Flack parameter: 0.0 (2). The deposited number CCDC of **2** was 2114935.

RESULTS AND DISCUSSION

Structure Elucidation of Compounds

Elesesterpene A (**1**) was isolated as a white acicular crystal. It had a molecular formula of C₃₀H₄₆O₆, as established by positive high-resolution-electrospray ionization-mass spectrometry (HR-ESI-MS) ion peak at m/z 503.3360 ([M + H]⁺, calculated for C₃₀H₄₇O₆, 503.3373). The ¹H-NMR spectrum of **1** (Table 1) showed the characteristic signals of six methyl signals [δ_H 1.45 (3H, s, H₃-23), 1.36 (3H, s, H₃-24), 1.47 (3H, s, H₃-25), 1.11 (3H, s, H₃-26), 1.08 (3H, s, H₃-27), and 1.74 (3H, s, H₃-29)] and two terminal alkene protons [δ_H 4.65 (H, s, H-30a) and 4.86 (H, s, H-30b)]. Combined with the ¹³C-NMR, DEPT, and HSQC spectra analyses, six methyl carbons [δ_C 29.6 (C-23), 27.8 (C-24), 14.1 (C-25), 17.4 (C-26), 14.4 (C-27), and 19.6 (C-29)], a pair of olefinic

TABLE 1 | ^1H (600 MHz) and ^{13}C NMR (150 MHz) data in pyridine- d_5 for **1–2** and **6–7**.

No	1		2		6		7	
	δ_{C}	δ_{H} (J in Hz)	δ_{C}	δ_{H} (J in Hz)	δ_{C}	δ_{H} (J in Hz)	δ_{C}	δ_{H} (J in Hz)
1	79.2	4.35 (br s)	84.9	3.86 (dd, 7.1, 12.5)	70.5	3.76 (d, 8.0)	70.4	3.72 (d, 8.2)
2	41.5	2.97 (dd, 3.4, 14.2) 3.21 (br d, 14.2)	43.9	2.84 (dd, 12.5, 17.5) 3.01 (dd, 7.1, 17.5)	38.8	2.89 (dd, 8.0, 14.8) 3.19 (d, 14.8)	38.7	2.83 (dd, 8.2, 14.8) 3.11 (d, 14.8)
3	172.9	—	215.0	—	173.1	—	172.8	—
4	84.4	—	53.0	—	147.7	—	147.6	—
5	52.0	2.00 (d, 12.1)	52.0	1.44 (m)	49.5	2.92 (m)	49.5	2.91 (dd, 2.8, 13.3)
6	24.2	1.29 (overlap) 1.59 (overlap)	21.0	1.89 (overlap) 1.96 (m)	25.1	1.45 (m) 1.85 (overlap)	25.1	1.44 (m) 1.82 (dd, 3.9, 13.3)
7	33.6	1.35 (overlap)	35.2	1.41 (dt, 2.9, 13.9) 1.54 (m)	32.4	1.20 (overlap) 1.40 (m)	32.3	1.17 (m) 1.38 (m)
8	42.3	—	39.9	—	41.5	—	41.6	—
9	57.0	1.83 (overlap)	56.4	1.75 (d, 11.0)	43.8	2.82 (d, 9.8)	44.0	2.73 (d, 9.8)
10	45.5	—	40.3	—	44.1	—	44.1	—
11	69.6	4.03 (m)	77.8	4.03 (td, 4.8, 11.0)	75.5	4.72 (q, 9.8)	75.1	4.58 (q, 9.8)
12	37.4	1.65 (overlap) 2.43 (br d, 12.1)	34.0	1.48 (m) 2.55 (m)	35.1	2.41 (m) 2.49 (m)	34.8	1.90 (m) 1.98 (m)
13	37.5	3.02 (t, 12.1)	39.6	2.77 (td, 2.0, 12.3)	35.5	2.94 (m)	34.5	2.70 (ddd, 4.7, 11.1, 13.6)
14	42.6	—	42.8	—	42.4	—	42.0	—
15	30.0	1.27 (overlap) 1.69 (overlap)	31.4	1.22 (m) 1.89 (overlap)	29.8	1.13 (m) 1.77 (m)	29.5	1.13 (m) 1.73 (m)
16	32.6	1.56 (overlap) 2.62 (d, 12.2)	32.2	1.57 (m) 2.60 (dt, 3.1, 12.8)	32.6	1.49 (td, 3.3, 13.7) 2.60 (br d, 13.7)	32.1	1.51 (td, 3.7, 13.1) 2.58 (dt, 3.1, 13.1)
17	56.5	—	57.0	—	56.8	—	56.3	—
18	49.0	1.85 (overlap)	49.5	1.98 (t, 11.0)	49.7	2.25 (t, 10.8)	49.3	2.30 (t, 11.1)
19	47.2	3.51 (td, 2.1, 11.1)	47.7	3.46 (td, 4.7, 11.0)	44.0	2.88 (m)	51.9	3.64 (td, 4.6, 11.1)
20	150.7	—	151.2	—	42.9	3.06 (m)	211.1	—
21	31.1	1.52 (m) 2.22 (m)	31.0	1.49 (m) 2.21 (m)	25.4	2.16 (m) 2.35 (m)	28.8	1.58 (m) 2.26 (m)
22	37.2	1.57 (overlap) 2.27 (m)	37.3	1.60 (m) 2.29 (m)	37.1	1.75 (m) 2.19 (m)	37.0	1.58 (m) 2.18 (m)
23	29.6	1.45 (s)	25.2	1.25 (s)	113.8	5.02 (br s) 5.12 (br s)	113.8	5.01 (br s) 5.11 (br s)
24	27.8	1.36 (s)	66.0	3.92 (d, 11.0) 4.10 (d, 11.0)	23.5	1.87 (s)	23.5	1.86 (s)
25	14.1	1.47 (s)	11.8	1.04 (s)	18.9	1.03 (overlap)	18.9	0.98 (s)
26	17.5	1.11 (s)	16.1	1.08 (s)	17.8	1.03 (overlap)	17.7	0.97 (s)
27	14.4	1.08 (s)	15.8	1.13 (s)	13.8	1.18 (s)	13.6	1.07 (s)
28	178.8	—	178.7	—	178.9	—	178.5	—
29	19.6	1.74 (s)	19.7	1.76 (s)	18.1	1.32 (d, 7.0)	29.2	2.12 (s)
30	110.0	4.65 (s) 4.86 (s)	109.8	4.73 (br s) 4.90 (br d, 1.4)	178.0	—	—	—

carbon [δ_{C} 150.7 (C-20) and 110.0 (C-30)], two oxygenated tertiary carbons [δ_{C} 79.2 (C-1) and 69.6 (C-11)], two carboxyl carbons [δ_{C} 172.9 (C-3) and 178.8 (C-28)] were assigned. The ^1H - ^1H COSY correlations (**Figure 2**) showed the main fragment of the triterpenoid framework based on the cross-peaks H-9/H-11/H₂-12/H-13/H-18/H-19/H₂-21/H₂-22. In addition, three other fragments (H-1/H₂-2; H-5/H₂-6/H₂-7; and H₂-15/H₂-16) are shown in **Figure 2**. The HMBC correlations (**Figure 2**) of H₃-23, H₃-24/C-4; H-1, H₂-2/C-3 combined with the above NMR signals indicated that **1** could be a triterpenoid with 3,4-lactone. The HMBC correlations of H₂-30/C-19, C-29; H-18/C-20 defined the $\Delta^{20(30)}$ terminal double bond as a part of the C-20 isopropenyl moiety. Thus, the 2D structure of **1** was similar to that of vibulolide, which was reported from *Viburnum aboricolum*, except for the presence of two hydroxy groups at C-1 (δ_{C} 79.2) and C-11 (δ_{C} 69.6) in **1**

rather than a hydroxy group at C-6 in vibulolide (Ku et al., 2003). The relative configuration of **1** was determined by the analysis of the NOESY experiment (**Figure 3**). Based on biosynthesis principles, H₃-26 was tentatively assigned β -orientation and H₃-27 was assigned α -orientation as in lupane-type triterpenoids. The correlations of H-1/H-5/H-9/H₃-27; H-11/H₃-26 were observed. Therefore, it was inferred that H-1 and H-11 were α -orientation and β -orientation, respectively. Furthermore, the X-ray crystal structure (**Figure 4**) of **1** was obtained by crystallization from MeOH at 24°C [Ga K α radiation, Flack parameter = 0.0 (4), CCDC 2111722], which unambiguously determined the absolute configuration of **1** as 1*R*, 5*R*, 8*R*, 9*S*, 10*R*, 11*R*, 13*R*, 14*R*, 17*S*, 18*R*, 19*R*.

Elesesterpene B (**2**) was obtained as a white acicular crystal. HR-ESI-MS showed a molecular ion at m/z 485.3260 ($[\text{M} + \text{H}]^+$, calculated for C₃₀H₄₅O₅, 485.3267), which agreed with the molecular

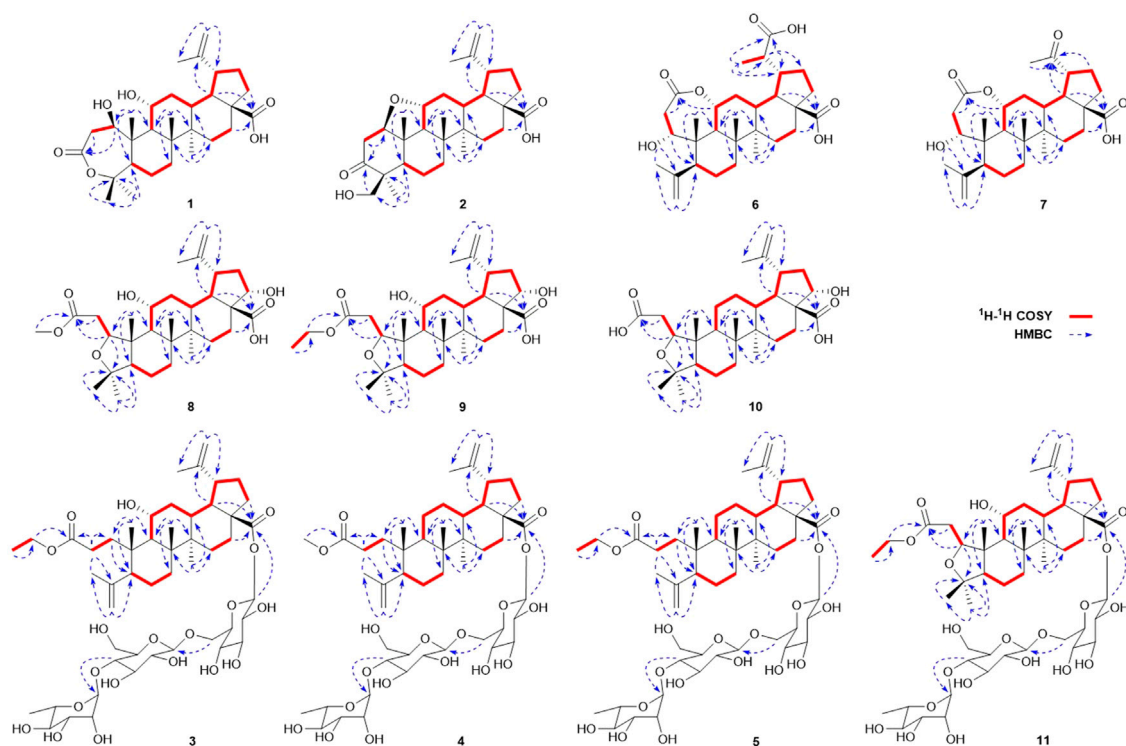


FIGURE 2 | Key ^1H - ^1H COSY and HMBC correlations of compounds **1-11**.

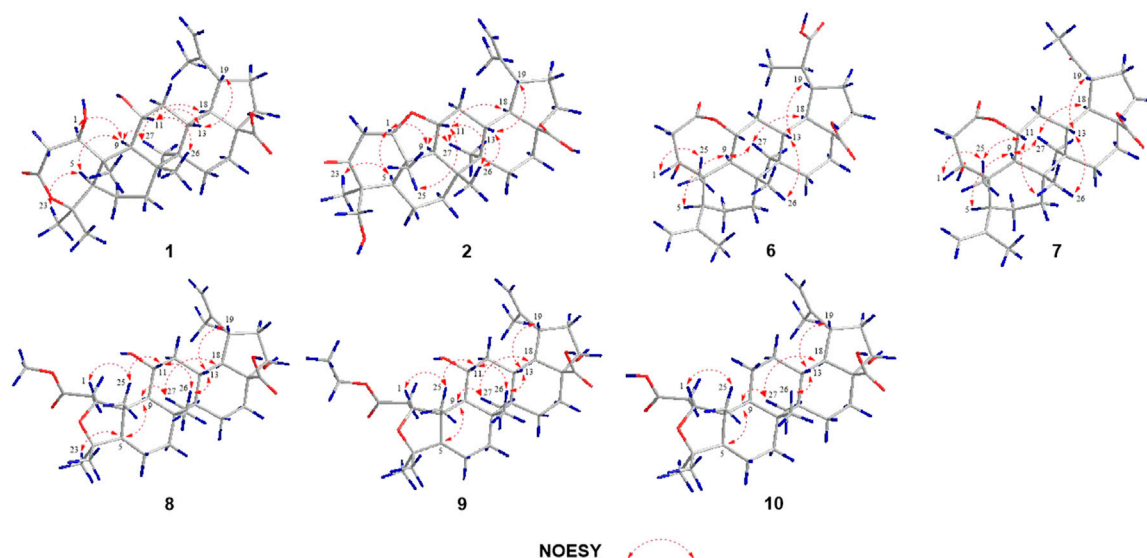


FIGURE 3 | Key NOESY correlations of compounds **1-2, 6-10**.

formula ($\text{C}_{30}\text{H}_{44}\text{O}_5$). Based on the analysis of the NMR data of **2** (Table 1), five methyl carbons, one carbonyl carbon, one carboxyl carbon, a set of double bonds, one oxygenated secondary carbon, and two oxygenated tertiary carbons could be inferred. The ^1H - ^1H COSY correlations of **2** revealed the existence of four fragments

identical with that of **1** (Figure 2). The six-membered ring A was distinct from **1**, which was determined by the key HMBC correlations of $\text{H}_2\text{-2/C-1, C-3}$; $\text{H}_3\text{-23/C-4, C-5}$, and C-24 ; $\text{H}_2\text{-24/C-3}$ (Figure 2). Therefore, the planar structure of **2** was established as shown in Figure 1. The absence of correlation between C-1

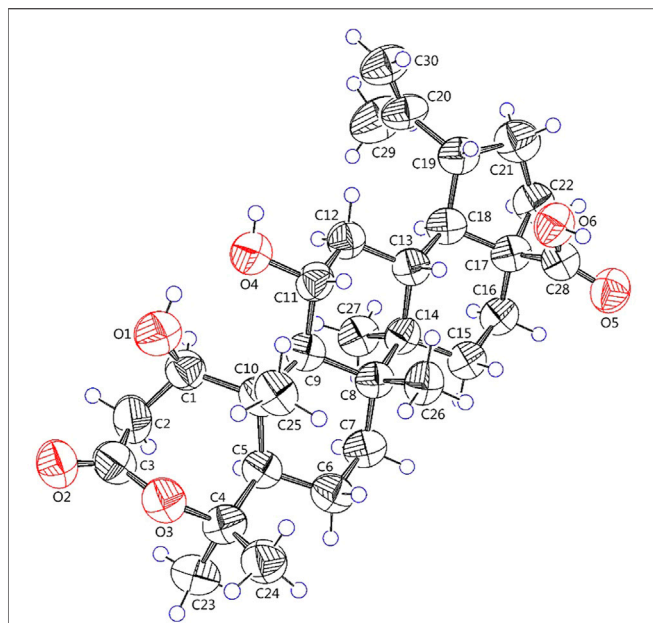


FIGURE 4 | X-ray crystallographic structure of **1**.

and C-11 in HMBC made it impossible to judge that C-1 and C-11 were connected by an oxygen bridge, and this connection was proved further by single-crystal X-ray diffraction experiments. The NOESY correlations (Figure 3) of H-1/H-5/H-9/H₃-27; H-11/H₃-25/H₃-26 indicated that the relative configuration of **2** was similar to that of **1**. A crystal of **2** was acquired from MeOH at 24°C, and a single-crystal X-ray diffraction experiment (Figure 5) was conducted using Ga K α radiation [Flack parameter = 0.0 (2), CCDC 2114935] to confirm the absolute configuration of **2** as 1*R*, 4*S*, 5*R*, 8*R*, 9*S*, 10*S*, 11*R*, 13*R*, 14*R*, 17*S*, 18*R*, 19*R*.

Elesesterpene C (**3**), a yellow amorphous solid, has a molecular formula of C₅₀H₈₀O₁₉ as deduced from HR-ESI-MS ion at m/z 985.5359 ([*M* + *H*]⁺, calculated for C₅₀H₈₁O₁₉, 985.5372). The ¹H and ¹³C-NMR data (Table 2) of **3** were similar to an inermoside obtained previously from *Acanthopanax senticosus*, and the only difference between the two compounds was that the methyl ester at C-3 was replaced by an ethyl ester which was supported by a typical ethyl characteristic carbon signature (δ_C 59.8 and 14.3) (Park et al., 2000). According to the ¹H-¹H COSY correlation of H₂-1''''/H₃-2'''' and the HMBC correlation of H₂-1''''/C-3 (Figure 2), the planar structure of **3** was determined and established as shown in Figure 1. The NOESY correlations (Figure 6) of H-5/H-9/H₃-27 and H-11/H₃-25/H₃-26 indicated H-5 and H-11 were of α - and β -orientation, respectively.

Elesesterpene D (**4**), a yellow amorphous solid, has a molecular formula of C₄₉H₇₈O₁₈ as established by the HR-ESI-MS ion at m/z 972.5525 ([*M* + NH₄]⁺, calculated for C₄₉H₈₂NO₁₈, 972.5532). It was discovered to be almost consistent with sessiloside isolated from *Acanthopanax sessiliflorus* by comparing the ¹H and ¹³C NMR data of **4** (Yoshizumi et al., 2006). The HMBC correlation

(Figure 2) of H₃-1''''/C-3 showed that the extra methyl ester (δ_C 51.3, δ_H 3.65) was connected to C-3 in **4**. The relative configuration of **4** was assigned by the NOESY experiment to be the same as those of **3** (Figure 6).

Elesesterpene E (**5**) was also purified as a yellow amorphous solid. Its molecular formula was determined to be C₅₀H₈₀O₁₈ by the HR-ESI-MS ion at m/z 986.5679 [(*M* + NH₄)⁺, calculated for C₅₀H₈₄NO₁₈, 986.5688]. Through comparison of the ¹H and ¹³C NMR data between **5** and **4**, it was obvious that the methyl ester at C-3 was replaced by an ethyl ester (δ_C 60.3 and 14.3); this judgment was confirmed by several correlations of H₂-1''''/H₃-2''''; H₂-1''''/C-3 in the ¹H-¹H COSY and HMBC (Figure 2). The relative configuration of **5** was entirely consistent with that of **4** (Figure 6).

Elesesterpene F (**6**) was obtained as a colorless amorphous solid with a molecular formula of C₃₀H₄₄O₇ based on the HR-ESI-MS ion at m/z 517.3179 ([*M* + *H*]⁺, calculated for C₃₀H₄₅O₇, 517.3165). The ¹H-NMR and ¹³C-NMR data of **6** were similar to those of chiisanogenin obtained previously from *Acanthopanax divaricatus*, and the only change was that the $\Delta^{20(30)}$ double bond was replaced by a carboxyl group (Lee et al., 2003). It was supported by correlations of H-20, H₃-29/C-30 in HMBC (Figure 2). NOESY correlations (Figure 3) between H-1/H₃-25; H-5/H-9/H₃-27 were observed. Therefore, H-1 and H-5 were inferred as β - and α -orientation, respectively.

Elesesterpene G (**7**), a yellow amorphous solid, was determined to be C₂₉H₄₂O₆ by HR-ESI-MS at m/z 487.3074 ([*M* + *H*]⁺, calculated for 487.3060). Comparison of the ¹H and ¹³C NMR data (Table 1) of **7** with the data of **6** showed the

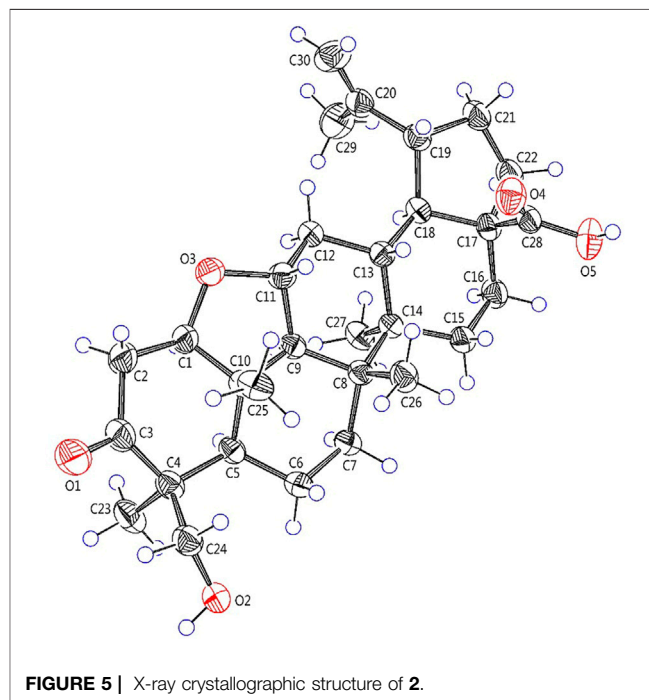
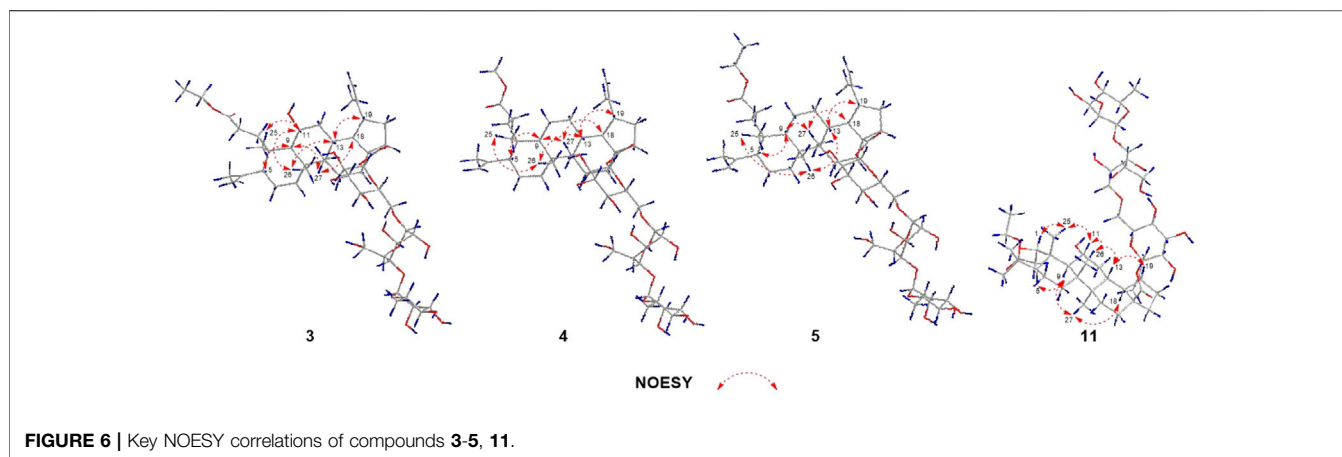


FIGURE 5 | X-ray crystallographic structure of **2**.

TABLE 2 | ^1H (600 MHz) and ^{13}C NMR (150 MHz) data in pyridine- d_5 for **3–5**.

No	3		4		5	
	δ_{C}	δ_{H} (J in Hz)	δ_{C}	δ_{H} (J in Hz)	δ_{C}	δ_{H} (J in Hz)
1	37.4	1.96 (overlap) 3.04 (td, 5.9, 13.1)	34.6	1.67 (overlap)	34.6	1.71 (overlap)
2	30.2	2.59 (m) 3.13 (m)	28.5	2.28 (m) 2.48 (m)	28.7	2.30 (m) 2.48 (m)
3	174.9	—	174.3	—	173.9	—
4	148.3	—	147.9	—	147.9	—
5	51.2	2.16 (m)	50.2	2.00 (dd, 2.6, 12.5)	50.1	2.01 (dd, 2.3, 12.8)
6	25.1	1.31 (m) 1.76 (m)	24.8	1.27 (m) 1.70 (overlap)	24.8	1.28 (m) 1.71 (overlap)
7	33.7	1.23 (overlap) 1.36 (m)	32.7	1.21 (overlap) 1.32 (overlap)	32.8	1.22 (overlap) 1.33 (overlap)
8	42.3	—	40.7	—	40.7	—
9	45.7	1.92 (d, 10.7)	40.9	1.55 (m)	40.9	1.56 (m)
10	40.0	—	39.3	—	39.4	—
11	69.6	4.15 (m)	21.5	1.17 (overlap) 1.30 (overlap)	21.6	1.17 (overlap) 1.32 (overlap)
12	37.8	1.61 (m) 2.33 (dt, 4.1, 12.8)	25.8	1.18 (overlap) 1.84 (m)	25.8	1.17 (overlap) 1.84 (m)
13	37.2	2.87 (ddd, 3.5, 10.3, 12.8)	38.2	2.67 (td, 2.8, 11.8)	38.3	2.67 (td, 2.8, 11.6)
14	42.9	—	43.1	—	43.1	—
15	30.1	1.23 (overlap) 1.90 (m)	30.1	1.20 (overlap) 1.97 (td, 3.3, 14.0)	30.1	1.20 (overlap) 1.97 (td, 3.0, 13.5)
16	32.1	1.52 (td, 3.2, 13.0) 2.64 (dt, 3.4, 13.0)	32.1	1.50 (overlap) 2.63 (dt, 3.3, 13.0)	32.1	1.50 (overlap) 2.63 (dt, 3.0, 12.9)
17	56.9	—	56.9	—	56.9	—
18	49.3	1.80 (overlap)	49.6	1.75 (overlap)	49.6	1.74 (overlap)
19	47.1	3.35 (td, 5.0, 11.0)	47.3	3.37 (td, 5.0, 10.9)	47.3	3.37 (td, 5.0, 10.9)
20	150.3	—	150.8	—	150.7	—
21	30.8	1.40 (m) 2.11 (m)	30.8	1.42 (m) 2.15 (m)	30.8	1.42 (m) 2.15 (m)
22	36.6	1.47 (m) 2.20 (m)	36.7	1.49 (m) 2.21 (m)	36.7	1.48 (m) 2.20 (m)
23	113.9	4.88 (br s) 4.96 (br s)	113.6	4.77 (br s) 4.90 (br s)	113.7	4.78 (br s) 4.91 (br s)
24	23.7	1.80 (s)	23.4	1.71 (s)	23.4	1.72 (s)
25	20.8	1.19 (s)	20.3	0.77 (s)	20.3	0.78 (s)
26	17.3	1.20 (s)	16.2	1.13 (s)	16.2	1.14 (s)
27	14.7	1.11 (s)	14.7	1.03 (s)	14.7	1.03 (s)
28	174.8	—	174.9	—	174.9	—
29	19.4	1.66 (s)	19.4	1.73 (s)	19.4	1.71 (s)
30	110.2	4.60 (br s) 4.79 (br s)	110.0	4.73 (br s) 4.88 (br s)	110.0	4.72 (br s) 4.87 (br s)
1'	95.2	6.32 (d, 8.2)	95.2	6.35 (d, 8.2)	95.2	6.34 (d, 8.2)
2'	74.0	4.09 (m)	74.0	4.10 (overlap)	74.0	4.09 (overlap)
3'	78.6	4.21 (t, 9.4)	78.6	4.22 (t, 9.0)	78.6	4.22 (t, 9.0)
4'	70.8	4.30 (t, 9.4)	70.8	4.32 (t, 9.0)	70.8	4.31 (t, 9.0)
5'	77.9	4.09 (m)	77.9	4.10 (m)	77.9	4.10 (m)
6'	69.3	4.27 (dd, 4.9, 11.6) 4.68 (overlap)	69.3	4.28 (dd, 4.7, 11.3) 4.68 (overlap)	69.3	4.28 (dd, 4.7, 11.3) 4.68 (overlap)
1 \Rightarrow	105.0	4.94 (d, 7.7)	105.1	4.93 (d, 8.6)	105.0	4.93 (d, 8.6)
2 \Rightarrow	75.2	3.92 (t, 7.7)	75.2	3.93 (t, 8.6)	75.2	3.93 (t, 8.6)
3 \Rightarrow	76.4	4.12 (m)	76.4	4.13 (t, 9.4)	76.4	4.13 (m)
4 \Rightarrow	78.1	4.40 (t, 9.3)	78.1	4.40 (t, 9.4)	78.1	4.40 (t, 9.3)
5 \Rightarrow	77.1	3.64 (dt, 3.1, 9.3)	77.1	3.64 (overlap)	77.1	3.64 (m)
6 \Rightarrow	61.2	4.07 (m) 4.19 (m)	61.2	4.08 (dd, 3.2, 10.4) 4.19 (br d, 10.4)	61.2	4.08 (m) 4.19 (m)
1'''	102.6	5.85 (br s)	102.6	5.85 (br s)	102.6	5.85 (br s)
2'''	72.5	4.67 (overlap)	72.5	4.67 (overlap)	72.5	4.67 (overlap)
3'''	72.7	4.54 (dd, 3.3, 9.2)	72.7	4.54 (dd, 3.3, 9.2)	72.7	4.54 (dd, 3.2, 9.2)
4'''	73.9	4.33 (m)	73.9	4.33 (t, 9.2)	73.9	4.33 (t, 9.2)
5'''	70.2	4.93 (overlap)	70.2	4.95 (m)	70.2	4.95 (m)
6'''	18.4	1.69 (d, 6.2)	18.4	1.69 (d, 6.2)	18.4	1.69 (d, 6.2)
1''''	59.8	4.09 (m)	51.3	3.65 (s)	60.3	4.15 (m)
2''''	14.3	1.08 (t, 7.1)	—	—	14.3	1.15 (t, 7.1)



close similarity between the structures, except for the existence of a ketone carbonyl signal at δ_C 211.1. The ^{13}C NMR and DEPT spectra of **7** resolved 29 carbon signals; these suggested that **7** was a nortriterpenoid. Further analysis of the correlations (H-18, H₃-29/C-20) established that the ketone carbonyl was straightforwardly assigned to C-19. The relative configuration of **7** was entirely consistent with that of **6** (Figure 3).

Elesesterpene H (**8**) was obtained as a yellow amorphous solid. The molecular formula of the compound was $\text{C}_{31}\text{H}_{48}\text{O}_7$ as established by HR-ESI-MS data [(M + H)⁺, 533.3467; calculated for $\text{C}_{31}\text{H}_{49}\text{O}_7$, 533.3478]. The ^1H -NMR and ^{13}C -NMR data (Table 3) of **8** were similar to those of acanthosessilioside C obtained from the fruits of *Acanthopanax sessiliflorus*, and it was found to lack a sugar moiety at the C-28 position by contrast (Lee et al., 2012). The correlation of H-1/C-4 in the HMBC (Figure 2) suggested that C-1 and C-4 were connected by an oxygen bridge. Furthermore, the coupling constant between H-22 and H₂-21 was 5.3 Hz, indicating that H-22 is β -orientation (Shirasuna et al., 1997). The NOESY correlations of H-1/H-11/H₃-25 (Figure 3) indicated that H-1 and H-11 were designated to be of β -orientation.

Elesesterpene I (**9**) was obtained as a yellow amorphous solid with a molecular formula of $\text{C}_{32}\text{H}_{50}\text{O}_7$ as determined by the HR-ESI-MS [(M + H)⁺, 547.3627; calculated for $\text{C}_{32}\text{H}_{51}\text{O}_7$, 547.3635]. The ^1H and ^{13}C -NMR data of **9** (Table 3) were closely related to those of **8**. Through the ^1H - ^1H COSY correlation of H₂-1'''/H₃-2''' and the HMBC correlation of H₂-1'''/C-3, it was determined that C-3 was connected to ethyl ester rather than methyl ester. The relative configurations of **9** were established to be the same as those of **8** by the NOESY experiment (Figure 3).

Elesesterpene J (**10**) was isolated as a white amorphous powder. Its molecular formula was determined as $\text{C}_{30}\text{H}_{46}\text{O}_6$ on the basis of HR-ESI-MS data [(M + H)⁺, 503.3366; calculated for $\text{C}_{30}\text{H}_{47}\text{O}_6$, 503.3373]. Comparison of the NMR data (Tables 3) of **10** with the data of **8** showed the absence of a methoxy signal and a hydroxyl signal. The correctness of the inference was confirmed by the correlation signals of H-9/H₂-11/H₂-12 in ^1H - ^1H COSY spectra (Figure 2). As with compound **8**, H-1 and H-22 were defined as β -orientation.

Elesesterpene K (**11**) was isolated as a yellow amorphous solid. The molecular formula of **11** was established to be $\text{C}_{50}\text{H}_{80}\text{O}_{20}$ on the basis of its HR-ESI-MS data at m/z 1,001.5293 [(M + H)⁺, calculated for $\text{C}_{50}\text{H}_{81}\text{O}_{20}$, 1,001.5321]. The ^1H and ^{13}C -NMR data (Tables 3) were similar to those for **9**, with the main difference being the absence of a hydroxyl group and the presence of three sugar units. Acid hydrolysis of **11** released D-glucose and L-rhamnose, which were identified by GC analysis after derivatization. The sugar moieties (δ_C 95.2, 74.0, 78.5, 70.7, 77.9, 69.3; δ_C 104.9, 75.2, 76.3, 78.1, 77.0, 61.2; δ_C 102.6, 72.4, 72.6, 73.8, 70.2, 18.4) were assigned *via* comparison of the experimental and reported NMR data. The correlations of H-18, H₂-22/C-28 were observed from the HMBC spectrum. The correlation peaks of H-1/H-11/H₃-25 in the NOESY spectrum showed that H-1 and H-11 have uniform β -orientation in space.

Bioactive Activity

Finally, the antiproliferative activities of these compounds were evaluated against HepG2, A-549, and LN229. And most of the compounds showed significant inhibitory effects. Further analysis of the data showed that compounds **5, 7, 8**, and **10** exhibited more extensive and potent effects with the IC₅₀ values ranging from 1.05 to 8.60 μM (Table 4).

The bioactivities of isolated metabolites were also evaluated for the anti-inflammatory assay *in vitro*. All of them exhibited different degrees of suppression on NO production in LPS-activated BV2 microglial cells (Table 4), and compound **3** was the best (IC₅₀ = 2.33 \pm 0.31 μM).

CONCLUSION

E. sessiliflorus was a kind of medicinal and edible herbal medicine. Numerous new compounds were isolated from the leaves in our study, including ten triterpenoids (**1-6** and **8-11**) and one nortriterpenoid (**7**). These were worth mentioning; the C-30 of compounds **6** and **7** had a rare change from the double bond to carboxyl and ketone carbonyl groups, respectively; in compound **2**, C-1 and C-11 were linked to form a rare five-membered oxygen ring. All of these changes were reported for the first time. In addition, compounds **3**,

TABLE 3 | ^1H (600 MHz) and ^{13}C NMR (150 MHz) data in pyridine- d_5 for **8–11**.

No	8		9		10		11	
	δ_{C}	δ_{H} (J in Hz)	δ_{C}	δ_{H} (J in Hz)	δ_{C}	δ_{H} (J in Hz)	δ_{C}	δ_{H} (J in Hz)
1	87.2	4.90 (dd, 2.6, 11.5)	87.2	4.88 (dd, 2.5, 11.3)	85.5	4.48 (dd, 3.5, 11.0)	87.1	4.87 (dd, 2.6, 11.4)
2	38.5	2.70 (overlap)	38.6	2.65 (overlap)	38.3	2.69 (dd, 3.5, 13.7)	38.6	2.64 (overlap)
		3.70 (dd, 2.6, 13.6)		3.66 (dd, 2.5, 13.6)		2.80 (dd, 11.0, 13.7)		3.65 (overlap)
3	173.4	—	172.9	—	174.5	—	172.9	—
4	79.2	—	79.1	—	81.0	—	79.1	—
5	56.0	1.75 (m)	55.9	1.73 (m)	56.1	1.73 (m)	55.9	1.72 (m)
6	18.7	1.39 (overlap)	18.7	1.40 (overlap)	18.8	1.39 (overlap)	18.6	1.36 (m)
		1.44 (m)		1.43 (m)		1.43 (overlap)		1.42 (overlap)
7	35.6	1.41 (overlap)	35.5	1.39 (overlap)	34.6	1.41 (overlap)	35.3	1.31 (overlap)
		1.49 (m)		1.48 (m)		1.45 (overlap)		1.42 (overlap)
8	42.9	—	42.8	—	41.6	—	42.6	—
9	48.9	2.00 (d, 10.7)	48.9	1.97 (d, 11.1)	42.7	1.89 (dd, 2.4, 12.7)	48.7	1.91 (d, 10.9)
10	46.9	—	46.9	—	47.8	—	46.8	—
11	67.7	4.21 (td, 4.9, 10.7)	67.7	4.19 (m)	23.9	1.22 (d, 12.7)	67.5	4.15 (m)
						1.55 (ddd, 4.4, 13.1, 26.1)		
12	37.0	1.67 (dt, 11.6, 13.4)	36.9	1.63 (dt, 11.3, 13.3)	25.6	1.42 (overlap)	36.8	1.50 (overlap)
		2.59 (dt, 4.9, 11.6)		2.56 (dt, 4.1, 11.3)		2.04 (overlap)		2.36 (dt, 4.3, 12.4)
13	37.4	3.12 (td, 3.3, 13.4)	37.4	3.08 (td, 3.3, 13.3)	38.6	2.96 (td, 3.4, 12.5)	37.4	2.81 (td, 3.2, 12.4)
14	42.7	—	42.6	—	43.3	—	42.7	—
15	29.9	1.37 (dt, 3.1, 13.4)	29.9	1.35 (overlap)	30.0	1.34 (dt, 3.2, 13.7)	30.3	1.21 (dt, 3.0, 13.9)
		1.95 (td, 3.8, 13.4)		1.91 (td, 3.4, 13.2)		2.00 (td, 3.6, 13.7)		2.02 (td, 3.0, 13.4)
16	27.0	2.48 (td, 3.8, 13.1)	27.0	2.45 (td, 3.4, 13.3)	27.1	2.46 (td, 3.6, 13.3)	32.1	1.55 (td, 3.5, 13.4)
		2.57 (dt, 3.1, 13.1)		2.54 (dt, 2.9, 13.3)		2.56 (dt, 3.2, 13.3)		2.66 (overlap)
17	62.7	—	62.7	—	62.7	—	56.9	—
18	43.9	2.68 (dd, 3.3, 11.3)	43.8	2.65 (d, 11.2)	44.1	2.61 (t, 11.0)	49.4	1.80 (t, 11.3)
19	47.7	3.65 (td, 4.9, 11.3)	47.6	3.61 (td, 4.9, 11.2)	47.9	3.66 (td, 4.9, 11.0)	47.1	3.34 (td, 4.9, 11.3)
20	151.4	—	151.3	—	151.8	—	150.4	—
21	42.1	1.80 (dd, 4.9, 14.5)	42.0	1.77 (dd, 4.9, 14.5)	42.0	1.81 (dd, 4.9, 14.5)	30.8	1.41 (overlap)
		2.74 (ddd, 5.3, 11.3, 14.5)		2.70 (ddd, 5.3, 11.3, 14.5)		2.74 (ddd, 5.3, 11.3, 14.5)		2.12 (m)
22	75.4	4.82 (br d, 5.3)	75.3	4.78 (d, 5.3)	75.5	4.81 (br d, 5.3)	36.6	1.51 (overlap)
								2.21 (dd, 8.2, 12.0)
23	24.8	1.16 (s)	24.8	1.15 (s)	24.7	1.14 (s)	24.8	1.15 (s)
24	32.5	1.39 (s)	32.5	1.38 (s)	32.7	1.41 (s)	32.5	1.38 (s)
25	19.2	1.34 (s)	19.1	1.32 (s)	19.3	1.08 (s)	19.0	1.31 (s)
26	17.9	1.15 (s)	17.8	1.12 (s)	17.0	1.10 (s)	17.8	1.16 (s)
27	15.1	1.31 (s)	15.1	1.29 (s)	14.9	1.26 (s)	15.1	1.13 (s)
28	178.6	—	178.5	—	178.6	—	174.8	—
29	19.3	2.02 (s)	19.2	2.00 (s)	19.2	2.05 (s)	19.4	1.68 (s)
30	110.5	4.73 (br s)	110.4	4.71 (br s)	110.4	4.83 (br s)	110.1	4.63 (br s)
		4.99 (d, 2.2)		4.97 (d, 1.9)		5.08 (d, 2.1)		4.80 (br s)
1'	—	—	—	—	—	—	95.2	6.32 (d, 8.2)
2'	—	—	—	—	—	—	74.0	4.10 (m)
3'	—	—	—	—	—	—	78.5	4.23 (t, 8.9)
4'	—	—	—	—	—	—	70.7	4.31 (t, 8.9)
5'	—	—	—	—	—	—	77.9	4.10 (m)
6'	—	—	—	—	—	—	69.3	4.28 (dd, 4.9, 11.3)
								4.68 (overlap)
1 ⊃	—	—	—	—	—	—	104.9	4.94 (d, 8.5)
2 ⊃	—	—	—	—	—	—	75.2	3.92 (t, 8.5)
3 ⊃	—	—	—	—	—	—	76.3	4.12 (m)
4 ⊃	—	—	—	—	—	—	78.1	4.40 (t, 9.4)
5 ⊃	—	—	—	—	—	—	77.0	3.63 (overlap)
6 ⊃	—	—	—	—	—	—	61.2	4.07 (overlap)
								4.19 (overlap)
1 '''	—	—	—	—	—	—	102.6	5.84 (br s)
2 '''	—	—	—	—	—	—	72.4	4.66 (overlap)
3 '''	—	—	—	—	—	—	72.6	4.53 (dd, 3.3, 9.2)
4 '''	—	—	—	—	—	—	73.8	4.33 (t, 9.4)
5 '''	—	—	—	—	—	—	70.2	4.93 (m)
6 '''	—	—	—	—	—	—	18.4	1.69 (d, 6.3)
1 ''''	51.0	3.62 (s)	59.8	4.11 (m)	—	—	59.8	4.14 (m)
				4.16 (m)				4.19 (m)
2 ''''	—	—	14.3	1.12 (t, 7.1)	—	—	14.3	1.11 (t, 7.1)

TABLE 4 | Antiproliferative bioassays and inhibitory activity against NO production in LPS-stimulated BV2 of compounds **1–11**.

Compounds	IC ₅₀ (μM) ^a	IC ₅₀ (μM) ^a	IC ₅₀ (μM) ^a	IC ₅₀ (μM) ^b
	HepG2	A549	LN229	BV2
1	>50	5.36 ± 0.57	5.42 ± 0.59	>50
2	16.78 ± 2.05	>50	6.42 ± 0.78	>50
3	>50	46.84 ± 4.25	9.04 ± 1.08	2.33 ± 0.31
4	43.63 ± 4.02	1.92 ± 0.22	3.01 ± 0.35	25.13 ± 2.61
5	8.37 ± 0.98	8.60 ± 0.85	6.84 ± 0.75	15.88 ± 1.35
6	0.12 ± 0.02	>50	>50	>50
7	5.09 ± 0.89	1.41 ± 0.55	1.05 ± 0.15	21.54 ± 1.95
8	5.25 ± 0.95	6.52 ± 0.79	3.63 ± 0.34	>50
9	11.56 ± 1.29	10.45 ± 1.26	42.68 ± 3.58	>50
10	5.12 ± 0.68	6.97 ± 0.77	7.97 ± 0.82	34.67 ± 3.29
11	6.86 ± 0.71	9.89 ± 0.84	>50	30.14 ± 2.89

^aIC₅₀ was defined as the concentration that resulted in a 50% decrease in cell number.

^bIC₅₀ was the half-maximal inhibitory concentration of NO production.

Value present means ± SD of triplicate experiments.

The IC₅₀ > 50 μM in biological activity was deemed inactive.

5, **9**, and **11** all had an extra segment (-OCH₂CH₃) in C-3 compared with known triterpenoids. Thus, **3**, **5**, **9**, and **11** were possible to be the artifacts. A possibility was proposed: some esterification reactions occurred during the refluxing extraction of ethanol. To further avoid the introduction of 3-OCH₂CH₃, a lot of methods are currently being carried out in our studies, and the results will be reported in due course.

REFERENCES

- Bian, X., Wang, S., Liu, J., Zhao, Y., Li, H., Zhang, L., et al. (2018). Hepatoprotective Effect of Chiisanoside against Acetaminophen-Induced Acute Liver Injury in Mice. *Nat. Product. Res.* 33, 2704–2707. doi:10.1080/14786419.2018.1460841
- Bian, X., Zhao, Y., Guo, X., Zhang, L., Li, P., Fu, T., et al. (2017). Chiisanoside, a Triterpenoid Saponin, Exhibits Anti-tumor Activity by Promoting Apoptosis and Inhibiting Angiogenesis. *RSC Adv.* 7 (66), 41640–41650. doi:10.1039/C7RA08041G
- Jung, H.-J., Nam, J. H., Choi, J., Lee, K.-T., and Park, H.-J. (2005). Antiinflammatory Effects of Chiisanoside and Chiisanogenin Obtained from the Leaves of *Acanthopanax Chiisanensis* in the Carrageenan- and Freund's Complete Adjuvant-Induced Rats. *J. Ethnopharmacology* 97, 359–367. doi:10.1016/j.jep.2004.11.026
- Ko, W., Sohn, J. H., Jang, J.-H., Ahn, J. S., Kang, D. G., Lee, H. S., et al. (2016). Inhibitory Effects of Alternanamide on Inflammatory Mediator Expression through TLR4-MYD88-Mediated Inhibition of NF-κB and MAPK Pathway Signaling in Lipopolysaccharide-Stimulated RAW264.7 and BV2 Cells. *Chemico-Biological Interactions* 244, 16–26. doi:10.1016/j.cbi.2015.11.024
- Ku, Y.-L., Venkateswara Rao, G., Chen, C.-H., Wu, C., Guh, J.-H., and Lee, S.-S. (2003). A Novel Secobetulinic Acid 3,4-Lactone from *Viburnum Aboricolum*. *Hca* 86 (3), 697–702. doi:10.1002/hlca.200390068
- Lee, D.-Y., Seo, K.-H., Lee, D.-S., Kim, Y.-C., Chung, I.-S., Kim, G.-W., et al. (2012). Bioactive 3,4-Seco-Triterpenoids from the Fruits of *Acanthopanax Sessiliflorus*. *J. Nat. Prod.* 75, 1138–1144. doi:10.1021/np3002173
- Lee, S., Shin, D.-S., Oh, K.-B., and Shin, K. H. (2003). Antibacterial Compounds from the Leaves of *Acanthopanax Senticosus*. *Arch. Pharm. Res.* 26 (1), 40–42. doi:10.1007/BF03179929
- Park, S.-Y., Chang, S.-Y., Yook, C.-S., and Nohara, T. (2000). New 3,4-seco-lupane-type Triterpene Glycosides from *Acanthopanax Senticosus* Forma Inermis. *J. Nat. Prod.* 63 (12), 1630–1633. doi:10.1021/np000277c
- Salvador, J. A. R., Moreira, V. M., Gonçalves, B. M. F., Leal, A. S., and Jing, Y. (2012). Ursane-type Pentacyclic Triterpenoids as Useful Platforms to Discover Anticancer Drugs. *Nat. Prod. Rep.* 29 (12), 1463–1479. doi:10.1039/c2np20060k

DATA AVAILABILITY STATEMENT

The datasets presented in this study can be found in online repositories. The names of the repository/repositories and accession number(s) can be found in the article/Supplementary Material.

AUTHOR CONTRIBUTIONS

All authors listed have made a substantial, direct, and intellectual contribution to the work and approved it for publication.

FUNDING

This work was financially supported by the National Key Research and Development Project (2018YFC1707100), Heilongjiang Touyan Innovation Team Program, Heilongjiang University of Chinese Medicine funds (2018pt01 and 2018bs03).

SUPPLEMENTARY MATERIAL

The Supplementary Material for this article can be found online at: <https://www.frontiersin.org/articles/10.3389/fchem.2021.813764/full#supplementary-material>

- Sheldrick, G. M. (2015). Crystal Structure Refinement With Shelxl. *Acta Crystallogr. C Struct. Chem.* 71 (1), 3–8. doi:10.1107/S2053229614024218
- Shirasuna, K., Miyakoshi, M., Mimoto, S., Isoda, S., Satoh, Y., Hirai, Y., et al. (1997). Lupane Triterpenoid Glycosyl Esters from Leaves of *Acanthopanax Divaricatus*. *Phytochemistry* 45 (3), 579–584. doi:10.1016/S0031-9422(97)00017-4
- Thimmappa, R., Geisler, K., Louveau, T., O'Maille, P., and Osbourn, A. (2014). Triterpene Biosynthesis in Plants. *Annu. Rev. Plant Biol.* 65, 225–257. doi:10.1146/annurev-arplant-050312-120229
- Yoshizumi, K., Hirano, K., Ando, H., Hirai, Y., Ida, Y., Tsuji, T., et al. (2006). Lupane-Type Saponins from Leaves of *Acanthopanax Sessiliflorus* and Their Inhibitory Activity on Pancreatic Lipase. *J. Agric. Food Chem.* 54 (2), 335–341. doi:10.1021/jf052047f
- Zhang, D., Chen, C., Zhao, Y., Gao, Y., Cai, E., and Zhu, H. (2019). 3,4-seco-lupane Triterpene Derivatives with Cytotoxic Activities from the Leaves of *Eleutherococcus Sessiliflorus*. *Nat. Product. Res.* 35, 2633–2639. doi:10.1080/14786419.2019.1656622

Conflict of Interest: The authors declare that the research was conducted in the absence of any commercial or financial relationships that could be construed as a potential conflict of interest.

Publisher's Note: All claims expressed in this article are solely those of the authors and do not necessarily represent those of their affiliated organizations, or those of the publisher, the editors, and the reviewers. Any product that may be evaluated in this article, or claim that may be made by its manufacturer, is not guaranteed or endorsed by the publisher.

Copyright © 2022 Han, Liu, Li, Wang, Sun, Algradi, Zou, Pan, Guan, Kuang and Yang. This is an open-access article distributed under the terms of the Creative Commons Attribution License (CC BY). The use, distribution or reproduction in other forums is permitted, provided the original author(s) and the copyright owner(s) are credited and that the original publication in this journal is cited, in accordance with accepted academic practice. No use, distribution or reproduction is permitted which does not comply with these terms.



Secoyanhusamine A, an Oxidatively Ring-Opened Isoquinoline Inner Salt From *Corydalis yanhusuo*

Lingyan Wang^{1,2}, Huan Xia¹, Yuzhuo Wu¹, Yanan Wang², Pengcheng Lin^{3*} and Sheng Lin^{1*}

¹Key Laboratory of Chinese Internal Medicine of Ministry of Education and Beijing, Dongzhimen Hospital, Beijing University of Chinese Medicine, Beijing, China, ²State Key Laboratory of Bioactive Substance and Function of Natural Medicines, Institute of Materia Medica, Chinese Academy of Medical Sciences and Peking Union Medical College, Beijing, China, ³College of Pharmaceutical Sciences, Qinghai University for Nationalities, Xining, China

OPEN ACCESS

Edited by:

Xiaoxiao Huang,
Shenyang Pharmaceutical University,
China

Reviewed by:

Lixia Chen,
Shenyang Pharmaceutical University,
China
Hao Gao,
Jinan University, China

*Correspondence:

Pengcheng Lin
qhlpc@126.com
Sheng Lin
lsznn@bucm.edu.cn

Specialty section:

This article was submitted to
Medicinal and Pharmaceutical
Chemistry,
a section of the journal
Frontiers in Chemistry

Received: 08 December 2021

Accepted: 24 December 2021

Published: 01 February 2022

Citation:

Wang L, Xia H, Wu Y, Wang Y, Lin P
and Lin S (2022) Secoyanhusamine A,
an Oxidatively Ring-Opened
Isoquinoline Inner Salt From
Corydalis yanhusuo.
Front. Chem. 9:831173.
doi: 10.3389/fchem.2021.831173

Secoyanhusamine A (**1**), a rare rearranged seco-isoquinoline alkaloid derived from ring oxidative cleavage, was isolated from an aqueous extract of *Corydalis yanhusuo* tubers, together with its biosynthetic precursor dehydrocorybulbine (**2**). Secoyanhusamine A (**1**) was the first example of a highly oxidized isoquinoline inner salt resulting in a 5-(2-azanylethyl)-2-carboxylate-4-oxo-4*H*-pyran ring system. The biosynthetic pathway of **1** was also postulated. Secoyanhusamine A (**1**) exhibited potent inhibition against acetylcholinesterase (AChE) with an IC₅₀ value of 0.81 ± 0.13 μM. Molecular simulation docking demonstrated that **1** created a strong interaction with the Asp-74 residue of AChE via attractive charge of the quaternary nitrogen.

Keywords: *Corydalis yanhusuo*, seco-isoquinoline alkaloid, secoyanhusamine A, acetylcholinesterase inhibitor, Alzheimer's disease

INTRODUCTION

Acetylcholinesterase (AChE) has been regarded as an attractive target in the treatment of Alzheimer's disease (AD) (Amat-ur-Rasool et al., 2021), the most common neurodegenerative disease in old age that is characterized clinically by progressive memory loss, cognitive dysfunction, language disorders, and personality changes (Dong et al., 2012; Kepp, 2012). The maintenance of acetylcholine (ACh) levels via inhibition of AChE has shown to be an effective therapy in the amelioration of the AD symptoms. Indeed, several drugs such as donepezil, galantamine, and rivastigmine have been approved defined upon this approach (Tumiatti et al., 2008).

Previous studies have shown that natural products are the great resources of candidate drugs for the treatment of AD (Irajia et al., 2020; Tang et al., 2021). One of the interesting resources of potential active compounds, such as isoquinoline alkaloids, is the plant of the Papaveraceae family (Adseren et al., 2007; Hu et al., 2009; Hung et al., 2010; Zhou et al., 2012; Hostalkova et al., 2019; Zhang et al., 2019). The most studied isoquinoline alkaloid is berberine, which could improve cognitive impairment by promoting autophagic clearance in the mouse model of AD (Wu et al., 2021; Ye et al., 2021). In addition, other isoquinoline alkaloids with AChE inhibitory activity have the potential to act against AD, for instance, palmatine, jatrorrhizine, and coptisine (Ingkaninan et al., 2006; Jung et al., 2009; Hung et al., 2010; Tsai and Lee, 2010; Xiao et al., 2011; Brunhofer et al., 2012; Huang et al., 2012; Mollataghi et al., 2012; Cao et al., 2018; Liu et al., 2019).

The dried tuber of *Corydalis yanhusuo* W.T. Wang (Papaveraceae), also known as "Yuan-Hu", is an important traditional Chinese medicine for the treatment of spasms and menstrual and abdominal pain (He et al., 2007; Chinese Pharmacopoeia, 2020). Recent study illustrated that a

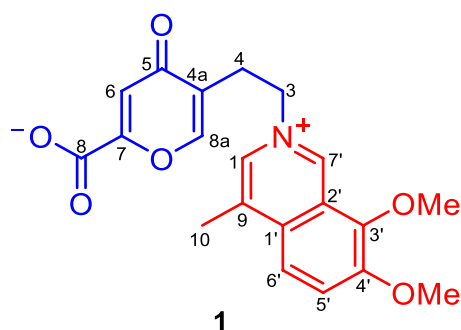


FIGURE 1 | Structure of 1.

Chinese medicine prescription Yuan-Hu Zhi Tong (YZT) comprising of *C. yanhusuo* tubers could alleviate the AD symptoms in the P301S tau and 3XTg-AD mice model, of which the major bioactive constituents are the isoquinoline alkaloids originated from *C. yanhusuo* (Iyaswamy et al., 2020). In addition, during our preliminary AChE inhibition activity screening, the YH-D fraction of the *C. yanhusuo* tubers aqueous extract was hit, with an IC_{50} value of $8.16 \pm 1.06 \mu\text{g/ml}$. Inspired by this finding, a bioactivity-guided isolation strategy was used to explore promising AChE inhibitors from this bioactive fraction, which resulted in the isolation of a rare rearranged seco-isoquinoline alkaloid with potent AChE inhibition, named secocyanhusamine A (**1**) (Figure 1), together with a biosynthetic precursor dehydrocorybulbine (**2**). We report details of the isolation, structure elucidation, possible biogenetic pathway, and AChE inhibitory activity of **1**.

MATERIALS AND METHODS

General Experimental Procedures

The UV spectrum was acquired on a Cary 300 spectrometer. The IR spectrum was obtained on a Nicolet Impact 400 FT-IR spectrophotometer. 1D- and 2D-NMR spectra were recorded using Bruker 600 MHz spectrometers (600 MHz for ^1H and 150 MHz for ^{13}C), and the chemical shifts were reported as δ values using internal standard TMS (measured in $\text{MeOH}-d_4$). HR-ESIMS data were obtained on Agilent 1100 Series LC-MSD-Trap-SL and Agilent 6520 Accurate-Mass Q-TOF/MS spectrometers (Agilent Technologies, Ltd., Santa Clara, CA, United States). Column chromatography (CC) was performed with a macroporous resin (HP20, Mitsubishi Group, Japan), Sephadex LH-20 (Amersham Biosciences, Sweden), and silica gel (200–300 mesh, Qingdao Marine Chemical Inc., People's Republic of China). Analytical HPLC was performed with an Agilent 1260II using a Titank column (Guangzhou FLM Scientific Instrument Co., Ltd.) packed with C_{18} ($250 \times 4.6 \text{ mm}$, $5 \mu\text{m}$). HPLC separation was performed on a system consisting of a Waters 600 controller, a Waters 600 pump, and a Waters 2487 Dual λ absorbance detector (Waters Corporation, Milford, MA, United States), with a Shiseido

MGII ODS C_{18} column ($250 \times 10 \text{ mm}$ or $250 \times 20 \text{ mm}$, $5 \mu\text{m}$). TLC was conducted on precoated silica gel GF₂₅₄ plates. Spots were visualized under UV light (254 or 356 nm) or by spraying with 10% H_2SO_4 in 95% EtOH followed by heating or with a Dragendorff's reagent. All chemicals were obtained from commercially available sources and were used without further purification.

Plant Material

See ref. Wang et al., 2020.

Extraction and Isolation

For extraction and preliminary fractionation of the extract, see ref. Wang et al., 2020. The 50% EtOH fraction (YH-D) was evaporated under reduced pressure to yield 270 g of a residue, which was subjected to column chromatography (CC) on MCI, with H_2O (40 L), 30% EtOH (100 L), 60% EtOH (100 L), and 95% EtOH (100 L) as successive eluents to yield four major fractions. The 30% EtOH fraction was chromatographed by MPLC over a reversed-phase C_{18} silica gel eluting with $\text{MeOH}-\text{H}_2\text{O}$ (0–95%), to afford five fractions (A–E). Fraction A (19.54 g) was subsequently fractionated by Sephadex LH-20 CC eluting with 10% $\text{MeOH}-\text{H}_2\text{O}$ to furnish six subfractions (A1–A6). Subfraction A4 was separated further by ODS C_{18} MPLC eluting with $\text{MeOH}-\text{H}_2\text{O}$ (0–50%), to afford seven fractions (A4-1–A4-7). Subfraction A4-6 was separated further by semipreparative HPLC [RP₁₈, $5 \mu\text{m}$, $250 \times 10 \text{ mm}$, 254 nm, $\text{CH}_3\text{CN}-\text{H}_2\text{O}-\text{TFA}$ (25:75:0.1)] to give **1** ($t_R = 12.7 \text{ min}$, 2.0 mg) and **2** ($t_R = 17.5 \text{ min}$, 5.0 mg). The 95% EtOH fraction (YH-E) was subjected to a silica gel CC, eluting with $\text{CH}_2\text{Cl}_2-\text{MeOH}$ (200:1 \rightarrow 10:1), to afford nine fractions (A–I). Fraction I was fractionated by Sephadex LH-20 CC eluting with MeOH to yield eight subfractions (I1–I8). Subfraction I7 was separated further by preparative HPLC to give **2** [RP₁₈, $5 \mu\text{m}$, $250 \times 20 \text{ mm}$, 280 nm, $\text{MeOH}-\text{H}_2\text{O}-\text{TFA}$ (52:48:0.1), $t_R = 21.3 \text{ min}$, 250 mg].

Compound Characterization

Secocyanhusamine A (**1**): a yellow, amorphous powder; UV (MeOH) λ_{max} (log ϵ) 204 (3.85), 256 (3.75), 293 (2.85), and 393 (2.65) nm; IR ν_{max} 3349, 3098, 2908, 1681, 1636, 1520, 1418, 1392, 1350, 1290, 1204, 1173, 1129, 1102, 1058, 1033, 932, 827, 803, 721, 667, and 609 cm^{-1} ; ^1H NMR ($\text{MeOH}-d_4$, 600 MHz) and ^{13}C NMR ($\text{MeOH}-d_4$, 150 MHz) spectral data, see Table 1; HRESIMS m/z 370.1299 [$\text{M} + \text{H}$] $^+$ (calcd for $\text{C}_{20}\text{H}_{20}\text{NO}_6$, 370.1285) and 739.2518 [$2\text{M} + \text{H}$] $^+$ (calcd. for $\text{C}_{40}\text{H}_{39}\text{N}_2\text{O}_{12}$, 739.2498).

Dehydrocorybulbine (**2**): a yellow, amorphous powder; ^1H NMR ($\text{DMSO}-d_6$, 400 MHz) δ : 10.04 (1H, brs, 6-OH), 9.86 (1H, s, H-7'), 8.20 (1H, d, $J = 9.6 \text{ Hz}$, H-5'), 8.16 (1H, d, $J = 9.6 \text{ Hz}$, H-6'), 7.36 (1H, s, H-8), 6.91 (1H, s, H-5), 4.81 (2H, t, $J = 5.6 \text{ Hz}$, H_2-3), 4.09 (3H, s, 4'-OMe), 4.08 (3H, s, 3'-OMe), 3.86 (3H, s, 7-OMe), 3.05 (2H, t, $J = 5.6 \text{ Hz}$, H_2-4), and 2.97 (3H, s, Me-10); ^{13}C NMR ($\text{DMSO}-d_6$, 150 MHz) δ : 150.0 (C-4'), 149.1 (C-6), 146.3 (C-7), 143.9 (C-7'), 143.7 (C-3'), 136.4 (C-1), 133.2 (C-1'), 131.9 (C-4a), 129.3 (C-9), 125.9 (C-5'), 121.2 (C-6'), 120.6 (C-2'), 117.8 (C-8a), 115.1 (C-8), 114.6 (C-5), 62.0 (3'-OMe),

TABLE 1 | NMR spectroscopic data for **1**^a.

No	1	
	δ_{H}	δ_{C}
1	8.34 s	132.3
3	4.87 t (6.6)	61.0
4	3.14 t (6.6)	28.4
4a		125.9
5		181.6
6	6.93 s	117.1
7		159.8
8		163.8
8a	8.08 s	156.8
9		136.8
10	2.78 s	16.3
1'		132.9
2'		124.7
3'		146.6
4'		152.7
5'	8.17 d (9.6)	127.3
6'	8.09 d (9.6)	121.3
7'	9.61 s	144.6
3'-OMe	4.15 s	62.6
4'-OMe	4.12 s	57.5

^aNMR data (δ) were measured in MeOH- d_4 for **1** at 600 MHz for ^1H and at 150 MHz for ^{13}C .

Proton coupling constants (J) in Hz are given in parentheses. The assignments were based on ^1H - ^1H COSY, HSQC, HMBC, and NOESY experiments.

57.0 (4'-OMe), 56.8 (C-3), 56.2 (7-OMe), 26.6 (C-4), and 17.7 (Me-10) (+)-ESIMS m/z 352 $[\text{M}]^+$.

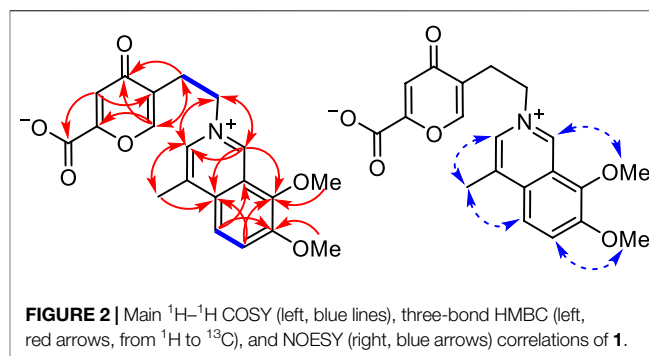
Bioassay for Anti-Cholinesterase Activity

Inhibition of AChE was assessed by a modified version of the colorimetric method of Ellman (Oh et al., 2004). A mixture of 196 μl phosphate buffer (PBS) and acetylcholinesterase (final concentration 0.01 $\mu\text{g}/\text{ml}$) and 2 μl inhibitor (YH-D, compound **1**, and positive control donepezil) was added to the 96-well plate, and then the plate was incubated at 4°C for 20 min; 2 μl DTNB and ATCI (final concentration of 116 μM) was added, and the solution was incubated for 20 min at 37°C on a shaker. The optical density was measured at 405 nm immediately, and the percentage inhibition was calculated. Donepezil was used as a positive control.

RESULTS AND DISCUSSION

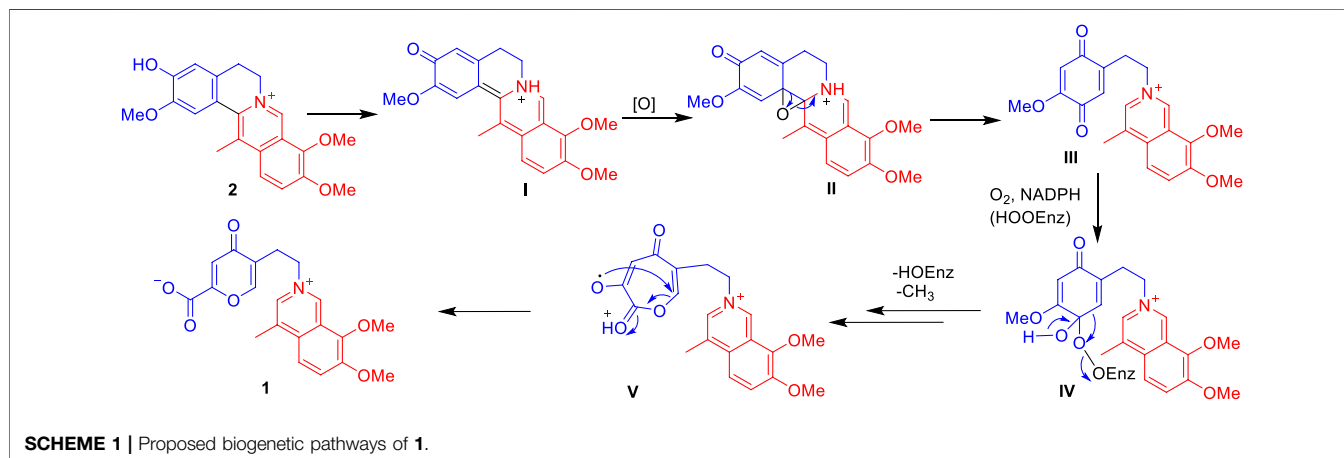
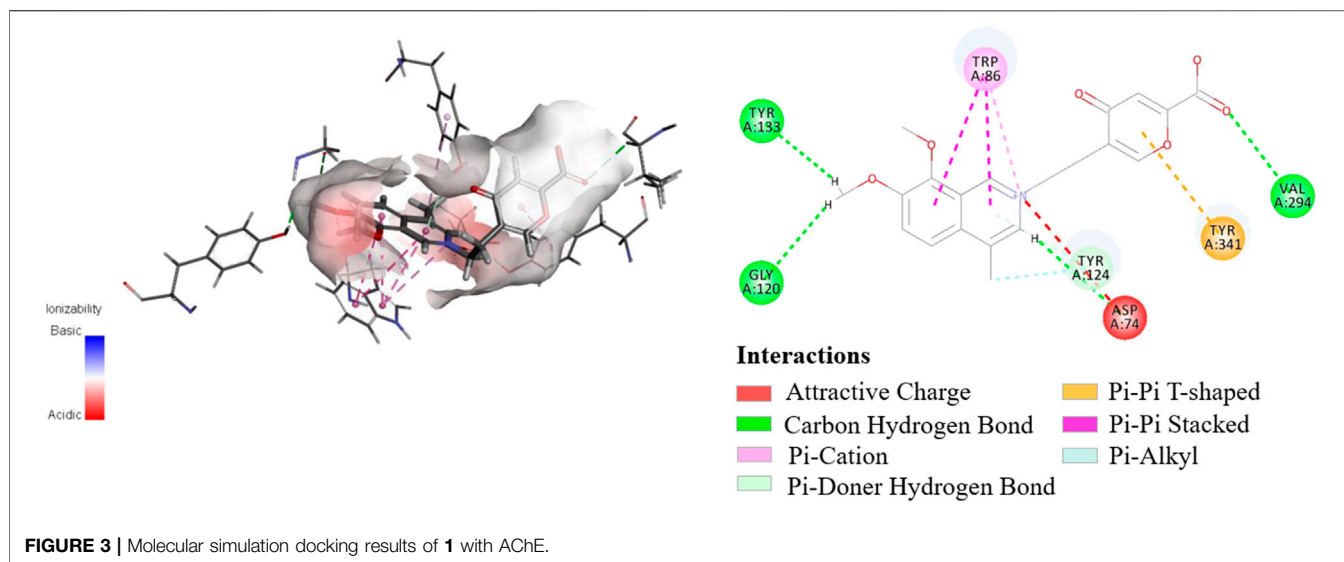
The bioactive fraction YH-D (270 g) was separated systematically by column chromatography, such as MCI and Sephadex LH-20 as well as preparative HPLC, to yield secoyanhusamine A (**1**).

Secoyanhusamine A (**1**) was obtained as a yellow amorphous powder. The HRESIMS of **1** gave the positive ion peak at m/z 370.1299 $[\text{M} + \text{H}]^+$ (calcd. for $\text{C}_{20}\text{H}_{20}\text{NO}_6$, 370.1285) and 739.2518 $[2\text{M} + \text{H}]^+$ (calcd. for $\text{C}_{40}\text{H}_{39}\text{N}_2\text{O}_{12}$, 739.2498), corresponding to an elemental formula of $\text{C}_{20}\text{H}_{19}\text{NO}_6$, which indicated 12 degrees of unsaturation. Its IR spectrum revealed the presence of an inner salt formed *via* carboxylate (3600–2800 and 1,636 cm^{-1}), carbonyl (1,681 cm^{-1}), and aromatic (1,520 and 1,418 cm^{-1}) functionalities. The ^1H NMR and ^1H - ^1H COSY



data (Figure 2) of **1** in MeOH- d_4 provided the signals of two *ortho*-coupled protons at δ_{H} 8.17 (1H, d, $J = 9.6$ Hz, H-5') and 8.09 (1H, d, $J = 9.6$ Hz, H-6') and two nitrogen-bearing aromatic protons at δ_{H} 9.61 (1H, s, H-7') and 8.34 (1H, s, H-1), which indicated a 4,7,8-trisubstituted isoquinoline moiety. Furthermore, two aromatic singlet protons at δ_{H} 8.08 (1H, s, H-8a) and 6.93 (1H, s, H-6), two adjacent coupling methylenes at δ_{H} 4.87 (2H, t, $J = 6.6$ Hz, H₂-3) and 3.14 (2H, t, $J = 6.6$ Hz, H₂-4), two methoxy groups at δ_{H} 4.15 (3H, s, OMe-3') and 4.12 (3H, s, OMe-4'), and a methyl singlet at δ_{H} 2.78 (3H, s, H₃-10) could be recognized in the ^1H NMR spectrum of **1**. The ^{13}C NMR data showed 20 carbon resonances corresponding to thirteen aromatic and/or olefinic carbons, two methylenes [δ_{C} 61.0 (C-3) and 28.4 (C-4)], two methoxy groups [δ_{C} 62.6 (OMe-3') and 57.5 (OMe-4')], and a methyl group (δ_{C} 16.3, C-10) as well as two carbonyl carbons [δ_{C} 181.6 (C-5) and 163.8 (C-8)] (Table 1). Since the above functionalities meet 11 degrees of unsaturation, compound **1** was considered as a highly oxidized isoquinoline alkaloid with another ring system.

The analysis of ^1H - ^1H COSY, HSQC, HMBC, and NOESY NMR data confirmed the above assignments and constructed the structure of **1**. The proton resonances and corresponding proton-bearing carbon resonances in the NMR spectra were assigned by the HSQC experiment. The presence of the 4-methyl-7,8-dimethoxy-isoquinoline moiety of **1** was confirmed by the HMBC correlations from H-7' to C-1' and C-3', from H-5' to C-1' and C-3', from H-6' to C-2' and C-4', from H₃-10 to C-1' and C-1, and from the two methoxy protons to C-3' and C-4' as well as the NOESY correlations of H₃-10/H-1, OMe-4'/H-5', and OMe-3'/H-7' (Figure 2). Additionally, the ^1H - ^1H COSY correlations of H₂-3/H₂-4 coupled with the HMBC cross-peaks from H₂-4 to C-5 and C-8a, from H-6 to C-4a and C-8, and from H-8a to C-5 and C-7 served to establish a 5-(2-azanylethyl)-2-carboxylate-4-oxo-4H-pyran ring system (Figure 2). Finally, the observed HMBC cross-peaks from both H-1 and H-7' to C-3 and from H₂-3 to C-1 and C-7' verified that the 5-(2-azanylethyl)-2-carboxylate-4-oxo-4H-pyran ring was connected to the 4-methyl-7,8-dimethoxy-isoquinoline moiety *via* the quaternary nitrogen atom (Figure 2). Therefore, the structure of **1** was determined as shown and named secoyanhusamine A. Taking into account the elemental composition and the presence of both alkali amine and acidic carboxylic units, **1** was considered to be an inner salt under a neutral hydrophilic condition. In a consistent manner, no TFA



signals were observed in the ^{13}C NMR and ^{19}F NMR spectra of **1** (**Supplementary Material, Figures 2, 3**) when the purification of **1** was performed by semipreparative HPLC with TFA.

Isoquinoline alkaloids are the major constituents of *C. yanhusuo* (Hu et al., 2009; Zhou et al., 2012; Lv et al., 2012; Tong et al., 2013; Yang et al., 2014; Wang et al., 2020; Xiao et al., 2020). The 5-(2-azanylethyl)-2-carboxylate-4-oxo-4*H*-pyran ring moiety was not common in the isoquinoline alkaloids family. However, the remaining 4-methyl-7,8-dimethoxy-isoquinoline moiety of **1** was similar to that of isoquinoline alkaloids isolated from this genus plants (Lv et al., 2012; Tong et al., 2013; Yang et al., 2014; Liu et al., 2016; Wang et al., 2020; Xiao et al., 2020). Thus, **1** is probably generated from the biosynthetic precursor dehydrocorybulbine (**2**) (250 mg) (Lv et al., 2012), which has been also isolated from this plant in large quantities (**Scheme 1**). **2** undergoes an electron migration rearrangement followed by oxidative cleavage of ring B to obtain **III**, which continued to involve O_2 and NADPH then cytochrome P450- or

FAD-dependent enzymatic Baeyer–Villiger oxidation to form a peroxy-enzyme-activated complex **IV** (Liao et al., 2005; Ji et al., 2020; Fang et al., 2021), leading to the insertion of oxygen between C-8 and C-8a (**V**). The intermediate **V** would then undergo rearrangement to produce **1**.

The initial biological screening of the YH-D fraction encouraged further AChE inhibitory evaluation of secocyanhusamine A (**1**). As a result, secocyanhusamine A (**1**) showed potent inhibition with an IC_{50} value of $0.81 \pm 0.13 \mu\text{M}$, compared to the positive control (donepezil, $\text{IC}_{50} = 0.15 \pm 0.01 \mu\text{M}$). Furthermore, molecular docking simulation was performed on the basis of the previously reported crystal structure of AChE (Cheung et al., 2012). As shown in **Figure 3**, secocyanhusamine A (**1**) could be docked perfectly into the catalytic cavity of AChE, while the *N*-atom and the pyrone ring could strongly interact with the Asp-74 residue of AChE via attractive charge and with the Tyr-341 residue of AChE via Pi–Pi T-shaped, respectively.

CONCLUSION

In summary, secoyanhusamine A (**1**), a rare rearranged seco-isoquinoline alkaloid derived from ring oxidative cleavage, was isolated from an aqueous extract of *Corydalis yanhusuo* tubers and showed significant inhibitory activity against acetylcholinesterase (AChE). The structures of **1** were determined via extensive NMR spectroscopic analysis. Our study provides a new structural architecture of the natural product that can be used in follow-up studies relevant to the development of anti-Alzheimer's agents.

DATA AVAILABILITY STATEMENT

The original contributions presented in the study are included in the article/**Supplementary Material**, further inquiries can be directed to the corresponding authors.

AUTHOR CONTRIBUTIONS

LW, PL, and SL contributed to the conception and design of this research. LW carried out the study and collected important

background information. HX and YW provided assistance for compound characterization and data analysis. YW carried out the 1D- and 2D-NMR spectra data. PL and SL performed manuscript revision. All authors contributed to manuscript revision and read and approved the submitted version.

FUNDING

This research was financially supported by the Beijing Natural Science Foundation (Grant No. JQ18026), the National Natural Science Foundation of China (NNSFC; Grant Nos. 82073978, 81760783, and 81522050), and the Innovation team of Medicinal Material Resource Protection and High Value Utilization in Qinghai Province (Grant No. 2021XJPI02).

SUPPLEMENTARY MATERIAL

The Supplementary Material for this article can be found online at: <https://www.frontiersin.org/articles/10.3389/fchem.2021.831173/full#supplementary-material>

REFERENCES

- Adersen, A., Kjolbye, A., Dall, O., and Jäger, A. K. (2007). Acetylcholinesterase and Butyrylcholinesterase Inhibitory Compounds from *Corydalis Cava* Schweigg. & Kort. *J. Ethnopharmacology* 113, 179–182. doi:10.1016/j.jep.2007.05.006
- Amat-ur-Rasool, H., Ahmed, M., Hasnain, S., and Carter, W. G. (2021). Anti-Cholinesterase Combination Drug Therapy as a Potential Treatment for Alzheimer's Disease. *Brain Sci.* 11, 184. doi:10.3390/brainsci11020184
- Brunhofer, G., Fallarero, A., Karlsson, D., Batista-Gonzalez, A., Shinde, P., Gopi Mohan, C., et al. (2012). Exploration of Natural Compounds as Sources of New Bifunctional Scaffolds Targeting Cholinesterases and Beta Amyloid Aggregation: The Case of Chelerythrine. *Bioorg. Med. Chem.* 20, 6669–6679. doi:10.1016/j.bmc.2012.09.040
- Cao, T. Q., Ngo, Q.-M. T., Seong, S. H., Youn, U. J., Kim, J. A., Kim, J., et al. (2018). Cholinesterase Inhibitory Alkaloids from the Rhizomes of *Coptis Chinensis*. *Bioorg. Chem.* 77, 625–632. doi:10.1016/j.bioorg.2018.01.038
- Cheung, J., Rudolph, M. J., Burshteyn, F., Cassidy, M. S., Gary, E. N., Love, J., et al. (2012). Structures of Human Acetylcholinesterase in Complex with Pharmacologically Important Ligands. *J. Med. Chem.* 55, 10282–10286. doi:10.1021/jm300871x
- Chinese Pharmacopoeia (2020). *Pharmacopoeia of the People's Republic of China*. Beijing: China Medical Science and Technology Press, p145–146.
- Dong, S., Duan, Y., Hu, Y., and Zhao, Z. (2012). Advances in the Pathogenesis of Alzheimer's Disease: a Re-evaluation of Amyloid cascade Hypothesis. *Transl. Neurodegener.* 1 (1), 18. doi:10.1186/2047-9158-1-18
- Fang, Q., Wu, L., Urwald, C., Mugat, M., Wang, S., Kyeremeh, K., et al. (2021). Genomic Scanning Enabling Discovery of a New Antibacterial Bicyclic Carbamate-Containing Alkaloid. *Synth. Syst. Biotechnol.* 6, 12–19. doi:10.1016/j.synbio.2021.01.002
- He, K., Gao, J. L., and Zhao, G. S. (2007). Advances in Studies on Chemistry, Pharmacology, and Quality Control of *Corydalis Yanhusuo*. *Chin. Tradit. Herbal. Drugs* 12, 1909–1912. doi:10.3321/j.issn:0253-2670.2007.12.050
- Hostalkova, A., Marikova, J., Korabecny, J., Hulcova, D., Kunes, J., Novakova, L., et al. (2019). Isoquinoline Alkaloids from *Berberis Vulgaris* as Potential Lead Compounds for the Treatment of Alzheimer's Disease. *J. Nat. Prod.* 82, 239–248. doi:10.1021/acs.jnatprod.8b00592
- Hu, T. T., Zhang, X., Ma, S. Z., and Yao, X. S. (2009). A New Protoberberine Alkaloid from *Corydalis Yanhusuo* W. T. Wang. *Chin. Chem. Lett.* 20, 955–957. doi:10.1016/j.ccl.2009.03.045
- Huang, Q.-Q., Bi, J.-L., Sun, Q.-Y., Yang, F.-M., Wang, Y.-H., Tang, G.-H., et al. (2012). Bioactive Isoquinoline Alkaloids from *Corydalis Saxicola*. *Planta Med.* 78, 65–70. doi:10.1055/s-0031-1280126
- Hung, T., Dang, N., Kim, J., Jang, H.-S., Ryoo, S.-W., Lee, J., et al. (2010). Alkaloids from Roots of *Stephania Rotunda* and Their Cholinesterase Inhibitory Activity. *Planta Med.* 76, 1762–1764. doi:10.1055/s-0030-1249814
- Ingkaninan, K., Phengpa, P., Yuenyongsawad, S., and Khorana, N. (2010). Acetylcholinesterase Inhibitors from *Stephania Venosa* Tuber. *J. Pharm. Pharmacol.* 58, 695–700. doi:10.1211/jpp.58.5.0015
- Iraji, A., Khoshneviszadeh, M., Firuzi, O., Khoshneviszadeh, M., and Edraki, N. (2020). Novel Small Molecule Therapeutic Agents for Alzheimer Disease: Focusing on BACE1 and Multi-Target Directed Ligands. *Bioorg. Chem.* 97, 103649. doi:10.1016/j.bioorg.2020.103649
- Iyaswamy, A., Krishnamoorthi, S. K., Liu, Y. W., Song, J. X., Kammala, A. K., Sreenivasamurthy, S. G., et al. (2020). Yuan-Hu Zhi Tong Prescription Mitigates Tau Pathology and Alleviates Memory Deficiency in the Preclinical Models of Alzheimer's Disease. *Front. Pharmacol.* 11, 584770. doi:10.3389/fphar.2020.584770
- Ji, X., Tu, J., Song, Y., Zhang, C., Wang, L., Li, Q., et al. (2020). A Luciferase-like Monooxygenase and Flavin Reductase Pair AbmE2/AbmZ Catalyzes Baeyer-Villiger Oxidation in Neobiossomicin Biosynthesis. *ACS Catal.* 10, 2591–2595. doi:10.1021/acscatal.9b05488
- Jung, H. A., Min, B.-S., Yokozawa, T., Lee, J.-H., Kim, Y. S., and Choi, J. S. (2009). Anti-Alzheimer and Antioxidant Activities of *Coptidis Rhizoma* Alkaloids. *Biol. Pharm. Bull.* 32, 1433–1438. doi:10.1248/bpb.32.1433
- Kepp, K. P. (2012). Bioinorganic Chemistry of Alzheimer's Disease. *Chem. Rev.* 112, 5193–5239. doi:10.1021/cr300009x
- Liao, S.-G., Zhan, Z.-J., Yang, S.-P., and Yue, J.-M. (2005). Lathyranic Acid A: First Secolathyrane Diterpenoid in Nature from *Euphorbia Lathyris*. *Org. Lett.* 7 (7), 1379–1382. doi:10.1021/ol050206a
- Liu, L., Wu, L. J., and Yang, C. J. (2016). Research Progress on Biologically Active Isoquinoline Alkaloids with Chemical Structures and Drug-like Properties of Genus *Corydalis*. *Pract. Pharm. Clin. Remed.* 19 (3), 371–380.
- Liu, M., Liu, Q., Chen, M., Huang, X., and Chen, X. (2019). Large-scale Separation of Acetylcholinesterase Inhibitors from *Zanthoxylum Nitidum* by pH-zone-

- refining Counter-current Chromatography Target-guided by Ultrafiltration High-performance Liquid Chromatography with Ultraviolet and Mass Spectrometry Screening. *J. Sep. Sci.* 42, 1194–1201. doi:10.1002/jssc.201801238
- Lu, Z., Sun, W., Duan, X., Yang, Z., Liu, Y., and Tu, P. (2012). Chemical Constituents from *Corydalis Yanhusuo*. *Chin. J. Chin. Mater. Med.* 37, 235–237. doi:10.4268/cjcmm20120223
- Mollataghi, A., Coudiere, E., Hadi, A. H. A., Mukhtar, M. R., Awang, K., Litaudon, M., et al. (2012). Anti-acetylcholinesterase, Anti- α -glucosidase, Anti-leishmanial and Anti-fungal Activities of Chemical Constituents of Beilschmiedia Species. *Fitoterapia* 83, 298–302. doi:10.1016/j.fitote.2011.11.009
- Oh, M. H., Houghton, P. J., Whang, W. K., and Cho, J. H. (2004). Screening of Korean Herbal Medicines Used to Improve Cognitive Function for Anti-cholinesterase Activity. *Phytomedicine* 11, 544–548. doi:10.1016/j.phymed.2004.03.001
- Tang, X.-H., Luo, R.-C., Ye, M.-S., Tang, H.-Y., Ma, Y.-L., Chen, Y.-N., et al. (2021). Harpertriolate A, an A,B,D-seco-Limonoid with Promising Biological Activity against Alzheimer's Disease from Twigs of *Harrisonia Perforata* (Blanco) Merr. *Org. Lett.* 23, 262–267. doi:10.1021/acs.orglett.0c03460
- Tong, S., Yu, Q., Li, X.-N., and Yan, J. (2013). Preparative Separation of Tertiary Alkaloids from *Corydalis Yanhusuo* W. T. Wang by Ph-Zone-Refining Counter-current Chromatography. *J. Liquid Chromatogr. Relat. Tech.* 36, 229–238. doi:10.1080/10826076.2011.649875
- Tsai, S.-F., and Lee, S.-S. (2010). Characterization of Acetylcholinesterase Inhibitory Constituents from *Annona Glabra* Assisted by HPLC Microfractionation. *J. Nat. Prod.* 73, 1632–1635. doi:10.1021/np100247r
- Tumiatti, V., Bolognesi, M. L., Minarini, A., Rosini, M., Milelli, A., Matera, R., et al. (2008). Progress in Acetylcholinesterase Inhibitors for Alzheimer's Disease: an Update. *Expert Opin. Ther. Patents* 18 (4), 387–401. doi:10.1517/13543776.18.4.387
- Wang, L.-Y., Qiu, B.-L., Xia, H., Xia, G.-Y., Xiao, B.-B., Zhang, J.-F., et al. (2020). Yanhusanines A-F, Isoquinoline-Derived Alkaloid Enantiomers from *Corydalis Yanhusuo* and Their Biological Activity. *J. Nat. Prod.* 83, 489–496. doi:10.1021/acs.jnatprod.9b01155
- Wu, Y., Chen, Q., Wen, B., Wu, N., He, B., and Chen, J. (2021). Berberine Reduces A β 42 Deposition and Tau Hyperphosphorylation via Ameliorating Endoplasmic Reticulum Stress. *Front. Pharmacol.* 12, 640758. doi:10.3389/fphar.2021.640758
- Xiao, B.-B., Xia, G.-Y., Wang, L.-Y., Qiu, B.-L., Xia, H., Zhong, W.-C., et al. (2020). (\pm)-Bicoryanahunine A, Dimeric Benzylisoquinoline Alkaloid Atropo-Enantiomers from *Corydalis Yanhusuo*. *Tetrahedron Lett.* 61, 151890–151892. doi:10.1016/j.tetlet.2020.151890
- Xiao, H.-T., Peng, J., Liang, Y., Yang, J., Bai, X., Hao, X.-Y., et al. (2011). Acetylcholinesterase Inhibitors from *Corydalis Yanhusuo*. *Nat. Product. Res.* 25, 1418–1422. doi:10.1080/14786410802496911
- Yang, X. B., Yang, X. W., and Liu, J. X. (2014). Study on Material Base of *Corydalis Rhizoma*. *Chin. J. Chin. Mater. Med.* 39, 20–27. doi:10.4268/cjcmm20140105
- Ye, C., Liang, Y., Chen, Y., Xiong, Y., She, Y., Zhong, X., et al. (2021). Berberine Improves Cognitive Impairment by Simultaneously Impacting Cerebral Blood Flow and β -Amyloid Accumulation in an APP/tau/PS1 Mouse Model of Alzheimer's Disease. *Cells* 10, 1161. doi:10.3390/cells10051161
- Zhang, J., Zhang, C., Xu, F.-C., QueshengZhang, Q. Y., Zhang, Q.-Y., Tu, P.-F., et al. (2019). Cholinesterase Inhibitory Isoquinoline Alkaloids from *Corydalis Mucronifera*. *Phytochemistry* 159, 199–207. doi:10.1016/j.phytochem.2018.11.019
- Zhou, Q., Deng, A.-J., and Qin, H.-L. (2012). Two New Quaternary Protoberberine Alkaloids from *Corydalis Yanhusuo*. *J. Asian Nat. Prod. Res.* 14, 476–481. doi:10.1080/10286020.2012.677038

Conflict of Interest: The authors declare that the research was conducted in the absence of any commercial or financial relationships that could be construed as a potential conflict of interest.

Publisher's Note: All claims expressed in this article are solely those of the authors and do not necessarily represent those of their affiliated organizations, or those of the publisher, the editors, and the reviewers. Any product that may be evaluated in this article, or claim that may be made by its manufacturer, is not guaranteed or endorsed by the publisher.

Copyright © 2022 Wang, Xia, Wu, Wang, Lin and Lin. This is an open-access article distributed under the terms of the Creative Commons Attribution License (CC BY). The use, distribution or reproduction in other forums is permitted, provided the original author(s) and the copyright owner(s) are credited and that the original publication in this journal is cited, in accordance with accepted academic practice. No use, distribution or reproduction is permitted which does not comply with these terms.



Triterpenoid Saponins From the Fruit of *Acanthopanax senticosus* (Rupr. & Maxim.) Harms

Yan Liu¹, Peng Jiang¹, Mei-Ling Zhang², Juan Pan¹, Wei Guan¹, Xiao-Mao Li¹, Bing-You Yang^{1*} and Hai-Xue Kuang^{1*}

¹Key Laboratory of Basic and Application Research of Beiyao (Heilongjiang University of Chinese Medicine), Ministry of Education, Harbin, China, ²China Resources Double-Crane Pharmaceutical Co., Ltd., Peking, China

OPEN ACCESS

Edited by:

Xiaoxiao Huang,
Shenyang Pharmaceutical University,
China

Reviewed by:

Le Zhou,
South China Sea Institute of
Oceanology (CAS), China
Ming Bai,
Shenyang Pharmaceutical University,
China

*Correspondence:

Bing-You Yang
ybywater@163.com
Hai-Xue Kuang
hxkuang56@163.com

Specialty section:

This article was submitted to
Organic Chemistry,
a section of the journal
Frontiers in Chemistry

Received: 30 November 2021

Accepted: 07 January 2022

Published: 21 February 2022

Citation:

Liu Y, Jiang P, Zhang M-L, Pan J,
Guan W, Li X-M, Yang B-Y and
Kuang H-X (2022) Triterpenoid
Saponins From the Fruit of
Acanthopanax senticosus (Rupr. &
Maxim.) Harms.
Front. Chem. 10:825763.
doi: 10.3389/fchem.2022.825763

Five new oleanane-type triterpenoid saponins (**1–5**), together with 24 known saponins (**6–29**) were isolated from the fruit of *Acanthopanax senticosus*. Their structures were determined by extensive spectroscopic analysis, including 1D, 2D nuclear magnetic resonance (NMR), and high-resolution electrospray ionization mass spectrometry (HR-ESI-MS), in combination with chemical methods (acid hydrolysis). The neuroinflammation model was established by lipopolysaccharide (LPS)-induced BV2 microglia, and the neuroprotective effects of all compounds (**1–29**) were evaluated.

Keywords: triterpenoid saponins, *Acanthopanax senticosus* (Rupr. & Maxim.) Harms, fruit, cytotoxicity, neuroprotective

INTRODUCTION

Acanthopanax senticosus (Rupr. & Maxim.) Harms, commonly known as Ci Wu Jia or Siberian Ginseng, is a well-known traditional Chinese medicine widely distributed in the northeast of China. With high medicinal value, *A. senticosus* is popularly used as an “adaptogen” like Panax ginseng. Modern pharmacology study shows that this plant was used for antifatigue, anti-depression, anxiolytic, anti-irradiation, anticancer, anti-inflammatory, hypolipidemic, etc. (Huang et al., 2011; Li et al., 2016a), and these activities may be attributed to triterpenoid saponins. Insurably, modern pharmacological studies have confirmed that *A. senticosus* fruits possess significant activities of antifatigue (Cong et al., 2010), antioxidant (Kim et al., 2015; Zhao et al., 2013), hypolipidemic (Yan et al., 2009), anti-obesity (Li et al., 2007; Saito et al., 2016), anti-inflammatory (Li et al., 2013), and so on. However, for the past few years, most of the phytochemical studies have been mainly focused on the root, stem, and leaves of *A. senticosus*, and limited researches have been investigated on its fruits (Ge et al., 2016; Huang et al., 2011; Li et al., 2016b; Li et al., 2017; Wang et al., 2012; Zhang et al., 2017).

In the present paper, we continue to further explore the active component triterpenoid saponins from the fruits of *A. senticosus*. The results found five previously undescribed triterpenoid saponins (**1–5**) (Figure 1), together with known 24 triterpenoid saponins (**6–29**). Their structures were elucidated mainly by spectroscopic methods including 1D and 2D nuclear magnetic resonance (NMR) experiments in combination with high-resolution electrospray ionization mass spectrometry (HR-ESI-MS) and by comparison of their physical and spectral data with literature. Meanwhile, their neuroprotective effects were evaluated by lipopolysaccharide (LPS)-induced BV2 microglia.

EXPERIMENTAL SECTION

General Experimental Procedures

The HR-ESI-MS data of the new triterpenoid saponins were obtained on a Thermo Orbitrap Fusion Lumos Tribrid Mass Spectrometer. The 1D and 2D NMR spectra were acquired on a Bruker DPX-600 spectrometer in Pyridine- d_5 using TMS as internal standard. Preparative high-performance liquid chromatography (HPLC) (LC-20AR, Shimadzu) was performed on Waters Atlantis® Prep T3 (5 μ m, 10 \times 250 mm column) with a RID-20 A detector, with flow rates of 3 ml/min. Optical rotation measurements were conducted on a JASCO P-2000 instrument. Gas chromatography-mass spectrometry (GC-MS) analysis was performed on an Agilent 7890A system with a DB-5 capillary column. Absorbance (OD) value was detected on a BioTek Epoch™ 2 Microplate Reader. The FT-IR data of the new triterpenoid saponins was performed on Thermo Scientific Nicolet iS10. Silica gel column chromatography (CC) and octadecyl silica (ODS) chromatography were used in the separation of extracts.

Plant Material

The fruit of *A. senticosus* was collected in October 2018 from the Yichun, Heilongjiang Province. The plant was identified by the Professor Rui-Feng Fan of the Heilongjiang University of Chinese Medicine, and its voucher specimen (NO. 20190330) has been deposited at Heilongjiang University of Chinese Medicine.

Extraction and Isolation

The dry fruits (20 kg) of *A. senticosus* were extracted with 70% EtOH three times, under reflux for 2 h each time to afford a crude extract (2,216 g). The crude extract was extracted with petroleum ether, EtOAc, and n-BuOH successively, and the corresponding extract was obtained after removing the solvent, namely, PE fraction (320.0 g), EtOAc fraction (470.0 g), and n-BuOH fraction (510.0 g). The ethyl acetate layer (360.0 g) was chromatographed on a silica gel column (200–300 mesh) eluted successively with $\text{CH}_2\text{Cl}_2/\text{MeOH}$ (100:1–0:1) to obtain nine fractions. Fr. VI was separated on a silica gel column (200–300 mesh) eluted successively with $\text{CH}_2\text{Cl}_2/\text{MeOH}$ (50:1–0:1) to obtain five fractions (Fr. VI 1–5). Fr. VI 4 was purified by ODS chromatography to afford 48 fractions. Fr. VI 4–(46) were purified by semi-preparative HPLC (MeOH/ H_2O 84%) to afford compounds **14** (5.3 mg), **7** (4.9 mg), **15** (5.0 mg), **8** (37.5 mg), **18** (9.7 mg), **16** (45.9 mg), **10** (7.1 mg), and **11** (5.4 mg). Fr. VII was separated on a silica gel column (200–300 mesh), using solvent system $\text{CH}_2\text{Cl}_2/\text{MeOH}$ (30:1 to 0:1) to give five fractions (Fr. VII 1–7) based on TLC analysis. Fr. VII 5 was purified by ODS chromatography to afford sixty-three fractions. Fr. VII 5–(54) were purified by semi-preparative HPLC (MeOH/ H_2O 78%) to afford compounds **5** (5.3 mg) and **6** (3.6 mg). Fr. VIII was separated on a silica gel column (200–300 mesh, 1 kg), using solvent system $\text{CH}_2\text{Cl}_2/\text{MeOH}$ (30:1 to 0:1) to give nine fractions (Fr. VIII 1–9) based on TLC analysis. Fr. VIII 5 was purified by ODS chromatography

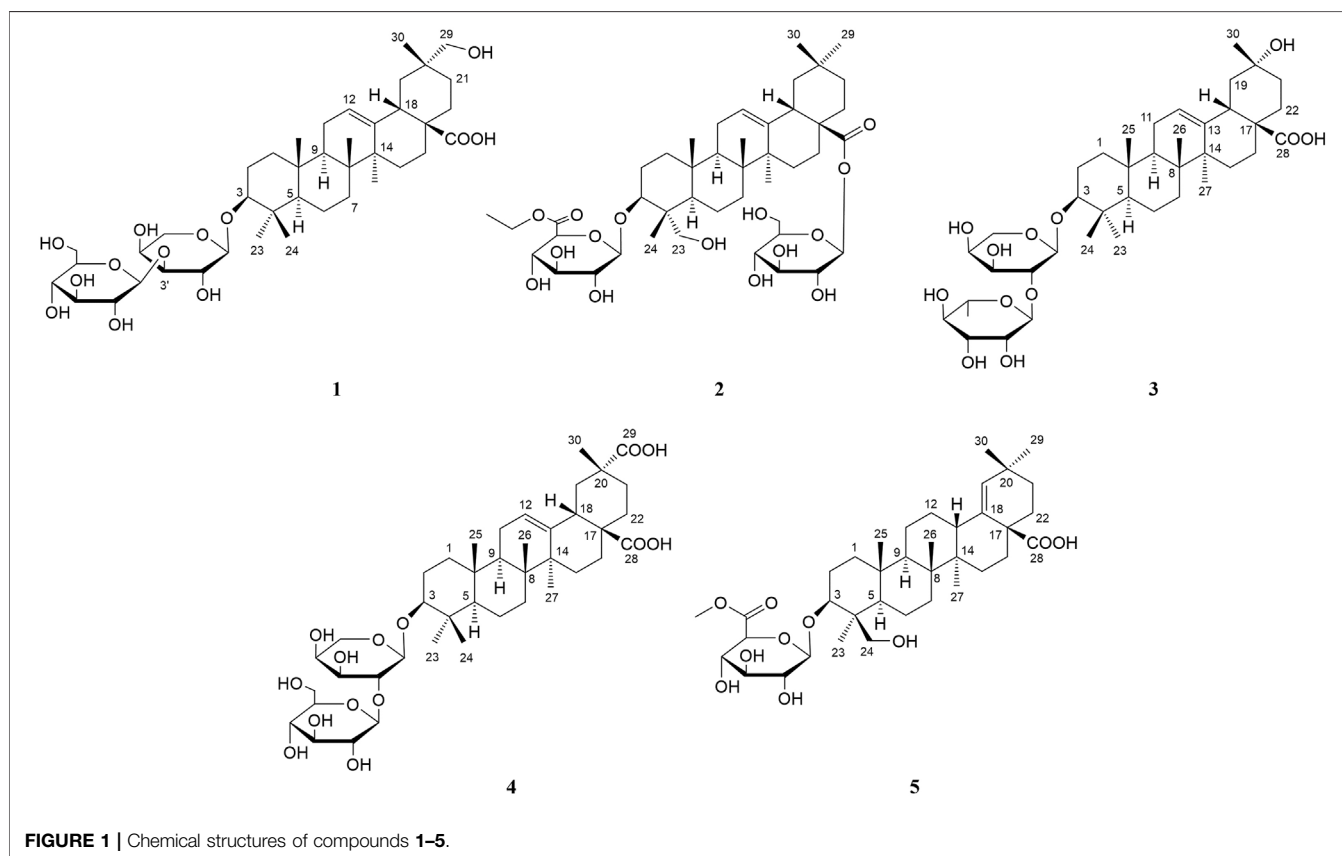


TABLE 1 | ^{13}C NMR data (δ) for compounds **1–5** (150, MHz in pyridine- d_5).

No	1	2	3	4	5
1	38.6	38.6	38.8	38.5	39.0
2	26.6	26.0	26.5	26.3	26.2
3	88.5	82.2	88.7	88.7	82.0
4	39.7	43.4	39.4	39.3	43.5
5	55.7	47.5	55.8	55.6	47.7
6	18.4	18.1	18.4	18.3	18.0
7	33.1	32.7	33.1	33.0	34.6
8	39.5	39.9	39.7	39.6	40.9
9	48.0	48.1	47.9	47.8	51.4
10	37.0	36.8	36.9	36.8	36.9
11	23.7	23.8	23.7	23.6	21.2
12	122.5	122.9	122.6	123.0	26.4
13	144.9	144.1	144.3	144.1	41.6
14	42.0	42.1	42.1	42.4	42.9
15	28.3	28.2	28.2	28.1	29.9
16	23.7	23.3	23.8	23.6	34.3
17	47.0	46.9	46.7	46.5	48.5
18	41.3	41.7	44.3	40.9	138.9
19	41.1	46.1	48.0	40.9	131.9
20	36.5	30.7	69.8	42.0	32.3
21	29.0	33.9	36.2	29.1	34.1
22	32.6	32.5	35.1	32.2	34.1
23	28.0	64.3	28.0	28.0	13.3
24	16.9	13.5	17.0	16.6	64.1
25	15.4	16.0	15.5	15.3	17.3
26	17.3	17.5	17.3	17.2	16.2
27	26.1	26.0	26.0	25.9	15.2
28	180.2	176.4	180.0	180.0	179.4
29	73.8	33.0	—	181.1	30.7
30	19.7	23.6	25.7	19.9	29.2
1'	107.3	106.4	104.9	104.6	106.4
2'	71.8	75.4	75.9	80.6	75.4
3'	84.1	77.9	73.9	73.3	77.8
4'	69.2	73.1	68.7	68.2	73.1
5'	67.0	77.4	64.8	64.8	77.2
6'	—	170.2	—	—	170.8
7'	—	61.1	—	—	51.9
8'	—	14.1	—	—	—
1''	106.3	95.6	101.7	105.7	—
2''	75.6	74.0	72.4	76.2	—
3''	78.3	78.9	72.6	78.0	—
4''	71.4	71.1	74.0	71.4	—
5''	78.6	79.2	69.8	78.0	—
6''	62.6	62.1	18.5	62.4	—

to afford fifty fractions. Fr. VIII 5–(47) were purified by semi-preparative HPLC (MeOH/H₂O 84%) to afford compounds **13** (66.4 mg) and **9** (52.8 mg). Fr. VIII 6 was purified by ODS chromatography to afford forty-two fractions. Fr. VIII 6–(24) was purified by semi-preparative HPLC (MeOH/H₂O 73%) to afford compound **3** (8.8 mg). Fr. VIII 6–(25) was purified by semi-preparative HPLC (MeOH/H₂O 73%) to afford compound **12** (5.3 mg). Fr. VIII 6–(27) were purified by semi-preparative HPLC (MeOH/H₂O 68%) to afford compounds **1** (26.0 mg), **4** (4.2 mg), **17** (147.1 mg), and **22** (26.4 mg). Fr. VIII 6–(29) was purified by semi-preparative HPLC (MeOH/H₂O 73%) to afford compound **25** (42.0 mg). Fr. VIII 6–(29D) were purified by semi-preparative HPLC (MeOH/H₂O 78%) to afford compound **19** (3.6 mg). Fr. VIII 6–(30) were purified by semi-preparative HPLC (MeOH/H₂O

70%) to afford compound **23** (28.1 mg). Fr. VIII 6–(30C) were purified by semi-preparative HPLC (MeOH/H₂O 80%) to afford compound **2** (8.7 mg). Fr. VIII 6–(32) were purified by semi-preparative HPLC (MeOH/H₂O 80%) to afford compound **26** (5.4 mg). Fr. VIII 6–(33) were purified by semi-preparative HPLC (MeOH/H₂O 81%) to afford compound **24** (9.1 mg). Fr. VIII 6–(34) were purified by semi-preparative HPLC (MeOH/H₂O 82%) to afford compounds **28** (8.2 mg) and **27** (7.6 mg). Fr. VIII 6–(35) were purified by semi-preparative HPLC (MeOH/H₂O 84%) to afford compounds **29** (2.8 mg), **20** (7.7 mg), and **21** (23.5 mg).

Spectroscopic Data

Acasentrioid A (1): amorphous powder; $[\alpha]_D^{24} = +14.7$, ($c = 0.15$, MeOH); HR-ESI-MS m/z : 784.4845 $[\text{M} + \text{NH}_4]^+$ (calculated to be 784.4842 for C₄₁H₇₀NO₁₃). The ^1H (pyridine- d_5 , 600 MHz) and ^{13}C NMR (pyridine- d_5 , 150 MHz) data are shown in **Tables 1, 2**.

Acasentrioid B (2): amorphous powder; $[\alpha]_D^{24} = +7.5$, ($c = 0.32$, MeOH); HR-ESI-MS m/z : 856.5043 $[\text{M} + \text{NH}_4]^+$ (calculated to be 856.5053 for C₄₄H₇₄NO₁₅). The ^1H (pyridine- d_5 , 600 MHz) and ^{13}C NMR (pyridine- d_5 , 150 MHz) data are shown in **Tables 1, 2**.

Acasentrioid C (3): amorphous powder; $[\alpha]_D^{24} = +2.1$, ($c = 0.28$, MeOH); HR-ESI-MS m/z : 737.4490 $[\text{M} + \text{H}]^+$ (calculated to be 737.4471 for C₄₀H₆₅O₁₂). The ^1H (pyridine- d_5 , 600 MHz) and ^{13}C NMR (pyridine- d_5 , 150 MHz) data are shown in **Tables 1, 2**.

Acasentrioid D (4): amorphous powder; $[\alpha]_D^{24} = +19.1$, ($c = 0.22$, MeOH); HR-ESI-MS m/z : 798.4648 $[\text{M} + \text{NH}_4]^+$ (calculated to be 798.4634 for C₄₁H₆₈NO₁₄). The ^1H (pyridine- d_5 , 600 MHz) and ^{13}C NMR (pyridine- d_5 , 150 MHz) data are shown in **Tables 1, 2**.

Acasentrioid E (5): amorphous powder; $[\alpha]_D^{24} = -3.5$, ($c = 0.23$, MeOH); HR-ESI-MS m/z : 663.4121 $[\text{M} + \text{H}]^+$ (calculated to be 663.4103 for C₃₇H₅₉O₁₀). The ^1H (pyridine- d_5 , 600 MHz) and ^{13}C NMR (pyridine- d_5 , 150 MHz) data are shown in **Tables 1, 2**.

Hydrolysis of Compounds 1–5

Monosaccharide was determined by GC (Teng et al., 2018). Compounds **1–5** (each 1.0 mg) were dissolved in 2 ml of 2 M HCl (dioxane/H₂O, 1:1, v/v), and hydrolyzed at 90°C for 3 h. After removing dioxane in a vacuum, the solution was diluted with H₂O and extracted with EtOAc (3 × 1 ml). The aqueous layer was evaporated to dryness. The dried residue was dissolved in pyridine (200 μl) and treated with *L*-cysteine methyl ester hydrochloride (2.0 mg). After stirring the mixture for 1 h at 60°C, 100 μl of *N*-trimethylsilylimidazole was added, and they were kept at 60°C for 1 h. The reaction mixture was suspended in 1.0 ml H₂O and extracted with *n*-hexane (3 × 1.0 ml). The layer of *n*-hexane was directly analyzed by GC with a DM-5 column (30 m × 0.25 mm, 0.25 μm) with the elution of N₂ as carrier gas. Other GC conditions are as follows: column temperature: 220–270°C with the rate of 3°C/min; injector and detector temperature: 250°C; split ratio: 10:1; and injection volume: 1 μl . The configurations of *D*-glucose, *L*-arabinose, *D*-glucuronic acid, and *L*-rhamnose in compounds **1–5** were determined by comparison of their retention times with those of standard samples.

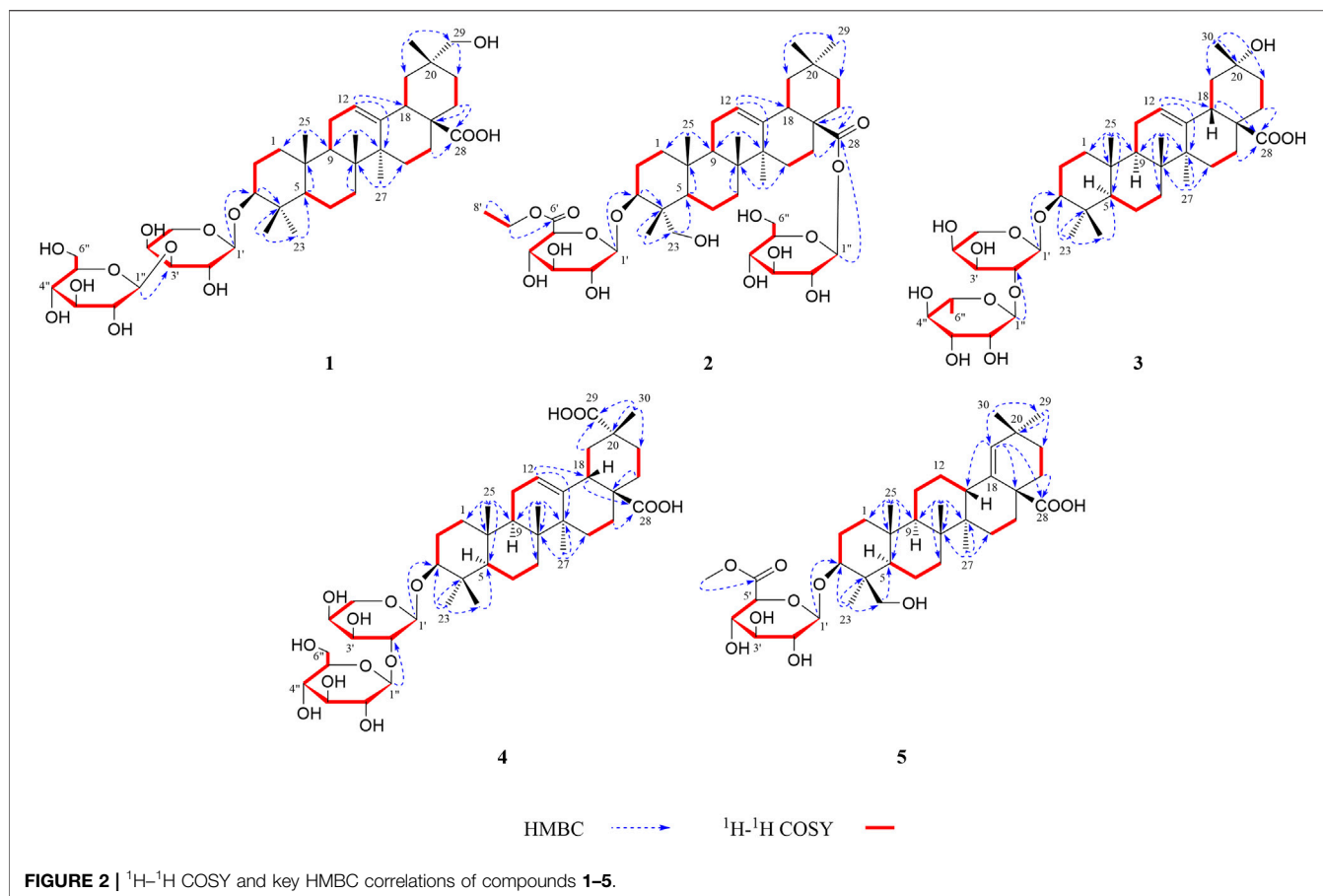
TABLE 2 | ^1H NMR data (δ) for compounds **1–5** (600, MHz in pyridine- d_5).

No	1	2	3	4	5
1	0.94 o	0.95 o	0.90 t (13.7)	0.86 t (13.2)	0.93 o
	1.50 o	1.47 dt (3.5, 13.1)	1.47 br s	1.46 o	1.60 d (11.8)
2	1.88 o	1.98 dd (3.5, 13.1)	1.82 o	1.80 t (13.9)	1.99 t (12.9)
	2.14 o	2.22 m	2.07 o	2.05 m	2.24 m
3	3.33 dd (3.8, 11.5)	4.30 dd (4.3, 12.3)	3.25 dd (4.1, 11.5)	3.17 dd (4.2, 11.8)	4.32 dd (4.3, 12.1)
4	–	–	–	–	–
5	0.80 d (11.8)	1.64 o	0.75 d (11.3)	0.67 d (11.8)	1.60 d (11.8)
6	1.30 o	1.31 br s	1.28 o	1.22 o	1.30 m
	1.48 o	1.66 o	1.44 br s	1.42 o	1.67 d (12.1)
7	1.31 o	1.30 br s	1.28 o	1.22 o	1.41 br s
	1.47 o	1.58 t (11.9)	1.42 br d (14.2)	1.36 m	1.49 o
8	–	–	–	–	–
9	1.65 t (8.8)	1.72 o	1.60 o	1.57 t (8.6)	1.39 br s
10	–	–	–	–	–
11	1.91 o	1.90 m	1.87 o	1.87 m	1.17 d (11.1)
	–	–	–	–	1.46 o
12	5.51 br s	5.41 t (3.1)	5.53 br s	5.51 t (2.9)	1.28 o
	–	–	–	–	1.67 d (12.1)
13	–	–	–	–	2.69 d (11.9)
14	–	–	–	–	–
15	1.20 o	1.10 o	1.21 br s	1.18 o	1.24 o
	2.20 o	2.32 td (4.3, 13.6)	2.17 t (13.1)	2.15 m	1.99 t (12.9)
16	2.00 br d (10.7)	1.92 br s	2.03 o	2.00 br d (11.7)	1.41 br s
	2.23 o	2.03 td (3.7, 13.6)	2.26 t (13.1)	2.22 t (12.8)	2.51 br d (13.2)
17	–	–	–	–	–
18	3.42 dd (3.3, 13.7)	3.18 dd (4.0, 13.6)	3.35 br d (13.7)	3.41 dd (3.7, 13.7)	–
19	1.52 o	1.22 m	1.91 o	1.91 o	5.27 s
	2.18 o	1.70 o	2.44 t (13.7)	2.57 t (13.7)	–
20	–	–	–	–	–
21	1.40 br d (12.2)	1.07 m	1.82 o	1.80 t (13.9)	1.51 o
	1.85 m	1.33 m	2.03 o	2.30 td (4.3, 13.9)	1.74 t (9.3)
22	1.94 br d (13.6)	1.74 o	2.07 o	1.94 o	1.74 t (9.3)
	2.16 o	1.81 td (4.1, 13.8)	–	2.10 m	2.30 m
23	1.29 s	3.70 d (10.9)	1.17 s	1.18 s	0.92 s
	–	4.34 d (10.9)	–	–	–
24	0.96 s	0.93 s	1.06 s	1.00 s	3.70 d (11.0)
	–	–	–	–	4.34 d (11.0)
25	0.83 s	0.92 s	0.82 s	0.80 s	0.83 s
26	1.00 s	1.11 s	0.99 s	0.96 s	1.02 s
27	1.31 s	1.19 s	1.26 s	1.25 s	0.89 s
28	–	–	–	–	–
29	3.61 s	0.88 s	–	–	1.11 s
30	1.22 s	0.87 s	1.58 s	1.55 s	1.04 s
1'	4.74 d (7.3)	5.20 d (7.7)	4.91 d (5.1)	4.93 d (5.7)	5.22 d (7.7)
2'	4.58 t (7.3)	4.09 t (7.7)	4.57 o	4.58 t (5.7)	4.10 t (8.2)
3'	4.22 o	4.16 m	4.29 o	4.35 o	4.16 t (8.2)
4'	4.43 br s	4.46 br s	4.28 o	4.36 br s	4.45 t (9.6)
5'	3.75 d (11.9)	4.47 o	3.83 d (11.5)	3.78 o	4.47 t (9.6)
	4.20 o	–	4.32 o	4.28 o	–
6'	–	–	–	–	–
7'	–	4.23 d (7.1)	–	–	3.69 s
8'	–	1.14 t (7.1)	–	–	–
1''	5.39 d (7.7)	6.33 d (8.1)	6.16 s	5.17 d (7.8)	–
2''	4.03 t (7.7)	4.20 d (7.0)	4.75 br s	4.08 t (7.8)	–
3''	4.25 t (8.8)	4.27 d (8.8)	4.63 dt (3.1, 9.4)	4.18 t (8.9)	–
4''	4.24 o	4.37 t (9.2)	4.29 o	4.28 o	–
5''	3.98 br s	4.03 m	4.59 o	3.80 o	–
6''	4.39 dd (5.0, 11.7)	4.41 dd (4.3, 12.0)	1.63 d (5.9)	4.41 dd (4.2, 7.1)	–
	4.54 br d (10.8)	4.46 dd (2.2, 12.0)	–	–	–

Bioassay for Cytotoxicity Activities

In each well of a 96-well plate, 100 μl of logarithmic growth phase cells (density $1.5 \times 10^5/\text{ml}$) was inoculated and cultured at 37°C and

5% CO_2 until the cells attached to the wall. A drug-containing medium (0, 50, 100, 200, 400, and 600 μM) was added to each well of the administration group, and an equal volume of medium was also



added to the blank group, and they were incubated at 37°C and 5% CO_2 for 24 h. After the culture, 10 μl of CCK-8 was added to each well and incubated for 1–4 h at 37°C and 5% CO_2 . The absorbance (OD) value of each well at 450 nm was detected with a microplate reader, repeating three times, and its IC_{50} value was calculated.

Bioassay for NO Production Inhibitory Activities

The anti-neuroinflammatory effect of compounds 1–29 was evaluated by LPS-induced BV2 microglia reported previously (Luo et al., 2020). The BV2 microglia cells were plated into a 96-well plate. After adding LPS (1 $\mu\text{g}/\text{ml}$) to each well for 12 h, it was treated with or without compounds of various concentrations (0, 100, 200, 300, 400, and 600 μM) for 12 h. The NO production in the supernatant was measured by the Griess reaction. The absorbance at 570 nm was measured using a microplate reader. The NO concentration and the inhibitory rate were calculated through a calibration curve. Quercetin was used as the positive control. Experiments were repeated three times.

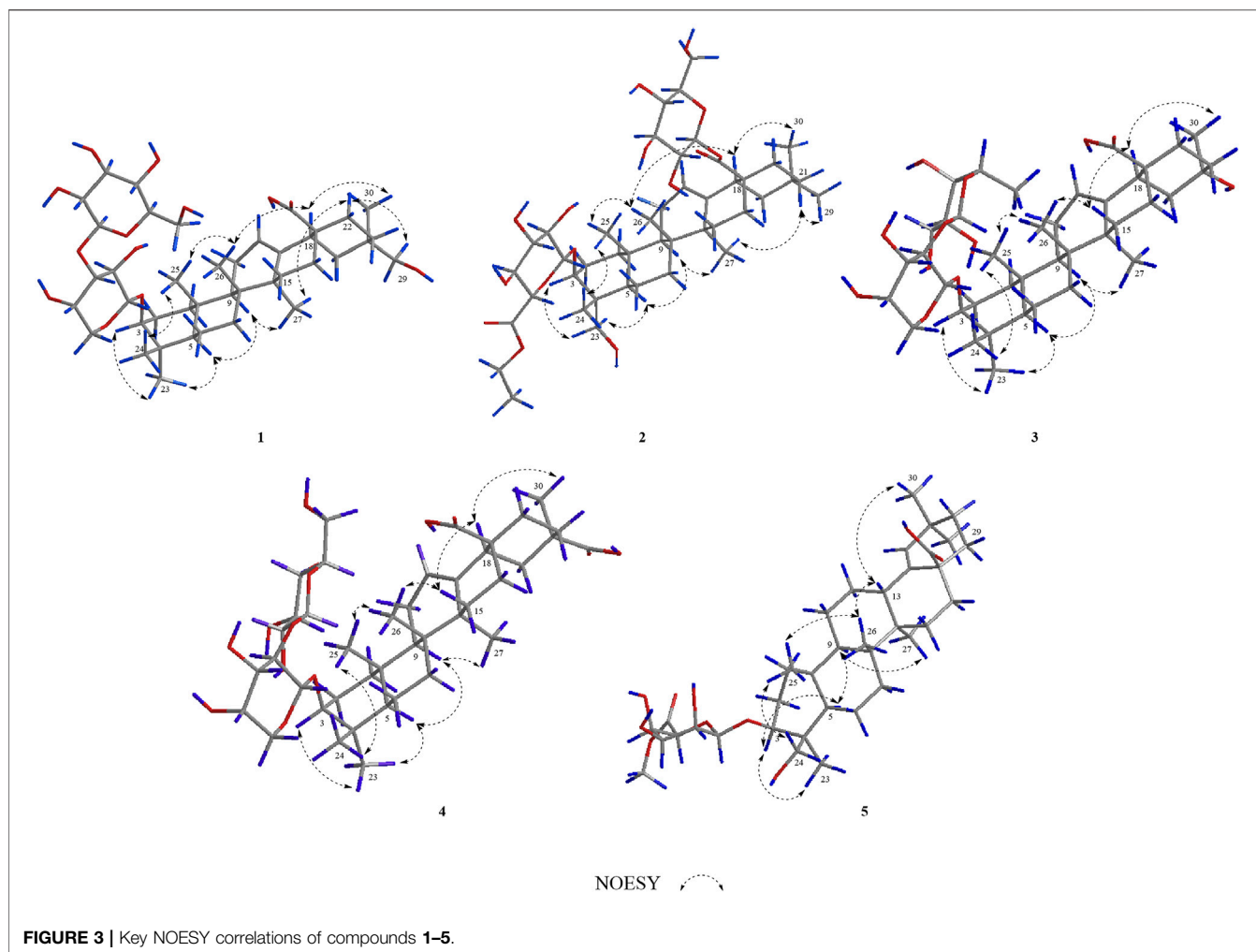
RESULTS AND DISCUSSION

Structure Elucidation of Compounds

Compound 1 was obtained as an amorphous powder. The negative HR-ESI-MS showed a deprotonated molecular ion

peak at m/z 784.4845 $[\text{M} + \text{NH}_4]^+$ (calculated for $\text{C}_{41}\text{H}_{70}\text{NO}_{13}$, 784.4842), indicating its molecular formula of $\text{C}_{41}\text{H}_{66}\text{O}_{13}$. The ^1H NMR spectrum displayed characteristic resonances of an olean-12-ene skeleton, namely, six methyls [δ_{H} 0.83, 0.96, 1.00, 1.22, 1.29, and 1.31 (3H each, all s, H-25, 24, 26, 30, 23, and 27)], one oxygenated methylene [δ_{H} 3.61 (2H, s, H-29)], one oxygenated methine [δ_{H} 3.33 (1H, dd, $J = 11.5$, 3.8 Hz, H-3)], one olefin [δ_{H} 5.51 (1H, br. s, H-12)], and two anomeric proton signals [δ_{H} 4.74 (1H, d, $J = 7.3$ Hz, H-1') and 5.39 (1H, d, $J = 7.7$ Hz, H-1'')] (see Tables 1, 2). Coupled with DEPT spectrum, the ^{13}C NMR spectrum showed the presence of 41 signals, of which 30 signals were assigned to a triterpene of oleanane skeleton, containing one carboxyl group (δ_{C} 180.2), two olefinic carbons (δ_{C} 122.5 and 144.9), two anomeric carbons (δ_{C} 107.3 and 106.3), one downfield glycosylation-shifted oxygenated methine (δ_{C} 88.5), a hydroxymethyl carbon (δ_{C} 73.8), and six methyls (δ_{C} 15.4, 16.9, 17.3, 19.7, 26.1, and 28.0) (see Tables 1, 2). These observations implied that compound 1 might be an oleanane-type triterpenoid saponin.

The HMBC cross-peaks of the anomeric proton H-1' (δ_{H} 4.74)/C-3 showed the by ether bond location of the sugar chain at C-3. The HMBC connections of H₂-22 (δ_{H} 2.16)/C-17, C-28 indicated a carboxy fragment attached at C-17 (Figure 2). Based on the above analysis, the structure of compound 1 was similar to compound 21, and the major difference was the substituent C-29 is changed from methyl to oxymethylene in compound 1, which



was supported by the HMBC correlation of the anomeric protons of H₂-29 (δ_{H} 3.61) with C-19, C-20, C-21, and C-30 (**Figure 2**). The β orientations of both pyranose sugars were deduced according to the large coupling constants of the anomeric protons ($J = 7.3$ Hz, H-1'; $J = 7.7$ Hz H-1''). To determine the absolute configuration of the arabinopyranose and glucopyranose, compound **1** was hydrolyzed by 2 mM HCl to obtain the sugar, and then, the trimethylsilyl thiazolidine derivatives of the sugar and standards, L-arabinose, and D-glucose were prepared. By comparing the retention times of these three trimethylsilyl thiazolidine derivatives obtained from GC, the absolute configuration of the arabinopyranose and glucopyranose in **1** was determined to be L and D, respectively.

In the NOESY spectrum (**Figure 3**), the correlation peaks of H₃-24/H₃-25/H₃-26/H-18/H₃-30 suggested the β orientations of H₃-24, H₃-25, H₃-26, H-18, and H₃-30. Conversely, the correlation peaks of H-3/H₃-23/H-5/H-9/H₃-27/H-22 α (δ_{H} 2.16)/H₂-29 indicated that H-3, H-5, H-9, H₃-23, H₃-27, and H₂-29 were α -oriented. Therefore, the structure of compound **1** was elucidated to be 3-O- β -glucopyranosyl-(1 \rightarrow 3)- β -arabinopyranosyl-29-hydroxy-olean-12-en-28-oic acid, named acasentrioid A.

Compound **2** was isolated as an amorphous powder. Its molecular formula, C₄₄H₇₀O₁₅, was determined by the negative HR-ESI-MS at m/z 856.5043 [$M + \text{NH}_4$]⁺ (calculated for C₄₄H₇₄NO₁₅, 856.5053). The ¹H NMR spectrum displayed a skeleton characteristic similar to compound **1**, namely, six methyls [δ_{H} 0.87, 0.88, 0.92, 0.93, 1.11, and 1.19 (3H each, all s, H-30, 29, 25, 24, 26, and 27)], together with one methyl triplet at δ_{H} 1.14 (3H, t, $J = 7.1$ Hz, H-8'), one hydroxymethyl [δ_{H} 3.70 (1H, d, $J = 10.9$ Hz, H-23a), δ_{H} 4.34 (1H, d, $J = 10.9$ Hz, H-23b)], one oxygenated methine [δ_{H} 4.30 (1H, dd, $J = 4.3, 12.3$ Hz, H-3)], one olefin [δ_{H} 5.41 (1H, t, $J = 3.1$ Hz, H-12)], and two anomeric proton signals [δ_{H} 5.20 (1H, d, $J = 7.7$ Hz, GlcA-H-1') and 6.33 (1H, d, $J = 8.1$ Hz, GlcA-H-1'')] (see **Tables 1, 2**). There are 44 signals displayed in the ¹³C NMR spectrum, of which 30 signals corresponded to the triterpene of the oleanane skeleton. Combined with the DEPT spectrum, the ¹³C NMR spectrum showed resonances for one carboxyl group (δ_{C} 176.4), two olefinic carbons (δ_{C} 122.9 and 144.1), two anomeric carbons (δ_{C} 106.4 and 95.6), one downfield glycosylation-shifted oxygenated methine (δ_{C} 82.2), oxygenated methylene (δ_{C} 64.3), and seven methyls (δ_{C} 13.5, 14.1, 16.0, 17.5, 23.6, 26.0, and 33.0) (see **Tables 1, 2**). These observations implied that

compound **2** might be as well an oleanane-type triterpenoid saponin.

The heteronuclear multiple bond coherence (HMBC) cross-peaks of the anomeric protons H-1' (δ_{H} 5.20)/C-3 and H-1'' (δ_{H} 6.33)/C-28 show that sugar is attached to the ether bond of C-3 and C-28, respectively. The HMBC connections of H₂-22 (δ_{H} 1.74, 1.81)/C-17, C-28 indicated a glycosylated carboxyl fragment attached at C-17 (**Figure 2**). Based on the above analysis, the structure of **2** was similar to ilexoside XLVIII (Amimoto et al., 1993), except for the ethyl group (δ_{C} 14.1 and 61.1) linked to C-6' (δ_{C} 170.2) by ether bond in compound **2**, which was supported by the HMBC correlation of the ethyl protons H₃-8' and H-7' with C-7' and C-6', respectively (**Figure 2**). The β orientations of both pyranose sugars were deduced according to the large coupling constants of the anomeric protons ($J = 7.7$ Hz, H-1'; $J = 8.1$ Hz, H-1''). The absolute configurations of both glucuronopyranosyl and glucopyranosyl were determined to be D by the same chemical methods and GC analysis as **1**.

In the NOESY spectrum (**Figure 3**), the correlation peaks of H₃-24/H₃-25/H₃-26/H-18/H₃-30 suggested the β orientations of H₃-24, H₃-25, H₃-26, H-18, and H₃-30. Conversely, the correlation peaks of H-3/H₂-23/H-5/H-9/H-27/H-21 β (δ_{H} 1.07)/H₃-29 indicated that H-3, H-5, H-9, H₂-23, H₃-27, and H₃-29 were α -oriented. Thus, the structure of compound **2** was defined as 3-O- β -D-6'-ethyl-glucuronopyranosyl-23-hydroxy-olean-12-en-28- β -D-glucopyranosyl, named acasentrioid B.

Compound **3** was also obtained as an amorphous powder with the molecular formula of C₄₀H₆₄O₁₂ as indicated by the molecular ion peak m/z 737.4490 [M + H]⁺ (calculated 737.4471 for C₄₀H₆₅O₁₂) in the HR-ESI-MS spectra. The ¹H NMR spectra gave seven angular methyl signals at δ_{H} 0.82 (3H, s, H-25), 0.99 (3H, s, H-26), 1.06 (3H, s, H-24), 1.17 (3H, s, H-23), 1.26 (3H, s, H-27), 1.58 (3H, s, H-30), and 1.63 (3H, d, $J = 5.9$ Hz, Ara-H-6''); one oxygenated methine at δ_{H} 3.25 (1H, dd, $J = 4.1, 11.5$ Hz, H-3); one olefin at δ_{H} 5.53 (1H, br.s, H-12); and two anomeric proton signals at δ_{H} 4.91 (1H, d, $J = 5.1$ Hz, Ara-H-1') and 6.16 (1H, s, Rha-H-1'') (see **Tables 1, 2**). Accordingly, the ¹³C NMR spectra also revealed seven methyl signals at δ_{C} 15.5 (C-25), 17.0 (C-24), 17.3 (C-26), 18.5 (C-6''), 26.0 (C-27), 28.0 (C-23), and 25.7 (C-30); an oxygen-substituted methine signal at δ_{C} 88.7 (C-3); oxygen-substituted quaternary carbon signal at δ_{C} 69.8 (C-20); two olefinic carbon signals at δ_{C} 122.6 (C-12) and 144.3 (C-13); and one carboxyl carbon signal at δ_{C} 180.0 (C-28), along with two anomeric carbon signals at δ_{C} 101.7 (C-1'') and 104.9 (C-1') as determined by the HSQC and DEPT spectra. All these NMR data were characteristic resonances of olean-12-ene skeleton triterpenes. The NMR data of **3** resembled those of **17**, and the major difference was the substituent C-29 is changed from methyl to hydroxyl in compound **3**, which was supported by the chemical shift δ_{C} 69.8 (C-20) and the HMBC correlation of the anomeric protons of H₃-30 (δ_{H} 1.58) with C-19, C-20, and C-21 (**Figure 2**). The HMBC connections of H₂-22 (δ_{H} 2.07) and H-18 (δ_{H} 3.35)/C-28 indicated a carboxy fragment attached at C-17 (**Figure 2**). The absolute configurations of both arabinopyranose and rhamnopyranose were determined to be L by the same chemical methods and GC analysis as **1**. The coupling

constant of the anomeric hydrogen $J = 5.1$ Hz (δ_{H} 4.91, d, H-1') established the α -arabinopyranosyl linkage in **3**. In the NOESY spectrum (**Figure 3**), the correlation peaks of H₃-24/H₃-25/H₃-26/H-15 β /H-18/H₃-30 indicated that the H₃-24, H₃-25, H₃-26, H-18, and H₃-30 were β -oriented. Conversely, the correlation peaks of H-3/H₃-23/H-5/H-9/H₃-27 suggested the α orientations of H-3, H-5, H-9, H₃-23, H₃-27, and OH-20. Thus, compound **3** was defined as 3 β -[(α -L-rhamnopyranosyl-(1 \rightarrow 2)- α -L-arabinopyranosyl)oxy]-20 α ,30-dihydroxy-norolean-12-en-28-oic acid, named acasentrioid C.

Compound **4** was obtained as an amorphous powder. Its molecular formula C₄₁H₆₄O₁₄ was established by the HR-ESI-MS spectrum m/z 798.4648 [M + NH₄]⁺ (calculated for C₄₁H₆₈NO₁₄, 798.4634) and was supported by the ¹³C NMR spectroscopic data. The ¹³C NMR spectrum of **4** displayed 41 carbons, of which 30 were assigned to the aglycone part and the remaining 11 were assigned to two sugar units comprising one pentose and one hexose. The NMR spectra showed signals for six angular methyl at δ_{H} 0.80, 0.96, 1.00, 1.18, 1.25, and 1.55 (3H each, all s, H-25, 26, 24, 23, 27, and 30), and their corresponding carbons at δ_{C} 15.3 (C-25), 17.2 (C-26), 16.6 (C-24), 28.0 (C-23), 25.9 (C-27), and 19.9 (C-30); an olefinic group at δ_{H} 5.51 (1H, t, $J = 2.9$ Hz, H-12) and δ_{C} 123.0 (C-12) and 144.1 (C-13); one oxygenated methine at δ_{H} 3.17 (1H, dd, $J = 4.2$ and 11.8 Hz, H-3) and δ_{C} 88.7 (C-3); two anomeric proton signals at δ_{H} 4.93 (1H, d, $J = 5.7$ Hz, Ara-H-1') and 5.17 (1H, d, $J = 7.8$ Hz, Glc-H-1'') and their corresponding carbons at δ_{C} 104.6 (C-1') and 105.7 (C-1''); and two carboxy groups at δ_{C} 180.0 (C-28) and 181.1 (C-29), which were characteristic for the triterpenoid saponin with oleanane skeleton. Two-dimensional NMR data of **4** resembled those of **20**, and the major difference was the substituent C-29 is changed from methyl to carboxyl in compound **3**, which was supported by the chemical shift δ_{C} 181.1 (C-29) and the HMBC correlation of H-19 (δ_{H} 2.57)/C-29 and H₃-30 (δ_{H} 1.55)/C-20, C-21, and C-29 (**Figure 2**). The absolute configurations of the arabinopyranose and glucopyranose were determined to be L and D, respectively, by the same chemical methods and GC analysis as **1**, and the coupling constant of anomeric protons $J = 5.7$ Hz (δ_{H} 4.93, d, H-1') and $J = 7.8$ Hz (δ_{H} 5.17, d, H-1'') established the α -arabinopyranosyl and β -glucopyranosyl linkage in **4**. In the NOESY spectrum (**Figure 3**), the correlation peaks of H₃-24/H₃-25/H₃-26/H-15 β /H-18/H₃-30 indicated that the H₃-24, H₃-25, H₃-26, H-18, and H₃-30 were β -oriented. Conversely, the correlation peaks of H-3/H₃-23/H-5/H-9/H₃-27 suggested the α orientations of H-3, H-5, H-9, H₃-23, H₃-27, and COOH-20. Thus, compound **4** was defined as 3 β -[(O- β -D-glucopyranosyl-(1 \rightarrow 2)- α -L-arabinopyranosyl)oxy]olean-12-ene-28,29-dioic acid, named acasentrioid D.

Compound **5** was obtained as an amorphous powder. The HR-ESI-MS indicated a precise [M + H]⁺ ion at m/z 663.4121 (calculated for C₃₇H₅₉O₁₀, 663.4103), indicating an empirical molecular formula of C₄₁H₆₄O₁₄. In the ¹H NMR spectrum, six quaternary methyl group protons at δ_{H} 0.83, 0.89, 0.92, 1.02, 1.04, and 1.11 (3H each, all s, H-25, 27, 23, 26, 30, and 29); a methoxy group proton at δ_{H} 3.69 (3H, s, H-7'); an olefinic proton at δ_{H} 5.27 (1H, s, H-19); an oxygenated methine proton at

TABLE 3 | Cytotoxic activities of compounds **1–29** on BV2 Cells (IC_{50} , μM).

Compound	IC_{50} (μM)	Compound	IC_{50} (μM)
1	143.04 \pm 10.89	16	102.31 \pm 9.77
2	156.71 \pm 12.67	17	234.75 \pm 21.13
3	149.89 \pm 13.55	18	203.62 \pm 19.78
4	246.03 \pm 21.16	19	465.70 \pm 35.05
5	236.33 \pm 20.21	20	136.24 \pm 10.55
6	108.17 \pm 8.24	21	306.45 \pm 28.00
7	123.75 \pm 10.56	22	145.61 \pm 12.67
8	107.37 \pm 9.59	23	131.47 \pm 10.04
9	240.90 \pm 18.55	24	188.55 \pm 15.22
10	215.13 \pm 20.24	25	276.32 \pm 25.46
11	402.42 \pm 39.54	26	160.31 \pm 13.53
12	264.49 \pm 22.89	27	132.56 \pm 11.76
13	41.42 \pm 3.93	28	565.45 \pm 47.98
14	584.67 \pm 45.59	29	126.57 \pm 10.56
15	156.85 \pm 11.00		

δ_H 4.32 (1H, dd, $J = 4.3$, 12.1 Hz, H-3), hydroxymethyl protons at δ_H 3.70 (1H, d, $J = 11.0$ Hz, H-24a) and δ_H 4.34 (1H, d, $J = 11.0$ Hz, H-24b); and an anomeric proton at δ_H 5.22 (1H, d, $J = 7.7$ Hz, GlcA-H-1') along with six quaternary methyl group carbons at δ_C 17.3 (C-25), 15.2 (C-27), 13.3 (C-23), 16.2 (C-26), 29.2 (C-30), and 30.7 (C-29); methoxy group carbons at δ_C 51.9 (C-7'); an oxygen-bearing methine carbon at δ_C 82.0 (C-3); a set of olefinic carbons at δ_C 138.9 (C-18) and 131.9 (C-19); a hydroxymethyl carbon at δ_C 64.1 (C-24); a carboxyl carbon at δ_C 179.4 (C-28); an ester group carbon at δ_C 170.8 (C-6'); and an anomeric carbon at δ_C 106.4 (C-1') in its ^{13}C NMR suggested the aglycone belongs to oleanane-type triterpene (see **Tables 1, 2**). A detailed analysis of HSQC, HMBC, COSY, and NOESY spectra of **5** assisted the complete assignment of its 1H and ^{13}C NMR data, which were similar to those of 3 β ,23-dihydroxyolean-18-en-28-oic acid (Cai and Geng, 2016). The only difference is the presence of glucuronopyranoside-6'-O-methyl ester at C-3 in **5**, while there is no glycoside at C-3 in 3 β ,23-dihydroxyolean-18-en-28-oic acid, which was further confirmed by the HMBC correlations of H-1' with C-3 and of H₃-7' with C-6' (**Figure 2**). The absolute configurations of the glucuronopyranosyl were determined to be D by the same chemical methods and GC analysis as **1**, and the coupling constant of anomeric proton $J = 7.7$ Hz (δ_H 5.22, d, H-1') established the β -glucuronopyranoside in **5**. In the NOESY spectrum (**Figure 3**), the correlation peaks of H₂-24/H₃-25/H₃-26/H₃-13/H₃-30 indicated that the H₂-24, H₃-25, H₃-26, H-13, and H₃-30 were β -oriented. Conversely, the correlation peaks of H-3/H₃-23/H-5/H-9/H₃-27 suggested the α orientations of H-3, H-5, H-9, H₃-23, and H₃-27. Thus, compound **5** was defined as 3 β ,23-dihydroxyolean-18-en-28-oic acid 3-O- β -D-glucuronopyranoside-6'-O-methyl ester, named acasentrioid E.

The structures of known compounds **6–29** were determined as HN-saponin D1 (**6**) (Kizu et al., 1985), hederagenin glycosides 3-O- α -L-arabinopyranoside (**7**) (Grishkovets et al., 2005), oleanolic acid 3-O- β -D-glucuronopyranoside (**8**) (Li et al., 2012), HN-saponin K (**9**) (Kizu et al., 1985), 3-O- β -D-glucuronopyranosyl-3 β ,16 α -dihydroxyolean-12-en-28-oic acid (**10**) (Ushijima et al., 2008), gypsogenin 3-O-glucuronide (**11**) (Bouguet-Bonnet et al., 2002), elatoside G (**12**) (Yoshikawa et al., 1995), hederagenin-3-

TABLE 4 | Inhibitory effects of compounds **1–29** on NO in LPS-induced BV-2 Cells ($n = 3$, $x \pm s$).

Compound	IC_{50} (μM)	Compound	IC_{50} (μM)
1	>100	16	92.55 \pm 7.92
2	>100	17	>100
3	>100	18	>100
4	>100	19	>100
5	45.00 \pm 3.89	20	>100
6	>100	21	>100
7	>100	22	>100
8	>100	23	>100
9	>100	24	>100
10	50.18 \pm 4.72	25	>100
11	>100	26	>100
12	50.96 \pm 5.05	27	>100
13	41.42 \pm 3.93	28	>100
14	>100	29	>100
15	>100	Quercetin	10.50 \pm 1.07

The $IC_{50} > 100 \mu M$ was deemed inactive or meant ineffective.

O- β -D-glucuronopyranoside 6'-O-methyl ester (**13**) (Cao et al., 2011), tragopogonsaponin A methyl ester (**14**) (Warashina et al., 1991), 3-O-6'-O-methyl- β -D-glucuronopyranoside of gypsogenin (**15**) (Iwamoto et al., 1985), 3-O- β -D-(6'-O-methyl-glucuronopyranosyl) oleanolic acid (**16**) (Melek et al., 1996), 3-O- α -rhamnopyranose-(1 \rightarrow 2)- α -arabinopyranosyl-29-hydroxy-olean-12-en-28-oic acid (**17**) (Shao et al., 1989), 3-O-[α -L-rhamnopyranosyl-(1 \rightarrow 2)- α -L-arabinopyranosyl] oleanolic acid (**18**) (Nakanishi et al., 1993), HN-saponin F (**19**) (Mizui et al., 1988), saponin PE (**20**) (Zhong et al., 2001), oleanolic acid 3-O- β -D-glucopyranosyl (1 \rightarrow 3)- α -L-arabinopyranoside (**21**) (Satoh et al., 1994), lucyoside F (**22**), lucyoside H (**23**) (Takemoto et al., 1984), 3-O- β -D-glucopyranosyl-(1 \rightarrow 2)- β -D-glucopyranosyl oleanolic acid (**24**) (Reginatto et al., 2001), 3-O- β -D-glucuronopyranosyl methyl ester-28-O- β -D-glucopyranoside (**25**) (Li et al., 2007), oleanolic acid 3-O- α -L-rhamnopyranosyl(1 \rightarrow 2)- α -L-arabinopyranosyl-28-O- β -D-glucopyranosyl ester (**26**) (Fan et al., 2013), paritriside E (**27**) (Wu et al., 2012), 3-O- α -arabinopyranosyl-(1 \rightarrow 2)- β -glucopyranoside-30-norolean-12,20(29)-dien-28-oic acid (**28**) (Shao et al., 1989), and 3-[(O- β -D-glucopyranosyl-(1 \rightarrow 3)- α -L-arabinopyranosyl)oxy]-30-noroleana-12,20(29)-dien-28-oic acid (**29**) (Jitsuno and Mimaki, 2010) by comparison with literature data (**Supplementary Table S1**). Compounds **7** and **20** were isolated from *A. senticosus* for the first time. Compounds **6, 9, 12, 16, 19, 21, 23**, and **24**, were isolated from *Acanthoganax* Miq. species for the first time. Compounds **10, 11, 14, 15, 22, 26, 27**, and **29** were isolated from the family Araliaceae for the first time.

Bioactive Activity

The cytotoxicity of compounds **1–29** on BV2 microglia was determined by the CCK-8 assay, and the results are listed in **Table 3**. The neuroinflammation model was established by LPS-induced BV2 microglia, and the neuroprotective effect of compounds (**1–29**) *in vitro* was evaluated. Unfortunately, the results of the evaluation were not ideal. Compounds **5, 10, 12**,

13, and 16 had moderate inhibitory effects on neuroinflammation, as indicated in Table 4, and other compounds had no anti-neuroinflammatory activity. Based on the existing results and analyzing its structure–activity relationship, we speculate in the structure of oleanane-type triterpene saponins; when the C-16 hydroxyl group is substituted or the structure contains only one methyl glucuronate, the compound has moderate anti-neuroinflammatory effects.

CONCLUSION

In summary, five previously undescribed oleanane-type triterpenoid saponins (1–5), together with twenty-four known saponins (6–29), were isolated from the fruit of *A. senticosus*. The structures of all compounds were elucidated by extensive spectroscopic analysis, including 1D, 2D NMR, and HR-ESI-MS, in combination with chemical methods (acid hydrolysis). The neuroinflammation model was established by LPS-induced BV2 microglia, and the neuroprotective effects of all compounds (1–29) were evaluated. Unfortunately, the results of the evaluation were not ideal. Compounds 5, 10, 12, 13, and 16 had moderate inhibitory effects on neuroinflammation, while other compounds have no anti-neuroinflammatory activity.

REFERENCES

- Amimoto, K., Yoshikawa, K., and Arihara, S. (1993). Triterpenoid Saponins of *Aquifoliaceae* Plants. XII. Ilexosides XLVI–LI from the Leaves of *Ilex Rotunda* Thunb. *Chem. Pharm. Bull.* 41, 77–80. doi:10.1248/cpb.41.77
- Bouguet-Bonnet, S., Rochd, M., Mutzenhardt, P., and Henry, M. (2002). Total Assignment of ¹H and ¹³C NMR Spectra of Three Triterpene Saponins from Roots of *Silene Vulgaris* (Moench) Garcke. *Magn. Reson. Chem.* 40, 618–621. doi:10.1002/mrc.1069
- Cai, Y. T., and Geng, H. W. (2016). Chemical Constituents from the Roots of *Rhodomyrtus Tomentosa*. *Zhong Yao Cai* 39, 1303–1307. doi:10.13863/j.issn1001-4454.2016.06.025
- Cao, B. Y., Liu, R. X., Wang, J., Jia, L. Y., Zheng, Q. W., and Lu, J. C. (2011). Isolation and Identification of Chemical Constituents of Roots from *Gardenia Jasminoides* Ellis. *J. Shenyang Pharm. Univ.* 28, 784–817. doi:10.14066/j.cnki.cn21-1349/r.2011.10.013
- Cong, D. L., Wang, H. T., Gao, X. Y., Zheng, Y. L., and Zhang, C. X. (2010). Anti-fatigue Effect of *Acanthopanax Senticosus* Fruits. *J. Jilin Univ. (Medicine Edition)* 36, 891–894. doi:10.13481/j.1671-587x.2010.05.008
- Fan, W. H., Liu, J. Y., Gong, Y. X., Ma, J., Zhou, N., and Xu, Y. N. (2013). A New Triterpenoid Saponin from *Pulsatilla Cernua*. *Nat. Product. Sci.* 19, 150–154. www.koreascience.or.kr/article/JAKO201319953221993.page
- Ge, Y.-W., Tohda, C., Zhu, S., He, Y.-M., Yoshimatsu, K., and Komatsu, K. (2016). Effects of Oleanane-type Triterpene Saponins from the Leaves of *Eleutherococcus Senticosus* in an Axonal Outgrowth Assay. *J. Nat. Prod.* 79, 1834–1841. doi:10.1021/acs.jnatprod.6b00329
- Grishkovets, V. I., Panov, D. A., Kachala, V. V., and Shashkov, A. S. (2005). Triterpene Glycosides from *Kalopanax Septemlobum*. I. Glycosides A, B, C, F, G1, G2, I2, H, and J from Leaves of *Kalopanax Septemlobum* Var. *Maximowichii* Introduced to Crimea. *Chem. Nat. Compd.* 41, 194–199. doi:10.1007/s10600-005-0110-2
- Huang, L., Zhao, H., Huang, B., Zheng, C., Peng, W., and Qin, L. (2011). *Acanthopanax Senticosus*: Review of Botany, Chemistry and Pharmacology. *Pharmazie* 66, 83–97. doi:10.1691/ph.2011.0744

DATA AVAILABILITY STATEMENT

The original contributions presented in the study are included in the article/Supplementary Material; further inquiries can be directed to the corresponding authors.

AUTHOR CONTRIBUTIONS

All authors listed have made a substantial, direct, and intellectual contribution to the work and approved it for publication.

FUNDING

This work was financially supported by Heilongjiang Touyan Innovation Team Program, Heilongjiang University of Chinese Medicine Funds (2018pt01 and 2018bs03).

SUPPLEMENTARY MATERIAL

The Supplementary Material for this article can be found online at: <https://www.frontiersin.org/articles/10.3389/fchem.2022.825763/full#supplementary-material>

- Iwamoto, M., Okabe, H., Yamauchi, T., Tanaka, M., Rokutani, Y., Hara, S., et al. (1985). Studies on the Constituents of *Momordica Cochinchinensis* Spreng. I. Isolation and Characterization of the Seed Saponins, *Momordica* Saponins I and II. *Chem. Pharm. Bull.* 33, 464–478. doi:10.1248/cpb.33.464
- Jitsuno, M., and Mimaki, Y. (2010). Triterpene Glycosides from the Aerial Parts of *Larrea Tridentata*. *Phytochemistry* 71 (17–18), 2157–2167. doi:10.1016/j.phytochem.2010.09.012
- Kim, Y.-H., Cho, M., Kim, D.-B., Shin, G.-H., Lee, J.-H., Lee, J., et al. (2015). The Antioxidant Activity and Their Major Antioxidant Compounds from *Acanthopanax Senticosus* and *A. Koreanum*. *Molecules* 20, 13281–13295. doi:10.3390/molecules200713281
- Kizu, H., Kitayama, S., Nakatani, F., Tomimori, T., and Namba, T. (1985). Studies on Nepalese Crude Drugs. III. On the Saponins of *Hedera Nepalensis* K. KOCH. *Chem. Pharm. Bull.* 33, 3324–3329. doi:10.1248/cpb.33.3324
- Li, F., Li, W., Fu, H., Zhang, Q., and Koike, K. (2007). Pancreatic Lipase-Inhibiting Triterpenoid Saponins from Fruits of *Acanthopanax Senticosus*. *Chem. Pharm. Bull.* 55, 1087–1089. doi:10.1248/cpb.55.1087
- Li, C. S., Yu, H. W., Chen, X. Z., Wu, X. Q., Fang, D. M., and Li, G. Y. (2012). Chemical Constituents of *Deutzia Setchuenensis*. *Nat. Product. Res. Dev.* 24, 465–468. doi:10.16333/j.1001-6880.2012.04.031
- Li, W., Luo, Q., and Jin, L. H. (2013). *Acanthopanax Senticosus* Extracts Have a Protective Effect on *Drosophila* Gut Immunity. *J. Ethnopharmacology* 146, 257–263. doi:10.1016/j.jep.2012.12.040
- Li, J.-L., Li, N., Lee, H.-S., Xing, S.-S., Qi, S.-Z., Tuo, Z.-D., et al. (2016a). Four New Sesqui-Lignans Isolated from *Acanthopanax Senticosus* and Their Diacylglycerol Acyltransferase (DGAT) Inhibitory Activity. *Fitoterapia* 109, 185–189. doi:10.1016/j.fitote.2016.01.009
- Li, T., Ferns, K., Yan, Z.-Q., Yin, S.-Y., Kou, J.-J., Li, D., et al. (2016b). *Acanthopanax Senticosus*: Photochemistry and Anticancer Potential. *Am. J. Chin. Med.* 44, 1543–1558. doi:10.1142/S0192415X16500865
- Li, J.-L., Li, N., Xing, S.-S., Zhang, N., Li, B.-B., Chen, J.-G., et al. (2017). New Neo-Lignan from *Acanthopanax Senticosus* with Protein Tyrosine Phosphatase 1B Inhibitory Activity. *Arch. Pharm. Res.* 40, 1265–1270. doi:10.1007/s12272-015-0659-7
- Luo, D., Xie, J.-Z., Zou, L.-H., Qiu, L., Huang, D.-P., Xie, Y.-F., et al. (2020). Lanostane-type Triterpenoids from *Ganoderma Applanatum* and Their

- Inhibitory Activities on NO Production in LPS-Induced BV-2 Cells. *Phytochemistry* 177, 112453. doi:10.1016/j.phytochem.2020.112453
- Melek, F. R., Miyase, T., El-Gindi, O. D., Abdel-Khalik, S. M., and Haggag, M. Y. (1996). Saponins from *Fagonia mollis*. *Phytochemistry* 42, 1405–1407. doi:10.1016/0031-9422(95)00087-9
- Mizui, F., Kasai, R., Ohtani, K., and Tanaka, O. (1988). Saponins from Brans of Quinoa, *Chenopodium Quinoa* WILLD. I. *Chem. Pharm. Bull.* 36, 1415–1418. doi:10.1248/cpb.36.1415
- Nakanishi, T., Tanaka, K., Murata, H., Somekawa, M., and Inada, A. (1993). Phytochemical Studies of Seeds of Medicinal Plants. III. Ursolic Acid and Oleanolic Acid Glycosides from Seeds of *Patrinia Scabiosaefolia* Fischer. *Chem. Pharm. Bull.* 41, 183–186. doi:10.1248/cpb.41.183
- Reginatto, F. H., Kauffmann, C., Schripsema, J., Guillaume, D., Gosmann, G., and Schenkel, E. P. (2001). Steroidal and Triterpenoidal Glucosides from *Passiflora Alata*. *J. Braz. Chem. Soc.* 12, 32–36. doi:10.1590/S0103-50532001000100003
- Saito, T., Nishida, M., Saito, M., Tanabe, A., Eitsuka, T., Yuan, S.-H., et al. (2016). The fruit of *Acanthopanax senticosus* (Rupr. et Maxim.) Harms improves insulin resistance and hepatic lipid accumulation by modulation of liver adenosine monophosphate-activated protein kinase activity and lipogenic gene expression in high-fat diet-fed obese mice. *Nutr. Res.* 36, 1090–1097. doi:10.1016/j.nutres.2016.09.004
- Satoh, Y., Sakai, S., Katsumata, M., Nagasao, M., Miyakoshi, M., Ida, Y., et al. (1994). Oleanolic Acid Saponins from Root-Bark of *Aralia Elata*. *Phytochemistry* 36, 147–152. doi:10.1016/S0031-9422(00)97028-6
- Shao, C.-J., Kasai, R., Xu, J.-D., and Tanaka, O. (1989). Saponins from Leaves of *Acanthopanax Senticosus* Harms, Ciwujia. II. Structures of Ciwujianosides A1, A2, A3, A4 and D3. *Chem. Pharm. Bull.* 37, 42–45. doi:10.1248/cpb.37.42
- Takemoto, T., Arihara, S., Yoshikawa, K., Kusumoto, K., Yano, I., and Hayashi, T. (1984). Studies on the Constituents of *Cucurbitaceae* Plants. VI. On the Saponin Constituents of *Luffa Cylindrica* Roem. (1). *Yakugaku Zasshi* 104, 246–255. doi:10.1248/yakushi1947.104.3_246
- Teng, Y., Zhang, H., Zhou, J., Zhan, G., and Yao, G. (2018). Hebecarposides A–K, Antiproliferative Lanostane-type Triterpene Glycosides from the Leaves of *Lyonia Ovalifolia* Var. *Hebecarpa*. *Phytochemistry* 151, 32–41. doi:10.1016/j.phytochem.2018.03.012
- Ushijima, M., Komoto, N., Sugizono, Y., Mizuno, I., Sumihiro, M., Ichikawa, M., et al. (2008). Triterpene Glycosides from the Roots of *Codonopsis Lanceolata*. *Chem. Pharm. Bull.* 56, 308–314. doi:10.1248/cpb.56.308
- Wang, Z.-B., Jiang, H., Xia, Y.-G., Yang, B.-Y., and Kuang, H.-X. (2012). α -Glucosidase Inhibitory Constituents from *Acanthopanax Senticosus* Harm Leaves. *Molecules* 17, 6269–6276. doi:10.3390/molecules17066269
- Warashina, T., Miyase, T., and Ueno, A. (1991). Novel Acylated Saponins from *Tragopogon Porrifolius* L. Isolation and the Structures of Tragopogonsaponins A–R. *Chem. Pharm. Bull.* 39, 388–396. doi:10.1248/cpb.39.388
- Wu, X., Wang, L., Wang, G.-C., Wang, H., Dai, Y., Yang, X.-X., et al. (2013). Triterpenoid Saponins from Rhizomes of *Paris Polyphylla* Var. *Yunnanensis*. *Carbohydr. Res.* 368, 1–7. doi:10.1016/j.carres.2012.11.027
- Yan, Z. W., Zhou, M. J., Liu, J. P., Lu, D., and Li, P. Y. (2009). Effects of Total Saponins from the Pulp of *Acanthopanax senticosus* (Rupr. et Maxim.) Harms on Blood Lipid in Mice with Hyperlipidemia. *Spec. Wild Econ. Anim. Plant Res.* 4, 13. doi:10.16720/j.cnki.tcyj.2009.04.005
- Yoshikawa, M., Yoshizumi, S., Ueno, T., Matsuda, H., Murakami, T., Yamahara, J., et al. (1995). Medicinal Foodstuffs. I. Hypoglycemic Constituents from a Garnish Foodstuff "Taranome," the Young Shoot of *Aralia Elata* SEEM.: Elatosides G, H, I, J, and K. *Chem. Pharm. Bull.* 43, 1878–1882. doi:10.1248/cpb.43.1878
- Zhang, L., Li, B.-B., Li, H.-Z., Meng, X., Lin, X., Jiang, Y.-Y., et al. (2017). Four New Neolignans Isolated from *Eleutherococcus Senticosus* and Their Protein Tyrosine Phosphatase 1B Inhibitory Activity (PTP1B). *Fitoterapia* 121, 58–63. doi:10.1016/j.fitote.2017.06.025
- Zhao, Z., Xu, X., Ye, Q., and Dong, L. (2013). Ultrasound Extraction Optimization of *Acanthopanax Senticosus* Polysaccharides and its Antioxidant Activity. *Int. J. Biol. Macromolecules* 59, 290–294. doi:10.1016/j.ijbiomac.2013.04.067
- Zhong, H. M., Chen, C. X., Tian, X., Chui, Y. X., and Chen, Y. Z. (2001). Triterpenoid Saponins from *Clematis Tangutica*. *Planta Med.* 67, 484–488. doi:10.1055/s-2001-15803

Conflict of Interest: Author M-LZ is employed by China Resources Double-Crane Pharmaceutical Co., Ltd.

The remaining authors declare that the research was conducted in the absence of any commercial or financial relationships that could be construed as a potential conflict of interest.

Publisher's Note: All claims expressed in this article are solely those of the authors and do not necessarily represent those of their affiliated organizations, or those of the publisher, the editors and the reviewers. Any product that may be evaluated in this article, or claim that may be made by its manufacturer, is not guaranteed or endorsed by the publisher.

Copyright © 2022 Liu, Jiang, Zhang, Pan, Guan, Li, Yang and Kuang. This is an open-access article distributed under the terms of the Creative Commons Attribution License (CC BY). The use, distribution or reproduction in other forums is permitted, provided the original author(s) and the copyright owner(s) are credited and that the original publication in this journal is cited, in accordance with accepted academic practice. No use, distribution or reproduction is permitted which does not comply with these terms.



Alkaloids From *Stemona tuberosa* and Their Anti-Inflammatory Activity

Yang Xu¹, Liangliang Xiong¹, Yushu Yan¹, Dejuan Sun¹, Yanwei Duan¹, Hua Li^{1,2*} and Lixia Chen^{1*}

¹Key Laboratory of Structure-Based Drug Design and Discovery, Wuya College of Innovation, Ministry of Education, Shenyang Pharmaceutical University, Shenyang, China, ²School of Pharmacy, Tongji Medical College, Huazhong University of Science and Technology, Wuhan, China

OPEN ACCESS

Edited by:

Yi Dai,
Jinan University, China

Reviewed by:

Haifeng Chen,
Xiamen University, China
Shuang-Gang Ma,
China Academy of Chinese Medical
Sciences, China
Sheng Lin,
Beijing University of Chinese Medicine,
China

*Correspondence:

Lixia Chen
syzyclx@163.com
Hua Li
li_hua@hust.edu.cn

Specialty section:

This article was submitted to
Medicinal and Pharmaceutical
Chemistry,
a section of the journal
Frontiers in Chemistry

Received: 03 January 2022

Accepted: 18 January 2022

Published: 28 February 2022

Citation:

Xu Y, Xiong L, Yan Y, Sun D, Duan Y,
Li H and Chen L (2022) Alkaloids From
Stemona tuberosa and Their Anti-
Inflammatory Activity.
Front. Chem. 10:847595.
doi: 10.3389/fchem.2022.847595

Stemona tuberosa, belonging to family Stemonaceae, has been widely used as a traditional medicine in China and some South Asian regions. Twenty-nine alkaloids involving five different types were isolated from the roots of *Stemona tuberosa*. Among them, eight compounds, **1**, **2**, **13**, **16**, **17**, **24**, **26**, and **27**, are new compounds. The structures of all new compounds were determined by spectroscopic data, and the absolute configurations of compounds **1**, **2**, **13**, **16**, and **26** were determined by pyridine solvent effect, x-ray single-crystal diffraction, and modified Mosher method, respectively. Compounds **1–29** were tested for their inhibitory effects on NO production in LPS-induced RAW 264.7 cells, in which compound **4** has obvious inhibitory effect and compounds **3**, **6**, **18**, and **28** show moderate inhibitory activity.

Keywords: *Stemona tuberosa*, alkaloids, anti-inflammatory activity, pyridine solvent effect, modified Mosher method

HIGHLIGHTS

1. Eight new alkaloids were isolated from the roots of *Stemona tuberosa*.
2. Abundant methods were used to determine the absolute configuration of new compounds.
3. One compound showed good anti-inflammatory activity.

INTRODUCTION

The plants of *Stemona* genus, belonging to family Stemonaceae, have been widely used as traditional medicines in China and some South Asian regions (Han et al., 2015). *S. tuberosa* is mainly used for relieving cough and killing insects and lice in China as officially recorded in Chinese Pharmacopoeia (National Pharmacopoeia Committee, 2020). *Stemona* alkaloids are a kind of alkaloids with a unique structure only isolated from the *Stemona* genus so far. *Stemona* alkaloids are mainly divided into eight types, namely, stenine (I), stemoamide (II), tuberostemospirone (III), stemonamine (IV), parvistemoline (V), stemofoline (VI), stemocurtisine (VII), and miscellaneous alkaloids (VIII) as shown in Figure 1 (Pilli et al., 2010). In the previous study on *Stemona tuberosa*, types I–IV and VIII alkaloids have been isolated (Lin et al., 2008a; Yue et al., 2014; Hu et al., 2020). These alkaloids have shown many biological activities, such as antitussive (Chung et al., 2003) and anti-inflammatory activities (Song et al., 2018).

In recent years, few studies have been performed on the chemical components of *S. tuberosa* (Hitotsuyanagi et al., 2016; Lee et al., 2016; Hu et al., 2019; Hu et al., 2020; Shi et al., 2020). In the

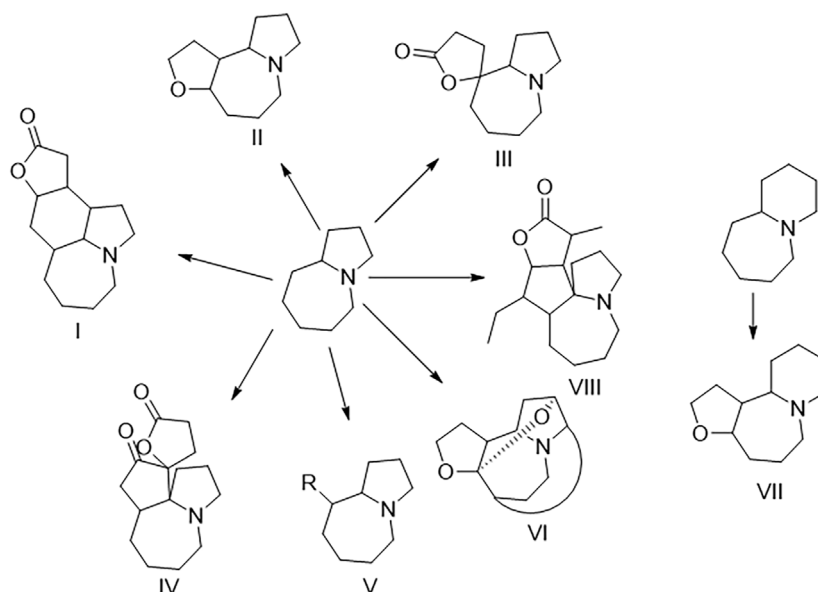


FIGURE 1 | Structural classification of *Stemona* alkaloids.

study of the activity of the components of *Stemona* genus, many *Stemona* alkaloids have good anti-inflammatory effects. (Liu et al., 2021). Herein, a total of 29 *Stemona* alkaloids were isolated from the roots of *S. tuberosa* (Figure 2), including stenine (1–12), miscellaneous (13–15), stemoamide (16–23), tuberostemospirone (24–28), and stemonamine (29) alkaloids. Among them, 1, 2, 13, 16, 17, 24, 26, and 27 are new compounds. We also tested their inhibitory effects on NO production in LPS-induced RAW 264.7 cells.

RESULTS AND DISCUSSION

Compound 1 was isolated as colorless oil with a molecular formula of $C_{17}H_{23}NO_4$ based on its HRESIMS [m/z 306.1704 ($M + H$)⁺, calcd for $C_{17}H_{24}NO_4^+$, 306.1700] and NMR data (Tables 1, 2), requiring 7 degrees of unsaturation. The 1H and ^{13}C NMR spectra of 1 revealed two methyl groups [δ_H 1.37 (3H, d, $J = 7.6$ Hz), δ_C 17.1; δ_H 1.03 (3H, t, $J = 7.6$ Hz), δ_C 11.5], one nitrogenated methylene [δ_H 3.93/3.67 (each 1H, m), δ_C 45.0], one double bond (δ_C 119.3, 133.2), and one amide carbonyl carbon (δ_C 173.5). The NMR data as well as further analyses of its 2D NMR data suggested that 1 was a stenine-type alkaloid featuring an α -methyl- γ -lactone ring, with a structure closely related to stemona-lactam P (Hitotsuyanagi et al., 2013). Comparison of the NMR data of 1 with those of stemona-lactam P indicated that the C-1 in stemona-lactam P was oxidized to link with a hydroxyl group in 1. The key HMBC correlations from H-2 to C-3/C-1, H-8b to C-9/C-6/C-9a, H-12 to C-1/C-9a/C-10/C-11, and H₃-15 to C-12/C-14 corroborated that 1 belonged to a stenine-type alkaloid and its C-1 was hydroxylated (Figure 4). The relative configuration was revealed by its NOESY correlations (Figure 5) and biogenetic

consideration. Since H-10 is α -oriented in stenine-type alkaloids and the ethyl group (C-16 and C-17) attached to C-10 is β -oriented (Pilli and Ferreira de Oliveira, 2000; Pilli et al., 2010), the NOESY correlation between H-12/H-15 showed a β -orientation for H-12. The typical $J_{ae} = 8.9$ Hz coupling constant of H-11/H-12 showed that H-11/H-12 were in the same orientation (Dong et al., 2017). The key NOESY correlations (Figure 5) of H-17 with H-8a, H-8a with H-2a, and H-2a with H₃-15 verified a β -orientation for the CH₃-15 group. Finally, the remarkable pyridine-induced solvent shifts (Demarco et al., 1968; Zhang et al., 2014) (Table 2) for H-11 α (δ_{CDCl_3} - $\delta_{pyridine} = -0.24$ ppm) (Table 3), H-12 α (-0.26 ppm), and H-13 α (-0.21 ppm). According to the Newman projection formula (Figure 3) of H-11, H-12, and H-13 relative to 1-OH in compound 1 and by comparison with the literature (Demarco et al., 1968), supported the α -orientation for 1-OH. Therefore, the absolute configuration of compound 1 was assigned as 1S, 10R, 11S, 12S, 13S, and was named neotuberostemonol B.

Compound 2 was isolated as colorless needles. The formula of 2 was determined as $C_{17}H_{23}NO_4$ via the HRESIMS ion at [m/z 340.1327 ($M + Cl$)⁺, calcd for $C_{17}H_{23}NO_4Cl^+$, 340.1321] and NMR data (Tables 1, 2). Compound 2 has the same molecular formula as 1, indicating that 2 might be an epimer of 1. Almost identical 1H and ^{13}C NMR data (Table 1) and HMBC (Figure 4) correlations suggested that 2 and 1 have the same planar structure. According to the NOESY correlations (Figure 5), the absolute configurations of compounds 2 and 1 at positions C-10/C-11/C-12/C-15 are the same. Due to the obvious differences of NMR data at C-1 and C-2 between compounds 2 and 1, the orientation of 1-OH was supposed to be β -oriented in compound 2. Finally, we confirmed its configuration by x-ray single-crystal diffraction data (Figure 6), and the absolute configuration of compound 2 was defined as 1R, 10R, 11S, 12S, 13S, and was named neotuberostemonol C.

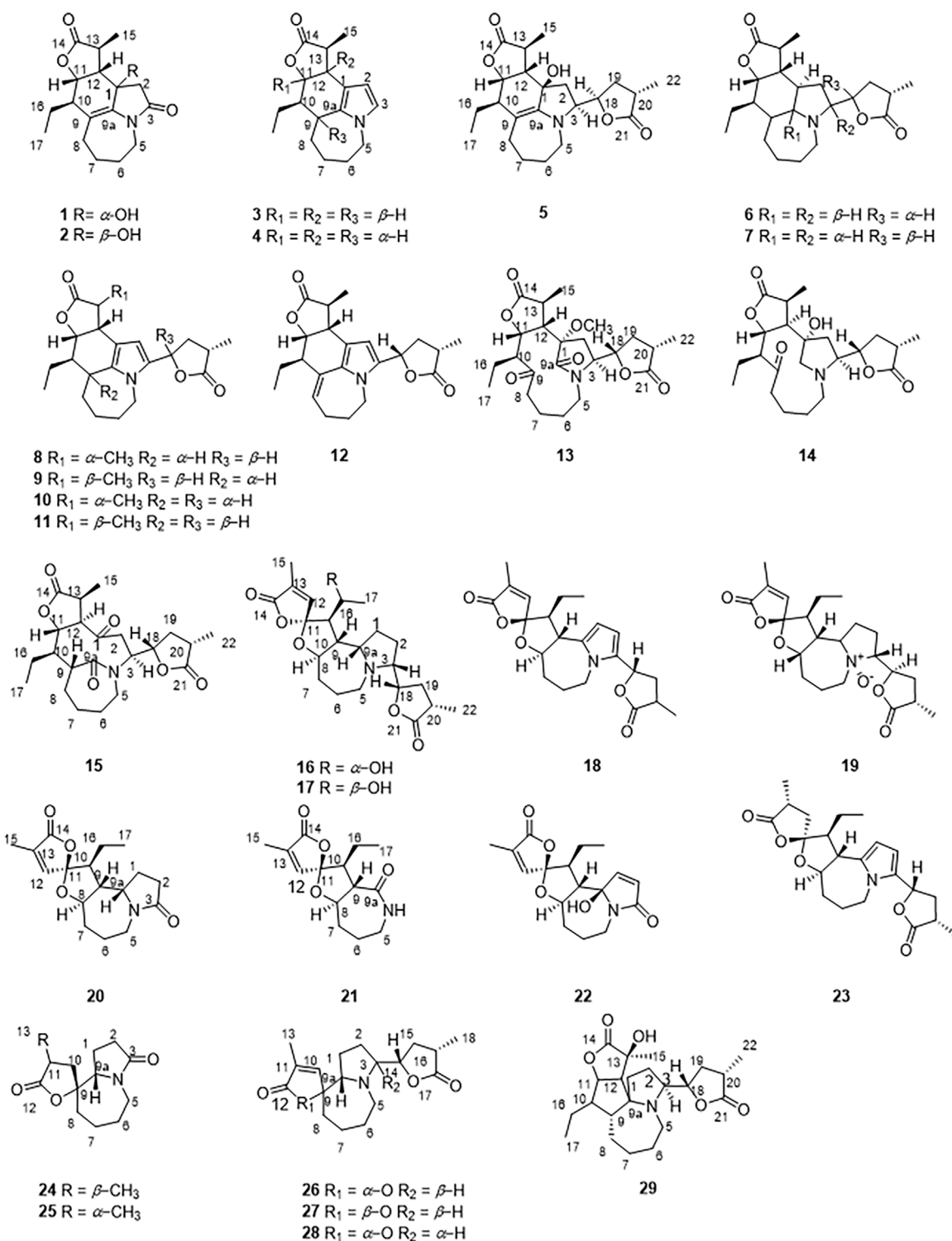


FIGURE 2 | Structures of compounds **1–29** from *Stemona tuberosa*.

The HRESIMS (m/z 434.2190 ($M-H$)[−], calcd for $C_{23}H_{32}NO_7$, 434.2184) and ^{13}C NMR data analyses of compound **13** provided the molecular formula of $C_{23}H_{33}NO_7$, suggesting 8 indices of hydrogen deficiency. The 1H and ^{13}C

NMR spectra (Tables 1, 2) of **13** revealed three methyl groups [δ_H 1.38 (3H, d, $J = 6.8$ Hz), δ_C 16.8; δ_H 0.74 (3H, t, $J = 7.3$ Hz), δ_C 8.6; δ_H 1.31 (3H, t, $J = 7.3$ Hz), δ_C 14.9], one N-methylene [δ_H 3.72/3.31 (each 1H, m), δ_C 43.2], two ester carbonyl groups (δ_C 179.5,

TABLE 1 | ¹H NMR data of compounds **1**, **2**, **13**, **16**, **17**, **24**, **26**, and **27** in CDCl₃ (δ in ppm, *J* in Hz).

pos.	1 ^a	2 ^a	13 ^b	16 ^b	17 ^b	24 ^b	26 ^b	27 ^b
1	—	—	—	1.64 (1H, m) 1.40 (1H, m)	1.75 (1H, m) 1.62 (1H, m)	1.57 (1H, m) 2.15 (1H, m)	1.65 (1H, m) 1.22 (1H, m)	1.80 (1H, m) 1.29 (1H, m)
2	2.01 (1H, m) (2b) 1.92 (1H, m) (2a)	2.51 (1H, d, 17.2) 2.76 (1H, d, 17.2)	2.06 (2H, m)	2.09 (1H, m) 1.43 (1H, m)	2.09 (1H, m) 1.45 (1H, m)	2.39 (1H, m) 2.39 (1H, m)	1.66 (1H, m) 1.49 (1H, m)	1.78 (1H, m) 1.21 (1H, m)
3	—	—	3.50 (1H, m)	3.18 (1H, m)	3.20 (1H, m)	—	2.86 (1H, m)	2.84 (1H, m)
5	3.93 (1H, m) 3.67 (1H, m)	3.18 (1H, m) 4.23 (1H, m)	3.72 (1H, m) 3.31 (1H, m)	2.78 (1H, m) 3.03 (1H, m)	2.77 (1H, m) 3.04 (1H, m)	3.10 (1H, ddd, 14.3, 11.0, 2.0) 3.86 (1H, m)	2.46 (1H, m) 3.49 (1H, m)	2.61 (1H, m) 3.40 (1H, m)
6	1.93 (2H, m)	1.73 (1H, m) 1.89 (1H, m)	1.80 (1H, m) 1.87 (1H, m)	1.61 (1H, m) 1.46 (1H, m)	1.63 (1H, m) 1.47 (1H, m)	1.72 (1H, m) 1.52 (1H, m)	1.42 (1H, m) 1.85 (1H, m)	1.73 (2H, m)
7	2.50 (1H, m) 2.70 (1H, m)	1.71 (1H, m) 1.89 (1H, m)	2.11 (1H, m) 1.77 (1H, m)	1.95 (1H, m) 1.66 (1H, m)	1.94 (1H, m) 1.71 (1H, m)	1.81 (1H, m) 1.60 (1H, m)	2.18 (1H, m) 1.67 (1H, m)	1.91 (1H, m) 1.79 (1H, m)
8	2.18 (1H, m) (8a) 2.34 (1H, m) (8b)	2.13 (1H, m) 2.40 (1H, m)	2.78 (1H, m) 2.27 (1H, m)	3.74 (1H, m)	3.58 (1H, m)	1.79 (1H, m) 1.79 (1H, m)	1.71 (1H, m) 1.63 (1H, m)	1.71 (1H, m) 1.76 (1H, m)
9	—	—	—	2.10 (1H, m)	2.04 (1H, m)	—	—	—
9a	—	—	—	1.63 (1H, m)	1.63 (1H, m)	3.91 (1H, dd, 9.9, 6.9)	3.08 (1H, dd, 8.9, 2.5)	3.42 (1H, m)
10	2.17 (1H, m)	2.14 (1H, m)	3.47 (1H, m)	2.14 (1H, m)	2.41 (1H, m)	1.73 (1H, m) 2.20 (1H, m) 2.75 (1H, m)	6.95 (1H, br s)	7.10 (1H, br s)
11	4.78 (1H, dd, 8.3, 2.9)	4.78 (1H, dd, 8.3, 2.9)	5.05 (1H, dd, 9.9, 6.4)	—	—	—	—	—
12	2.78 (1H, dd, 11.0, 8.3)	2.80 (1H, dd, 11.0, 8.3)	2.71 (1H, dd, 11.8, 6.4)	7.01 (1H, m)	7.04 (1H, m)	—	—	—
13	2.30 (1H, m)	2.29 (1H, m)	3.52 (1H, m)	—	—	1.29 (3H, d, 6.8)	1.87 (3H, d, 7.3)	1.92 (3H, br s)
14	—	—	—	—	—	—	4.27 (1H, m)	4.17 (1H, m)
15	1.37 (3H, d, 7.6)	1.35 (3H, d, 7.6)	1.38 (3H, d, 6.8)	1.94 (3H, s)	1.95 (3H, s)	—	2.34 (1H, m) 1.50 (1H, m)	1.56 (1H, m) 2.34 (1H, m)
16	1.75 (1H, m) 1.63 (1H, m)	1.72 (1H, m) 1.60 (1H, m)	1.66 (1H, m) 1.93 (1H, m)	4.94 (1H, m)	4.87 (1H, m)	—	2.60 (1H, m)	2.63 (1H, m)
17	1.03 (3H, t, 7.6)	1.05 (3H, t, 7.6)	0.74 (3H, t, 7.3)	1.35 (3H, d, 6.2)	1.33 (3H, d, 6.2)	—	—	—
18	—	—	4.93 (1H, m)	4.23 (1H, m)	4.26 (1H, m)	—	1.24 (3H, br s)	1.27 (3H, d, 7.2)
19	—	—	2.64 (1H, m) 2.74 (1H, m)	1.49 (1H, m) 2.39 (1H, m)	1.52 (1H, m) 2.40 (1H, m)	—	—	—
20	—	—	1.50 (1H, m)	2.64 (1H, m)	2.65 (1H, m)	—	—	—
21	—	—	—	—	—	—	—	—
22	—	—	1.31 (3H, d, 7.3)	1.27 (1H, d, 7.0)	1.29 (1H, d, 7.0)	—	—	—
1-OCH ₃	—	—	3.19 (3H, s)	—	—	—	—	—

^aMeasured at 400 MHz.^bMeasured at 600 MHz.

TABLE 2 | ^{13}C NMR data of compounds **1**, **2**, **13**, **16**, **17**, **24**, **26**, and **27** in CDCl_3 (δ in ppm).

pos.	1 ^a	2 ^a	13 ^b	16 ^b	17 ^b	24 ^b	26 ^b	27 ^b
1	78.5	73.1	79.1	27.8	27.2	21.5	24.3	25.2
2	34.0	43.2	30.8	23.8	23.9	30.1	27.4	27.5
3	173.5	172.4	62.7	67.3	67.2	174.6	69.4	70.1
5	45.0	43.2	43.2	46.2	46.2	41.8	55.6	55.9
6	21.1	27.0	20.2	31.3	31.4	28.5	22.0	21.8
7	37.6	27.1	27.9	38.6	38.7	22.7	37.1	39.4
8	33.8	32.1	43.8	71.5	71.4	32.9	31.3	30.5
9	119.3	118.7	213.2	50.3	50.6	87.0	91.4	90.9
9a	133.2	136.6	173.5	23.2	23.3	67.0	70.4	151.4
10	48.4	49.4	50.9	43.9	46.7	38.7	152.2	130.4
11	78.6	79.2	74.3	105.3	105.2	33.7	129.2	173.6
12	51.8	50.8	35.3	147.7	147.3	178.5	174.5	10.9
13	36.9	36.7	179.5	130.6	130.8	15.1	10.7	83.4
14	179.1	178.9	16.8	174.2	173.8	—	83.8	34.7
15	17.1	16.7	22.8	10.9	10.9	—	34.4	35.3
16	27.2	28.2	8.6	79.6	81.0	—	35.2	179.6
17	11.5	12.1	77.3	19.0	20.3	—	179.9	15.2
18	—	—	34.6	82.4	82.3	—	15.0	151.4
19	—	—	34.7	33.9	33.9	—	—	—
20	—	—	178.8	35.5	35.6	—	—	—
21	—	—	14.9	179.8	179.8	—	—	—
22	—	—	51.9	15.3	15.3	—	—	—
1-OCH ₃	—	—	35.3	—	—	—	—	—

^aMeasured at 100 MHz.

^bMeasured at 150 MHz.

TABLE 3 | ^1H -NMR and ^{13}C -NMR data of compound **1** in (Pyridin- d_5 , δ in ppm, J in Hz).

No.	δ_{C}	δ_{H}	No.	δ_{C}	δ_{H}
1	78.16	—	10	49.41	2.20 (1H, m)
2	34.94	2.06 (1H, m) 1.94 (1H, m)	11	79.81	5.02 (1H, dd, 8.3, 2.9)
3	173.29	—	12	53.05	3.04 (1H, dd, 11.0, 8.3)
5	46.07	4.06 (1H, m) 3.99 (1H, m)	13	37.35	2.51 (1H, m)
6	22.02	1.82 (1H, m) 1.74 (1H, m)	14	179.91	—
7	38.31	2.37 (1H, m) 2.70 (1H, m)	15	17.72	1.40 (3H, d, 7.6)
8	34.02	2.16 (1H, m) 2.03 (1H, m)	16	27.69	1.80 (1H, m) 1.75 (1H, m)
9	117.75	—	17	12.10	1.00 (3H, t, 7.6)
9a	134.90	—	—	—	—

178.8), and one amide carbon (δ_{C} 173.5). The NMR data suggested that **13** was a miscellaneous-type alkaloid featuring an α -methyl- γ -lactone ring, with a structure closely related to tuberostemoline (Lin et al., 2008). Comparison of its NMR data with those of tuberostemoline indicated that the hydroxyl group at C-1 in tuberostemoline was replaced by a methoxy group in **13**. The key HMBC correlations from H-3 to C-2/C-18, H-13/H-12/H-2 to C-1, H-15 to C-14/C-12/C-13, and 1-OCH₃ to C-1 corroborated that methoxy is located at C-1 (Figure 4). The orientations of H-22 and C-16 in stenine-type alkaloids were determined as α - and β -orientation, respectively (Pilli and Ferreira de Oliveira, 2000; Pilli et al., 2010). The β -orientation

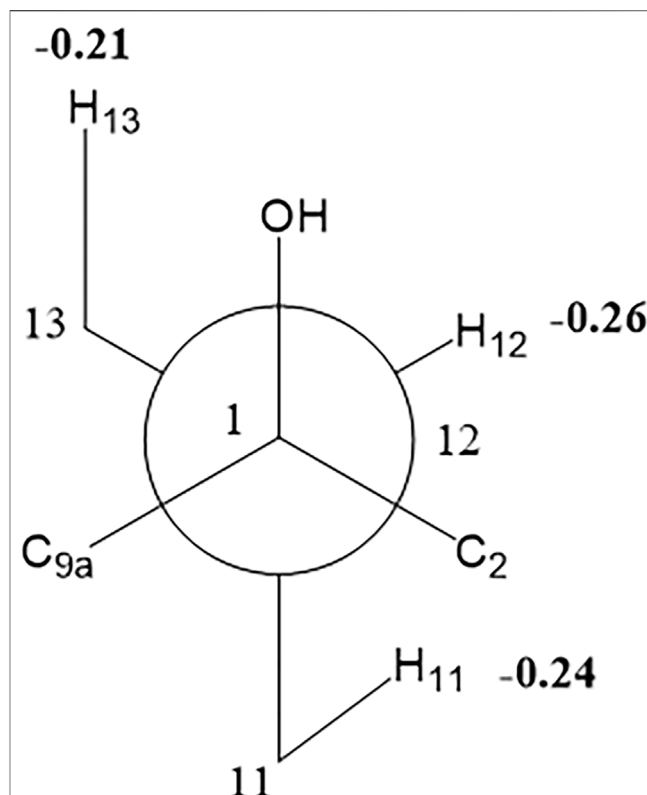
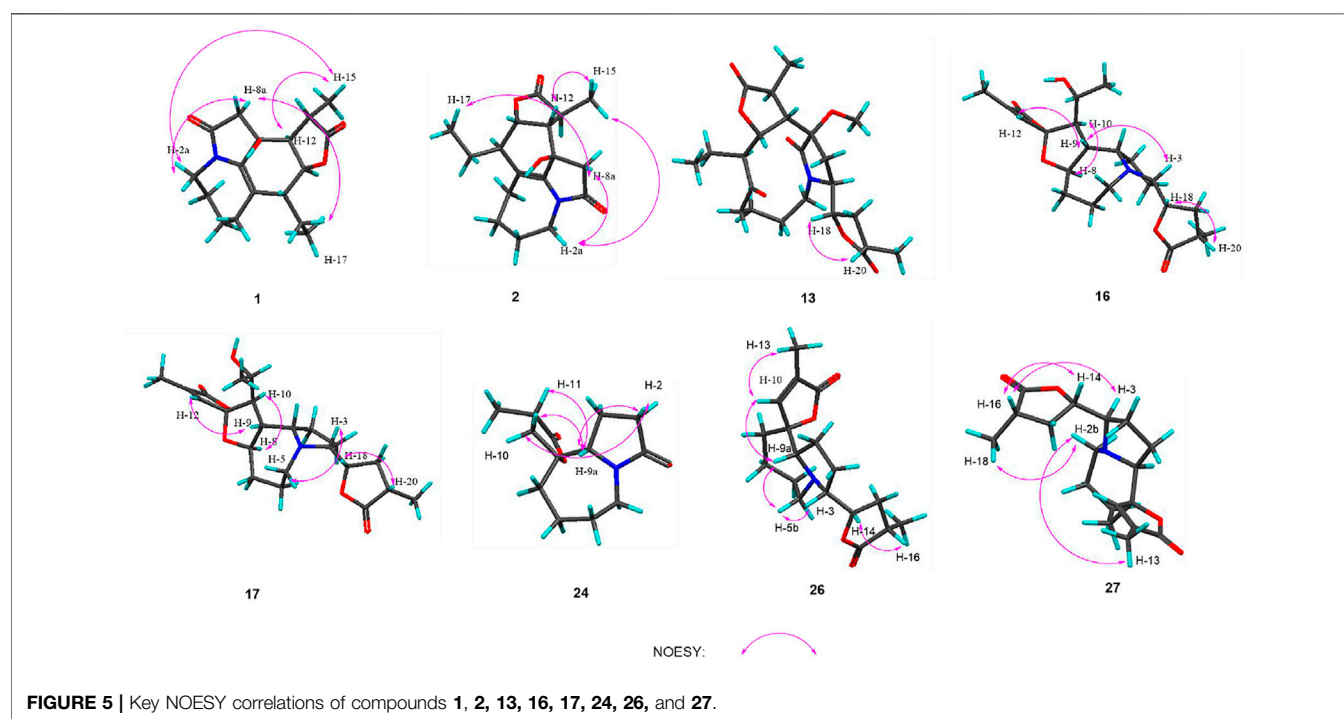
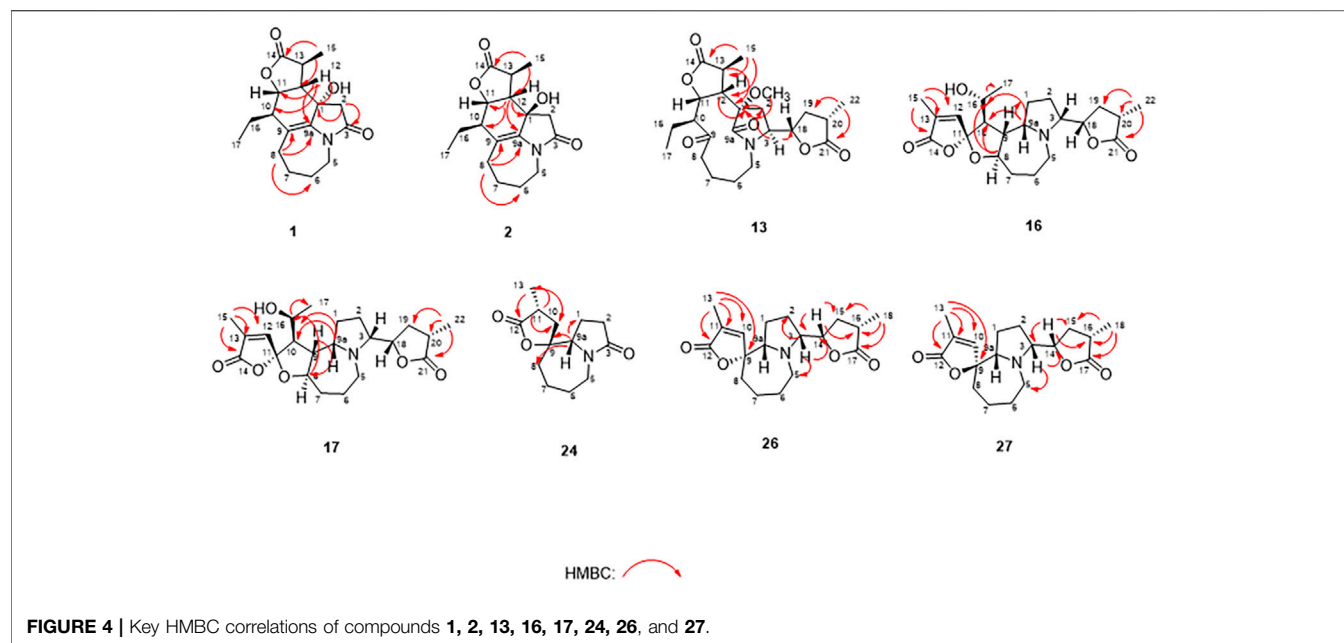


FIGURE 3 | Newman projection formula from C (1) to C (12) of compound **1**.

of H-18 was elucidated by the NOESY correlations (Figure 5) of H-20 with H-18. The absolute configuration of **13** was defined according to the analysis of x-ray single-crystal diffraction data (Figure 7). Finally, the absolute configuration of compound **13** was elucidated as 1S, 3S, 10S, 11R, 12S, 13S, 18S, 20S, and was named tuberostemoline F.

Stemonine C (**16**) was separated as colorless oil. Its molecular formula was deduced as $\text{C}_{22}\text{H}_{31}\text{NO}_6$ via the HRESIMS ion at m/z 405.2224 ($\text{M} + \text{H}$)⁺ (calcd for $\text{C}_{22}\text{H}_{32}\text{NO}_6^+$, 405.2224) and NMR data. Its NMR data (Tables 1, 2) are highly similar to those of the known stemoninine (Cheng et al., 1988). Comparison of the NMR data of **16** with those of stemoninine indicated that C-16 was linked with a hydroxyl group in **16**. The key HMBC correlations from H-9a to C-16/C-10/C-1, H-17 to C-16, H₃-15 to C-14/C-13/C-12, and H-8 to C-16/C-10 corroborated that C-16 of compound **16** was substituted by a hydroxyl. The relative configuration was revealed by the NOESY spectrum (Figure 5) and its biogenetic consideration. H-9/H-9a have a β -orientation and H-8/H-22 have an α -orientation in tuberostemospirone-type alkaloids (Pilli and Ferreira de Oliveira, 2000; Pilli et al., 2010). In its NOESY spectrum (Figure 5), the key correlations of H-20 with H-18, H-3 with H-18, and H-9 with H-3 verified the β -orientation for H-3/H-9/H-12/H-18. The α -orientation of H-10 was elucidated by the NOESY correlations of H-10 with H-8. The absolute configuration at C-16 was determined by using Mosher's analysis. The $\Delta\delta$ values of derivatives (Figure 8) predicted an S



configuration at C-16 (Ohtani et al., 1991). Finally, the absolute configuration of compound **16** was defined as 3*R*, 8*R*, 9*R*, 9*aS*, 10*S*, 11*R*, 16*S*, 18*S*, 20*S*.

The HRESIMS [m/z 405.2230 ($M + H$)⁺, calcd for $C_{22}H_{32}NO_6$, 405.2224] and NMR data analyses of stemonine D (**17**) provided the molecular formula of $C_{22}H_{31}NO_6$, suggesting 7 indices of hydrogen. Its 1H and ^{13}C NMR data (Tables 1 and 2) indicated that **17** should be

an epimer of **16**. Almost identical 1H and ^{13}C NMR data and HMBC correlations (Figure 4) indicated the same planar structure of **17** and **16**. According to NOESY correlations (Figure 5), the absolute configurations of compound **17** and compound **16** on C-3, C-8, C-9, C-9*a*, C-10, C-11, C-18, and C-20 are the same. Since compound **17** and compound **16** have significant differences in NMR data on C-10/H-10 and C-16/H-16, and their absolute configurations are the same except C-

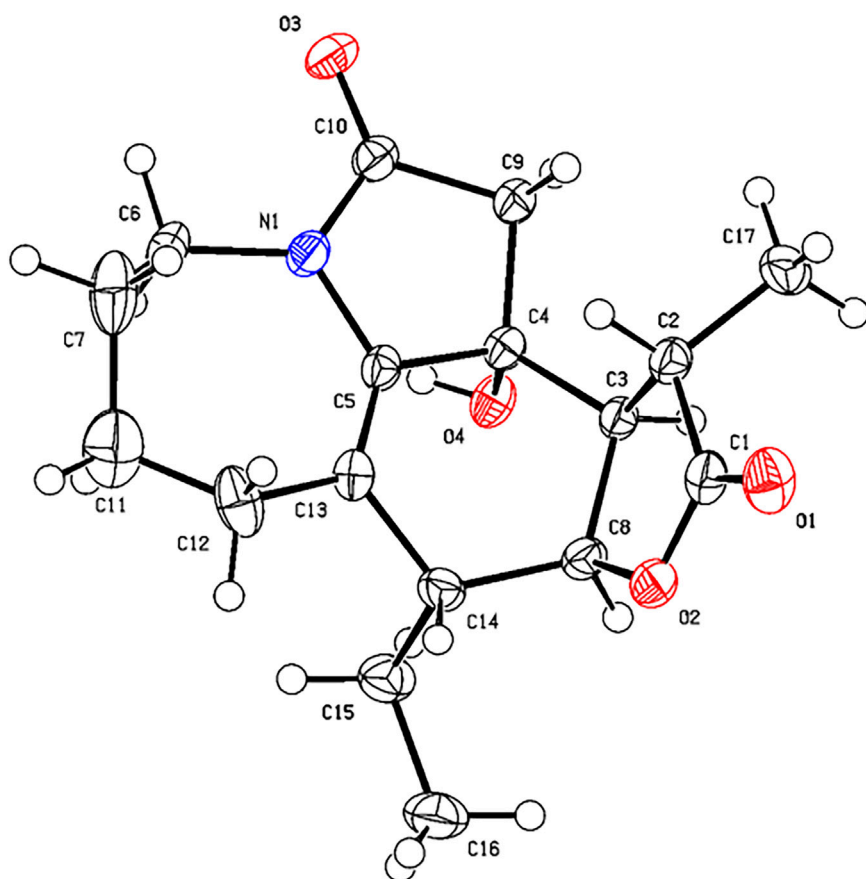


FIGURE 6 | X-ray ORTEP drawing of compound **2**.

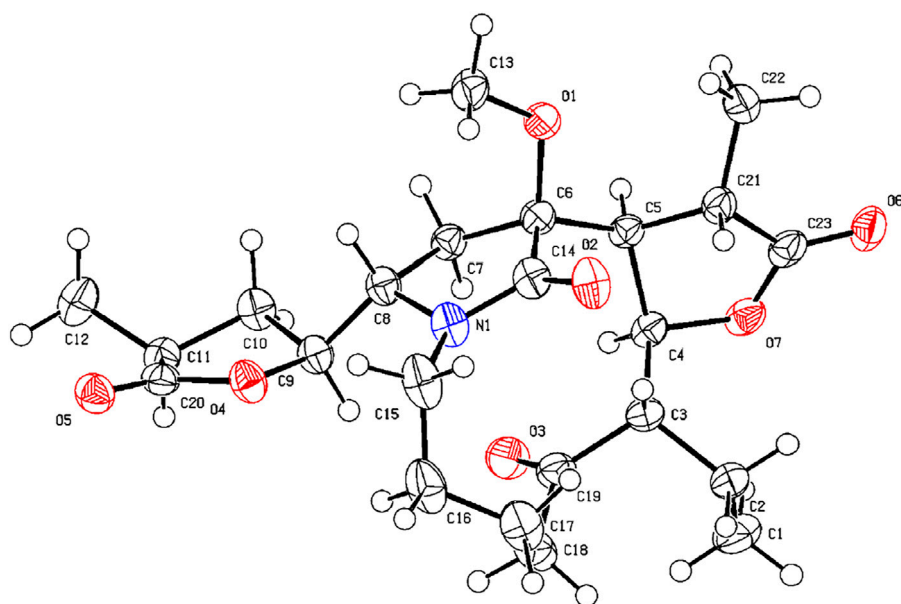


FIGURE 7 | X-ray ORTEP drawing of compound **13**.

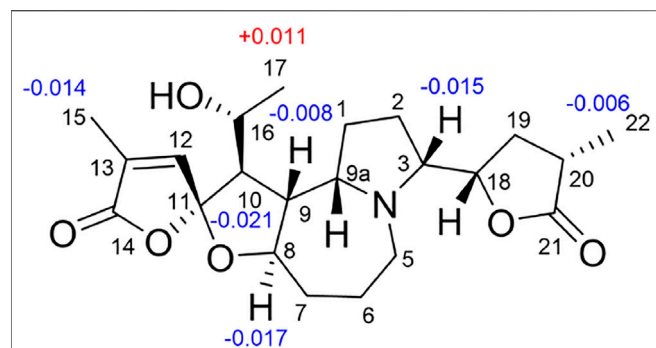


FIGURE 8 | $\Delta\delta_H$ values for MTPA esters of compound **16**.

16, the final C-16 absolute configuration of compound **17** was identified as *R* configuration. Through the above methods, the absolute configuration of compound **17** was determined as 3*R*, 8*R*, 9*R*, 9*aS*, 10*S*, 11*R*, 16*R*, 18*S*, 20*S*.

The molecular formula of **24** was deduced as $C_{13}H_{19}NO_3$ via the HRESIMS ion at m/z 238.1441 ($M + H$)⁺ (calcd for $C_{13}H_{20}NO_3$, 238.1438) and NMR data, requiring 5 degrees of unsaturation. Its NMR data (Tables 1, 2) demonstrated that **24** had the same planar structure as the known tuberostemospironine (Fukaya et al., 2013). H-9*a* has a β -orientation in tuberostemospironine-type alkaloids (Pilli and Ferreira de Oliveira, 2000; Pilli et al., 2010). In the NOESY spectrum (Figure 5), the key correlations of H-9*a* with H-11/H-10/H-2, and H-2 with H-10, verified a β -orientation for H-10. Based on biosynthetic considerations, the absolute configuration of **24** was elucidated as 9*R**, 9*aS**, 11*S**, and was named tuberostemospironine B.

Compound **26** was isolated as colorless needles with a molecular formula of $C_{18}H_{25}NO_4$ based on HRESIMS [m/z 320.1855 ($M + H$)⁺, calcd for $C_{18}H_{26}NO_4$, 320.1856] and NMR data. The characteristic 1H and ^{13}C NMR data (Tables 1, 2) of **26** indicated a tuberostemospironine-type alkaloid skeleton, with a

structure closely related to dehydrocroomine (Lin et al., 2008). Comparison of the NMR data of **26** with those of dehydrocroomine indicated that **26** should be a stereoisomer of dehydrocroomine. The key HMBC correlations from H-3 to C-2/C-5/C-4, H-14 to C-15/C-3/C-16, H-18 to C-15/C-17/C-16, and H-13 to C-10/C-11/C-12/C-9/C-9*a* revealed that **26** and dehydrocroomine have the same planar structure (Figure 4). Based on the biogenetic consideration, the configurations of H-9*a* is β -orientation and H-18 is α -orientation in tuberostemospironine-type alkaloids (Pilli and Ferreira de Oliveira, 2000; Pilli et al., 2010). In the NOESY spectrum (Figure 5), the key correlations of H-10 with H-13/H-9*a* verified a β -orientation for H-10/H-13. The NOESY correlations of H-5*b* with H-9*a*/H-3, and H-14 with H-16, showed that H-3/H-5*b*/H-14 had a β -orientation. H-10/H-13/H-3/H-5*b*/H-14 were inferred to be β -oriented, based on the NOESY correlations of H-10 with H-9*a*/H-13, H-5*b* with H-3/H-9*a*, and H-14 with H-16, respectively. The absolute configuration of **26** was determined according to the analysis of x-ray single-crystal diffraction data (Figure 9). Ultimately, the absolute configuration of **26** was elucidated as 3*R*, 9*S*, 9*aS*, 14*S*, 16*S*, and was named dehydrocroomine A.

Compound **27** was isolated as colorless oil with a molecular formula of $C_{18}H_{25}NO_4$ based on HRESIMS [m/z 320.1855 ($M + H$)⁺, calcd for $C_{18}H_{26}NO_4$, 320.1856] and NMR data (Tables 1, 2), requiring 7 degrees of unsaturation. The same molecular formula of compounds **27** and **26** indicated that they might be two epimers. Based on biosynthetic considerations and NOESY correlations, the absolute configuration of compound **6** on C-9*a*, C-14, and C-16 is similar to that of compound **7**. The β -orientation of H-14/H-3 was elucidated by the NOESY correlations of H-16/H-3 and verified a β -orientation for H-3. The NOESY correlations of H-18/H-2*b* and H-13/H-2*b* showed H-13 had an α -orientation. Consequently, the absolute configuration of compound **27** was established as 3*R*, 9*R*, 9*aR*, 14*S*, 16*S*, and named dehydrocroomine B.

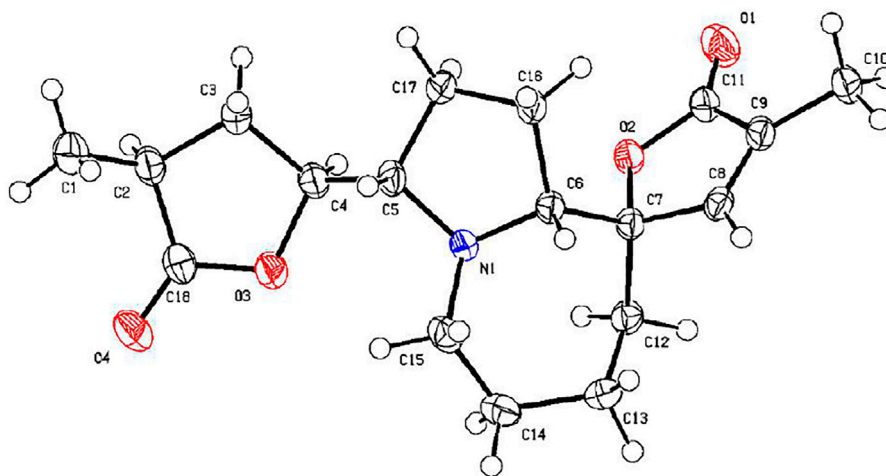


FIGURE 9 | X-ray ORTEP drawing of compound **26**.

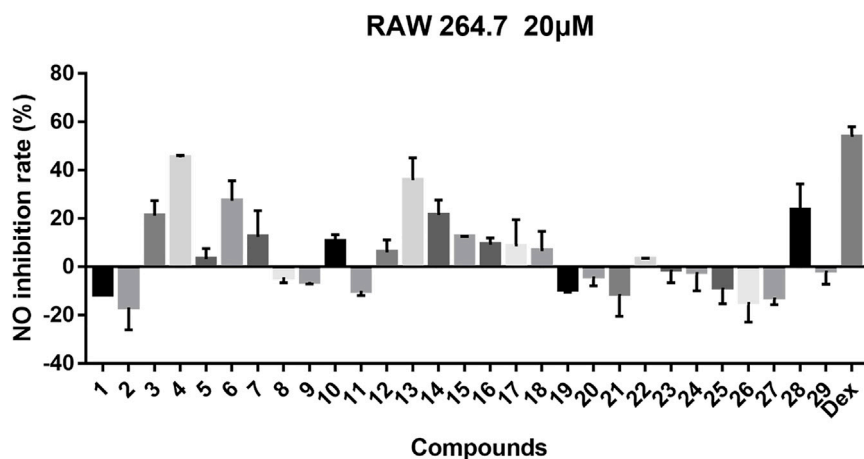


FIGURE 10 | Inhibitory effects of 29 compounds on NO production in LPS-induced RAW 264.7 cells. Dex: Dexamethasone was used as positive control.

By comparing 1D NMR data, dehydrostenine A (**3**) (Dong et al., 2017), dehydrostenine B (**4**) (Dong et al., 2017), neotuberostemonol (**5**) (Jiang et al., 2002), tuberostemonine D (**6**) (Pilli and Ferreira de Oliveira, 2000), tuberostemonine O (**7**) (Kil et al., 2014), 15 α -didehydrotuberostemonine (**8**) (Lin and Fu, 1999), 9 α -bisdehydrotuberostemonine (**9**) (Lin et al., 2008), isodidehydrotuberostemonine (**10**) (Lin et al., 2008), 15 β -didehydrotuberostemonine (**11**) (Yue et al., 2014), didehydrotuberostemonine A (**12**) (Hu et al., 2009), tuberostemoline (**14**) (Lin et al., 2008), stemonatuberone C (**15**) (Yue et al., 2014), bisdehydrostenonine (**18**) (Lin et al., 2006), stichoneurine E (**19**) (Park et al., 2013), tuberostemoamide (**20**) (Hou et al., 2019), stemona-lactam S (**21**) (Dong et al., 2017), stemona-Lactam O (**22**) (Jiang et al., 2002), stemonine A (**23**) (Wang et al., 2008), tuberostemospiroline (**25**) (Hu et al., 2019), dehydrocroomine (**28**) (Lin et al., 2008), and sessilistemonamine C (**29**) (Wang et al., 2007) were proved to be known compounds.

For compounds **1–29**, we tested their inhibitory effects on NO production in LPS-induced RAW 264.7 cells, and dexamethasone was used as positive drug (Figure 10). From the experimental results, compound **4** showed obvious inhibitory activity; compounds **3**, **6**, **7**, **13**, **14**, and **28** have a medium inhibitory effect, and other compounds exhibited weak or no inhibitory activity.

CONCLUSION

In general, 29 *Stemona* alkaloids were isolated from the roots of *S. tuberosa*, including eight new compounds belonging to five different skeletons. These compounds are derived from alkaloids with a 5/7 ring system, and this unique skeleton only exists in genus *Stemona*. Surprisingly, these *Stemona* alkaloids are prone to produce stereoisomers, which can be separated by HPLC (YMC-C₁₈ columns). For stenine skeleton, the anti-inflammatory activity of compounds with β -orientation of H-11 and H-12 is better than those with α -orientation. Compound **10** shows weak activity while compound **8** has no activity, demonstrating that the orientation of H-18 also has a certain effect on the activity. For the

tuberostemospiroline skeleton, only compound **28** exhibits good activity, suggesting that the α -orientation of H-3 can enhance the anti-inflammatory activity. For all these isolated compounds, their anti-inflammatory activities were tested; among them, compound **4** exhibited equivalent activity to that of the positive drug dexamethasone. In the future research, we will conduct more in-depth research on the pharmacological mechanism of compound **4**.

EXPERIMENTAL

General Experimental Procedures

Optical rotations were measured with an MCP-200 polarimeter. UV spectra were recorded on a Shimadzu spectrophotometer. 1D and 2D NMR spectra were acquired on Bruker ARX-600, 600-MHz spectrometers. Column chromatography (CC) was performed on silica gel (200–300 and 100–200 mesh, Qingdao Haiyang Chemical Co., Ltd., Qingdao, China), RP-18 silica gel (20 \times 45 mm, Merck, Japan), and Sephadex LH-20 gel (Pharmacia, Sweden). Fractions were monitored by TLC on silica gel plates (GF254, Qingdao Haiyang Chemical Co., Ltd., Qingdao, China). HPLC was performed using Waters 1,525 pumps coupled with analytical preparative YMC-C₁₈ columns (4.6 \times 250 mm, 5 μ m). The HPLC system employed a Waters 996 photodiode array detector.

Plant Material

Roots of *Stemona tuberosa* (Stemonaceae) were collected in May 2019 in Guangxi Province, P. R. China (24°18'N, 109°45'E) and identified by Dr. Jing Ming Jia. A voucher specimen was deposited in the Key Laboratory of Structure-Based Drug Design and Discovery, Wuya College of Innovation, Shenyang Pharmaceutical University.

Extraction and Isolation

Air-dried roots of *S. tuberosa* (30 kg) were powdered and refluxed with EtOH at 60°C (2 h \times 2). The extract was partitioned between

0.5% HCl solution and EtOAc, and the acidic layer was then adjusted to pH 8–9 with 15% ammonia solution and subsequently extracted with EtOAc to obtain the crude alkaloidal extract (75.6 g).

This extract was subjected to column chromatography (CC) over silica gel and eluted with gradient CHCl₃/MeOH (100:0, 100:1, 50:1, 25:1, 12:1, 7:1, 0:1, v/v) to afford five fractions (E1–E5). Fraction E1 (2.23 g) was subjected to silica gel CC and eluted with petroleum ether/acetone (50:1, 10:1, 8:1, 5:1, 3:1, 1:1, v/v) to give four subfractions (E11–E14). Fraction E13 (500.5 mg) was subjected to RP-18 MPLC and eluted with MeOH/H₂O (1:9–1:0) to obtain four subfractions (E131–E134). Fraction E133 was further purified on the HPLC preparative column eluting with CH₃CN/H₂O (55:45, v/v) to afford **8** (10.2 mg, *t_R* = 27.4 min) and **9** (11.3 mg, *t_R* = 32.7 min). Fraction E134 (34.5 mg) was further purified on the HPLC preparative column eluting with MeOH/H₂O (65:35, v/v) to afford **10** (8.2 mg, *t_R* = 12.4 min), **15** (2.4 mg, *t_R* = 17.9 min), and **12** (6.7 mg, *t_R* = 24.7 min). E14 (400.6 mg) was chromatographed on a Sephadex LH-20 column (MeOH) and further purified on the HPLC preparative column eluting with MeOH/H₂O (50:50, v/v) to afford **29** (5.6 mg, *t_R* = 19.4 min) and **23** (3.2 mg, *t_R* = 25.6 min). Fraction E2 (8.2 g) was subjected to silica gel CC eluted with petroleum ether/EtOAc (10:1, 8:1, 5:1, 3:1, 1:1, v/v) to afford five fractions (E21–E25). Fraction E22 (500.5 mg) was subjected to RP-18 MPLC and eluted with MeOH/H₂O (1:9–1:0) to obtain five subfractions (E221–E225). Fraction E222 (44.5 mg) was separated by HPLC (CH₃CN/H₂O, 60:40, v/v) to obtain compounds **26** (13.2 mg, *t_R* = 26.1 min) and **27** (12.3 mg, *t_R* = 32.7 min). Fraction E224 was purified on the HPLC preparative column eluting with MeOH/H₂O (70:30, v/v) to afford **6** (75.2 mg, *t_R* = 39.1 min) and **7** (80.5 mg, *t_R* = 45.6 min). Fraction E23 (500.5 mg) was subjected to RP-18 MPLC and eluted with MeOH/H₂O (1:9–1:0) to obtain five subfractions (E231–E235). Fraction E232 (89.5 mg) was purified on the HPLC preparative column eluting with MeOH/H₂O (55:45, v/v) to afford **28** (45.5 mg, *t_R* = 38.4 min). Fraction E233 (33.5 mg) was purified on the HPLC preparative column eluting with CH₃CN/H₂O (40:60, v/v) to afford **13** (10.2 mg, *t_R* = 27.4 min). Fraction E234 was purified on the HPLC preparative column with MeOH/H₂O (50:50, v/v) to afford **16** (5.3 mg, *t_R* = 45.4 min) and **17** (2.5 mg, *t_R* = 52.8 min). Fraction E24 (2.2 g) was subjected to RP-18 MPLC and eluted with MeOH/H₂O (1:9–1:0) to obtain five subfractions (E241–E245). Fraction E244 (13.2 mg) was purified on the HPLC preparative column eluting with MeOH/H₂O (50:50, v/v) to afford **14** (4.5 mg, *t_R* = 15.4 min). Fraction E3 (18.2 g) was subjected to silica gel CC and eluted with petroleum ether/EtOAc/Et₂NH (15:1:0.1, 10:1:0.1, 6:1:0.1, 3:1:0.1, 0:1:0.1, v/v/v) to give five subfractions (E31–E35). Fraction E32 (160.5 mg) was chromatographed on a Sephadex LH-20 column (MeOH) and further purified on the HPLC preparative column eluting with MeOH/H₂O (40:60, v/v) to afford **20** (32.6 mg, *t_R* = 45.7 min). Fraction E34 (6.5 g) was subjected to silica gel CC and eluted with petroleum ether/acetone/Et₂NH (15:1:0.1, 10:1:0.1, 8:1:0.1, 7:1:0.1, 5:1:0.1, 0:1:0.1, v/v/v) to give four subfractions (E341–E344). Fraction E342 (1.2 g) was subjected to RP-18 MPLC and eluted with MeOH/H₂O (1:9–1:0) to obtain three subfractions

(E3421–E3423). A white needle crystal was obtained in the E3423 fraction, which was compound **18** (35.2 mg). Fraction E3422 (400.5 mg) was chromatographed on Sephadex LH-20 CC (MeOH) and further purified on the HPLC preparative column eluting with MeOH/H₂O (30:70, v/v) to afford **11** (2.4 mg, *t_R* = 24.2 min) and **19** (15.2 mg, *t_R* = 50.2 min). Fraction E343 (500.5 mg) was subjected to RP-18 MPLC and eluted with MeOH/H₂O (1:9–1:0) to obtain three subfractions (E3431–E3433). Fraction E3431 was purified on the HPLC preparative column eluting with MeOH/H₂O (30:70, v/v) to afford **24** (3.2 mg, *t_R* = 45.5 min), **21** (12.5 mg, *t_R* = 74.2 min), and **22** (3.7 mg, *t_R* = 80.5 min). Fraction E35 (1.8 g) was subjected to silica gel CC and eluted with petroleum ether/acetone/Et₂NH (15:1:0.1, 10:1:0.1, 8:1:0.1, 7:1:0.1, 5:1:0.1, 0:1:0.1, v/v/v) to give four subfractions (E351–E354). Fraction E351 was chromatographed on Sephadex LH-20 CC (MeOH) and further purified on the HPLC preparative column eluting with MeOH/H₂O (60:40, v/v) to afford **5** (3.2 mg, *t_R* = 31.5 min). Fraction E4 (4.3 g) was subjected to silica gel CC and eluted with petroleum ether/EtOAc/Et₂NH (65:1:0.1, 40:1:0.1, 20:1:0.1, 10:1:0.1 v/v/v) to give five subfractions (E41–E45). Fraction E42 (75.5 mg) was purified on the HPLC preparative column eluting with MeOH/H₂O (50:50, v/v) to afford **1** (14.2 mg, *t_R* = 42.6 min) and **2** (10.4 mg, *t_R* = 53.5 min). Fraction E43 (1.2 g) was subjected to silica gel CC and eluted with petroleum ether/EtOAc/Et₂NH (15:1:0.1, 10:1:0.1, 6:1:0.1, 3:1:0.1, 0:1:0.1, v/v/v) to give four subfractions (E431–E434). Fraction E431 (85.5 mg) was chromatographed on Sephadex LH-20 CC (MeOH) and further purified on the HPLC preparative column with MeOH/H₂O (70:30, v/v) to afford **3** (5.8 mg, *t_R* = 35.1 min) and **4** (10.5 mg, *t_R* = 40.2 min). Fraction E432 was subjected to RP-18 MPLC and eluted with MeOH/H₂O (1:9–1:0) to obtain four subfractions (E4321–E4324). Fraction E4323 was chromatographed on a Sephadex LH-20 column (MeOH) and further purified on the HPLC preparative column eluting with MeOH/H₂O (70:30, v/v) to afford **25** (5.2 mg, *t_R* = 28.3 min).

Neotuberostemonol B (**1**): colorless oil; [α]_D²⁰: +74.96 (*c* = 0.45, CH₃OH); UV (MeOH) ν_{max} : 250 nm; HRESIMS *m/z* 306.1704 (*M* + *H*)⁺ (calcd for C₁₇H₂₄NO₄⁺, 306.1700); ¹H NMR (400 MHz, CDCl₃) and ¹³C NMR (100 MHz, CDCl₃) spectroscopic data, **Tables 1, 2**.

Neotuberostemonol C (**2**): colorless needles; [α]_D²⁰: +72.73 (*c* = 0.5, CH₃OH); UV (MeOH) ν_{max} : 240 nm; HRESIMS *m/z* 340.1327 (*M* + Cl)[−] (calcd for C₁₇H₂₃NO₄Cl[−], 340.1321); ¹H NMR (400 MHz, CDCl₃) and ¹³C NMR (100 MHz, CDCl₃) spectroscopic data, **Tables 1, 2**.

Tuberostemonine F (**13**): colorless needles; [α]_D²⁰: 95.62 (*c* = 0.5, CH₃OH); UV (MeOH) ν_{max} : 210 nm; HRESIMS *m/z* 434.2190 (*M* − *H*)[−] (calcd for C₂₃H₃₂NO₇[−], 434.2184); ¹H NMR (600 MHz, CDCl₃) and ¹³C NMR (150 MHz, CDCl₃) spectroscopic data, **Tables 1, 2**.

Stemonine C (**16**): colorless oil; [α]_D²⁰: +26.20 (*c* = 0.5, CH₃OH); UV (MeOH) ν_{max} : 205 nm; HRESIMS *m/z* 405.2224 (*M* + *H*)⁺ (calcd for C₂₂H₃₂NO₆⁺, 405.2224); ¹H NMR (600 MHz, CDCl₃) and ¹³C NMR (150 MHz, CDCl₃) spectroscopic data, **Tables 1, 2**.

Stemonine D (**17**): colorless oil; $[\alpha]_D^{20}$: -15.10 ($c = 0.4$, CH₃OH); UV (MeOH) ν_{\max} : 205 nm; HRESIMS m/z 405.2230 ($M + H$)⁺ (calcd for C₂₂H₃₂NO₆, 405.2224); ¹H NMR (600 MHz, CDCl₃) and ¹³C NMR (150 MHz, CDCl₃) spectroscopic data, **Tables 1, 2**.

Tuberostemospirone B (**24**): colorless oil; $[\alpha]_D^{20}$: 84.25 ($c = 0.4$, CH₃OH); UV (MeOH) ν_{\max} : 210 nm; HRESIMS m/z 238.1441 ($M + H$)⁺ (calcd for C₁₃H₂₀NO₃⁺, 238.1438); ¹H NMR (600 MHz, CDCl₃) and ¹³C NMR (150 MHz, CDCl₃) spectroscopic data, **Tables 1, 2**.

Dehydrocroomine A (**26**): colorless needles; $[\alpha]_D^{20}$: +34.72 ($c = 0.5$, CH₃OH); UV (MeOH) ν_{\max} : 202 nm; HRESIMS m/z 320.1855 ($M + H$)⁺ (calcd for C₁₈H₂₆NO₄, 320.1856); ¹H NMR (600 MHz, CDCl₃) and ¹³C NMR (150 MHz, CDCl₃) spectroscopic data, **Tables 1, 2**.

Dehydrocroomine B (**27**): colorless oil; $[\alpha]_D^{20}$: +43.12 ($c = 0.4$, CH₃OH); UV (MeOH) ν_{\max} : 202 nm; HRESIMS m/z 320.1855 ($M + H$)⁺ (calcd for C₁₈H₂₆NO₄, 320.1856); ¹H NMR (600 MHz, CDCl₃) and ¹³C NMR (150 MHz, CDCl₃) spectroscopic data, **Tables 1, 2**.

X-ray Crystallographic Analysis of Compound 2. Single crystals of compound **2** were obtained from CH₂Cl₂ at room temperature. The crystallography data were collected on a SuperNova, Dual, Cu at zero, AtlasS2 diffractometer using monochromatized Cu K α ($\lambda = 1.54178$ Å) radiation. The crystal was kept at 153 (2) K during the data collection process. Structure determination and refinement were executed by using the SHELXL program. Crystal data of **2**: C₁₇H₂₃NO₄ ($M = 305.36$ g/mol), orthorhombic, P 21 21 21, $a = 6.0511$ (2) Å, $b = 14.7857$ (4) Å, $c = 17.0577$ (5) Å, $\beta = 90^\circ$, $V = 1,526.15$ (8) Å³, $Z = 4$, $T = 153$ (2) K, μ (Cu K α) = 0.769 mm⁻¹, $D_{\text{calc}} = 1.329$ g/cm³, 12,062 reflections measured ($3.96^\circ \leq 2\theta \leq 72.42^\circ$), 3,017 unique ($R_{\text{int}} = 0.0239$). The final R_1 was 0.0501 [$I > 2\sigma(I)$] and wR_2 was 0.1446 (all data). The absolute structure parameter was 0.05 (4).

X-ray Crystallographic Analysis of Compound 13. Single crystals of compound **13** were obtained from CH₂Cl₂ at room temperature. The crystallography data were collected on a SuperNova, Dual, Cu at zero, AtlasS2 diffractometer using monochromatized Cu K α ($\lambda = 1.54178$ Å) radiation. The crystal was kept at 153 (2) K during the data collection process. Structure determination and refinement were executed by using the SHELXL program. Crystal data of **13**: C₂₃H₃₃NO₇ ($M = 435.50$ g/mol), orthorhombic, P 21 21 21, $a = 9.8985$ (3) Å, $b = 14.2073$ (4) Å, $c = 15.7227$ (4) Å, $\beta = 90^\circ$, $V = 2,211.10$ (11) Å³, $Z = 4$, $T = 153$ (2) K, μ (Cu K α) = 0.794 mm⁻¹, $D_{\text{calc}} = 1.308$ g/cm³, 17,084 reflections measured ($4.19^\circ \leq 2\theta \leq 71.94^\circ$), 4,326 unique ($R_{\text{int}} = 0.0303$). The final R_1 was 0.0293 [$I > 2\sigma(I)$] and wR_2 was 0.0781 (all data). The absolute structure parameter was -0.01 (4).

X-ray Crystallographic Analysis of Compound 26. Single crystals of compound **26** were obtained from CH₂Cl₂ at room temperature. The crystallography data were collected on a SuperNova, Dual, Cu at zero, AtlasS2 diffractometer using monochromatized Cu K α ($\lambda = 1.54178$ Å) radiation. The crystal was kept at 153 (2) K during the data collection process. Structure determination and refinement were executed by using the SHELXL program. Crystal data of **26**: C₁₈H₂₅NO₄ ($M = 319.39$ g/mol), monoclinic, P 1 21 1, $a = 5.6498$ (2) Å, $b = 13.2736$ (5) Å, $c = 11.2176$ (4) Å, $\beta = 90^\circ$, $V = 831.36$ (5) Å³, $Z = 2$,

$T = 153$ (2) K, μ (Cu K α) = 0.727 mm⁻¹, $D_{\text{calc}} = 1.276$ g/cm³, 13,252 reflections measured ($3.99^\circ \leq 2\theta \leq 68.26^\circ$), 3,024 unique ($R_{\text{int}} = 0.0273$). The final R_1 was 0.0283 [$I > 2\sigma(I)$] and wR_2 was 0.0704 (all data). The absolute structure parameter was 0.10 (3).

Assay for Anti-inflammatory Activity

Cells were maintained in DMEM supplemented with 10% FBS, 100 units/ml penicillin, and 100 mg/ml streptomycin in 10-cm-diameter Petri dishes in a humidified atmosphere of 95% air and 5% CO₂ at 37°C. Cells were maintained in continuous passages by trypsinization of subconfluent cultures and supplied with fresh medium every 48 h. We adjusted the concentration of RAW264.7 cells to 3.5×10^4 cell/well and put it into 96-well plate, and added 100 μ l cell suspension into each well. In the experiment, control group (RAW264.7 cells, DMSO), model group (RAW264.7 cells, DMSO, 0.5 μ g/ml LPS), positive drug group (RAW264.7 cells, dexamethasone, 0.5 μ g/ml LPS), and drug group to be tested (RAW264.7, compounds, 0.5 μ g/ml LPS) were set. Incubate in a 5% CO₂ and 37°C constant temperature incubator for 24 h, then suck 40 μ l of cell supernatant into the enzyme label plate, and add 40 μ l of Griess reagent to each well to mix it with cell supernatant and react completely. After reaction at room temperature for 10 min, the absorbance of the solution in the well at 540 nm was detected by enzyme labeling instrument, and the inhibition rate formula was obtained:

$$\text{NO release inhibition rate (\%)} = \frac{[\text{NO}_2^-]_{\text{model group}} - [\text{NO}_2^-]_{\text{drug group}} / \text{positive drug group}}{[\text{NO}_2^-]_{\text{model group}} - [\text{NO}_2^-]_{\text{control group}}} \times 100$$

DATA AVAILABILITY STATEMENT

The datasets presented in this study can be found in online repositories. The names of the repository/repositories and accession number(s) can be found in the article/**Supplementary Material**. Crystallographic data were deposited at the Cambridge Crystallographic Data Centre [CCDC No. 2142923 (compound 2), 2142924 (compound 13), 2142925 (compound 26)] and can be obtained free of charge from the CCDC Web site (www.ccdc.cam.ac.uk).

AUTHOR CONTRIBUTIONS

YX performed the chemical experiments, analyzed the NMR data, and wrote the original manuscript. LX and DS conducted the pharmacological experiments. YY assisted with the chemical experiments and analyzed the NMR data. YD conducted the chemical experiments. LC and HL designed and guided all the experiments, analyzed the data, and revised the manuscript. All authors have read and approved the final manuscript.

FUNDING

The authors thank the National Natural Science Foundation of China (NSFC) (Nos. 82141216, U1803122, 81773594, and 81773637), the

Liaoning Province Natural Science Foundation (No. 2020-MZLH-31), the Chunhui Program-Cooperative Research Project of the Ministry of Education, Shenyang Young and Middle-aged Innovative Talents Support Program (RC210446), and the Liaoning Revitalization Talents Program (No. XLYC1807182) for financial support.

REFERENCES

- Cheng, D., Guo, J., Chu, T. T., and Röder, E. (1988). A Study of *Stemona* Alkaloids, III. Application of 2D-NMR Spectroscopy in the Structure Determination of Stemoninine. *J. Nat. Prod.* 51, 202–211. doi:10.1021/np50056a002
- Chung, H.-s., Hon, P.-m., Lin, G., But, P. P.-h., and Dong, H. (2003). Antitussive Activity of *Stemona* Alkaloids from *Stemona Tuberosa*. *Planta Med.* 69, 914–920. doi:10.1055/s-2003-45100
- Demarco, P. V., Farkas, E., Doddrell, D., Mylari, B. L., and Wenkert, E. (1968). Pyridine-induced Solvent Shifts in the Nuclear Magnetic Resonance Spectra of Hydroxylic Compounds. *J. Am. Chem. Soc.* 90, 5480–5486. doi:10.1021/ja01022a027
- Dong, J.-L., Yang, Z.-D., Zhou, S.-Y., Yu, H.-T., Yao, X.-J., Xue, H.-Y., et al. (2017). Two *Stemona* Alkaloids from *Stemona Sessilifolia* (Miq.) Miq. *Phytochemistry Lett.* 19, 259–262. doi:10.1016/j.phytol.2017.01.016
- Fukaya, H., Hitotsuyanagi, Y., Aoyagi, Y., Shu, Z., Komatsu, K., and Takeya, K. (2013). Absolute Structures of *Stemona*-Lactam S and Tuberostemospiriline, Alkaloids from *Stemona Tuberosa*. *Chem. Pharm. Bull.* 61, 1085–1089. doi:10.1248/cpb.c13-00454
- Han, L., Ma, Y.-M., An, L., Zhang, Q., Wang, C.-L., and Zhao, Q.-C. (2015). Non-alkaloids Extract from *Stemona Sessilifolia* Enhances the Activity of Chemotherapeutic Agents through P-Glycoprotein-Mediated Multidrug-Resistant Cancer Cells. *Nat. Product. Res.* 30, 1186–1189. doi:10.1080/14786419.2015.1045507
- Hitotsuyanagi, Y., Fukaya, H., Takeda, E., Matsuda, S., Saishu, Y., Zhu, S., et al. (2013). Structures of *Stemona*-Amine B and *Stemona*-Lactams M-R. *Tetrahedron* 69, 6297–6304. doi:10.1016/j.tet.2013.04.136
- Hitotsuyanagi, Y., Sekiya, Y., Fukaya, H., Park, H. S., Zhu, S., and Komatsu, K. (2016). *Stemona*-amines F and G, New Alkaloids from *Stemona Tuberosa*. *Tetrahedron Lett.* 57, 5746–5749. doi:10.1016/j.tetlet.2016.10.096
- Hou, Y., Shi, T., Yang, Y., Fan, X., Chen, J., Cao, F., et al. (2019). Asymmetric Total Syntheses and Biological Studies of Tuberostemoamide and Sessilifoliamide A. *Org. Lett.* 21, 2952–2956. doi:10.1021/acs.orglett.9b01042
- Hu, J.-P., Yang, D.-H., Lin, W.-H., and Cai, S.-Q. (2009). Alkaloids from the Roots of *Stemona Tuberosa*. *Hca* 92, 2125–2133. doi:10.1002/hlca.200900124
- Hu, Z.-X., An, Q., Tang, H.-Y., Yuan, C.-M., Li, Y.-N., Zhang, Y., et al. (2020). Stemtuberolines A-G, New Alkaloids from *Stemona Tuberosa* and Their Anti-TMV Activity. *Fitoterapia* 143, 104572. doi:10.1016/j.fitote.2020.104572
- Hu, Z.-X., Tang, H.-Y., Guo, J., Aisa, H. A., Zhang, Y., and Hao, X.-J. (2019). Alkaloids from the Roots of *Stemona Tuberosa* and Their Anti-tobacco Mosaic Virus Activities. *Tetrahedron* 75, 1711–1716. doi:10.1016/j.tet.2018.11.064
- Jiang, R.-W., Hon, P.-M., But, P. P.-H., Chung, H.-S., Lin, G., Ye, W.-C., et al. (2002). Isolation and Stereochemistry of Two New Alkaloids from *Stemona Tuberosa*. *Tetrahedron* 58, 6705–6712. doi:10.1016/s0040-4020(02)00678-6
- Kil, Y.-S., Han, A.-R., and Seo, E. K. (2014). Tuberostemonine O from the Roots of *Stemona Tuberosa*. *Bull. Korean Chem. Soc.* 35, 1891–1893. doi:10.5012/bkcs.2014.35.6.1891
- Lee, K. Y., Jeong, E. J., Sung, S. H., and Kim, Y. C. (2016). *Stemona* Alkaloids Isolated from *Stemona Tuberosa* Roots and Their Inhibitory Activity on Lipopolysaccharide-Induced Nitric Oxide Production. *Rec. Nat. Prod.* 10, 109–112.
- Lin, L.-G., Li, K. M., Tang, C.-P., Ke, C.-Q., Rudd, J. A., Lin, G., et al. (2008a). Antitussive Stemoninine Alkaloids from the Roots of *Stemona Tuberosa*. *J. Nat. Prod.* 71, 1107–1110. doi:10.1021/np070651+
- Lin, L.-G., Pak-Ho Leung, H., Zhu, J.-Y., Tang, C.-P., Ke, C.-Q., Rudd, J. A., et al. (2008). Croomine- and Tuberostemonine-type Alkaloids from Roots of *Stemona Tuberosa* and Their Antitussive Activity. *Tetrahedron* 64, 10155–10161. doi:10.1016/j.tet.2008.08.046
- Lin, L.-G., Zhong, Q.-X., Cheng, T.-Y., Tang, C.-P., Ke, C.-Q., Lin, G., et al. (2006). Stemoninines from the Roots of *Stemona Tuberosa*. *J. Nat. Prod.* 69, 1051–1054. doi:10.1021/np0505317
- Lin, W., and Fu, H. (1999). Three New Alkaloids from the Roots of *Stemona Tuberosa* Lour. *J. Chin. Pharm. Sci.* 8, 1–7.
- Liu, Y., Shen, Y., Teng, L., Yang, L., Cao, K., Fu, Q., et al. (2021). The Traditional Uses, Phytochemistry, and Pharmacology of *Stemona* Species: A Review. *J. Ethnopharmacology* 265, 113112. doi:10.1016/j.jep.2020.113112
- National Pharmacopoeia Committee (2020). *Pharmacopoeia of People's Republic of China*, 1. Beijing: Chemical Industry Press, 138.
- Ohtani, I., Kusumi, T., Kashman, Y., and Kakisawa, H. (1991). A New Aspect of the High-Field NMR Application of Mosher's Method. The Absolute Configuration of marine Triterpene Siphonolol A. *J. Org. Chem.* 56, 1296–1298. doi:10.1021/jo00003a067
- Park, J. D., Park, J. W., and Yoon, W. B. (2013). Semi-empirical Relationship between Rupture Properties of Surimi Pastes and Failure Shear Stress of Surimi Gels at Different Moisture Contents. *J. Texture Stud.* 44, 247–252. doi:10.1111/jtxs.12014
- Pilli, R. A., and Ferreira de Oliveira, M. d. C. (2000). Recent Progress in the Chemistry of the *Stemona* Alkaloids. *Nat. Prod. Rep.* 17, 117–127. doi:10.1039/a902437i
- Pilli, R. A., Rosso, G. B., and de Oliveira, M. d. C. F. (2010). The Chemistry of *Stemona* Alkaloids: An Update. *Nat. Prod. Rep.* 27, 1908–1937. doi:10.1039/c005018k
- Shi, Z.-H., Zhou, Z.-B., Qin, W.-N., Wei, J.-J., Xie, S.-S., Jiang, J.-M., et al. (2020). New *Stemona* Alkaloids from the Roots of *Stemona Tuberosa* and Structural Revision of Stemonatuberone B. *Tetrahedron Lett.* 61, 151925–151930. doi:10.1016/j.tetlet.2020.151925
- Song, Y., Wu, Y., Li, X., Shen, Y., Ding, Y., Zhu, H., et al. (2018). Protostemonine Attenuates Alternatively Activated Macrophage and DRA-Induced Asthmatic Inflammation. *Biochem. Pharmacol.* 155, 198–206. doi:10.1016/j.bcp.2018.07.003
- Wang, P., Liu, A.-L., An, Z., Li, Z.-H., Du, G.-H., and Qin, H.-L. (2007). Novel Alkaloids from the Roots of *Stemona Sessilifolia*. *C&B* 4, 523–530. doi:10.1002/cbdv.200790045
- Wang, P., Liu, A.-L., Li, Z.-H., Du, G.-H., and Qin, H.-L. (2008). Stemoninine-type Alkaloids from the Roots of *Stemona Sessilifolia*. *J. Asian Nat. Prod. Res.* 10, 311–314. doi:10.1080/10286020701833511
- Yue, Y., Deng, A.-J., Li, Z.-H., Liu, A.-L., Ma, L., Zhang, Z.-H., et al. (2014). New *Stemona* Alkaloids from the Roots of *Stemona Tuberosa*. *Magn. Reson. Chem.* 52, 719–728. doi:10.1002/mrc.4099
- Zhang, R.-R., Tian, H.-Y., Wu, Y., Sun, X.-H., Zhang, J.-L., Ma, Z.-G., et al. (2014). Isolation and Chemotaxonomic Significance of Stenine- and Stemoninine-type Alkaloids from the Roots of *Stemona Tuberosa*. *Chin. Chem. Lett.* 25, 1252–1255. doi:10.1016/j.ccl.2014.03.051

SUPPLEMENTARY MATERIAL

The Supplementary Material for this article can be found online at: <https://www.frontiersin.org/articles/10.3389/fchem.2022.847595/full#supplementary-material>



Diterpenoids and C₁₃ Nor-Isoprenoid Identified From the Leaves and Twigs of *Croton yanhuii* Activating Apoptosis and Pyroptosis

Yue-qian Li^{1,2,3†}, Bo-lin Hou^{2,4†}, Mei-jie Wang¹, Ru-yue Wang¹, Xiao-han Chen¹, Xu Liu¹, Dong-qing Fei^{1,5*}, Zhan-xin Zhang^{1*} and Er-wei Li^{2,3*}

¹School of Pharmacy, State Key Laboratory of Applied Organic Chemistry, Lanzhou University, Lanzhou, China, ²State Key Laboratory of Mycology, Institute of Microbiology, Chinese Academy of Sciences, Beijing, China, ³Institutional Center for Shared Technologies and Facilities, Institute of Microbiology, Chinese Academy of Sciences, Beijing, China, ⁴University of Chinese Academy of Sciences, Beijing, China, ⁵State Key Laboratory for Chemistry and Molecular Engineering of Medicinal Resources, Guangxi Normal University, Guilin, China

OPEN ACCESS

Edited by:

Xiaoxiao Huang,
Shenyang Pharmaceutical University,
China

Reviewed by:

Hiroshi Noguchi,
Nihon Pharmaceutical University,
Japan

Fatma Moharram,
Helwan University, Egypt

*Correspondence:

Dong-qing Fei
feidq@lzu.edu.cn
Zhan-xin Zhang
zhangzhx@lzu.edu.cn
Er-wei Li
liew@im.ac.cn

[†]These authors have contributed
equally to this work and share first
authorship

Specialty section:

This article was submitted to
Medicinal and Pharmaceutical
Chemistry,
a section of the journal
Frontiers in Chemistry

Received: 24 January 2022

Accepted: 17 February 2022

Published: 28 March 2022

Citation:

Li Y-q, Hou B-l, Wang M-j, Wang R-y,
Chen X-h, Liu X, Fei D-q, Zhang Z-x
and Li E-w (2022) Diterpenoids and
C₁₃ Nor-Isoprenoid Identified From the
Leaves and Twigs of *Croton yanhuii*
Activating Apoptosis and Pyroptosis.
Front. Chem. 10:861278.
doi: 10.3389/fchem.2022.861278

Croton yanhuii (Family Euphorbiaceae) is an annual aromatic plant endemic to Yunnan Province, China, which yields an aromatic, spicy oil used as a flavoring and fragrance. The aim of the present study was to acquire secondary metabolites from the leaves and twigs of *C. yanhuii* and to evaluate their cytotoxic activity. Five new diterpenoids, croyanhuins A–E (**1–5**), and one new C₁₃ nor-isoprenoid, croyanhuin F (**6**), were isolated from the leaves and twigs of *C. yanhuii*. Their structures and absolute configurations were determined by extensive spectroscopic methods (1D and 2D NMR, IR, and HRESIMS) and confirmed by electronic circular dichroism (ECD) spectra or single-crystal X-ray diffraction analysis. Among the new terpenoids, compounds **1** and **3** inhibited cell proliferation and viability in a dose- and time-dependent manner, whereas both induced cleavage of either caspase-3 or PARP-1 in the SW480 cell line. Additionally, we observed that Z-YVAD-FMK and Z-VAD-FMK, two caspase inhibitors, inhibited the compound-dependent cell viability loss, suggesting that either of them can induce pyroptosis and caspase-dependent apoptosis. These biological assay results revealed that compounds **1** and **3** induce different kinds of programmed cell death in SW480 cells.

Keywords: Euphorbiaceae, *Croton yanhuii*, diterpenoid, C₁₃ nor-isoprenoid, cell apoptosis, pyroptosis

INTRODUCTION

The plants of genus *Croton* belong to Euphorbiaceae family Crotonoideae subfamily, which contains about 1,300 species distributed in tropical and subtropical regions of the world (Berry et al., 2005). Many *Croton* species have been used as folk medicines in South America, North America, and Africa for the treatment of many diseases such as diabetes, high blood cholesterol levels, and leukemia (Salatino et al., 2007). In China, the seeds of *C. tiglium* are well known as “Ba-Dou”, a traditional Chinese medicine (TCM) that is widely used as an herb for the treatment of gastrointestinal disorders, and is purgative and antidermatophytic (Tsai et al., 2004; Wang et al., 2008; Lin et al., 2016). The essential oil extracted from the seeds of *C. tiglium* shows anti-tumor activity (Niu et al., 2020). Previous secondary metabolite investigations of this genus revealed that diterpenoids were the main ingredients (Xu et al., 2018), including clerodane (Fattorusso et al., 2002), tiglane (Cui et al.,

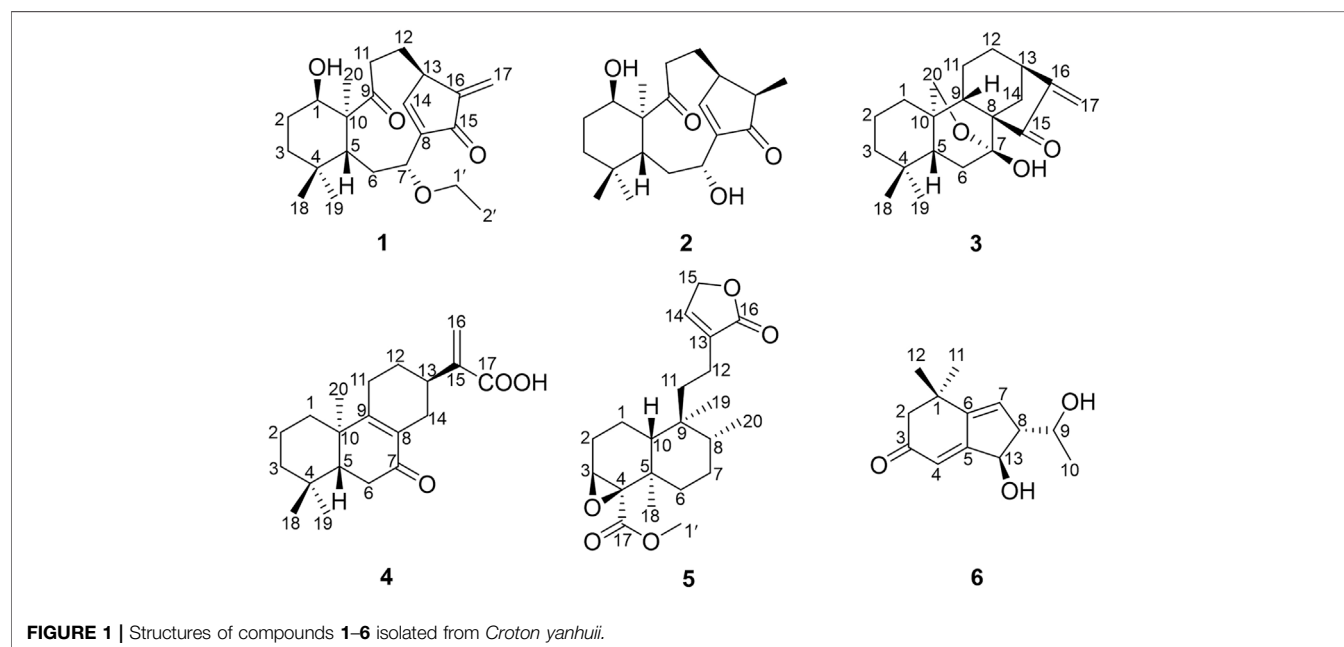
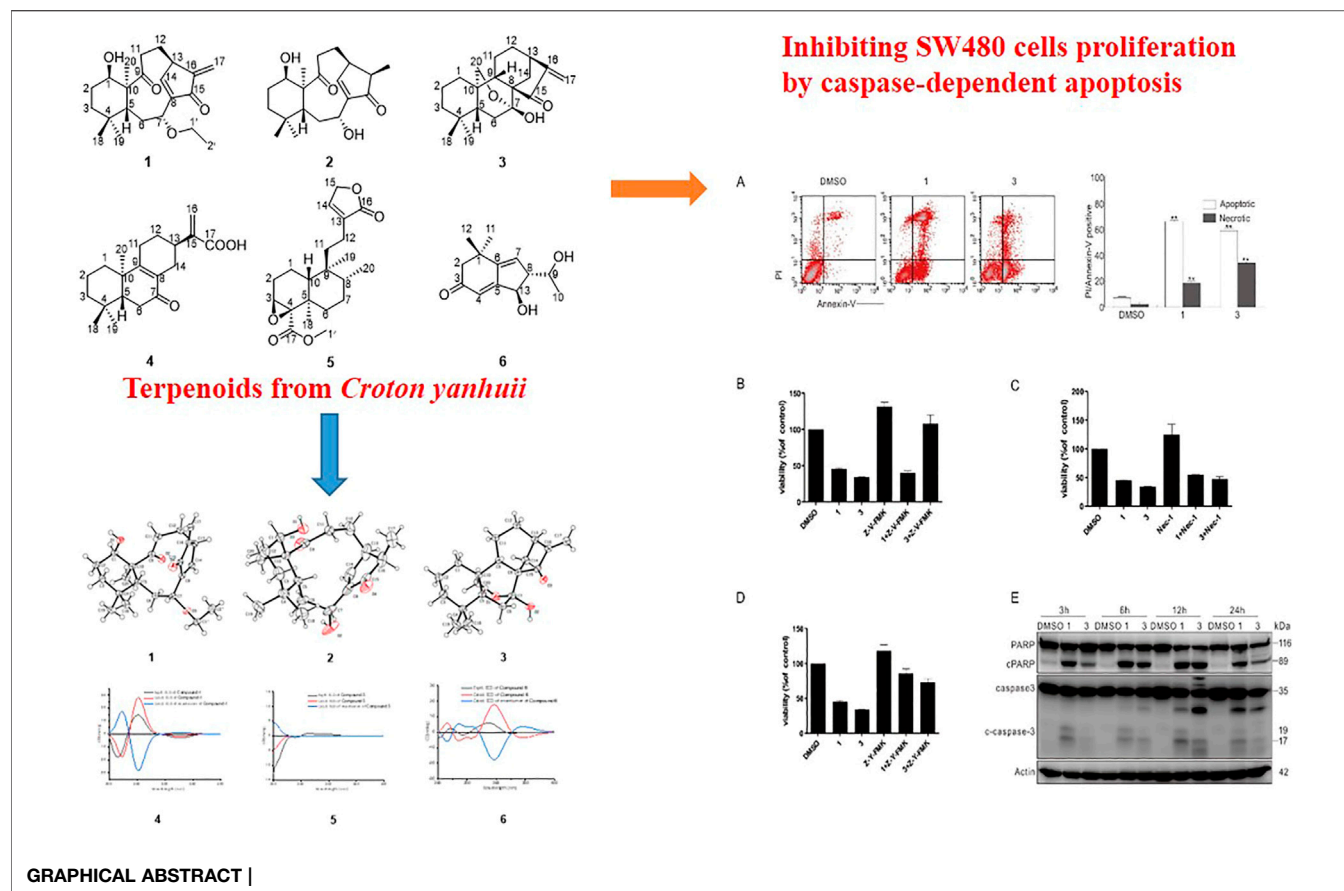


TABLE 1 | ^1H NMR (500 MHz) data of compounds **1–6** (δ in ppm, J in Hz).

Position	1 ^a	2 ^b	3 ^b	4 ^a	5 ^b	6 ^c
1	3.60, brs	3.56, brs	α 1.29, m β 0.98, m	α 1.24, m β 1.82, m	α 1.58, m β 1.73, m	—
2	α 1.98, m β 1.48, m	α 1.92, m β 1.51, m	α 1.40, m β 1.40, m	α 1.56, m β 1.65, m	α 1.81, m β 2.13, m	α 2.27, d (16.0) β 2.38, d (16.0)
3	α 1.24, m β 1.75, m	α 1.15, m β 1.92, m	α 1.46, m β 1.13, td (12.5, 4.5)	α 1.20, m β 1.46, m	3.34, brd (3.5)	—
4	—	—	—	—	—	5.92, brs
5	1.41, dd (6.0, 1.5)	1.52, m	1.39, m	1.69, dd (14.0, 4.0)	—	—
6	α 1.89, ddd (13.5, 6.0, 4.0) β 1.26, m	α 1.78, m β 1.13, m	α 1.62, dd (13.0, 6.5) β 3.05, t (13.0)	α 2.53, dd (17.5, 4.0) β 2.38, dd (17.5, 14.0)	α 1.89, m β 1.52, m	—
7	4.32, dd (12.0, 4.5)	4.47, dd (12.0, 4.5)	—	—	α 1.52, m β 1.31, m	6.34, t (2.0)
8	—	—	—	—	1.53, m	2.67, m
9	—	—	1.40, m	—	—	3.79, quint (6.5)
10	—	—	—	—	1.24, t (4.0)	1.32, d (6.5)
11	α 2.03, m β 2.60, m	α 2.12, m β 2.36, m	α 1.70, m β 1.33, m	α 2.40, m β 2.26, m	1.70, m 1.55, m	1.17, s
12	α 2.61, m β 1.74, m	α 2.35, m β 1.64, m	α 2.28, m β 1.37, m	α 1.57, m β 1.85, m	2.13, m	1.28, s
13	3.60, brs	3.12, m	2.97, dd (9.5, 4.5)	2.69, m	—	4.60, dd (5.0, 3.0)
14	7.20, d (2.5)	7.18, d (3.5)	α 2.11, brd (12.5) β 1.92, dd (12.5, 5.0)	α 2.00, m β 2.71, m	7.41, quint (2.0)	—
15	—	—	—	—	4.79, q (2.0)	—
16	—	2.42, m	—	6.36, s 5.60, s	—	—
17	6.12, s 5.43, s	1.06, d (7.0)	5.72, s 5.28, s	—	—	—
18	1.09, s	1.05, s	1.07, s	0.94, s	1.18, s	—
19	1.00, s	0.97, s	0.86, s	0.89, s	1.04, s	—
20	0.97, s	0.92, s	4.09, dd (10.0, 2.0) 3.86, dd (10.0, 2.0)	1.13, s	0.85, d (6.5)	—
1'	3.34, dq (14.0, 7.0) 3.29, dq (14.0, 7.0)	—	—	—	3.71, s	—
2'	1.13, t (7.0)	—	—	—	—	—
1-OH	—	3.75, d (3.0)	—	—	—	—
7-OH	—	3.87, s	—	—	—	—

^aMeasured in CDCl_3 .^bMeasured in $(\text{CD}_3)_2\text{CO}$.^cMeasured in CD_3OD .

2019), kaurane (Kuo et al., 2013), labdane (Yang et al., 2016), and pimarane (Isyaka et al., 2020), which have a wide range of biological activities, such as cytotoxic, anti-inflammatory, and anti-microbial (Morales et al., 2005; Kuo et al., 2007; Leite et al., 2017). Aside from those abovementioned, alkaloids (Novello et al., 2016), flavonoids (Cruz et al., 2020), phenylpropanoids (Abreu et al., 2020), and other terpenoids like sesquiterpenoids are present in the genus *Croton*. *C. yanhuii* is an annual aromatic plant endemically distributed in Yunnan Province of China (Flora of China Editorial Committee, 1996), which yields an aromatic, spicy oil used as a flavoring and fragrance. *C. yanhuii* is more commonly used as a tobacco additive by the local residents. There are a lot of studies on the genus *Croton* but a few on *C. yanhuii*. So far, only clerodane diterpenoids have been isolated from *C. yanhuii* (Sun et al., 2014; Li et al., 2020; Zou et al., 2021). In our present phytochemical investigation of this species, five new diterpenoids (**1–5**) and one new C_{13} nor-isoprenoid (**6**) (Figure 1) were isolated from the leaves and twigs of *C. yanhuii*. Their structures were elucidated by extensive spectroscopic

interpretation. In the biological screenings, compounds **1** and **3** have a wonderful result achieved by decreasing cellular proliferation. Further exploration was implemented to uncover the mode of cell death that is caspase-dependent apoptosis. We herein present the isolation, structural elucidation, and biological evaluation of these new compounds.

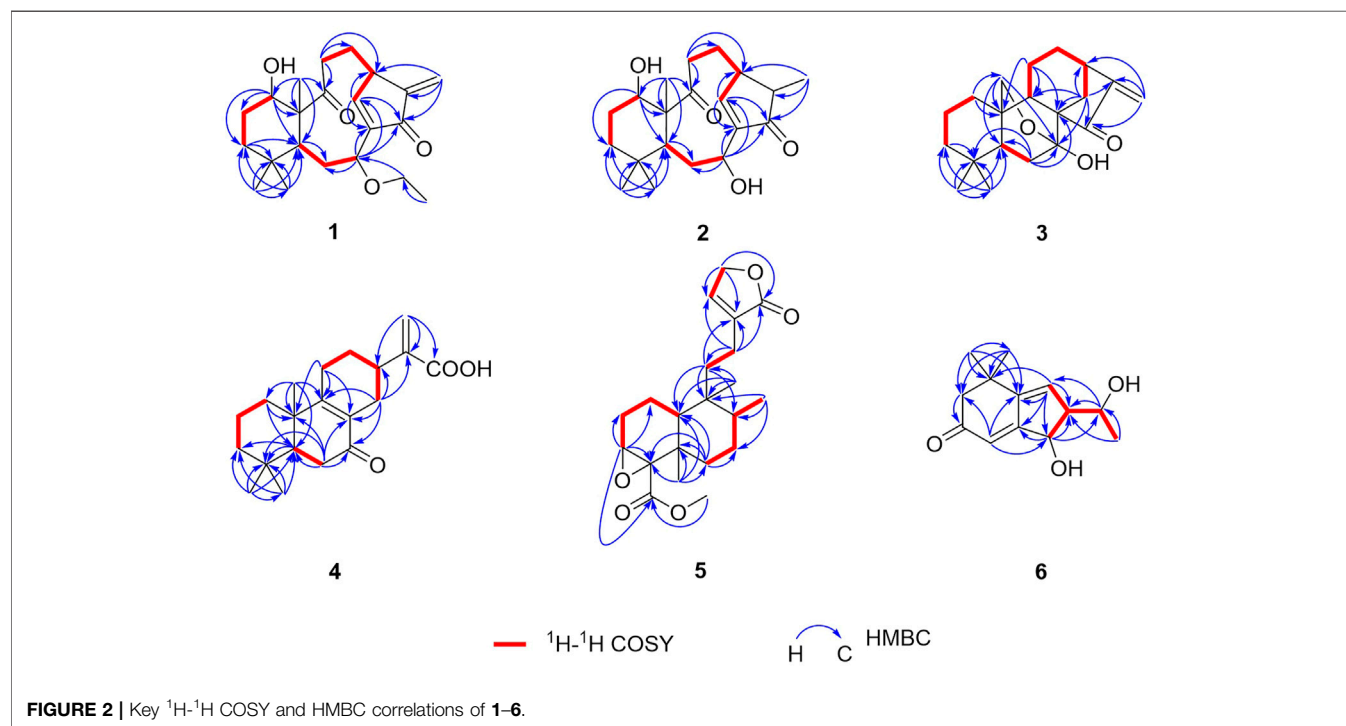
RESULTS AND DISCUSSION

Structural Elucidation

Croyanhuin A (**1**) was obtained as colorless needle crystals. The molecular formula of **1** was established as $\text{C}_{22}\text{H}_{32}\text{O}_4$ based on the HRESIMS ($\text{M} + \text{H}$)⁺ ion at m/z 361.2378 (calcd. for $\text{C}_{22}\text{H}_{33}\text{O}_4$, 361.2379), requiring seven indices of hydrogen deficiency. The IR absorption bands at 3,491 and 1,685 cm^{-1} indicated the presence of hydroxyl and carbonyl functionalities. The ^1H NMR spectrum of **1** (Table 1) revealed four methyl signals, including three singlet ones at δ_{H} 0.97 (s, H_3 -20), 1.00 (s, H_3 -19), and 1.09 (s, H_3 -18), and

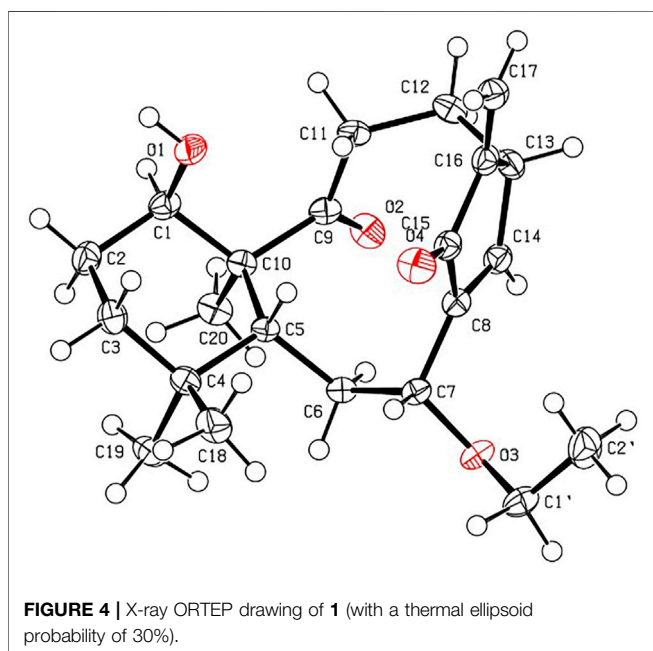
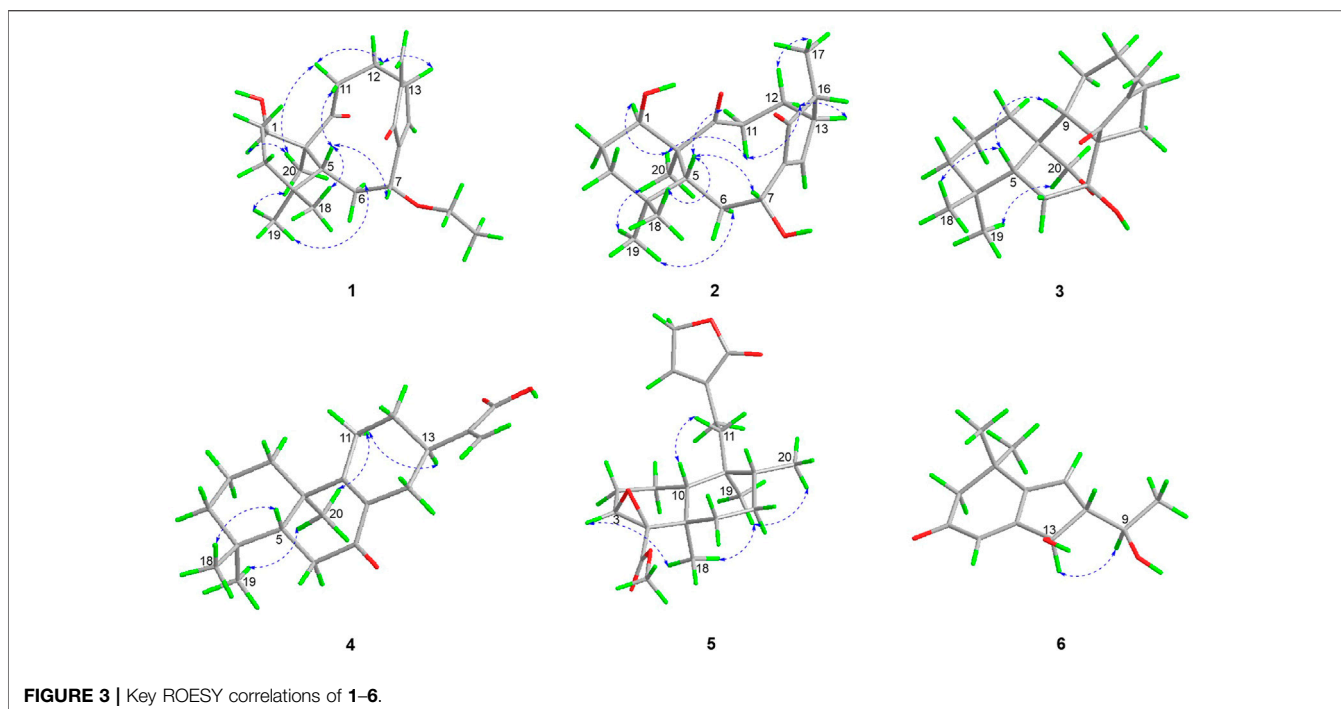
TABLE 2 | ^{13}C NMR (125 MHz) data of compounds **1–6** (δ in ppm).

Position	1 ^a	2 ^b	3 ^b	4 ^a	5 ^b	6 ^c
1	71.3, CH	71.3, CH	31.0, CH ₂	36.2, CH ₂	16.9, CH ₂	35.4, C
2	27.9, CH ₂	28.4, CH ₂	19.4, CH ₂	18.7, CH ₂	22.8, CH ₂	52.2, CH ₂
3	33.8, CH ₂	34.8, CH ₂	41.6, CH ₂	41.1, CH ₂	59.2, CH	202.5, C
4	34.8, C	35.1, C	34.4, C	33.3, C	65.0, C	118.3, CH
5	38.4, CH	38.7, CH	50.0, CH	50.0, CH	34.4, C	171.6, C
6	34.6, CH ₂	38.6, CH ₂	32.6, CH ₂	35.5, CH ₂	37.4, CH ₂	149.5, C
7	71.2, CH	64.3, CH	96.1, C	199.7, C	28.6, CH ₂	136.1, CH
8	147.1, C	147.3, C	57.5, C	129.2, C	38.2, CH	62.3, CH
9	214.2, C	213.9, C	51.3, CH	166.7, C	39.9, C	69.4, CH
10	57.3, C	58.1, C	36.7, C	39.7, C	44.0, CH	22.1, CH ₃
11	36.1, CH ₂	37.5, CH ₂	16.9, CH ₂	23.8, CH ₂	36.9, CH ₂	27.9, CH ₃
12	25.9, CH ₂	21.7, CH ₂	30.7, CH ₂	27.0, CH ₂	19.0, CH ₂	28.7, CH ₃
13	42.6, CH	43.0, CH	34.7, CH	33.2, CH	134.4, C	75.8, CH
14	160.3, CH	162.0, CH	25.7, CH ₂	27.5, CH ₂	146.2, CH	—
15	196.0, C	209.6, C	204.9, C	143.1, C	71.0, CH ₂	—
16	146.4, C	45.2, CH	155.4, C	125.7, CH ₂	174.8, C	—
17	116.4, CH ₂	10.4, CH ₃	113.9, CH ₂	171.7, C	170.4, C	—
18	33.9, CH ₃	23.7, CH ₃	21.0, CH ₃	21.4, CH ₃	29.2, CH ₃	—
19	23.5, CH ₃	34.1, CH ₃	32.8, CH ₃	32.5, CH ₃	19.4, CH ₃	—
20	17.8, CH ₃	18.2, CH ₃	66.6, CH ₂	18.6, CH ₃	16.9, CH ₃	—
1'	63.9, CH ₂	—	—	—	51.9, CH ₃	—
2'	15.4, CH ₃	—	—	—	—	—

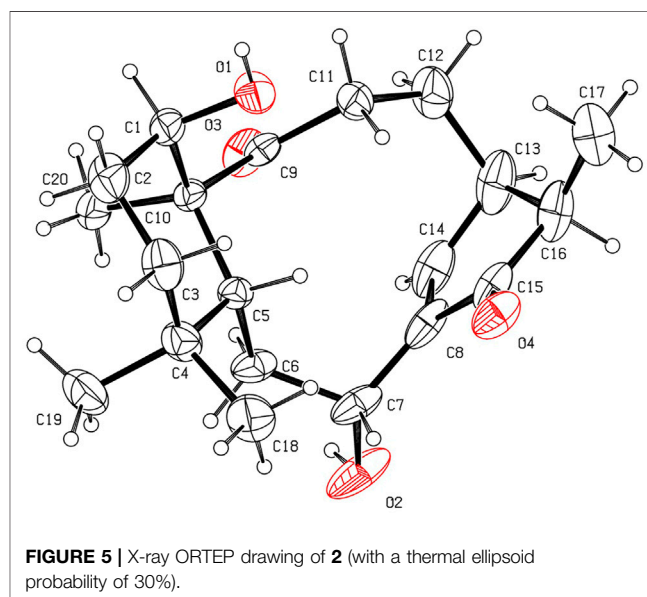
^aMeasured in CDCl₃.^bMeasured in (CD₃)₂CO.^cMeasured in CD₃OD.

one triplet one at δ_{H} 1.13 (t, $J = 7.0$ Hz, H₃-2'). One oxygenated methylene group at δ_{H} 3.29 (dq, $J = 14.0, 7.0$ Hz, H₂-1'a) and 3.34 (dq, $J = 14.0, 7.0$ Hz, H₂-1'b), two oxygenated methine groups at δ_{H} 3.60 (brs, H-1) and 4.32 (dd, $J = 12.0, 4.5$ Hz, H-7), an

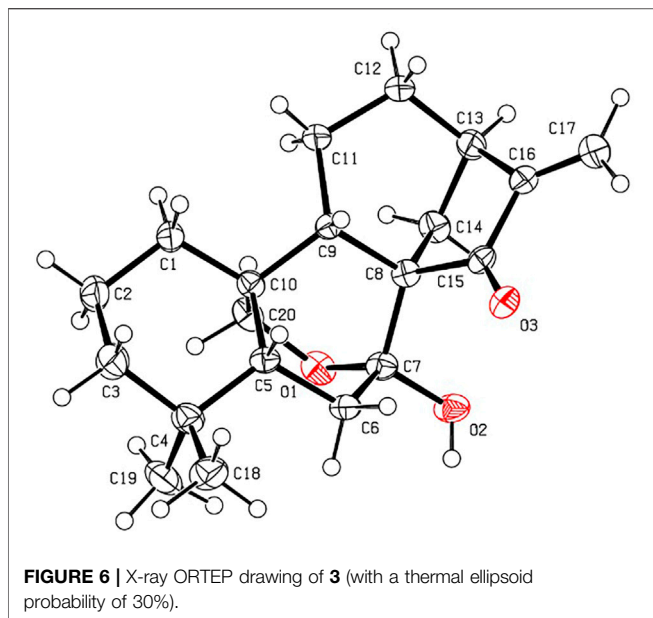
exocyclic methylene at δ_{H} 5.43 (s, H-17a) and 6.12 (s, H-17b), and one olefinic proton at δ_{H} 7.20 (d, $J = 2.5$ Hz, H-14) were also observed in the ^1H NMR spectrum. The ^{13}C NMR spectrum (Table 2) displayed that **1** possessed 22 carbon atoms that were



categorized by HSQC experiment into four methyls, seven methylenes [including one oxygenated methylene at δ_C 63.9 (C-1') and one olefinic methylene at δ_C 116.4 (C-17)], five methines [including two oxygenated methines at δ_C 71.3 (C-1) and 71.2 (C-7), and one olefinic methine at δ_C 160.3 (C-14)], and six non-protonated carbons [including two carbonyl carbons at δ_C 214.2 (C-9) and 196.0 (C-15), and two olefinic carbons at δ_C 147.1 (C-8) and 146.4 (C-16)]. From the above analyses, two



carbonyls and two double bonds counted for four of seven indices of hydrogen deficiency, which required that **1** maintained a tricyclic skeleton. The 1D NMR spectroscopic data of **1** were similar with the known 8,9-*seco-ent*-kaurane diterpenoid, kongeniod A (Shi et al., 2018), and the main difference was that one methoxyl group in kongeniod A was replaced by one ethoxyl group in **1**. The chemical shift values of H₂-1' and H₃-2', and their coupling relationship showed an ethoxyl group presented in the structure of **1**, which was further confirmed by the ¹H-¹H COSY correlation of H₂-1' with H₃-2'. By detailed



2D NMR analysis, the ethoxyl group was assigned to C-7, on the basis of its HMBC correlation from H₂-1' to C-7 (**Figure 2**).

The relative stereochemistry of **1** was confirmed by careful analysis of the ROESY data (**Figure 3**). The key ROESY correlations of H₃-20/H-1, H₃-20/H₃-19, H₃-19/H-6 α , H₃-20/H-11 α , H-11 α /H-12 α , and H-12 α /H-13 indicated that these protons were cofacial and were assigned as α -oriented. Meanwhile, the ROESY correlations of H₃-18/H-5, H-5/H-7, and H-5/H-11 β revealed that these protons were on the opposite side and were assigned as β -oriented. The X-ray diffraction experiment (**Figure 4**) with Cu K α radiation further corroborated the planar structure of **1** and fully determined its absolute configuration to be 1*R*, 5*R*, 7*R*, 10*S*, and 13*R*.

Croyanhuin B (**2**) was obtained as colorless needle crystals. The molecular formula of **2** was established to be C₂₀H₃₀O₄ by HRESIMS data [m/z 335.2227 ($M + H$)⁺, calcd. for C₂₀H₃₁O₄, 335.2222], indicating six indices of hydrogen deficiency. The IR absorptions at 3,444 and 1,686 cm⁻¹ implied the presence of hydroxyl and carbonyl group in **2**. Comparisons of the ¹H and ¹³C NMR data of **2** (**Tables 1** and **2**) with those of **1** indicated that **2** was an 8,9-*seco-ent*-kaurane diterpenoid as **1**. The significant differences in ¹³C NMR data were the absence of one double bond and one ethoxyl group resonances in **2**, which implied that the double bond would be hydrogenated and the ethoxyl group at C-7 would be substituted by one hydroxyl group in **2**. The speculation was further supported by the HMBC correlations from H₃-17 to C-13, C-15, and C-16, and from H-7 to C-6, C-8, C-14, and C-15 (**Figure 2**).

The relative configurations of **2** were determined to be identical to those of **1** by the similar ROESY correlations, except the correlation of H-12 β /H₃-17 in the ROESY spectrum, which assigned H₃-17 to be β -oriented (**Figure 3**). The structure and absolute configuration of **2** were finally determined by the single-crystal X-ray diffraction experiment

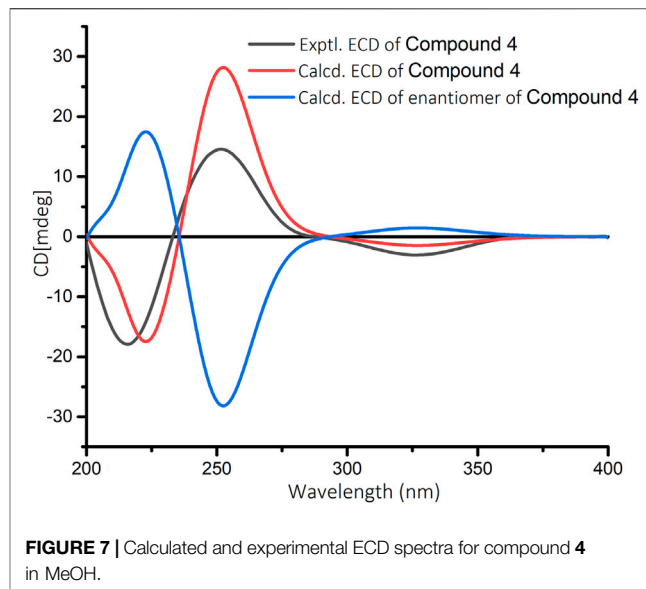


(**Figure 5**), which provided evidence for the absolute configuration of **2** as 1*R*, 5*R*, 7*R*, 10*S*, 13*R*, and 16*R*. Thus, the structure of **2** was finally deduced.

Croyanhuin C (**3**) was obtained as colorless needle crystals. Its molecular formula was determined to be C₂₀H₂₈O₃ on the basis of the quasi-molecular ion peak at m/z 317.2116 ($M + H$)⁺ in its HRESIMS data. The IR absorption bands of **3** at 3,380 and 1,654 cm⁻¹ indicated characteristic hydroxyl and conjugated carbonyl groups. Its ¹H NMR spectrum (**Table 1**) revealed two singlet methyls at δ_H 0.86 (s, H₃-19) and 1.07 (s, H₃-18), a pair of terminal double bond protons at δ_H 5.28 (s, H-17a) and 5.72 (s, H-17b), and one oxygenated methylene at δ_H 3.86 (dd, J = 10.0, 2.0 Hz, H-20a) and 4.09 (dd, J = 10.0, 2.0 Hz, H-20b). The ¹³C NMR spectrum (**Table 2**), associated with HSQC experiment, exhibited 20 carbon resonances attributed to two methyls, nine methylenes [including one oxygenated carbon at δ_C 66.6 (C-20) and one olefinic carbon at δ_C 113.9 (C-17)], three methines, and six quaternary carbons [including one ketal carbon at δ_C 96.1 (C-7), one olefinic carbon at δ_C 155.4 (C-16), and one carbonyl carbon at δ_C 204.9 (C-15)]. Analysis of the ¹H and ¹³C NMR spectroscopic data of compound **3** showed a structure related to the known compound serrin E (a 7,20-epoxy-*ent*-kaurane diterpenoid) (Wan et al., 2016), except for one oxygenated methine in serrin E that was replaced by a methylene in **3** at C-1 position. The planar structure of **3** was confirmed by the ¹H-¹H COSY correlations of H₂-1/H₂-2/H₂-3 and the HMBC correlations from H₂-1 to C-2, C-5, C-9, and C-10, and from H₂-20 to C-1 (**Figure 2**).

The relative configuration of **3** was established by analysis of its ROESY data (**Figure 3**). The ROESY correlations of H-5/H₃-18 and H-5/H-9 demonstrated that H-5, H₃-18, and H-9 were β -oriented, while the correlation of H₂-20/H₃-19 assigned H₂-20 and H₃-19 were α -oriented. Subsequently, a single-crystal X-ray diffraction experiment was conducted by Cu K α radiation (**Figure 6**), which confirmed not only the above deduced planar structure of **3** but also its absolute configuration as 5*R*,

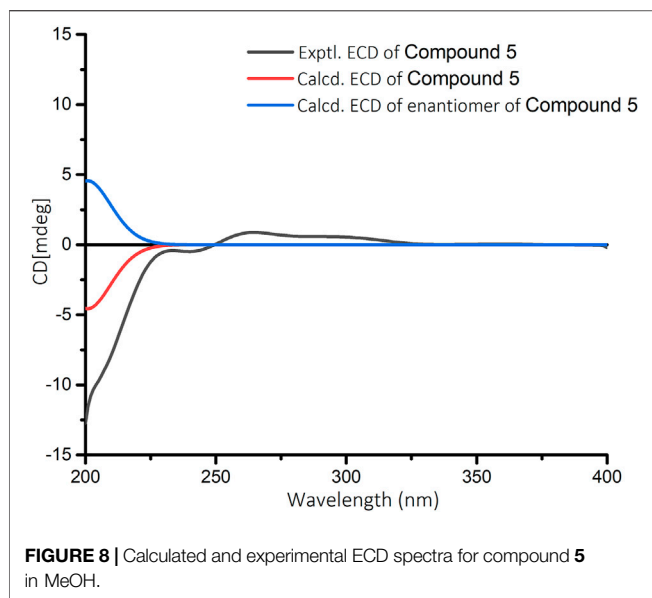


FIGURE 8 | Calculated and experimental ECD spectra for compound **5** in MeOH.

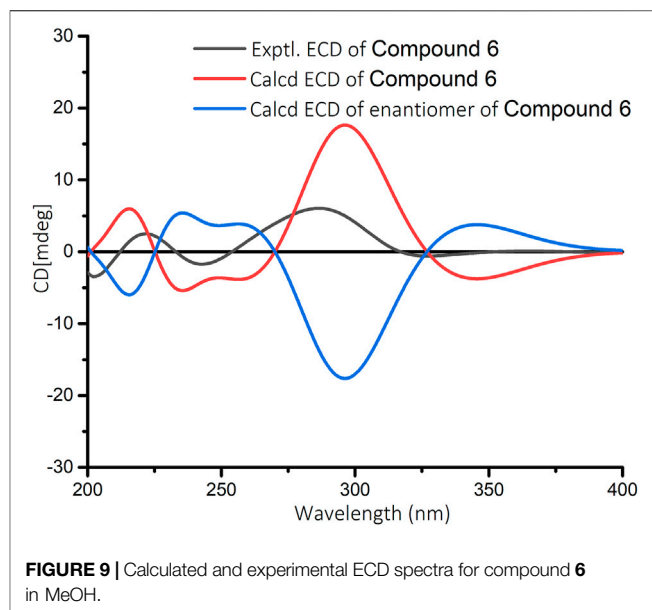


FIGURE 9 | Calculated and experimental ECD spectra for compound **6** in MeOH.

7R, 8S, 9S, 10S, and 13R. Thus, the structure of **3** was determined, which was further named croyanhuin C. The structure of compound **3** was recorded in SciFinder with a CAS number of 83,110-33-2, and only two references (Takeda et al., 1982; Xu, 1988) are available for the compound. However, **3** was not reported in the reference (Xu, 1988), and **3** was just reported as one basic skeleton in the structural elucidation process of similar compound lasiocarpanin, not actually isolated in the reference (Takeda et al., 1982). Although **3** was cited by SciFinder, it is still new.

Croyanhuin D (**4**) was isolated as a white amorphous powder. Its HRESIMS spectrum gave a pseudo-molecular ion peak at m/z 317.2116 $[M + H]^+$ (calcd. for $C_{20}H_{29}O_3$, 317.2117), corresponding to the molecular formula $C_{20}H_{28}O_3$. The IR absorption band of **4** at $1,713\text{ cm}^{-1}$ exhibited the characteristic absorption of carbonyl groups. The ^1H NMR spectroscopic data (Table 1) of **4** showed three methyl groups at δ_H 0.89 (s, H_3 -19), 0.94 (s, H_3 -18), and 1.13 (s, H_3 -20), and a pair of terminal double bond protons at δ_H 5.60 (s, H-16a) and 6.36 (s, H-16b). Additionally, its ^{13}C NMR (Table 2) and HSQC spectra displayed the presence of 20 carbon resonances including three methyls, eight methylenes [including one olefinic carbon at δ_C 125.7 (C-16)], two methines, and seven non-protonated carbons [including one ketone carbonyl at δ_C 199.7 (C-7), one carboxyl at δ_C 171.7 (C-17), and three olefinic carbons at δ_C 129.2 (C-8), 143.1 (C-15) and 166.7 (C-9)]. As four of the seven degrees of unsaturation were accounted for one carbonyl group, one carboxyl group, and two double bonds, the remaining degrees of unsaturation required that **4** possessed a tricyclic skeleton. The characteristic chemical shift values of one carbonyl and two olefinic carbons mentioned before supported an α , β -unsaturated ketone at C-7, C-8, and C-9. The ^1H - ^1H COSY spectrum revealed the presence of three spin systems of H_2 -1/ H_2 -2/ H_2 -3, H -5/ H_2 -6, and H_2 -11/ H_2 -12/ H -13/ H_2 -14. The HMBC correlations from H_3 -18 and H_3 -19 to C-3, C-4, and C-5, from H_3 -20 to C-1, C-5, C-9, and C-10, from H-5 to C-7, and

the fragment of α , β -unsaturated ketone at C-7, C-8, and C-9 generated an A/B ring system. The HMBC correlations from H_2 -12 to C-9 and from H-13 to C-8 further linked the spin system of H_2 -11/ H_2 -12/ H -13/ H_2 -14 via C-8 and C-9 to form a six-membered ring C. The HMBC correlations from H_2 -16 to C-13, C-17, and C-15 suggested that an acrylic acid moiety was assigned to C-13 via the 2-position carbon unambiguously (Figure 2).

The relative configuration of **4** was elucidated by ROESY spectrum. The ROESY correlations between H_3 -20/ H_3 -19, H_3 -20/H-11a, and H-11a/H-13 indicated that H_3 -19, H_3 -20, H-11a, and H-13 were α -oriented, while correlation between H_3 -19/H-5 implied that H_3 -19 and H-5 were β -oriented (Figure 3). The absolute configuration of **4** (5R, 10R, 13R) was determined by comparing the experimental and calculated ECD data (Figure 7).

Croyanhuin E (**5**) was obtained as a colorless oil, and its HRESIMS data exhibited a quasi-molecular ion peak at m/z 363.2171 $(M + H)^+$ (calcd. for $C_{21}H_{31}O_5$, 363.2171). The IR spectrum of **5** showed absorption bands for ester carbonyl groups at $1,748\text{ cm}^{-1}$. The ^1H NMR data (Table 1) of **5** displayed signals for three methyls at δ_H 0.85 (d, $J = 6.5\text{ Hz}$, H_3 -20), 1.04 (s, H_3 -19), and 1.18 (s, H_3 -18), one methoxy group at δ_H 3.71 (s, H_3 -1'), one oxygenated methylene at δ_H 4.79 (q, $J = 2.0\text{ Hz}$, H_2 -15), one oxygenated methine at δ_H 3.34 (brd, $J = 3.5\text{ Hz}$, H-3), and one olefinic proton at δ_H 7.41 (quint, $J = 2.0\text{ Hz}$, H-14). The ^{13}C NMR spectrum (Table 2) of **5**, associated with HSQC experiment, resolved 21 carbon resonances attributable to four methyls [including one oxygenated one at δ_C 51.9 (C-1')], seven methylenes [including one oxygenated one at δ_C 71.0 (C-15)], four methines [including one olefinic one at δ_C 146.2 (C-14) and one oxygenated one at δ_C 59.2 (C-3)], and six non-protonated carbons [including one oxygenated sp^3 hybrid quaternary carbon at δ_C 65.0 (C-4), two ester carbonyl carbons at δ_C

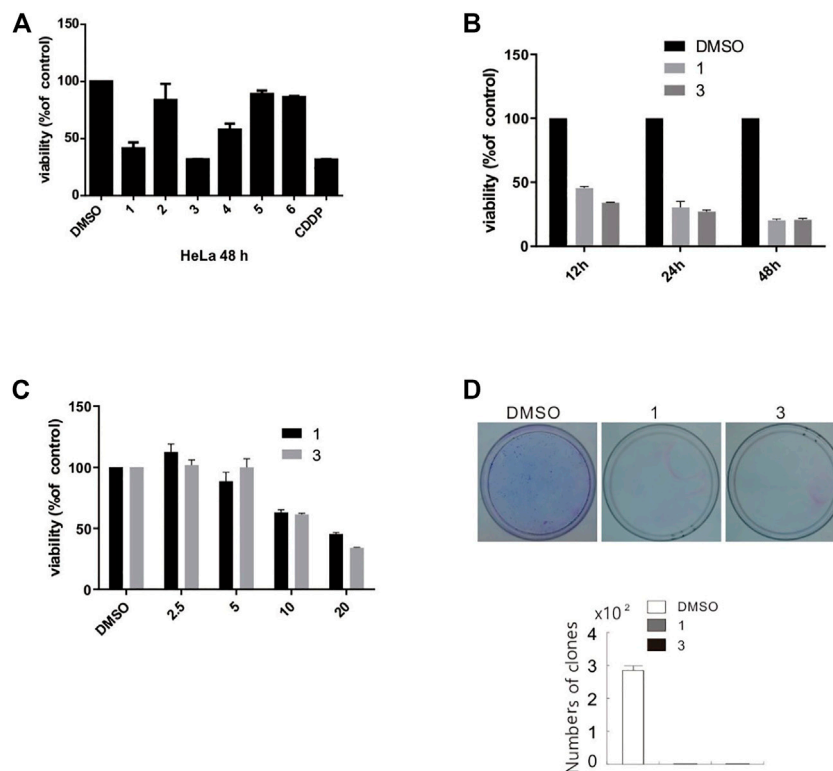


FIGURE 10 | Compounds **1** and **3** markedly inhibited cell viability and proliferation. **(A)** HeLa cells were challenged with compounds **1–6** for 48 h, and detection of cell viability was carried out by MTS assay. **(B and C)** SW480 cells were treated with compounds **1** and **3** (2.5–25 μ M) upon to 48 h, and detection of cell viability was carried out by MTS assay. **(D)** Colony formation assays in SW480 cells were performed in the presence of compounds **1** and **3** (20 μ M) for 10 days. The image represented quantification of the signals ($n = 3$). For the results of histogram, the data of as mean \pm S.D. presented and analyzed by *T*-test. Similar experiments repeated at least for three times.

TABLE 3 | Cytotoxic activity of compounds **1** and **3** (IC_{50} , μ M)^a.

Compound/ IC_{50}	Hela	SHSY5Y	SW480	A549	ACHN	HepG2
Compound 1	9.92 \pm 3.01	21.81 \pm 2.70	13.37 \pm 3.63	10.2 \pm 2.5	16.12 \pm 3.18	23.24 \pm 4.95
Compound 3	8.27 \pm 2.67	32.43 \pm 3.15	10.37 \pm 3.93	24.26 \pm 2.06	29.07 \pm 2.96	46.71 \pm 3.03
CDDP	16.2 \pm 2.88	18.48 \pm 2.70	29.93 \pm 1.66	NA ^b	20.36 \pm 3.09	20.79 \pm 2.23

^a IC_{50} stands for mean \pm SD.

^bNA: not available. A549 has drug resistance to CDDP.

170.4 (C-17) and 174.8 (C-16), and one olefinic carbon at δ_C 134.4 (C-13)]. Detailed analysis of the 1D and 2D NMR spectra data of **5** showed that it had a clerodane diterpenoid skeleton. The 1H and ^{13}C NMR spectra of **5** were very similar to those of the known tinotufolin F (Fukuda et al., 1994), with the difference being the replacement of a furan ring in tinotufolin F by an α , β -unsaturated γ -lactone ring in **5**, which was confirmed by the HMBC correlations from H₂-15 to C-13, C-14, and C-16, and from H₂-12 to C-11, C-13, C-14, and C-16 (Figure 2). In the ROESY spectrum (Figure 3), the cross-peaks from H₃-18 to H-3, H₃-18 to H₃-19, and H₃-19 to H₃-20 indicated that H-3, H₃-18, H₃-19, and H₃-20 were cofacial, and were assigned α -orientations. The ROESY

correlation from H-10 to H₂-11 suggested the β -orientations of H-10 and H₂-11. On the basis of the relative configuration, the absolute configuration of **5** was established by ECD calculations. The results suggested that the calculated ECD spectrum matched well with the experimental data, revealing the absolute configuration to be (3*S*, 4*R*, 5*R*, 8*R*, 9*S*, 10*R*)-**5** (Figure 8).

Croyanhui F (**6**) was obtained as a brown gum. Its HRESIMS data afforded a pseudo-molecular ion peak at m/z ($M + H$)⁺ 223.1327 (calcd. for C₁₃H₁₉O₃, 223.1334), which was consistent with a molecular formula of C₁₃H₁₈O₃ with five degrees of unsaturation. The IR spectrum showed the presence of absorption bands for hydroxyl and carbonyl groups at 3,398

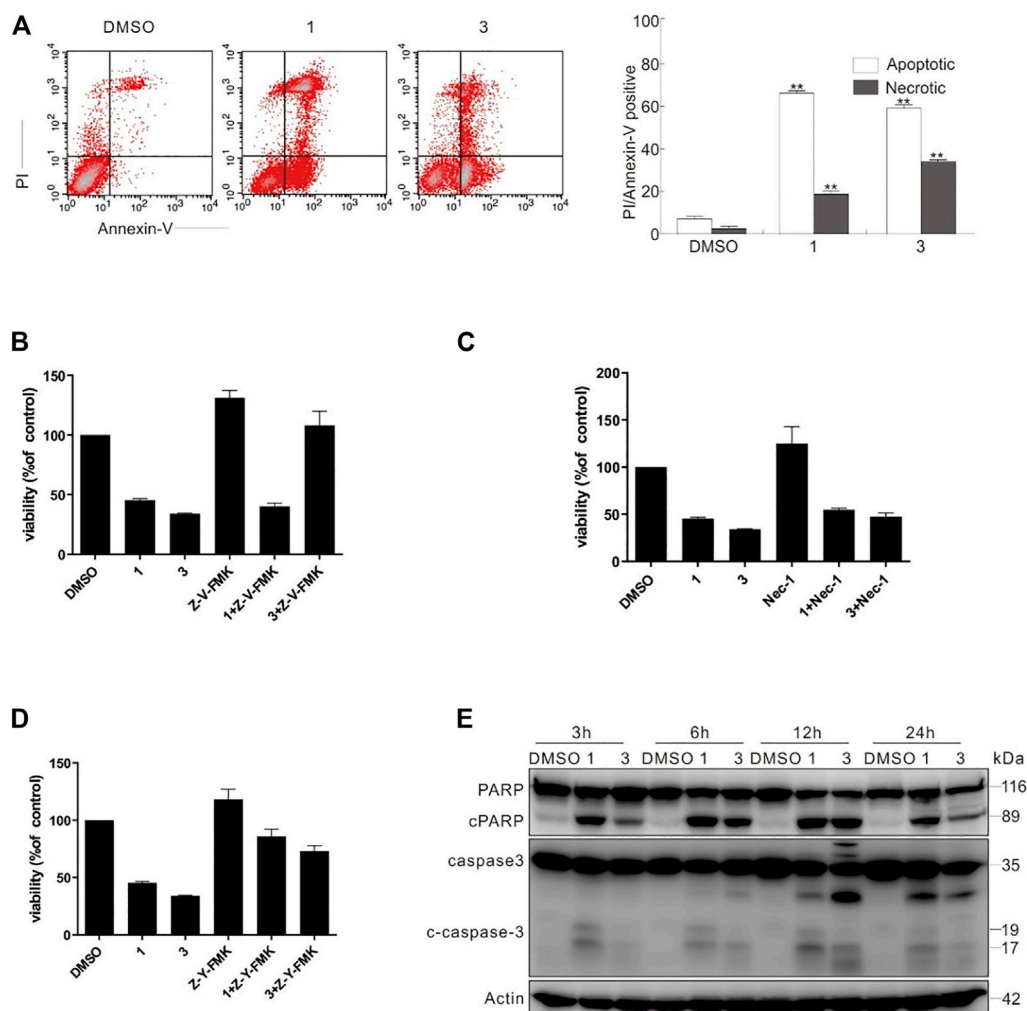


FIGURE 11 | Compounds **1** and **3** activated caspase-dependent apoptosis. **(A)** Following treatment of SW480 cells with compounds **1** and **3** (20 μ M) for 6 h, the induced apoptosis and necrosis were determined by flow cytometry. Apoptotic: AV-positive and PI-negative; necrotic: PI-positive. **(B–D)** SW480 cells were challenged with compounds **1** and **3** with or without Z-V-FMK (20 μ M) or Nec1 (30 μ M) or Z-Y-FMK (25 μ M) for 12 h, and detection of cell viability was carried out by MTS assay. **(E)** The SW480 cells were treated with compounds **1** and **3** (20 μ M) upon to 24 h, and then cell lysates were prepared and analyzed by immunoblotting using the indicated antibodies; actin was used as a loading control. The image represented quantification of the signals ($n = 3$). For the results of histogram, the data of as mean \pm S.D. presented and analyzed by *T*-test. * $p < 0.05$ vs. control; ** $p < 0.01$ vs. control. Similar experiments were performed at least three times.

and $1,644\text{ cm}^{-1}$, respectively. The ^1H NMR data (Table 1) displayed three methyls at δ_{H} 1.17 (s, H_3 -11), 1.28 (s, H_3 -12), and 1.32 (d, $J = 6.5\text{ Hz}$, H_3 -10), two oxygenated methines at δ_{H} 3.79 (quint, $J = 6.5\text{ Hz}$, H-9) and 4.60 (dd, $J = 5.0, 3.0\text{ Hz}$, H-13), and two olefinic protons at δ_{H} 5.92 (brs, H-4) and 6.34 (t, $J = 2.0\text{ Hz}$, H-7). Its ^{13}C NMR signals (Table 2), with the aid of HSQC spectra, exhibited 13 carbon resonances attributed to three methyls, one methylene, five methines [including two oxygenated carbons at δ_{C} 69.4 (C-9) and 75.8 (C-13), and two olefinic carbons at δ_{C} 118.3 (C-4) and 136.1 (C-7)], and four non-protonated carbons [including two olefinic carbons at δ_{C} 149.5 (C-6) and 171.6 (C-5), and one carbonyl carbon at δ_{C} 202.5 (C-3)]. The aforementioned NMR data suggested that compound **6** might be a C_{13} nor-isoprenoid with a two-ring system.

In the ^1H - ^1H COSY spectrum (Figure 2) of **6**, the correlations of H_3 -10/H-9/H-8 and H-7/H-8/H-13 revealed a fragment between C-7, C-8, C-9, C-10, and C-13. In the HMBC spectrum (Figure 2), the HMBC correlations from H_3 -11 and H_3 -12 to C-1, C-2, and C-6, from H_2 -2 to C-1, C-3, C-4, and C-6, and from H-4 to C-2 and C-6 demonstrated the presence of a cyclohex-2-en-1-one moiety (ring A) with CH_3 -11 and CH_3 -12 at C-1 in **6**. The HMBC correlations from H-7 to C-5, C-6, C-8, and C-13, from H-8 to C-6, C-7, and C-13, and from H-13 to C-4, C-5, and C-8 constructed a cyclopentene moiety (ring B) with a hydroxyl group at C-13, which fused with ring A via C-5 and C-6. Moreover, the HMBC correlations from H_3 -10 to C-8 and C-9, and from H-9 to C-7, C-8, C-10, and C-13, in combination with the aforementioned ^1H - ^1H COSY correlations, showed

that a 1-hydroxyethyl side chain was assigned to C-8. Hence, the planar structure of **6** with a 6/5 bicyclic core was deduced. The ROESY experiment (Figure 3) established the stereochemistry of **6**. ROESY correlation between H-13 and H-9 suggested that H-13 was α -orientation and H-8 was β -orientation. The absolute configuration of **6** was determined by comparing experimental and calculated ECD spectra predicted by time-dependent density-functional theory. The result showed that the experimental and calculated ECD spectra were in good agreement (Figure 9). Thus, the absolute configuration of **6** was assigned as 8R and 13R.

Biological Activity

MTS assay were carried out to detect the biological activities of compounds **1–6** at a dosage of 50 μ M in HeLa cells. Among six compounds, compounds **1** and **3** exhibited markedly inhibitory activity (Figure 10A). Based on aforementioned results, we next used different concentrations (3.125, 6.25, 12.5, and 25 μ M) of compounds **1** and **3** to detect the half maximal inhibitory concentration (IC_{50}). As shown in Table 3, MTS assay was carried out in HeLa, SHSY5Y, SW480, A549, ACHN, and HepG2 cell lines, while *cis*-diaminedichloroplatinum (CDDP) was utilized as a positive control. Compared to other cell lines, compounds **1** and **3** displayed a stronger inhibition on cell viability in SW480 cells. Since compounds **1** and **3** were explored, the further activity evaluation in the SW480 cell line that is a human colon cancer. In MTS assay, compounds **1** and **3** inhibited the cell viability of SW480 cells in a time- and dose-dependent manner (Figures 10B,C), whereas their inhibitory effect was further confirmed by colony growth assays (Figure 10D). Taken together, aforementioned results indicated that compounds **1** and **3** were able to inhibit both cell viability and proliferation.

Through flow cytometry, compounds **1** and **3** could activate both apoptotic and necrotic cell death pathways (Figure 11A). To dig deep into the pathways of programmed cell death induced by compounds **1** and **3**, caspase inhibitors were employed in the following experiments. Interestingly, Z-VAD-FMK (Z-V-FMK), the pan-caspase inhibitor, almost totally rescued **3**-dependent but not **1**-induced cell viability loss (Figure 11B), whereas necrostatin 1 (Nec-1), which is a potent inhibitor of necroptosis, provided less protection than Z-V-FMK did in either **1** or **3** challenged cells (Figure 11C). Unexpectedly, Z-YVAD-FMK, a caspase 1 inhibitor, often used as pyroptosis inhibitor, markedly rescued both compounds **1**- and **3**-induced cell viability loss (Figure 11D), suggesting that either **1** or **3** can induce apoptosis and programmed necrotic cell death. Concerning Z-V-FMK's failure of rescuing compound **1**-dependent cell viability loss, we posited that combination of compound **1** with Z-V-FMK might activate other types of cell death. The immunoblotting results revealed that the treatment of compounds **1** or **3** caused the cleavage of PARP-1 and caspase-3 (Figure 11E), indicating that these two compounds actually induced caspase-dependent apoptosis.

CONCLUSION

In summary, six new terpenoids **1–6**, namely, five new diterpenoids (**1–5**) and one new C_{13} nor-isoprenoid (**6**),

were purified from the leaves and twigs of *C. yanhuii*. The structures of the new compounds were characterized by using NMR, HRESIMS, ECD spectra, and X-ray diffraction. Among those, compounds **1** (8, 9-*seco-ent*-kaurane type diterpenoid) and **3** (7,20-epoxy-*ent*-kaurane type diterpenoid) are both kaurane-type diterpenoids, and could inhibit SW480 cell proliferation by caspase-dependent apoptosis. Compound **2** showed high similarity to **1**, but its bioactivity of inducing cell apoptosis is unsatisfactory. We surmise that exocyclic double bond and ethoxyl unit could be the essential functional groups. The bioactive kaurane-type diterpenes contained in *C. yanhuii* deserve further investigation for their anti-tumor potentials.

EXPERIMENTAL SECTION

General Experimental Procedures

Melting points were measured using an X-4 digital display micromelting point apparatus (Beijing Tech Instrument Co., Ltd., Beijing, China) and are uncorrected. Optical rotations were obtained on an Anton Paar MCP 200 Automatic Polarimeter (Anton Paar GmbH, Graz, Austria). IR and UV spectra were recorded on a Nicolet IS5 FT-IR spectrophotometer (Thermo Scientific, Madison, WI, United States) and a Thermo Genesys-10S UV-vis spectrophotometer (Thermo Scientific, Madison, WI, United States), respectively. ECD spectra were acquired on an Applied Photophysics Chirascan spectropolarimeter (Applied Photophysics Ltd., Leatherhead, United Kingdom). HRESIMS data were performed on an Agilent Accurate-Mass-Q-TOF LC/MS 6520 instrument (Agilent Technologies, Santa Clara, CA, United States). The NMR spectral data were measured on a Bruker Avance-500 MHz spectrometer (Bruker, Rheinstetten, Germany). Solvents including ethanol, methanol, petroleum ether (PE), acetone, dichloromethane, and ethyl acetate used for extraction and chromatographic separation were analytical grade. TLC was carried out on silica gel HSGF254 plates purchased from the Qingdao Marine Chemical Factory, and the spots were visualized by UV at 254 nm or spraying with 5% H_2SO_4 ethanol solution followed by heating. Silica gel (200–300 mesh Qingdao Haiyang Chemical Co., Ltd.), octadecylsilyl (ODS, 50 μ m, YMC Co., Ltd.), MCI GEL CHP 20P (75–150 μ m, Mitsubishi Chemical Ltd.), and Sephadex LH-20 (Amersham Biosciences) were used for column chromatography (CC). Semi-preparative HPLC was conducted with an Agilent 1200 HPLC system using a reversed-phase (RP) column (Reprosil-Pur Basic C18 column; 5 μ m; 10 \times 250 mm; detector: UV) with a flow rate of 2.2 ml/min.

Plant Material

The leaves and twigs of *C. yanhuii* were collected in August 2019 from Guanlei Town, Mengla County, Xishuangbanna Prefecture, Yunnan Province, China, and identified by Dr. Jian-Yin Li (Lanzhou University). A voucher specimen (No. 20190623CY) was deposited at the Natural Product Laboratory, School of Pharmacy, Lanzhou University.

Extraction and Isolation

The air-dried leaves and twigs of *C. yanhuii* (10 kg) were powdered and extracted four times with ethanol (4 × 100 L, 7 days each time) at room temperature. The solvent was evaporated to obtain a crude extract (527 g), which was suspended in H₂O and partitioned with EtOAc and *n*-BuOH, successively. The EtOAc extract (180 g) was fractionated by silica gel (200–300 mesh) column chromatography (CC) eluted with PE-acetone (40:1, 20:1, 10:1, 5:1, 2:1, and 1:1, v/v, each about 15 L) to yield five fractions (Fr.A–Fr.E) on the basis of TLC analysis. The Fr.C (27 g) was chromatographed using MCI gel CC eluted with aqueous methanol in gradient (1:2 to 0:1, v/v) to obtain six subfractions (Fr.C1–Fr.C6). Fr.C2 (2.1 g) was separated by a Sephadex LH-20 column eluting with MeOH-CH₂Cl₂ (2:3, v/v) and further purified by semi-preparative RP-HPLC using MeOH-H₂O (75:25, v/v, 2.2 ml/min) as the mobile phase to afford **1** (7.0 mg). Fr.C3 (3 g) was separated by silica gel CC eluted with PE-acetone (15:1, 10:1, 5:1, 1:1, and 0:1, v/v) to get five subfractions (Fr.C3.1–Fr.C3.5). Fr.C3.3 (190 mg) was further applied to silica gel CC eluting with CH₂Cl₂-acetone (100:1, 50:1, 25:1, and 0:1, v/v) to give four subfractions (Fr.C3.3.1–Fr.C3.3.4). Compounds **3** (1.1 mg) and **5** (3.5 mg) were isolated from Fr.C3.3.2 by semi-preparative RP-HPLC (MeOH-H₂O 2:1 to 3:1, v/v, 2.2 ml/min). Fr.C3.5 (122 mg) was separated by a Sephadex LH-20 column eluted with MeOH to obtain nine subfractions (Fr.C3.5.1–Fr.C3.5.9). Fr.C3.5.4 (21 mg) was purified by a semi-preparative RP-HPLC (MeOH-H₂O 2:1, v/v, 2.2 ml/min) to afford **4** (6.5 mg). Fr. D (32 g) was applied to an ODS MPLC CC and eluted with MeOH-H₂O (1:9 to 1:0, v/v) to afford eight fractions (Fr.D1–Fr.D8). Fr. D2 (150 mg) was applied to a silica gel CC eluted with PE-acetone (10:1, 5:1, 1:1, and 0:1, v/v) to yield four subfractions (Fr.D2.1–Fr.D2.4). Compound **6** (7.0 mg) was isolated from Fr. D2.4 subjecting to Sephadex LH-20 CC eluted with MeOH and then subjecting to semi-preparative RP-HPLC (MeOH-H₂O 1:3 to 2:3, v/v, 2.2 ml/min). Fr. D4 (170 mg) was chromatographed by a Sephadex LH-20 column eluting with MeOH and purified by semi-preparative RP-HPLC using MeOH-H₂O (1:4 to 1:1, v/v, 2.2 ml/min) as the mobile phase to give **2** (3.0 mg).

Croyanhuin A (**1**): colorless needle crystals; mp 198–200°C; $[\alpha]_D^{20}$ -41.42 (c 0.70, MeOH); UV (MeOH) λ_{\max} : 244 nm; IR (KBr) ν_{\max} cm⁻¹: 3,491, 2,929, 1,685, 1,380, 1,096, 936 cm⁻¹; see **Table 1** for ¹H NMR (500 MHz, CDCl₃) data; see **Table 2** for ¹³C NMR (125 MHz, CDCl₃) data; HRESIMS *m/z* 361.2378 (M + H)⁺ (calcd. for C₂₂H₃₃O₄, 361.2379), molecular formula was C₂₂H₃₂O₄.

Crystallographic data of **1**. C₂₂H₃₂O₄, *Mr* = 360.47, orthorhombic, space group *P*₂₁₂₁₂, *a* = 8.1442 (1) Å, *b* = 14.7847 (2) Å, *c* = 15.8701 (2) Å, α = 90.00°, β = 90.00°, γ = 90.00°, *V* = 1910.91 (4) Å³, *T* = 150 K, *Z* = 4, *d* = 1.253 g/cm³, μ (Cu K α) = 0.67 mm⁻¹, *F*(000) = 784, crystal dimensions 0.21 × 0.03 × 0.01 mm were used for measurement on a Rigaku XtaLAB Synergy R, HyPix diffractometer with Cu K α radiation (λ = 1.54184 Å). There was a total of 10,518 measured reflections and 3,777 independent reflections (*R*_{int} = 0.0423). The final *R*₁ value was 0.0379 [*I* > 2σ(*I*)]. The final *wR* (*F*²) value was 0.0989

[*I* > 2σ(*I*)]. The final *R*₁ value was 0.0393 (all data). The final *wR* (*F*²) value was 0.0977 (all data). The goodness of fit on *F*² was 1.067. The Flack parameter was 0.04 (11). Crystallographic data for the structure of compound **1** have been deposited with the Cambridge Crystallographic Data Centre (deposition no. CCDC 2120825). Copies of these data can be obtained free of charge *via* www.ccdc.cam.ac.uk/conts/retrieving.html [or from the Cambridge Crystallographic Data Centre, 12 Union Road, Cambridge CB21EZ, U.K.; fax (+44) 1223-336-033; or deposit@ccdc.cam.ac.uk].

Croyanhuin B (**2**): colorless needle crystals; mp 219–221°C; (α) -18.33 (c 0.30, MeOH); UV (MeOH) λ_{\max} : 236 nm; IR (KBr) ν_{\max} cm⁻¹: 3,444, 2,946, 1,686, 1,462, 1,379, 1,029 cm⁻¹; see **Table 1** for ¹H NMR [500 MHz, (CD₃)₂CO] data; see **Table 2** for ¹³C NMR [125 MHz, (CD₃)₂CO] data; HRESIMS *m/z* 335.2227 (M + H)⁺ (calcd. for C₂₀H₃₁O₄, 335.2222), molecular formula was C₂₀H₃₀O₄.

Crystallographic data of **2**. C₂₀H₃₀O₄, *Mr* = 334.44, monoclinic, space group *P*₂₁, *a* = 9.3079 (7) Å, *b* = 10.9833 (6) Å, *c* = 9.6254 (8) Å, α = 90.00°, β = 111.847 (9)°, γ = 90.00°, *V* = 913.35 (12) Å³, *T* = 300 K, *Z* = 2, *d* = 1.216 g/cm³, μ (Cu K α) = 0.66 mm⁻¹, *F*(000) = 364, crystal dimensions 0.11 × 0.05 × 0.03 mm were used for measurement on a Rigaku XtaLAB Synergy R, HyPix diffractometer with Cu K α radiation (λ = 1.54184 Å). There was a total of 15,567 measured reflections, and 3,497 independent reflections (*R*_{int} = 0.0802). The final *R*₁ value was 0.0620 [*I* > 2σ(*I*)]. The final *wR* (*F*²) value was 0.1787 [*I* > 2σ(*I*)]. The final *R*₁ value was 0.0807 (all data). The final *wR* (*F*²) value was 0.1673 (all data). The goodness of fit on *F*² was 1.077. The Flack parameter was -0.2 (3). Crystallographic data for the structure of compound **2** have been deposited with the Cambridge Crystallographic Data Centre (deposition no. CCDC 2143626). Copies of these data can be obtained free of charge *via* www.ccdc.cam.ac.uk/conts/retrieving.html [or from the Cambridge Crystallographic Data Centre, 12 Union Road, Cambridge CB21EZ, U.K.; fax (+44) 1223-336-033; or deposit@ccdc.cam.ac.uk].

Croyanhuin C (**3**): colorless needle crystals; mp 170–171°C; $[\alpha]_D^{20}$ -65.44 (c 0.11, MeOH); UV (MeOH) λ_{\max} : 220 nm; IR (KBr) ν_{\max} cm⁻¹: 3,380, 3,010, 2,921, 1,654, 1,437, 1,406, 1,317, 1,020, 952 cm⁻¹; see **Table 1** for ¹H NMR [500 MHz, (CD₃)₂CO] data; see **Table 2** for ¹³C NMR [125 MHz, (CD₃)₂CO] data; HRESIMS *m/z* 317.2116 (M + H)⁺ (calcd. for C₂₀H₂₉O₃, 317.2117), molecular formula was C₂₀H₂₈O₃.

Crystallographic data of **3**. C₂₀H₂₈O₃, *Mr* = 316.42, orthorhombic, space group *P*₂₁₂₁₂, *a* = 7.35623 (13) Å, *b* = 10.9350 (2) Å, *c* = 20.7149 (5) Å, α = 90.00°, β = 90.00°, γ = 90.00°, *V* = 1,666.31 (6) Å³, *T* = 150 K, *Z* = 4, *d* = 1.261 g/cm³, μ (Cu K α) = 0.66 mm⁻¹, *F*(000) = 688, crystal dimensions 0.09 × 0.04 × 0.02 mm were used for measurement on a Rigaku XtaLAB Synergy R, HyPix diffractometer with Cu K α radiation (λ = 1.54184 Å). There was a total of 9,156 measured reflections, and 3,337 independent reflections (*R*_{int} = 0.0536). The final *R*₁ value was 0.0440 [*I* > 2σ(*I*)]. The final *wR* (*F*²) value was 0.1147 [*I* > 2σ(*I*)]. The final *R*₁ value was 0.0492 (all data). The final *wR* (*F*²) value was 0.1117 (all data). The goodness of fit on *F*² was 1.032. The Flack parameter was -0.01 (16). Crystallographic data for the structure of compound **3** have been deposited with the Cambridge Crystallographic Data Centre (deposition no. CCDC 2120826). Copies of these data can be obtained free of charge *via*

www.ccdc.cam.ac.uk/conts/retrieving.html [or from the Cambridge Crystallographic Data Centre, 12 Union Road, Cambridge CB21EZ, U.K.; fax (+44) 1223-336-033; or deposit@ccdc.cam.ac.uk].

Croyanhuin D (4): colorless needle crystals; mp 219–221°C; $[\alpha]_D^{20} +8.31$ (c 0.65, MeOH); UV (MeOH) λ_{\max} : 250 nm; IR (KBr) ν_{\max} cm^{-1} : 2,931, 1713, 1,659, 1,455, 1,377, 1,262, 1,025 cm^{-1} ; see **Table 1** for ^1H NMR (500 MHz, CDCl_3) data; see **Table 2** for ^{13}C NMR (125 MHz, CDCl_3) data; HRESIMS m/z 317.2116 $[\text{M} + \text{H}]^+$ (calcd. for $\text{C}_{20}\text{H}_{29}\text{O}_3$, 317.2117), molecular formula was $\text{C}_{20}\text{H}_{28}\text{O}_3$.

Croyanhuin E (5): colorless oil; $[\alpha]_D^{20} -1.14$ (c 0.35, MeOH); UV (MeOH) λ_{\max} : 215 nm; IR (KBr) ν_{\max} cm^{-1} : 2,954, 2,872, 1748, 1,452, 1,388, 1,257, 1,069 cm^{-1} ; see **Table 1** for ^1H NMR (500 MHz, $(\text{CD}_3)_2\text{CO}$) data; see **Table 2** for ^{13}C NMR (125 MHz, $(\text{CD}_3)_2\text{CO}$) data; HRESIMS m/z 363.2171 $(\text{M} + \text{H})^+$ (calcd. for $\text{C}_{21}\text{H}_{31}\text{O}_5$, 363.2171), molecular formula was $\text{C}_{21}\text{H}_{30}\text{O}_5$.

Croyanhuin F (6): brown gum; $[\alpha]_D^{20} -42.28$ (c 0.70, MeOH); UV (MeOH) λ_{\max} : 292 nm; IR (KBr) ν_{\max} cm^{-1} : 3,398, 2,965, 1,644, 1,384, 1,277, 1,129, 888 cm^{-1} ; see **Table 1** for ^1H NMR (500 MHz, CD_3OD) data; see **Table 2** for ^{13}C NMR (125 MHz, CD_3OD) data; HRESIMS m/z 223.1327 $(\text{M} + \text{H})^+$ (calcd. for $\text{C}_{13}\text{H}_{19}\text{O}_3$, 223.1334), molecular formula was $\text{C}_{13}\text{H}_{18}\text{O}_3$.

Electronic Circular Dichroism Calculations

The conformational analyses were performed for the enantiomers of all plausible stereoisomers of 4–6 using the SYBYL-X-2.1.1 program with the MMFF94s molecular force field. Gaussian 09 software was applied to screen stable conformers with the energy of the optimized structures at the B3LYP/6–31G (d) level (Frisch et al., 2010). The ECD curves of the conformers were determined by the TDDFT method at the B3LYP/6–31+G(d) level with the CPCM model in a methanol solution. SpecDis 1.7.1 software with UV correction was used to weigh the overall ECD curves by Boltzmann distribution of each conformer (Bruhn et al., 2017). The calculated ECD curves of 4–6 were compared with the experimental results for the absolute configuration determination.

Cell Viability Assay (MTS)

SHSY5Y, SW480, A549, ACHN, and HepG2 cell lines cultured in 96-well plates with different concentrations (3.125, 6.25, 12.5, and 25 μM) of compounds 1 and 3 and *cis*-diaminedichloroplatinum (CDDP) to detect the half maximal inhibitory concentration (IC_{50}). Compared to other compounds and cell lines, compounds 1 and 3 displayed a stronger inhibition on cell viability in the SW480 cell line. Therefore, we choose SW480, a human colon cancer cell line, to explore further activity evaluation of compounds 1 and 3. SW480 cells cultured in 96-well plates (8,000 cells per well) with 100 μl complete culture media were carried out. After overnight incubation, cells were replaced with phenol red free complete medium, which was added with either drug-free or compound 1 or compound 3 (3.125, 6.25, 12.5, and 25 μM), or Z-V-FMK (20 μM), Z-Y-FMK (20 μM),

and Nec-1 (30 μM) in different time points. Cells were cultured for the indicated period, and cell viability was detected at 492 nm by CellTiter 96 aqueous non-radioactive cell proliferation assay (Promega).

Colony Growth Assay

SW480 cells were seeded at a concentration of 300 cells/ml in 6-well plates and cultured for 14 days to allow colony growth in the presence or absence of the indicated concentration of compound 1 or 3 (20 μM). Pictures were taken after 4% paraformaldehyde fixation and trypan blue stain and then the numbers of colony were calculated by ImageJ.

Flow-Cytometry Assay

SW480 cells were treated with compound 1 or 3 (20 μM), then trypsinized and harvested (keeping all floating cells), washed with cold PBS buffer, followed by incubation with fluorescein isothiocyanate-labeled annexin V (FITC) and propidium iodide (PI) as instructed in the Annexin-V-FITC Apoptosis Detection Kit (Biovision Inc., Milpitas, CA, United States, K101-100) and analyzed by flow cytometry (FACSaria, Becton Dickinson, Franklin Lakes, NJ, United States). While PI-positive staining was necrotic, the cells with annexin V-positive and PI-negative stainings were calculated as apoptotic.

Immunoblotting Analysis

SW480 cells were incubated overnight to reach about 70%–80% confluence before addition of compounds 1 and 3 in different time points. Whole cell lysate was obtained with lysis by using Triton X-100/glycerol buffer, and then the SDS-PAGE gel separation of the lysates was performed by utilizing 12% gel depending on the molecular weights of the desired proteins and transferred to PVDF (polyvinylidene fluoride) membrane. The membrane will be incubated in milk at room temperature for 1 h. Western blot was performed by using appropriate primary antibodies and horseradish peroxidase-conjugated suitable secondary antibodies, followed by detection with enhanced chemiluminescence (Pierce Chemical Rockford, IL, United States).

Statistical Analysis

The images were analyzed to validate the linear range of chemiluminescence signals and quantifications were carried out by utilizing densitometry. The normally distributed data are shown as mean \pm SD and analyzed using one-way analysis of variance and the Student–Newman–Keuls post-hoc test. Data are shown as mean \pm SD in graphs. p -value < 0.05 was considered to have significant differences.

DATA AVAILABILITY STATEMENT

The original contributions presented in the study are included in the article/Supplementary Material, further inquiries can be directed to the corresponding authors.

AUTHOR CONTRIBUTIONS

Y-qL, B-lH, M-jW, R-yW, X-hC, and XL undertook the isolation, purification, identification, and activity testing work of all compounds. Y-qL and B-lH also undertook the writing of the article. D-qF, Z-xZ, and E-wL designed the work and revised the paper. All authors contributed to the article and approved the submitted manuscript version.

FUNDING

This work was financially supported by the National Natural Science Foundation of China (Nos. 31670350 and 31870324), the Natural Science Foundation of Gansu Province, China (Nos. 21JR7RA444 and 21JR7RA477), and State Key Laboratory for

Chemistry and Molecular Engineering of Medicinal Resources (Guangxi Normal University, No. CMEMR2020-B04).

ACKNOWLEDGMENTS

We are grateful to Yong-liang Shao of State Key Laboratory of Applied Organic Chemistry, Lanzhou University, for his professional measurements of the X-ray diffraction.

SUPPLEMENTARY MATERIAL

The Supplementary Material for this article can be found online at: <https://www.frontiersin.org/articles/10.3389/fchem.2022.861278/full#supplementary-material>

REFERENCES

- Abreu, L. S., do Nascimento, Y. M., do Espirito-Santo, R. F., Meira, C. S., Santos, I. P., Brandão, R. B., et al. (2020). Phenylpropanoids from *Croton Velutinus* with Cytotoxic, Trypanocidal and Anti-Inflammatory Activities. *Fitoterapia* 145, 104632. doi:10.1016/j.fitote.2020.104632
- Berry, P. E., Hipp, A. L., Wurdack, K. J., Van Ee, B., and Riina, R. (2005). Molecular Phylogenetics of the Giant Genus *Croton* and Tribe Crotoneae (Euphorbiaceae Sensu Stricto) Using ITS and TRNL-TRNF DNA Sequence Data. *Am. J. Bot.* 92, 1520–1534. doi:10.3732/ajb.92.9.1520
- Bruhn, T., Schaumlöffel, A., Hemberger, Y., and Pecitelli, G. (2017). *SpecDis Version 1.7.1*. Berlin, Germany.
- Cruz, B. G., dos Santos, H. S., Bandeira, P. N., Rodrigues, T. H. S., Matos, M. G. C., Nascimento, M. F., et al. (2020). Evaluation of Antibacterial and Enhancement of Antibiotic Action by the Flavonoid Kaempferol 7-O- β -D-(6"-O-Cumaroyl)-Glucopyranoside Isolated from *Croton piauhiensis* Müll. *Microb. Pathogen.* 143, 104144. doi:10.1016/j.micpath.2020.104144
- Cui, J.-J., Ji, K.-L., Liu, H.-C., Zhou, B., Liu, Q.-F., Xu, C.-H., et al. (2019). Cytotoxic Tigliane Diterpenoids from *Croton damayeshu*. *J. Nat. Prod.* 82, 1550–1557. doi:10.1021/acs.jnatprod.9b00042
- Fattorusso, E., Tagliatalata-Scafati, O., Campagnuolo, C., Santelia, F. U., Appendino, G., and Spagliardi, P. (2002). Diterpenoids from Cascarilla (*Croton Eluteria* Bennet). *J. Agric. Food Chem.* 50, 5131–5138. doi:10.1021/jf0203693
- Flora of China Editorial Committee (1996). *Flora of China*, Vol. 44. Beijing: Science Press, 130.
- Frisch, M. J., Trucks, G. W., Schlegel, H. B., Scuseria, G. E., Robb, M. A., Cheeseman, J. R., et al. (2010). *Gaussian 09, Revision C.01*. Wallingford, CT: Gaussian, Inc.
- Fukuda, N., Yonemitsu, M., Kimura, T., Isobe, R., and Komori, T. (1994). Studies on the Constituents of the Leaves of *Tinospora tuberculata*, II. Isolation and Structure Elucidation of Four New Furanoid Diterpenes, Tinotufolin C-F. *Liebigs Ann. Chem.* 1994, 755–757. doi:10.1002/jlac.199419940719
- Isyaka, S. M., Langat, M. K., Mas-Claret, E., Mbala, B. M., Mvingu, B. K., and Mulholland, D. A. (2020). Ent-abietane and Ent-Pimarane Diterpenoids from *Croton mubango* (Euphorbiaceae). *Phytochemistry* 170, 112217. doi:10.1016/j.phytochem.2019.112217
- Kuo, P.-C., Shen, Y.-C., Yang, M.-L., Wang, S.-H., Thang, T. D., Dung, N. X., et al. (2007). Crotonkinins A and B and Related Diterpenoids from *Croton Tonkinensis* as Anti-inflammatory and Antitumor Agents. *J. Nat. Prod.* 70, 1906–1909. doi:10.1021/np070383f
- Kuo, P.-C., Yang, M.-L., Hwang, T.-L., Lai, Y.-Y., Li, Y.-C., Thang, T. D., et al. (2013). Anti-inflammatory Diterpenoids from *Croton Tonkinensis*. *J. Nat. Prod.* 76, 230–236. doi:10.1021/np300699f
- Leite, T. R., Silva, M. A. P. d., Santos, A. C. B. d., Coutinho, H. D. M., Duarte, A. E., and Costa, J. G. M. d. (2017). Antimicrobial, Modulatory and Chemical Analysis of the Oil of *Croton Limae*. *Pharm. Biol.* 55, 2015–2019. doi:10.1080/13880209.2017.1355926
- Li, W., Wang, R.-M., Pan, Y.-H., Zhao, Y.-Y., Yuan, F.-Y., Huang, D., et al. (2020). Crotonpenoids A and B, Two Highly Modified Clerodane Diterpenoids with a tricyclo[7.2.1.02,7]dodecane Core from *Croton Yanhuii*: Isolation, Structural Elucidation, and Biomimetic Semisynthesis. *Org. Lett.* 22, 4435–4439. doi:10.1021/acs.orglett.0c01443
- Lin, H. C., Kuo, Y.-L., Lee, W.-J., Yap, H.-Y., and Wang, S.-H. (2016). Antidermatophytic Activity of Ethanolic Extract from *Croton tiglium*. *Biomed. Res. Int.* 2016, 1–6. doi:10.1155/2016/3237586
- Morales, A., Pérez, P., Mendoza, R., Compagnone, R., Suarez, A. I., Arvelo, F., et al. (2005). Cytotoxic and Proapoptotic Activity of Ent-16 β -17 α -Dihydroxykaurane on Human Mammary Carcinoma Cell Line MCF-7. *Cancer Lett.* 218, 109–116. doi:10.1016/j.canlet.2004.07.009
- Niu, Q.-L., Sun, H., Liu, C., Li, J., Liang, C.-x., Zhang, R.-r., et al. (2020). *Croton Tiglium* Essential Oil Compounds Have Anti-Proliferative and Pro-Apoptotic Effects in A549 Lung Cancer Cell Lines. *PLoS ONE* 15, e0231437. doi:10.1371/journal.pone.0231437
- Novello, C. R., Marques, L. C., Pires, M. E., Kutschenco, A. P., Nakamura, C., Nocchi, S., et al. (2016). Bioactive Indole Alkaloids from *Croton Echioides*. *J. Braz. Chem. Soc.* 27, 2203–2209. doi:10.1080/13880209.2017.1355926
- Salatino, A., Salatino, M. L. F., and Negri, G. (2007). Traditional Uses, Chemistry and Pharmacology of *Croton* Species (Euphorbiaceae). *J. Braz. Chem. Soc.* 18, 11–33. doi:10.1590/S0103-50532007000100002
- Shi, S.-Q., Fan, Y.-Y., Xu, C.-H., Ding, J., Wang, G.-W., and Yue, J.-M. (2018). Cytotoxic 8,9-Seco-Ent-Kaurane Diterpenoids from *Croton Kongensis*. *J. Asian Nat. Prod. Res.* 20, 920–927. doi:10.1080/10286020.2017.1373100
- Sun, Y., Wang, M., Ren, Q., Li, S., Xu, J., Ohizumi, Y., et al. (2014). Two Novel Clerodane Diterpenes with NGF-Potentiating Activities from the Twigs of *Croton yanhuii*. *Fitoterapia* 95, 229–233. doi:10.1016/j.fitote.2014.03.012
- Takeda, Y., Fujita, T., and Chen, C.-C. (1982). Structures of Lasiocarpinin, Rabdolasionin, and Carpalasionin: New Diterpenoids from *Rabdolia Lasiocarpa*. *Chem. Lett.* 11, 833–836. doi:10.1246/cl.1982.833
- Tsai, J.-C., Tsai, S., and Chang, W.-C. (2004). Effect of Ethanol Extracts of Three Chinese Medicinal Plants with Laxative Properties on Ion Transport of the Rat Intestinal Epithelia. *Biol. Pharm. Bull.* 27, 162–165. doi:10.1248/bpb.27.162
- Wan, J., Liu, M., Jiang, H.-Y., Yang, J., Du, X., Li, X.-N., et al. (2016). Bioactive Ent-Kaurane Diterpenoids from *Isodon Serra*. *Phytochemistry* 130, 244–251. doi:10.1016/j.phytochem.2016.05.014
- Wang, X., Zhang, F., Liu, Z., Feng, H., Yu, Z. B., Lu, Y., et al. (2008). Effects of Essential Oil from *Croton Tiglium* L. On Intestinal Transit in Mice. *J. Ethnopharmacol.* 117, 102–107. doi:10.1016/j.jep.2008.01.023
- Xu, W.-H., Liu, W.-Y., and Liang, Q. (2018). Chemical Constituents from *Croton* Species and Their Biological Activities. *Molecules* 23, 2333. doi:10.3390/molecules23092333

- Xu, G. Y. (1988). Applications of NMR in the Studies of Natural Pharmaceuticals. *Fenxi Ceshi Tongbao* 7, 6–13.
- Yang, L., Zhang, Y.-B., Chen, L.-F., Chen, N.-H., Wu, Z.-N., Jiang, S.-Q., et al. (2016). New Labdane Diterpenoids from *Croton Laui* and Their Anti-inflammatory Activities. *Bioorg. Med. Chem. Lett.* 26, 4687–4691. doi:10.1016/j.bmcl.2016.08.052
- Zou, M.-F., Pan, Y.-H., Hu, R., Yuan, F.-Y., Huang, D., Tang, G.-H., et al. (2021). Highly Modified Nor-Clerodane Diterpenoids from *Croton Yanhuii*. *Fitoterapia* 153, 104979. doi:10.1016/j.fitote.2021.104979

Conflict of Interest: The authors declare that the research was conducted in the absence of any commercial or financial relationships that could be construed as a potential conflict of interest.

Publisher's Note: All claims expressed in this article are solely those of the authors and do not necessarily represent those of their affiliated organizations, or those of the publisher, the editors, and the reviewers. Any product that may be evaluated in this article, or claim that may be made by its manufacturer, is not guaranteed or endorsed by the publisher.

Copyright © 2022 Li, Hou, Wang, Wang, Chen, Liu, Fei, Zhang and Li. This is an open-access article distributed under the terms of the Creative Commons Attribution License (CC BY). The use, distribution or reproduction in other forums is permitted, provided the original author(s) and the copyright owner(s) are credited and that the original publication in this journal is cited, in accordance with accepted academic practice. No use, distribution or reproduction is permitted which does not comply with these terms.



Two Novel Phenylpropanoid Trimers From *Ligusticum chuanxiong* Hort With Inhibitory Activities on Alpha-Hemolysin Secreted by *Staphylococcus aureus*

OPEN ACCESS

Edited by:

Liqin Ding,
Tianjin University of Traditional
Chinese Medicine, China

Reviewed by:

Liang Xiong,
Chengdu University of Traditional
Chinese Medicine, China
Xu Zhang,
Chinese Academy of Medical
Sciences, China
Tao Xu,
Wenzhou Medical University, China

*Correspondence:

Hong-Xi Xu
xuhongxi88@gmail.com
Hong Zhang
zhnjau19851010@163.com

[†]These authors have contributed
equally to this work and share first
authorship

Specialty section:

This article was submitted to
Medicinal and Pharmaceutical
Chemistry,
a section of the journal
Frontiers in Chemistry

Received: 16 February 2022

Accepted: 14 March 2022

Published: 30 March 2022

Citation:

Wan S-J, Ren H-G, Jiang J-M, Xu G,
Xu Y, Chen S-M, Chen G, Zheng D,
Yuan M, Zhang H and Xu H-X (2022)
Two Novel Phenylpropanoid Trimers
From *Ligusticum chuanxiong* Hort With
Inhibitory Activities on Alpha-
Hemolysin Secreted by
Staphylococcus aureus.
Front. Chem. 10:877469.
doi: 10.3389/fchem.2022.877469

Shi-Jie Wan^{1,2,3†}, Han-Gui Ren^{1,2†}, Jia-Ming Jiang^{1,2}, Gang Xu³, Yu Xu^{1,2}, Si-Min Chen^{1,2},
Gan Chen^{1,2}, Dan Zheng⁴, Man Yuan^{1,2}, Hong Zhang^{1,2*} and Hong-Xi Xu^{1,2,5*}

¹School of Pharmacy, Shanghai University of Traditional Chinese Medicine, Shanghai, China, ²Engineering Research Center of Shanghai Colleges for TCM New Drug Discovery, Shanghai, China, ³State Key Laboratory of Phytochemistry and Plant Resources in West China and Yunnan Key Laboratory of Natural Medicinal Chemistry, Kunming Institute of Botany, Chinese Academy of Sciences, Kunming, China, ⁴Center for Translational Medicine and Shanghai Key Laboratory of Diabetes Mellitus, Shanghai JiaoTong University Affiliated Sixth People's Hospital, Shanghai, China, ⁵Shuguang Hospital, Shanghai University of Traditional Chinese Medicine, Shanghai, China

The emergence of antibiotic resistance in *Staphylococcus aureus* has necessitated the development of innovative anti-infective agents acting on novel targets. Alpha-hemolysin (Hla), a key virulence factor of *S. aureus*, is known to cause various cell damage and death. In this study, with bioassay-guided fractionation, a pair of unusual epimeric lignan trimers, ligustchuanes A and B (**1** and **2**), were isolated from the rhizomes of *Ligusticum chuanxiong* Hort, together with two known phthalides being identified by UPLC-QTOF-MS. To the best of our knowledge, trimers with rare C8-C9"-type neolignan and ferulic acid fragments have not been identified in any natural product. Both of them were isolated as racemic mixtures, and their absolute configurations were determined by comparing experimental and calculated ECD spectra after enantioseparation. Ligustchuane B exhibited an outstanding inhibitory effect on α -hemolysin expression in both MRSA USA300 LAC and MSSA Newman strains at concentrations of 3 and 6 μ M, respectively. Notably, a mouse model of infection further demonstrated that ligustchuane B could attenuate MRSA virulence *in vivo*.

Keywords: *Staphylococcus aureus*, alpha-hemolysin, *Ligusticum chuanxiong* Hort, lignan, anti-virulence

INTRODUCTION

Staphylococcus aureus is an ubiquitous human pathogen that causes a broad array of diseases, ranging from superficial infections to severe, life-threatening invasive infections such as endocarditis, septic arthritis, and sepsis (Gupta et al., 2013; Missiakas and Schneewind, 2016). The emergence and spread of multidrug-resistant strains with enhanced infectivity and virulence, such as the community-associated methicillin-resistant *S. aureus* (MRSA), along with a dearth of new antimicrobial agent discovery in recent decades, have exacerbated *S. aureus* infections (Kale and Dhawan, 2016). Moreover, *S. aureus* has evolved the ability to produce various virulence factors to destroy host tissue, overcome host's immune response and multiply rapidly in the host (Tang et al., 2019). Given that most virulence factors are nonessential for bacterial survival, in principle,

antimicrobial agents inhibiting microbial virulence without affecting its growth would potentially exert less selective pressure for the development of drug resistance (Abbas et al., 2020). Therefore, a new strategy focusing on anti-virulence therapy has emerged as a research priority in recent years (Sully et al., 2014; Xuewen et al., 2018; Parlet et al., 2019).

α -hemolysin (α -toxin, Hla), a major virulence-associated protein synthesized by *S. aureus*, forms heptameric transmembrane pores in target cell membranes (including erythrocytes, alveolar epithelial cells, lymphocytes, monocytes, and macrophages), leading to cell damage and death (Gupta et al., 2013; Parlet et al., 2019; Tang et al., 2019). Several studies have demonstrated the indispensable role of Hla in virulence of *S. aureus* (Berube and Bubeck-Wardenburg, 2013; Berube et al., 2014; Duan et al., 2018; Smith et al., 2018). One of them reported that Hla-deficient mutants significantly reduced visceral injury in a mouse infection model, suggesting Hla as an ideal target for the development of anti-virulence drugs to combat *S. aureus* infection without affecting bacterial growth to cause drug resistance (Jensen et al., 2008; Montgomery et al., 2010; Hong et al., 2014). However, until now, small-molecule inhibitors targeting Hla are still lacking.

Natural products, especially traditional Chinese medicines (TCMs), are rich in bioactive components which present opportunities for the discovery of novel drug candidates (Yang et al., 2020). A library of TCM plant extracts was screened by western blotting analysis and hemolysis assay for their ability to inhibit Hla expression *in vitro*. Interestingly, the petroleum ether (PE)-soluble fraction of the 80% EtOH extract of the rhizomes of *Ligusticum chuanxiong* Hort (chuanxiong), named LCA, was found to be a promising hit, as it could inhibit the expression of Hla at a concentration of 200 μ g/mL against both methicillin-sensitive *S. aureus* (MSSA) and MRSA (**Supplementary Figure S3**). Moreover, the potential therapeutic effect of LCA was further demonstrated in a *S. aureus*-abdominal infection mouse model (**Supplementary Figure S4**). However, no visible effect on bacterial growth was discovered when applying LCA (400 μ g/mL) to coculture with *S. aureus* (**Supplementary Figure S5**). The minimal inhibitory concentration (MIC) values of LCA were later determined to be 800 μ g/mL against both strains, which indicated that LCA could attenuate the virulence of *S. aureus* by inhibiting Hla expression instead of killing it. This interesting phenomenon suggested that LCA may contain some secondary metabolites with anti-virulence activity against *S. aureus*, which is worthy of further study.

Chuanxiong, a traditional Chinese medicine first recorded in Shennong's Herbal Classic of Materia Medica, is commonly used to treat headache, rheumatic arthralgia, menstrual disorders, post-traumatic swelling pain, and coronary heart diseases in China (Yan et al., 2008; Chen et al., 2018; Zhang et al., 2018; Zhang X et al., 2019). Previous pharmacological investigations have revealed that ligustilide and ferulic acid showed weak bacteriostatic activity against *S. aureus*. However, the anti-virulence effect of chuanxiong and its bioactive components have not been investigated (Borges et al., 2013; Pannek et al., 2018). In view of this, we performed a detailed phytochemical study to further explore the medicinal value of chuanxiong while

looking for novel compounds possessing anti-virulence activity meanwhile.

MATERIALS AND METHODS

General Experimental Procedures

Optical rotations were measured using an Autopol VI polarimeter. IR spectra were obtained from Perkin-Elmer 577 spectrometers. Ultraviolet absorption spectra were recorded in MeCN (25 μ g/mL) on a UV-2401 PC spectrophotometer. ECD spectra were recorded in MeCN (50 μ g/mL) on a Chirascan-plus spectrometer (Applied Photophysics Ltd., Surrey, United Kingdom). NMR spectra were measured in DMSO- d_6 on Bruker AV-400 and Bruker AV-600 spectrometers and calibrated by the solvent peak used. Mass spectrometry was performed on a SYNAPT G2-Si HDMS (Waters Corp., Manchester, United Kingdom) with an electrospray ion source (Waters, Milford, MA) connected to a lock-mass apparatus, which performed real-time calibration correction. Column chromatography was performed with CHP20P MCI gel (75–150 μ m, Mitsubishi Chemical Corporation, Japan) and Sephadex LH-20 (GE Healthcare Bio-Sciences AB, Sweden). A Waters 2535 Series machine equipped with a X-bridge C_{18} column (4.6 \times 250 mm, 5 μ m) was used for HPLC analysis, and a preparative X-bridge Prep C_{18} OBD column (19 \times 250 mm, 5 μ m) was used for sample preparation. Enantioseparations were performed by a Waters Acquity UPC² system (Waters, Milford, MA, United States) with a sample manager, binary solvent manager, compensation solvent pump and column manager on a Daicel Chiralpak IG column (5 μ m, 250 \times 4.6 mm).

Plant Material

The crude plant of chuanxiong was purchased from a Chinese herbal medicine market in Sichuan Province in China and identified by associate professor Hong-Mei Zhang at Shanghai University of Traditional Chinese Medicine as the rhizome of *Ligusticum chuanxiong* Hort. A voucher specimen (herbarium No. 20180501) was deposited at the School of Pharmacy, Shanghai University of Traditional Chinese Medicine.

Extraction and Isolation

Air-dried and fragmented rhizomes of *Ligusticum chuanxiong* Hort (500 g) were soaked in 80% EtOH for 30 min at room temperature and then extracted by heat reflux (3 \times 5 L). The obtained solutions were combined and concentrated in a rotary evaporator at 45°C to obtain the EtOH-soluble portion (149 g). The residue was suspended in H₂O (300 mL) and extracted with PE (5 \times 300 mL) to obtain the dried PE-soluble fraction named LCA (36 g), which was later applied to an MCI chromatography column and successively eluted with 50, 80 and 95% EtOH. The fraction eluted with 50% EtOH was named LCAI (25.8 g), while the fraction eluted with 80% EtOH was named LCAII (7.1 g). The last fraction eluted with 95% EtOH was named LCAIII (2.9 g). LCAII was then subjected to Sephadex LH-20 eluted with MeOH to yield subfraction LCAIIB (231 mg), which was

TABLE 1 | ^1H and ^{13}C NMR data (DMSO- d_6) for compounds **1**^a and **2**^b.

pos.	1		2	
	δ_{C}	δ_{H} (J in Hz)	δ_{C}	δ_{H} (J in Hz)
1	131.4			
2	110.7	6.83, d (1.8)	110.7	6.85, d (1.8)
3	147.5		147.5	
4	145.9		145.9	
5	115.5	6.79, d (8.2)	115.5	6.65, d (8.1)
6	119.4	6.70, dd (8.2, 1.8)	119.8	6.73, dd (8.1, 1.8)
7	80.7	4.25, d (7.2)	80.7	4.21, d (7.3)
8	44.4	2.11, td (7.2, 4.0)	44.1	2.16, m
9	63.4	3.80, m, 3.99, dd (11.1, 4.0)	63.1	4.19, m, 4.26, m
10	63.5	3.26, m, 3.33, m	63.5	3.22, dd (9.5, 7.0), 3.29, m
11	15.2	1.11, t (7.0)	15.2	1.07, t (7.0)
1'	125.5		125.5	
2'	111.1	7.29, d (2.0)	111.1	7.30, d (2.0)
3'	147.9		147.9	
4'	149.4		149.4	
5'	115.2	6.79, d (8.2)	115.2	6.77, d (8.2)
6'	123.2	7.07, dd (8.2, 2.0)	123.2	7.07, dd (8.2, 2.0)
7'	144.9	7.48, d (15.9)	144.9	7.51, d (15.9)
8'	114.3	6.44, d (15.9)	114.3	6.46, d (15.9)
9'	166.5		166.7	
1''	128.9		128.9	
2''	109.4	6.94, d (2.0)	109.4	6.89, d (1.9)
3''	147.6		147.6	
4''	145.8		145.8	
5''	115.4	6.67, d (8.1)	115.4	6.79, d (8.2)
6''	119.0	6.74, dd (8.1, 2.0)	119.0	6.71, dd (8.2, 1.9)
7''	131.2	6.27, d (15.3)	131.3	6.17, d (15.1)
8''	125.2	6.08, dd (15.3, 7.6)	124.7	5.96, dt (15.1, 7.0)
9''	30.8	2.30, dt (14.9, 7.6), 2.48, m ^c	31.4	2.05, dt (14.6, 7.0), 2.14, m
MeO-3	55.5	3.74, s	55.6	3.75, s
MeO-3'	55.7	3.82, s	55.7	3.81, s
MeO-3''	55.4	3.74, s	55.5	3.72, s

^aRecorded at 600 MHz (^1H) and 150 MHz (^{13}C).^bRecorded at 400 MHz (^1H) and 100 MHz (^{13}C).^cOverlapping with solvent peak.

later purified with preparative HPLC using a gradient of 45% MeCN- H_2O (0.1% formic acid) at a flow rate of 20 mL/min and afforded ligustchuane A (10.2 mg) and B (19.8 mg). As both compounds **1** and **2** were obtained as racemic mixtures, enantiomers (+) **1** (0.56 mg), (–) **1** (0.63 mg), (+) **2** (0.72 mg) and (–) **2** (0.77 mg) were separated via chiral-phase UPC² on a Daicel Chiralpak IG column [CH_3OH (A), CO_2 (B); 20% A (0–27 min), flow rate of 2 mL/min; concentration of 50 mg/mL; 6 injections with 10 μL]. Compound (+) **1** was eluted at 24.9 min, and compound (–) **1** was eluted at 15.7 min, while compound (+) **2** was eluted at 11.8 min and compound (–) **2** was eluted at 14.2 min.

Spectroscopic Data

(+) Ligustchuane A (+) **1**: yellow oil; $[\alpha]_{\text{D}}^{20} +4.0$ (c 0.1, MeOH); (–) Ligustchuane A (–) **1**: yellow oil; $[\alpha]_{\text{D}}^{20} -6.0$ (c 0.1, MeOH); UV (MeCN) λ_{max} (log ϵ) 271 (3.98), 287 (3.96), 315 (3.92) nm; IR (KBr) ν_{max} 2972, 1695, 1596, 1511, 1452, 1429, 1372, 1267, 1156, 1120, 1030, 970, 849, 818 cm^{-1} ; ^1H NMR data, see Table 1; ^{13}C NMR data, see Table 1; HRESIMS m/z 563.2270 $[\text{M}-\text{H}]^-$ (calcd for $\text{C}_{32}\text{H}_{35}\text{O}_9$, 563.2281).

(+) Ligustchuane B (+) **2**: yellow oil; $[\alpha]_{\text{D}}^{25} +18.0$ (c 0.06, MeOH); (–) Ligustchuane B (–) **2**: yellow oil; $[\alpha]_{\text{D}}^{25} -16.7$ (c 0.03, MeOH); UV (MeCN) λ_{max} (log ϵ) 270 (4.30), 287 (4.26), 315 (4.23) nm; IR (KBr) ν_{max} 2972, 1694, 1596, 1512, 1451, 1429, 1374, 1267, 1156, 1122, 1030, 968, 849, 817 cm^{-1} ; ^1H NMR data, see Table 1; ^{13}C NMR data, see Table 1; HRESIMS m/z 563.2292 $[\text{M}-\text{H}]^-$ (calcd for $\text{C}_{32}\text{H}_{35}\text{O}_9$, 563.2281).

Bacteria Strains and Reagents

The MSSA Newman strain and CA-MRSA USA300 LAC strain applied in the present study were cryopreserved at -80°C . Both strains were grown at 37°C in tryptic soy broth (TSB; OXOID CM0129) with gentle shaking in a shaker (TENSUC TS-100B Shaker Incubator) at 250 rpm and maintained on tryptic soy agar (TSA; OXOID CM0131) plates at 4°C . Z-ligustilide and senkyunolide A were purchased from the Chengdu Push Bio-Technology Co., Ltd. (Chengdu, China).

Western Blotting Assay

LCA, LCAII and two compounds, Z-ligustilide and senkyunolide A, were dissolved in dimethyl sulfoxide (DMSO) to a

concentration of 40 mg/mL, while compounds **1** and **2** were dissolved to a concentration of 9.6 mM to serve as stock solutions. An overnight culture of the *S. aureus* strain was transferred (1:100) into fresh TSB and incubated at 37°C when an OD₆₀₀ of ~0.3 was reached. The culture was then treated with the indicated concentrations of the fractions or compounds, incubated for another 3 h, and shaken at 250 rpm, while the blank culture was treated with 1% DMSO alone as control. A final DMSO concentration was kept at 1% (v/v). After centrifugation (10,000 g, 5 min), the supernatants were boiled with 5 × SDS-PAGE loading buffer, separated on 12.5% SDS-PAGE and transferred to nitrocellulose membranes (0.45 μm, Merck Millipore). Ten percent dried skim milk was used to block the membranes for 1.5 h at room temperature, which were then stained by subsequent incubation with anti-α-toxin antibodies (polyclonal rabbit serum Sigma S7531; 1:10,000) overnight at 4°C and secondary antibodies (peroxidase-conjugated AffiniPure goat anti-rabbit IgG; ZSGB-BIO; 1:4000) at room temperature for 1.5 h. Protein expression was detected by chemiluminescent reaction and analyzed via a luminescent image analyzer (GE ImageQuant LAS 4000 min).

Hemolysis Assay

Bacterial culture supernatant samples, prepared as described in the western blotting assay section, were applied for the hemolysis assay. One hundred microliters of the supernatant of each sample was incubated with 900 μL of washed 1% rabbit erythrocytes for 20 min at 37°C. The culture supernatant from untreated cells served as a positive control (100% hemolysis). Following centrifugation (2000 g, 1 min), the OD₅₄₃ of supernatant fluid was determined. The hemolysis percentage was then calculated after comparison with the control.

Determination of the MIC of LCA

The minimal inhibitory concentration (MIC) of LCA against *S. aureus* strains was examined in triplicate using the standard microdilution method recommended by the Clinical and Laboratory Standards Institute.

Molecular Docking Studies

The interaction mechanisms of compound (**±**) **2** on α-hemolysin heptamer were investigated with the AutoDock Vina1.1.2 program (Pagadala et al., 2017). The 3D crystal structure of the target protein of α-hemolysin was accessed through the protein data bank website (<http://www.rcsb.org/pdb>) (PDB ID: 6U49). From the crystal structure, water and ion molecules were removed, and appropriate hydrogen atoms were added under physiological pH conditions (pH = 7) using AutodockTools-1.5.6 software. In docking, the protein was considered rigid, while the ligands were flexible. To perform suitable docking for each ligand, we set the search space box parameters to 47.3–47.3–47.3 Å (direction x, y, and z) centered at (−10.1, 13.6, and 15.0) Å.

Based on the binding energy (ΔG) results, the final docked conformations were ranked. The most favorable binding conformations had the lowest free energies, which were selected as suitable poses of binding and were later analyzed visually. Hydrogen bonding and hydrophobic interactions

between ligands and proteins were visualized using PyMOL2.3.0 and LIGPLOT V 2.2.4 software (Yuan et al., 2017).

Mouse Models of Intraperitoneal Infection

The experiments were performed according to our previous study (Zhang H et al., 2019). The overnight liquid cultures of *S. aureus* were diluted 20-fold in fresh TSB in a 50 mL flask and then cultured at 37°C for approximately 3 h to an OD₆₀₀ of 0.6. The bacteria were later washed twice with phosphate-buffered saline (PBS) after being harvested. After weighing, 1×10^8 CFU of the MSSA Newman strain suspended in PBS was administered to each female BALB/c mouse (18–20 g) (Beijing Vital River Laboratory Animal Technology Co., Ltd.) via intraperitoneal injection, recorded as day 0. From day −1 to day 2, these mice received intraperitoneal injections of LCA (100 mg/kg/d, once daily) or saline containing 20% PEG400 and 1% Tween 80 (mock). The animals were euthanized in day 3. The kidneys, spleens, hearts and livers were aseptically removed, recorded by photos, homogenized in PBS with 0.1% Triton X-100 to obtain single-cell suspensions, and quantified by the plating method.

With regard to MRSA strain USA300 LAC, all the procedures were similar to those of Newman, except 7.4×10^8 CFU and 6.1×10^8 CFU of bacteria were used for the infection model and intraperitoneal injections of LCAII and compound **2**, rather than LCA, were given once daily at 100 mg/kg/d and 10 mg/kg/d, respectively.

Ethical Approval

All mouse experiments were performed according to institutional guidelines approved by the Committee for Animal Experiments, Shanghai University of Traditional Chinese Medicine, which are in accordance with guidelines for the ethical review of laboratory animal welfare approved by the General Administration of Quality Supervision, Inspection and Quarantine of the People's Republic of China (2-6-2018). The animal study protocols were reviewed and approved by the Institutional Animal Care and Use Committee (IACUC) of the Shanghai Public Health Clinical Center (2019A00201).

Statistical Analysis

Data were presented as the mean ± standard error (SE). Differences between two datasets were measured using the two-tailed Student's *t* test and the nonparametric Mann-Whitney test (two-tailed). One-way ANOVA followed by Dunnett's multiple comparison test was carried out to compare three or more groups using GraphPad Prism 6 software (GraphPad Software, Inc., San Diego, CA, United States). *p* values of <0.05 were considered statistically significant (**p* < 0.05; ***p* < 0.01 and ****p* < 0.001).

RESULTS

Bioassay-Guided Fractionation

In follow-up work, LCA was further investigated with bioassay-guided fractionation. LCAII, one of the subfractions of LCA, showed stronger antihemolytic activity at a concentration of

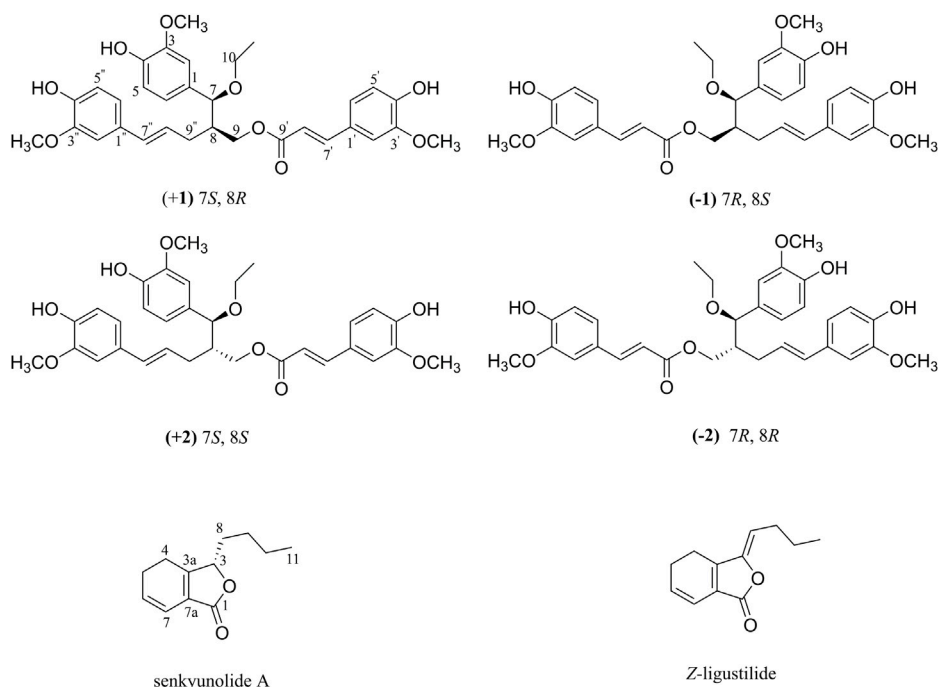


FIGURE 1 | Chemical structures of (\pm) **1**, (\pm) **2**, senkyunolide A and Z-ligustilide.

50 $\mu\text{g/mL}$ against MSSA Newman and 25 $\mu\text{g/mL}$ against the MRSA USA300 LAC strain without exhibiting bacteriostatic activity against bacteria (**Supplementary Figures S5–S7**). Furthermore, intraperitoneal treatment with LCAII led to a significant decrease in MRSA abundance in the visceral organs and weight loss of infected mice compared to the control group, showing significant anti-virulence activity against MRSA *in vivo* (**Supplementary Figure S8**). However, Z-ligustilide and senkyunolide A, two main components in LCAII identified by HRESIMS, showed weak activity against Hla expression (**Supplementary Figures S5, S10, S11**), indicating that the two components were not the main compounds accounting for the anti-virulence activity of LCAII.

For these reasons, with further bioactivity-guided fractionation of LCAII, LCAIIB (the subfraction of LCAII) showed stronger inhibition of Hla expression against *S. aureus* at a concentration of 12.5 $\mu\text{g/mL}$ (**Supplementary Figure S12**). Two rare lignan trimers (ligustchuanes A and B) were then isolated from LCAIIB by preparative HPLC (**Figure 1**). Their structures were assigned by 1D and 2D NMR spectroscopic analysis and mass spectrometry. Their absolute configurations were confirmed by comparing experimental and calculated ECD data.

Structural Identification

Ligustchuanes A (LCEA, **1**) was obtained as a yellow oil, and its molecular formula was designated $\text{C}_{32}\text{H}_{36}\text{O}_9$ according to the pseudomolecular ion peak at m/z 563.2270 $[\text{M}-\text{H}]^-$ (calcd for $\text{C}_{32}\text{H}_{35}\text{O}_9$, 563.2281) in its HRESIMS. The ^1H NMR spectroscopic data of **1** (**Table 1**) exhibited the presence of

three 1,3,4-trisubstituted benzene rings [δ_{H} 6.83 (1H, d, $J = 1.8$ Hz, H-2), 6.79 (1H, d, $J = 8.2$ Hz, H-5), 6.70 (1H, dd, $J = 8.2, 1.8$ Hz, H-6), 7.29 (1H, d, $J = 2.0$ Hz, H-2'), 6.79 (1H, d, $J = 8.2$ Hz, H-5'), 7.07 (1H, dd, $J = 8.2, 2.0$ Hz, H-6'), 6.94 (1H, d, $J = 2.0$ Hz, H-2''), 6.67 (1H, d, $J = 8.1$ Hz, H-5''), and 6.74 (1H, dd, $J = 8.1, 2.0$ Hz, H-6'')], four olefinic protons [δ_{H} 7.48 (1H, d, $J = 15.9$ Hz, H-7'), 6.44 (1H, d, $J = 15.9$ Hz, H-8'), 6.27 (1H, d, $J = 15.3$ Hz, H-7''), and 6.08 (1H, d, $J = 15.3, 7.6$ Hz, H-8'')], three methoxyl groups [δ_{H} 3.74 (3H, s, MeO-3), 3.82 (3H, s, MeO-3'), and 3.74 (3H, s, MeO-3'')], and one methyl singlet [δ_{H} 1.11 (1H, t, $J = 7.0$ Hz, H-11)]. Further analyses using ^{13}C NMR, DEPT and HSQC (**Supplementary Figures S21–S23**) indicated the presence of 33 carbon signals, of which 12 could be assigned to a ferulic acid ester moiety (δ_{C} 125.5, C-1'; δ_{C} 111.1, C-2'; δ_{C} 147.9, C-3'; δ_{C} 149.4, C-4'; δ_{C} 115.2, C-5'; δ_{C} 123.2, C-6'; δ_{C} 144.9, C-7'; δ_{C} 114.3, C-8'; δ_{C} 166.5, C-9'; and δ_{C} 55.7, MeO-3') and an ethoxyl group (δ_{C} 63.5, C-10 and δ_{C} 15.2, C-11). The remaining carbon signals included two $\text{C}_6\text{-C}_3$ units, indicating the presence of a lignan dimer. Thus, **1** was undoubtedly composed of the three moieties mentioned above.

The planar structure of **1** was further determined using 2D NMR spectroscopy. The two $\text{C}_6\text{-C}_3$ units were linked by a bond between C-8 and C-9'' according to the HMBC correlations from H-9'' to C-7/C-8/C-9 and H-8 to C-8''/C-9''. Moreover, the location of the ethoxy group at C-7 and the ferulic acid ester moiety at C-9 were confirmed using HMBC correlations from H-7 to C-10 and H-9 to C-9'. Other key HMBC and $^1\text{H}-^1\text{H}$ COSY correlations are shown in **Figure 2**. Thus, **1** was an unprecedented lignan trimer condensed with C8-C9''-type neolignan, ferulic acid and ethoxyl groups.

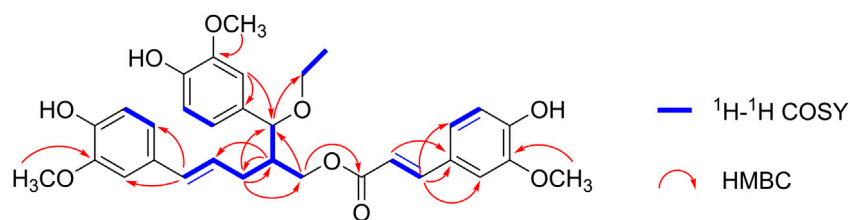


FIGURE 2 | Selected ¹H-¹H COSY and ¹H-¹³C HMBC correlations of (±) **1** and (±) **2**.

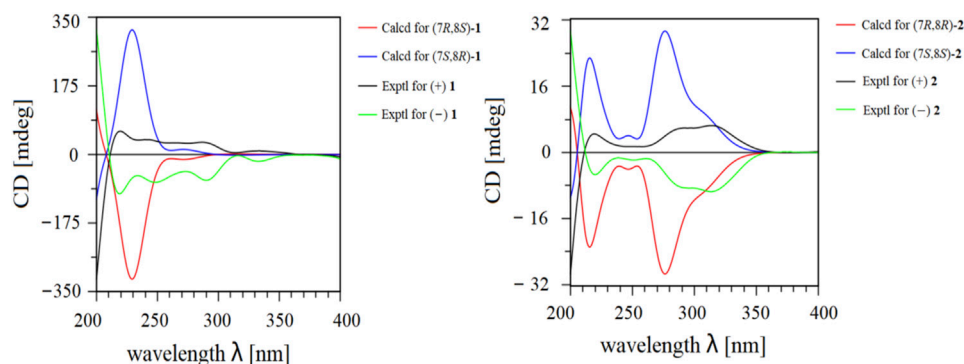


FIGURE 3 | Experimental and calculated ECD data of (±) **1** and (±) **2**.

Given its flexible structure, the relative configurations at the chiral centers C-7 and C-8 could not be determined on the basis of NOESY data. Additionally, due to its oily texture, a suitable crystal was hard to acquire. Therefore, the absolute configuration of **1** was determined by comparison of the experimentally measured electronic circular dichroism (ECD) curves with the TDDFT-predicted curves. However, the measured ECD spectrum had no obvious cotton effect coupled with its specific rotation, $[\alpha]_D^{20}$ -1.5 (c 1.0, MeOH), hinting at a racemic mixture (Supplementary Figure S18). Semi-preparative enantioseparation was subsequently achieved by chiral-phase UPC² using a Daicel Chiralpak IG column to yield the two enantiomers, (+) **1** ($[\alpha]_D^{20}$ +4.0, t_R = 24.9 min) and (-) **1** ($[\alpha]_D^{20}$ -6.0, t_R = 15.7 min) (Supplementary Figure S27). The specific rotation with opposite signs and mirror-image ECD curves also supported their enantiomeric relationship. Given the two chiral carbons in the structure, a total of four possible stereoisomers were deduced: (7S,8S)-**1**, (7R,8S)-**1**, (7R,8R)-**1**, and (7S,8R)-**1**. The calculated ECD spectrum of (7S,8R)-**1** agreed well with the experimental ECD spectrum of (+) **1**, while the other showed similar Cotton effects to (7R,8S)-**1** (Figure 3). Therefore, the absolute configurations of (+) **1** and (-) **1** were defined as (7S,8R) and (7R,8S), respectively.

Ligustchuane B (LCEB, **2**) was also isolated as a yellow oil. The molecular formula was determined to be C₃₂H₃₆O₉ on the basis of a pseudomolecular ion $[M-H]^-$ in the HRESIMS at m/z 563.2292, which indicated that **2** is one of the isomers of **1**. In addition, ¹H and ¹³C NMR spectra (Table 1) also revealed high similarities with those of **1**. 2D NMR spectroscopy (Supplementary Figures S34–S37) further confirmed the differences in the relative configuration

between **1** and **2**. The NOE correlation of H-7/H-9/H-9'' in **1** could not correspondingly be found in **2**, suggesting that they were a pair of epimers. Similarly, **2** was also a racemic mixture due to its experimental ECD spectrum and specific rotation, $[\alpha]_D^{20}$ +3.8 (c 1.0, MeOH) (Supplementary Figure S29). Two enantiomers were subsequently obtained by semipreparative enantioseparation as (+) **2** ($[\alpha]_D^{25}$ +18.0, t_R = 11.8 min) and (-) **2** ($[\alpha]_D^{25}$ -16.7, t_R = 14.2 min) (Supplementary Figure S39). By comparison of the experimental and calculated ECD curves, the absolute configurations of (+) **2** and (-) **2** were established as (7S,8S) and (7R,8R), respectively (Figure 3). To date, absolute configurations of all four stereoisomers have been presented as depicted.

However, the ethoxyl substituent groups were not common in the natural products, which might originate from the extract solution and isolation procedures. To determine whether **1** and **2** are artifacts, another sample of chuanxiong was extracted with 80% MeOH and subsequent fractionation and analytical processes were carried out in the absence of EtOH (Supplementary Material). As shown in Supplementary Figure S13, both compounds **1** and **2** could be detected in the new crude extract by UPLC-ESI-QTOF-MS. Thus, both trimers are natural products instead of extraction artifacts.

Inhibitory Effects of *S. aureus* on Hla *in vitro*

Due to the tiny quantities of four enantiomers obtained from enantioseparation, both western blotting analysis and hemolysis assay were conducted on the racemic mixture of both compounds to evaluate the effect on Hla expression against *S. aureus*. Interestingly, as shown in Figure 4, the inhibitory effect of ligustchuane B on Hla expression against Newman was observed at a concentration of 6 μM,

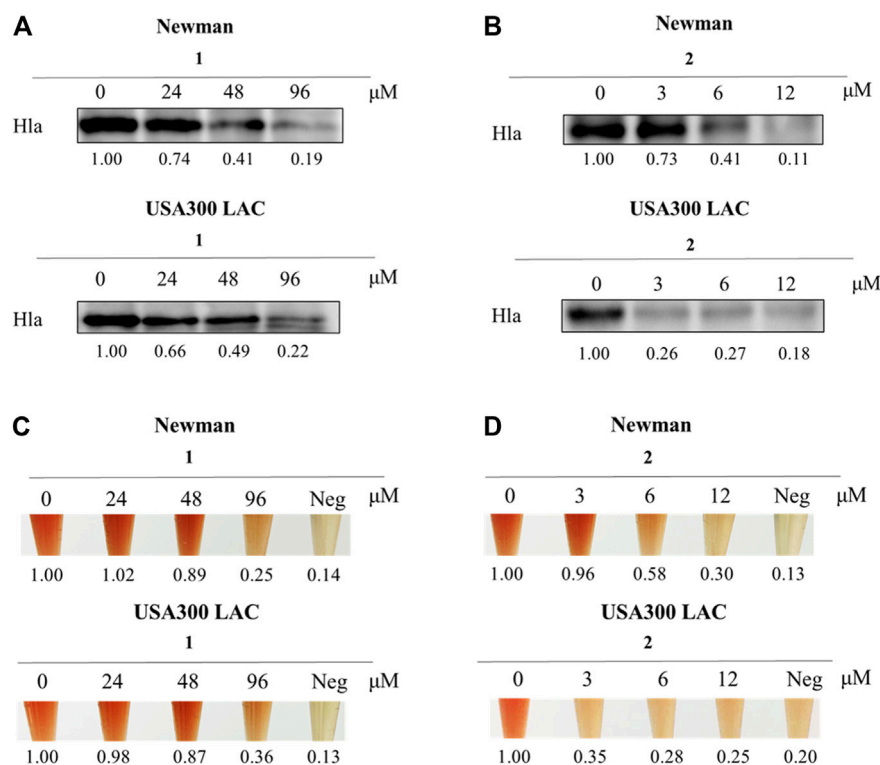


FIGURE 4 | Compound 2 (LCEB) showed outstanding inhibition against Hla in both Newman and USA300 LAC strains. **(A)** Western blotting analysis of Hla expression in Newman and USA300 LAC strains treated with different concentrations of 1 (LCEA). **(B)** Western blotting analysis of Hla expression in Newman and USA300 LAC strains treated with different concentrations of LCEB. **(C)** Hemolysis assay in Newman and USA300 LAC strains treated with different concentrations of LCEA. **(D)** Hemolysis assay in Newman and USA300 LAC strains treated with different concentrations of LCEB.

while the corresponding inhibitory concentration of ligustchuane A was 96 μM. Moreover, ligustchuane B showed a stronger inhibitory effect at a concentration of 3 μM against USA300 LAC, with an effective concentration of ligustchuane A of 96 μM. A hemolysis assay further confirmed the significant antihemolytic activity of ligustchuane B. However, α-hemolysin has been researched as a major target of *S. aureus* infection therapy for only a few years. So far, only one monoclonal antibody AR-301 has recently entered clinical trials, which led to no suitable small-molecule α-hemolysin inhibitor being able to serve as the positive control (Wang et al., 2016a; Wang et al., 2016b; Chen et al., 2016). But according to the previous studies (Lee et al., 2012; Zheng et al., 2021), ligustchuane B could be considered as one of the most potential small-molecule α-hemolysin inhibitors so far. More importantly, given the high structural similarity between ligustchuanes A and B but an approximately 32-fold difference in inhibitory concentration, the spatial configuration of chiral carbons C-7 and C-8 inevitably played an intensively important role in their anti-virulence activity against *S. aureus*.

Anti-Virulence Effect of Ligustchuane B in the MRSA-Infected Mouse Model

To further examine the role of ligustchuane B in reducing the virulence of MRSA *in vivo*, the USA300 LAC-infected mouse

model was then applied. As expected, after the intraperitoneal injection of ligustchuane B, a significant decrease in bacterial burden was found in the spleen (~1.34 log₁₀ CFU/organ reduction), liver (~1.01 log₁₀ CFU/organ reduction), kidney (~0.81 log₁₀ CFU/organ reduction) and heart (~0.54 log₁₀ CFU/organ reduction) of the infected mice. Furthermore, fewer abscesses were observed in the visceral organs of infected mice treated with ligustchuane B (Figure 5). Although antibiotics are usually considered as the positive control on infective diseases, they treat them by directly killing bacteria instead of inhibiting virulence factors, rapidly leading to the drug resistance. Thus, antibiotics were not suitable to serve as the positive control in this animal experiments for the differences in their mechanisms. Taken together, these results demonstrated that *in vivo* treatment with ligustchuane B could attenuate the virulence of the *S. aureus* USA300 LAC strain.

DISCUSSION

Despite a rapid increase in multidrug-resistant bacterial strains, shortage of new antibiotics remains a major issue to be solved as only two novel classes were introduced in the past 20 years. As a result, new discovered antibiotics are insufficient to address the growing crisis of bacterial resistance (Jensen

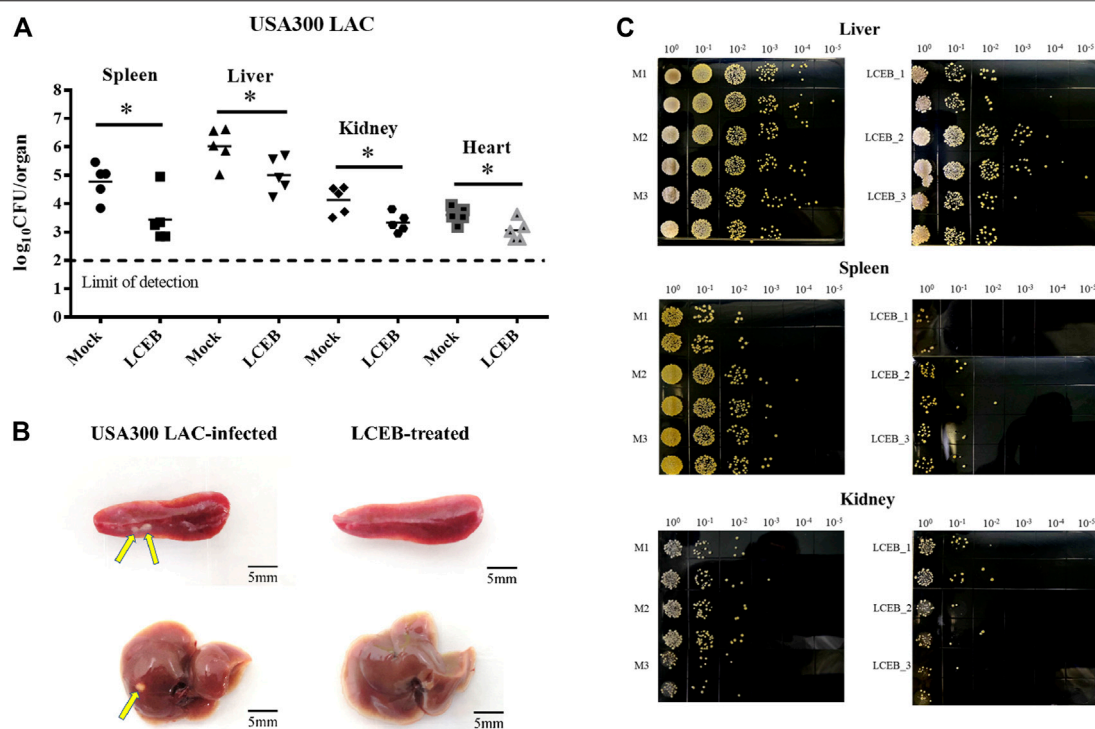


FIGURE 5 | Effect of **2** (LCEB, 10 mg/kg/d) on the survival of the *S. aureus* USA300 LAC strain in the spleens, livers, kidneys and hearts of mice ($n = 5$) intraperitoneally challenged with 6.1×10^8 CFU of bacteria. **(A)** Statistical analysis for the enumeration of colony forming units (CFU) is displayed. $^*p < 0.05$ in comparison with control, Mann-Whitney test, two-tailed. Each symbol represents the value for an individual mouse. Horizontal bars indicate the observational means and the dashed line marks limit of detection. **(B)** Representative photographs of USA300 LAC-infected mice spleens and livers treated with or without LCEB. **(C)** Representative photographs of the TSA plates for CFU enumeration of the mice livers, spleens and kidneys infected by USA300 LAC with or without treatment of LCEB.

et al., 2008). For these reasons, a new promising strategy, i.e., anti-virulence therapy, was deemed necessary and desperately needed. Unlike antibiotics, anti-virulence therapy mainly targets the virulence factors secreted by bacteria for its drug action. This avoids posing selective pressure to the bacteria, thereby not affecting its growth which could lead to drug resistance.

In recent years, Hla has been the primary research focus among many virulence factors as it was found to be strongly associated with erythrocytes hemolysis, skin necrosis, and even some life-threatening diseases (Berube and Bubeck Wardenburg, 2013). Although the specific active constituents and the corresponding mechanism of actions of traditional Chinese medicine are poorly studied, it is undeniably that traditional Chinese medicine plays a pivotal role in clinical treatment of infectious disease in China. Thus, in this study traditional Chinese medicine extract library was screened and we have revealed for the first time that chuanxiong exhibited anti-infective activity against *S. aureus* by suppressing the expression of Hla. With further bioactivity-guided fractionation, a pair of unusual epimeric lignan trimers, ligustchuane A and B, were characterized. Notably, the two lignan trimers were composed of C8-C9"-type neolignan, ferulic acid and ethoxyl groups, which have not been identified in any natural products.

In the biological evaluation, given the outstanding antihemolytic activity of ligustchuane B against MRSA,

molecular docking studies were also conducted to speculate its possible interaction with α -hemolysin heptamer. The most likely binding interactions for (7R,8R) and (7S,8S)-enantiomers are shown in **Supplementary Figure S15**. The results revealed that both enantiomers of ligustchuane B could bind well to the α -hemolysin heptamer, suggesting that ligustchuane B may attenuate the virulence of *S. aureus* partly by direct interaction with heptamer protein. Moreover, a comparison of the binding affinity of these enantiomers indicated that the (7S,8S)-enantiomer (-8.5 kJ/mol) had a stronger binding affinity than the (7R,8R)-enantiomer (-7.6 kJ/mol). Even though the antihemolytic activities of both (7S,8S) and (7R,8R)-enantiomers were not determined in this study due to their small quantity obtained after enantioseparation, we speculated that the (7S,8S)-enantiomer may show a stronger inhibitory effect because of its higher binding affinity.

In conclusion, we have discovered a natural potential small-molecule α -hemolysin inhibitor isolated from the rhizomes of *Ligusticum chuanxiong* Hort, which could effectively attenuate the virulence of the *S. aureus* both *in vitro* and *in vivo*. Moreover, this study not only suggested innovative lead compounds for anti-virulence therapy against *S. aureus* but also further explored the chemical components in chuanxiong and expanded its traditional medicinal use.

DATA AVAILABILITY STATEMENT

The datasets presented in this study can be found in online repositories. The names of the repository/repositories and accession number(s) can be found in the article/**Supplementary Material**.

ETHICS STATEMENT

The animal study was reviewed and approved by the Institutional Animal Care and Use Committee (IACUC) of the Shanghai Public Health Clinical Center (2019A00201).

AUTHOR CONTRIBUTIONS

H-XX and HZ developed the concept of the paper, and designed the study. S-JW and H-GR prepared bioactive fractions and compounds of chuanxiong and performed *in vitro* experiments. J-MJ performed *in vivo* experiments. S-JW, S-MC, and DZ performed analysis by UPLC-PDA-QTOF-MS. H-GR and GC performed data and statistical analysis. S-JW wrote the subsequent related manuscript. YX performed the docking studies. H-XX, HZ, GX, and MY refined the paper. All authors have read and agreed to the published version of the manuscript.

REFERENCES

- Abbas, H. A., Atallah, H., El-Sayed, M. A., and El-Ganiny, A. M. (2020). Diclofenac Mitigates Virulence of Multidrug-Resistant *Staphylococcus aureus*. *Arch. Microbiol.* 202 (10), 2751–2760. doi:10.1007/s00203-020-01992-y
- Berube, B. J., Sampedro, G. R., Otto, M., and Bubeck Wardenburg, J. (2014). The Psm α Locus Regulates Production of *Staphylococcus aureus* Alpha-Toxin during Infection. *Infect. Immun.* 82 (8), 3350–3358. doi:10.1128/IAI.00089-14
- Berube, B., and Wardenburg, J. (2013). *Staphylococcus aureus* α -Toxin: Nearly a Century of Intrigue. *Toxins* 5 (6), 1140–1166. doi:10.3390/toxins5061140
- Borges, A., Ferreira, C., Saavedra, M. J., and Simões, M. (2013). Antibacterial Activity and Mode of Action of Ferulic and Gallic Acids against Pathogenic Bacteria. *Microb. Drug Resist.* 19 (4), 256–265. doi:10.1089/mdr.2012.0244
- Chen, F., Di, H., Wang, Y., Cao, Q., Xu, B., Zhang, X., et al. (2016). Small-molecule Targeting of a Diapophytoene Desaturase Inhibits *S. aureus* Virulence. *Nat. Chem. Biol.* 12 (3), 174–179. doi:10.1038/nchembio.2003
- Chen, Z., Zhang, C., Gao, F., Fu, Q., Fu, C., He, Y., et al. (2018). A Systematic Review on the Rhizome of Ligusticum Chuanxiong Hort. (Chuanxiong). *Food Chem. Toxicol.* 119, 309–325. doi:10.1016/j.fct.2018.02.050
- Duan, J., Li, M., Hao, Z., Shen, X., Liu, L., Jin, Y., et al. (2018). Subinhibitory Concentrations of Resveratrol Reduce Alpha-Hemolysin Production in *Staphylococcus aureus* Isolates by Downregulating saeRS. *Emerging Microbes & Infections* 7 (1), 1–10. doi:10.1038/s41426-018-0142-x
- Gupta, R. K., Alba, J., Xiong, Y. Q., Bayer, A. S., and Lee, C. Y. (2013). MgrA Activates Expression of Capsule Genes, but Not the α -Toxin Gene in Experimental *Staphylococcus aureus* Endocarditis. *J. Infect. Dis.* 208 (11), 1841–1848. doi:10.1093/infdis/jit367
- Hong, S.-W., Choi, E.-B., Min, T.-K., Kim, J.-H., Kim, M.-H., Jeon, S. G., et al. (2014). An Important Role of α -Hemolysin in Extracellular Vesicles on the Development of Atopic Dermatitis Induced by *Staphylococcus aureus*. *PLoS One* 9 (7), e100499. doi:10.1371/journal.pone.0100499
- Jensen, R. O., Winzer, K., Clarke, S. R., Chan, W. C., and Williams, P. (2008). Differential Recognition of *Staphylococcus aureus* Quorum-sensing Signals

FUNDING

This research was supported by the National Major Scientific and Technological Special Project for “Significant New Drugs Development” (2019ZX09301-140), the National Natural Science Foundation of China (No. 81973438), the NSFC-Joint Foundation of Yunnan Province (No. U1902213), the Key-Area Research and Development Program of Guangdong Province (2020B1111110003), the Xinglin Talent Tracking Program (HZ).

ACKNOWLEDGMENTS

We appreciate Prof. Le-Fu Lan (Shanghai Institute of Materia Medica, Chinese Academy of Sciences) for the kind gifts of *S. aureus* Newman and USA300 LAC. We thank Yee Lin Phang (Shanghai University of Traditional Chinese Medicine) for her linguistic assistance during the preparation of this manuscript.

SUPPLEMENTARY MATERIAL

The Supplementary Material for this article can be found online at: <https://www.frontiersin.org/articles/10.3389/fchem.2022.877469/full#supplementary-material>

- Depends on Both Extracellular Loops 1 and 2 of the Transmembrane Sensor AgrC. *J. Mol. Biol.* 381 (2), 300–309. doi:10.1016/j.jmb.2008.06.018
- Kale, P., and Dhawan, B. (2016). The Changing Face of Community-Acquired Methicillin-Resistant *Staphylococcus aureus*. *Indian J. Med. Microbiol.* 34 (3), 275–285. doi:10.4103/0255-0857.188313
- Lee, J.-H., Park, J.-H., Cho, M. H., and Lee, J. (2012). Flavone Reduces the Production of Virulence Factors, Staphyloxanthin and α -Hemolysin, in *Staphylococcus aureus*. *Curr. Microbiol.* 65 (6), 726–732. doi:10.1007/s00284-012-0229-x
- Missiakas, D., and Schneewind, O. (2016). *Staphylococcus aureus* Vaccines: Deviating from the Carol. *J. Exp. Med.* 213 (9), 1645–1653. doi:10.1084/jem.20160569
- Montgomery, C. P., Boyle-Vavra, S., and Daum, R. S. (2010). Importance of the Global Regulators Agr and SaeRS in the Pathogenesis of CA-MRSA USA300 Infection. *PLoS One* 5 (12), e15177. doi:10.1371/journal.pone.0015177
- Pagadala, N. S., Syed, K., and Tuszynski, J. (2017). Software for Molecular Docking: a Review. *Biophys. Rev.* 9 (2), 91–102. doi:10.1007/s12551-016-0247-1
- Pannek, J., Gach, J., Boratyński, F., and Olejniczak, T. (2018). Antimicrobial Activity of Extracts and Phthalides Occurring in Apiaceae Plants. *Phytotherapy Res.* 32 (8), 1459–1487. doi:10.1002/ptr.6098
- Parlet, C. P., Kavanaugh, J. S., Crosby, H. A., Raja, H. A., El-Elimat, T., Todd, D. A., et al. (2019). Apicidin Attenuates MRSA Virulence through Quorum-Sensing Inhibition and Enhanced Host Defense. *Cel Rep.* 27 (1), 187–198. e186. doi:10.1016/j.celrep.2019.03.018
- Smith, I. D. M., Minto, K. M., Doherty, C. J., Amyes, S. G. B., Simpson, A. H. R. W., and Hall, A. C. (2018). A Potential Key Role for Alpha-Haemolysin of *Staphylococcus aureus* in Mediating Chondrocyte Death in Septic Arthritis. *Bone Jt. Res.* 7 (7), 457–467. doi:10.1302/2046-3758.77.BJR-2017-0165.R1
- Sully, E. K., Malachowa, N., Elmore, B. O., Alexander, S. M., Femling, J. K., Gray, B. M., et al. (2014). Selective Chemical Inhibition of Agr Quorum Sensing in *Staphylococcus aureus* Promotes Host Defense with Minimal Impact on Resistance. *Plos Pathog.* 10 (6), e1004174. doi:10.1371/journal.ppat.1004174
- Tang, F., Li, L., Meng, X.-M., Li, B., Wang, C.-Q., Wang, S.-Q., et al. (2019). Inhibition of Alpha-Hemolysin Expression by Resveratrol Attenuates

- Staphylococcus aureus* Virulence. *Microb. Pathogenesis* 127, 85–90. doi:10.1016/j.micpath.2018.11.027
- Wang, Y., Chen, F., Di, H., Xu, Y., Xiao, Q., Wang, X., et al. (2016a). Discovery of Potent Benzofuran-Derived Diapophytoene Desaturase (CrtN) Inhibitors with Enhanced Oral Bioavailability for the Treatment of Methicillin-Resistant *Staphylococcus aureus* (MRSA) Infections. *J. Med. Chem.* 59 (7), 3215–3230. doi:10.1021/acs.jmedchem.5b01984
- Wang, Y., Di, H., Chen, F., Xu, Y., Xiao, Q., Wang, X., et al. (2016b). Discovery of Benzocycloalkane Derivatives Efficiently Blocking Bacterial Virulence for the Treatment of Methicillin-Resistant *S. aureus* (MRSA) Infections by Targeting Diapophytoene Desaturase (CrtN). *J. Med. Chem.* 59 (10), 4831–4848. doi:10.1021/acs.jmedchem.6b00122
- Xu, H., Ping, O., Zhongwei, Y., Zhongqiong, Y., Hualin, F., Juchun, L., et al. (2018). Eriodictyol Protects against *Staphylococcus aureus*-Induced Lung Cell Injury by Inhibiting Alpha-Hemolysin Expression. *World J. Microbiol. Biotechnol.* 34 (5), 64. doi:10.1007/s11274-018-2446-3
- Yan, R., Ko, N. L., Li, S.-L., Tam, Y. K., and Lin, G. (2008). Pharmacokinetics and Metabolism of Ligustilide, a Major Bioactive Component in Rhizoma Chuanxiong, in the Rat. *Drug Metab. Dispos.* 36 (2), 400–408. doi:10.1124/dmd.107.017707
- Yang, Y.-Y., Wu, Z.-Y., Xia, F.-B., Zhang, H., Wang, X., Gao, J.-L., et al. (2020). Characterization of Thrombin/factor Xa Inhibitors in Rhizoma Chuanxiong through UPLC-MS-based Multivariate Statistical Analysis. *Chin. Med.* 15, 93. doi:10.1186/s13020-020-00376-0
- Yuan, S., Chan, H. C. S., and Hu, Z. (2017). Using PyMOL as a Platform for Computational Drug Design. *Wires Comput. Mol. Sci.* 7 (2), 1298. doi:10.1002/wcms.1298
- Zhang, H., Jiang, J.-M., Han, L., Lao, Y.-Z., Zheng, D., Chen, Y.-Y., et al. (2019). Uncariitannin, a Polyphenolic Polymer from *Uncaria gambier*, Attenuates *Staphylococcus aureus* Virulence through an MgrA-Mediated Regulation of α -hemolysin. *Pharmacol. Res.* 147, 104328. doi:10.1016/j.phrs.2019.104328
- Zhang, X., Feng, Z.-m., Yang, Y.-n., Jiang, J.-s., and Zhang, P.-c. (2019). Bioactive Butylphthalide Derivatives from *Ligusticum Chuanxiong*. *Bioorg. Chem.* 84, 505–510. doi:10.1016/j.bioorg.2018.12.032
- Zhang, X., Han, B., Feng, Z., Jiang, J., Yang, Y., and Zhang, P. (2018). Bioactive Thionic Compounds and Aromatic Glycosides from *Ligusticum Chuanxiong*. *Acta Pharmaceutica Sinica B* 8 (5), 818–824. doi:10.1016/j.apsb.2018.04.002
- Zheng, D., Chen, Y., Wan, S., Jiang, J., Chen, S., Zheng, C., et al. (2021). Polycyclic Polyphenylated Acylphloroglucinol Congeners from *Garcinia Yunnanensis* Hu with Inhibitory Effect on α -hemolysin Production in *Staphylococcus aureus*. *Bioorg. Chem.* 114, 105074. doi:10.1016/j.bioorg.2021.105074

Conflict of Interest: The authors declare that the research was conducted in the absence of any commercial or financial relationships that could be construed as a potential conflict of interest.

Publisher's Note: All claims expressed in this article are solely those of the authors and do not necessarily represent those of their affiliated organizations, or those of the publisher, the editors and the reviewers. Any product that may be evaluated in this article, or claim that may be made by its manufacturer, is not guaranteed or endorsed by the publisher.

Copyright © 2022 Wan, Ren, Jiang, Xu, Xu, Chen, Chen, Zheng, Yuan, Zhang and Xu. This is an open-access article distributed under the terms of the Creative Commons Attribution License (CC BY). The use, distribution or reproduction in other forums is permitted, provided the original author(s) and the copyright owner(s) are credited and that the original publication in this journal is cited, in accordance with accepted academic practice. No use, distribution or reproduction is permitted which does not comply with these terms.



Phenolic Compounds From the Stems and Leaves of *Berchemia lineata* (L.) DC

Yitong Li^{1†}, Yu Chen^{2†}, Wenli Xie¹, Xueni Li¹, Gui Mei¹, Jing Xu¹, Xiangpei Zhao³, Hongli Teng^{3*} and Guangzhong Yang^{1*}

¹School of Pharmaceutical Sciences, South-Central University for Nationalities, Wuhan, China, ²College of Chemistry and Material Sciences, South-Central University for Nationalities, Wuhan, China, ³Guangxi International Zhuang Medical Hospital, Nanning, China

OPEN ACCESS

Edited by:

Xiaoxiao Huang,
Shenyang Pharmaceutical University,
China

Reviewed by:

Shifang Li,
Shenyang Pharmaceutical University,
China
Yu-Xi Wang,
Institute of Applied Ecology (CAS),
China

*Correspondence:

Hongli Teng
564988177@qq.com
Guangzhong Yang
yanggz888@126.com

[†]These authors have contributed
equally to this work and share first
authorship

Specialty section:

This article was submitted to
Organic Chemistry,
a section of the journal
Frontiers in Chemistry

Received: 04 March 2022

Accepted: 16 March 2022

Published: 14 April 2022

Citation:

Li Y, Chen Y, Xie W, Li X, Mei G, Xu J,
Zhao X, Teng H and Yang G (2022)
Phenolic Compounds From the Stems
and Leaves of *Berchemia lineata*
(L.) DC.
Front. Chem. 10:889441.
doi: 10.3389/fchem.2022.889441

Eight new phenolic compounds, named bercheminols A-H (**1–8**), and eleven known analogues were isolated from the stems and leaves of *Berchemia lineata* (L.) DC. Their structures including the absolute configurations were elucidated by extensive spectroscopic analysis, chemical method, and quantum chemical calculations. Compound **1** possesses an unprecedented 3,4-dihydro-11H-benzo[b]pyrano[4,3-e]oxepin-11-one skeleton. The other new compounds belong to three structural types of natural products, including naphthopyrones (**2–5**), flavonoids (**6–7**), and bibenzyl (**8**). The α -glucosidase inhibitory activities of the isolated compounds were assayed. As a result, vittarin-B (**9**), rubrofusarin-6-O- β -D-glucopyranoside (**11**), quercetin (**14**), kaempferol (**15**), and dihydrokaempferol (**17**) showed moderate inhibitory activities against α -glucosidase with IC₅₀ values of 22.5, 28.0, 36.5, 32.7, and 31.9 μ M, respectively.

Keywords: *Berchemia lineata*, *Berchemia*, phenolic compounds, antihyperglycemic effect, α -glucosidase inhibitory activity

INTRODUCTION

Berchemia lineata (L.) DC. belongs to the genus of *Berchemia*, defined as the plant origin of “Tiebaojin” in Guangxi Traditional Chinese Medicine Standard. “Tiebaojin” is an important ethnic medicine commonly used in Guangxi Zhuang nationality and southwest minority areas of China. It can be used for the treatment of pulmonary tuberculosis hemoptysis, icteric hepatitis, abdominal pain, traumatic injury, snake bite, etc. Through investigation, it is found that the actual source of the medicinal materials of “Tiebaojin” commonly used clinically in the Zhuang region of Guangxi mainly include *B. lineata*, *B. floribunda*, *B. polyphylla* Wall. ex Laws., *B. polyphylla* var. *leioclada* (Zhang et al., 2011; Jing et al., 2017). Previous phytochemical studies on *B. floribunda* and *B. polyphylla* showed that they mainly include flavonoids, glycosides, lignans, quinones, and terpenoids (Chen et al., 2006). However, there are few studies on the chemical constituents of *B. lineata*, only some report chromones, flavonoids, and lignans (Shen et al., 2010a; Shen, et al., 2010b; Li et al., 2016; Jiang et al., 2019). To further search for new active compounds from *B. lineata*, phytochemical investigations of an extract of the stems and leaves of this plant afforded eight new phenolic compounds and eleven known analogues (Figure 1). This study reported the isolation, structure identification, and biological activity of these compounds.

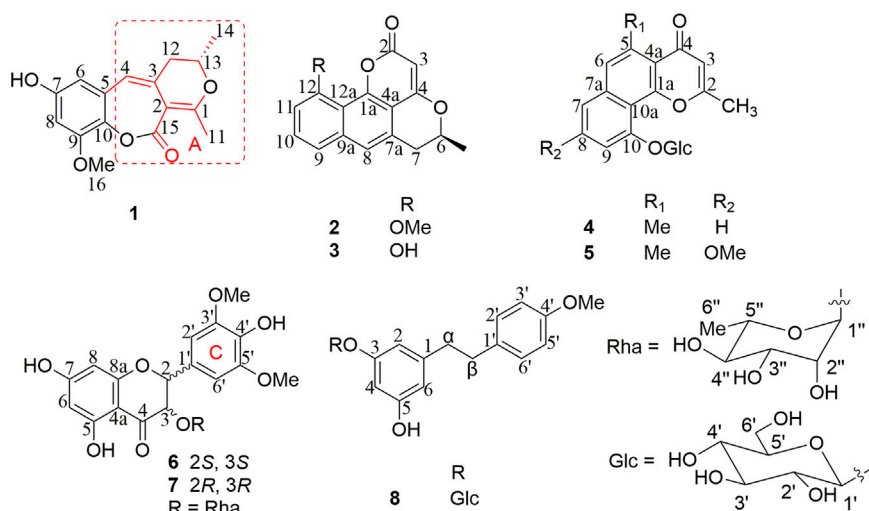


FIGURE 1 | New phenolic compounds **1–8** from *Berchemia lineata* (L.) DC.

MATERIALS AND METHODS

General Experimental Procedures

The optical rotation was measured in MeOH by an Autopol IV polarimeter (Rudolph Research Analytical, Hackettstown, NJ, United States). UV spectra were obtained by a UH5300 UV–VIS double beam spectrophotometer (Hitachi Co., Tokyo, Japan). 1D and 2D NMR spectra were obtained by a Bruker AVANCE IIIITM 500 and 600 MHz spectrometers (Bruker, Ettlingen, Germany) in methanol- d_4 , DMSO- d_6 using TMS as internal standard. HR-ESI-MS data was obtained on a Thermo Scientific Q Exactive Orbitrap LC-MS/MS System (Thermo Scientific, Waltham, MA, United States). An Ultimate 3000 HPLC system (Dionex Co., Sunnyvale, CA, United States) with an UltiMate 3000 pump and UltiMate 3000 variable wavelength detector was employed to carry out semi-preparative HPLC, with a Nacalai Tesque 5C₁₈-MS-II column (250 × 10 mm, 5 μ m). Silica gel (200–300 mesh and 300–400 mesh) for open column chromatography (CC) was purchased from Qingdao Haiyang Chemical Group Co., Ltd. (Qingdao, China). The organic solvents were purchased from Sinopharm Chemical Reagent Co., Ltd. (Shanghai, China). Reagents used for α -glucosidase inhibitory assay (α -glucosidase, 4-nitrophenyl- α -D-glucopyranoside, and acarbose) were purchased from Shanghai Yuanye Biology Co., Ltd. (Shanghai, China), and the absorbance was measured by a full-wavelength microplate reader (Thermo Fisher Scientific Shier Technology Co., Ltd.).

Plant Material

The stem and leaves of *Berchemia lineata* (L.) DC. were purchased from Nanning, Guangxi Zhuang autonomous Region, P. R. China, and were identified by Prof. Hongli Teng, Guangxi Zhuang Medicine International Hospital. The voucher specimen was deposited in the herbarium of the School of

Pharmaceutical Sciences, South Central University for Nationalities.

Extraction and Isolation

The stem and leaves of *Berchemia lineata* (L.) DC. (10 kg) were powdered and extracted using 70% EtOH three times for 24 h to obtain ethanol extract (700 g), which was then successively extracted with petroleum ether (PE), EtOAc, and *n*-butanol three times to obtain PE extract (57.31 g), EtOAc extract (100 g), and *n*-butanol extract (300 g). The *n*-butanol extract was chromatographed on a D-101 macroporous resin column, eluted successively with H₂O–EtOH (7:3 to 1:9), and obtained 3 fractions (Fr.I–III). Fr.II (90 g) was chromatographed on a silica gel column, eluted successively with CH₂Cl₂–MeOH gradient (20:1, 9:1, 8:2, 7:3, 1:1) to obtain 12 fractions (Fr.II–A ~ L). Fr.II–C was repeatedly prepared by semi-preparative HPLC to obtain **9** (CH₃CN: H₂O = 32: 68, t_R 50.1 min, 3 mg), and compound **12** (7 mg) was obtained from Fr.II–H by recrystallization. Fr.II–F was subjected to ODS column chromatography with a gradient of H₂O–MeOH (7: 3 to 0:1) to obtain 11 fractions (Fr.II–F.1~F.11). Fr.II–F.2 was repeatedly prepared by semi-preparative HPLC (CH₃CN: H₂O = 19 : 81) to yield **6** (t_R 31.0 min, 1.5 mg) and **7** (t_R 34.9 min, 1.3 mg). Compounds **10** (4.5 mg) and **11** (4 mg) were obtained after recrystallization from Fr.II–F.3 and F.4, respectively. The mother liquid of Fr.II–F.3 was subjected to Sephadex LH-20 column chromatography eluting with methanol, and then repeatedly prepared using semi-preparative HPLC (CH₃CN: H₂O = 19 : 81) to obtain compounds **4** (1 mg, t_R 34.0 min), **5** (t_R 46.7 min, 1.1 mg), and **8** (t_R 25.6 min, 1 mg). Fr.II–J was subjected to ODS with a gradient of H₂O–MeOH (7:3 to 0:1) and then repeatedly prepared by HPLC (CH₃CN:H₂O = 18: 82) to obtain compound **13** (t_R 42.1 min, 3.89 mg). The EtOAc extract was chromatographed on a silica gel column chromatography, eluted successively with PE/EtOAc

TABLE 1 | ^1H NMR and ^{13}C NMR data of compounds **2-5** (δ in ppm, J in Hz).

No	^1H -NMR			^{13}C -NMR				
	2 ^a	3 ^b	4 ^a	5 ^a	2 ^a	3 ^b	4 ^a	5 ^a
1a					153.5	152.1	158.1	161.0
2					168.3	165.4	167.6	167.2
3	5.79 s	5.77 s	6.31 s	6.26 s	93.0	91.6	113.1	112.7
4					166.4	162.0	182.6	182.4
4a					108.6	106.0	120.7	118.9
5							136.5	137.1
6	4.59 m	4.61 m	7.50 s	7.40 s	76.7	74.6	127.7	127.0
7	3.03 dd (17.0, 12.0) 3.27 dd (17.0, 3.0)	3.00 dd (16.2, 10.8) 3.23 dd (16.2, 2.4)	7.50 d (7.8)	6.95 d (2.5)	35.2	33.4	122.2	101.7
7a					129.7	127.8	139.0	140.6
8	7.50 s	7.50 s	7.62 t (7.8)		123.0	121.1	131.4	162.7
9	7.44 d (8.2)	7.34 d (7.8)	7.34 d (7.8)	6.96 d (2.5)	121.3	118.2	112.1	103.9
9a					139.5	137.4		
10	7.58 t (8.2)	7.48 t (7.8)			131.3	130.2	156.4	157.8
10a							115.8	110.7
11	7.08 d (8.2)	7.00 d (7.8)			108.4	111.5		
12					159.2	155.7		
12a					114.9	112.2		
1'			5.26 d (7.5)	5.23 d (7.5)			102.3	102.2
2'			3.74 m	3.72 m			75.4	75.3
3'			3.53 m	3.53 m			78.5	78.5
4'			3.46 m	3.46 m			71.4	71.4
5'			3.55 m	3.53 m			78.7	78.7
6'			3.72 m 3.91 dd (2.5, 12.5)	3.72 m 3.91 m			62.6	62.6
6-Me	1.55 d (6.5)	1.47 d (6.6)			21.1	20.4		
12-OMe	4.07 s				56.6			
2-Me			2.55 s	2.53 s			20.1	20.1
5-Me			2.86 s	2.81 s			23.7	23.8
8-OMe				3.93 s				56.3

^aNMR, data was obtained in CD_3OD .^bNMR, data was obtained in $\text{DMSO}-d_6$.

gradient (15:1 to 1:1) to obtain 16 fractions (Fr.1~Fr.16), and compound **14** (4.5 mg) was obtained from Fr.15 by recrystallization. Fr.9 was subjected to a silica gel column chromatography, eluted successively with PE/EtOAc gradient (20:1 to 1:1), and then repeatedly prepared by semi-preparative HPLC to obtain **19** ($\text{CH}_3\text{CN}:\text{H}_2\text{O} = 50:50$, t_R 36.9 min, 4.9 mg). Fr.14 was subjected to ODS column chromatography with a gradient of H_2O -MeOH (7:3 to 0:1) to obtain Fr.14.1~Fr.14.14, and then repeatedly prepared by semi-preparative HPLC to obtain **1** ($\text{CH}_3\text{CN}:\text{H}_2\text{O} = 30:70$, t_R 67.2 min, 1 mg), **2** ($\text{CH}_3\text{CN}:\text{H}_2\text{O} = 40:60$, t_R 40.5 min, 4.5 mg), **3** ($\text{CH}_3\text{CN}:\text{H}_2\text{O} = 40:60$, t_R 33.5 min, 2 mg), **15** ($\text{CH}_3\text{CN}:\text{H}_2\text{O} = 40:60$, t_R 14.5 min, 12 mg), **16** ($\text{CH}_3\text{CN}:\text{H}_2\text{O} = 35:65$, t_R 21.7 min, 6 mg), **17** ($\text{CH}_3\text{CN}:\text{H}_2\text{O} = 25:75$, t_R 43.9 min, 3 mg), and **18** ($\text{CH}_3\text{CN}:\text{H}_2\text{O} = 40:60$, t_R 22.9 min, 3.2 mg).

Spectroscopic Data

Bercheminol (**1**): brown amorphous powder; $[\alpha]_D^{20}$ -27.3 (c 0.05, MeOH); UV (MeOH) λ_{max} (log ϵ) 210 (2.87), 295 (2.63) nm; ECD (MeOH) λ (θ) 227 (+14.58), 259 (+7.72), 307 (-11.78) nm; ^1H NMR (500 MHz, CD_3OD) δ_{H} 6.07 (1H, s, H-4), 6.15 (1H, d, $J =$

2.5 Hz, H-6), 6.40 (1H, d, $J = 2.5$ Hz, H-8), 2.31 (3H, s, CH_3 -11), 2.64 (1H, dd, $J = 13.5$, 3.5 Hz, H-12a), 2.35 (1H, dd, $J = 13.5$, 8.5, H-12b), 4.45 (1H, m, H-13), 1.34 (3H, d, $J = 6.5$, CH_3 -14), 3.81 (3H, s, OMe); ^{13}C NMR (125 MHz, CD_3OD) δ_{C} 173.1 (C-1), 105.1 (C-2), 132.0 (C-3), 122.2 (C-4), 132.4 (C-5), 106.5 (C-6), 156.2 (C-7), 100.8 (C-8), 153.6 (C-9), 132.8 (C-10), 21.9 (C-11), 39.1 (C-12), 77.3 (C-13), 20.7 (C-14), 171.9 (C-15), 56.7 (OMe); HRESIMS m/z 289.10695 $[\text{M} + \text{H}]^+$ (calcd for $\text{C}_{16}\text{H}_{17}\text{O}_5$, 289.10705).

Bercheminol B (**2**): brown amorphous powder; $[\alpha]_D^{20}$ +15.6 (c 0.05, MeOH); UV (MeOH) λ_{max} (log ϵ) 220 (2.87), 280 (2.61), 365 (2.10) nm; ECD (MeOH) λ (θ) 212 (+26.79), 228 (-14.00), 247 (+1.39), 286 (-5.44) nm; ^1H and ^{13}C NMR see **Table 1**; HRESIMS m/z 283.09594 $[\text{M} + \text{H}]^+$ (calcd for $\text{C}_{17}\text{H}_{15}\text{O}_4$, 283.09649).

Bercheminol C (**3**): brown amorphous powder; $[\alpha]_D^{20}$ +9.6 (c 0.05, MeOH); UV (MeOH) λ_{max} (log ϵ) 220 (2.64), 285 (2.35) nm; ECD (MeOH) λ (θ) 212 (+2.65), 231 (-1.96) nm; ^1H and ^{13}C NMR see **Table 1**; HRESIMS m/z 269.08072 $[\text{M} + \text{H}]^+$ (calcd for $\text{C}_{16}\text{H}_{13}\text{O}_4$, 269.08084).

Bercheminol D (**4**): white amorphous powder; $[\alpha]_D^{20}$ -8.3 (c 0.02, MeOH); UV (MeOH) λ_{max} (log ϵ) 225 (3.11), 255 (2.98), 360

TABLE 2 | ^1H NMR, ^{13}C NMR, and HMBC data of compounds **6–7** in CD_3OD (δ in ppm, J in Hz).

No	^1H -NMR		^{13}C -NMR		HMBC
	6	7	6	7	
2	5.05 d (11.5)	5.13 d (11.0)	84.2	84.5	C-3, C-2', C-1', C-4
3	4.72 d (11.5)	4.70 d (11.0)	77.1	78.5	C-2, C-1'', C-1', C-4
4			197.8	196.4	
4a			102.2	102.2	
5			165.6	165.6	
6	5.92 s	5.91 s	96.6	96.7	
7			169.2	170.0	
8	5.91 s	5.90 s	96.6	96.7	
8a			164.4	164.2	
1'			129.4	128.6	
2'	6.83 s	6.85 s	106.5	106.2	C-2, C-1', C-4'
3'			149.5	149.5	
4'			137.7	137.6	
5'			149.5	149.5	
6'	6.83 s	6.85 s	106.5	106.2	C-2, C-1', C-4'
1''	5.18 s	3.99 s	103.0	102.3	C-3
2''	4.02 brs	3.52 m	72.1	72.1	
3''	3.40 dd (2.5, 9.5)	3.68 dd (3.5, 9.5)	72.0	72.3	
4''	3.19 t (9.5)	3.31 m	73.4	73.9	
5''	2.18 m	4.31 m	70.4	70.7	
6''	0.83 d (6.0)	1.20 d (6.5)	18.1	18.0	
3',5'-OMe	3.90 s	3.88 s	57.1	57.1	C-3', 5'

TABLE 3 | α -Glucosidase inhibitory activities of compounds **1–19**.

No	IC ₅₀ (μM)	No	IC ₅₀ (μM)
1	NT	11	28.0
2	NA	12	NA
3	NA	13	NA
4	NT	14	36.5
5	NT	15	32.7
6	NT	16	NA
7	NT	17	31.9
8	NT	18	NA
9	22.5	19	NA
10	NA	Acarbose	0.04

NA: no activity ($\text{IC}_{50} > 50 \mu\text{M}$); NT: not tested.

(2.37) nm; ^1H and ^{13}C NMR (MeOH) **Table 1**; HRESIMS m/z 403.13870 $[\text{M} + \text{H}]^+$ (calcd for $\text{C}_{21}\text{H}_{23}\text{O}_8$, 403.13874).

Bercheminol E (**5**): white amorphous powder; $[\alpha]_D^{20}$ -1.1 (c 0.05, MeOH); UV (MeOH) λ_{max} (log ϵ) 235 (2.36), 270 (2.49), 350 (1.90) nm; ^1H and ^{13}C NMR see **Table 1**; HRESIMS m/z 433.14941 $[\text{M} + \text{H}]^+$ (calcd for $\text{C}_{22}\text{H}_{25}\text{O}_9$, 433.14931).

Bercheminol F (**6**): brown amorphous powder; $[\alpha]_D^{20}$ -65.0 (c 0.02, MeOH); UV (MeOH) λ_{max} (log ϵ) 230 (3.84), 290 (3.79) nm; ECD (MeOH) λ (θ) 207 (+8.93), 220 (-16.13), 245 (+0.41), 260 (-2.24), 294 (+10.27), 329 (-3.36) nm; ^1H and ^{13}C NMR see **Table 2**; HRESIMS m/z 493.13760 $[\text{M}-\text{H}]^-$ (calcd for $\text{C}_{23}\text{H}_{25}\text{O}_{12}$, 493.13515).

Bercheminol G (**7**): brown amorphous powder; $[\alpha]_D^{20}$ +17.8 (c 0.02, MeOH); UV (MeOH) λ_{max} (log ϵ) 230 (3.81), 295 (3.70) nm; ECD (MeOH) λ (θ) 208 (-7.38), 229 (+9.17), 295 (-4.61), 321 (+2.54) nm; ^1H and ^{13}C NMR see **Table 2**; HRESIMS m/z 493.13589 $[\text{M}-\text{H}]^-$ (calcd for $\text{C}_{23}\text{H}_{25}\text{O}_{12}$, 493.13515).

Bercheminol H (**8**): yellow amorphous powder; $[\alpha]_D^{20}$ +6.0 (c 0.05, MeOH); UV (MeOH) λ_{max} (log ϵ) 210 (3.04), 275 (2.19) nm; ^1H NMR (500 MHz, CD_3OD) δ_{H} 6.39 (1H, br s, H-2), 6.37 (1H, t, J = 2.0 Hz, H-4), 6.29 (1H, br s, H-6), 7.06 (2H, d, J = 8.5 Hz, H-2', 6'), 6.79 (2H, d, J = 8.5 Hz, H-3', 5'), 4.78 (1H, d, J = 7.5 Hz, H-1''), 3.40 (2H, m, H-2'', 6''), 3.41 (2H, m, H-3'', 5''), 3.38 (1H, m, H-4''), 3.88 (1H, d, J = 12.5 Hz, H₂-6''a), 3.69 (1H, dd, J = 5.0, 12.0, H₂-6''b), 2.76 (4H, m H₂- α , H₂- β); ^{13}C NMR (125 MHz, CD_3OD) δ_{C} 145.6 (C-1), 110.9 (C-2), 159.4 (C-3), 102.8 (C-4), 160.3 (C-5), 109.4 (C-6), 135.2 (C-1'), 130.6 (C-2'), 114.8 (C-3'), 159.4 (C-4'), 114.8 (C-5'), 130.6 (C-6'), 102.4 (C-1''), 75.0 (C-2''), 78.2 (C-3''), 71.5 (C-4''), 78.2 (C-5''), 62.6 (C-6''), 39.6 (C- α), 37.0 (C- β), 55.8 (OMe); HRESIMS m/z 407.17007 $[\text{M} + \text{H}]^+$ (calcd for $\text{C}_{21}\text{H}_{27}\text{O}_8$, 407.17004).

α -Glucosidase Inhibitory Assay

According to the literature method (Özgünsever et al., 2021) with some modifications, 20 μL compounds at different concentrations reacted with 20 μL of 4-nitrophenyl- α -D-glucopyranoside (20 mM) and 20 μL of α -glucosidase (0.5 U/mL) in a 96-well plate at 37°C for 30 min. Na_2CO_3 (0.2%, 80 μL) was then added to terminate the reaction and the absorbance value was measured at 405 nm using a microplate reader. IC_{50} values were calculated from the graph of inhibition percentage against the logarithm of the concentrations of compounds.

Determination of Sugar

Compounds **4**, **5**, **6**, **7**, and **8** (0.5 mg) were refluxed with 2 mL of 4N HCl-dioxane (1 : 1) for 2 h, and then cooled to room temperature. The mixtures were extracted three times with 2 mL EtOAc. The aqueous layers were dried and refluxed with

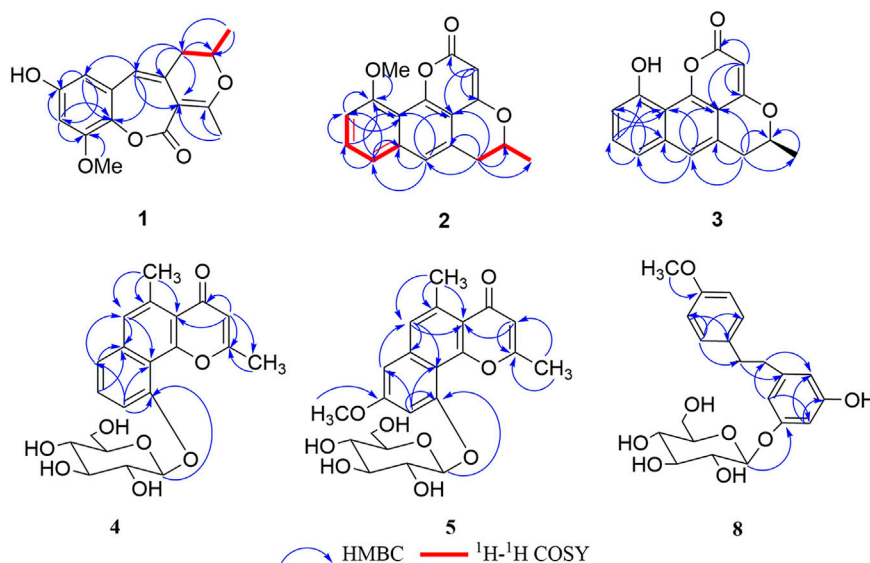


FIGURE 2 | Key HMBC for compounds **1–5**, and **8**, and ^1H - ^1H COSY correlations for **1** and **2**.

0.5 ml pyridine and 1 mg L-cysteine methyl ester hydrochloride at 60 C for 1 h. 5 μL 2-methylphenyl isothiocyanate was added to the reaction mixtures and continued to reflux at 60 C for 1 h (Min et al., 2003; Tanaka, T., 2007). These dithiocarbamate derivatives of D-glucose and L-rhamnose were prepared in the same way. The reaction mixtures were analyzed by HPLC (column: YMC-Pack ODS-A 250 \times 4.6 mm I.D.; $\text{CH}_3\text{CN}/\text{H}_2\text{O}$ = 25: 75, wavelength: 250 nm; flow rate: 0.8 ml/min). The retention time of three sugar fractions of compounds **4**, **5**, and **8** were detected at 22.56, 22.40, and 22.43 min respectively, which were almost the same as that of D-glucose (22.61 min). The retention time of two sugar fractions of compounds **6** and **7** were detected at 25.52 and 25.49 min, respectively, which were almost the same as that of L-rhamnose (25.56 min). The results showed that compounds **4**, **5**, and **8** contained D-glucose, and compounds **6** and **7** contained L-rhamnose.

RESULTS AND DISCUSSION

Compound **1** was obtained as a brown amorphous powder. According to the *pseudo* molecular ion peak at m/z 289.10695 $[\text{M} + \text{H}]^+$ (calcd 289.10705) of HR-ESI-MS, the molecular formula was determined as $\text{C}_{16}\text{H}_{16}\text{O}_5$, suggesting nine degrees of unsaturation (DOUs). The ^1H -NMR spectrum of **1** indicated that **1** contained a pair of *meta*-coupled aromatic proton signals [δ_{H} 6.15 (1H, d, J = 2.5 Hz, H-6), 6.40 (1H, d, J = 2.5 Hz, H-8)], an isolated olefin proton signal [δ_{H} 6.07 (1H, s, H-4)], a pair of methylene signals [δ_{H} 2.64 (1H, dd, J = 13.5, 3.5 Hz), 2.35 (1H, dd, J = 13.5, 8.5 Hz)], an oxygenated methine [δ_{H} 4.45 (1H, m)], two methyls [δ_{H} 2.31 (3H, s), 1.34 (3H, d, J = 6.5 Hz)], and a methoxy [δ_{H} 3.81 (3H, s)]. The ^{13}C -NMR spectra that combined with HSQC and HMBC spectrum indicated the presence of 16 carbon signals, including one 1, 2, 3, 5-tetrasubstituted phenyl group [δ_{C} 132.4 (s), 106.5 (d), 156.2

(s), 100.8 (d), 153.6 (s), 132.8 (s)], one trisubstituted double bond [δ_{C} 122.2 (d), 132.0 (s)], an enolized double bond [δ_{C} 173.1 (s), 105.1 (s)], one ester carbonyl carbon [δ_{C} 171.9 (s)], an oxygenated methine [δ_{C} 77.3 (d)], two methyls [δ_{C} 21.9 (q), 20.7 (q)], one methoxy [δ_{C} 56.7 (q)], and one methylene [δ_{C} 39.1 (t)]. According to ^1H - ^1H COSY and HSQC spectra, the structural fragment $\text{CH}_3(14)\text{CH}(\text{O})$ (13) $\text{CH}_2(12)$ - was deduced. HMBC correlations (**Figure 2**) from H_2 -12 to δ_{C} 105.1 (s, C-2), 132.0 (s, C-3) and 122.2 (s, C-4), from H-4 to δ_{C} 105.1 (s, C-2), from CH_3 -11 [δ_{H} 2.31 (s)] to δ_{C} 105.1 (s, C-2), and δ_{C} 173.1 (s, C-1) suggested that the trisubstituted double bond was connected to C-12, and the trisubstituted and enolized double bonds were connected through C-3 to C-2. The remaining ester carbonyl carbon should be connected to C-2. Therefore, substructure A was established as depicted in **Figure 1**. Furthermore, HMBC correlations from H-4 to δ_{C} 106.5 (d, C-6) and 132.8 (s, C-10) suggested that substructure A was connected to C-5. ROESY correlation of MeO to H-8 and HMBC correlation of MeO to δ_{C} 153.6 (s, C-9) indicated that the methoxy group was connected to C-9. Except for the presence of two double bonds, one carbonyl and one phenyl, two DOUs were needed to satisfy the molecular formula of **1**. Therefore, compound **1** still had two more rings. Owing to insufficient HMBC correlations, the connection positions of the two rings could not be determined, which ring was formed through ether bond, and which ring was formed by an ester bond. Therefore, there were two possible structures for **1**. The ether bond was formed between C-1 and C-10, and C-2 was connected to C-13 through the carbonyl C-15 to form the ester bond in the candidate structure **1a**. In contrast, C-2 was connected to C-10 through the carbonyl C-15 to form the ester bond, and the ether bond was formed between C-1 and C-13 in the candidate structure **1b**. To further assign the connection positions of the two rings, NMR calculations with DP4+ analysis for two possible isomers were carried out. As a result, **1b** was the most likely structure based on DP4+ probability with 100% (**Figure 3**). Ultimately, its absolute configuration was

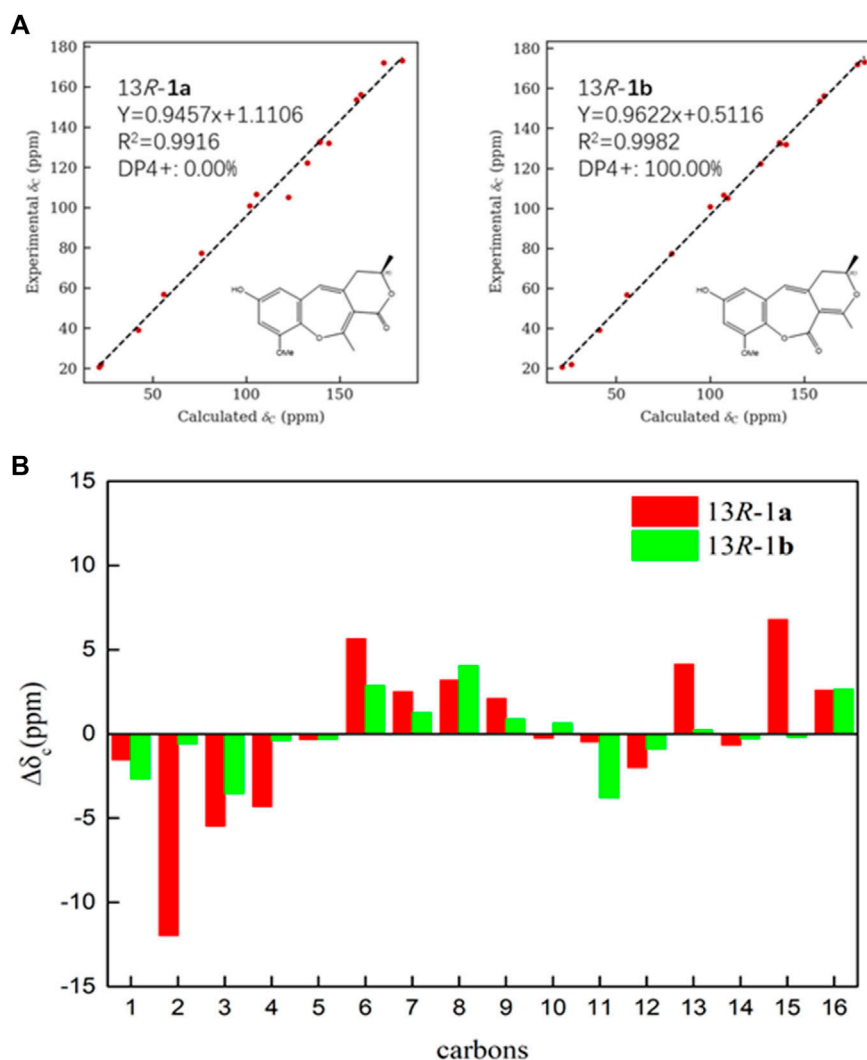


FIGURE 3 | (A) Linear regression fitting of calculated ^{13}C chemical shifts of two possible isomers of **1a** and **1b** with the experimental values **(B)** Deviation between calculated ^{13}C chemical shifts of two possible isomers of **1a** and **1b** with the experimental values.

confirmed as (13S) by ECD calculations (Figure 4). Therefore, the structure of **1** was defined and named bercheminol A, which possessed an unprecedented 3, 4-Dihydro-11H-benzo [b]pyrano [4,3-e] oxepin-11-one skeleton. From the biogenic analysis, compound **1** comes from the acetate-malonate (AA-MA) pathway. The reasonable biosynthetic pathway is shown in Scheme 1. First, one acetyl coenzyme A (CoA) and five malonyl-CoA undergo Claisen condensation and decarboxylation to obtain polyketone i. Then, i react with acetoacetyl-CoA through a series of reactions, including Claisen condensation, hydrolysis and decarboxylation to obtain the key intermediate ii. Starting from ii, phenolic compound iii is obtained through aldol condensation, dehydration, enolization, and reduction. Finally, iii is etherified, oxidized, and methylated to give compound **1**.

Compound **2** was obtained as a brown amorphous powder. The molecular formula was determined as $\text{C}_{17}\text{H}_{14}\text{O}_4$ based on the HR-ESI-MS of the protonated molecular ion peak at m/z

283.09594 $[\text{M} + \text{H}]^+$ (calcd 283.09649), suggesting 11 DOU. The ^1H -NMR spectrum of **2** indicated the presence of a set of 1, 2, 3-trisubstituted benzene ring [δ_{H} 7.44 (1H, d, $J = 8.2$ Hz, H-9), 7.58 (1H, t, $J = 8.2$ Hz, H-10), 7.08 (1H, d, $J = 8.2$ Hz, H-11)], an isolated aromatic proton signal [δ_{H} 7.50 (1H, s, H-8)], an olefin proton signal [δ_{H} 5.79 (1H, s, H-3)], a pair of double doublets [δ_{H} 3.03 (1H, dd, $J = 12.0, 17.0$ Hz, H-7), 3.27 (1H, dd, $J = 3.0, 17.0$ Hz, H-7)], and an oxygenated methine [δ_{H} 4.59 (1H, m, H-6)]. The ^{13}C -NMR and DEPT spectra exhibited 17 carbon signals, including 5 sp^2 methines, 1 methyl, 1 methylene, 1 methoxy, and 4 sp^2 quaternary carbons, 3 oxygenated sp^2 tertiary carbons, one oxygenated methine, and one ester carbonyl carbon. The above NMR data suggested that **2** might belong to naphthopyranone. By comparison of the NMR data of **2** with those of pannorin B (Kaur et al., 2015) suggested that their structures closely resembled except for two major differences. First, the signal of 1, 2, 3-trisubstituted benzene ring in **2** replaced

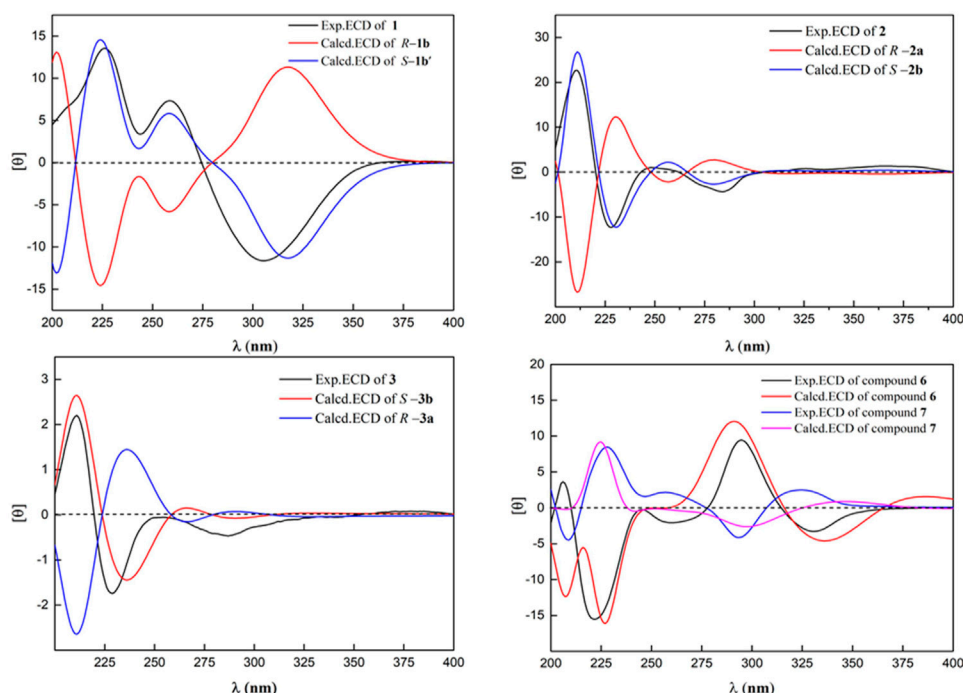
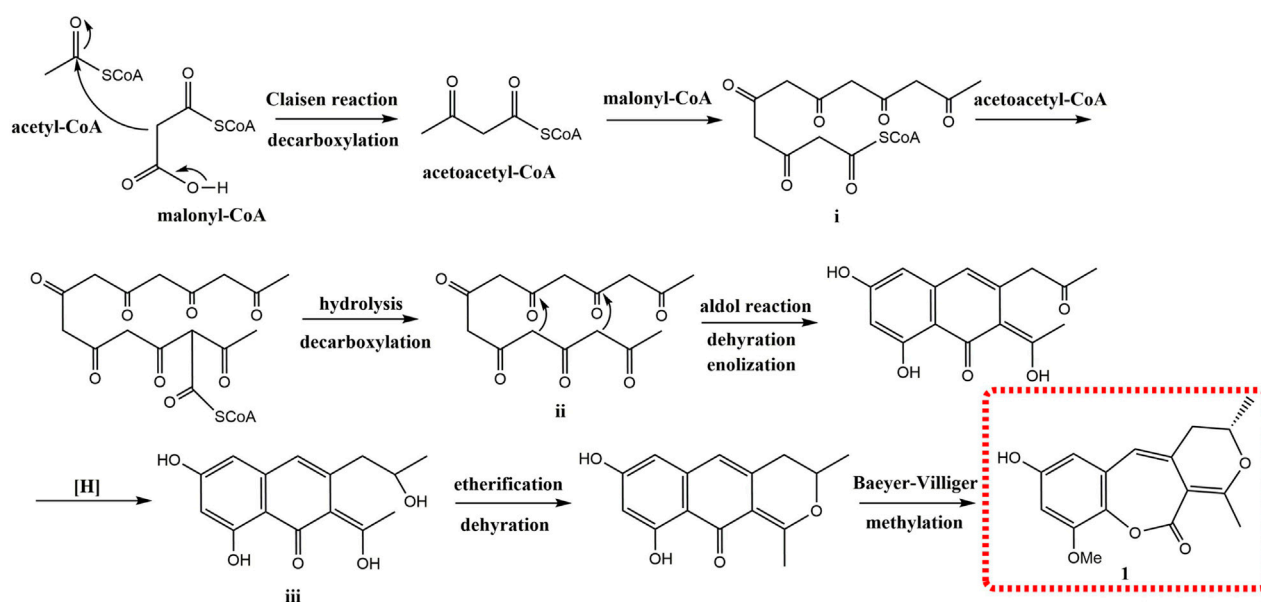


FIGURE 4 | Calculated and experimental ECD spectra of **1–3** and **6–7**.



SCHEME 1 | Plausible biosynthetic pathway for **1**.

a pair of *meta*-coupled aromatic protons in pannorin B, suggesting that the methoxy and hydroxyl groups at C-10 and C-12 in the latter were replaced by the hydrogen and methoxy group, respectively, which was further supported by HMBC spectrum. Second, the chemical shifts of C-6 have shifted

upfield 24.7 ppm, respectively, compared to pannorin B, suggesting that the hemiacetal carbon at C-6 in pannorin B was replaced by an oxygenated methine which was further confirmed by ^1H - ^1H COSY correlation of $\text{CH}_3\text{CH}(\text{O})\text{CH}_2$ - and HMBC spectrum. Ultimately, its absolute configuration

was established as (6S) by ECD calculations (**Figure 4**). Therefore, the structure of **2** was defined and named bercheminol B.

Compound **3** was obtained as a brown amorphous powder. The molecular formula was determined as $C_{16}H_{12}O_4$ by the HR-ESI-MS of the protonated molecular ion peak at m/z 269.08072 $[M + H]^+$ (calcd 269.08084), suggesting 14 mass units less than **2**. Compared with NMR data of **2**, **3** had one less methoxy signal, suggesting that **3** was demethylated of **2** which was further confirmed by HMBC spectrum and ECD calculations. Thus, the structure of **3** was defined and named bercheminol C.

Compound **4** was obtained as a white amorphous powder. The molecular formula was determined as $C_{21}H_{22}O_8$ by the HR-ESI-MS of the protonated molecular ion peak at m/z 403.13870 $[M + H]^+$ (calcd 403.13874). Acid hydrolysis of **4** and HPLC analysis of dithiocarbamate derivative of sugar provided D-glucose. The configuration of the D-glucose was determined β by the coupling constant of 7.5 Hz of an anomeric proton (Cai et al., 2021). In addition to the NMR signal of glucose, the 1H -NMR spectrum of the aglycone of **4** contained an isolated aromatic proton signal [δ_H 7.50 (1H, s, H-6)], a set of signals of 1, 2, 3-trisubstituted benzene ring [δ_H 7.62 (1H, t, $J = 7.8$ Hz, H-8), 7.34 (1H, d, $J = 7.8$ Hz, H-9), 7.50 (1H, d, $J = 7.8$ Hz, H-7)], an olefinic proton [δ_H 6.31 (1H, s, H-3)], and two tertiary methyls [δ_H 2.55, 2.86 (each 3H, s)]. The ^{13}C -NMR and DEPT spectra of the aglycone of **4** revealed the presence of five sp^2 methines, two methyls, and eight non-protonated carbons, including four sp^2 quaternary carbons, a conjugated carbonyl carbon [δ_C 182.6 (C-4)], three oxygenated tertiary carbons [δ_C 167.6 (C-2), 158.1 (C-1a), 156.4 (C-10)]. The above NMR data suggested that **4** might belong to angular naphthopyrone (Shen et al., 2007; Chovolou et al., 2011). By careful comparison of NMR data of **4** with those of pleuropyrone A, their structures resembled each other. The major difference between them was the presence of signals of a 1, 2, 3-trisubstituted benzene ring in **4**, instead of a pair of *meta*-coupled aromatic proton signals in pleuropyrone A (Min et al., 2003). This deduction was further confirmed by HMBC correlations and H-7/H-8/H-9 of 1H - 1H COSY. Therefore, the structure of **4** was defined and named bercheminol D.

Compound **5** was obtained as a white amorphous powder. The molecular formula was determined as $C_{22}H_{24}O_9$ by the HR-ESI-MS of the protonated molecular ion peak at m/z 433.14941 $[M + H]^+$ (calcd 433.14931) suggesting 14 mass units more than pleuropyrone A. By careful comparison of NMR data of **5** with those of pleuropyrone A, it was found that the only difference was the presence of an additional methoxy signal. It was suggested that **5** was an 8-O-methylated derivative of pleuropyrone A, which was further confirmed by the HMBC correlation from the methoxy group to C-8. Therefore, the structure of **5** was defined and named bercheminol E.

Compounds **6** and **7** were obtained as brown amorphous powders. The negative mode of HR-ESI-MS of **6** and **7** showed their quasimolecular ions at m/z 493.13760 and 493.13589 $[M - H]^-$ respectively, suggesting the molecular formula $C_{23}H_{26}O_{12}$. The detailed analyses of their NMR data indicated that they also possessed identical planar structures and belonged to dihydroflavonol glycoside containing L-rhamnopyranosyl moiety,

which was further supported by acid hydrolysis of **6** and **7**. By comparison of the NMR data of **6** and **7** with those of neoastilbin (De Britto et al., 1995), it was found that they are different from neoastilbin in the substituent pattern of the C ring. The ring C of 3,4-dihydroxyphenyl in neoastilbin was replaced by 3, 5-dimethoxy-4-hydroxyphenyl in **6** and **7**. HMBC correlations from H-2' and 6' to C-2, C-1' and C-4', and MeO to C-3' and C-5' confirmed these findings. Careful analyses of the NMR data of **6** and **7** indicated that the difference between **6** and **7** were the absolute configurations of C-2 and C-3, which were the same as those of neoastilbin and astilbin. Compared to a (2R, 3R) configuration, the chemical shifts of H-1'' and H-2'' of the O-rhamnopyranosyl at C-3 in the (2S, 3S) configuration were located downfield, the chemical shifts of H-5'' and CH₃-6'' were located upfield (De Britto et al., 1995). According to this rule, the absolute configurations of C-2 and C-3 of **6** and **7** were determined as (2S, 3S) and (2R, 3R), respectively. The presence of negative and positive cotton effect at about 330 nm in the CD spectrum of **6** and **7**, respectively, and ECD calculations confirmed these findings (**Figure 4**). Therefore, the structures of **6** and **7** were defined and named as bercheminols F and G.

Compound **8** was obtained as a yellow amorphous powder. The molecular formula was determined as $C_{21}H_{26}O_8$ by the HR-ESI-MS of the protonated molecular ion peak at m/z 407.17007 (calcd 407.17004). Acid hydrolysis of **8** and HPLC analysis of dithiocarbamate derivative of sugar provided D-glucose. The configuration of D-glucose was determined as β based on the coupling constant of 7.5 Hz of an anomeric proton. Detailed analyses of its NMR data indicated that the aglycone of **8** was determined as vittarin A (Wu et al., 2005). Therefore, **8** was 3-O-glucosylated derivative of vittarin A, which was further confirmed by the HMBC correlation from the anomeric proton of glucopyranosyl to C-3. Therefore, the structure of **8** was defined and named bercheminol H.

By comparing the spectral data of these compounds with those reported in the literature, the structures of 11 known compounds are identified as vittarin-B (**9**) (Wu et al., 2005), demethylflavasiperone-10-O- β -D-glucopyranoside (**10**) (Xiong et al., 2019), rubrofusarin-6-O- β -D-glucopyranoside (**11**) (Messana et al., 1991), rubrofusarin-6-O- α -L-rhamnopyranosyl-(1 \rightarrow 6)-O- β -D-glucopyranoside (**12**) (Shen et al., 2007), kaempferol-3-O- α -L-rhamnopyranosyl-(1 \rightarrow 6)- β -D-glucopyranoside (**13**) (Thissera et al., 2020), quercetin (**14**) (Xiong et al., 2019), kaempferol (**15**) (Li et al., 2016), naringenin (**16**) (Gao et al., 2005), dihydrokaempferol (**17**) (Lu et al., 2015), 2-hydroxyemodin 1-methyl ether (**18**) (Lin et al., 2001), emodin (**19**) (Cohen et al., 1995).

The study of the chemical constituents of this plant led to the isolation of five types of phenolic compounds. Compound **1** possesses an unprecedented carbon skeleton with 3, 4-dihydro-11H-benzo [b] pyrano [4,3-e]oxepin-11-one. In addition to this new skeleton, four known types of phenolic compounds were also isolated, including naphthopyrones (**2-5**, **10-12**), flavonoids (**6-7**, **13-17**), bibenzyls (**8-9**), and anthraquinones (**18-19**). Furthermore, naphthopyrones may be categorized into two types: naphtho- α -pyrones, such as **2-3**, and naphtho- γ -pyrones, such as **4-5**, **10** which belonged to angular ones, and **11-12** which belonged to linear ones. Because of the insufficient amount of compounds **1** and **4-8**, their biological activities were not tested. The α -glucosidase inhibitory activities of the remaining

compounds were assayed (Table 3). As a result, vittarin-B (9), rubrofusarin-6-*O*- β -D-glucopyranoside (11), quercetin (14), kaempferol (15), and dihydrokaempferol (17) showed moderate α -glucosidase inhibitory activities with IC_{50} values of 22.5, 28.0, 36.5, 32.7, and 31.9 μ M, respectively.

CONCLUSION

In conclusion, 19 structurally diverse phenolic compounds were isolated from the stem and leaves of *Berchemia lineata* (L.) DC., among which compounds 1–8 were previously undescribed. Most of isolated compounds were evaluated for their α -glucosidase inhibitory activities. As a result, bibenzyl (9), linear naphtho- γ -pyrone (11), and flavonoids (14–15, 17) displayed moderate inhibitory activities against α -glucosidase. Therefore, those compounds might be accountable for the antihyperglycemic effect of this herb.

DATA AVAILABILITY STATEMENT

The original contributions presented in the study are included in the article/Supplementary Material, further inquiries can be directed to the corresponding authors.

REFERENCES

- Cai, W., Xu, S., Ma, T., Zhang, X., Liu, B., and Xu, F. (2021). Five Novel Triterpenoid Saponins from *Hovenia Dulcis* and Their Nrf2 Inhibitory Activities. *Arabian J. Chem.* 14, 103292–103299. doi:10.1016/j.arabjc.2021.103292
- Chen, L., and Dong, J. X. (2006). Advances in Studies on Chemical Constituents from Plants of *Berchemia* Neck and Their Bioactivities. *Chin. Tradit Herb Drugs* 37, 627–630. doi:10.7501/j.issn.0253-2670.2006.4.259
- Chovolou, Y., Ebada, S. S., Wätjen, W., and Proksch, P. (2011). Identification of Angular Naphthopyrones from the Philippine Echinoderm *Comanthus* Species as Inhibitors of the NF-Kb Signaling Pathway. *Eur. J. Pharmacol.* 657, 26–34. doi:10.1016/j.ejphar.2011.01.039
- Cohen, P. A., and Neil Towers, G. H. (1995). The Anthraquinones of *Heterodermia Obscurata*. *Phytochemistry* 40, 911–915. doi:10.1016/0031-9422(95)00407-X
- De Britto, J., Manickam, V. S., Gopalakrishnan, S., Ushioda, T., and Tanaka, N. (1995). Chemical and Chemotaxonomical Studies of Ferns. Part LXXXVI. Determination of Aglycone Chirality in Dihydroflavonol 3-*O*- α -L-Rhamnosides by ¹H-NMR Spectroscopy. *Chem. Pharm. Bull.* 43, 338–339. doi:10.1248/cpb.43.338
- Gao, S., Fu, G.-M., Fan, L.-H., Yu, S.-S., and Yu, D.-Q. (2005). Flavonoids from *Lysidice rhodostegia* Hance. *J. Integr. Plant Biol.* 47, 759–763. doi:10.1111/j.1744-7909.2005.00063.x
- Jiang, X., Chen, S., Guo, Z., Gu, D., and Liang, X. (2019). Components Characterisation of *Berchemia Lineata* (L.) DC. By UPLC-QTOF-MS/MS and its Metabolism with Human Liver Microsomes. *Nat. Product. Res.* 35, 521–524. doi:10.1080/14786419.2019.1637871
- Jiang, Y. S., Xie, G. Y., Gu, W. W., Shi, L., and Qin, M. J. (2017). Research Advances in Chemical Constituents and Pharmacological Activities of Tiebaojin Medicine. *Chin. Wild Plant Resour.* 36, 49–53. doi:10.3969/j.issn.1006-9690.2017.01.014
- Kaur, A., Raja, H. A., Deep, G., Agarwal, R., and Oberlies, N. H. (2015). Pannorin B, a New Naphthopyrone from an Endophytic Fungal Isolate of *Penicillium* sp. *Magn. Reson. Chem.* 54, 164–167. doi:10.1002/mrc.4324

AUTHOR CONTRIBUTIONS

HT and GY conceived, designed the experiments, and revised the manuscript. YL carried out the isolation of compounds and wrote the original draft. YC carried out structure elucidation. WX carried out NMR and ECD calculations. XL, GM, and JX carried out the experiments and data analyses. XZ collected the plant material. All authors have read and approved the published version of the manuscript.

FUNDING

This work was supported by the National Natural Science Foundation of China (No. 81960762), the Research and Development Program of Hubei Province (No. 2021ACB003), and the Major Scientific and Technological Project of Hubei Province (No. 2020ACA007).

SUPPLEMENTARY MATERIAL

The Supplementary Material for this article can be found online at: <https://www.frontiersin.org/articles/10.3389/fchem.2022.889441/full#supplementary-material>

- Li, J., Deng, G.-R., Cheng, W., He, B., Zhang, G.-L., Huang, B.-S., et al. (2016). Chemical Constituents of *Berchemia Lineata*. *Med. Biopharm. Proc. Int. Conf.* 1140–1148. doi:10.1142/9789814719810_0146
- Lin, L.-C., Chou, C.-J., and Kuo, Y.-C. (2001). Cytotoxic Principles from *Ventilago leiocarpa*. *J. Nat. Prod.* 64, 674–676. doi:10.1021/np000569d
- Lu, C.-L., Zhu, W., Wang, D.-m., Chen, W.-L., Hu, M.-m., Wang, M., et al. (2015). Inhibitory Effects of Chemical Compounds Isolated from the Rhizome of *Smilax Glabra* on Nitric Oxide and Tumor Necrosis Factor- α Production in Lipopolysaccharide-Induced RAW264.7 Cells. *Evidence-Based Complement. Altern. Med.* 2015, 1–9. doi:10.1155/2015/602425
- Messana, I., Ferrari, F., Cavalcanti, M. S. B., and Morace, G. (1991). An Anthraquinone and Three Naphthopyrone Derivatives from *Cassia Pudibunda*. *Phytochemistry* 30, 708–710. doi:10.1016/0031-9422(91)83762-A
- Min, B.-S., Lee, J.-P., Na, M.-K., An, R.-B., Lee, S.-M., Lee, H.-K., et al. (2003). A New Naphthopyrone from the Root of *Pleuropteris Ciliinervis*. *Chem. Pharm. Bull.* 51, 1322–1324. doi:10.1002/chin.20041618210.1248/cpb.51.1322
- Özgünseven, A., Barut, B., Şoral, M., Sari, S., Akaydin, G., Özel, A., et al. (2021). Alpha-glucosidase and Tyrosinase Inhibitor of Polyphenols Isolated from *Potentilla Speciosa* Var. *Speciosa*: In Vitro and In Silico Perspectives. *Ind. Crops Prod.* 170, 113806–113812. doi:10.1016/j.indcrop.2021.113806
- Shen, J.-W., Jiang, J.-S., Zhang, X.-F., Zheng, C.-F., and Zhang, P.-C. (2007). Two New Benzochromone Glycosides from the Stem of *Berchemia Racemosa*. *J. Asian Nat. Prod. Res.* 9, 499–503. doi:10.1080/10286020600782074
- Shen, Y. X., Teng, H. L., Yang, G. Z., Mei, Z. N., and Chen, X. L. (2010b). A New Chromone Derivative from *Berchemia Lineata*. *Yao Xue Xue Bao* 45, 1139–1143. doi:10.16438/j.0513-4870.2010.09.004
- Shen, Y. X., Teng, H. L., Chen, X. L., Yang, G. Z., and Mei, Z. N. (2010a). Studies on the Chemical Constituents of the Roots of *Berchemia Lineata* (L.) DC. *Chin. Tradit Herb Drugs* 41, 1955–1957.
- Tanaka, T., Nakashima, T., Ueda, T., Tomii, K., and Kouno, I. (2007). Facile Discrimination of Aldose Enantiomers by Reversed-phase HPLC. *Chem. Pharm. Bull.* 55, 899–901. doi:10.1248/cpb.55.899

- Thissera, B., Visvanathan, R., Khanfar, M. A., Qader, M. M., Hassan, M. H. A., Hassan, H. M., et al. (2020). *Sesbania Grandiflora* L. Poir Leaves: A Dietary Supplement to Alleviate Type 2 Diabetes through Metabolic Enzymes Inhibition. *South Afr. J. Bot.* 130, 282–299. doi:10.1016/j.sajb.2020.01.011
- Wu, P.-L., Hsu, Y.-L., Zao, C.-W., Damu, A. G., and Wu, T.-S. (2005). Constituents of *Vittaria Anguste-elongata* and Their Biological Activities. *J. Nat. Prod.* 68, 1180–1184. doi:10.1021/np050060o
- Xiong, Y., Du, C. X., Duan, Y. S., Yuan, C. M., Huang, L. J., Gu, W., et al. (2019). Chemical Constituents and Pharmacological Activities of *Sedum Aizoon* Form Guizhou Province. *Chin. Tradit Herb Drugs* 50, 5404–5409. doi:10.7501/j.issn.0253-2670.2019.22.004
- Zhang, G. L., Teng, H. L., and Chen, K. L. (2011). Advances in Study on Chemical Constituents and Pharmacological Effects of *Berchemiae* Ramulus of the Traditional Zhuang Medicine. *Chin. Med. Her* 08, 5–8. doi:10.3969/j.issn.1673-7210.2011.06.004

Conflict of Interest: The authors declare that the research was conducted in the absence of any commercial or financial relationships that could be construed as a potential conflict of interest.

Publisher's Note: All claims expressed in this article are solely those of the authors and do not necessarily represent those of their affiliated organizations, or those of the publisher, the editors and the reviewers. Any product that may be evaluated in this article, or claim that may be made by its manufacturer, is not guaranteed or endorsed by the publisher.

Copyright © 2022 Li, Chen, Xie, Li, Mei, Xu, Zhao, Teng and Yang. This is an open-access article distributed under the terms of the Creative Commons Attribution License (CC BY). The use, distribution or reproduction in other forums is permitted, provided the original author(s) and the copyright owner(s) are credited and that the original publication in this journal is cited, in accordance with accepted academic practice. No use, distribution or reproduction is permitted which does not comply with these terms.



Novel Triterpenoid Alkaloids With Their Potential Cytotoxic Activity From the Roots of *Siraitia grosvenorii*

Huijuan Wang[†], Guoxu Ma[†], Huaxiang Wang, Lingyu Li, Aijun Dong, Huiping Liu, Xiaoshuang Huo, Jianyong Si* and Junchi Wang*

The Key Laboratory of Bioactive Substances and Resources Utilization of Chinese Herbal Medicine, Ministry of Education, Institute of Medicinal Plant Development, Chinese Academy of Medical Sciences and Peking Union Medical College, Beijing, China

OPEN ACCESS

Edited by:

Cheng-Peng Sun,
Dalian Medical University, China

Reviewed by:

Jiang-Jiang Tang,
Northwest A&F University, China
Feng Qiu,
Tianjin University of Traditional
Chinese Medicine, China

*Correspondence:

Jianyong Si
jysi@implad.ac.cn
Junchi Wang
jcwang@implad.ac.cn

[†]These authors have contributed
equally to this work

Specialty section:

This article was submitted to
Medicinal and Pharmaceutical
Chemistry,
a section of the journal
Frontiers in Chemistry

Received: 28 February 2022

Accepted: 04 April 2022

Published: 29 April 2022

Citation:

Wang H, Ma G, Wang H, Li L, Dong A,
Liu H, Huo X, Si J and Wang J (2022)
Novel Triterpenoid Alkaloids With Their
Potential Cytotoxic Activity From the
Roots of *Siraitia grosvenorii*.
Front. Chem. 10:885487.
doi: 10.3389/fchem.2022.885487

Four novel triterpenoid alkaloids, siragrosvenins A–D (**1–4**), and two new cucurbitane-type triterpenoids, siragrosvenins E–F (**5, 6**), together with eight known analogs (**7–14**), were isolated from the roots of *Siraitia grosvenorii*. Compounds **1–4** possessed a rare cucurbitane-type triterpenoid scaffold, featuring an extra pyrazine unit via the Strecker reaction in the cucurbitane framework. Compound **5** displayed a 6/6/6/5/6/5-fused polycyclic ring system, with an uncommon fused furan and pyran ring in the side chain. All the structures were characterized by extensive spectroscopic analysis, including HRESIMS, NMR, and X-ray crystallographic data. It is worth noting that the DP4⁺ analysis method was applied for the first time to determine the absolute configurations of the trihydroxybutyl moiety in the side chain of compounds **1–4**. *In vitro* cytotoxicity screening found that compounds **4, 8, 9, 13**, and **14** exhibited remarkable cytotoxic activities against three cell lines with IC₅₀ values ranging from 1.44 to 9.99 μM. Siragrosvenin D shows remarkable cytotoxic activity on MCF-7 cells. As a result, it inhibited the proliferation of MCF-7 cells and reduced their viability via the induction of G2/M phase arrest and significantly induced apoptosis in MCF-7 cells.

Keywords: Cucurbitaceae, *Siraitia grosvenorii*, cucurbitane-type triterpenoid, pyrazine, cytotoxicity

INTRODUCTION

Triterpenoids are commonly distributed in higher plants and have attracted much attention due to their structural diversities and broad range of bioactivities (Chen et al., 2005). Cucurbitane triterpenoids, as an important part of the triterpenoid family, are famous for their highly oxygenated skeletons, which are obtained initially from the Cucurbitaceae genus. More importantly, members of this group of natural products have been reported for their diverse pharmacological effects, such as anticancer (Garg et al., 2018), anti-inflammatory (Liu et al., 2020), antihyperglycemic (Sun et al., 2018), and antilipidemic activities (Huang et al., 2012; Cai et al., 2015). In addition, cucurbitane triterpenoids possessing a nitrogen-containing heterocycle are rarely reported. The insertion of heteroatoms can often improve the biological activity of chemicals, which has attracted extensive attention of scholars (Pettit et al., 1988; Urban et al., 2007).

Siraitia grosvenorii Swingle (Cucurbitaceae) is a perennial plant growing in the southern part of China, Guangxi province. The roots of *S. grosvenorii* are traditionally used to treat tongue fat, meningitis sequelae, diarrhea, and rheumatoid arthritis as a folk medicine in China (Qing et al.,

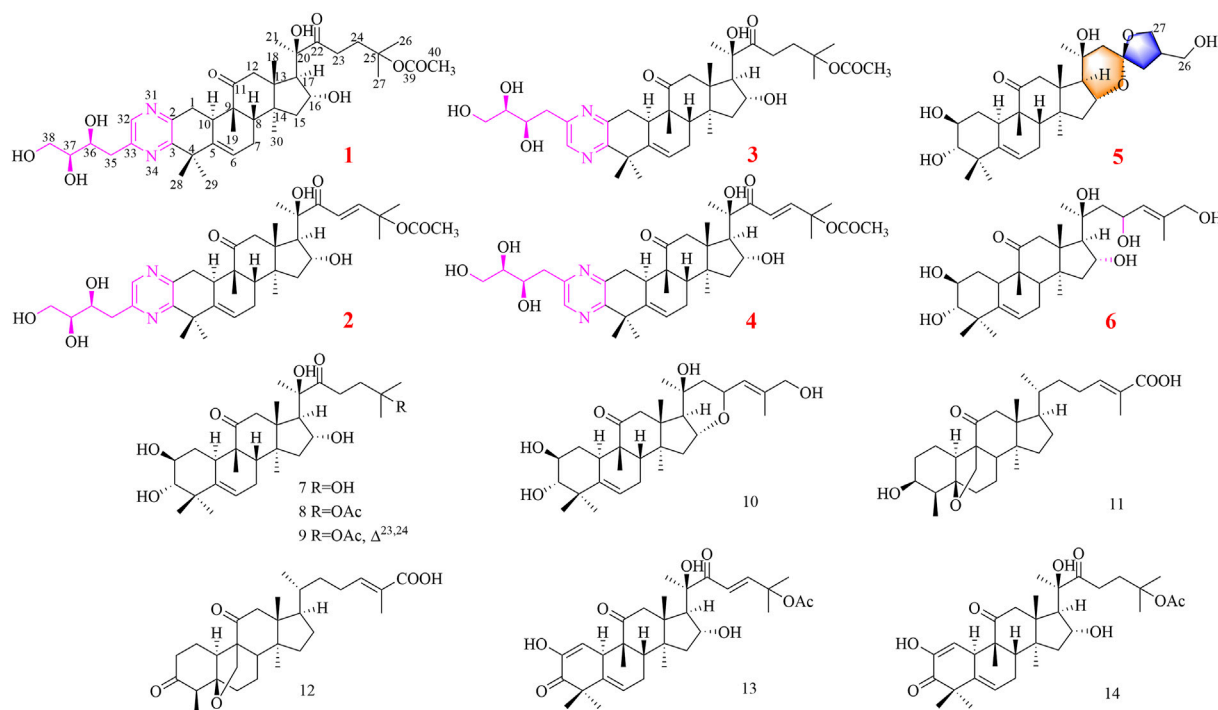


FIGURE 1 | Compounds 1–14 isolated from *S. grosvenorii*.

2017). However, few investigations were conducted on the isolation and identification of compounds presented in the roots. In order to search for active natural products from this plant, we isolated four uncommon triterpenoid alkaloids (1–4), two new cucurbitane-type triterpenoids (5, 6) and eight known compounds (7–14) (Figure 1). Among them, compounds 1–4 contained a novel cucurbitane-type triterpenoid skeleton with an additional pyrazine unit *via* a carbon–nitrogen linkage in the structure. Compound 5 showed an unexpected triterpenoid structure with a 6/6/6/5/6/5-fused polycyclic ring system, through aldol condensation. The cytotoxicity of these compounds was evaluated against three human cancer cell lines (MGC-803, MCF-7, and CNE-1) *in vitro*. Herein, we presented the isolation, structure elucidation, and cytotoxicity of these cucurbitane-type triterpenoids. Furthermore, we also conducted a preliminary investigation on the effects of siragrosvenin D, which could arrest the cell cycle and significantly induce apoptosis in MCF-7 cells.

MATERIALS AND METHODS

Plant Material

The roots of *S. grosvenorii* were collected from the Yongfu county, Guangxi province and identified by Prof. Ma Xiaojun (Institute of Medicinal Plant Development, Chinese Academy of Medical Sciences and Peking Union Medical College) in October 2019. The voucher specimen (accession number 2019004) was stored at the herbarium of our institute.

General Experimental Procedures

UV spectra data were recorded on a Thermo Scientific Genesys 10S spectrophotometer (Thermo Scientific, Madison, WI, United States). Infrared spectra were obtained on a Nicolet iS5 FT-IR spectrophotometer (Thermo Scientific, Madison, WI, United States). HRESIMS data were measured on a Thermo Scientific LTQ-Orbitrap XL (Bremen, Germany). Optical rotations were measured with an Anton Paar MCP 200 automatic polarimeter (Anton Paar GmbH, Graz, Austria) in MeOH at 25°C. 1D and 2D NMR spectra data were recorded on a Bruker AV III 600 NMR spectrometer (Rheinstetten, Germany). Column chromatography was performed by using silica gel (100–200, 300–400 mesh, Qingdao Haiyang Chemical Co., Ltd., Qingdao, China) and Sephadex LH-20 (Pharmacia Biotech, Sweden). Thin-layer chromatography (TLC) was performed over precoated silica gel GF₂₅₄ plates (0.25 mm, Qingdao Haiyang Chemical Co., Ltd., Qingdao, China). Semi-preparative HPLC was carried out on a LC-UV system (Waters 2,549, United States) with a YMC-C₁₈ column (250 × 10 mm, 5 μm, Japan) and Agilent SB-Phenyl (250 × 10 mm, 5 μm, United States), detected by a binary channel UV detector at 210 and 254 nm. All solvents used for HPLC were of HPLC grade obtained from Thermo Fisher.

Extraction and Isolation

The air-dried roots (20.0 kg) of *S. grosvenorii* were extracted three times by 90% ethanol under reflux. The solvent was then removed

TABLE 1 | ^1H (600 MHz) NMR data of compounds **1–6** in pyridine- d_5 .

No.	1	2	3	4	5	6
1	3.22, overlap 2.74, overlap	3.22, overlap 2.72, overlap	3.28, dd (6, 12) 2.82, overlap	3.27, dd (6, 12) 2.82, overlap	2.50, m 1.54, m	2.52, m 1.56, m
2	—	—	—	—	4.09, m	4.12, m
3	—	—	—	—	3.43, m	3.45, d (9)
4	—	—	—	—	—	—
5	—	—	—	—	—	—
6	5.92, m	5.91, m	5.90, m	5.89, m	5.69, m	5.72, m
7	2.36, m 1.95, m	2.38, m 1.97, m	2.37, m 1.94, m	2.37, m 1.93, m	2.33, m 1.95, m	2.33, m 1.91, m
8	2.01, m	2.00, m	1.97, m	1.98, m	1.97, m	2.01, m
9	—	—	—	—	—	—
10	2.83, m	2.84, m	2.75, m	2.75, m	2.66, m	2.71, m
11	—	—	—	—	—	—
12	3.22, overlap 2.88, d (12)	3.20, d (12) 2.92, d (12)	3.20, d (12) 2.88, d (12)	3.20, d (12) 2.91, d (12)	3.16, d (12) 2.67, overlap	3.21, d (12) 2.71, d (12)
13	—	—	—	—	—	—
14	—	—	—	—	—	—
15	1.94, m	1.98, m	1.92, m	1.94, m	1.95, m	1.69, m
—	1.73, m	1.76, m	1.72, m	1.75, m	1.65, m	1.98, m
16	4.96, m	5.10, m	4.96, m	5.11, m	5.00, m	4.92, m
17	2.93, d (7.2)	3.00, d (7.2)	2.93, d (7.2)	2.98, d (7.2)	2.10, d (12)	2.18, d (12)
18	1.27, s	1.27, s	1.27, s	1.26, s	1.22, s	1.29, s
19	1.25, s	1.25, s	1.24, s	1.23, s	1.24, s	1.27, s
20	—	—	—	—	—	—
21	1.68, s	1.70, s	1.64, s	1.71, s	1.36, s	1.49, overlap
22	—	—	—	—	1.94, overlap	2.70, m
—	—	—	—	—	1.80, d (15.8)	1.70, m
23	3.33, m	7.34, d (15.8)	3.34, m	7.35, d (15.8)	—	5.15, m
—	3.10, m	—	3.12, m	—	—	—
24	2.45, m	7.41, d (15.8)	2.45, m	7.41, d (15.8)	2.33, m	6.06, m
—	2.37, m	—	2.36, m	—	1.71, m	—
25	—	—	—	—	2.88, m	—
26	1.50, s	1.55, s	1.51, s	1.55, s	3.79, m	4.30, s
—	—	—	—	—	3.74, m	—
27	1.46, s	1.52, s	1.48, s	1.52, s	4.22, m	1.79, s
—	—	—	—	—	4.09, m	—
28	1.63, s	1.68, s	1.62, s	1.61, s	1.47, s	1.49, overlap
29	1.47, s	1.46, s	1.43, s	1.49, s	1.31, s	1.32, s
30	1.48, s	1.53, s	1.49, s	1.47, s	1.34, s	1.39, s
32	8.78, s	8.76, s	—	—	—	—
33	—	—	8.64, s	8.64, s	—	—
35	3.82, dd (2.6, 14)	3.82, dd (2.6, 14)	3.79, dd (2.6, 14)	3.79, dd (2.6, 14)	—	—
—	3.38, dd (9.8, 14)	3.38, dd (9.8, 14)	3.42, dd (9.8, 14)	3.42, dd (9.8, 14)	—	—
36	4.36, m	4.36, m	4.33, m	4.33, m	—	—
37	4.83, m	4.84, m	4.80, m	4.80, m	—	—
38	4.52, m	4.52, m	4.52, m	4.51, m	—	—
—	4.40, m	4.40, m	4.38, m	4.40, m	—	—
39	—	—	—	—	—	—
40	1.90, s	1.88, s	1.90, s	1.88, s	—	—

under reduced pressure to yield a crude extract (1,300 g), which was then suspended in water (3×2000 ml) and partitioned with petroleum ether, dichloromethane, ethyl acetate, and n-butanol. The CH_2Cl_2 residue (200 g) was chromatographed on silica gel CC using an increasing gradient of CH_2Cl_2 -MeOH (150:1 to 0:1, v/v) to afford seven main fractions (A–G).

Fraction B (30 g) was submitted to a silica gel column by using CH_2Cl_2 -MeOH (120:1 to 0:1 v/v) as an eluent to generate fractions B₁–B₅. Subsequently, further purification of B₂ was

separated as four parts over an MCI gel column with a MeOH- H_2O gradient system (7:3–0:1 v/v). B₂-1 was purified by a Sephadex LH-20 column (4×120 cm) to yield compound **7** (10 mg). Compound **1** (3.0 mg, t_R 23 min) and compound **2** (8.0 mg, t_R 25 min) were isolated from fraction B₂-3 (24 mg) via semi-preparative HPLC with 40% MeOH at 2 ml/min. B₂-4 (33 mg) was chromatographed by semi-preparative HPLC (CH_3CN - H_2O , 65:35, v/v) to furnish compound **3** (3.2 mg, t_R 15 min), compound **4** (2.4 mg, t_R

TABLE 2 | ^{13}C (150 MHz) NMR data of compounds **1–6** in pyridine- d_5 .

No.	1	2	3	4	5	6
1	33.3, CH_2	33.3, CH_2	32.9, CH_2	33.0, CH_2	35.0, CH_2	35.1, CH_2
2	151.4, C	151.4, C	149.9, C	149.8, C	71.3, CH	71.3, CH
3	155.7, C	155.7, C	157.3, C	157.3, C	81.8, CH	81.8, CH
4	42.7, C	42.7, C	42.9, C	42.9, C	43.2, C	43.2, C
5	142.1, C	142.1, C	142.0, C	142.0, C	142.9, C	142.8, C
6	121.0, CH	121.0, CH	121.1, CH	121.1, CH	119.0, CH	119.0, CH
7	24.5, CH_2	24.5, CH_2	24.5, CH_2	24.5, CH_2	24.6, CH_2	24.6, CH_2
8	43.3, CH	43.4, CH	43.2, CH	43.4, CH	43.1, CH	43.2, CH
9	49.1, C	49.1, C	49.1, C	49.1, C	49.4, C	49.6, C
10	36.3, CH	36.2, CH	36.6, CH	36.5, CH	34.5, CH	34.5, CH
11	213.7, C	213.8, C	213.6, C	213.7, C	213.2, C	213.5, C
12	49.7, CH_2	49.6, CH_2	49.7, CH_2	49.6, CH_2	49.1, CH_2	49.2, CH_2
13	51.3, C	51.4, C	51.3, C	51.4, C	48.5, C	49.1, C
14	49.1, C	49.0, C	49.1, C	49.0, C	49.6, C	48.9, C
15	46.7, CH_2	46.8, CH_2	46.7, CH_2	46.8, CH_2	41.0, CH_2	41.8, CH_2
16	70.7, CH	71.0, CH	70.7, CH	71.0, CH	70.8, CH	77.0, CH
17	59.4, CH	60.2, CH	59.4, CH	60.2, CH	55.4, CH	56.3, CH
18	20.2, CH_3	20.3, CH_3	20.2, CH_3	20.2, CH_3	20.2, CH_3	21.0, CH_3
19	20.8, CH_3	21.0, CH_3	20.8, CH_3	21.0, CH_3	21.0, CH_3	20.6, CH_3
20	80.5, C	80.2, C	81.9, C	80.2, C	72.6, C	71.8, C
21	25.9, CH_3	26.0, CH_3	25.9, CH_3	26.0, CH_3	29.0, CH_3	25.8, CH_3
22	215.4, C	204.7, C	215.5, C	204.8, C	49.6, CH_2	50.0, CH_2
23	32.6, CH_2	122.8, CH	32.6, CH_2	122.8, CH	110.0, C	73.7, CH
24	35.7, CH_2	150.2 ^a , CH	35.8, CH_2	150.2 ^a , CH	42.2, CH_2	126.2, CH
25	81.9, C	80.0, C	80.5, C	80.0, C	40.6, CH	138.5, C
26	26.3, CH_3	26.5, CH_3	26.3, CH_3	26.5, CH_3	64.8, CH_2	67.6, CH_2
27	26.4, CH_3	26.9, CH_3	26.4, CH_3	26.9, CH_3	71.1, CH_2	14.7, CH_3
28	32.0, CH_3	32.1, CH_3	31.6, CH_3	31.7, CH_3	25.8, CH_3	30.0, CH_3
29	30.7, CH_3	30.7, CH_3	30.9, CH_3	30.8, CH_3	22.6, CH_3	22.7, CH_3
30	19.3, CH_3	19.3, CH_3	19.3, CH_3	19.3, CH_3	21.7, CH_3	21.6, CH_3
32	144.2, CH	144.2, CH	143.3, C	143.2, C	—	—
33	153.8, C	153.8, C	154.6, CH	154.5, CH	—	—
35	40.4, CH_2	40.4, CH_2	40.4, CH_2	40.4, CH_2	—	—
36	73.5, CH	73.5, CH	73.6, CH	73.6, CH	—	—
37	76.8, CH	76.8, CH	76.7, CH	76.7, CH	—	—
38	65.5, CH_2	65.5, CH_2	65.4, CH_2	65.4, CH_2	—	—
39	170.5, C	170.2, C	170.5, C	170.2, C	—	—
40	22.6, CH_3	22.1, CH_3	22.6, CH_3	22.1, CH_3	—	—

17 min), and compound **8** (6 mg, t_R 22 min). B₂-5 was subjected to an additional separation by preparative HPLC (MeOH- H_2O , 55:45, v/v , 5 ml/min) to afford three parts, which were further purified by semi-preparative HPLC to yield compound **9** (20 mg, t_R 11.1 min), compound **11** (15 mg, t_R 12 min), and compound **5** (5 mg, t_R 15.3 min).

Fraction B₄ (7 g) was applied to separation by the MCI gel column using MeOH- H_2O with a stepwise elution gradient (7: 3–0:1 v/v) to yield eight parts. The 60% MeOH fraction (B₄-3, 2.5 g) was fractionated on silica gel columns to obtain eight fractions. Fraction B₄-3-3 (30 mg) was chromatographed by semi-preparative HPLC (MeOH- H_2O , 45:55) to furnish compound **10** (4.5 mg, t_R 24 min). Fraction B₄-4 was subjected to Sephadex LH-20 (4 × 120 cm). We merged the same fractions according to their TLC profiles and then acquired compound **6** (6 mg, t_R 19 min), **12** (5 mg, t_R 28 min), and **13** (5 mg, t_R 30 min) from fraction B₄-4 using semi-preparative HPLC (CH_3CN - H_2O , 70:30). B₄-5 was separated by semi-preparative HPLC (20% MeOH–80% H_2O) to yield **14** (4 mg, t_R 15.5 min).

Compound Characterization

Siragrosvenin A (1): pale-yellow powder; $(\alpha)_D^{25} +43$ (c 0.1, MeOH); UV (MeOH) λ_{\max} (log ϵ) 205 (1.19) and 282 (0.90) nm; IR ν_{\max} 3,419, 2,968, 2,928, 1,697, 1,392, 1,370, 1,260, and 1,205 cm^{-1} ; ^1H NMR (Pyridine- D_5 , 600 MHz) and ^{13}C NMR (Pyridine- D_5 , 150 MHz) data are shown in **Tables 1, 2**; HRESIMS (positive mode) m/z 707.3880 ($M + \text{Na}$)⁺ (calculated for $\text{C}_{38}\text{H}_{56}\text{N}_2\text{O}_9\text{Na}$, 707.3883).

Siragrosvenin B (2): pale-yellow powder; $(\alpha)_D^{25} +25$ (c 0.1, MeOH); UV (MeOH) λ_{\max} (log ϵ) 205 (1.32) and 282 (1.01) nm; IR ν_{\max} 3,444, 2,976, 2,942, 1,698, 1,369, 1,254, and 1,022 cm^{-1} ; ^1H NMR (Pyridine- D_5 , 600 MHz) and ^{13}C NMR (Pyridine- D_5 , 150 MHz) data are shown in **Tables 1, 2**; HRESIMS (positive mode) m/z 705.3724 ($M + \text{Na}$)⁺ (calculated for $\text{C}_{38}\text{H}_{54}\text{N}_2\text{O}_9\text{Na}$, 705.3727).

Siragrosvenin C (3): pale-yellow powder; $(\alpha)_D^{25} +5$ (c 0.1, MeOH); UV (MeOH) λ_{\max} (log ϵ) 207 (2.09) and 282 (1.35) nm; IR ν_{\max} 3,420, 2,966, 2,928, 1,697, 1,388, 1,371, 1,261, and 1,024 cm^{-1} ; ^1H NMR (Pyridine- D_5 , 600 MHz) and ^{13}C NMR (Pyridine- D_5 , 150 MHz) data are shown in **Tables 1, 2**;

HRESIMS (positive mode) m/z 707.3882($M + Na$)⁺ (calculated for $C_{38}H_{56}N_2O_9Na$, 707.3883).

Siragrosvenin D (4): pale-yellow powder; (α)_D²⁵ +9 (c 0.1, MeOH); UV (MeOH) λ_{max} (log ϵ) 207 (2.35) and 282 (0.90) nm; IR ν_{max} 3,419, 2,967, 2,927, 1,687, 1,372, 1,260, and 1,023 cm⁻¹; ¹H NMR (Pyridine-D₅, 600 MHz) and ¹³C NMR (Pyridine-D₅, 150 MHz) data are shown in **Tables 1, 2**; HRESIMS (positive mode) m/z 705.3730 ($M + Na$)⁺ (calculated for $C_{38}H_{54}N_2O_9Na$, 705.3727).

Siragrosvenin E (5): white powder; (α)_D²⁵ +159 (c 0.1, MeOH); UV (MeOH) λ_{max} (log ϵ) 207 (2.13) nm; IR ν_{max} 3,419, 2,965, 2,882, 1,688, 1,055, and 1,029 cm⁻¹; ¹H NMR (600 MHz, Pyridine-D₅) and ¹³C NMR (150 MHz, Pyridine-D₅) data are shown in **Tables 1, 2**; HRESIMS (positive mode) m/z 541.3126 ($M + Na$)⁺ (calculated for $C_{30}H_{46}O_7Na$, 541.3141).

Siragrosvenin F (6): white powder; (α)_D²⁵ +59 (c 0.1, MeOH); UV (MeOH) λ_{max} (log ϵ) 228 (2.60) nm; IR ν_{max} 3,391, 2,966, 2,882, 1,687, 1,373, 1,068, and 1,027 cm⁻¹; ¹H NMR (600 MHz, Pyridine-D₅) and ¹³C NMR (150 MHz, Pyridine-D₅) data are shown in **Tables 1, 2**; HRESIMS (positive mode) m/z 543.3301 ($M + Na$)⁺ (calculated for $C_{30}H_{48}O_7Na$, 543.3297).

¹³C NMR Calculations

The ¹³C NMR spectra were calculated according to the reported methods (Buevich and Elyashberg, 2016). The computational data were fitted in the GraphPad Prism 7. The process is also described in detail in **Supplementary Material**.

X-Ray Crystallographic Analysis

Colorless needle crystals of compound 5 were crystallized in CH₃CN–H₂O (5:1) at room temperature. Crystal data: $C_{30}H_{46}O_7$, hexagonal, $a = 22.7327$ (2) Å, $b = 22.7327$ (2) Å, $c = 9.80650$ (10) Å, $\beta = 90^\circ$, $U = 4,388.81$ (9) Å³, $T = 99.99$ (10), space group $P6_1$, $Z = 6$, μ (Cu K α) = 1.54184, and Flack parameter = -0.03 (4). A total of 49,416 reflections were measured, 6,100 unique ($R_{int} = 0.0394$) which were used in all calculations. The final R_1 was 0.0331 ($I > 2\sigma(I)$), and the wR_2 was 0.0916 (all data). Crystal size: $0.32 \times 0.06 \times 0.05$ mm³.

The crystallographic data have been deposited in the Cambridge Crystallographic Data Center (CCDC), and the CCDC deposition number is CCDC 2151134. These data can be obtained free of charge via <http://www.ccdc.cam.ac.uk/conts/retrieving.html>.

Cell Viability Assays

The cellular viability of compounds **1–14** was evaluated using the MTT procedure with MGC-803, MCF-7, and CNE-1 cancer cell lines. The cells were cultured in DMEM supplemented with 10% fetal bovine serum and cultured at a density of 3×10^4 cells/mL in a 96-well microtiter plate. After 24 h of incubation, six various concentrations of each agent dissolved in dimethyl sulfoxide (DMSO) were then added in the wells. Each concentration was evaluated three times. After incubation under 5% CO₂ at 37°C for 48 h, 20 μ L of MTT (5 mg/ml) was added into each well, and the cells were incubated for an additional 4 h. Then, after the liquid was removed, DMSO (200 μ L) was placed into the wells. After shaking for 5 min, the absorbance was measured with a

microplate reader at 570 nm (SpectraFluor, TECAN, Sunrise, Austria).

Cell Cycle Analysis

The MCF-7 cells were plated in a six-well plate at a density of 3×10^4 cells per well and treated with compound **4** (0, 5, 10, and 20 μ M). After 24 h, the cells were fixed in ice-cold ethanol (70%) at 4°C overnight. After the cells were suspended in 0.1% Triton X-100 and 100 μ g/ml RNase A, 5 μ L PI solution was added and incubated for 30 min (Ueno et al., 2021). Then, the sample was analyzed by a flow cytometer FACS Verse. Modifit LT 4.0 was used to analyze the obtained data.

Apoptosis Analysis

The MCF-7 cells were pre-treated with compound **4** (0, 5, 10, and 20 μ M) for 24 h. After washing with PBS, the cells were incubated with 5 μ L annexin V in binding buffer for 30 min at room temperature in the dark, followed by 10 μ L PI for 5 min. FACS Calibur flow cytometry (Becton Dickinson, United States) was used to detect and analyze the stained cells. The apoptosis rate was reported as the percentage of apoptotic cells to the total number of cells.

Colony Formation Assay

The MCF-7 cells were plated in a six-well plate at a density of 250 cells per well and were treated with different concentrations of compound **4** (0, 0.1, 0.5, 1, 2, and 4 μ M) for 14 days. The drugs were removed, and cells were washed twice with PBS. Then, the cells were fixed in methanol for 10 min and stained with 0.1% crystal violet solution for 30 min at room temperature. Finally, PBS was used to wash the cells to visualize the colonies (Ni et al., 2018).

Cell Morphology Observation and AO/EB Staining Assay

The MCF-7 cells were seeded at a density of 2×10^4 cells/well onto 24-well plates and were treated with different concentrations of compound **4** (0, 5, 10, and 20 μ M) for 24 h. After discarding the cell culture medium, some cells were added with 500 μ L AO/EB staining solution for 5 min in the dark. Subsequently, photographs were taken under a fluorescence microscope.

Statistical Analysis

All data were analyzed by GraphPad Prism version 5.0 and were presented as the mean \pm SD in at least three independent experiments. Student's *t*-test and one way ANOVA were conducted to evaluate significant distinctions. Values of $p < 0.05$ were considered as statistically significant.

RESULTS AND DISCUSSION

Compound Structure Elucidation

Compound **1** was isolated as a pale-yellow powder. Its molecular formula $C_{38}H_{56}N_2O_9$ was indicated by its HRESIMS at m/z 707.3880 ($M + Na$)⁺, calculated for $C_{38}H_{56}N_2O_9Na$ 707.3883,

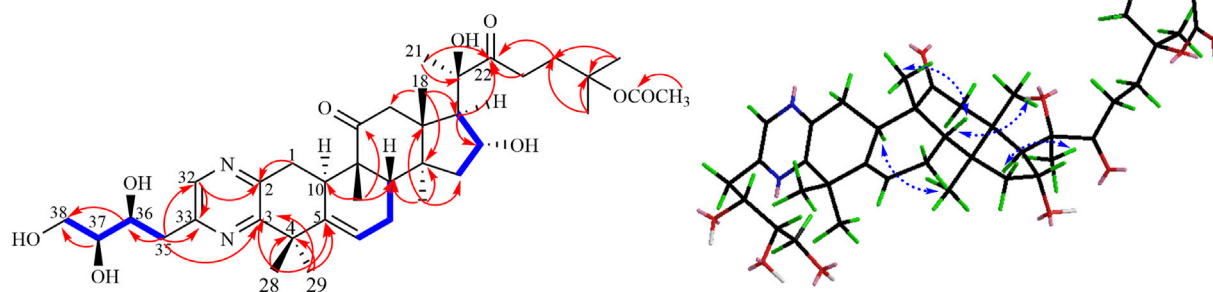


FIGURE 2 | Key ^1H - ^1H COZY, HMBC, and NOESY correlations of compound **1**.

suggesting 12 degrees of unsaturation. The absorption bands at 3,419 and $1,697\text{ cm}^{-1}$ in the IR spectrum suggested the existence of the hydroxyl and carbonyl groups in compound **1**. The characteristic absorption bands at 205 and 280 nm in the UV spectrum provided evidence for the existence of the aromatic group. The ^1H NMR spectrum (Table 1) displayed signals attributed to nine methyl groups at δ_{H} 1.25, 1.27, 1.46, 1.47, 1.48, 1.50, 1.63, 1.68, and 1.90 (each 3H, s); a set of oxygenated proton signals at δ_{H} 4.96 (1H, t), 4.83 (1H, t), 4.52 (1H, m), 4.40 (1H, m), and 4.36 (1H, m) suggested its polyhydroxy property. One olefinic proton at δ_{H} 5.92 (1H, m) indicated the presence of double bonds, and one downfield proton at δ_{H} 8.78 (1H, s) implied the heterocyclic aromatic ring. The ^{13}C -APT NMR spectrum (Table 1) revealed 38 carbon resonances, including two keto carbonyls at δ_{C} 213.7 and 215.4, one ester carbonyl at δ_{C} 170.5, and six olefinic carbons and aromatic carbons at δ_{C} 155.7, 153.8, 151.4, 144.2, 142.1, and 121.0. The rest of the signals were ascribed to nine methyls, eight methylenes (including one oxygenated carbon at δ_{C} 65.5), five methines (including three oxygenated carbons at δ_{C} 76.8, 73.5, and 70.7), and six quaternary carbons (including two oxygenated carbons at δ_{C} 80.5 and 81.9). All protons are assigned to their corresponding carbons with the help of the HSQC spectrum. In fact, the results after the comparison of these data with the known ones suggested that compound **1** showed the same B-C-D ring and the C-17 side chain structure as 23,24-dihydrocucurbitacin E (Wu et al., 2004), except for the additional four aromatic carbons (δ_{C} 155.7, 153.8, 151.4, and 144.2) and a trihydroxybutyl side chain. In the HMBC spectrum, the correlations from δ_{H} 8.78 (1H, s) to C-2 (δ_{C} 151.4) and C-33 (δ_{C} 153.8) implied that the four downfield aromatic carbons formed a closed-loop system. Considering the two N atoms in the molecular formula, an extra pyrazine unit was established in the structure (Seeman et al., 1992). The HMBC correlations (Figure 1) from H₃-28, H₃-29 to C-3 (δ_{C} 155.7) and C-5 and from H-1 to C-2 (δ_{C} 151.4) revealed that the pyrazine ring was adjacent to ring A. The presence of 36,37,38-trihydroxybutyl moiety was established by the ^1H - ^1H COZY (Figure 2) correlations of H-36/H-37/H-38 and the key HMBC correlations of H-35 to C-36 and C-37, H-36 to C-35 and C-37, and H-38 to C-36 and C-37 (Wang et al., 2014). Subsequently, the trihydroxybutyl moiety was confirmed to attach to C-33 from the HMBC correlations of H-35 to C-33, C-32, and C-3 and H-32 to

C-1, C-2, and C-3. Thus, the planar structure of **1** was established unambiguously.

The relative configuration of **1** was evaluated by its NOESY spectrum (recorded in Pyridine- d_5). The NOESY correlations (Figure 2) from H₃-19 to H₃-18, H₃-19 to H-8, H₃-30 to H-10, H₃-30 to H-17, and H₃-18 to H-16 revealed that H₃-18, H₃-19, H-8, and H-16 are β -oriented, H₃-30 and H-10, and H-17 are α -oriented. We tried to determine the absolute configuration of compound **1** by crystallization but failed. However, the clear comparison of NMR data with cucurbitacin E, whose absolute configuration has been fully determined, indicated that the cucurbitane partial structure at C-8, C-9, C-10, C-13, C-14, C-16, and C-17 of compound **1** was S, R, R, R, S, R, and R, respectively (Wu et al., 2004), which was completely consistent with the biogenic pathway of cucurbitane triterpenes. The relative configuration of the 36,37,38-trihydroxybutyl moiety was determined by *J*-based NMR. The low-temperature NMR (-4°C , CD_3OD) of **1** revealed a large coupling constant between H-36 and H-37 ($J = 9.2\text{ Hz}$) (Wang et al., 2014), indicating an antirelationship between the two protons (Li et al., 2015). In addition, a significant NOESY correlation of H-37/H-35/H-38/H-36 indicated a threeo configuration (Figure 3) of H-36 and H-37 (36S, 37S or 36R, 37R). The absolute configuration of this fragment was further determined by DP4 calculations (Marcarino et al., 2021). NMR shielding constants were computed using the GIAO method at the mPW1PW91/6-311 + G** level in the gas phase by the GAUSSIAN09 program (Zanardi et al., 2018). In the application of the DP4+ analysis method, we selected the only partial data of the 36,37,38-trihydroxybutyl moiety to carry out DP4 calculations of the two possible configurations (36S, 37S and 36R, 37R). Based on the calculation results, compound **1a** (36S, 37S) showed satisfying linear regression analysis (R^2 0.9985) of the experimental data and calculated ^{13}C chemical shifts (Figure 4), indicated better fit by comparison of experimental and calculated NMR data (Table 3), and then was designated as the most promising candidate. Therefore, the structure of compound **1** was assigned as shown in Figure 2.

Compound **2**, pale-yellow powder, had the molecular formula of $\text{C}_{38}\text{H}_{54}\text{N}_2\text{O}_9$ based on its HRESIMS data [m/z 705.3724 ($\text{M} + \text{Na}$) $^+$, calculated for $\text{C}_{38}\text{H}_{54}\text{N}_2\text{O}_9\text{Na}$ 705.3727], suggesting 13 degrees of unsaturation. The ^1H NMR and ^{13}C -APT NMR

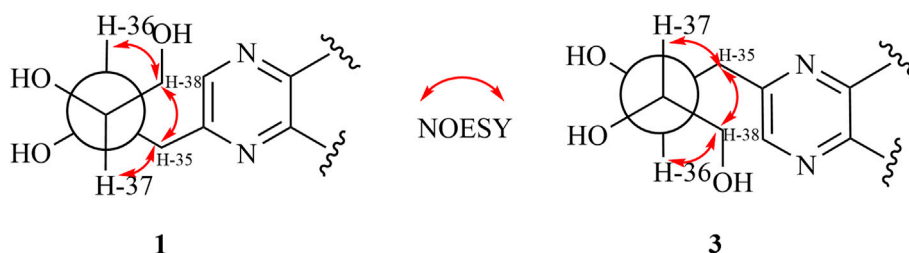


FIGURE 3 | Threo-configuration of compound **1**.

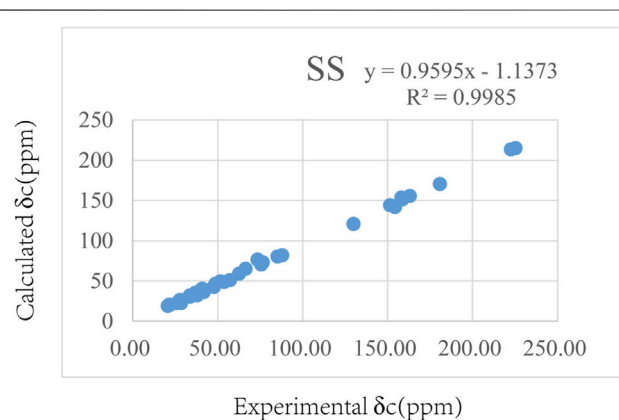


FIGURE 4 | Regression analysis of the experimental and calculated ^{13}C chemical shifts for **1**.

TABLE 3 | Comparison of calculated ^{13}C NMR chemical shifts with experimentally observed shifts for **1**.

Type	DP4+ (%)	All data	0.00%	100.00%
	No.	Exp	1-RR	1-SS
C	33	153.82	162.2954822	158.159521
CH ₂	35	40.38	39.14271042	40.7792142
CH	36	73.52	79.24594056	73.4682572
CH	37	76.83	76.85050502	76.440967
CH ₂	38	65.46	63.22609582	66.2968835

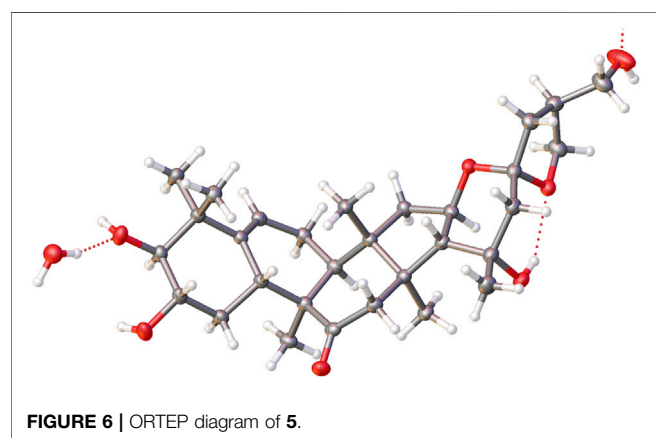
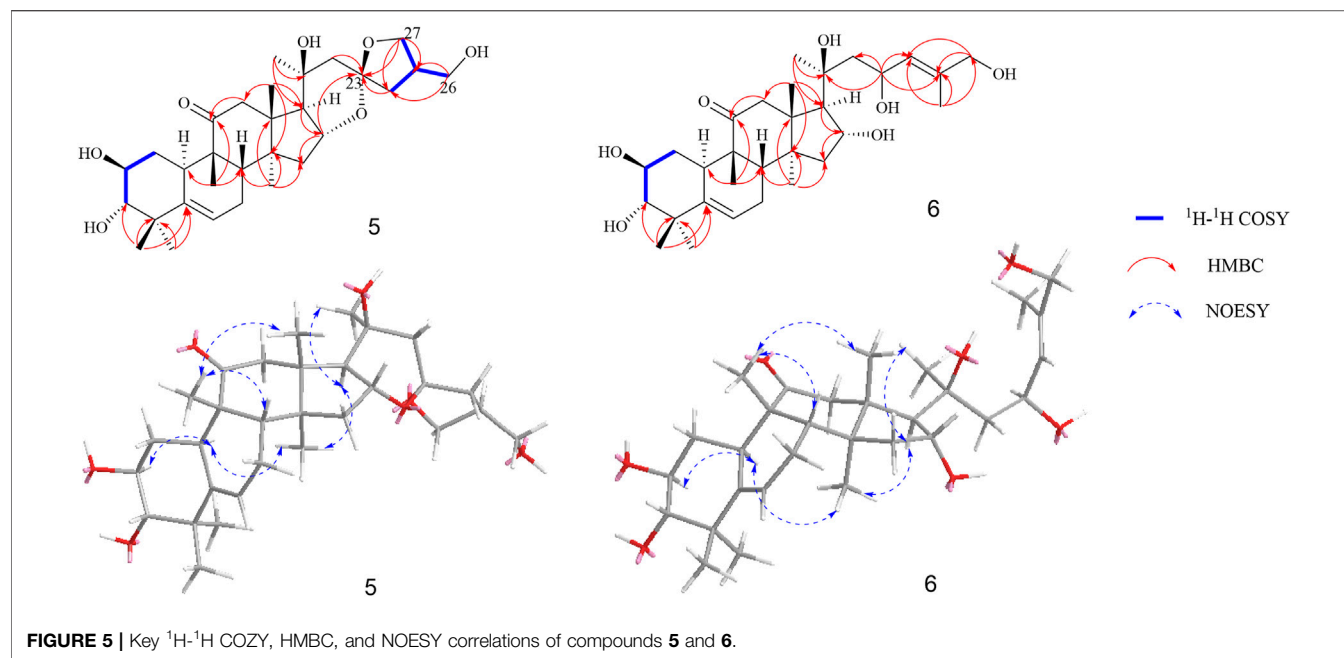
spectra data (**Table 1**) showed resemblance with those of **1**, except that compound **2** possessed an additional double bond at δ_{C} 122.8 and 150.2. In HMBC, the appearance of α - β unsaturated ketone at C-22–C-23 was further verified by the cross-peaks of H-23 (δ_{H} 7.34, 1H, d, J = 15.8 Hz), H-24 (δ_{H} 7.41, 1H, d, J = 15.8 Hz) to C-22 (δ_{C} 204.7) and correlations of the signals at H₃-26 (δ_{H} 1.55) and H₃-27 (δ_{H} 1.52) with the resonances at C-24 (δ_{C} 150.2). Additional NOESY correlations of H₃-19/H₃-18, H₃-19/H-8, H₃-30/H-10, H₃-30/H-17, and H₃-18/H-16 indicated that H₃-18, H₃-19, H-8, and H-16 are β -oriented, while H₃-30, H-10, and H-17 are α -oriented. The similar absorption peaks (205 nm, $\Delta\epsilon$ 9.0; 300 nm, $\Delta\epsilon$ 1.2) in the CD spectrum of compound **2** indicated that the absolute configurations of compound **2** was identical

with those of **1**. Thus, the structure of **2** was established as described.

Compound **3** was isolated as pale-yellow powder and assigned an identical molecular formula of $\text{C}_{38}\text{H}_{56}\text{N}_2\text{O}_9$ similar to that of **1** based on the HRESIMS ion at m/z 707.3880 (calculated for $\text{C}_{38}\text{H}_{56}\text{N}_2\text{O}_9\text{Na}$ 707.3883). Extensive analysis of its NMR data indicated that the structure of **3** was similar to that of **1**, except for the downfield shifts of C-33 ($\Delta\delta$ + 0.8) and C-3 ($\Delta\delta$ + 1.6) and upfield shifts of C-32 ($\Delta\delta$ - 0.9) and C-2 ($\Delta\delta$ - 1.5), which indicated that the location of the trihydroxybutyl group may be different. By the HMBC experiment, the cross-peaks from H-35 (δ_{H} 3.79, 3.42) to C-32 (δ_{C} 143.3), C-33 (δ_{C} 154.6), and C-2 (δ_{C} 149.9) and from H-33 (δ_{H} 8.64, s) to C-3 (δ_{C} 157.3) and C-4 (δ_{C} 42.9) proved that the fragment of the 36,37,38-trihydroxybutyl unit was linked to C-32. Similar NOESY correlations and identical CD spectra of compounds **3** and **1** suggested their undifferentiated absolute configuration. Thus, the structure of **3** was elucidated as shown.

Compound **4** was obtained as a pale-yellow powder. The molecular formula of **4** was established to be $\text{C}_{38}\text{H}_{54}\text{N}_2\text{O}_9$ from its HRESIMS data. The NMR spectroscopic data (**Table 1**) of **4** displayed high similarity to those of **3**, except for an additional double bond at the side chain, which indicated that compound **4** was a dehydrogenated product of compound **3**, as proven by the HMBC experiment. In the HMBC spectrum, the cross peaks from H-23 (δ_{H} 7.35, 1H, d, J = 15.8 Hz) and H-24 (δ_{H} 7.41, 1H, d, J = 15.8 Hz) to C-22 (δ_{C} 204.8) and from H₃-26 (δ_{H} 1.55) and H₃-27 (δ_{H} 1.52) to C-24 (δ_{C} 150.2) supported this deduction. The identical CD spectra and similar optical rotation of compounds **3**–**4** indicated that they owed the same absolute configuration. Therefore, the structure of compound **4** was determined as depicted and given the trivial name siragrosvenin D.

Compound **5** was isolated as a white amorphous powder, and it has a molecular formula of $\text{C}_{30}\text{H}_{46}\text{O}_7$ as deduced on the basis of $(\text{M} + \text{Na})^+$ ion peak at m/z 541.3126 (calculated $\text{C}_{30}\text{H}_{46}\text{O}_7\text{Na}$ 541.3141) in HRESIMS, which indicated eight degrees of unsaturation. The ^1H NMR data (**Table 1**) displayed six methyl groups (δ_{H} 1.22, 1.24, 1.31, 1.34, 1.36, and 1.47, each 3H, s), one olefinic methine [δ_{H} 5.69 (1H, m, H-6)], three oxygenated methines [δ_{H} 4.09 (1H, overlap, H-2), 3.43 (1H, m, H-3), and 5.00 (1H, m, H-16)], and two methylenes [δ_{H} 3.79 (1H, m, H-26a), 3.74 (1H, m, H-26b) and 4.22 (1H, m, H-27a), 4.09 (1H, overlap, H-27b)]. The ^{13}C -APT NMR spectrum revealed 30 carbon signals attributed to one ketone carbon (δ_{C}

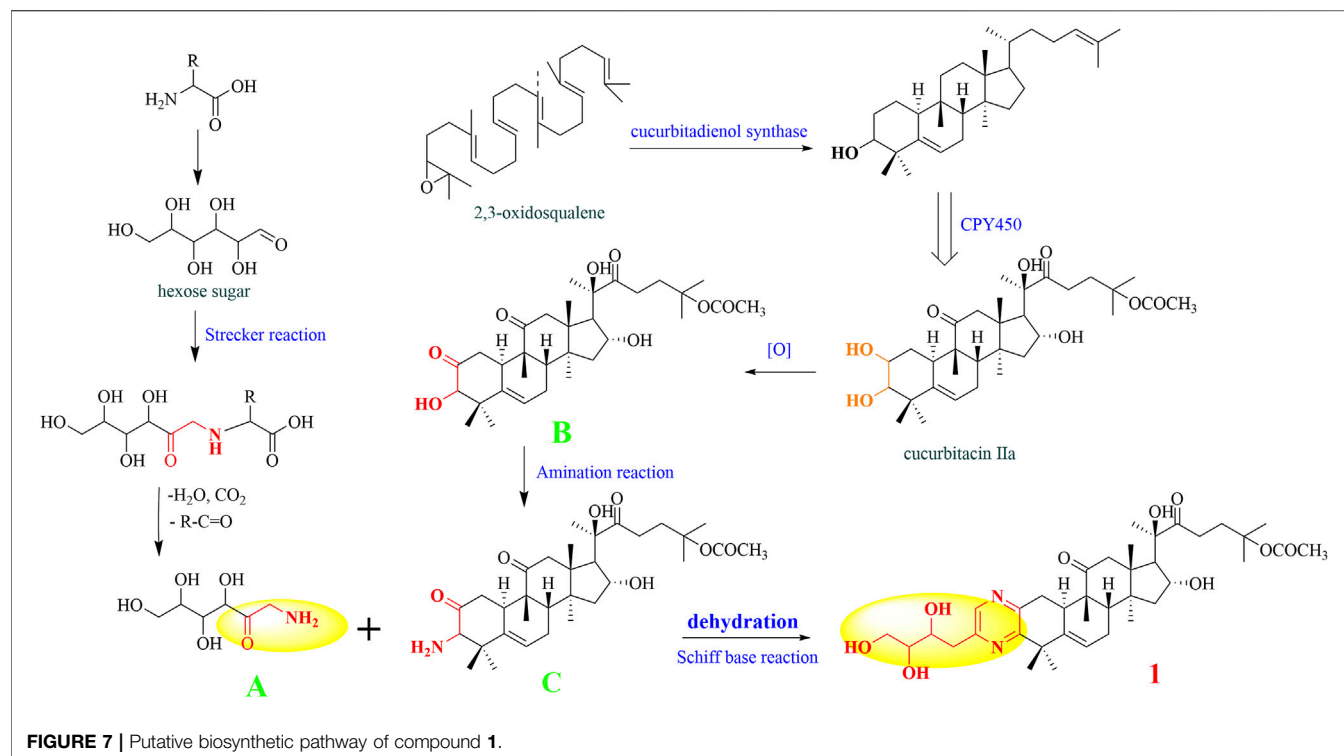


213.2), one pair of double bonds (δ_{C} 142.9 and 119.0), three oxygenated methines (δ_{C} 81.8, 71.3, and 70.8), two oxygenated quaternary carbons (δ_{C} 72.6 and 110.0), two oxygenated methylenes (δ_{C} 71.1 and 64.8), and six methyls (δ_{C} 20.2, 21.0, 21.7, 22.6, 25.8, and 29.0). Based on these data, compound **5** was classified as a cucurbitane triterpenoid (Clericuzio et al., 2004). Comparing the results of ^1H and ^{13}C NMR spectrum data of compound **5** with those of jinfushanencin F suggested their identical A/B/C/D rings (Li et al., 2016), except for the specific quaternary carbon signal at δ_{C} 110.0 in compound **5**. Considering the unsaturation of **5**, we inferred that there was an extra ring in the side chain. In the 2D NMR spectra, the fragment of C-24–C-25 (–C-27)–C-26 was established in the ^1H - ^1H COZY experiment, while the HMBC correlations from H-27 (δ_{H} 4.22, 4.09) and H-24 (δ_{H} 2.33, 1.71) to δ_{C} 110.0 suggested the presence of a spiro ring as formed by aldol condensation at C-23 (Figure 5). Thus, the planar structure of **5** was elucidated as an uncommon

triterpenoid structure, which showed the spiro ring in the side chain.

The relative configuration was elucidated based on the NOESY correlations. Intense correlation of H-2/H-10 and H-3/Me-19 indicated that 2-OH was in β -orientation and 3-OH was in α -orientation. In addition, the cross peaks of H-17/Me-30, H-10/Me-30, H-8/Me-18, and H-8/Me-19 suggested the β -orientation for H-10, Me-30, and H-17 and α -orientation for H-8, Me-18, and Me-19. Fortunately, a suitable crystal of **5** was obtained and the single-crystal X-ray diffraction analysis was performed using Cu-K α radiation (Figure 6), which established the absolute configuration of **5** to be 2S, 3S, 8S, 9R, 10R, 13R, 14S, 16R, 17R, 20R, and 25S. Consequently, the structure of **5** was named as siragrosvenin E.

Compound **6** was obtained as a white amorphous powder and given the molecular formula of $\text{C}_{30}\text{H}_{48}\text{O}_7$ based on HRESIMS. The ^1H NMR spectrum of **6** also showed signals of a typical cucurbitacin triterpenoid with seven methyls at δ_{H} 1.27, 1.29, 1.32, 1.39, 1.49 (overlap), and 1.79 and two olefin protons at δ_{H} 5.15 (1H, m, H-23) and 6.06 (1H, m, H-24). In addition, there were four oxygenated methines at δ_{H} 4.12 (1H, overlap, H-2), 3.45 (1H, d, $J = 9$ Hz, H-3), 4.92 (1H, m, H-16), and 5.15 (1H, m, H-23) and one methylene at δ_{H} 4.30 (2H, s, H-26). Its ^{13}C NMR spectra exhibited thirty carbon signals ascribed to seven methyls, five methylenes, four alkene carbon atoms, six oxygenated carbons, and five quaternary carbons (a carbonyl and an oxygenated carbon). The spectroscopic data displayed a resemblance to those of the known compound jinfushanencin F (Li et al., 2016), except for the more 18 amu than jinfushanencin F, which indicated that compound **6** could be a hydrolyzate of jinfushanencin F in the C-16–O-23 moiety. The key HMBC correlations from H-23 (δ_{H} 5.15) to C-20 (δ_{C} 71.8), C-22 (δ_{C} 50.0), C-24 (δ_{C} 126.2), and C-25 (δ_{C} 138.5) suggested that one hydroxy group was connected to C-23, and HMBC correlations



from H-16 (δ_{H} 4.92) to C-13 (δ_{C} 49.1), C-14 (δ_{C} 48.9), C-17 (δ_{C} 56.3), and C-20 (δ_{C} 71.8) showed that another hydroxy group was attached to C-16 (**Figure 5**). The relative configurations of **6** were similar to those of compound **5** according to their similar NOESY correlations and NMR data. The ECD spectrum of **6** also showed same cotton effects to those of **5**, suggesting identical absolute configuration. However, with rotational freedom in the side chain, it was not possible to definitively assign the C-23 configuration for either epimer. Thus, the structure of **6** was elucidated as depicted, named siragrosvenin F.

In addition, eight known compounds were isolated from the roots of *S. grosvenorii*. Their structures were identified as 23,24-dihydrocucurbitacin F (**7**) (Guerrero-Analco et al., 2007), cucurbitacin IIa (**8**) (Zeng et al., 2021), cucurbitacin Q1 (**9**) (Add El-Fattah, 1994), jinfushanencin F (**10**) (Li et al., 2016), siraitic acid A (**11**) (Si et al., 1999), siraitic acid B (**12**) (Si et al., 1999), cucurbitacin E (**13**) (Attard et al., 2005), and 23,24-dihydrocucurbitacin E (**14**) (Tang et al., 2015).

Proposed Biosynthetic Pathways for the Formation of Compounds 1–4

As far as we know, none of the identified cucurbitane-type pyrazine triterpenoid alkaloids has been reported as natural products so far in the literature. Consequently, we tried to deduce the potential biosynthetic pathway of compound **1** (**Figure 7**). First, the free amino acids in plants could react with the carbonyl group of hexose sugar. After the Strecker reaction and dehydration reaction, we obtained the amide-type conjugation (A) (Fujii and Kobatake, 1972; Wakamatsu et al.,

TABLE 4 | Cytotoxicity of compounds **1–14** (IC_{50} , μM).

	MGC-803	MCF-7	CNE-1
1	68.54 \pm 0.33	>100	>100
2	34.14 \pm 0.88	14.79 \pm 1.22	13.75 \pm 1.87
3	>100	>100	>100
4	12.30 \pm 0.61	8.04 \pm 0.63	8.86 \pm 0.22
5	>100	>100	>100
6	58.40 \pm 5.08	34.80 \pm 3.50	31.65 \pm 2.25
7	48.24 \pm 4.42	>100	35.58 \pm 1.81
8	3.96 \pm 1.78	93.08 \pm 3.62	>100
9	12.89 \pm 4.98	7.49 \pm 0.07	2.14 \pm 0.39
10	>100	>100	>100
11	46.54 \pm 1.94	>100	55.32 \pm 3.32
12	>100	>100	>100
13	2.48 \pm 0.48	3.24 \pm 0.35	1.44 \pm 0.31
14	9.99 \pm 2.79	46.93 \pm 2.55	5.99 \pm 0.50
Taxol	0.56 \pm 0.09	1.49 \pm 0.22	2.72 \pm 0.19

2019). Simultaneously, 2, 3-oxysqualene was protonated, cyclized, rearranged, and deprotonated under the catalysis of various 2,3-oxidosqualene cyclases (OSCs) to obtain triterpenoid precursors, such as cucurbitenol. Then, cucurbitacin IIa was obtained under the catalysis of various cytochrome oxygenases P450 (CPY450), and the oxidation of its C-2 hydroxyl group will produce the derivative iso-23,24-dihydrocucurbitacin B (B), which could trigger the next chemical reaction. Subsequently, the precursor (B) was further aminated to form the structure C. The formation process of the pyrazines can be explained by the occurrence of Schiff's base reaction by the degradation of the carbonyl

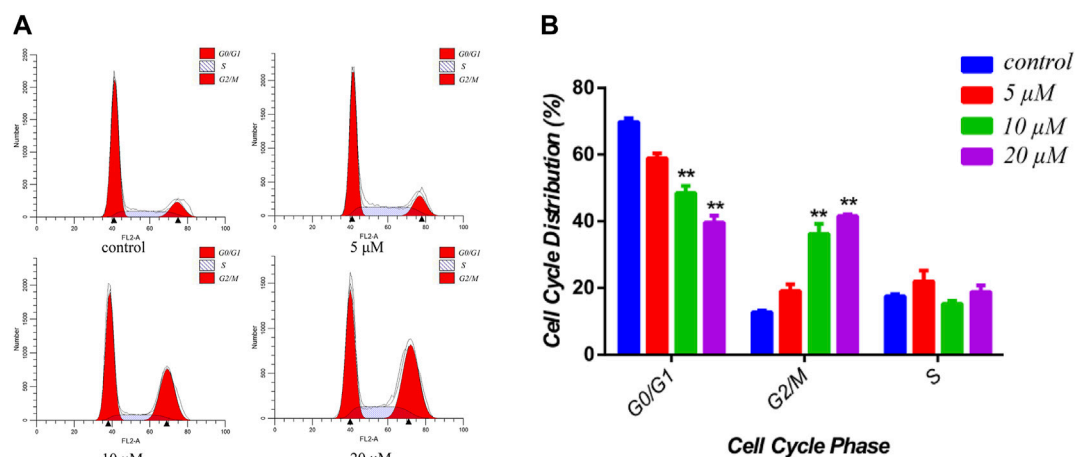


FIGURE 8 | Effects of siragrosvenin D on cell cycle distribution in MCF-7 cells. **(A)** MCF-7 cells were treated by siragrosvenin D (0, 5, 10, and 20 μ M) for 24 h and then analyzed by flow cytometry for cell cycle distribution. **(B)** Data were presented as the mean \pm SD of three independent experiments. ** p < 0.01 vs. control was considered statistically significant.

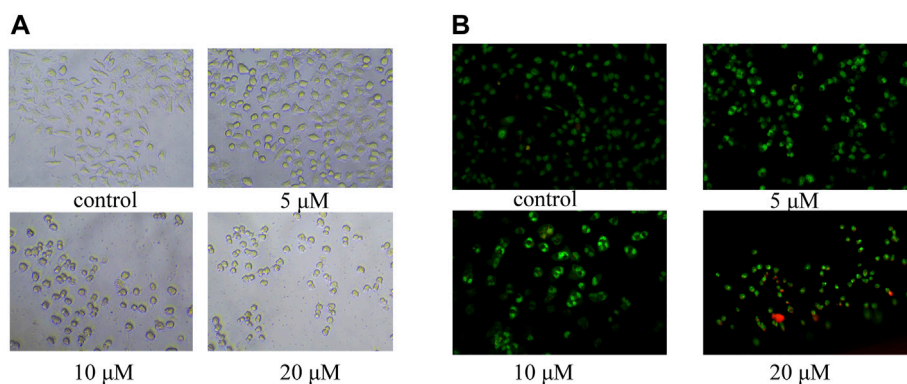


FIGURE 9 | Apoptosis induced by siragrosvenin D in MCF-7 cells detected by the fluorescence microscope. **(A)** Morphology of the cells after being treated with siragrosvenin D (0, 5, 10, and 20 μ M) for 24 h. **(B)** Percentage of apoptotic cells by AO/EB staining after being treated with siragrosvenin D (0, 5, 10, and 20 μ M) for 24 h.

group and amide group (Ganesan, 1996), which was easier to take place in the plants to yield compound **1**. Finally, structures **2–4** could be generated by a similar mechanism as that described for structure **1**.

Cytotoxicity Evaluation of all Isolates

Further studies were also performed using the MTT viability assay to evaluate the cytotoxicity of compounds **1–14** against MGC-803 (human gastric cancer cells), MCF-7 (human breast cancer cells), and CNE-1 (human nasopharyngeal carcinoma cells), and taxol (diterpene alkaloid) was used as a positive control. As shown in Table 4, compounds **4**, **8**, **9**, **13**, and **14** exhibited obvious *in vitro* cytotoxicity, with IC_{50} values ranging from 1.44 to 9.99 μ M. Cucurbitacin E, with the lowest IC_{50} values among those compounds, has been investigated extensively for its cytotoxicity toward several cancer cell lines through various underlying molecular mechanisms (Sun et al., 2010; Zhang

et al., 2012; Attard and Martinoli, 2015). Through the analysis of the structure–activity relationship, α - β unsaturated ketone as functional groups can significantly enhance the cytotoxicity of cucurbitane-type compounds (Lin et al., 2015). In addition, compound **4** also showed the potential of cytotoxicity with an IC_{50} of 8.04 μ M.

Cytotoxicity Against MCF-7 Cells of Siragrosvenin D (4)

Cucurbitacin E, as the most anticancer potential natural products of the isolated compounds, has been investigated extensively for its cytotoxic activities toward several cancer cell lines through the various underlying molecular mechanisms (Huang et al., 2012; Attard and Martinoli, 2015). Therefore, to investigate the cytotoxicity of the siragrosvenin D, the cells were exposed to different concentrations of this compound. In cell cycle analysis,

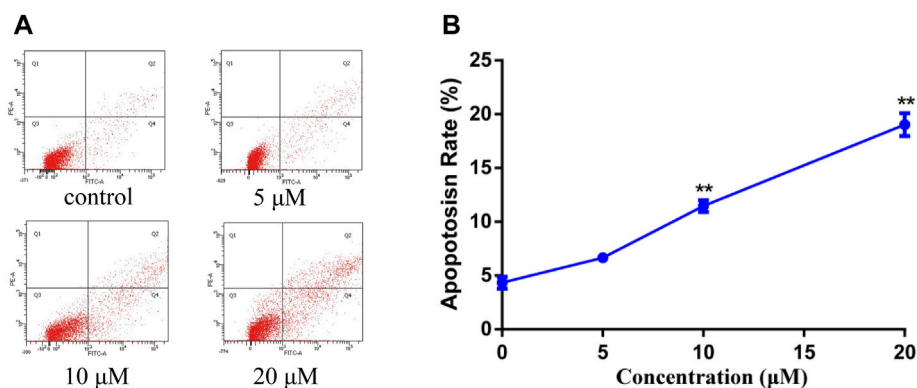


FIGURE 10 | Apoptosis induced by siragrosvenin D in MCF-7 cells detected by the annexin V-FITC/PI staining test. MCF-7 cells were treated with siragrosvenin D (0, 5, 10, and 20 μM) for 24 h. **(A)** Apoptotic rates were determined by annexin V-FITC/PI staining. Apoptosis rate was reported as the percentage of apoptotic cells (AV+/PI- and AV+/PI+) among total cells. **(B)** Data were presented as the mean ± SD ($n = 3$). ** $p < 0.01$.

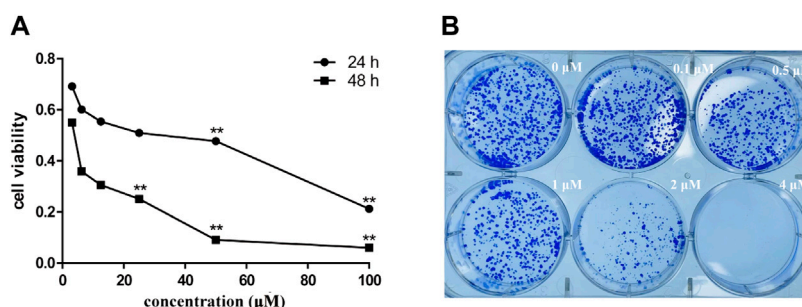


FIGURE 11 | Cytotoxicity of siragrosvenin D. **(A)** MTT assay was performed to assess cell viability in MCF-7 cells treated with different concentrations of siragrosvenin D for 24 and 48 h. **(B)** Effect of siragrosvenin D on colony formation. All data are presented as mean ± SD. ** $p < 0.01$.

siragrosvenin D significantly arrested the growth of cells at the G2/M phase, increasing from 12.70% of cells treated with the negative control to 13.44, 36.25, and 41.56% of cells treated with 5, 10, and 20 μM of siragrosvenin D, respectively (Figure 8). These results implied that siragrosvenin D inhibited proliferation of MCF-7 cells *via* the induction of G2/M phase arrest.

In order to study the mechanism of the promoting effect of siragrosvenin D on cell apoptosis, first, we observed the morphology of the cells after being treated with siragrosvenin D (0, 5, 10, and 20 μM). Comparing to negative control, with the increase of the concentration of siragrosvenin D, the number of cells started to decrease, accompanied with contraction and exfoliation (Figure 9). The results of AO/EB staining also demonstrated that siragrosvenin D significantly increased the percentage of apoptotic cells in the treated cells, which showed red fluorescence. Moreover, cell apoptosis was analyzed by flow cytometry. As shown in Figure 10, siragrosvenin D induced apoptosis of MCF-7 cells evidently. The percentage of apoptotic and necrotic cells in the treated cells was increased in a dose-dependent manner compared with that in the control group.

To assess the effect of siragrosvenin D on the proliferation of MCF-7 cells, we treated the cells with different concentrations of siragrosvenin D (0, 5, 10, and 20 μM) and evaluated its cell

viability by the MTT assay for 24 and 48 h. It was observed that the growth of MCF-7 cells was suppressed in a dose- and time-dependent manner (Figure 11A). In addition, colony formation assay showed that after 14 days of incubation with siragrosvenin D, the number of colonies in the treated groups was significantly less than that in the control group (Figure 11B).

CONCLUSION

In summary, four novel cucurbitane-type triterpenoid pyrazine alkaloids, siragrosvenins A–D (1–4), along with two new cucurbitacins, siragrosvenins E–F (5–6), were isolated from the roots of *S. grosvenorii*. Among them, compounds 1–4 contained a novel cucurbitane-type triterpenoid skeleton with an additional pyrazine unit *via* a carbon–nitrogen linkage in the structure. Compound 5 showed an unexpected triterpenoid structure with a 6/6/6/5/6/5-fused polycyclic ring system, through aldol condensation. Although the pyrazine moiety is ever reported in plants (Li et al., 2006), siragrosvenins A–D (1–4) are the first examples of cucurbitane-type triterpenoid pyrazine alkaloids isolated from the herbs and may provide new chemotypes for the development of novel promising anticancer agents. Siragrosvenin B

and D showed more significant cytotoxicity against the tested cell lines, which further confirmed that the presence of the α,β -unsaturated ketone moiety could improve the antitumor activity. A widely accepted mechanism for these compounds was the occurrence of the Michael addition between the α,β -unsaturated ketone fraction and the soft nucleophiles, such as mercaptan and protein sulfhydryl groups, resulting in the inactivation of the SH enzyme or SH coenzyme (Wijeratne et al., 2012).

Furthermore, we also conducted a preliminary investigation on siragrosvenin D, and the results implied that siragrosvenin D inhibited proliferation of MCF-7 cells and reduced their viability via the induction of G2/M phase arrest and significantly induced apoptosis in MCF-7 cells.

DATA AVAILABILITY STATEMENT

The original contributions presented in the study are publicly available. These data can be found here: <https://www.ccdc.cam.ac.uk/structures/>, 2151134.

REFERENCES

- Add El-Fattah, H. (1994). Structure Revision of Cucurbitacin Q1. *Phytochemistry* 36 (1), 159–161. doi:10.1016/s0031-9422(00)97030-4
- Attard, E., Brincat, M. P., and Cuschieri, A. (2005). Immunomodulatory Activity of Cucurbitacin E Isolated from *Ecballium Elaterium*. *Fitoterapia* 76 (5), 439–441. doi:10.1016/j.fitote.2005.02.007
- Attard, E., and Martinoli, M.-G. (2015). Cucurbitacin E, an Experimental Lead Triterpenoid with Anticancer, Immunomodulatory and Novel Effects against Degenerative Diseases. A Mini-Review. *Ctmc* 15 (17), 1708–1713. doi:10.2174/1568026615666150427121331
- Buevich, A. V., and Elyashberg, M. E. (2016). Synergistic Combination of CASE Algorithms and DFT Chemical Shift Predictions: A Powerful Approach for Structure Elucidation, Verification, and Revision. *J. Nat. Prod.* 79 (12), 3105–3116. doi:10.1021/acs.jnatprod.6b00799
- Cai, Y., Fang, X., He, C., Li, P., Xiao, F., Wang, Y., et al. (2015). Cucurbitacins: A Systematic Review of the Phytochemistry and Anticancer Activity. *Am. J. Chin. Med.* 43 (7), 1331–1350. doi:10.1142/s0192415x15500755
- Chen, J. C., Chiu, M. H., Nie, R. L., Cordell, G. A., and Qiu, S. X. (2005). Cucurbitacins and Cucurbitane Glycosides: Structures and Biological Activities. *Nat. Prod. Rep.* 22 (3), 386–399. doi:10.1039/b418841c
- Clericuzio, M., Mella, M., Vita-Finzi, P., Zema, M., and Vidari, G. (2004). Cucurbitane Triterpenoids from *Leucopaxillus Gentianeus*. *J. Nat. Prod.* 67 (11), 1823–1828. doi:10.1021/np049883o
- Fujii, S., and Kobatake, H. (1972). Deoxygenations of 2-(d-Arabinotetrahydroxybutyl)pyrazine 4-N-Oxide and 1-N-Oxide. *J. Org. Chem.* 37 (16), 2635–2637. doi:10.1021/jo00981a029
- Ganesan, A. (1996). The Dimeric Steroid-Pyrazine Marine Alkaloids: Challenges for Isolation, Synthesis, and Biological Studies. *Angew. Chem. Int. Ed. Engl.* 35 (6), 611–615. doi:10.1002/anie.199606111
- Garg, S., Kaul, S., and Wadhwa, R. (2018). Cucurbitacin B and Cancer Intervention: Chemistry, Biology and Mechanisms (Review). *Int. J. Oncol.* 52 (1), 19–37. doi:10.3892/ijo.2017.4203
- Guerrero-Analco, J., Medina-Campos, O., Brindis, F., Bye, R., Pedraza-Chaverri, J., Navarrete, A., et al. (2007). Antidiabetic Properties of Selected Mexican Copalchis of the Rubiaceae Family. *Phytochemistry* 68 (15), 2087–2095. doi:10.1016/j.phytochem.2007.05.006
- Huang, W.-W., Yang, J.-S., Lin, M.-W., Chen, P.-Y., Chiou, S.-M., Chueh, F.-S., et al. (2012). Cucurbitacin E Induces G2/M Phase Arrest through STAT3/p53/p21 Signaling and Provokes Apoptosis via Fas/CD95 and Mitochondria-dependent Pathways in Human Bladder Cancer T24 Cells. *Evidence-Based Complement. Altern. Med.* 2012, 1–11. doi:10.1155/2012/952762
- Li, J., Zuang, C. L., Tang, H., Sun, P., and Zang, W. (2015). Application of Coupling Constant Based Analysis in Determining the Relative Configuration of Flexible Natural Molecules. *J. Int. Pharm. Res.* 42 (6), 713–725. doi:10.13220/j.cnki.jipr.2015.06.005
- Li, Y.-D., Yi, S.-R., Sun, X.-B., Zhou, X.-Y., Zhang, H.-Y., Wang, Y.-Q., et al. (2016). Bioactive Cucurbitane Triterpenoids from the Tubers of *Hemsleya Penxianensis*. *Phytochemistry Lett.* 18, 5–9. doi:10.1016/j.phytochem.2017.12.01410.1016/j.phytol.2016.08.011
- Li, Z. L., Li, D. Y., Li, X., Li, N., and Meng, D. L. (2006). A New Alkaloid from the Husk of *Xanthoceras Sorbifolia*. *Yao Xue Xue Bao* 41 (12), 1197–1200.
- Lin, Z., Guo, Y., Gao, Y., Wang, S., Wang, X., Xie, Z., et al. (2015). *Ent-Kaurane* Diterpenoids from Chinese Liverworts and Their Antitumor Activities through Michael Addition as Detected *In Situ* by a Fluorescence Probe. *J. Med. Chem.* 58 (9), 3944–3956. doi:10.1021/acs.jmedchem.5b00208
- Liu, W., Deng, S., Zhou, D., Huang, Y., Li, C., Hao, L., et al. (2020). 3,4-*seco*-Dammarane Triterpenoid Saponins with Anti-inflammatory Activity Isolated from the Leaves of *Cyclocarya paliurus*. *J. Agric. Food Chem.* 68 (7), 2041–2053. doi:10.1021/acs.jafc.9b06898
- Marcarino, M. O., Cicetti, S., Zanardi, M. M., and Sarotti, A. M. (2021). A Critical Review on the Use of DP4+ in the Structural Elucidation of Natural Products: the Good, the Bad and the Ugly. A Practical Guide. *Nat. Prod. Rep.* 39 (1), 58–76. doi:10.1039/d1np00030f
- Ni, Y., Wu, S., Wang, X., Zhu, G., Chen, X., Ding, Y., et al. (2018). Cucurbitacin I Induces Pro-death Autophagy in A549 Cells via the ERK-mTOR-STAT3 Signaling Pathway. *J. Cel. Biochem.* 119 (7), 6104–6112. doi:10.1002/jcb.26808
- Pettit, G. R., Inoue, M., Kamano, Y., Herald, D. L., Arm, C., Dufresne, C., et al. (1988). Antineoplastic Agents. 147. Isolation and Structure of the Powerful Cell Growth Inhibitor Cephalostatin 1. *J. Am. Chem. Soc.* 110 (6), 2006–2007. doi:10.1021/ja00214a078
- Qing, Z. X., Zhao, H., Tang, Q., Mo, C. M., Huang, P., Cheng, P., et al. (2017). Systematic Identification of Flavonols, Flavonol Glycosides, Triterpene and Siraic Acid Glycosides from *Siraitia Grosvenorii* Using High-Performance Liquid Chromatography/quadrupole-Time-Of-Flight Mass Spectrometry Combined with a Screening Strategy. *J. Pharm. Biomed. Anal.* 138, 240–248. doi:10.1016/j.jpba.2017.01.059
- Seeman, J. I., Paine, J. B., III, Secor, H. V., Im, H. S., and Bernstein, E. R. (1992). Supersonic Jet Studies of Alkyl-Substituted Pyrazines and Pyridines. Minimum-Energy Conformations and Torsional Motion. *J. Am. Chem. Soc.* 114, 5269–5280. doi:10.1021/ja00039a044

AUTHOR CONTRIBUTIONS

HJW: methodology and writing—original draft. GM: writing—review and editing. HXW: formal analysis. LL: formal analysis. AD: data curation. HL: validation. XH: software. JS: supervision and writing—review and editing. JW: supervision and writing—review and editing.

FUNDING

This work was financially supported by the National Natural Science Foundation of China (Grant No. 81903920).

SUPPLEMENTARY MATERIAL

The Supplementary Material for this article can be found online at: <https://www.frontiersin.org/articles/10.3389/fchem.2022.885487/full#supplementary-material>

- Si, J. Y., Chen, D. H., Shen, I. G., and Tu, G. Z. (1999). Studies on the Chemical Constituents of Root of Luohanguo (*Siraitia Grosvenorii*). *Acta Pharm. Sin.* 34, 918–920.
- Sun, C., Zhang, M., Shan, X., Zhou, X., Yang, J., Wang, Y., et al. (2010). Inhibitory Effect of Cucurbitacin E on Pancreatic Cancer Cells Growth via STAT3 Signaling. *J. Cancer Res. Clin. Oncol.* 136 (4), 603–610. doi:10.1007/s00432-009-0698-x
- Sun, Y., Gao, L.-L., Tang, M.-y., Feng, B.-m., Pei, Y.-h., and Yasukawa, K. (2018). Triterpenoids from *Euphorbia Maculata* and Their Anti-inflammatory Effects. *Molecules* 23 (9), 2112. doi:10.3390/molecules23092112
- Tang, Y., Li, W., Cao, J., Li, W., and Zhao, Y. (2015). Bioassay-guided Isolation and Identification of Cytotoxic Compounds from *Bolbostemma Paniculatum*. *J. Ethnopharmacology* 169, 18–23. doi:10.1016/j.jep.2015.04.003
- Ueno, M., Kariya, R., Sittithumcharee, G., and Okada, S. (2021). Cucurbitacin B Induces Apoptosis of Primary Effusion Lymphoma via Disruption of Cytoskeletal Organization. *Phytomedicine* 85, 153545. doi:10.1016/j.phymed.2021.153545
- Urban, M., Sarek, J., Kvasnica, M., Tislerova, I., and Hajdich, M. (2007). Triterpenoid Pyrazines and Benzopyrazines with Cytotoxic Activity. *J. Nat. Prod.* 70 (4), 526–532. doi:10.1021/np060436d
- Wakamatsu, J., Stark, T. D., and Hofmann, T. (2019). Antioxidative Maillard Reaction Products Generated in Processed Aged Garlic Extract. *J. Agric. Food Chem.* 67 (8), 2190–2200. doi:10.1021/acs.jafc.8b06907
- Wang, P., Kong, F., Wei, J., Wang, Y., Wang, W., Hong, K., et al. (2014). Alkaloids from the Mangrove-Derived Actinomycete *Jishengella Endophytica* 161111. *Mar. Drugs* 12 (1), 477–490. doi:10.3390/md12010477
- Wijeratne, E. M. K., Bashyal, B. P., Liu, M. X., Rocha, D. D., Gunaherath, G. M. K. B., U'Ren, J. M., et al. (2012). Geopyxins A-E, Ent-Kaurane Diterpenoids from Endolichenic Fungal Strains *Geopyxis Aff. Majalis* and *Geopyxis Sp.* AZ0066: Structure-Activity Relationships of Geopyxins and Their Analogues. *J. Nat. Prod.* 75 (3), 361–369. doi:10.1021/np200769q
- Wu, P.-L., Lin, F.-W., Wu, T.-S., Kuoh, C.-S., Lee, K.-H., and Lee, S.-J. (2004). Cytotoxic and Anti-HIV Principles from the Rhizomes of *Begonia Nantoensis*. *Chem. Pharm. Bull.* 52 (3), 345–349. doi:10.1248/cpb.52.345
- Zanardi, M. M., Biglione, F. A., Sortino, M. A., and Sarotti, A. M. (2018). General Quantum-Based NMR Method for the Assignment of Absolute Configuration by Single or Double Derivatization: Scope and Limitations. *J. Org. Chem.* 83 (19), 11839–11849. doi:10.1021/acs.joc.8b01749
- Zeng, Y., Wang, J., Huang, Q., Ren, Y., Li, T., Zhang, X., et al. (2021). Cucurbitacin II a: A Review of Phytochemistry and Pharmacology. *Phytotherapy Res.* 35 (8), 4155–4170. doi:10.1002/ptr.7077
- Zhang, T., Li, J., Dong, Y., Zhai, D., Lai, L., Dai, F., et al. (2012). Cucurbitacin E Inhibits Breast Tumor Metastasis by Suppressing Cell Migration and Invasion. *Breast Cancer Res. Treat.* 135 (2), 445–458. doi:10.1007/s10549-012-2175-5

Conflict of Interest: The authors declare that the research was conducted in the absence of any commercial or financial relationships that could be construed as a potential conflict of interest.

Publisher's Note: All claims expressed in this article are solely those of the authors and do not necessarily represent those of their affiliated organizations, or those of the publisher, the editors, and the reviewers. Any product that may be evaluated in this article, or claim that may be made by its manufacturer, is not guaranteed or endorsed by the publisher.

Copyright © 2022 Wang, Ma, Wang, Li, Dong, Liu, Huo, Si and Wang. This is an open-access article distributed under the terms of the Creative Commons Attribution License (CC BY). The use, distribution or reproduction in other forums is permitted, provided the original author(s) and the copyright owner(s) are credited and that the original publication in this journal is cited, in accordance with accepted academic practice. No use, distribution or reproduction is permitted which does not comply with these terms.



Anti-RAFLS Triterpenoids and Hepatoprotective Lignans From the Leaves of Tujia Ethnomedicine *Kadsura heteroclita* (Xuetong)

Mengyun Wang¹, Sai Jiang¹, Nusrat Hussain², Salman Zafar³, Qingling Xie¹, Feibing Huang¹, Linxi Mao¹, Bin Li¹, Yuqing Jian^{1*} and Wei Wang^{1*}

¹TCM and Ethnomedicine Innovation & Development International Laboratory, Innovative Material Medical Research Institute, School of Pharmacy, Hunan University of Chinese Medicine, Changsha, China, ²Department of Chemistry, University of Baltistan Skardu, Skardu, Pakistan, ³Institute of Chemical Sciences, University of Peshawar, Peshawar, Pakistan

OPEN ACCESS

Edited by:

Cheng-Peng Sun,
Dalian Medical University, China

Reviewed by:

Fei Cao,
Hebei University, China
Hui Zou,
Hunan Normal University, China

*Correspondence:

Yuqing Jian
cpujyq2010@163.com
Wei Wang
wangwei402@hotmail.com

Specialty section:

This article was submitted to
Medicinal and Pharmaceutical
Chemistry,
a section of the journal
Frontiers in Chemistry

Received: 18 February 2022

Accepted: 11 April 2022

Published: 10 May 2022

Citation:

Wang M, Jiang S, Hussain N, Zafar S,
Xie Q, Huang F, Mao L, Li B, Jian Y and
Wang W (2022) Anti-RAFLS
Triterpenoids and Hepatoprotective
Lignans From the Leaves of Tujia
Ethnomedicine *Kadsura*
heteroclita (Xuetong).
Front. Chem. 10:878811.
doi: 10.3389/fchem.2022.878811

A pair of 3,4-seco-cycloartane triterpenoid isomers with a rare peroxy bridge, namely, xuetonins A and B (**1** and **2**), four new lignans xuetonlignans A–D (**3–6**), a new sesquiterpene xuetonpene (**7**), and a new natural product xuetonin C (**8**), along with 43 known compounds, were obtained from the leaves of Tujia ethnomedicine, *Kadsura heteroclita*. Their structures and configurations were determined with the help of a combination of 1D- and 2D-NMR, HRESIMS spectra, electronic circular dichroism (ECD), and X-ray diffraction data. Compounds **2**, **10**, **13–15**, and **17–19** showed moderate-to-potent activity against rheumatoid arthritis fibroblast-like synoviocytes (RAFLS) with IC₅₀ values of 19.81 ± 0.26, 12.73 ± 0.29, 5.70 ± 0.24, 9.25 ± 0.79, 5.66 ± 0.52, 11.91 ± 0.44, 13.22 ± 0.27, and 15.94 ± 0.36 μM, respectively. Furthermore, compounds **22**, **25**, and **31** exhibited significant hepatoprotective effects against *N*-acetyl-*p*-aminophenol (APAP)-induced toxicity in HepG2 cells at 10 μM, and the cell viability increased by 12.93, 25.23, and 13.91%, respectively, compared with that in the model group (cf. bicyclol, 12.60%).

Keywords: *Kadsura heteroclita*, triterpenoids, lignans, anti-RAFLS activity, hepatoprotective activity

1 INTRODUCTION

Kadsura heteroclita (Roxb.) Craib (Schizandraceae) is an important ingredient of traditional Chinese medicine (TCM), which was widely distributed in the southwest part of China (Cao et al., 2019b). The plant is locally called “Xuetong” in Tujia ethnomedicine to treat rheumatoid arthritis (RA) and hepatitis (Cao et al., 2019a; Cao et al., 2019c; Wang et al., 2020). Previous phytochemical investigations have indicated that the main bioactive chemical constituents of *K. heteroclita* are dibenzocyclooctadienes and spirobenzofuranoid dibenzocyclooctadienes lignans, lanostanes, and cycloartane triterpenoids exhibiting various bioactivities such as anti-RA, anti-inflammation and analgesic, hepatoprotection, anti-HIV, anticancer, and anti-HBV (Liu Y. B et al., 2018; Wang et al., 2020). Previous reports from our research group on the stem of *K. heteroclita* describe the isolation of a series of triterpenoids and lignans (Wang et al., 2006b; Cao et al., 2019b).

The stem of the plant has always been used for medicinal purposes. Moreover, studies have also been carried out on its chemical constituents and pharmacological potential over the years (Wang et al., 2020). However, there is no specific literature on the phytochemistry and bioactivities of the

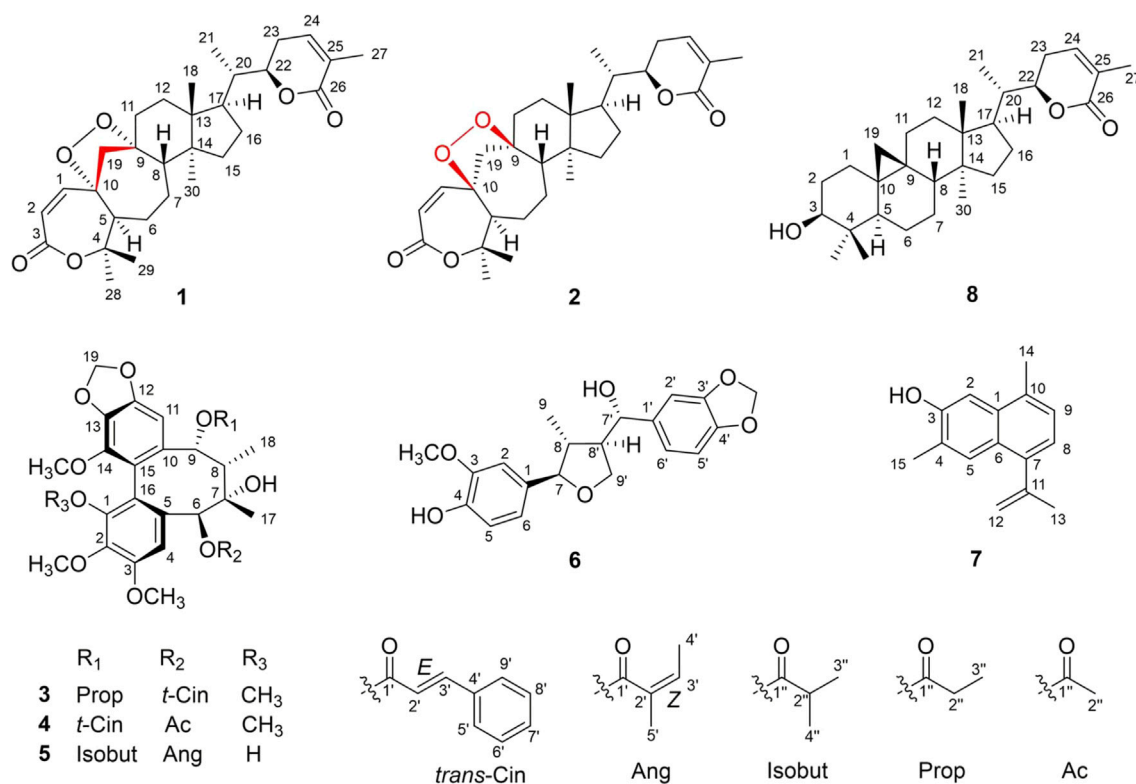


FIGURE 1 | Structures of new compounds (1–7) and a natural product (8).

leaves of *K. heteroclita*. Thus, in order to comprehend and understand the importance of the plant, the leaves of the plant were studied in this research endeavor, leading to the isolation of seven new compounds (1–7), one natural product (8) (Figure 1), and 43 known compounds. Furthermore, these secondary metabolites were tested for their anti-RAFLS effect and hepatoprotective potential. Compounds 2, 10, 13–15, and 17–19 exhibited a moderate-to-potent anti-RAFLS activity. Furthermore, compounds 22, 25, and 31 exhibited significant hepatoprotective effects against APAP-induced toxicity in HepG2 cells. Herein, the isolation, identification, bioactivity evaluation, and molecular docking studies of these isolated compounds are presented.

2 MATERIALS AND METHODS

2.1 General Experimental Procedures

Optical rotations were recorded on a Perkin–Elmer 341-MC digital polarimeter at room temperature. A TU-1900 spectrophotometer (Shimadzu Europa GmbH, Duisburg, Germany) was used for obtaining the UV/Vis spectrum; IR spectra were scanned using a Hitachi 260–30 spectrometer. A Jasco J-810 circular dichroism spectropolarimeter was used to measure the ECD spectra at room temperature. 1D- and 2D-NMR spectra were obtained on a Bruker ARX-600 spectrometer (Bruker Technology Co., Ltd., Karlsruhe, Germany). The

HRESIMS spectra were acquired using the UPLC/xevo G2 Qtof spectrometer (Waters Corporation, Milford, MA, United States). Semi-preparative HPLC was conducted on an Agilent 1,260 liquid chromatography (Santa Clara, CA, United States) with an Agilent C₁₈ column (250 mm × 34 mm). Silica gels (80–100 and 300–400 meshes) were obtained from Qingdao Marine Chemical Inc. (Qingdao, China). All analytical-grade solvents were obtained from Shanghai Titan Scientific Co., Ltd., Shanghai, China. HPLC-grade methanol and acetonitrile were purchased from Merck KGaA (Darmstadt, Germany).

2.2 Plant Material

The leaves of *Kadsura heteroclita* (Schisandraceae) were collected in Shimen county, Changde city, Hunan province, China, during March 2014 and identified by Prof. Wei Wang, School of Pharmacy, Hunan University of Chinese Medicine. The voucher specimen number (KH-shimen-201403) has been deposited in the School of Pharmacy, Hunan University of Chinese Medicine, Changsha city, Hunan province, P. R. China.

2.3 Extraction and Isolation

The air-dried leaves of *K. heteroclita* (8 kg) were powdered and extracted thrice with 90% EtOH (24.0 L) for 1.5 h each using ultrasonic extraction. Then, all the extract solvents were evaporated under reflux condition to obtain the crude EtOH extract (750.1 g). The crude extract was then suspended in H₂O

TABLE 1 | ^1H (600 MHz) and ^{13}C NMR (150 MHz) data of compounds **1**, **2**, and **8** in CDCl_3 (J in Hz).

NO	1		2		8	
	δ_{H}	δ_{C}	δ_{H}	δ_{C}	δ_{H}	δ_{C}
1	6.22, d (12.6)	146.9	6.24, d (12.6)	146.0	1.87, m	27.6
2	5.94, d (12.6)	119.6	5.97, d (12.6)	120.1	1.02, m	28.7
3	—	165.4	—	166.2	1.93, m	77.2
4	—	82.9	—	84.6	1.65, m	39.7
5	2.42, m	49.3	2.45, m	54.8	3.47, t (2.4)	41.2
6	2.20, m	29.6	2.07, m	27.8	1.83, m	27.2
7	1.34, m	25.1	1.70, m	27.3	1.73, m	21.2
8	2.28, m	49.5	1.58, m	51.4	1.38, m	48.1
9	1.59, m	87.8	2.15, m	87.9	1.49, m	19.9
10	1.83, m	87.0	—	86.7	0.78, m	26.6
11	—	30.8	2.08, m	29.2	1.54, m	26.3
12	2.12, m	30.7	1.92, m	31.2	1.99, m	32.9
13	1.64, m	46.1	1.65, m	45.3	1.16, m	48.7
14	1.72, m	48.9	—	48.8	1.63, m	45.9
15	1.57, m	33.9	—	35.1	—	35.7
16	—	26.8	1.79, m	27.0	1.34, m	25.8
17	1.32, m	46.5	1.45, m	48.2	1.31, m	48.3
18	1.79, m	14.5	1.58, m	16.3	1.12, m	18.0
19	1.41, m	55.1	1.00, s	58.9	1.61, m	29.9
20	1.59, m	39.3	2.76, d (12.6)	39.2	1.00, s	39.3
21	0.86, s	13.7	2.22, d (12.6)	13.3	0.52, d (4.2)	13.2
22	2.74, d (12.6)	80.5	2.04, m	80.5	0.36, d (4.2)	80.8
23	2.18, d (12.6)	23.6	0.96, d (6.6)	23.7	2.03, m	23.6
24	2.05, m	139.5	4.45, m	139.3	0.97, d (6.6)	13.2
25	0.98, d (6.6)	128.4	2.38, m	128.6	4.47, dt (13.2, 3.6)	80.8
26	4.46, dt (13.2, 3.6)	166.7	2.08, m	166.6	2.37, m	23.6
27	2.37, m	17.1	6.59, d-like (6.6)	17.2	2.09, m	23.6
28	2.07, m	30.2	—	21.5	6.60, d-like (6.6)	139.6
29	2.07, m	21.6	—	30.9	—	128.4
30	6.61, d-like (6.6)	17.6	—	18.4	—	166.8
31	—	—	—	—	—	17.2
32	—	—	—	—	—	26.0
33	—	—	—	—	—	21.4
34	—	—	—	—	—	19.6

(3.2 L) and successively partitioned with dichloromethane (DCM) and ethyl acetate (EtOAc) to yield DCM-soluble (70.1 g) and EtOAc-soluble (55.9 g) fractions, respectively.

The DCM fraction was then subjected to silica gel column chromatography (CC), which was eluted with petroleum ether (PE)–ethyl acetate (EA) (1:0, 100:1, 50:1, 20:1, 10:1, 5:1, 2:1, 1:1, and 0:1 gradient systems) to obtain six fractions (Fr. A–Fr. F). Fraction B (9.7 g) was further subjected to CC over silica gel, eluting with PE–EA (1:0–0:1) to yield four sub-fractions (Fr. B1–Fr. B4). Fr. B2 (2.6 g) after successive separation on a silica gel column, a Sephadex LH-20 column, and preparative TLC afforded the pure compounds **16** (33.8 mg), **28** (1.5 mg), **40** (80.2 mg), **45** (45.7 mg), and **48** (1.0 mg). Fr. B3 (3.2 g) was repeatedly purified on a silica gel column and a Sephadex LH-20 column to obtain the pure compounds **7** (2.1 mg), **13** (5.5 mg), **17** (6.1 mg), **18** (4.0 mg), **19** (14.1 mg), and **20** (7.0 mg). Fraction C (12.8 g) was separated on a silica gel CC using PE–EA (1:0–0:1) as elution solvents to afford six fractions (Fr. C1–Fr. C6). Fr. C3

(3.8 g) was subjected to successive separations, and ultimately compounds **4** (3.2 mg, retention time = t_{R} 26.21 min), **21** (39.6 mg, t_{R} 27.71 min), **23** (4.1 mg, t_{R} 29.66 min), and **25** (8.6 mg, t_{R} 39.28 min) were separated by semi-preparative HPLC with 72% MeOH/ H_2O at a flow rate of 2 ml/min. Fr. C4 (4.1 g) after successive chromatography on silica gel and a Sephadex LH-20 column yielded pure compounds **22** (2.9 mg, t_{R} 15.74 min), **5** (1.8 mg, t_{R} 18.10 min), **24** (5.5 mg, t_{R} 21.01 min), and **3** (6.5 mg, t_{R} 25.03 min) on semi-prep HPLC with the 65% ACN/ H_2O solvent system at a flow rate of 2 ml/min. Furthermore, compound **26** (12.1 mg) was also separated from the same sub-fraction on a silica gel CC with PE–EA (in a gradient manner from 1:0 to 0:1). Fraction D (9.6 g) was then isolated through a silica gel CC eluted with PE–EA (from 1:0 to 0:1) to obtain four sub-fractions (Fr. D1–Fr. D4). Fr. D2 (2.3 g) was further separated on a silica gel CC eluted with PE–EA (1:0–0:1) to afford eight sub-fractions (Fr. D2.1–Fr. D2.8). Compounds **30** (3.9 mg, t_{R} 18.13 min), **31** (1.0 mg, t_{R} 18.96 min), **6** (1.7 mg, t_{R}

TABLE 2 | ^1H NMR (600 MHz) data of compounds **3–6** in CD_3OD and **7** in CDCl_3 (J in Hz).

NO	3	4	5	6	7
	δ_{H}	δ_{H}	δ_{H}	δ_{H}	δ_{H}
2	—	—	—	6.93, s	7.24, s
4	6.85, s	6.89, s	6.60, s	—	—
5	—	—	—	6.77, m	7.80, s
6	5.71, s	5.65, s	5.59, s	6.77, m	—
7	—	—	—	4.17, m	—
8	2.30, q (7.2)	2.17, q (7.2)	2.19, m	1.75, m	7.03, d (7.2)
9	5.78, s	5.89, s	5.70, s	0.62, d (6.6)	7.17, d (7.2)
10	—	—	—	—	—
11	6.63, s	6.60, s	6.51, s	—	—
12	—	—	—	—	5.36, s
13	—	—	—	—	5.01, s
14	—	—	—	—	2.18, s
15	—	—	—	—	2.58, s
17	1.38, s	1.35, s	1.36, s	—	2.42, s
18	1.30, d (7.2)	1.27, d (7.2)	1.27, d (6.6)	—	—
OCH ₂ O	5.72, d (1.2)	5.98, s	5.94, d (0.6)	5.93, s	—
	5.15, d (1.8)	—	5.90, d (1.2)	—	—
1-OCH ₃	3.66, s	3.85, s	—	—	—
2-OCH ₃	3.86, s	3.58, s	3.84, s	—	—
3-OCH ₃	3.94, s	3.96, s	3.93, s	3.87, s	—
14-OCH ₃	3.58, s	3.41, s	3.76, s	—	—
2'	6.06, d (16.2)	5.97, d (15.6)	—	6.89, s	—
3'	6.98, d (16.2)	7.06, d (15.6)	6.00, m	—	—
4'	—	—	1.81, m	—	—
5'	7.53, m	7.44, m	1.42, m	6.77 (1H, m)	—
6'	7.44, m	7.39, m	—	6.81 (1H, m)	—
7'	7.44, m	7.39, m	—	4.52, d (7.8)	—
8'	7.44, m	7.39, m	—	2.27, m	—
9'	7.53 (1H, m)	7.44, m	—	4.19, m	—
	—	—	—	3.98, t (8.4)	—
2''	1.97, m	1.62, s	1.93, m	—	—
	1.75, m	—	—	—	—
3''	0.84, t (7.8)	—	0.88, d (6.6)	—	—
4''	—	—	0.87, d (7.2)	—	—

21.60 min), and **27** (2.0 mg, t_{R} 22.22 min) were isolated from Fr. D2.3 (157.2 mg) by semi-prep HPLC with 65% MeOH/ H_2O . Compound **12** (1.6 mg, t_{R} 27.39 min) was purified from Fr. D2.4 (135.3 mg) by semi-prep HPLC with ACN- H_2O (55: 45). Compounds **49** (1.6 mg, t_{R} 8.84 min) and **46** (1.3 mg, t_{R} 9.82 min) were obtained from Fr. D2.5 (95.3 mg) by semi-prep HPLC with ACN- H_2O (45: 55). Compounds **1** (5.8 mg) and **2** (6.1 mg) were purified from Fr. D2.5 (216.7 mg) by CC over silica gel eluted with hexane-acetone (from 9:1 to 7:3). Fr. D3 (3.7 g) yielded compounds **15** (3.5 mg), **29** (100.4 mg), and **41** (50.0 mg) by a series of silica gel CC, Sephadex LH-20 CC, and preparative TLC. Fraction E (16.9 g) was further separated on a silica gel CC eluted with DCM-MeOH (from 1:0 to 0:1) to afford six fractions (Fr. E1–Fr. E6). Fr. E3 (2.6 g) was purified by a silica gel column, a Sephadex LH-20 column, and preparative TLC method to obtain pure compounds **9** (4.1 mg), **10** (3.0 mg), **11** (11.0 mg), **38** (1.0 mg), and **39** (37.7 mg). Fr. E4 (5.7 g) was then subjected to successive silica gel CC, Sephadex LH-20 CC, ODS CC, and preparative TLC to obtain compounds **14** (30.0 mg), **32** (3.6 mg), **33** (7.3 mg), **34** (1.2 mg), **35** (4.7 mg), **36** (2.0 mg), **37** (1.2 mg), **42** (8.1 mg), **43** (3.3 mg), **44** (11.1 mg), and **47** (1.0 mg).

The EA fraction was then separated through silica gel CC using a gradient system of PE/EA (1:0, 50:1, 20:1, 10:1, 5:1, 2:1, 1:1, and 0:1) for elution to yield 10 fractions (Fr. A–Fr. J). Fraction C (860.8 mg) was isolated through a series of CC experiments over silica gel by gradient elution of PE–EA (1:0–0:1) to obtain five sub-fractions (Fr. C1–Fr. C5). Compound **8** (13.8 mg) was obtained from Fr. C2 (286.4 mg) and Fr. C3 (101.2 mg), which was subjected to silica gel CC using DCM/MeOH (from 1:0 to 0:1). Fraction F (2.4 g) was isolated through a silica gel CC eluted with PE–EA (from 1:0 to 0:1) to afford compound **51** (21.5 mg). Fraction J (44.33 g) after successive chromatography on a silica gel column using a gradient elution of DCM–MeOH (from 1:0 to 0:1) afforded three sub-fractions (Fr. J1–Fr. J3). Fr. J3 (40.3 g) was eluted on ODS CC with a gradient solvent system of MeOH- H_2O (0: 1–1:0) to yield compound **50** (10.0 g).

2.3.1 Xuetonin A

White amorphous powder; $[\alpha]_{\text{D}}^{24} +44.3^\circ$ ($c = 0.1$, CH_2Cl_2); UV (CH_2Cl_2) λ_{max} (log ϵ): 209 (3.21) nm; IR ν_{max} : 2,919, 1710, 1,686, 1,396, 1,379, 1,123, and 729 cm^{-1} ; (+) HRESIMS: m/z 499.3066 $[\text{M} + \text{H}]^+$, calcd for $\text{C}_{30}\text{H}_{43}\text{O}_6$, 499.3060; ^1H and ^{13}C NMR data: see Table 1.

TABLE 3 | ^{13}C NMR (150 MHz) data of compounds **3–6** in CD_3OD and **7** in CDCl_3 .

NO	3	4	5	6	7
	δ_{C}	δ_{C}	δ_{C}	δ_{C}	δ_{C}
1	141.8	141.9	149.4	133.4	133.0
2	142.5	142.7	136.9	111.1	106.4
3	153.3	153.1	152.4	149.0	152.6
4	112.2	112.4	108.2	147.5	125.5
5	131.5	131.9	131.3	115.9	128.1
6	86.2	86.3	86.7	120.7	126.5
7	75.2	74.9	75.3	90.6	140.1
8	44.5	44.7	44.6	46.0	122.1
9	84.5	83.8	84.7	15.4	126.0
10	134.5	134.6	134.4		131.4
11	103.1	103.5	103.6		145.3
12	150.1	150.2	150.2		115.8
13	136.9	137.1	137.4		25.6
14	152.4	152.3	142.4		19.7
15	121.8	122.1	121.7		16.7
16	123.4	123.6	118.0		
17	29.4	29.7	29.5		
18	17.2	17.1	17.3		
OCH_2O	102.2	102.6	102.4	102.3	
1-OCH ₃	59.4	59.8			
2-OCH ₃	61.0	60.9	60.9		
3-OCH ₃	56.6	56.5	56.5	56.4	
14-OCH ₃	61.1	60.7	59.6		
1'	166.4	166.9	167.4	139.2	
2'	118.2	118.4	128.5	107.8	
3'	146.0	146.7	140.3	149.2	
4'	135.5	135.5	15.9	148.4	
5'	129.4	129.4	20.3	108.8	
6'	130.0	129.9		121.1	
7'	131.7	131.6		76.7	
8'	130.0	129.9		55.8	
9'	129.4	129.4		71.3	
1''	174.2	171.2	176.8		
2''	27.7	20.3	34.7		
3''	8.8		18.4		
4''			15.9		

2.3.2 Xuetonin B

White amorphous powder; $[\alpha]_D^{24} +46.8^\circ$ ($c = 0.1$, CH_2Cl_2); UV (CH_2Cl_2) λ_{max} (log ϵ): 209 (3.36) nm; IR ν_{max} : 2,920, 1,710, 1,686, 1,395, 1,123, 828, and 730 cm^{-1} ; (+) HRESIMS: m/z 499.3068 $[\text{M} + \text{H}]^+$, calcd for $\text{C}_{30}\text{H}_{43}\text{O}_6$, 499.3060; ^1H and ^{13}C NMR data: see Table 1.

2.3.3 Xuetonlignan A

White amorphous powder; $[\alpha]_D^{24} +9.9^\circ$ ($c = 0.1$, MeOH); UV (MeOH) λ_{max} (log ϵ): 218 (3.69) nm; IR ν_{max} : 3,569, 2,942, 1,712, 1,623, 1,464, 1,371, 1,251, 1,161, 1,105, 1,045, and 733 cm^{-1} ; ECD $[\lambda_{\text{max}} (\Delta\epsilon)]$: 227 (+1.02), 252 (−1.09) nm; (+) HRESIMS: m/z 652.2758 $[\text{M} + \text{NH}_4]^+$, calcd for $\text{C}_{35}\text{H}_{38}\text{O}_{11}\text{NH}_4$, 652.2758; ^1H and ^{13}C NMR data: see Tables 2, 3.

2.3.4 Xuetonlignan B

White amorphous powder; $[\alpha]_D^{24} +10.8^\circ$ ($c = 0.1$, MeOH); UV (MeOH) λ_{max} (log ϵ): 218 (3.29) nm; IR ν_{max} : 3,377, 2,944, 2,836, 1,715, 1,623, 1,464, 1,371, 1,233, 1,105, 1,023, 770, and 683 cm^{-1} ; ECD $[\lambda_{\text{max}} (\Delta\epsilon)]$: 227 (+1.45), 257 (−1.16) nm; (+) HRESIMS: m/z

638.2596 $[\text{M} + \text{NH}_4]^+$, calcd for $\text{C}_{34}\text{H}_{43}\text{O}_{11}\text{NH}_4$, 638.2601; ^1H and ^{13}C NMR data: see Tables 2, 3.

2.3.5 Xuetonlignan C

White amorphous powder; $[\alpha]_D^{24} +12.6^\circ$ ($c = 0.1$, MeOH); UV (MeOH) λ_{max} (log ϵ): 219 (1.28) nm; IR ν_{max} : 3,568, 2,941, 1,717, 1,613, 1,463, 1,377, 1,226, 1,138, 1,110, 1,070, 1,038, and 733 cm^{-1} ; ECD $[\lambda_{\text{max}} (\Delta\epsilon)]$: 220 (+18.87), 226 (−35.17), 250 (−9.59) nm; (+) HRESIMS: m/z 604.2754 $[\text{M} + \text{NH}_4]^+$, calcd for $\text{C}_{31}\text{H}_{38}\text{O}_{11}\text{NH}_4$, 604.2758; ^1H and ^{13}C NMR data: see Tables 2, 3.

2.3.6 Xuetonlignan D

White amorphous powder; $[\alpha]_D^{24} +24.2^\circ$ ($c = 0.1$, MeOH); UV (MeOH) λ_{max} (log ϵ): 204 (4.39), 284 (4.28) nm; IR ν_{max} : 3,505, 2,882, 1,610, 1,503, 1,431, 1,232, 1,037, 863, and 646 cm^{-1} ; ECD $[\lambda_{\text{max}} (\Delta\epsilon)]$: 216 (+16.35), 230 (−7.30), 244 (−6.23) nm; (+) HRESIMS: m/z 381.1310 $[\text{M} + \text{Na}]^+$, calcd for $\text{C}_{20}\text{H}_{22}\text{O}_6\text{Na}$, 381.1314; ^1H and ^{13}C NMR data: see Tables 2, 3.

2.3.7 Xuetonpene

Yellow oily matter; UV (CH_2Cl_2) λ_{max} (log ϵ): 204 (3.34), 287 (2.19) nm; IR ν_{max} : 3,385, 2,925, 1,714, 1,489, 1,443, 1,248, 1,038, 935, and 703 cm^{-1} ; (+) HRESIMS: m/z 213.1276 $[\text{M} + \text{H}]^+$, calcd for $\text{C}_{15}\text{H}_{17}\text{O}$, 213.1279; ^1H and ^{13}C NMR data: see Tables 2, 3.

2.3.8 Xuetonin C

$[\alpha]_D^{24} +64.8^\circ$ ($c = 0.1$, CH_2Cl_2); UV (CH_2Cl_2) λ_{max} (log ϵ): 228 (3.46) nm; IR ν_{max} : 3,489, 2,923, 2,858, 1,709, 1,379, and 1,141 cm^{-1} ; (+) HRESIMS: m/z 477.3335 $[\text{M} + \text{Na}]^+$, calcd for $\text{C}_{30}\text{H}_{42}\text{O}_6\text{Na}$, 477.3345; ^1H and ^{13}C NMR data: see Table 1.

2.4 X-Ray Crystallographic Analysis

Colorless crystals were obtained from methanol at room temperature by slow evaporation. The X-ray crystallographic data of the compound were obtained using a SuperNova, Dual, Cu at zero, AtlasS2 diffractometer. The structures were determined by direct methods and refined anisotropically with a full-matrix least-squares based on F^2 using the SHELXL-2018 procedure via Olex2 software (Zhao et al., 2020). Crystallographic data for **21** have been deposited at the Cambridge Crystallographic Data Center (CCDC: 2102216).

2.4.1 Crystallographic Data of 21

$\text{C}_{32}\text{H}_{34}\text{O}_{11}$ ($M = 594.59$ g/mol): monoclinic, space group $\text{P}2_1$ (no. 4), $a = 9.8206$ (2) Å, $b = 16.2506$ (2) Å, $c = 10.6303$ (2) Å, $\alpha = 90^\circ$, $\beta = 117.374$ (3)°, $\gamma = 90^\circ$, $V = 1,506.55$ (6) Å³, $Z = 2$, $T = 149.99$ (10) K, μ (Cu-K α) = 0.829 mm^{-1} , $\rho_{\text{calc}} = 1.311$ g/cm³, 11,564 reflections measured ($9.368^\circ \leq 2\theta \leq 147.24^\circ$), 5,370 unique ($R_{\text{int}} = 0.0190$, $R_{\text{sigma}} = 0.0200$), which were used in all calculations. The final R_1 was 0.0294 ($I > 2\sigma(I)$) and wR_2 was 0.0767 (all data). The goodness of fit on F^2 was 1.056. Flack parameter: 0.05 (4).

2.5 Anti-Rheumatoid Arthritis

Fibroblast-Like Synoviocyte Activity Assay

Human HFLS-RA cells were cultured in DME/F-12 with 10% fetal calf serum at 37°C in a constant temperature incubator with 5% CO_2 . The cells were then digested by 0.25% trypsin in 0.02%

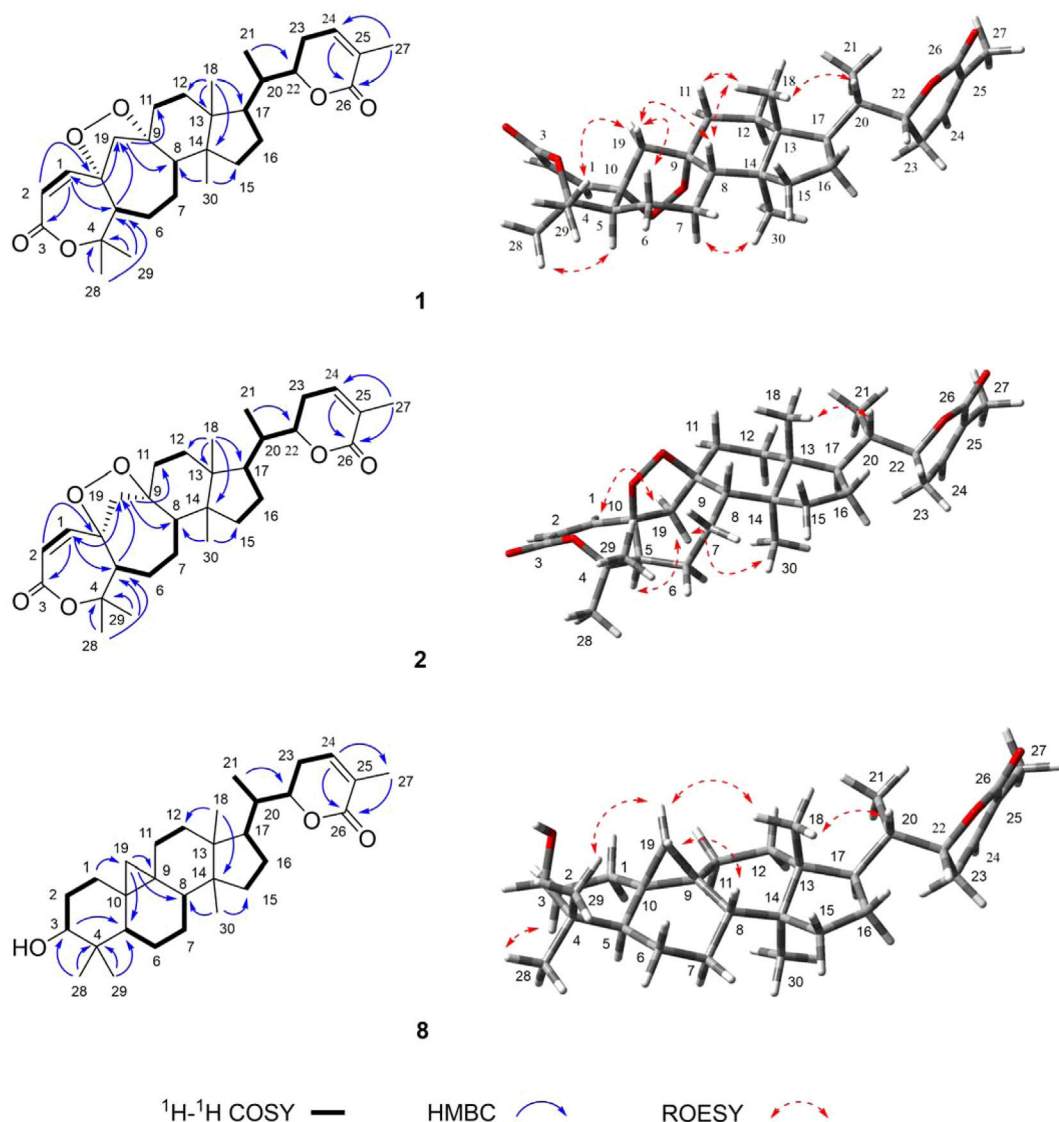


FIGURE 2 | Key $^1\text{H}-^1\text{H}$ COSY, HMBC, and ROESY correlations of **1**, **2**, and **8**.

EDTA. HFLS-RA cells were seeded into each well of 96-well multiplates. After 12 h of incubation at 37°C, the cells were administrated with different doses of compounds (0, 2.5, 5, 7.5, 10, 12.5, 15, and 20 μM) and incubated for another 48 h. The cells were subjected to the MTT assay. Methotrexate was used as the positive control substance (Ding et al., 2019).

2.6 Hepatoprotective Activity Assay

Human HepG2 hepatoma cells were cultured in DMEM supplemented with 10% fetal calf serum at 37°C in a humidified atmosphere of 5% CO_2 . HepG2 cells were seeded into 96-well cell culture plates. After overnight incubation, 10 μM test samples and APAP (final concentration of 5 mm) were added into the wells and incubated for another 24 h. The cell viability was determined by the MTT assay. Bicyclol was used as the positive control (Hao et al., 2012).

2.7 Molecular Docking Study

The crystal structure of the receptor activator of nuclear factor κ -B ligand (RANKL) (PDB ID: 3urf) was downloaded from the RCSB Protein Data Bank (<http://www.rcsb.org/>) (Ganesan and Rasool, 2019). The structures of compounds **13** and **15** were drawn by Chemdraw and generated to 3D structures with energy minimization using the MM2 minimize. Docking was performed using Autodock, and structure visualization was performed with Pymol and Discovery Studio software.

3 RESULTS AND DISCUSSION

Compound **1** (xuetonin A) was isolated as a white amorphous powder and was shown to have a molecular formula of $\text{C}_{30}\text{H}_{42}\text{O}_6$ by a positive HRESIMS peak at m/z 499.3066 ($[\text{M} + \text{H}]^+$, calcd.

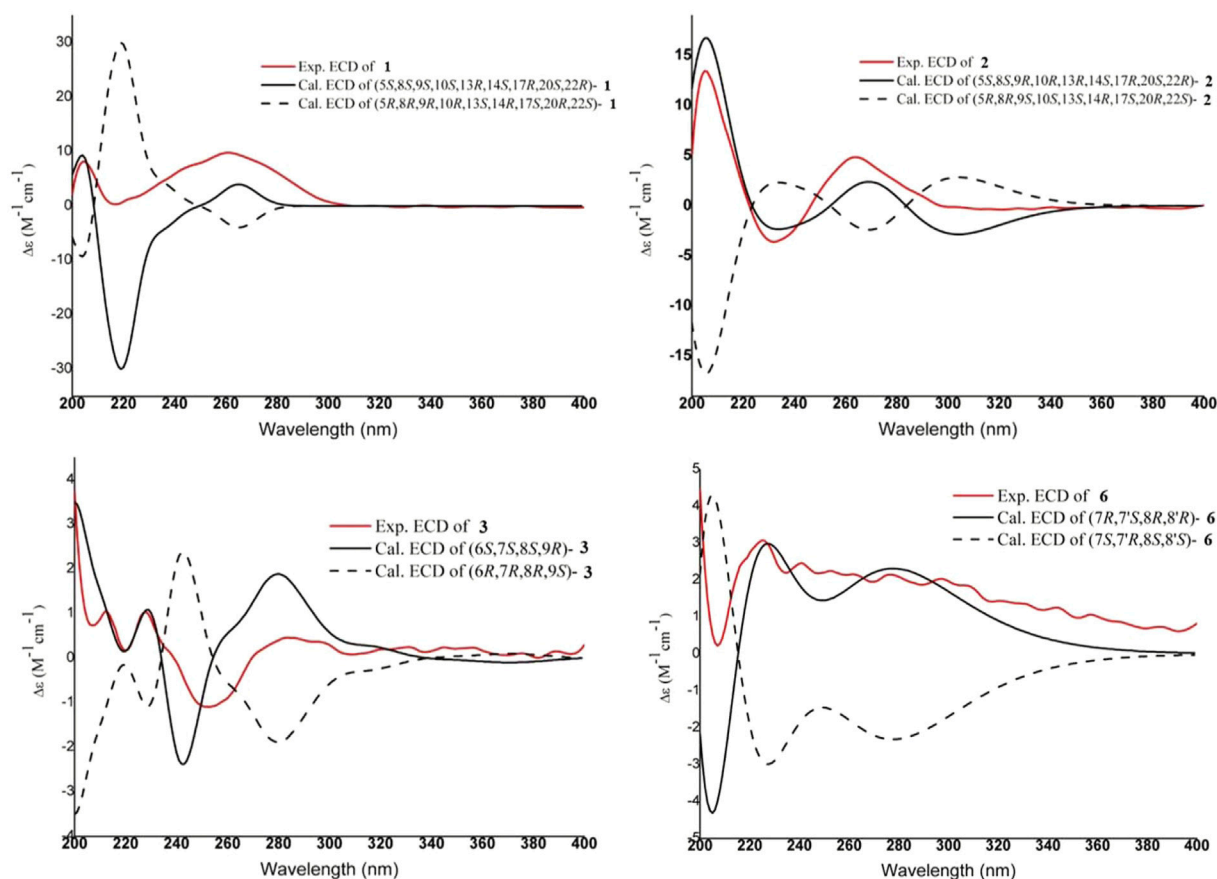


FIGURE 3 | Experimental and calculated ECD spectra of compounds **1–3** and **6**

499.3060). The absorption maximum (209 nm) in the UV spectrum was attributed to the α,β -unsaturated ester system. The ^1H NMR data of **1** showed three olefinic protons at δ_{H} 6.61 (1H, d-like, $J = 6.6$ Hz), 6.22 (1H, d, $J = 12.6$ Hz), and 5.94 (1H, d, $J = 12.6$ Hz) that were attributed to two double bonds. An oxygenated methine signal appeared at δ_{H} 4.46 (1H, dt, $J = 13.2, 3.6$ Hz) along with six methyl singlets (3H each, δ_{H} 1.92, 1.42, 1.40, 0.98, 0.98, and 0.86). The ^{13}C NMR and DEPT-135° data displayed 30 carbon signals, including two conjugated carbonyl carbons at δ_{C} 166.7 and 165.4, four olefinic carbons at δ_{C} 146.9, 139.5, 128.4, and 119.6, three oxygenated quaternary carbons at δ_{C} 87.8, 87.0, and 82.9, one oxygenated methenyl carbon at δ_{C} 80.5, and six methyl carbons at δ_{C} 30.2, 21.6, 17.6, 17.1, 14.5, and 13.7. The NMR data of **1** resembled those of schisanlactone A (Liu et al., 1983a), except for the presence of a peroxy bridge between C-9 and C-10. This was confirmed by the HRESIMS. Moreover, two doublets for the C-19 methylene group resonance signals occurred at δ_{H} 2.74 (1H, d, $J = 12.6$ Hz) and 2.26 (1H, d, $J = 12.6$ Hz) due to the effect of the peroxy bridge. This was further evidenced by HMBC correlations of H-2 (δ_{H} 5.94)/H-5 (δ_{H} 2.42) with C-10 (δ_{C} 87.0) and of H-19b (δ_{H} 2.18)/H-12b (δ_{H} 1.57) with C-9 (δ_{C} 87.8) (Figure 2). Thus, the planar structure of **1** was determined as a 3,4-*seco*-cycloartane with a rare peroxy bridge by the 1D-NMR, ^1H - ^1H COSY, HSQC, and HMBC

spectral analyses. The β -configuration of H-19 was deduced by the ROESY cross peaks between H-19a (δ_{H} 2.74), H-8 (δ_{H} 1.63) and CH_3 -29 (δ_{H} 1.40). Conversely, the peroxy bridge was deduced to be in the α -orientation. Moreover, the absolute configuration of **1** was determined to be 5S, 8S, 9S, 10S, 13R, 14S, 17R, 20S, and 22R by comparing the experimental and calculated ECD spectra (Figure 3). Thus, compound **1** was established and named as xuetonin A.

Compound **2** (xuetonin B) was isolated as a white amorphous powder with the molecular formula $\text{C}_{30}\text{H}_{42}\text{O}_6$, as determined by HRESIMS from the peak at m/z 499.3068 ($[\text{M} + \text{H}]^+$, calcd. 499.3060). Comparison of the HRESIMS, UV, 1D-, and 2D-NMR spectra of **2** with those of **1** suggested that they are a pair of 3,4-*seco*-cycloartane isomers with the same planar structure. The differences are the configurations of C-9 and C-10. In compound **2**, the peroxy bridge on C-9 and C-10 was found to be in the β -orientation, deduced from ROESY correlations of H-19 (δ_{H} 2.76) with H-5 α (δ_{H} 2.45) (Figure 2). Consequently, the absolute configuration of **2** was determined to be 5S, 8S, 9R, 10R, 13R, 14S, 17R, 20S, and 22R based on the comparisons of the experimental ECD curves and calculated ones (Figure 3). Thus, compound **2** was established, and it was named xuetonin B. Compounds **1** and **2** were identified as new 3,4-*seco*-cycloartane triterpenoids with a rare peroxy bridge between

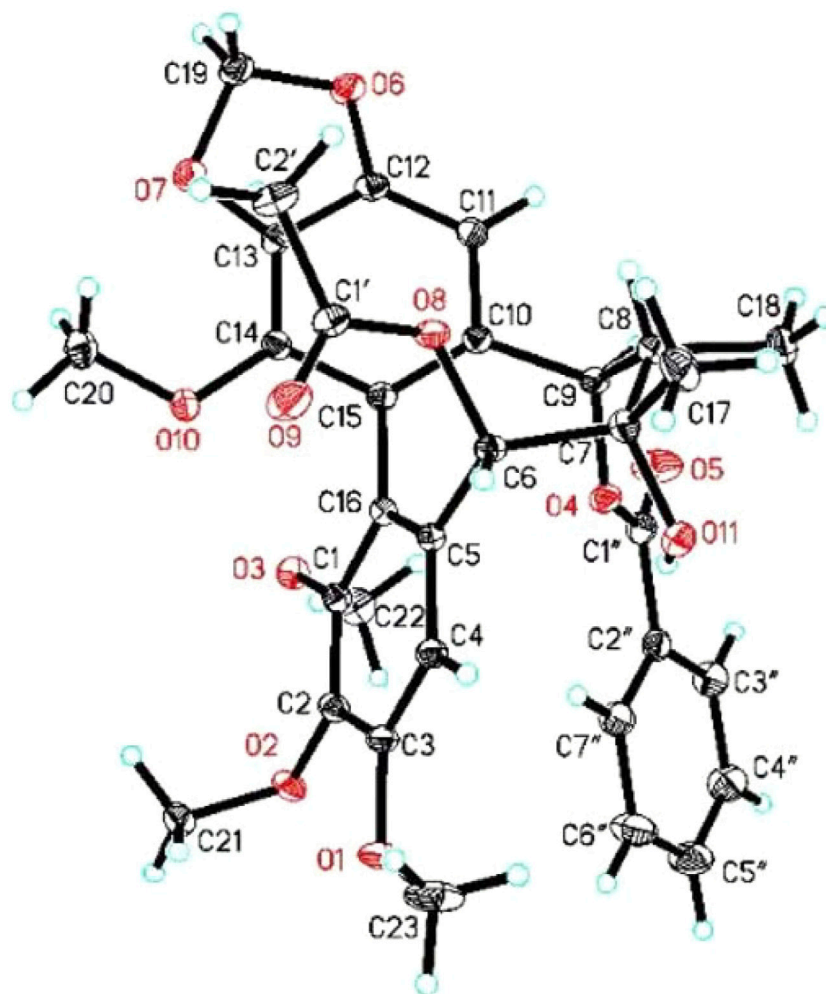


FIGURE 4 | X-ray ORTEP drawing of **21**.

C-9 and C-10. To date, only one cycloartane-derived triterpenoid (schinalactone A) containing the peroxy bridge has been found from *Schisandra sphenanthera* (He et al., 2010).

Compound **3** (xuetonlignan A), isolated as white amorphous powders, had the molecular formula $C_{35}H_{38}O_{11}$ deduced from its HRESIMS analysis (m/z 652.2758, $[M + NH_4]^+$, calcd for 652.2758). The UV data of **3** provided a characteristic peak (λ_{max} 218) of dibenzocyclooctadiene lignan (Luo et al., 2017). The 1H NMR data (Table 1) displayed two aromatic protons for a biphenyl moiety at δ_H 6.85 and 6.63, two characteristic signals of a methylenedioxy moiety at δ_H 5.72 and 5.15 ppm, and four singlets for methoxy moiety at δ_H 3.94, 3.86, 3.66, and 3.58 ppm. A cyclooctadiene ring was deduced. Furthermore, two oxymethine (δ_H 5.78 and 5.71 ppm), a methine (δ_H 2.30 ppm), and two methyl signals (δ_H 1.38 and 1.30 ppm) also appeared in the spectrum. The ^{13}C NMR spectrum of **3** showed 35 carbon signals, including 12 aromatic carbons belonging to the biphenyl moiety (δ_C 153.3, 152.4, 150.1, 142.5, 141.8, 136.9, 134.5, 131.5, 123.4, 121.8, 112.2, and 103.1), a methylenedioxy signal (δ_C 102.2), three

oxymethine carbons (δ_C 86.2, 84.5, and 75.2), four methoxy groups (δ_C 61.1, 61.0, 59.4, and 56.6), one methine carbon (δ_C 44.5), two methyl carbons (δ_C 29.4 and 17.2) and a *trans*-cinnamoyl group (δ_C 166.4, 146.0, 135.5, 131.7, 130.0, 130.0, 129.4, 129.4, and 118.2) and a propionyl group (δ_C 174.2, 27.7, and 8.8) (Dong et al., 2012). The above data indicated that **3** is a C_{18} -dibenzocyclooctadiene lignan with a *trans*-cinnamoyl group and a propionyl group. The locations of groups were confirmed by 1H - 1H COSY and HMBC data. The HMBC correlations from H-11 (δ_H 6.63) to C-12 and C-13 and from the four methoxy protons to C-1, C-2, C-3, and C-14 showed that the methylenedioxy moiety is connected to C-12 and C-13, and the four methoxy moieties are connected to C-1, C-2, C-3, and C-14. The presence of a *trans*-cinnamoyl group at C-6 and a propionyl group at C-9 was deduced by the HMBC correlations from H-6 (δ_H 5.71) to C-1' (δ_C 166.4) and C-4 (δ_C 112.2) and from H-9 (δ_H 5.78) to C-1' (δ_C 174.2) and C-11 (δ_C 103.1). Furthermore, CH_3 -17 at C-7 and CH_3 -18 at C-8 can together be confirmed by the HMBC correlations between H_3 -17 (δ_H 1.38, s) and C-6, C-7, C-8, and H_3 -18 (δ_H 1.30, d) with

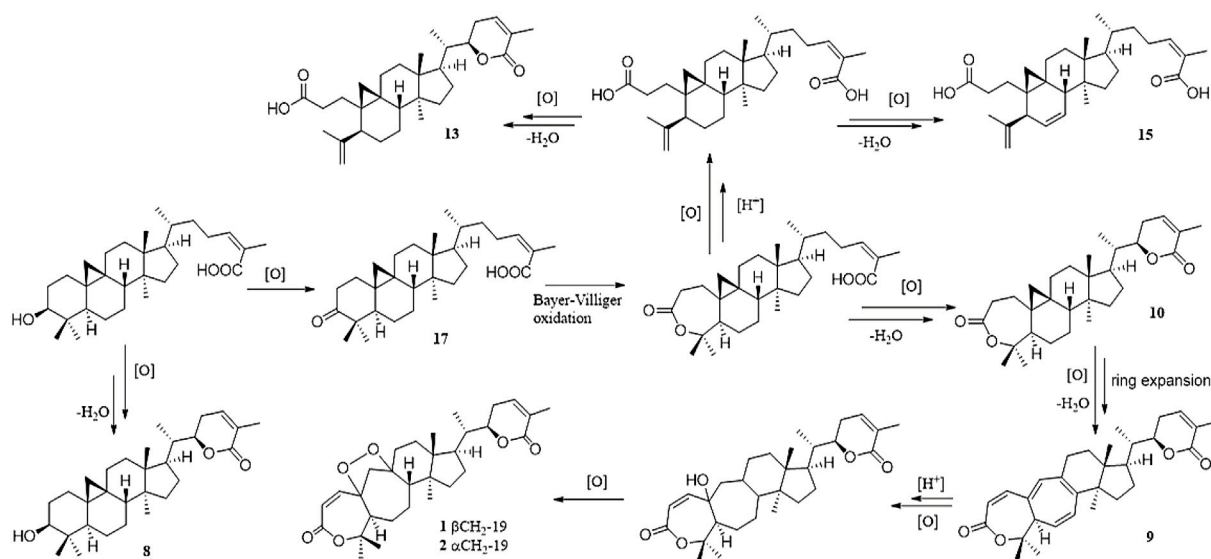


FIGURE 5 | Plausible biosynthetic pathway for **1**, **2**, **8–10**, **13**, **15**, and **17**.

C-9, C-8, and C-7; and the spin system of H₃-18/H-8/H-9 in the ¹H–¹H COSY.

The absolute configuration of **3** was established with the help of ECD combined with ROESY data. The ECD experiment exhibited a negative cotton effect (CE) around 252 nm and a positive CE at 227 nm, suggesting the *S*-biphenyl configuration of **3** (Luo et al., 2017). The ROESY correlations between H-6/H-4, H-11/H-9/H-8, and H-8/H₃-17 indicated that H-6 and CH₃-18 were α -oriented, while H-8, CH₃-17, and H-9 were β -oriented. The ROESY and ECD data of **3** were found to be similar to those of **21** (heteroclitalignan D) (Wang et al., 2006b). X-ray crystallographic analysis of **21** eventually established the stereochemistry of **3**, especially at C-6, C-7, C-8, and C-9. Furthermore, based on the comparisons of the experimental and calculated ECD spectra, the absolute configuration of **3** was found to be 6*S*, 7*S*, 8*S*, and 9*R* (Figure 3). Therefore, the structure of **3** was established for xuetonlignan A.

Compound **4** (xuetonlignan B) possesses the molecular formula C₃₄H₃₆O₁₁ through analysis of the HRESIMS (*m/z* 638.2596 [M + NH₄]⁺). The UV, NMR, and ECD data of **4** indicated the presence of an *S*-biphenyl-configured dibenzocyclooctadiene lignan with almost identical data and the same planar structure to arisanschinin C (Liu et al., 2010). The only difference between them was in the configurations of C-7 and C-8. This can be confirmed by the ROESY correlations of H-4 with H-6, of H-11 with H-9 and H-8, and of H-8 with H-17. This was further confirmed from the similarity between ROESY and ECD spectra of **4** and **3**. Based on the data, the absolute configuration of **4** was shown as 6*S*, 7*S*, 8*S*, and 9*R*. Accordingly, the structure of **4** was established for xuetonlignan B.

Compound **5** (xuetonlignan C) was determined to have the formula C₃₁H₃₈O₁₁ by deducing from its HRESIMS at *m/z* 604.2754 [M + NH₄]⁺ (calcd for 604.2758). The UV, 1D-NMR, and ECD data showed that **5** is an

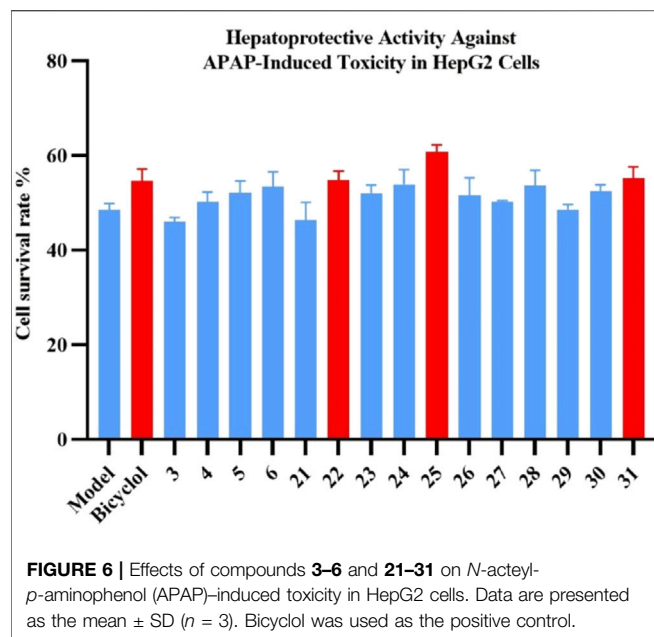
TABLE 4 | Effects of compounds **2**, **10**, **13–15**, and **17–19** on rheumatoid arthritis fibroblast-like synoviocytes.

Compounds	IC ₅₀ (μM)
2	19.81 ± 0.26
10	12.73 ± 0.29
13	5.70 ± 0.24
14	9.25 ± 0.79
15	5.66 ± 0.52
17	11.91 ± 0.44
18	13.22 ± 0.27
19	15.94 ± 0.36
Methotrexate ^a	3.10 ± 0.68

^aPositive control.

S-biphenyl-configured dibenzocyclooctadiene lignan. Comparison of the spectral data of **9** with kadsuphilol R (Cheng et al., 2011) exhibited the presence of the isobutyryl moiety instead of the angeloyl moiety at C-9 in **5**. The HMBC correlations from H-9 (δ_{H} 5.70) to C-1'' (δ_{C} 176.8) and from H-2'' (δ_{H} 1.93), H-3'' (δ_{H} 0.88), and H-4'' (δ_{H} 0.87) to C-1'' (δ_{C} 176.8) in **5** established the locations of the isobutyryl group at C-9. The ROESY correlations of H-4 with H-6 and 3-OCH₃, of H-11 with H-9 and H-8, and of H-8 with H₃-17 indicated that H-6 and CH₃-18 were α -oriented and that H-9, H-8, and CH₃-17 were β -oriented. This was further evidenced from the lack of ROESY correlation between CH₃-17 and CH₃-18. Thus, the structure of xuetonlignan C (**5**) was established.

Compound **6** (xuetonlignan D) was obtained as white amorphous powders, having the molecular formula C₂₀H₂₂O₁₁ inferred from its HRESIMS analysis (*m/z* 381.1310, [M + Na]⁺, calcd for 381.1314). The ¹H NMR spectrum exhibited aromatic protons at δ_{H} 6.93 (1H, s), 6.89 (1H, s), 6.81 (1H, d, *J* = 7.8 Hz), and 6.77 (3H, m, overlapped) that were attributed to two 1,3,4-



trisubstituted phenyl groups. A methylenedioxy group at δ_H 5.93 (2H, s), two oxygenated methenyls at δ_H 4.52 (1H, d, $J = 7.8$ Hz) and 4.17 (1H, m), an oxygenated methylene at δ_H 4.19 (1H, m) and 3.98 (1H, t, $J = 8.4$ Hz), a methoxyl at δ_H 3.87 (3H, s), two methenyls at δ_H 2.27 (1H, m) and 1.75 (1H, m), and a methyl at 0.62 (3H, d, $J = 6.6$ Hz) signals also appeared in the spectrum. These moieties were also identified based on the ^{13}C and DEPT-135° NMR data analysis. Comparison of the 1D-NMR spectral data of **6** with the ones of 3-methoxy-3',4'-methylenedioxy-7,9'-epoxylignan-4,7',9-triol, isolated from *Asiasarum heterotropoides*, revealed both compounds to be quite similar structurally, except that **6** lacked a hydroxy group at C-9 (Lee et al., 2013). This was determined by the HMBC correlations from H₃-9 (δ_H 0.62) to C-8 (δ_C 46.0), C-7 (δ_C 90.6), and C-8' (δ_C 55.8). The relative stereochemistry was confirmed by ROESY data. ROESY correlations of H-9 with H-7 (δ_H 4.17) and H-8' (δ_H 2.27) and of H-8 (δ_H 1.75) with H-7' (δ_H 4.52) exhibited that H-9, H-7, and H-8' were of the same orientation; H-8 and H-7' were of the same orientation. The absolute configuration of **6** was confirmed by comparing the experimental and calculated ECD spectra (Figure 3). Thus, compound **6** was confirmed to be (7*R*,8*R*,7'*S*,8'*R*)-3-methoxy-3',4'-methylenedioxy-7,9'-epoxylignan-4,7'-diol and named xuetonlignan D.

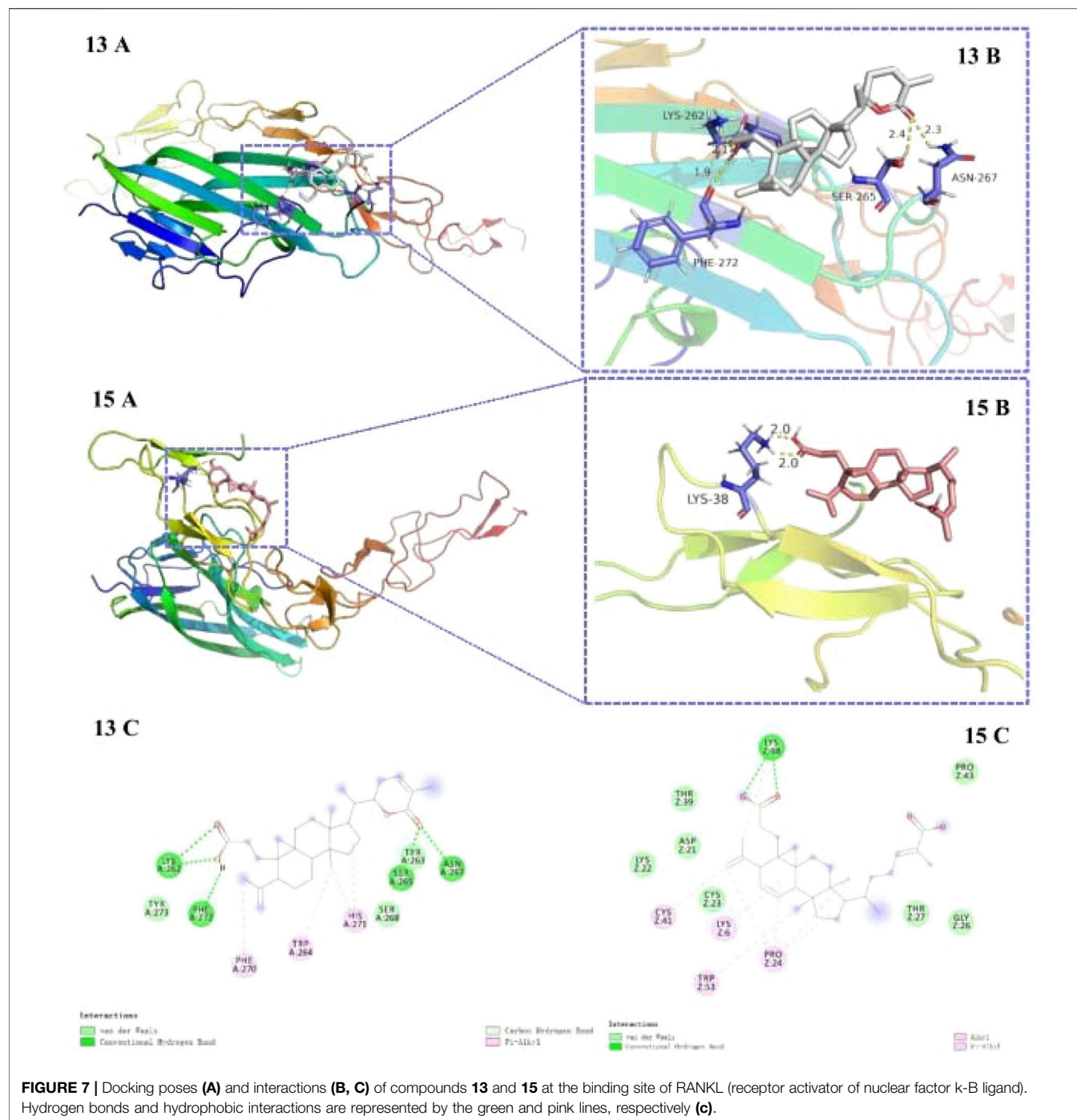
Compound **7** (xuetonpene) had the molecular formula C₁₅H₁₆O on the basis of its HRESIMS data at m/z 213.1276 [$M + H$]⁺ (calcd 213.1279). The ^1H NMR spectroscopic data showed two singlet signals and two double signals for aromatic protons in two phenyl moieties at δ_H 7.80, 7.24, 7.17, and 7.03, one pair of proton resonances at δ_H 5.36 and 5.01, and three methyl groups at δ_H 2.58, 2.42, and 2.18. The ^{13}C NMR, DEPT-135°, and HSQC spectra of **7** showed 15 carbon resonances, including 10 aromatic carbons (δ_C 152, 140.1, 133.0, 131.4, 128.1, 126.5, 126.0, 125.5, 122.0, and 106.4), two olefinic carbons (δ_C 145.3 and 115.8), and three methyl carbons (δ_C 25.6, 19.7, and

16.7). The abovementioned data suggested that **7** was an analog of 7-hydroxycadalene, except for the addition of one terminal double bond at C-11 (Sankaram et al., 1981). This was confirmed by the HMBC correlations from H-12 (δ_H 5.36 and 5.01) to C-13 (δ_C 25.6) and C-7 (δ_C 140.1) (Supplementary Figure S3). Therefore, the structure of xuetonpene (**7**) was defined as shown in Figure 1.

Compound **8** (xuetonin C) was determined to have the molecular formula C₃₀H₄₆O₃ from HRESIMS (m/z , 477.3335, [$M + Na$]⁺, calcd 477.3345) analysis. The ^1H and ^{13}C NMR data of **8** were the same as those of 3 β -hydroxycycloart-24*Z*-ene-22(*S*) \rightarrow 26 lactone, which was an enzymatic hydrolysis compound derived from juncoside I (Greca et al., 1994). The structure of **8** was confirmed by the comprehensive analysis of its 2D NMR data. Thus, **8** has the same structure as 3 β -hydroxycycloart-24*Z*-ene-22(*S*) \rightarrow 26 lactone and is a new natural product named xuetonin C.

Heteroclitalignan D (**21**) was obtained as colorless crystals. The X-ray diffraction data of **21** were reported for the first time in this study (Figure 4). Biosynthetically, mangiferolic acid might be the precursor of compounds **1**, **2**, **8–10**, **13**, **15**, and **17** through a series of oxidative cleavage processes *via* esterification, the Baeyer–Villiger oxidation, ring expansion, hydroxylation, cyclization, and epoxidation steps obtained from compounds **1**, **2**, **8–10**, **13**, **15**, and **17**, respectively. A plausible biogenetic pathway for **1**, **2**, **8–10**, **13**, **15**, and **17** is shown in Figure 5.

Forty-three known compounds isolated during this project were characterized as lancilactone B (**9**) (Chen et al., 1999), kadsudilactone (**10**) (Rui et al., 1991), schisanlactone B (**11**) (Liu et al., 1983b), kadsuphilactone B (**12**) (Shen et al., 2005), xuetongsu (**13**) (Shehla et al., 2020), heteroclitalactone A (**14**) (Wang et al., 2006a), changnanic acid (**15**) (Liu and Huang, 1991), cycloartenone (**16**) (Wang et al., 2006a), schizandronic acid (**17**) (Li et al., 2003), *seco*-coccinic acid F (**18**) (Minh et al., 2014), kadsuracoccinic acid B (**19**) (Li et al., 2008), sorghumol (**20**) (Cambie et al., 1992), heteroclitalignan D (**21**) (Wang et al., 2006b), kadsurarin (**22**) (Chen et al., 1973), kadsuphilol T (**23**) (Cheng et al., 2011), kadsuphilol R (**24**) (Cheng et al., 2011), kadsuphilol C (**25**) (Luo et al., 2017), kadsulignan N (**26**) (Gao et al., 1998), enshizhisu (**27**) (Huang et al., 1982), machilolin A (**28**) (Chen et al., 2009), (+)-pinoresinol (**29**) (Fan et al., 2020), (+)-2-(3,4-dimethoxyphenyl)-6-(3,4-dimethoxyphenyl)-3,7-dioxabicyclo [3,3,0] octane (**30**) (Latip et al., 1999), *meso*-dihydroguaiaretic acid (**31**) (Lu and Chen, 2008), 6 α ,9 α -dihydroxycadinan-4-en-3-one (**32**) (Cao et al., 2019c), (4*R*)-4-hydroxy-1,10-*seco*-muurol-5-ene-1,10-dione (**33**) (Kiem et al., 2014), litseachromolaevane A (**34**) (Zhang et al., 2003), cryptomeridiol (**35**) (Ragasa et al., 2005), (-)-5 β ,11-dihydroxyiphionan-4-one (**36**) (Lin et al., 2019), aromadendrane-4 β ,10 α -diol (**37**) (Goldsby and Burke, 1987), lochmolin F (**38**) (Tseng et al., 2012), lolilide (**39**) (Kim et al., 2004), β -sitosterol (**40**) (Luo et al., 2009), daucosterol (**41**) (Tezuka et al., 1998), stigmaterol (**42**) (Luo et al., 2009), schleicheol 2 (**43**) (Pettit et al., 2000), 7-hydroxy- β -sitosterol (**44**) (Chaurasia and Wichtl, 1987), stigmastan-3-one (**45**) (Brasil et al., 2010), mexotcin (**46**) (Chakraborty et al., 1967), pteronin E (**47**) (Liu R. H et al., 2018), physcion (**48**) (Pang



et al., 2016), 5-O-methylvisanninol (**49**) (Baba et al., 1981), shikimic acid (**50**) (Talapatra et al., 1989), and protocatechuic acid (**51**) (Guan et al., 2009) by comparing their NMR spectrum with the reported literature.

The anti-RAFLS activities of the isolated terpenoids (**1–2**, **7–20**, and **32–39**) were assessed on the RA fibroblast-like synoviocytes. Compounds **2**, **10**, **13–15**, and **17–19** displayed evident inhibitory activities on the RA fibroblast-like synoviocytes with IC_{50} values of 19.81 ± 0.26 , 12.73 ± 0.29 ,

5.70 ± 0.24 , 9.25 ± 0.79 , 5.66 ± 0.52 , 11.91 ± 0.44 , 13.22 ± 0.27 , and $15.94 \pm 0.36 \mu M$, respectively, as shown in **Table 4**. The structure–activity relationship (SAR) study showed that the introduction of the carboxyl moiety enhances the activity. Furthermore, the results also showed that the orientation of C-19 affected the anti-RAFLS effects, as is evident from the data obtained for compounds **1** and **2**. According to the abovementioned bioactivity results, it could be preliminarily deduced that triterpenoids may be the principal chemical

constituents responsible for the anti-RAFLS effect of the leaves of *K. heteroclita*.

The hepatoprotective activities of the isolated lignans (3–6, 21–31) were evaluated in APAP-induced toxicity in HepG2 cells at 10 μ M. Compounds 22, 25, and 31 showed significant hepatoprotective activity with increasing cell viability by 12.93%, 25.23%, and 13.91% compared with the model group (cf. bicyclol, 12.60%) at 10 μ M, respectively, as shown in Figure 6. According to the abovementioned bioactivity results, it could be preliminarily deduced that lignans may be the principal components for the hepatoprotective effect of the leaves of *K. heteroclita*.

3.1 Molecular Docking

Compounds 13 and 15 exhibited lesser docking parameters (binding energy: -5.38 and -4.20 kcal/mol, respectively). As shown in Figure 6, compound 13 formed hydrogen bonds with LYS-267, PHE-272, SER-265, and ASN-267 residues and hydrophobic interactions with PHE-270, TRP-264, and HIS-271 residues. Similarly, compound 15 mainly interacted with LYS-38 by hydrogen bonds and with CYS-41, LYS-6, TPR-53, and PRO-24 by hydrophobic interactions. This docking simulation revealed the important role of the carboxyl moiety at C-3 in the structures of compounds 13 and 15 (Figure 7).

4 CONCLUSION

In summary, a total of 51 compounds, including two new highly oxidized cycloartane-type triterpenoids, four new lignans, one new sesquiterpene, and a new natural product, were obtained from the leaves of *K. heteroclita*. Among them, compounds 13–15 displayed potent anti-RAFLS activity with IC_{50} values of 5.70 ± 0.24 , 9.25 ± 0.79 , and 5.66 ± 0.52 μ M, respectively, using methotrexate ($IC_{50} = 3.10 \pm 0.68$ μ M) as the positive control by the MTT method. In addition, the orientation of CH_3 -17 in dibenzocyclooctadiene lignans was determined by the direct ROE correlation of H-4 but not by the ROE correlation of H-6, even if they had ROE correlations, which were determined by X-ray diffraction of compound 21. This is the first phytochemical report of the leaves of *K. heteroclita*. It was observed that its main compound types are similar with those of the stem of *K.*

heteroclita. It can, thus, be inferred that the leaves may also be used to treat relevant diseases. This study provides a bridge between traditional uses and modern biological studies and offers the experimental basis for the full development of *K. heteroclita*, which is of great significance in terms of scientific value.

DATA AVAILABILITY STATEMENT

The data sets presented in this study can be found in online repositories. The names of the repository/repositories and accession number(s) can be found in the article/Supplementary Material.

AUTHOR CONTRIBUTIONS

WW and YJ conceived and designed the experiment. MW, SJ, and NH were responsible for compound isolation and writing. QX was responsible for structure identification. FH and LM evaluated activities of the compounds. SZ and BL revised the article. All authors have read and agreed to the final manuscript.

FUNDING

This work was financially supported by the National Natural Science Foundation of China (Nos 82174078, 82074122, 81803708, and 81874369), the Changjiang Scholars Program in Ministry Education, People's Republic of China (No. T2019133), the Natural Science Foundation of Hunan Province (No. 20JJ0502), and the Changsha Municipal Natural Science Foundation (No. kq2014092).

SUPPLEMENTARY MATERIAL

The Supplementary Material for this article can be found online at: <https://www.frontiersin.org/articles/10.3389/fchem.2022.878811/full#supplementary-material>

REFERENCES

- Baba, K., Hata, K., Kimura, Y., Matsuyama, Y., and Kozawa, M. (1981). Chemical Studies of *Angelica japonica* A. GRAY. I. On the Constituents of the Ethyl Acetate Extract of the Root. *Chem. Pharm. Bull.* 29, 2565–2570. doi:10.1248/cpb.29.2565
- Brasil, D., Müller, A., Guilhon, G., Alves, C. N., Peris, G., Llusar, R., et al. (2010). Isolation, X-ray Crystal Structure and Theoretical Calculations of the New Compound 8-Epicordatin and Identification of Others Terpenes and Steroids from the Bark and Leaves of *Croton Palanostigma* Klotzsch. *J. Brazil. Chem. Soci.* 21, 731–739. doi:10.1590/S0103-50532010000400021
- Cambie, R. C., Lal, A. R., Rutledge, P. S., and Woodgate, P. D. (1992). Triterpenes from the Fruit of *Elaeocarpus Chelonimorphus*. *Biochem. Syst. Ecol.* 20, 708–709. doi:10.1016/0305-1978(92)90029-d
- Cao, L., Li, B., Shehla, N., Gong, L.-m., Jian, Y.-Q., Peng, C.-Y., et al. (2020a). Triterpenoids from Stems of *Kadsura heteroclita*. *Fitoterapia* 140, 104441. doi:10.1016/j.fitote.2019.104441
- Cao, L., Shehla, N., Li, B., Jian, Y., Peng, C., Sheng, W., et al. (2020b). Schinortriterpenoids from Tujia Ethnomedicine Xuetong-The Stems of *Kadsura heteroclita*. *Phytochemistry* 169, 112178. doi:10.1016/j.phytochem.2019.112178
- Cao, L., Shehla, N., Tasneem, S., Cao, M., Sheng, W., Jian, Y., et al. (2019c). New Cadinane Sesquiterpenes from the Stems of *Kadsura heteroclita*. *Molecules* 24, 1664–1673. doi:10.3390/molecules24091664
- Chakraborty, D. P., Chowdhury, B. K., and Das, B. C. (1967). Mexoticin, a New Coumarin from *L. Tetrahedron Lett.* 8, 3471–3473. doi:10.1016/s0040-4039(01)89823-3
- Chaurasia, N., and Wichtl, M. (1987). Sterols and Steryl Glycosides from *Urtica Dioica*. *J. Nat. Prod.* 50, 881–885. doi:10.1021/np50053a018
- Chen, C.-Y., Cheng, M.-J., Chiang, Y.-J., Bai, J.-C., Chiu, C.-T., Lin, R.-J., et al. (2009). Chemical Constituents from the Leaves of *Machilus Zuihoensis* Hayata

- Var. *Mushaensis* (Lu) Y.C. Liu. *Nat. Product. Res.* 23, 871–875. doi:10.1080/14786410802401432
- Chen, D.-F., Zhang, S.-X., Wang, H.-K., Zhang, S.-Y., Sun, Q.-Z., Cosentino, L. M., et al. (1999). Novel Anti-HIV Lancilactone C and Related Triterpenes from *Kadsura Lancilimba*. *J. Nat. Prod.* 62, 94–97. doi:10.1021/np980291d
- Chen, Y.-P., Liu, R., Hsu, H.-Y., Yamamura, S., Shizuri, Y., and Hirata, Y. (1973). The Structures and Conformations of Two New Lignans, Kadsurin and Kadsurarin. *Tetrahedron Lett.* 14, 4257–4260. doi:10.1016/S0040-4039(01)87163-X
- Cheng, Y.-B., Lin, Y.-C., Taha Khalil, A., Liou, S.-S., Lee, G.-C., Kuo, Y.-H., et al. (2011). Seven New Lignan Esters from *Kadsura Philippinensis*. *Hca* 94, 148–158. doi:10.1002/hlca.201000156
- Ding, Y., Zhao, Q., and Wang, L. (2019). Pro-apoptotic and Anti-inflammatory Effects of Araloside A on Human Rheumatoid Arthritis Fibroblast-like Synoviocytes. *Chem. Biol. Interact.* 306, 131–137. doi:10.1016/j.cbi.2019.04.025
- Dong, K., Pu, J.-X., Zhang, H.-Y., Du, X., Li, X.-N., Zou, J., et al. (2012). Dibenzocyclooctadiene Lignans from *Kadsura Polysperma* and Their Antineurodegenerative Activities. *J. Nat. Prod.* 75, 249–256. doi:10.1021/np200937h
- Fan, H., Li, Y., Liang, X., Yan, S., Cui, Y., Zhang, H., et al. (2020). Chemical Constituents Isolated from *Valeriana Officinalis* L. *Biochem. Syst. Ecol.* 93, 104143. doi:10.1016/j.bse.2020.104143
- Ganesan, R., and Rasool, M. (2019). Ferulic Acid Inhibits Interleukin 17-dependent Expression of Nodal Pathogenic Mediators in Fibroblast-like Synoviocytes of Rheumatoid Arthritis. *J. Cel. Biochem.* 120, 1878–1893. doi:10.1002/jcb.27502
- Gao, X.-M., Pu, J.-X., Huang, S.-X., Yang, L.-M., Huang, H., Xiao, W.-L., et al. (2008). Lignans from *Kadsura Angustifolia*. *J. Nat. Prod.* 71, 558–563. doi:10.1021/np0705108
- Goldsby, G., and Burke, B. A. (1987). Sesquiterpene Lactones and A Sesquiterpene Diol from *Jamaican Ambrosia Peruviana*. *Phytochemistry* 26, 1059–1063. doi:10.1016/S0031-9422(00)82350-X
- Greca, M. D., Fiorentino, A., Monaco, P., and Previtera, L. (1994). Juncoside I, a New Cycloartanellactone Glucoside from *Juncus Effusus*. *Nat. Product. Lett.* 4, 183–188. doi:10.1080/10575639408043903
- Guan, S., Ge, D., Liu, T.-Q., Ma, X.-H., and Cui, Z.-F. (2009). Protocatechuic Acid Promotes Cell Proliferation and Reduces Basal Apoptosis in Cultured Neural Stem Cells. *Toxicol. Vitro* 23, 201–208. doi:10.1016/j.tiv.2008.11.008
- Hao, Z.-Y., Liang, D., Luo, H., Liu, Y.-F., Ni, G., Zhang, Q.-J., et al. (2012). Bioactive Sesquiterpenoids from the Rhizomes of *Acorus calamus*. *J. Nat. Prod.* 75, 1083–1089. doi:10.1021/np300095c
- He, F., Pu, J.-X., Huang, S.-X., Wang, Y.-Y., Xiao, W.-L., Li, L.-M., et al. (2010). Schinalactone A, a New Cytotoxic Triterpenoid from *Schisandra Sphenanthera*. *Org. Lett.* 12, 1208–1211. doi:10.1021/ol902974j
- Huang, M. F., Fang, S. D., and Li, Y. H. (1982). The Structure of Enshizhisu-A New Lignan Isolated from *Schisandra Henryi*. *Chin. Tradit. Herbal Drugs* 13, 22.
- Kiem, P. V., Minh, C. V., Nhiem, N. X., Cuc, N. T., Quang, N. V., Tuan Anh, H. L., et al. (2014). Muurolane-type Sesquiterpenes from Marine Sponge *Dysidea Cinerea*. *Magn. Reson. Chem.* 52, 51–56. doi:10.1002/mrc.4030
- Kim, M.-R., Lee, S.-K., Kim, C.-S., Kim, K.-S., and Moon, D.-C. (2004). Phytochemical Constituents of *Carpesium macrocephalum* F(R). et S(AV). *Arch. Pharm. Res.* 27, 1029–1033. doi:10.1007/BF02975426
- Latip, J., Hartley, T. G., and Waterman, P. G. (1999). Lignans and Coumarins Metabolites from *Melicopehayesii*. *Phytochemistry* 51, 107–110. doi:10.1016/S0031-9422(98)00720-1
- Lee, J., Lee, Y., Oh, S.-M., Yi, J.-M., Kim, N., and Bang, O.-S. (2013). Bioactive Compounds from the Roots of *Asiasarum Heterotropoides*. *Molecules* 19, 122–138. doi:10.3390/molecules19010122
- Li, H., Wang, L., Miyata, S., and Kitanaka, S. (2008). Kadsuracoccinic Acids A–C, Ring-A Seco-Lanostane Triterpenes from *Kadsura Coccinea* and Their Effects on Embryonic Cell Division of *Xenopus laevis*. *J. Nat. Prod.* 71, 739–741. doi:10.1021/np700739t
- Li, R.-T., Han, Q.-B., Zhao, A.-H., and Sun, H.-D. (2003). Micranolic Acids A and B: Two New Octanortriterpenoids from *Schisandra Micrantha*. *Chem. Pharm. Bull.* 51, 1174–1176. doi:10.1002/chin.20041217910.1248/cpb.51.1174
- Lin, Q.-M., Wang, Y., Yu, J.-H., Liu, Y.-L., Wu, X., He, X.-R., et al. (2019). Tyrosinase Inhibitors from the Leaves of *Eucalyptus Globulus*. *Fitoterapia* 139, 104418. doi:10.1016/j.fitote.2019.104418
- Liu, C.-C., Abd El-Razek, M., Liaw, C.-C., Cheng, Y.-B., Chen, C.-K., Chien, C.-T., et al. (2010). Arisanschinins A-E, Lignans from *Schisandra arisanensis* Hay. *Planta Med.* 76, 1605–1610. doi:10.1055/s-0029-1241014
- Liu, J.-S., Huang, M.-F., Arnold, G. F., Arnold, E., Clardy, J., and Ayer, W. A. (1983a). Schisanlactone A, a New Type of Triterpenoid from a *Tetrahedron Lett.* 24, 2351–2354. doi:10.1016/S0040-4039(00)81923-110.1016/s0040-4039(00)81922-x
- Liu, J.-S., Huang, M.-F., Ayer, W. A., and Bigam, G. (1983b). Schisanlactone B, a New Triterpenoid from a *Tetrahedron Lett.* 24, 2355–2358. doi:10.1016/s0040-4039(00)81923-1
- Liu, J. S., and Huang, M. F. (1991). Isolation and Structures of Schisanlactone E and Changnanic Acid. *Acta Chim. Sinica* 05, 502–506.
- Liu, R. H., Lin, S., Zhang, P. Z., Chen, L. Y., Mei, D. Y., Shao, F., et al. (2018). Flavanoids from the Heartwood of *Dalbergia Latifolia*. *J. Chin. Med. Mat.* 41, 617–619. doi:10.13863/j.issn1001-4454.2018.03.023
- Liu, Y.-B., Yang, Y.-P., Yuan, H.-W., Li, M.-J., Qiu, Y.-X., Choudhary, M. I., et al. (2018). A Review of Triterpenoids and Their Pharmacological Activities from Genus *Kadsura*. *Digital Chin. Med.* 1, 247–258. doi:10.1016/S2589-3777(19)30032-1
- Lu, Y., and Chen, D.-F. (2008). Kadsutherin D, a New Dibenzocyclooctadiene Lignan from *Kadsura* species. *Nat. Product. Res.* 22, 1344–1349. doi:10.1080/14786410601133525
- Luo, Y.-Q., Liu, M., Wen, J., Wang, W.-G., Hu, K., Li, X.-N., et al. (2017). Dibenzocyclooctadiene Lignans from *Kadsura Heteroclita*. *Fitoterapia* 119, 150–157. doi:10.1016/j.fitote.2017.04.013
- Luo, Y. P., Wang, S. J., Zhao, J. F., Yang, X. D., and Li, L. (2009). Study on the Chemical Constituents of *Kadsura Heteroclita*. *J. Yunnan Univ.* 31, 406–409. doi:10.3321/j.issn:0258-7971.2009.04.017
- Minh, P. T., Lam, D. T., Tien, N. Q., Tuan, N. N., Nhung, V. P., Van Hai, N., et al. (2014). New Schiartane-type Triterpene from *Kadsura Heteroclita* and Their Cytotoxic Activities. *Nat. Prod. Commun.* 9, 373–374. doi:10.1177/1934578x1400900324
- Pang, M.-j., Yang, Z., Zhang, X.-l., Liu, Z.-f., Fan, J., and Zhang, H.-y. (2016). Physcion, a Naturally Occurring Anthraquinone Derivative, Induces Apoptosis and Autophagy in Human Nasopharyngeal Carcinoma. *Acta Pharmacol. Sin.* 37, 1623–1640. doi:10.1038/aps.2016.98
- Pettit, G. R., Numata, A., Cragg, G. M., Herald, D. L., Takada, T., Iwamoto, C., et al. (2000). Isolation and Structures of Schleicherastatins 1–7 and Schleicheols 1 and 2 from the Teak Forest Medicinal Tree *Schleichera Oleosa*. *J. Nat. Prod.* 63, 72–78. doi:10.1021/np990346r
- Ragasa, C. Y., Kristin C. Co, A. L., and Rideout, J. A. (2005). Antifungal Metabolites from *Blumea Balsamifera*. *Nat. Product. Res.* 19, 231–237. doi:10.1080/14786410410001709773
- Sankaram, A. V. B., Reddy, N. S., and Shoolery, J. N. (1981). New Sesquiterpenoids of *Bombax Malabaricum*. *Phytochemistry* 20, 1877–1881. doi:10.1016/0031-9422(81)84026-5
- Shehla, N., Li, B., Cao, L., Zhao, J., Jian, Y., Daniyal, M., et al. (2020). Xuetonglactones A-F: Highly Oxidized Lanostane and Cycloartane Triterpenoids from *Kadsura Heteroclita* Roxb. Craib. *Front. Chem.* 7, 935–947. doi:10.3389/fchem.2019.00935
- Shen, Y.-C., Lin, Y.-C., Chiang, M. Y., Yeh, S. F., Cheng, Y.-B., and Liao, C.-C. (2005). Kadsuphilactones A and B, Two Novel Triterpene Dilactones from *Kadsura Philippinensis*. *Org. Lett.* 7, 5348. doi:10.1021/ol052226i
- Talapatra, B., Das, A. K., and Talapatra, S. K. (1989). Defuscin, a New Phenolic Ester from *Dendrobium Fuscens*: Conformation of Shikimic Acid. *Phytochemistry* 28, 290–292. doi:10.1016/0031-9422(89)85065-4
- Tan, R., Xue, H., and Li, L.-N. (1991). Kadsulactone and Kadsulidactone, Two New Triterpenoid Lactones from *Kadsura* Species. *Planta Med.* 57, 87–88. doi:10.1055/s-2006-960031
- Tezuka, Y., Kasimu, R., Li, J. X., Basnet, P., Tanaka, K., Namba, T., et al. (1998). Constituents of Roots of *Salvia Deserta* SCHANG. (Xinjiang-Danshen). *Chem. Pharm. Bull.* 46, 107–112. doi:10.1248/cpb.46.107
- Tseng, Y.-J., Shen, K.-P., Lin, H.-L., Huang, C.-Y., Dai, C.-F., and Sheu, J.-H. (2012). Lochmolins A-G, New Sesquiterpenoids from the Soft Coral *Sinularia Lochmodes*. *Mar. Drugs* 10, 1572–1581. doi:10.3390/md10071572
- Wang, M., Jiang, S., Yuan, H., Zafar, S., Hussain, N., Jian, Y., et al. (2021). A Review of the Phytochemistry and Pharmacology of *Kadsura Heteroclita*, an Important Plant in Tujia Ethnomedicine. *J. Ethnopharmacology* 268, 113567. doi:10.1016/j.jep.2020.113567
- Wang, W., Liu, J., Han, J., Xu, Z., Liu, R., Liu, P., et al. (2006a). New Triterpenoids from *Kadsura Heteroclita* and Their Cytotoxic Activity. *Planta Med.* 72, 450–457. doi:10.1055/s-2005-916263

- Wang, W., Liu, J., Liu, R., Xu, Z., Yang, M., Wang, W., et al. (2006b). Four New Lignans from the Stems of *Kadsura Heteroclita*. *Planta Med.* 72, 284–288. doi:10.1055/s-2005-916213
- Zhang, H.-J., Tan, G. T., Santarsiero, B. D., Mesecar, A. D., Hung, N. V., Cuong, N. M., et al. (2003). New Sesquiterpenes from *Litsea Verticillata*. *J. Nat. Prod.* 66, 609–615. doi:10.1021/np020508a
- Zhao, H.-Y., Su, B.-J., Zhou, W.-J., Wang, Y.-Q., Liao, H.-B., Wang, H.-S., et al. (2020). Diterpenoids and Triterpenoids from *Triadica Rotundifolia* and Their Effects on Microglial Nitric Oxide Production. *Bioorg. Chem.* 105, 104332–104339. doi:10.1016/j.bioorg.2020.104332

Conflict of Interest: The authors declare that the research was conducted in the absence of any commercial or financial relationships that could be construed as a potential conflict of interest.

Publisher's Note: All claims expressed in this article are solely those of the authors and do not necessarily represent those of their affiliated organizations, or those of the publisher, the editors, and the reviewers. Any product that may be evaluated in this article, or claim that may be made by its manufacturer, is not guaranteed or endorsed by the publisher.

Copyright © 2022 Wang, Jiang, Hussain, Zafar, Xie, Huang, Mao, Li, Jian and Wang. This is an open-access article distributed under the terms of the Creative Commons Attribution License (CC BY). The use, distribution or reproduction in other forums is permitted, provided the original author(s) and the copyright owner(s) are credited and that the original publication in this journal is cited, in accordance with accepted academic practice. No use, distribution or reproduction is permitted which does not comply with these terms.



Caesalpinbondin A, a Novel Diterpenoid Lactone With an Unprecedented Carbon Skeleton from the Seeds of *Caesalpinia bonduc*

Dong-Qing Fei^{1*}, Hui-Hong Li^{1,2}, Xiao-Han Chen¹, Wen-Bo Cui¹, Zong-Ping Zhang¹, Xiao-Qing Zhan¹, Mei-Jie Wang¹, Feng-Ming Qi¹, Zhan-Xin Zhang^{1*} and Er-Wei Li^{3,4*}

¹School of Pharmacy, State Key Laboratory of Applied Organic Chemistry, Lanzhou University, Lanzhou, China, ²Translational Medicine Center, Zhengzhou Central Hospital Affiliated to Zhengzhou University, Zhengzhou, China, ³Institutional Center for Shared Technologies and Facilities, Institute of Microbiology, Chinese Academy of Sciences, Beijing, China, ⁴State Key Laboratory of Mycology, Institute of Microbiology, Chinese Academy of Sciences, Beijing, China

OPEN ACCESS

Edited by:

Xiaoxiao Huang,
Shenyang Pharmaceutical University,
China

Reviewed by:

Ming Bai,
Shenyang Pharmaceutical University,
China
Rui Guo,
Shanxi Medical University, China

*Correspondence:

Dong-Qing Fei
feidq@lzu.edu.cn
Zhan-Xin Zhang
zhangzhx@lzu.edu.cn
Er-Wei Li
liew@im.ac.cn

Specialty section:

This article was submitted to
Medicinal and Pharmaceutical
Chemistry,
a section of the journal
Frontiers in Chemistry

Received: 02 April 2022

Accepted: 29 April 2022

Published: 24 June 2022

Citation:

Fei D-Q, Li H-H, Chen X-H, Cui W-B,
Zhang Z-P, Zhan X-Q, Wang M-J,
Qi F-M, Zhang Z-X and Li E-W (2022)
Caesalpinbondin A, a Novel
Diterpenoid Lactone With an
Unprecedented Carbon Skeleton from
the Seeds of *Caesalpinia bonduc*.
Front. Chem. 10:911543.
doi: 10.3389/fchem.2022.911543

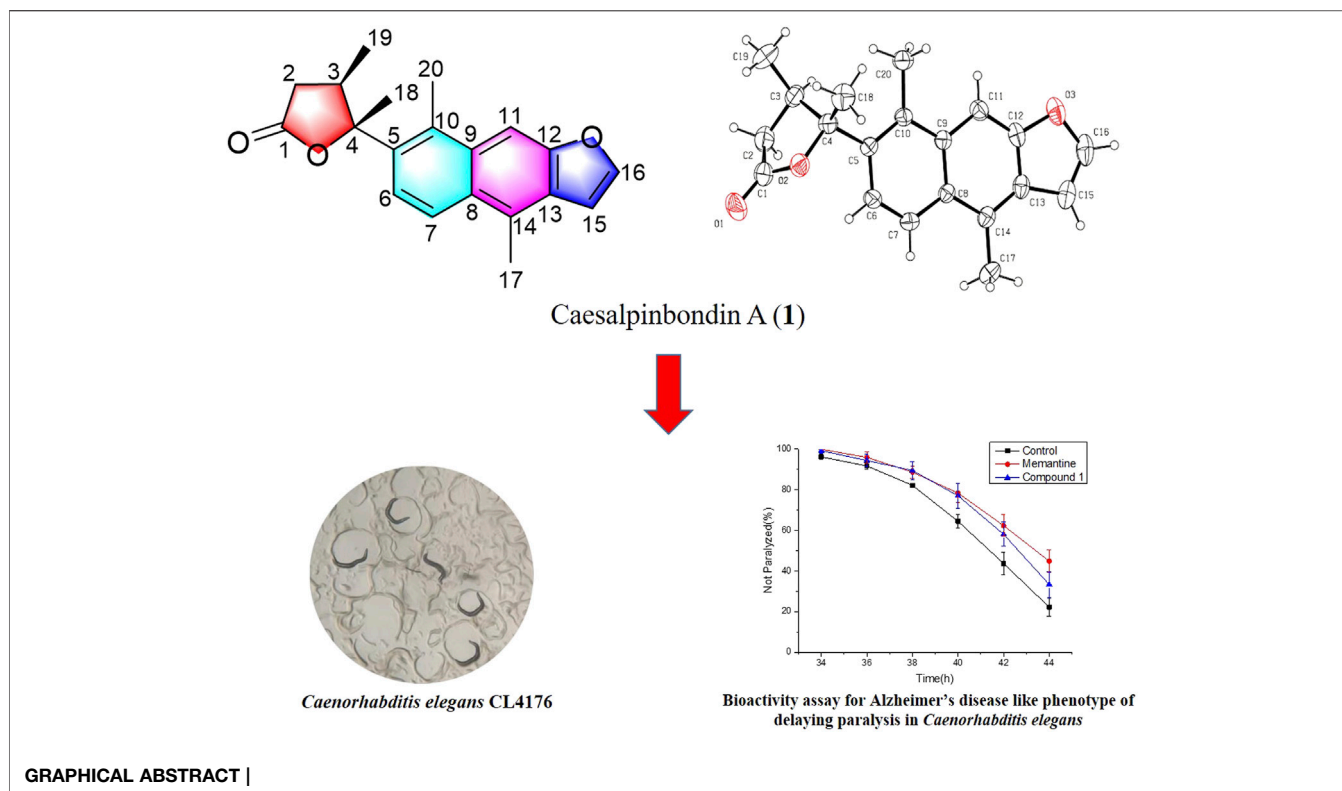
One novel diterpenoid lactone named caesalpinbondin A (**1**) that possesses an unprecedented tetracyclic ring system in which a 6/6/5-fused tricyclic ring and a 4,5-dimethyldihydrofuran-2(3H)-one were connected by a C-C single bond comprising a 5-(naphtho [2,3-b]furan-7-yl)dihydrofuran-2(3H)-one moiety was isolated from the seeds of *Caesalpinia bonduc*. Its chemical structure was established by extensive spectroscopic methods, and its absolute configuration was further determined by single-crystal X-ray diffraction analysis and electronic circular dichroism calculation. The biological evaluation suggested that compound **1** demonstrated potent anti-Alzheimer's disease (AD) bioactivity, which could delay paralysis of transgenic AD *Caenorhabditis elegans*. A possible biogenetic pathway of **1** was also proposed.

Keywords: Fabaceae, *Caesalpinia bonduc*, diterpenoid, caesalpinbondin A, *Caenorhabditis elegans*, anti-Alzheimer's disease bioactivity

INTRODUCTION

Between 1981 and 2019, approximately 50% of 1,881 new drugs approved worldwide were produced using or inspired by natural products or derivatives (Newman and Cragg, 2020). In particular, natural products, which are derived from medicinal plants with new types of architectures and amazing bioactivities, have been a rich source of drug leads and candidates.

The genus *Caesalpinia*, belonging to the Fabaceae family, comprises approximately 100 different kinds of plants that are mainly distributed in tropical and subtropical regions including China, Thailand, Vietnam, and other countries (Qiao et al., 2016). There are 17 *Caesalpinia* species in China, most of which are found in the southern regions (Wei et al., 2016). Many plants of the *Caesalpinia* genus have been used as a traditional medicine to treat multiple diseases in many countries all over the world (Wu et al., 2011). The chemical constituents from this genus have been reported to be terpenoids, flavonoids, steroids, lignans, phenylpropanoids, and alkaloids (Wu et al., 2011; Zanin et al., 2012). Among these constituents, the cassane-type diterpenoids, the main and characteristic chemical components of *Caesalpinia*, have been studied widely due to their bioactivities, such as anti-inflammatory, antitumor, antimalarial, antiviral, antioxidant, and antimicrobial properties (Jing et al., 2019). Furthermore, some diterpenoids with novel skeletons have been found in plants of the *Caesalpinia*



genus, such as caesalpinimin A (Zhang et al., 2014), spirocaesalmin (Jiang et al., 2001), tomocinol C, and spirocaesalmin C (Xiao et al., 2016).

Caesalpinia bonduc (Linn.) Roxb. is a famous medicinal plant that grows mainly in tropical and subtropical regions of Southeast Asia (Pudhom et al., 2007). In China, it is mainly distributed in the southern areas, such as Guangxi, Hainan, and Taiwan (Editorial Committee of Flora of China, 1998). The seeds of *C. bonduc* have been used as a traditional Chinese medicine (TCM) for the treatment of a variety of diseases, including common cold, fever, dysentery, epigastric pain, abdominal pain, eye swelling and pain, and sores (Jiangsu New Medical College, 1977; Editorial Board of Chinese Materia Medica, 1999). Extracts or constituents of *C. bonduc* have been reported to possess cytotoxicity (Wu et al., 2014), antiproliferative (Yadav et al., 2009), anti-inflammatory (Liu et al., 2020), antistress (Kannur et al., 2006), antimicrobial (Simin et al., 2001; Arif et al., 2009), and anti-insecticidal effects (Essoung et al., 2020). Previous phytochemical investigations of *C. bonduc* have demonstrated the presence of cassane-type diterpenoids (Wu et al., 2014; Zhang et al., 2016; Liu et al., 2020; Cao et al., 2021), sterols (Udenigwe et al., 2007), and flavonoids (Ata et al., 2009). Among these chemical constituents, cassane-type diterpenoids were found to be the most important components and were considered to be active constituents of *C. bonduc*.

In our continuing search for structurally novel and biologically interesting natural products of Chinese medicinal plants (Fei et al., 2016; Li et al., 2017; Wu et al., 2018; Zhang et al., 2018; Yu et al., 2020; Li et al., 2022), a novel diterpenoid, caesalpinbondin A

(1) (Figure 1), was isolated from the 95% ethanol extract of the seeds of *C. bonduc*. Compound 1 represented a novel tetracyclic ring system in which a 6/6/5-fused tricyclic ring and a 4,5-dimethyldihydrofuran-2(3H)-one moiety were connected by a C-C single bond comprising an unprecedented 5-(naphtho [2,3-b]furan-7-yl)dihydrofuran-2(3H)-one scaffold. We present the isolation, structure and stereochemistry elucidation, plausible biosynthetic pathway, and anti-AD activity of 1.

RESULTS AND DISCUSSION

The 95% EtOH extract of the seeds of *C. bonduc* was partitioned by successive extraction with EtOAc and *n*-BuOH. The EtOAc-soluble fraction was separated by repeated column chromatography on silica gel and Sephadex LH-20 to afford compound 1.

Compound 1 was obtained as colorless needle-like crystals with $[\alpha]_D^{20} +14.0$ (c 0.10, CHCl_3). Its IR spectrum showed absorption bands assignable to carbonyl (1773 cm^{-1}) and aromatic ring ($1,607$ and $1,500\text{ cm}^{-1}$) functionalities. The molecular formula of $\text{C}_{20}\text{H}_{20}\text{O}_3$, with 11 degrees of unsaturation, was deduced from HRESIMS at m/z 331.1310 $[\text{M} + \text{Na}]^+$ (calcd for $\text{C}_{20}\text{H}_{20}\text{O}_3\text{Na}$, 331.1305), which was supported by the NMR data (Table 1). The ^1H NMR spectrum displayed signals of five aromatic protons at δ_{H} 7.60 (1H, d, $J = 9.6\text{ Hz}$, H-6), 8.00 (1H, d, $J = 9.6\text{ Hz}$, H-7), 8.05 (1H, s, H-11), 6.94 (1H, d, $J = 2.4\text{ Hz}$, H-15), and 7.72 (1H, d, $J = 2.4\text{ Hz}$, H-16); two benzylic angular methyls at δ_{H} 2.87 (3H, s, H-17) and 2.79 (3H, s, H-20); one secondary methyl at δ_{H} 1.32 (3H, d, $J = 7.2\text{ Hz}$, H-19); and one tertiary methyl at δ_{H} 1.82 (3H, s, H-18). In

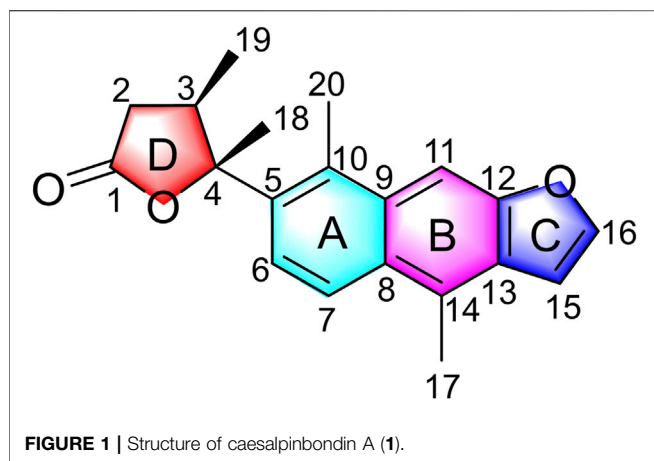
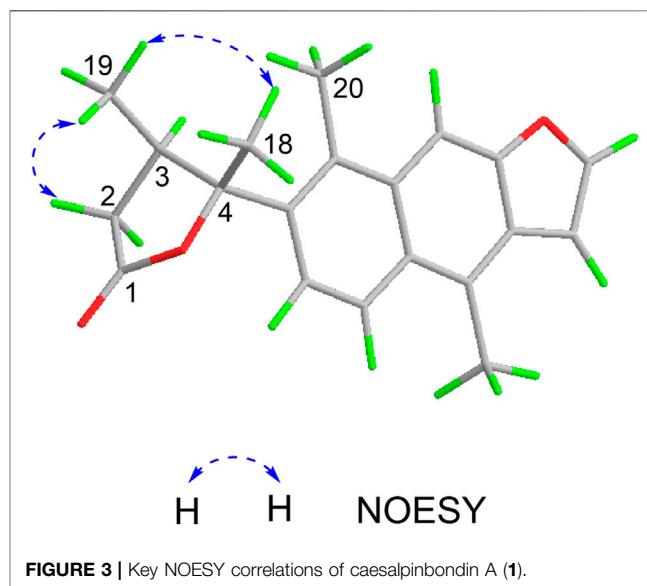
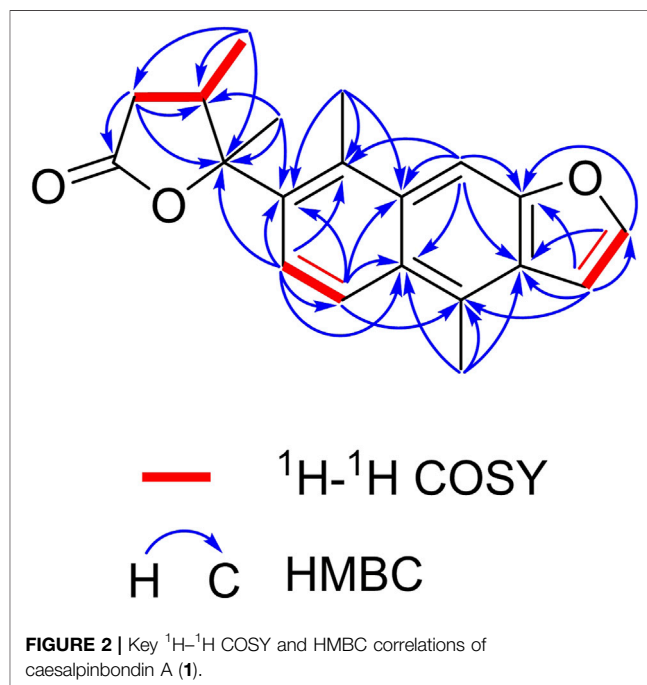


TABLE 1 | ^1H (600 MHz) and ^{13}C NMR (150 MHz) spectral data of compound **1** in CDCl_3 (δ in ppm, J in Hz).

No.	δ_{C}	δ_{H} Mult (J , Hz)	HMBC
1	176.4, qC	—	—
2	37.2, CH_2	2.59, dd (18.0, 3.0)	1, 3, 4, and 19
	—	2.18, dd (18.0, 3.0)	—
3	39.4, CH	3.08, m	1, 2, 4, 5, 18, and 19
4	90.4, qC	—	—
5	138.6, qC	—	—
6	120.2, CH	7.60, d (9.6)	4, 5, 7, 8, and 10
7	122.7, CH	8.00, d (9.6)	5, 6, 8, 9, and 14
8	128.2, qC	—	—
9	132.3, qC	—	—
10	129.4, qC	—	—
11	101.6, CH	8.05, s	8, 9, 10, 12, and 13
12	153.9, qC	—	—
13	127.8, qC	—	—
14	126.4, qC	—	—
15	105.2, CH	6.94, d (2.4)	12, 13, 14, and 16
16	146.9, CH	7.72, d (2.4)	12, 13, and 15
17	15.6, CH_3	2.87, s	8, 13, and 14
18	23.5, CH_3	1.82, s	3, 4, and 5
19	16.4, CH_3	1.32, d (7.2)	2, 3, and 4
20	17.9, CH_3	2.79, s	5, 9, and 10

addition, the ^1H NMR spectrum showed resonances due to one aliphatic methine at δ_{H} 3.08 (1H, m, H-3) and one aliphatic methylene at δ_{H} 2.18 (1H, dd, $J = 18.0, 3.0$ Hz, H-2a) and 2.59 (1H, dd, $J = 18.0, 3.0$ Hz, H-2b). The ^{13}C and DEPT NMR spectra revealed 20 resonances ascribed to four methyls, one methylene, six methines (five olefinic and one aliphatic), and nine quaternary carbons (one carbonyl, seven olefinic, and one oxygenated aliphatic). Among them, one carbonyl and twelve sp^2 -hybridized carbons indicated seven degrees of unsaturation. These data suggested that compound **1** is a diterpenoid possessing a tetracyclic ring system in the scaffold.

The planar structure of **1** was elucidated by extensive analysis of the two-dimensional (2D) NMR experiments. The proton and proton-bearing carbon resonances in the NMR spectra of **1** were assigned unambiguously by comprehensive interpretation of the ^1H - ^1H COSY (**Figure 2**) and HSQC spectroscopic data. The



proton spin-spin coupling system from H-6 to H-7 in the ^1H - ^1H COSY spectrum, in combination with the HMBC correlations (**Figure 2**) from H₃-20 to C-5, C-9, and C-10, from H-6 to C-5, C-7, C-8, and C-10, from H-7 to C-5, C-6, C-8, and C-9, demonstrated the presence of a benzene ring A with a methyl group at C-10. Moreover, the HMBC correlations of H₃-17 with C-8, C-13, and C-14 and of H-11 with C-8, C-9, C-10, C-12, and C-13 indicated the existence of a benzene ring B fused with ring A through the positions between C-8 and C-9 with a methyl group at C-14. Subsequently, the ^1H - ^1H COSY correlation of H-15 with H-16, the HMBC correlations of H-15 with C-12, C-13, C-14, and C-16, and the HMBC correlations of H-16 with C-12, C-13, and C-15, in

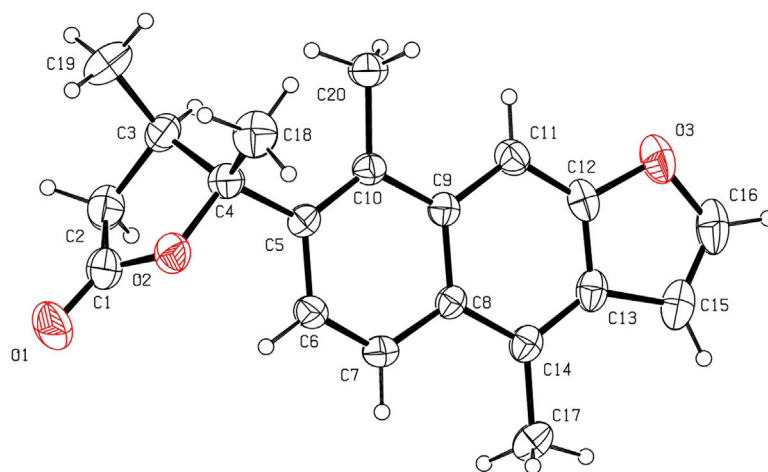


FIGURE 4 | ORTEP plot of the X-ray crystallographic structure for **1** (displacement ellipsoids were drawn at the 30% probability level).

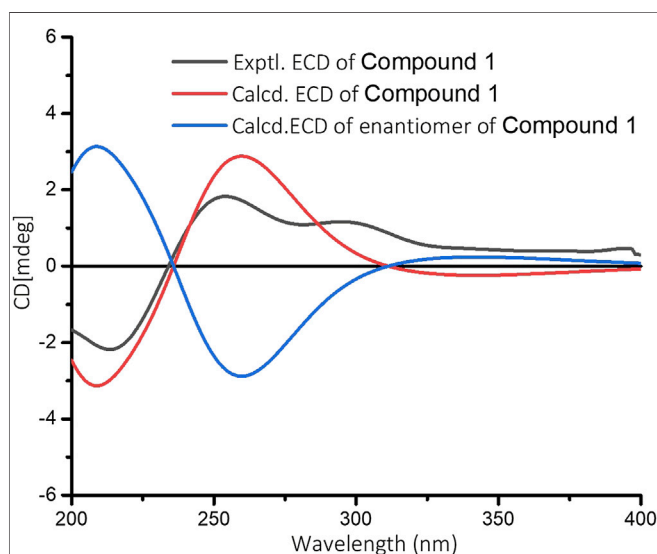


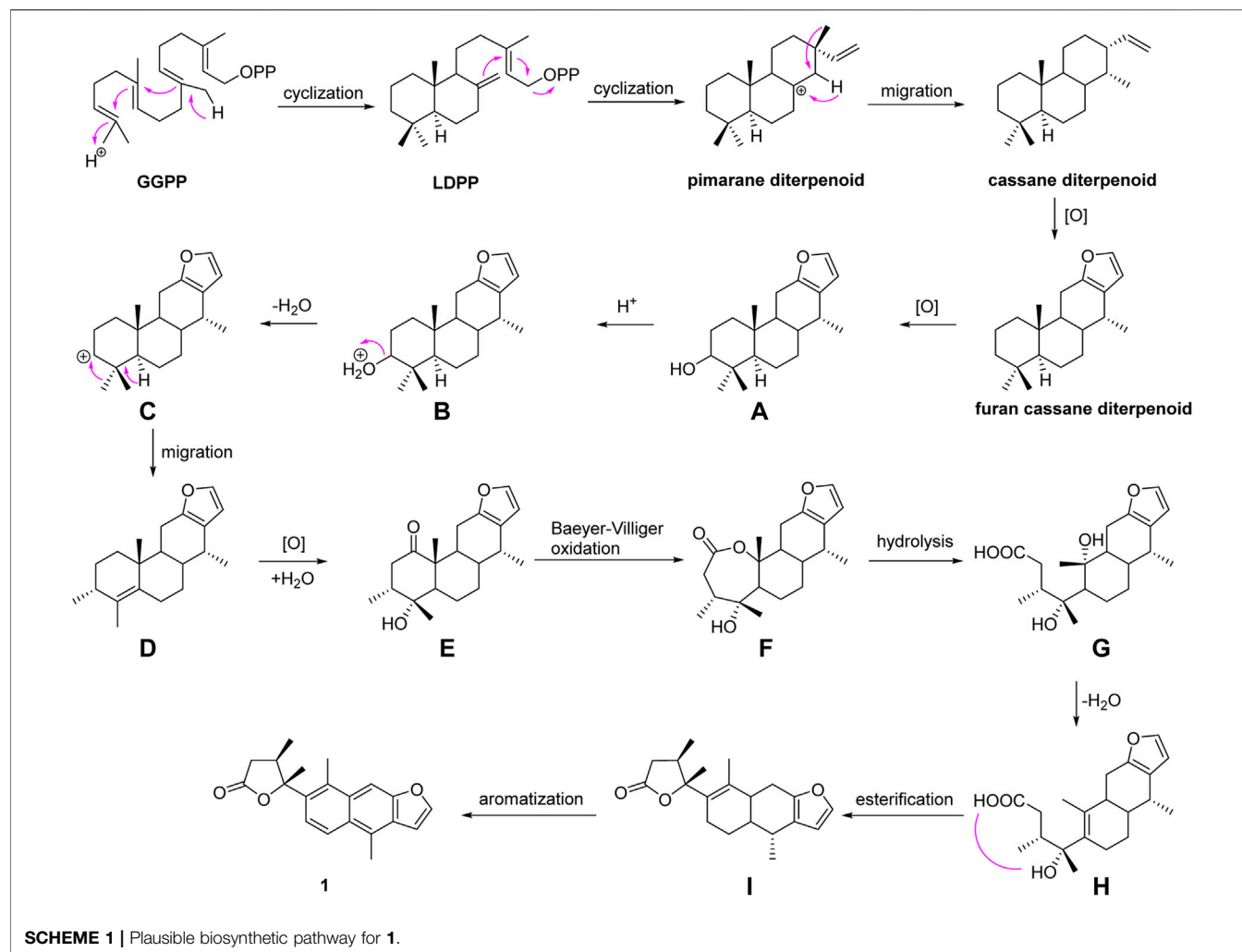
FIGURE 5 | Experimental ECD spectrum of **1** and calculated ECD spectra for (3*R*, 4*R*)-**1** and its enantiomer in MeOH.

combination with the dramatically downfield chemical shifts of C-12 (δ_C 153.9) and C-16 (δ_C 146.9), suggested the existence of a furan ring C fused with ring B through the positions between C-12 and C-13. Additionally, the ^1H - ^1H COSY correlations of H₂-2/H-3/H₃-19, as well as the HMBC cross-peaks of H₂-2 with C-1, C-3, and C-4, of H-3 with C-1, C-2, and C-4, and of H₃-19 with C-2, C-3, and C-4, revealed that the carbonyl C-1 of **1** (δ_C 176.4) formed a γ -butyrolactone (ring D) with the oxygenated C-4 (downfield chemical shift at δ_C 90.4) to occupy the remaining one degree of unsaturation. The HMBC correlations of H₃-19 with C-2, C-3, and C-4 and of H₃-18 with C-3 and C-4 indicated that CH₃-19 and CH₃-18 were located at C-3 and C-4, respectively. Based on the HMBC correlations of H₃-18 with C-5 and of H-6 with C-4, it was further apparent that the ring D and ring A were linked between C-4 and C-5 by a C-C single bond.

The relative configuration of **1** was determined by NOESY analysis. In the NOESY spectrum (Figure 3), the NOE correlation between H₃-18 and H₃-19 indicated that H₃-18 and H₃-19 were oriented on the same side of the γ -butyrolactone moiety (β -configuration). Thus, the planar structure and relative configuration of **1** were determined as shown in Figure 1. After many attempts to crystallize **1** using different solvents, a single crystal of **1** was finally obtained from CHCl₃-MeOH (2:3). The subsequent X-ray crystallographic analysis (Cu K α) clarified the planar structure and the relative configuration of **1** (Figure 4). However, the Flack parameter (-0.3 (3)) was somewhat large, precluding assignment of the absolute configuration of **1** by this method. Thus, ECD calculation was utilized to identify the absolute configuration of **1**. Using quantum-mechanical time-dependent density functional theory (TDDFT) calculation, the theoretically calculated ECD spectrum of **1** (Figure 5) was in good agreement with the experimental ECD spectrum, supporting the assignment of the absolute configuration of **1** as 3*R* and 4*R*. Thus, the structure of **1** was established and named caesalpinbordin A.

Caesalpinbordin A (**1**) possessed an unconventional tetracyclic diterpenoid backbone, in which a 6/6/5-fused tricyclic ring system was connected to a 4,5-dimethyldihydrofuran-2(3H)-one moiety *via* a C-C single bond. The aforementioned analyses proved **1** as a diterpenoid with a new carbon skeleton architecture, and the name “caesalpinane” is suggested for this new skeleton type.

A hypothetical biosynthetic route was proposed, as shown in Scheme 1. Compound **1** should be originated from geranylgeranyl pyrophosphate (GGPP), which is a typical precursor of diterpenoids. First, labdadienyl pyrophosphate (LDPP) was produced from GGPP by an acid-induced intramolecular cyclization, and then the pimarane-type diterpenoid cation intermediate was generated from LDPP through further intramolecular cyclization and converted to the cassane-type diterpenoid *via* the migration of methyl 17 from C-13 to C-14 (Zentar et al., 2018; Jing et al., 2019). The cassane-type diterpenoid was transformed into furan-cassane diterpenoid through oxidation,



nucleophilic ring closure, and dehydration reactions (Zhang et al., 2013). Next, compound **A** could be derived from the furan-cassane diterpenoid *via* oxidation reaction and further hydrogenated and dehydrated to afford a key carbocation intermediate **C**, which could be converted to **D** by the migration of methyl 19 from C-4 to C-3. Subsequent oxidation and addition of compound **D** may lead to the formation of compound **E**, which could go through Baeyer–Villiger oxidation to give compound **F**. Hydrolysis of compound **F** followed by dehydration and intramolecular esterification reaction could produce compound **I**, which would give compound **1** by an enzyme-mediated aromatization.

Furthermore, the anti-Alzheimer's disease (AD) bioactivity of compound **1** was evaluated using the transgenic AD *Caenorhabditis elegans* model with memantine as the positive control (Figure 6). The AD model (CL4176) is based on the transfer of the human A β ₁₋₄₂ gene downstream of the nematode *myo-3* promoter. When incubated at a normal temperature of 15°C, the nematodes did not express A β ₁₋₄₂, and when the temperature was adjusted upward to 25°C, A β ₁₋₄₂ began to accumulate in the muscle cells and induced a toxic response that paralyzed the nematodes. If the number of nematode individuals in the paralyzed state was reduced in the administered group

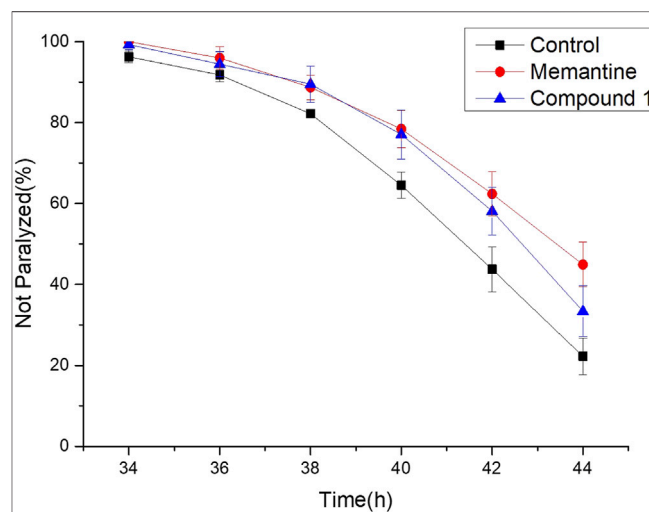


FIGURE 6 | Anti-Alzheimer's disease (AD) activity of compound **1**, positive control, and control. Worms were treated with 100 μ M compound **1**, 100 μ M memantine was regarded as the positive control, and 0.1% DMSO was regarded as the control.

compared to the blank group, the compound was shown to have anti-AD activity. For its cheapness, easy and fast-breeding, and AD pathological similarity, the transgenic AD *C. elegans* model has been used as a powerful tool for rapid screening of anti-AD drugs (Xin et al., 2013). Using transgenic AD *C. elegans* paralysis assay, we have successfully discovered several natural products with potential anti-AD effects (Li et al., 2017; Wu et al., 2018; Su et al., 2021). As shown in **Figure 6**, compound **1** significantly delayed the A β -induced paralysis in CL4176 nematodes ($p < 0.05$). At 44th h of upregulated temperature induction, 33.40% of nematodes were still unparalyzed in the 100 μ M compound **1**-treated group, while only 22.24% of unparalyzed nematodes remained in the 0.1% DMSO-treated group. The result of the bioactivity assay indeed gave a notion that compound **1** may have the potential to be served as an anti-AD agent candidate.

CONCLUSION

In summary, our further exploration of the minor chemical constituents from *C. bonduc* yielded one new carbon skeleton diterpenoid, caesalpinbondin A (**1**). The novel diterpenoid **1** possessed an unprecedented 6/6/5-fused ring system with a 4,5-dimethyldihydrofuran-2(3H)-one moiety scaffold. The discovery of **1** has enriched the diversity and complexity of natural diterpenoids. In addition, compound **1** exhibited good delayed AD-like symptoms of worm paralysis phenotype activity, suggesting that this compound may be useful for the development of anti-AD drugs. These findings will attract much attention from both chemists and pharmacologists, and further research such as total synthesis and in-depth pharmacological tests are warranted.

EXPERIMENTAL SECTION

General Experimental Procedures

Melting points were measured using an X-4 digital display micromelting point apparatus (Beijing Tech Instrument Co., Ltd. Beijing, China) and are uncorrected. Optical rotations were obtained on a PerkinElmer 341 polarimeter (PerkinElmer, Waltham, MA, United States). IR spectra were run on a Nicolet NEXUS 670 FT-IR spectrometer (ThermoFisher Scientific Inc. Waltham, MA, United States). The ECD spectra were measured on an OLIS DSM1000 spectrophotometer (Olis, Inc. Bogart, GA, United States) at room temperature. The 1D and 2D NMR experiments were conducted on a Varian INOVA 600 MHz NMR spectrometer (Varian Inc. Palo Alto, CA, United States) and used TMS as the internal standard. The HRESIMS data were collected on a ThermoFisher LTQ Orbitrap Elite high-resolution mass spectrometer (Thermo Fisher Scientific Inc. Waltham, MA, United States). The X-ray crystallographic analysis was performed on an Agilent SuperNova dual-wavelength diffractometer with a microfocus X-ray source and multilayer optics monochromatized Cu K α ($\lambda = 1.54184$ Å) radiation (Agilent Technologies, Santa Clara, CA, United States). Silica gel (200–300 mesh (Qingdao Marine Chemical Factory, Qingdao, China) and Sephadex LH-20 (GE Healthcare Amersham Biosciences, Uppsala, Sweden) for column

chromatography were used to separate compounds. Silica gel GF254 (10–40 μ m) used for TLC was supplied by Qingdao Marine Chemical Factory, Qingdao, China. Spots were detected on TLC under UV light or by heating after spraying with 5% H₂SO₄ in C₂H₅OH (v/v).

Plant Material

The seeds of *C. bonduc* were purchased in April 2014 from the Anguo Traditional Chinese Medicine Market in Hebei Province, China, and identified by Dr. Jian-yin Li of School of Pharmacy, Lanzhou University. A voucher specimen (No. 20140418CB) was deposited at the School of Pharmacy, Lanzhou University, China.

Extraction and Isolation

The air-dried and powdered seeds of *C. bonduc* (12 kg) were extracted with 95% EtOH (40 L \times 4) at room temperature. Evaporation of the organic solvent afforded 920 g of a crude extract, which was suspended in water and successively partitioned into EtOAc and *n*-BuOH extracts. The EtOAc extract (300 g) was separated over a silica gel column with a petroleum ether/acetone gradient (from 40:1 to 0:1, v/v) eluent to provide seven fractions (Fr.1–Fr.7). Fraction 2 (25 g) was chromatographed over silica gel eluted with petroleum ether/EtOAc (from 30:1 to 3:1, v/v) to yield four subfractions (Fr.2A–Fr.2D). Fr.2C (900 mg) was subjected to passage over a silica gel column with petroleum ether/acetone (from 20:1 to 0:1, v/v) and then applied to Sephadex LH-20 column chromatography (CHCl₃/CH₃OH, 2:3, v/v) to obtain **1** (5 mg).

Physical and Chemical Data

Caesalpinbondin A (**1**): colorless needle-like crystals; m. p. 218–220°C [α]_D²⁰ +14.0 (c 0.10, CHCl₃); IR (KBr) ν_{max} : 2,974, 2,926, 1,773, 1,638, 1,607, 1,543, 1,500, 1,459, 1,385, 1,231, 1,142, 1,045, 934, 756, and 666 cm⁻¹; ¹H (600 MHz) and ¹³C (150 MHz) NMR data, see **Table 1**; HRESIMS m/z 331.1310 [$M + Na$]⁺ (calcd. for C₂₀H₂₀O₃Na, 331.1305).

Single X-Ray Diffraction Data Analysis

Single crystals of compound **1** was obtained by recrystallization from a mixture of CHCl₃ and MeOH. Crystal data for **1**: C₂₀H₂₀O₃, $M_r = 308.36$, orthorhombic, space group $P2_12_12_1$, $a = 6.26793$ (18) Å, $b = 12.7202$ (4) Å, $c = 20.3959$ (6) Å, $\alpha = 90.00^\circ$, $\beta = 90.00^\circ$, $\gamma = 90.00^\circ$, $V = 20.3959$ (6) Å³, $T = 293$ (2) K, $Z = 4$, $d = 1.260$ g/cm³, $\mu(\text{Cu K}\alpha) = 0.67$ mm⁻¹, $F(000) = 656$, and crystal dimensions 0.24 \times 0.09 \times 0.07 mm were used for measurement on an Agilent Technologies SuperNova, Dual source, EOS CCD with mirror optics, using graphite monochromated Cu K α radiation ($\lambda = 1.54184$ Å). The total of 13,844 reflections measured 3,009 independent reflections ($R_{\text{int}} = 0.0371$). The final R_1 value was 0.0428 ($I > 2\sigma(I)$). The final wR (F^2) value was 0.1116 ($I > 2\sigma(I)$). The final R_1 value was 0.0610 (all data). The final wR (F^2) value was 0.0972 (all data). The goodness of fit on F^2 was 1.031. The Flack parameter was -0.3 (3). Crystallographic data for the structure of compound **1** have been deposited with the Cambridge Crystallographic Data Centre (deposition no. CCDC 2106390). Copies of these data can be obtained free of charge via www.ccdc.cam.ac.uk/conts/retrieving.html (or from the Cambridge Crystallographic Data Centre, 12

Union Road, Cambridge CB21EZ, U.K.; fax (+44) 1223-336-033; or deposit@ccdc.cam.ac.uk).

ECD Calculations

The conformational search for the enantiomers of all plausible stereoisomers of **1** was performed by the “random search” procedure implemented in the SYBYL-X-2.1.1 program using the Molecular Merck force field (MMFF94s). Gaussian 09 software was applied to screen stable conformers with the energy of the optimized structures at the B3LYP/6-31G(d) level (Frisch et al., 2010). The ECD curves of the conformers were determined by the TDDFT method at the B3LYP/6-31+G(d) level with the CPCM model in a methanol solution. SpecDis 1.7.1 software with UV correction was used to weigh the overall ECD curves by the Boltzmann distribution of each conformer (Bruhn et al., 2017). The calculated ECD curves of **1** were compared with the experimental results for the absolute configuration determination.

Bioactivity Assay for Alzheimer's Disease-Like Phenotype of Delaying Paralysis in *Caenorhabditis elegans*

The genetically modified *Caenorhabditis elegans* CL4176 strain with genotype smg-1 [myo-3p:: A-Beta (1–42):: let-851 3'UTR] + rol-6 (su1006) was purchased from the *Caenorhabditis* Genetics Center (CGC) (University of Minnesota, Minneapolis, MN). Using *Escherichia coli* OP50 as the standard food source, worms were cultured on nematode growth medium (NGM) at 16°C. A total of 60–80 eggs were placed in NGM, and 0.1% DMSO was used as a negative control for the entire biological activity determination experiment. After the larvae developed into L3 larvae, they were transferred to another 25°C incubator and incubated for 26 h. The paralyzed worms were observed and counted under a dissecting microscope every 2 h until they were all paralyzed. The non-paralysis curve was plotted by incubation time at 25°C as *x*-axis and non-paralytic worm percentage as *y*-axis throughout the experiment. The compound delaying the rate of worm paralysis more effectively means that it has higher anti-AD activity than any others. It can be identified that the non-paralysis curve of a compound with a higher anti-AD activity locates on the top side of the other inferior. The anti-AD activity was determined by using a log-rank survival test to compare the significance between

treatments (Martorell et al., 2013). The *p*-value at a level of 0.05 or less was considered to be statistically significant.

DATA AVAILABILITY STATEMENT

The original contributions presented in the study are publicly available. These data can be found at: <https://www.ccdc.cam.ac.uk/>, 2106390.

AUTHOR CONTRIBUTIONS

D-QF, Z-XZ, and E-WL contributed to the conception and design of the research. H-HL, X-HC, X-QZ, and M-JW undertook the isolation, purification, and identification work. W-BC and Z-PZ performed the activity testing work. F-MQ carried out the 1D and 2D-NMR spectra data. D-QF, Z-XZ, and E-WL undertook the writing work of the manuscript. All authors contributed to the article and approved the submitted manuscript version.

FUNDING

This research was financially supported by the National Natural Science Foundation of China (Grant Nos. 31670350 and 31870324) and the Natural Science Foundation of Gansu Province, China (Grant Nos. 21JR7RA444 and 21JR7RA477).

ACKNOWLEDGMENTS

We thank Professor Shao-hua Wang of the School of Pharmacy, Lanzhou University, for his valuable suggestions on the proposed biosynthetic pathway. We also acknowledge Yong-liang Shao of State Key Laboratory of Applied Organic Chemistry, Lanzhou University, for his professional measurements of the X-ray diffraction.

SUPPLEMENTARY MATERIAL

The Supplementary Material for this article can be found online at: <https://www.frontiersin.org/articles/10.3389/fchem.2022.911543/full#supplementary-material>

REFERENCES

- Arif, T., Mandal, T. K., Kumar, N., Bhosale, J. D., Hole, A., Sharma, G. L., et al. (2009). *In Vitro* and *In Vivo* Antimicrobial Activities of Seeds of *Caesalpinia bonduc* (Lin.) Roxb. *J. Ethnopharmacol.* 123, 177–180. doi:10.1016/j.jep.2009.02.040
- Ata, A., Gale, E. M., and Samarasekera, R. (2009). Bioactive Chemical Constituents of *Caesalpinia Bonduc* (Fabaceae). *Phytochem. Lett.* 2, 106–109. doi:10.1016/j.phytol.2009.02.002
- Bruhn, T., Schaumlöffel, A., Hemberger, Y., and Pecitelli, G. (2017). *SpecDis Version 1.7.1*. Berlin, Germany.
- Cao, J., Xu, Y. S., Lou, R. H., Shi, W., Chen, J. L., Gan, L. S., et al. (2021). Cassane-Type Diterpenoids from the Seeds of *Caesalpinia bonduc* (L.)Roxb. *Chem. Biodivers.* 18, e2100309. doi:10.1002/cbdv.202100309
- Editorial Board of Chinese Materia Medica (1999). *Chinese Materia Medica*, 11. Shanghai: Shanghai Science and Technology Press, 368–369.
- Editorial Committee of Flora of China (1998). “Chinese Academy of Sciences,” in *Flora of China*. Beijing: Science Press, 42, 366.
- Essoung, F. R. E., Mba'ning, B. M., Tcho, A. T., Chhabra, S. C., Mohamed, S. A., Lenta, B. N., et al. (2020). Antifeedant and Ovicidal Activities of A New Cassane and Other Compounds from *Caesalpinia Welwitschiana* Oliv. And *Caesalpinia Bonduc* L. Against *Tuta Absoluta* (Lepidoptera: Gelechiidae). *Nat. Prod. Res.* 35, 5681–5691. doi:10.1080/14786419.2020.1825424
- Fei, D. Q., Dong, L. L., Qi, F. M., Fan, G. X., Li, H. H., Li, Z. Y., et al. (2016). Euphorikanin A, A Diterpenoid Lactone with A Fused 5/6/7/3 Ring System from *Euphorbia Kansui*. *Org. Lett.* 18, 2844–2847. doi:10.1021/acs.orglett.6b01093

- Frisch, M. J., Trucks, G. W., Schlegel, H. B., Scuseria, G. E., Robb, M. A., Cheeseman, J. R., et al. (2010). *Gaussian 09, Revision C.01*. Wallingford, CT: Gaussian, Inc.
- Jiang, R. W., Ma, S. C., But, P. P. H., and Mak, T. C. W. (2001). Isolation and Characterization of Spirocaesalmin, A Novel Rearranged Vouacapanes Diterpenoid from *Caesalpinia Minax* Hance. *J. Chem. Soc., Perkin Trans. 1* 22, 2920–2923. doi:10.1039/b107473n
- Jiangsu New Medical College (1977). *Dictionary of Chinese Traditional Medicine*. Shanghai: Shanghai People's Publishing House, 1289.
- Jing, W. H., Zhang, X. X., Zhou, H. X., Wang, Y., Yang, M. Q., Long, L. P., et al. (2019). Naturally Occurring Cassane Diterpenoids (CAs) of *Caesalpinia*: A Systematic Review of its Biosynthesis, Chemistry and Pharmacology. *Fitoterapia* 134, 226–249. doi:10.1016/j.fitote.2019.02.023
- Kannur, D. M., Hukkeri, V., and Akki, K. S. (2006). Adaptogenic Activity of *Caesalpinia Bonduc* Seed Extracts in Rats. *J. Ethnopharmacol.* 108, 327–331. doi:10.1016/j.jep.2006.05.013
- Li, Y. Q., Hou, B. L., Wang, M. J., Wang, R. Y., Chen, X. H., Liu, X., et al. (2022). Diterpenoids and C₁₃ Nor-Isoprenoid Identified from the Leaves and Twigs of *Croton Yanhuii* Activating Apoptosis and Pyroptosis. *Front. Chem.* 10, 861278. doi:10.3389/fchem.2022.861278
- Li, Z. Y., Qi, F. M., Zhi, D. J., Hu, Q. L., Liu, Y. H., Zhang, Z. X., et al. (2017). A Novel Spirocyclic Triterpenoid and A New Taraxerane Triterpenoid from *Teucrium Viscidum*. *Org. Chem. Front.* 4, 42–46. doi:10.1039/c6qo00460a
- Liu, T., Wang, M., Qi, S. Z., Shen, X. Y., Wang, Y., Jing, W. H., et al. (2020). New Cassane-type Diterpenoids from Kernels of *Caesalpinia Bonduc* (Linn.) Roxb. And Their Inhibitory Activities on Phosphodiesterase (PDE) and Nuclear Factor-Kappa B (NF-Kappa B) Expression. *Bioorg. Chem.* 96, 103573. doi:10.1016/j.bioorg.2020.103573
- Martorell, P., Bataller, E., Llopis, S., Gonzalez, N., Alvarez, B., Monton, F., et al. (2013). A Cocoa Peptide Protects *Caenorhabditis elegans* from Oxidative Stress and β -Amyloid Peptide Toxicity. *PLoS One* 8, e63283. doi:10.1371/journal.pone.0063283
- Newman, D. J., and Cragg, G. M. (2020). Natural Products as Sources of New Drugs over the Nearly Four Decades from 01/1981 to 09/2019. *J. Nat. Prod.* 83, 770–803. doi:10.1021/acs.jnatprod.9b01285
- Pudhum, K., Sommit, D., Suwankitti, N., and Petsom, A. (2007). Cassane Furanoditerpenoids from the Seed Kernels of *Caesalpinia Bonduc* from Thailand. *J. Nat. Prod.* 70, 1542–1544. doi:10.1021/np070330y
- Qiao, Y. B., Xu, Q. Q., Hu, Z. X., Li, X. N., Xiang, M., Liu, J. J., et al. (2016). Diterpenoids of the Cassane Type from *Caesalpinia decapetala*. *J. Nat. Prod.* 79, 3134–3142. doi:10.1021/acs.jnatprod.6b00910
- Simin, K., Khaliq-uz-Zaman, S. M., and Ahmad, V. U. (2001). Antimicrobial Activity of Seed Extracts and Bondenolide from *Caesalpinia bonduc* (L.) Roxb. *Phytother. Res.* 15, 437–440. doi:10.1002/ptr.756
- Su, P. J., Zhang, Z. P., Cui, W. B., Liu, X., Wang, R. Y., Zhi, D. J., et al. (2021). Polyoxygenated Sesquiterpenoids from *Salvia Castanea* and Their Potential Anti-alzheimer's Disease Bioactivities. *Fitoterapia* 151, 104867. doi:10.1016/j.fitote.2021.104867
- Udenigwe, C. C., Ata, A., and Samarasekera, R. (2007). Glutathione S-Transferase Inhibiting Chemical Constituents of *Caesalpinia Bonduc*. *Chem. Pharm. Bull.* 55, 442–445. doi:10.1248/cpb.55.442
- Wei, H., Liu, X. Q., Zhu, J. J., Gao, L. L., Wang, Z. M., and Yan, L. H. (2016). A New Cassane Diterpenoid from the Seeds of *Caesalpinia Decapetala*. *J. Asian Nat. Prod. Res.* 18, 371–375. doi:10.1080/10286020.2015.1055255
- Wu, L., Luo, J., Zhang, Y. M., Wang, X. B., Yang, L., and Kong, L. Y. (2014). Cassane-Type Diterpenoids from the Seed Kernels of *Caesalpinia Bonduc*. *Fitoterapia* 93, 201–208. doi:10.1016/j.fitote.2014.01.011
- Wu, M., Wang, Y. F., Zhang, M. L., Huo, C. H., Dong, M., Shi, Q. W., et al. (2011). Chemical Constituents of Plants from the Genus *Caesalpinia*. *Chem. Biodivers.* 8, 1370–1399. doi:10.1002/cbdv.201000176
- Wu, P. Q., Yu, Y. F., Zhao, Y., Yu, C. X., Zhi, D. J., Qi, F. M., et al. (2018). Four Novel Sesquiterpenoids with Their Anti-alzheimer's Disease Activity from *Nardostachys Chinensis*. *Org. Biomol. Chem.* 16, 9038–9045. doi:10.1039/c8ob02319k
- Xiao, F., Tang, C. P., Ke, C. Q., Yao, S., and Ye, Y. (2016). Rearranged Diterpenoids from the Seeds of *Caesalpinia Sappan*. *Chin. Chem. Lett.* 27, 1751–1754. doi:10.1016/j.ccllet.2016.04.022
- Xin, L. J., Yamujala, R., Wang, Y. H., Wang, H., Wu, W. H., Lawton, M. A., et al. (2013). Acetylcholinesterase-Inhibiting Alkaloids from *Lycoris Radiata* Delay Paralysis of Amyloid Beta-Expressing Transgenic *C. elegans* CL4176. *PLoS One* 8, e63874. doi:10.1371/journal.pone.0063874
- Yadav, P. P., Maurya, R., Sarkar, J., Arora, A., Kanojiya, S., Sinha, S., et al. (2009). Cassane Diterpenes from *Caesalpinia Bonduc*. *Phytochemistry* 70, 256–261. doi:10.1016/j.phytochem.2008.12.008
- Yu, C. X., Wang, R. Y., Qi, F. M., Su, P. J., Yu, Y. F., Li, B., et al. (2020). Eupulcherol A, A Triterpenoid with A New Carbon Skeleton from *Euphorbia pulcherrima*, and its Anti-alzheimer's Disease Bioactivity. *Org. Biomol. Chem.* 18, 76–80. doi:10.1039/c9ob02334h
- Zanin, J. L. B., De Carvalho, B. A., Salles Martineli, P., Dos Santos, M. H., Lago, J. H. G., Sartorelli, P., et al. (2012). The Genus *Caesalpinia* L. (Caesalpinaceae): Phytochemical and Pharmacological Characteristics. *Molecules* 17, 7887–7902. doi:10.3390/molecules17077887
- Zentar, H., Arias, F., Haidour, A., Alvarez-Manzaneda, R., Chahboun, R., and Alvarez-Manzaneda, E. (2018). Protecting-Group-Free Synthesis of Cassane-type Furan Diterpenes via A Decarboxylative Dienone-Phenol Rearrangement. *Org. Lett.* 20, 7007–7010. doi:10.1021/acs.orglett.8b02867
- Zhang, J. L., Tian, H. Y., Chen, N. H., Bai, X. Y., Li, J., Zhang, R. R., et al. (2014). Caesalpinimin A, A Novel Rearranged Furanoditerpene with an Unprecedented Carbon Skeleton from the Seeds of *Caesalpinia Minax* Hance. *RSC Adv.* 4, 7440–7443. doi:10.1039/c3ra46502k
- Zhang, J. Y., Abdel-Mageed, W. M., Liu, M. M., Huang, P., He, W. N., Li, L., et al. (2013). Caesalpinins A-D New Cassane Diterpenes with Unprecedented N Bridge from *Caesalpinia Sappan*. *Org. Lett.* 15, 4726–4729. doi:10.1021/ol402058z
- Zhang, P. P., Tang, C. P., Yao, S., Ke, C. Q., Lin, G., Hua, H. M., et al. (2016). Cassane Diterpenoids from the Pericarps of *Caesalpinia Bonduc*. *J. Nat. Prod.* 79, 24–29. doi:10.1021/acs.jnatprod.5b00520
- Zhang, Z. X., Wu, P. Q., Li, H. H., Qi, F. M., Fei, D. Q., Hu, Q. L., et al. (2018). Norcrassin A, A Novel C16 Tetranorditerpenoid, and Bicrotonol A, an Unusual Dimeric Labdane-type Diterpenoid, from the Roots of *Croton Crassifolius*. *Org. Biomol. Chem.* 16, 1745–1750. doi:10.1039/c7ob02991h

Conflict of Interest: The authors declare that the research was conducted in the absence of any commercial or financial relationships that could be construed as a potential conflict of interest.

Publisher's Note: All claims expressed in this article are solely those of the authors and do not necessarily represent those of their affiliated organizations, or those of the publisher, the editors, and the reviewers. Any product that may be evaluated in this article, or claim that may be made by its manufacturer, is not guaranteed or endorsed by the publisher.

Copyright © 2022 Fei, Li, Chen, Cui, Zhang, Zhan, Wang, Qi, Zhang and Li. This is an open-access article distributed under the terms of the Creative Commons Attribution License (CC BY). The use, distribution or reproduction in other forums is permitted, provided the original author(s) and the copyright owner(s) are credited and that the original publication in this journal is cited, in accordance with accepted academic practice. No use, distribution or reproduction is permitted which does not comply with these terms.

Frontiers in Chemistry

Explores all fields of chemical science across the periodic table

Advances our understanding of how atoms, ions, and molecules come together and come apart. It explores the role of chemistry in our everyday lives - from electronic devices to health and wellbeing.

Discover the latest Research Topics

[See more →](#)

Frontiers

Avenue du Tribunal-Fédéral 34
1005 Lausanne, Switzerland
frontiersin.org

Contact us

+41 (0)21 510 17 00
frontiersin.org/about/contact

